A.I.Ch.E. JOURNAL

CHEMICAL ENGINEERING RESEARCH AND DEVELOPMENT / SEPTEMBER 1959

THE UNIVERSITY OF MICHIGAN
OCT 2 1959
ENGINEERING LIBRARY

ENGIN. LIB.

CONTENTS

Rate Constants and Molecular Structure	Harold S. Johnston and Kenneth S. Pitzer
The Phase Behavior and Solubility Relations of the Benzene-Water System	Charles J. Rebert and Webster B. Kay
Performance of Packed Columns: V. Effect of Solute Concentration on Gas-Phase Mass Transfer Rates	H. L. Shulman and L. J. Delaney
Multicomponent Distillation on a Large Digital Computer: II. Generalization with Side-Stream Stripping	N. R. Amundson, A. J. Pontinen, and J. W. Tierney
Effective Collision Diameters and Correlation of Some Thermodynamic Properties of Solutions	J. M. Prausnitz and P. R. Benson
A Computer Study of a Free-Radical Mechanism of Ethane Pyrolysis	R. H. Snow, R. E. Peck, and C. G. Von Fredersdorf
Particle Fluidization and Sedimentation of Spheres	A. L. Loeffler, Jr., and B. F. Ruth
Effect of Liquid on Interparticle Forces in Gas-fluidized Beds	Harry W. Parker and William F. Stevens
Formation of Gas Bubbles at Submerged Orifices	W. B. Hayes, III, B. W. Hardy, and C. D. Holland
Longitudinal Laminar Flow Between Cylinders Arranged in Regular Array	E. M. Sparrow and A. L. Loeffler, Jr.
Some Aspects of Fluid Mechanics in Chemical Engineering	B. H. Sage
Diffusion-controlled Chemical Reactions	H. L. Toor and S. H. Chiang
Mechanism of Drying Thick Porous Bodies During the Falling-Rate Period: II. A Hygroscopic Material	J. R. Bell and A. H. Nissan
Initiation of the Homogeneous *n*-Butane Oxidation	J. F. Skrivan and H. E. Hoelscher
Experimental Foundations of Chemical Engineering	R. R. White and S. W. Churchill
Vinyl Chloride from Acetylene and Hydrogen Chloride: Catalytic-Rate Studies	R. D. Wesselhoft, J. M. Woods, and J. M. Smith
Thermal Conductivity of Diatomic Gases: Liquid and Gaseous States	Charles A. Schaefer and George Thodos
Ion Exchange Kinetics for Systems of Nonlinear Equilibrium Relationships	Chi Tien and George Thodos
Theory of Solvent Extraction of Phosphoric and Hydrochloric Acids	W. H. Seaton and C. J. Geankoplis
Continuous Stirred Tank Reactors: Designs for Maximum Conversions of Raw Material to Desired Product. Homogeneous Reactions	P. J. Trambouze and Edgar L. Piret
Studies of the Cation Exchange System Fe^{+++} -H^{+} I. Equilibrium Studies II. Rate Studies in Concentrated Solutions	R. C. Vasishth and M. M. David
Fluid Dynamics and Diffusion Calculations for Laminar Liquid Jets	L. E. Scriven and R. L. Pigford
Film Boiling of Helium I and Other Liquefied Gases on Single Wires	T. H. K. Frederking

With a

PACE® *Computer you can*

TORTURE A CAT CRACKER . . .

simulate

any dynamic problem!

These men are simulating the performance of a catalytic cracking tower on a PACE Electronic Analog Computer. They are developing the ideal combination of pressure, temperature and flow for better process control and improved refinery efficiency.

This ability to study dynamic characteristics on electronic analog computers and to test equipment to destruction before it is built—is aiding a variety of industries in upgrading processes and developing new designs. Analog computers simulate machine or process performance and chart accurate graphic pictures of what happens under extremes of speed, pressure, temperature, etc. When destruction or breakdown occurs, the reason is clearly indicated. This helps engineers to "design-out" problems before pilots or prototypes are built. It means new and safer methods of operation can be found—with less engineering time and expense.

Electronic Associates, the world's largest manufacturer of general purpose electronic analog computers, offers a complete line of analog computing equipment and accessories. And you'll be surprised to learn how easy this equipment is to operate.

To help you solve specific problems and gain first-hand knowledge of the benefits of analog simulation, EAI operates three Computation Centers.

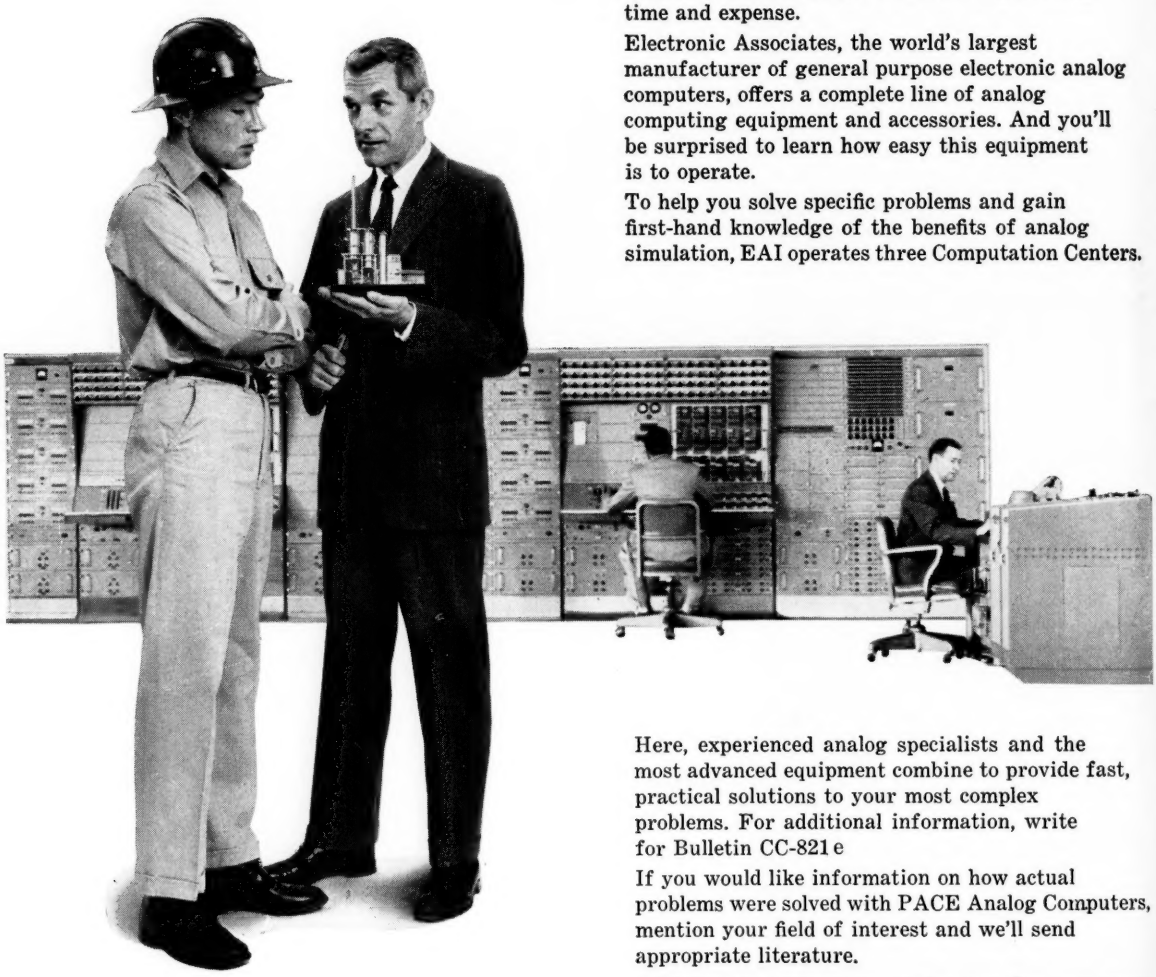

Here, experienced analog specialists and the most advanced equipment combine to provide fast, practical solutions to your most complex problems. For additional information, write for Bulletin CC-821 e

If you would like information on how actual problems were solved with PACE Analog Computers, mention your field of interest and we'll send appropriate literature.

Outstanding career opportunities for engineers with proven ability—résumés invited.

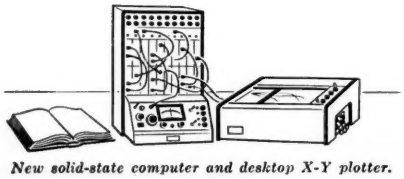

New solid-state computer and desktop X-Y plotter.

EAI

ELECTRONIC ASSOCIATES, INCORPORATED

Long Branch, New Jersey

A.I.Ch.E. JOURNAL

SEPTEMBER, 1959 ● VOL. 5, NO. 3

The A.I.Ch.E. Journal, an official publication of the American Institute of Chemical Engineers, is devoted in the main to theoretical developments and research in chemical engineering and allied branches of engineering and science. Manuscripts should be submitted to the New York office.

PUBLISHER

F. J. Van Antwerpen

EDITOR

Harding Bliss

ASSISTANT PUBLISHER

L. T. Dupree

MANAGING EDITOR

Sylvia Fourdrinier

ADVERTISING MANAGER

P. A. Jolcuvar

ADVISORY BOARD

C. M. Cooper	R. H. Newton
O. E. Dwyer	R. L. Pigford
W. C. Edmister	E. L. Piret
E. R. Gilliland	J. M. Smith
A. N. Hixson	Theodore Vermeulen
H. F. Johnstone	R. R. White
W. R. Marshall, Jr.	R. H. Wilhelm

Publication Office, Richmond, Virginia. Published quarterly in March, June, September, and December by the American Institute of Chemical Engineers, 25 West 45 Street, New York 36 New York. Manuscripts and other communications should be sent to the New York office. Correspondence with the editor may be addressed to him at Yale University, 225 Prospect Street, New Haven 11, Connecticut. Statements and opinions in the *A.I.Ch.E. Journal* are those of the contributors, and the American Institute of Chemical Engineers assumes no responsibility for them. Subscriptions: one year, member $4.50, nonmember $9.00; two years, member $7.50, nonmember $15.00; additional yearly postage, Canada 50 cents, Pan American Union $1.50, other foreign $2.00 (foreign subscriptions payable in advance). Single copies: $3.00. Second-class mail privileges authorized at Richmond, Virginia. Copyright 1959 by the American Institute of Chemical Engineers. National headquarters of A.I.Ch.E. is concerned about nondelivery of copies of the *A.I.Ch.E. Journal* and urgently requests subscribers to give prompt notification of any change of address. Sixty days must be allowed for changes to be made in the records.

Conservation and Engineering: I. Dreams and Reality 275

Rate Constants and Molecular Structure ..*Harold S. Johnston and Kenneth S. Pitzer* 277

The Phase Behavior and Solubility Relations of the Benzene-Water System
Charles J. Rebert and Webster B. Kay 285

Performance of Packed Columns: V. Effect of Solute Concentration on Gas-Phase Mass Transfer Rates .....*H. L. Shulman and L. J. Delaney* 290

Multicomponent Distillation on a Large Digital Computer:
II. Generalization with Side-Stream Stripping
N. R. Amundson, A. J. Pontinen, and J. W. Tierney 295

Effective Collision Diameters and Correlation of Some Thermodynamic Properties of Solutions .....*J. M. Prausnitz and P. R. Benson* 301

A Computer Study of a Free-Radical Mechanism of Ethane Pyrolysis
R. H. Snow, R. E. Peck, and C. G. Von Fredersdorf 304

Particle Fluidization and Sedimentation of Spheres
A. L. Loeffler, Jr., and B. F. Ruth 310

Effect of Liquid on Interparticle Forces in Gas-fluidized Beds
Harry W. Parker and William F. Stevens 314

Formation of Gas Bubbles at Submerged Orifices
W. B. Hayes, III, B. W. Hardy, and C. D. Holland 319

Longitudinal Laminar Flow Between Cylinders Arranged in Regular Array
E. M. Sparrow and A. L. Loeffler, Jr. 325

Some Aspects of Fluid Mechanics in Chemical Engineering .....*B. H. Sage* 331

Diffusion-controlled Chemical Reactions .....*H. L. Toor and S. H. Chiang* 339

Mechanism of Drying Thick Porous Bodies During the Falling-Rate Period:
II. A Hygroscopic Material .....*J. R. Bell and A. H. Nissan* 344

Initiation of the Homogeneous *n*—Butane Oxidation
J. F. Skrivan and H. E. Hoelscher 348

Experimental Foundations of Chemical Engineering
R. R. White and S. W. Churchill 354

Vinyl Chloride from Acetylene and Hydrogen Chloride: Catalytic-Rate Studies
R. D. Wesselhoft, J. M. Woods, and J. M. Smith 361

Thermal Conductivity of Diatomic Gases: Liquid and Gaseous States
Charles A. Schaefer and George Thodos 367

Ion Exchange Kinetics for Systems of Nonlinear Equilibrium Relationships
Chi Tien and George Thodos 373

Theory of Solvent Extraction of Phosphoric and Hydrochloric Acids
W. H. Seaton and C. J. Geankoplis 379

Continuous Stirred Tank Reactors: Designs for Maximum Conversions of Raw Material to Desired Product. Homogeneous Reactions
P. J. Trambouze and Edgar L. Piret 384

Studies of the Cation Exchange System Fe^{+++} -H^{+}
R. C. Vasishth and M. M. David

I. Equilibrium Studies 391

II. Rate Studies in Concentrated Solutions 394

Fluid Dynamics and Diffusion Calculations for Laminar Liquid Jets
L. E. Scriven and R. L. Pigford 397

Film Boiling of Helium I and Other Liquefied Gases on Single Wires
T. H. K. Frederking 403

Communications to the Editor

The Uselessness of Raffinate Reflux .....*J. F. Wehner* 406

The Uselessness of Total Reboiling .....*J. F. Wehner* 407

Semifluidization: Mass Transfer in Semifluidized Beds
Liang-Tseng Fan, Yung-Chia Yang, and Chin-Yung Wen 407

The Ratio of Fluids to Solid Temperature and/or Concentration in Fixed-Bed Processes .....*H. E. Hoelscher* 410

Thermodynamic Consistency Test for Multicomponent Solutions
J. M. Prausnitz and G. D. Snider 7S

Books 276

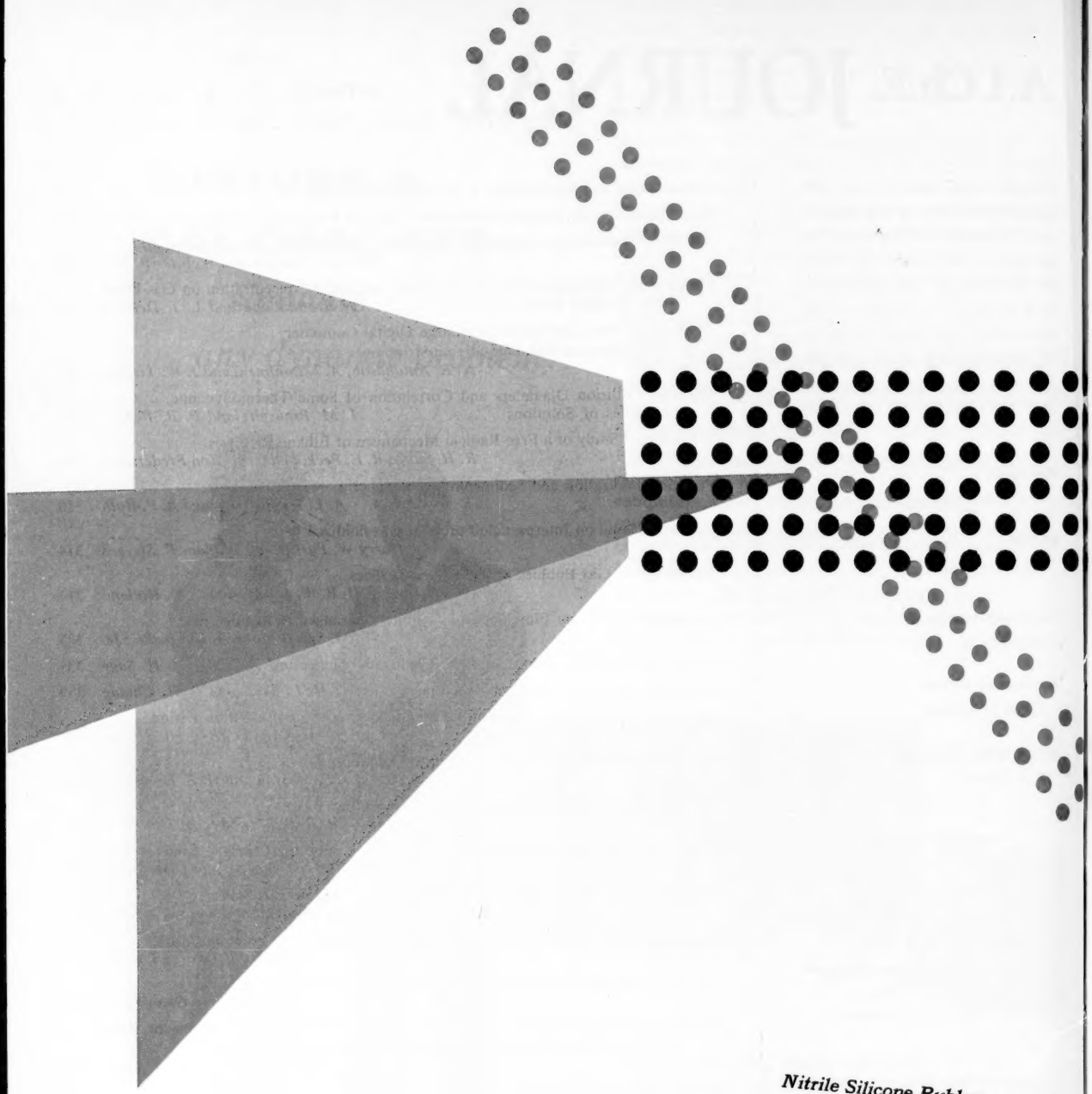

Nitrile Silicone Rubber

Tomorrow's Light Is Here

The World's Hottest Alloys

Is There Really a Shortage of Engineers?

Motivating the Technical Mind

Reinforcing the Plastics Revolution

A.I.Ch.E. JOURNAL

Conservation and Engineering

I. Dreams and Reality

We live in a dream world of sorts, a world in which the economists tell us that a 5% (or 3% or 7%, depending on the axe being ground) growth of production is required or is normal—or is essential to keep ahead of the Russians. We are bombarded with propaganda from Washington and from Wall Street purporting to demonstrate the wonder world of tomorrow when our population will have increased by 50% (or 100%, again depending on the axe). It is supposed that this increased population will consume more, generating greater and greater profits and taxes, but the economic seers are strangely silent on the sources of the food and materials to be thus consumed. The simple facts of the matter are that these dreams of the future disregard some elemental considerations. Also they are based on a simple and childlike faith that science and engineering will provide. Such faith, while flattering, has little foundation in fact. Technology can do a lot to help—indeed, the essence of this series of editorials will be to show many things which can be done—but technology has its limitations.

Excessive population growth, such as is being experienced in many countries, including the United States, is no cause for joy. Growth rates leading to a double world population in the next 50 years or less are going to lead, also, to some very acute problems with which more and more of us must concern ourselves. Billions of mouths to feed, bodies to clothe, and jobs to create are going to meet us head on just when another unhappy development may arise.

That development is that our past and continuing abuses of the earth are beginning to catch up with us. The future promises that we may have somdifficulty in providing food and materials for oue present peoples just about when the population exr plosion hits us. We cannot grow food on eroded land washing away to the sea, we cannot drink water from rivers converted to open sewers, and we cannot employ people in manufacturing when the raw materials are gone.

The Conservationists have been saying these things for years, and the interested student should acquaint himself with their literature. They have been almost alone; it is time that we engineers joined them. Everyone of ability and good will will be needed.

The reality of this matter is that the two factors—population growth and the abuses of our earth—are leading us to a period of stresses and strains of considerable magnitude. The consequent sociological and political ramifications such as the spread of communism and the constant threat of war are accurately described by Huxley in "Brave New World Revisited."

Our best hope of alleviating these problems is technology. Probably only alleviation is possible through technology unless and until other branches of human skills lead us to a cure for overpopulation. In the words of Harrison Brown, "Whether we like it or not, we have passed a major point-of-no-return and have become completely dependent on our science and technology for our personal and cultural survival."

Some specific cases in which technology can help will be described in later issues.

H.B.

Built by
HEVI-DUTY
specialists in
electric heat

"Multiple Unit"
MUFFLE FURNACE
Temperatures to 1850° F.

This furnace is a complete self-contained unit with the temperature indicating and controlling devices conveniently located in the pyramidal base. Four interchangeable and reversible heating units of heavy gauge Nickel Chromium Wire installed in grooved refractory plates completely surround the heating chamber.

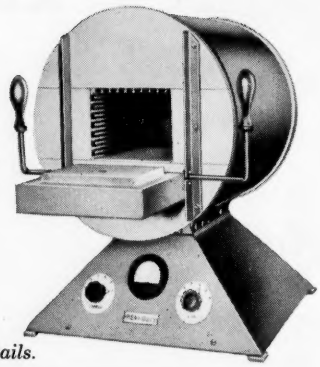

Write for Bulletin 849 for complete details.

Type	Watts	Chamber			Price
		W.	L.	H.	
051-PT	1150	5¼	8	4	$ 145.00
052-PT	1440	4¼	10	3	210.00
054-PT	2070	5¼	12	4	245.00
056-PT	3400	7½	14	5	315.00
012148-PT*	6500	11¼	14	8	1050.00

Operating voltage either 115 or 230 volts A.C. only except 012148-PT is 230 volt only.
*Automatic temperature control $230.00 additional.

FOR GENERAL AND SPECIALIZED LABORATORY APPLICATIONS

HEVI-DUTY "Multiple Unit"
TUBE TYPE COMBUSTION FURNACES
in Two Temperature Ranges, 1850° F. or 2200° F.

Hevi-Duty Combustion Tube Furnaces are available in either the split* (illustrated) or solid type and can be used horizontally or modified for vertical operation. Long-life "Multiple Unit" brand heating units offer fast heat-up because the heat is radiated directly into the heating chamber. The heated length may be divided for zone temperature control which gives greater temperature uniformity over a specified length. A few of the standard furnaces are shown below. Many sizes are in stock. Special sizes with diameters up to 16 inches can be built to your specifications.
*5-in. and smaller diameters are hinged.

HINGED-TYPE TUBE FURNACE FOR 1850° F.					
TYPE	CHAMBER		RATING WATTS	SHIPPING WEIGHT	PRICE
	DIA.	LENGTH			
70	1¼"	12"	750	35	$ 75.00
M-2012	2⅜"	12"	1400	90	$ 165.00
M-3024	3"	24"	3400	135	$ 250.00
M-5036	5"	36"	7500	325	$ 650.00
M-8040	8"	40"	14500	520	$1180.00

Write for Bulletin 552 for complete details.

HEVI-DUTY ELECTRIC CO.
Milwaukee 1, Wisconsin

• LABORATORY FURNACES
TRADE MULTIPLE UNIT MARK
• ELECTRIC EXCLUSIVE

BOOKS

An Introduction to Chemical Engineering, C. E. Littlejohn and G. F. Meenaghan Reinhold Publishing Corporation, New York (1959). 271 pages. $6.50.

Of the worthwhile texts available for first courses in chemical engineering, "An Introduction to Chemical Engineering" merits a place by performing the service of living up to its title—the student is introduced to the various facets of the profession of chemical engineering. The authors have kept in mind that there are many questions confronting chemical engineering students in dealing with the nature of the profession itself. These questions have as much to do with such topics as what does a chemical engineer do, as they do with the theories and computations which the student will meet in the years of his engineering career. As is pointed out, ". . . all too often persons enter an academic curriculum with only the haziest of notions as to their interest, the demands of the discipline, and what professionalism is." From the first two chapters in this book, entitled "The Profession of Engineering" and "Sources of Information in Chemical Engineering," the student should develop from the beginning a correct idea of what the profession of chemical engineering is, what it works on, and what it works with.

The logical extension of the first part of the text is to turn to matters more technical, and this is accomplished from simple graphical representation methods at the beginning to combined material and energy balances at the end. Among the material in the text which serves to convey the student between the aforementioned points are sections entitled "Process Variables," "*P-V-T* Relations for Gases," "Mixtures of Vapors and Gases," "Material Balances," "Energy Balances," and "Equilibria in Chemical Systems." Among these topics there are several which deserve special mention. The difference between force and mass is clearly defined early in the text, and the proper use of these terms is retained throughout, as mentioned in a pointed footnote. The ideal-gas concept is well presented, and the authors have introduced material on equations of state and compressibility factors in such a manner that the student should obtain an idea as to the uses of the various *P-V-T* computation methods and their relationships to each other. Useful concepts for energy balances, such as enthalpy and specific heat, are developed from basic thermodynamic relationships before use of them is made in the text. Unfortunately correspondingly complete derivations of the over-all energy balance and the phase rule are not included. The material dealing with equilibria includes introductory material on reaction kinetics and chemical equilibria, as well as a discussion of phase equilibria in binary and ternary systems. Problems are included at the end of each chapter.

In general the text is to be recommended, for it attains the stated goal of introducing the student to chemical engineering.

JOHN B. BUTT

(*Continued on page 8S.*)

Rate Constants and Molecular Structure

HAROLD S. JOHNSTON and KENNETH S. PITZER

University of California, Berkeley, California

The methods of relating parameters in the Arrhenius rate equation to fundamental molecular properties are briefly reviewed. The limited applicability of purely theoretical methods is noted, the use and limitations of the standard semiemprical method are surveyed, and recent work based on empirical molecular structure and spectroscopy is described in detail. The recent method makes no attempt to calculate activation energy, but within a limited range of cases it does provide a reliable method of estimating the preexponential factor in the Arrhenius equation and calculating the kinetic isotope effect. In this way the method provides a check on the credibility of experimental data and on the assignment of mechnaism. If the mechanism is correct, it provides a method of estimating activation energy from rate data taken at only one temperature. Further developments of this method are anticipated.

Although the equilibrium state of a chemical reaction

$$A + B = C + D \qquad (1)$$

does not depend on the mechanism or the rate of attainment of equilibrium, the rate may be of great practical importance as well as of theoretical interest. In Figure 1 there is proposed a mechanism for reaction [Equation (1)] involving eight rates and three structural intermediates, excited reactant pairs (A, B)*, excited product pairs (C, D)*, and the *transition state*, or *activated complex* (*1*). The activated complex is some structure intermediate between excited reactants and excited products, processing the same energy. A unique specification of the activated complex is made possible from considerations of a reaction coordinate. The excited pair (A, B)* undergoes violent internal motions, vibrations, and internal rotations. A component of these motions is a change in atomic arrangements which causes (A, B)* to go over to (C, D)*. This structural rearrangement is opposed by a potential energy barrier which however eventually reaches a maximum and decreases toward the formation of (C, D)*. The distance along the path of lowest potential energy which effects this structural change is the *reaction coordinate*. The activated complex is the complex for which the reaction coordinate is localized as closely as possible above its maximum in potential energy, while the rest of the structure has any configuration open to it. Most of the excitation energy of (A, B)*, largely internal kinetic energy, has in the activated complex gone into the potential energy of the reaction coordinate. Thus the rest of the activated complex is typically not highly distorted or highly agitated; it is in fact largely like a normal molecule except for the reaction coordinate.

A few examples of reaction coordinate will be given. For the reaction

$$D + H_2 = DH + H \qquad (2)$$

the activated complex is linear; the reaction path is the simultaneous extension of the H–H distance and the shortening of the D–H distance; the reaction coordinate is the difference in D–H and H–H distances and very closely resembles the antisymmetric-stretching normal mode of the linear D–H–H structure. For the reaction

$$H_2 + I_2 = 2HI \qquad (3)$$

the activated complex is planar, and the reaction path is a simultaneous stretching of H–H and I–I bonds with the shortening of two H–I distances. For substitution with inversion about a tetrahedral carbon atom

$$X + H_3CY = XCH_3 + Y \qquad (4)$$

the reaction path is the shortening of the X–C distance, the lengthening of the C–Y bond, and the left-to-right advancing of the three hydrogen atoms. This illustrates that atoms may participate in the reaction coordinate, even though they are not directly involved in the bonds formed or broken.

REVIEW OF CHEMICAL EQUILIBRIUM

If reaction (1) is in chemical equilibrium, then every process and its exact reverse occur at the same average rate and in terms of the mechanism of Figure 1, $R_1 = R_2$, $R_3 = R_4$, $R_5 = R_6$, $R_7 = R_8$. It is not necessary to measure or know these rates however to establish the existence of equilibrium; one uses the principle of approach from either side for the over-all reaction. The equilibrium state is given by the well-known relations (*2*)

$$K = \frac{[C][D]}{[A][B]} \qquad (5)$$

$$= e^{\Delta S^\circ/R} e^{-\Delta H^\circ/RT} \qquad (6)$$

$$= \frac{Q_C Q_D}{Q_A Q_B} e^{-\Delta H_0^\circ/RT} \qquad (7)$$

where brackets refer to activity or concentration for approximate considerations.

$$Q = \sum_i g_i e^{-\epsilon_i/kT} \qquad (8)$$

If all reactants and products are isolatable chemical species, the entropy of each may be evaluated by the measurement of heat capacities from 0°K. to the temperature of interest, and the enthalpy of each relative to the elements in their standard state may be evaluated by calorimetric studies. From the thermal properties of A, B, C, and D one may bypass all mechanistic considerations, such as Figure 1, and evaluate the equilibrium constant from Equation (6).

Also thermodynamic quantities can be related to the structures and mechanical properties of the reactants and products. For favorable cases the difference in standard enthalpy at absolute zero can be found from bond energies obtained by photochemical, electron-impact, and other

methods. The entropy of reactants and products can be calculated to various degrees of approximation from atomic weights, bond lengths, vibration frequencies, or force constants for stretching and bending of bonds, barriers hindering internal rotation, and electronic multiplicities. From these considerations, applied to each reactant and to each product molecule, one can calculate the equilibrium constant from Equations (7) and (8).

For certain species of interest, for example free radical reactants or products or high-temperature species, there may be no thermodynamic data and even no spectroscopic or structural data. Nevertheless approximate values of the entropy can be found if the structural and mechanical properties of the molecules of interest can be predicted theoretically or from empirical rules of molecular structure and molecular spectroscopy. By analogy with similar stable molecules one could for a particular species predict the molecular shape, the bond lengths, force constants, barriers to internal rotation, and electronic ground state. In this case the quality of the entropy factor in the computed equilibrium constant depends exclusively on the accuracy with which structural and mechanical properties are assigned. To predict ΔH°_0 in Equation (7) one must make an accurate estimate of all bond energies in the labile reactants or products; so far the prediction of enthalpies or bond energies has been much more difficult and less reliable than the prediction of entropies for such species.

REVIEW OF THE RATE EXPRESSION FOR ELEMENTARY BIMOLECULAR REACTION

For the initial rate of reaction (1) there are no products and no excited product pairs in terms of the mechanism in Figure 1. Even so the rate expression is particularly simple, provided that the reactants are essentially in equilibrium with excited reactant pairs. In terms of the mechanism of Figure 1 the requirement is that $R_1 \approx R_2$ or that $R_2 \gg R_3$. If this condition is met, the rate constant given by

$$\text{Rate} = -d[\text{A}]/dt = k[\text{A}][\text{B}] \qquad (9)$$

has the simple well-known form (*1*)

$$k = \kappa \frac{Q^\ddagger}{Q_A Q_B} \frac{\mathbf{k}T}{h} e^{-\Delta H_0^\ddagger/\mathbf{R}T} \qquad (10)$$

THE PROBLEM

The problem of computing a rate constant from Equation (10) is very nearly the same as that of computing an equilibrium constant from Equation (7), for the case where a product or a reactant is a free radical or other reactive species of unknown structure and unknown spectra. The structure, mechanical properties, and energy of the labile reactants and products must somehow be estimated. Similar information for the activated complex must be estimated for rate calculations.

Typically the kineticist reports his data in terms of the two parameters, **A** and **E**, of the Arrhenius equation

$$k = \mathbf{A}e^{-\mathbf{E}/\mathbf{R}T} \qquad (11)$$

Often the **E** term is regarded as purely empirical, and the **A** factor is related to the structural and mechanical properties of the activated complex. A small amount of numerical work with the rotational, vibrational, and internal rotational partition functions shows one that these functions are rather sensitive to bond distances, force constants, and barriers to internal rotation. If the kineticist takes the structure of the activated complex to be his adjustable parameter, then the theory is infinitely flexible; it can explain anything and predict nothing. If however one holds to the principle used in the derivation of Equation (10) that the activated complex is like a normal molecule aside from the single separable reaction coordinate, then one can appeal to the results of molecular theory, structure, and spectroscopy to determine the structure and properties of the activated complex. If these properties of the activated complex are fixed by considerations external to kinetics, then the predictions of **A** by means of the theory are precise to perhaps a factor of four and quite useful under certain circumstances. To predict **E** by theoretical methods or with empirical methods (with the empiricism in fields external to kinetics itself), one must make very accurate estimates of all bond energies in the activated complex; so far the prediction of **E** has been much more difficult and less reliable than the prediction of **A** in Equation (11).

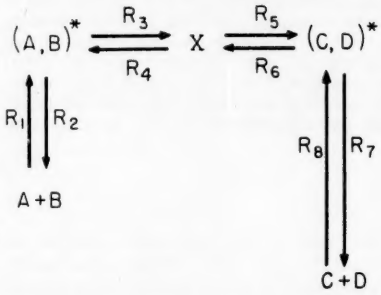

Fig. 1. A mechanism for attainment of chemical equilibrium for the reaction A + B = C + D. A + B represents the bulk normal state of the reactants; (A, B)* represents an excited, high-energy state for a pair of reactants; *X* represents an activated complex, the critical intermediate state between reactants and products; (C, D)* represents a pair of excited product molecules; and C + D represents normal product molecules. The vertical distance in the figures corresponds to an increase in energy; the transition between (A, B)* and (C, D)* is a constant energy path for the molecule pairs as a whole. R refers to rate.

METHODS OF FIXING STRUCTURE AND PROPERTIES OF ACTIVITATED COMPLEXES

Theoretical Methods

Purely theoretical methods have been limited to the simplest of all chemical reactions with the H_3 activated complex, reaction (2) for example, or ortho-para hydrogen conversion represented by

$$\text{H} + \text{H}_2 = \text{H}_2 + \text{H} \qquad (12)$$

London (*3*), discussing this problem in terms of quantum mechanics, showed that a linear complex was the one of lowest energy. Such a complex may be regarded as a superposition of three diatomic molecules

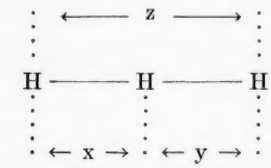

(13)

To a rather gross approximation the energies of these diatomic molecules are

$$\begin{aligned} E_x &= A + \alpha \\ E_y &= B + \beta \\ E_z &= C + \gamma \end{aligned} \qquad (14)$$

To the same rough approximation the energy of the complex in (13) is

$$E = A + B + C \pm \{\tfrac{1}{2}[(\alpha - \beta)^2 + (\beta - \gamma)^2 + (\gamma - \alpha)^2]\}^{1/2} \qquad (15)$$

As in (14), each integral is a function of interatomic distance. Upon evaluation of the integrals one finds from Equation (14) for the dissociation energy of H_3: calculated, 53 kcal.; observed, 103 kcal.; for activation energy based on (15) calculated, 19 kcal.; observed, 6 kcal.

Some of the crude approximations of this theory can be modified by the addition of extra terms to the functions used. Hirschfelder (*4*) made an extensive study of this type; however the accurately convergent method which gives the correct properties (*5*) for hydrogen is so complicated that it has not yet been applied to the H_3 complex. By the most advanced method which he used Hirschfelder concluded that the activated complex was symmetrical, $r_x = r_y$, and there is no tendency toward the formation of a stable or metastable H_3 complex; that is, there is no potential energy well in the top of the pass. From the value of the

distance which gives the maximum energy along the reaction coordinate, the size and thus moments of inertia of the complex are obtained. By variation of both distances around the value which gives the lowest maximum energy along the reaction coordinate, the force constant for the symmetrical stretching vibration is obtained. By repeating the calculation for slight bending of the linear complex, one can obtain the force constant for bending. From vibration frequencies of the complex and of H_2, zero-point energy corrections and therefore activation energy are calculated. Thus a completely theoretical evaluation of all parameters (aside from κ, which is about unity) in Equation (10) is carried out. Results are about as good or as poor as those for H_2 itself by the same method: dissociation of H_2, 67 calculated, 103 observed; activation energy, 25 calculated, 6 observed. Other calculated quantities are given in Table 2. These computations are highly instructive; the structural and mechanical quantities are presumably quite good; and the energies are far too inaccurate to be useful.

Recently Barker and Eyring (*6*) have been active in further refinements of the purely quantum mechanical treatment of H_3, but this work remains unfinished.

A somewhat different approach to the problem has been made by the molecular orbital-approximation method (*7*). A general qualitative conclusion based on considerations of H_3 and H_4 is that the activation energy for radical-radical reactions should be low, for radical-molecule reactions medium, and for molecule-molecule reactions relatively high, where unsaturated molecules are excluded. For H_3 it is concluded that the activated complex is symmetrical. A very tedious single computation gives 8 kcal. for the activation energy, 6 observed. These computations are too complicated to permit, so far, variation of distances to give vibration frequencies. An attempt to produce a simple, tractable molecular-orbital method of computation gave highly inaccurate energies.

Semiempirical Method

Eyring and coworkers (*1*, *8*) have developed and extensively used a method of computing the energies of H_3 and H_4 as a function of distances which is relatively simple to apply and gives results which are qualitatively instructive and quantitatively useful in certain cases. The method is based on Equations (14) and (15). In Equation (14) A is assumed at all distances to be a constant fraction of E_x; the fraction is taken to be something between about 0.10 and 0.20. For H_2 the fraction varies slowly, 0.10 to 0.14, with distance (at large distances, 1.5 to 5Å.), but it changes very rapidly, 0.10 to 0, at distances between 1.5 and about 0.8 Å. Since E_x as a function of distance can be observed spectroscopically and expressed conveniently as the Morse function, one can thus evaluate A and α as a function of distance; similarly B and β, C and γ can be found. These values are substituted into Equation (15) to give the total energy of H_3. A three-dimensional plot of potential energy against r_x and r_y reveals the reaction coordinate as a conspicuous canyon (Figure 2). The floor of the canyon goes through a maximum energy at easily determined distances in terms of r_x and r_y; thus activation energy and the size of the activated complex are given. Variations of distances around the saddle point of the complex give force constants and thus vibration

$$E = [2E_x + E_s] - (1 - f)[E_x + 2E_s] \qquad (16)$$

The first term in brackets in Equation (16) is sum of the energy of three diatomic molecules, and the second term is an additive correction based on the London theory with its order of magnitude held strictly in check by spectroscopic parameters. Upon purely theoretical evaluation of terms in (15) itself, extremely large errors can accumulate within a minor range of permissible assumptions (*9*).

On the other hand the semiempirical method seems to be subject to a major qualitative error. Hirschfelder's (*4*) improved theoretical treatment showed no well in the top of the energy maximum, that is, no tendency toward metastable H_3. The semiempirical method does find such a shallow well for H_3 and much deeper wells for certain other cases. In terms of the London theory itself $f = A/E_x$ is roughly constant at large distances for H_2 but decreases rapidly at small distances. The assumption about constancy of f is worst at short distances corresponding to the activated complex itself. In view of this one should distrust detailed shapes and curvatures (and thus force constants) of the potential-energy surface in the close vicinity of the activated complex itself. One can vary f to give the observed activation energy; the resultant potential-energy surface identifies the reaction coordinate and establishes the essential geometry of the activated complex. It probably fails to give good values of vibration frequencies,

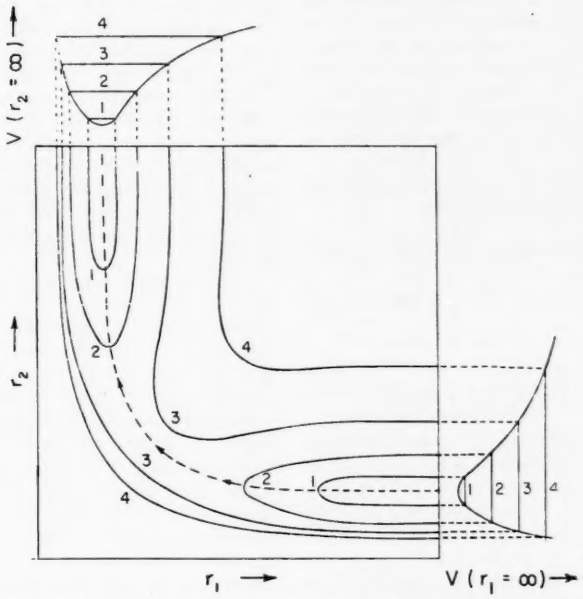

Fig. 2 Potential-energy surface for the reaction $H + H_2 = H_2 + H$, represented by contours of constant potential energy.

frequencies. The application of this method to chemical problems and to cases much more complicated than hydrogen systems has been given in detail by Glasstone, Laidler, and Eyring (*1*).

This method gives results which are surprisingly good (*9*) in view of the crudeness of Equations (14) and (15). To some extent success is due to the sensitivity of the calculated activation energy to the fitted parameter, $f = A/E_x$, which becomes three fitted parameters if the atoms X–Y–Z are different. To a greater extent success arises from the fact that use of spectroscopic values of E_x, E_y, and E_z automatically keeps dominant quantities to the correct order of magnitude, and the crude London theory gives in essence a correction term to the simple sum of energies from the three diatomic molecules. For the symmetric activated complex shown in (13) the energy is

and thus the semiempirical method is not necessarily a very good way to test or use Equation (10).

Empirical Methods

In view of the considerable body of knowledge and techniques accumulated in the fields of molecular structure and molecular spectroscopy, it has seemed worthwhile to try completely different methods of fixing the structure and mechanics of the activated complex (*10* to *13*). These data would determine the **A** factor in Equation (11); the activation energy is then taken from measured rates. There are several different approaches to this problem, some being simpler than others, some more precise (that is less dependent on the investigator's judgment). In view of the uncertainties in experimental **A** factors, an order of magnitude or more in many cases, it is not necessary for the model used to be particularly refined. Several recent approaches of this type will be reviewed.

These methods will be illustrated with reference to three examples

$$H + H_2 = H_2 + H \qquad (17)$$

$$O_3 + NO = O_2 + NO_2 \qquad (18)$$

$$(CH_3)_3CH + Cl = (CH_3)_3C + HCl \qquad (19)$$

The general shape of the activated complex is determined by the rule of equivalence with respect to reactants and products and by use of the principle that the purely *s* type of bond has no directional properties, and *p* or *sp* hydrides are directional in character. Thus reaction (17) has a linear symmetrical activated complex; that for reaction (18) may be taken as planar (for molecules or complexes with free internal rotations the simplest structure may be taken as reference model)

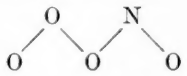

(20)

and the complex for (19) is

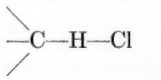

(21)

The bond orders are fixed by assigning reasonable valence-bond structures to the complexes. The H_3 complex is given the structures

$$H{:}H\dot{H} \qquad \dot{H}H{:}H \qquad (22)$$

which means that each bond is to be regarded as half order. For the complex of reaction (18) (when one ignores angles for the sake of more clearly showing electron-dot structures) the following structures are approximately equal in energy:

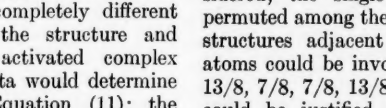

(23)

indicating that the bonds may be regarded as of the order 3/2, 1, 1, 3/2. Other electron-dot structures could be considered; the single electron could be permuted among the atoms, and no-bond structures adjacent to the transferred atoms could be invoked. Orders such as 13/8, 7/8, 7/8, 13/8, or other sequences could be justified. Differences of this magnitude have negligible effect on the computed **A** factors; the important point here is to utilize some consideration of molecular structure to avoid gross errors in assigning bond distances. For reaction (19) the bonds in the activated complex may be regarded as the same as those in the reactant except for those adjacent to the transferred hydrogen atom. The C–H and H–Cl bonds there may be taken as half order in each case; considerations of electronegativity and bond strength might lead to slightly different orders, say 0.4, 0.6, but again such differences are inconsequential to this discussion.

There are empirical rules, based on the structure of molecules, which give bond lengths in terms of bond order. Pauling (*14*) gives a table of normal covalent radii for single, double, and triple bonds. Also Pauling (*15*) has given an empirical formula for correcting integral-order bond lengths to lengths for fractional bonds; for example half-order bonds are 0.18 Å. longer than single bonds, and three-halves-order bonds are the geometric mean of single and double bond lengths. For these examples the bond lengths in Angstroms in the activated complex would be 0.92, 0.92 for (17); 1.20, 1.32, 1.36, 1.25 for (18); and 1.25, 1.47 for (19).

The assignment of bond angles is more arbitrary than that of bond lengths. The important decision is between linear or bent configurations, and considerations of *s* or *p* orbitals usually gives the clue here. For bent bonds it is convenient to assume 120-deg. angles, in the absence of any definite information.

Badger (*16*) has proposed an empirical rule which relates the stretching-force constant to bond distance:

$$k_r = 1.86 \times 10^5/(r - d_{ij})^3 \text{ dynes/cm.} \qquad (24)$$

For the bond between hydrogen and an atom of the first row of the periodic table, $d_{H_1} = 0.34$. Other values are $d_{H_2} = 0.59$, $d_{H_3} = 0.65$, $d_{11} = 0.68$, $d_{12} = 0.90$, and $d_{22} = 1.18$. Stretching-force constants for H–H and C–H half bonds happen to be equal and are, for example, 2.6×10^5 dynes/cm.

Bending-force constants may be assigned by comparison with roughly equivalent stable molecules. For bending about X–H–X half bonds the force constant derived from hydrogen-bonded systems was assigned (*11*) as 0.16×10^{-11} erg./radian.^{2} By the fitting of force constants to the kinetic data for the reaction $H_2 + Cl = H + HCl$, the value for bending of H–H–Cl was assigned (*13*) the value 0.046×10^{-11} erg./radian^2. Angular force constants are often divided by the product of the two included bond lengths to give force constants in units of dynes/cm. A few values of this sort taken from more extensive tables (*17*, *18*) include H–O–H, 0.69×10^5; H–C–H in CH_4, 0.30×10^5; F–C–F in CF_4, 0.71×10^5.

For exact partition-function calculations one needs vibration frequencies, not force constants, for the activated complex. However the force constants suffice for the classical partition function, which is discussed in a later section and yields a satisfactory approximation in some cases. For the activated complex of reaction (17) it is easy to carry out a complete vibrational analysis (*11*), including the introduction of a cross-product potential-energy term which reduces to zero the vibration frequency of the antisymmetric stretching mode and thus converts it very naturally to the reaction coordinate. By modifying the activated complex of reaction (18) in the direction of greater symmetry, that is, treating the nitrogen atom as if it were an oxygen atom, one can easily solve the vibrational problem here, finding six in-plane normal-mode frequencies plus one reaction coordinate (*10*, *12*). Alternatively the frequencies for this complex may be transferred directly from corresponding motions in similar stable molecules, NO_2, N_2O_4, and O_3, after they are classified as three stretching modes, one reaction coordinate, and three bending modes. This classification could be arrived at from general symmetry considerations (*10*), or more simply the complex may be regarded as a bent triatomic molecule

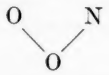

with one stretching mode, one bending mode, and one reaction coordinate, with the addition of the end atoms giving rise to four vibrations, symmetric and antisymmetric stretching and bending. Thus reaction (18) can be subjected to a relatively rigorous vibrational analysis or treated by the more empirical methods used for more complicated activated complexes. For reaction (19) the activated complex is so large that a detailed vibrational analysis is hopelessly complicated and unnecessary. For the activated complex in (19) there will be extensive duplication of frequencies between the complex and the hydrocarbon reactant. In Equation (10) these identical vibration frequencies give rise to identical

terms in the numerator and denominator and hence cancel. It is preferable to cancel in advance all equivalent vibration frequencies (and methyl-group internal rotations) rather than to evaluate each set for reactant and complex and then to cancel them in the calculations. All vibrations and methyl-group internal rotations of the $(CH_3)_3C$ group may be taken as the same in reactant and activated complex; these may be canceled without being evaluated, and in subsequent considerations the $(CH_3)_3C$ group is to be regarded as a rigid body, not as a mass point. Thus the vibration problem for the reactant is reduced to the three vibrations (one stretch, two bends) of the hydrogen atom against the massive rigid body. The vibration problem for the activated complex is reduced to that of a linear triatomic molecule (symmetric stretch, reaction coordinate, and two bends which are largely motions of hydrogen) plus two wagging motions of the rigid body against the rest of the molecule. For the vibration frequencies of the three-body problem one may make use of the convenient formulas collected by Herzberg (*19*); for the wagging vibrations one may use the approximate relation

$$\nu = 4.1 \times 10^8 (k_\theta/I)^{1/2} \text{ cm.}^{-1} \qquad (25)$$

A corresponding expression holds for bending at right angles to this axis.

Equation (25) is a valid approximation only if the moment of inertia of the wagging group is small as compared with the molecule about a parallel axis. If the two moments are of comparable size, a better approximation is obtained by use of the reduced moment in Equation (25)

$$I = I_1 I_2/(I_1 + I_2) \qquad (26)$$

This treatment for reaction (19) can be extended to any type of atom transfer process

$$X - y + Z \rightarrow X + yZ \qquad (27)$$

where the complex may be linear or bent. Considerable cancellation can be expected between X in the reactant and in the complex when these are complicated groups. After the exploitation (without computation) of this cancellation the group so treated is regarded as rigid. The degrees of freedom which must be considered in a partition-function calculation for various cases are listed in Table 1. In all cases vibration frequencies for the three-atom problem can be found from Herzberg's relations (*19*), the wagging vibrations can be treated as simple separate problems depending on moments of inertia of the wagging groups and bending force constants, and the internal rotations can be treated by the following simple method.

Internal rotations are characterized by reduced moments of inertia and barriers to internal rotation. The reduced moment of inertia is given by Equation (26), which was introduced above for wagging motions. I_1 and I_2 are moments of inertia of the two groups about axes parallel to the axis of internal rotation and passing through the center of gravity of each group. For coaxial symmetric tops this treatment is exact; I_1 is simply the moment of inertia of one group about the common axis, and I_2 is the moment of inertia of the second group about the axis. For less symmetrical internal rotations the exact treatment of internal rotation becomes more complex (*20a*). However a simple approximate method (*10*) may be used in connection with Equation (26). If an internal rotation is about some bond, one should imagine the bond to be cut, thus separating the molecule into two pieces; find the center of mass of one piece; pass a line through this point parallel to the severed bond; and compute I_1 as the moment of inertia about this line. Next one should find the center of mass of the second piece, pass a line through this point parallel to the severed bond, and compute I_2 as the moment of inertia about this second line.

Unless there is conspicuous steric hindrance, internal rotation about fractional bonds in the activated complex is usually regarded as essentially free. In case there is conspicuous evidence for a barrier, each case must be considered separately (*20b*).

The electronic multiplicity of the activated complex can be predicted, subject to some uncertainty, from the rules for stable molecules. If there are an even number of electrons, the multiplicity is usually one. The molecule O_2 is anomalous in having a multiplicity of three. This sort of anomaly, which is understood in terms of advanced quantum theories of valence, is possible only for certain highly symmetrical systems. It is usually safe to predict an electronic multiplicity of one for activated complexes.

If there are an odd number of electrons, the electronic multiplicity must be at least two, and it usually is two for systems of low symmetry. However in highly symmetrical systems orbital degeneracy may be present in addition to the spin degeneracy of two. Thus the Cl atom has a $^2P_{3/2}$ ground state with a multiplicity of four, and NO has a ground state ($^2\pi_{1/2}$) of multiplicity two but a low energy-excited state ($^2\pi_{3/2}$) of multiplicity four. The less symmetrical molecule NO_2 has multiplicity two. Thus one can usually predict the correct multiplicity, but in exceptional cases there may be an uncertainty of not more than a factor of three.

These considerations (all outside the field of kinetics itself) establish, with the uncertainties as pointed out, all the structural and mechanical features of the activated complex.

Table 1. Degrees of Freedom in Atom Transfer Reactions Which Do Not Cancel and Must Be Considered in Partition-Function Calculations for $Xy + Z = X + yZ$

		Noncanceling degrees of freedom							
			Vibrations						
Model*	T_r	R I.R.	Sym. str.	Antisym. str.	Bend	wag	Total number External	Internal
z	3						3	
X	3	3					6	
x − y	3	2	1				5	1
X − y	3	3	1		2‡		6	3
x − y − z linear	3	2	1	1†	2		5	4
x − y − z bent	3	3	1	1†	1		6	3
X − y − z linear	3	3	1	1†	2‡	2	6	6
X − y − z bent	3	3	1	1	1†	1	2	6	6
X − y − Z linear	3	3	1	1	1†	2‡	4	6	9
X − y − Z bent	3	3	2	1	1†	1	4	6	9

*Lower case x, y, or z stands for atoms; upper case X or Z stands for complex groups regarded as rigid bodies.
†The reaction coordinate.
‡To a fair approximation, especially for light y, these bending frequencies are the same in reactant and complex.

Comparisons of the Methods in Establishing the Properties of the Complex H_3.

It is only for reaction (17) with the H_3 complex that fairly detailed, even though still highly approximate, quantum mechanical computations have been carried out. This complex also has been extensively examined by the semiempirical method. It is one of the cases treated by the empirical method described above. Also recent, carefully obtained kinetic data (*21*) on this reaction have been so extensive and so precise that the activation energy and vibration frequencies could be found solely as a best fit to

TABLE 2. STRUCTURE AND PROPERTIES OF THE H_3 COMPLEX AS OBTAINED BY THEORETICAL SEMIEMPIRICAL, AND EMPIRICAL METHODS

	Bond distance, Å	Vibration frequencies, sec.$^{-1} \times 10^{-13}$ Stretch	Bend	Ref.
Theoretical	0.96	9.5	3.3	*4*
Semiempirical ($f = 0.14$)	0.88	*	2.7	*1*
Empirical	0.92	8.8	3.6	*11*
Kinetic	†	9.6	3.6	*21*

*The approximation of constant f breaks down badly at small distances. The shape of the potential energy function at the top of the pass is too uncertain to justify evaluation of the stretching frequencies.

†An unsymmetrical complex was taken from the potential energy surface which shows a small, false (*4*) well in the top of the pass. Distances of 0.85 and 1.25 Å. were used in the computation of vibration frequencies.

the experimental data, within the framework of the general activated-complex theory. In Table 2 there is a comparison of bond distance, frequency of symmetric stretching vibration, and frequency of the bending vibrations for the four methods mentioned above: theoretical, semiempirical, empirical, and kinetic. All these methods for this reaction agree as to the structure and mechanical properties of the activated complex.

CALCULATION OF A FACTORS FOR BIMOLECULAR REACTIONS

Evaluation of Separated Partition Functions

Experimental rate data are usually reported in terms of the Arrhenius equation

$$k = \mathbf{A} \exp(-\mathbf{E}/\mathbf{R}T) \qquad (11)$$

whereas theoretical rate expressions take the form

$$k = \mathbf{B}(T) \exp(-\mathbf{W}/\mathbf{R}T) \qquad (28)$$

The relations between these two quantities are

$$\mathbf{E} = \mathbf{W} + \theta\mathbf{R}T \qquad (29)$$

$$\mathbf{A} = \mathbf{B} \exp \theta \qquad (30)$$

where the quantity θ is given by

$$\Theta = Td \ln \mathbf{B}/dT \qquad (31)$$

In terms of the activated complex theory discussed here the rate factor **A** in units of cc.(mole^{-1})(sec.$^{-1}$) is

$$\mathbf{A} = 3.41 \times 10^{34} \kappa T \pi_p \mathbf{A}_p \qquad (32)$$

where κ is the transmission coefficient taken as unity in the absence of more detailed information (*22*), and $\pi_p\mathbf{A}_p$ is the product of partition functions for all kinds of energy, each of the form

$$\mathbf{A}_p = \exp(\theta_p) Q^{\ddagger}/Q_A Q_B \qquad (33)$$

The product includes translational, rotational vibrational, internal rotational, and electronic degrees of freedom.

In c.g.s. units translational partition functions per cc. are given by

$$Q_{tr} = 1.88 \times 10^{20} (MT)^{3/2} \qquad (34)$$

$$\theta_{tr} = 3/2 \qquad (35)$$

The translational **A** factor, including the term in θ, is

$$\mathbf{A}_{tr} = 1.18 \times 10^{-21} (M^{\ddagger}/M_A M_B T)^{3/2} \qquad (36)$$

Rotational partition functions for linear (gram-molecular weight and Angstrom units) molecules of moment of inertia are given by

$$Q_r^{\,L} = 0.0412\, IT/\sigma \qquad (37)$$

$$\theta_r^{\,L} = 1 \qquad (38)$$

and for a nonlinear molecule with three principal moments of inertia, I_1, I_2, I_3, are

$$Q_r^{\,N} = 0.0148 (I_1 I_2 I_3)^{1/2} T^{3/2}/\sigma \qquad (39)$$

$$\theta_r^{\,N} = 3/2 \qquad (40)$$

It is not necessary to evaluate the individual moments of inertia; their product can be found much more simply (*23*) by means of any Cartesian coordinate system with the center of mass as the origin by means of

$$I_1 I_2 I_3 = \begin{vmatrix} +I_{xx} & -I_{xy} & -I_{xz} \\ -I_{xy} & +I_{yy} & -I_{yz} \\ -I_{xz} & -I_{yz} & +I_{zz} \end{vmatrix} \qquad (41)$$

where $I_{xx} = \sum m_i(y_i^2 + z_i^2)$, $I_{xy} = \sum m_i x_i y_i$, etc.

For each free internal rotation the partition function is

$$Q_{fir} = 0.360\, (IT)^{1/2}/\sigma \qquad (42)$$

The effect of symmetry numbers may be evaluated in either of two ways: (1) the rotational symmetry number may be found for each reactant, for the activated complex, and for each internal rotation of both reactants and complex and (2) on the other hand, one may forget about symmetry numbers; omit them from Equations (37), (39), and (42); and find the integral value of the product

$$\pi\sigma_A\sigma_B/\sigma^{\ddagger} \qquad (43)$$

simply by inspection. The product in Equation (43) is the number of equivalent reaction coordinates, if one permutes both reactants about all equivalent modes of attack. For example for the reaction

$$\begin{aligned} CH_4 + Cl &\rightarrow H_3C - H - Cl \\ &\rightarrow CH_3 + HCl \end{aligned} \qquad (44)$$

the symmetry number of methane is twelve, Cl is one, and the complex is three. The ratio (12)(1)/3 is equal to four, the number of equivalent hydrogen atoms in methane. For calculations based on one structure the symmetry numbers in the rotational and internal rotational partition functions automatically account for this multiplicity of identical reaction sites. One must be careful not to apply this factor twice or to be inconsistent between reactants and complex.

Vibrational partition functions in terms of normal mode frequencies in cm.$^{-1}$ are given by

$$Q_v = 1 - \exp(-1.44\nu/T)^{-1} \qquad (45)$$

$$\theta_v = \frac{1.44\nu/T}{\exp(1.44\nu/T) - 1} \qquad (46)$$

When $1.44\nu \ll T$, the vibrational partition functions take on their classical value

$$Q_v' = T/1.44\nu, \qquad \theta_v = 1 \qquad (47)$$

Electronic partition functions are based simply on the fundamental definition

$$Q_e = \sum_i g_i \exp(-\epsilon_i/\mathbf{k}T) \qquad (48)$$

$$\theta_e = T\, d \ln Q_e/dT \qquad (49)$$

Often the sum in (48) is only the single term, the ground-state multiplicity. For nitric oxide at ordinary temperatures it is a sum of two terms. For reactions at high temperatures, say above 2,000°K., the higher terms in the sum over electronic states may become very important.

Evaluation of Partition Functions by Classical Mechanics (*13*)

Up to this point partition functions on the basis of the quantum energy levels of each system have been discussed. For many molecular motions however the separation of the energy levels is less than kT at temperatures of practical interest, and in such cases the partition function may be evaluated by classical mechanics. This method is advantageous because less detailed information is required. In particular one does not have to solve the dynamical-vibration problem; knowledge of the potential-energy function suffices.

Rotational and translational motions may always be treated classically; hence the criterion of validity of the classical

method lies in the treatment of vibration. If one arbitrarily selects 0.2 cal./deg. mole as a maximum error in the entropy of vibration (or 10% in the rate), then the classical method is valid for frequencies (in cm.$^{-1}$) such that $\nu \leq 1.1T$, where the temperature is in °K. While many vibrations in stable molecules lie above this boundary, most of these vibrations are essentially unchanged in the activated complex and hence may be canceled. The key decision concerns the new motions which arise in the activated complex but were not present in either reactant. If these motions are of low frequency, then the classical method is valid and useful.

The classical partition function (also called the *phase integral*) may be written

$$Q = \frac{q_e \mathbf{C}}{\sigma} \int \cdots \int e^{-V/\mathbf{k}T}\, dx_1 \cdots dz_n \qquad (50)$$

$$\mathbf{C} = \left(\frac{2\pi \mathbf{k}T}{h^2}\right)^{3n/2} \prod_{i=1}^{n} m_i^{3/2} \qquad (51)$$

One may of course transform from Cartesian coordinates to some other coordinate system. If a few vibrational motions have too high frequencies, one may correct this partition function by multiplication of the ratio ($Q_{q.m.}/Q_{class}$) of the quantum partition function to the classifical function for each high frequency. Also groups such as CH_2, CH_3, etc., may be regarded as single particles in the classical calculation and the quantum partition function for their internal motions introduced later.

One convenient method of integrating Equation (50) is a serial procedure in which the first atom is placed anywhere in the container, and the successive atoms are described by coordinates relative to the preceding atoms. In these calculations groups such as CH_3, CH_2, or CH are regarded as single atoms, and the hydrogen vibrations are treated separately by the quantum method or canceled out.

This method was applied (*13*) to the reaction of a chlorine atom with a hydrocarbon, but the calculations are equally applicable to any reaction of the type

$$X - H + z \rightarrow X + H - z \qquad (52)$$

The serial integration starts in an identical fashion for both the hydrocarbon reactant and the activated complex. Consequently all the earlier factors cancel in the desired ratio $Q\ddagger/Q_{R-H}$ of the partition functions of the activated complex and the reactant hydrocarbon. There remain just the additional factor introduced by the chlorine atom and the effect of released constraints on the reacting hydrogen. Only a single reaction site, a single C–H bond, is being considered.

It is easiest to consider the reacting hydrogen in a CH group, and a detailed model is given in Figure 3. The reacting hydrogen has a stretching motion and two bending motions in the CH group of the reactant hydrocarbon. The complete partition function contains the factor for these three quantized vibrations. In the activated complex the C–H stretching motion becomes the reaction coordinate and is omitted, but there are still the two C–H bending motions for which quantum mechanical partition-function factors must be included. The C–H stretching frequency in the reactant molecule is so high that it does not contribute significantly at moderate temperatures. Consequently it yields a partition-function factor of unity. The two hydrogen bending frequencies may be shifted somewhat by the formation of the complex. It is difficult to estimate how large this shift will be, but as the frequencies are so high that their contribution is small, this factor may also be neglected.

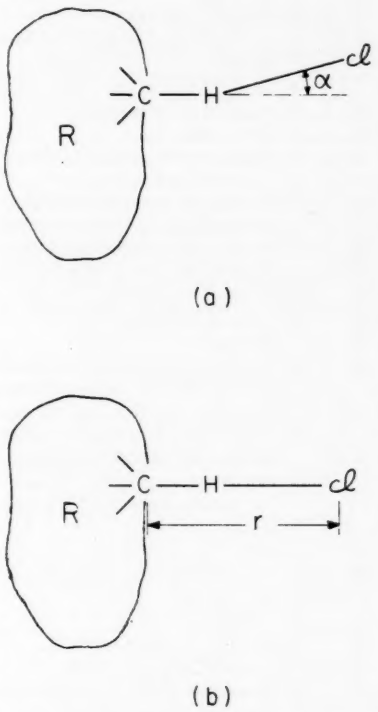

Fig. 3. The coordinates of a chlorine atom in an activated complex for reaction with the hydrocarbon R-H.

If the reacting hydrogen is in a CH_3 or CH_2 group (instead of a CH group), the situation is more complex. Nevertheless one C–H stretching mode becomes the reaction coordinate with the same resulting effect on the partition functions as described above. Also the same number of C–H bending modes will be present in the activated complex as in the reactant molecule, and the corresponding small quantum partition-function factors may be assumed to cancel one another in reasonable approximation.

The contribution to the partition function by the chlorine atom is not small, but now the frequencies are low and the classical method is appropriate. For the chlorine atom polar coordinates about the equilibrium position of the hydrogen atom at the reaction site (Figure 3) were chosen, and

$$\frac{Q}{Q_{R-H}} = q_e \left(\frac{2\pi \mathbf{k}T m_{Cl}}{h^2}\right)^{3/2} \cdot \iiint e^{-V(r,\theta,\phi)/\mathbf{k}T} \cdot r^2 \sin\theta\, dr\, d\theta\, d\phi \qquad (53)$$

was obtained.

The potential function has been estimated (*13*) in reasonable approximation, and the resulting integral yields agreement with the **A** factor observed in kinetic measurements. The potential function would be expected to be about the same for each exposed hydrogen atom in a hydrocarbon molecule. The total energy increase to the activated complex may vary somewhat from one reacting hydrogen to another, but this effect is in the activation energy for that particular reaction. The additional energy required for nonoptimal values of the coordinates in V should be nearly the same for each site. Consequently one sees that Equation (53) yields the same result for each site, and the kinetic **A** value is the same for each site. The experimental data (*24*) for several hydrocarbons follow this prediction approximately (within a factor of about two).

The preceding conclusion illustrates the power of the classical method. It sweeps away unimportant factors and emphasizes the essential features of the potential-energy function of the activated complex. At the present time this method is being extended to other types of reaction.

Evaluation and Summary

The application of theoretical and semiempirical methods to problems in reaction kinetics has been summarized by Glasstone, Laidler, and Eyring (*1*). By rather difficult computations results were found which were moderately successful quantitatively but very instructive qualitatively and which gave the thermodynamic formulation

$$k = (\mathbf{k}T/h) e^{\Delta S\ddagger/\mathbf{R}}\, e^{-\Delta H\ddagger/\mathbf{R}T} \qquad (54)$$

of rate constants. This relation has proved very valuable in the correlation of rate data, especially for organic reactions. One utilizes the rate constant and its temperature dependence to evaluate $\Delta H\ddagger$ and $\Delta S\ddagger$; as a check on the theory one looks

to the internal consistency for a class of reactions and to the reasonableness of entropy values obtained.

Recent efforts to apply theorems of molecular structure and molecular spectroscopy to these problems have sought to avoid the overwhelming complications of the theoretical approach and yet to provide predictions, not just correlations, at the level of accuracy of experimental kinetics. For the **A** factors in the Arrhenius equation there is relatively little (maybe a factor of 4) flexibility or spread in the values deduced from these considerations of molecular spectroscopy and structure. By these methods computations have been carried through for twenty-four bimolecular gas-phase reactions, involving a fairly diverse series of reactants and reaction types. In twenty-two of these cases there is agreement within the limit of experimental error between calculation and experimental result; in two cases the experimental A factors were much too high, a factor of 200 in one case and a factor of 10^5 in the other. In both cases the reaction was one of many occurring in a chain reaction, and it is easy to produce large errors in such a case by a wrong assignment in the mechanism, aside from errors in experimental technique. It is proposed that such an error in mechanism is involved in these cases.

Predictions of the energy of activation have not yet attained any comparable degree of accuracy, and at present it is usually best to regard the energy of activation as an empirical quantity to be obtained from experimental rate data or from general thermochemical correlations.

In some cases the activation energy of a dissociation reaction may be just the energy of dissociation; that is, the reverse reaction of recombination has no activation energy at all. Where this condition holds, the activation energy may be calculated from thermochemical data. In other cases this condition may not hold strictly, but a reasonable estimate may be made of the correction.

One may also note that the reaction rate becomes less sensitive to a given error in the activation energy as the temperature increases. Thus it becomes more feasible to predict reaction rates at high temperatures than at low.

In some experimental systems it is possible to measure the rate constant at only one temperature or over only a narrow range of temperature. With this method of calculating **A** in Equation (11) one can reliably estimate the activation energy **E** even from such meager data.

NOTATION

A, B, C, D = chemical species in a reaction

A, B, C = coulombic energy in London equation for energy of H_2 and H_3

A = preexponential factor in the Arrhenius equation

B = preexponential factor in general

C = term defined in Equation (51)

d_{ij} = constant depending on i and j

E = energy

E_x = energy for diatomic molecule with distance r_x

E_s = energy of diatomic molecule with distance $2r_x = r_s$

E = activation energy in the Arrhenius equation

f = fraction of coulombic energy in London theory

g = number of energy states with the same energy, the degeneracy factor

H = enthalpy

h = Planck's constant

i, j = rows of periodic table of two atoms

I = moment of inertia

K = equilibrium constant

k = rate constant

k_θ = angular-force constant for wagging, erg/radian^2

k = Boltzmann's constant, R/N

k_r = bond stretching-force constant

k_ϕ = bond bending-force constant

M = gram molecular weight

m = mass

m_i = mass of ith atom

P = product

Q = partition function or weighted sum over all energy states

$Q\ddagger$ = partition function for all motions of the activated complex except the reaction coordinate

q_e = electronic partition function (or multiplicity for a single state)

R = rate

R = gas constant

r = bond length

S = entropy

T = absolute temperature, °K.

V = potential energy

X = transition state or activated complex

X, Z = atom or groups of atoms

y = atom

Greek Letters

α, β, γ = exchange energy in London equation for energy of H_2 and H_3

ϵ = atomic or molecular energy level

κ = transmission coefficient, $R_b/(R_a + R_b)$ in Figure 1

ν = vibration frequency

θ, ϕ = spherical polar coordinate

Θ = term defined in Equation (31)

σ = symmetry number, equivalent structures produced by real rotations

$\ddagger$ = symbol identifying the activated complex

ΔS^0 = difference in standard entropy between products and reactants

ΔH^0 = similar difference in standard enthalpy

ΔH_0^0 = ΔH^0 at absolute zero

$\Delta H_0\ddagger$ = energy of activation at absolute zero

LITERATURE CITED

1. Glasstone, Samuel, K. J. Laidler Henry Eyring, "Theory of Rate Processes," McGraw-Hill, New York (1941).
2. Herzberg, Gerhard, *Molecular Spectra and Molecular Structure*, p. 501, Van Nostrand, New York (1945).
3. London, Fritz, "Probleme der modernen Physik, Sommerfeld Festschrift," p. 104, S. Hirzel, Leipzig (1928); *Z. Elektrochem.*, **35**, 552 (1929).
4. Hirschfelder, J. O., Henry Eyring, and Nathan Rosen, *J. Chem. Phys.*, **4**, 121, 130 (1936); Hirschfelder, J. O. Henry Eyring, and B. Topley, *J. Chem. Phys.*, **4**, 170 (1936); J. O. Hirschfelder, D. P. Stevenson, and Henry Eyring, *J. Chem. Phys.*, **5**, 896 (1937); D. P. Stevenson, and J. O. Hirschfelder, *J. Chem. Phys.*, **5**, 933 (1937); J. O. Hirschfelder, *J. Chem. Phys.*, **6**, 795 (1938); J. O. Hirschfelder, and C. N. Weygandt, *J. Chem. Phys.*, **6**, 806 (1938).
5. James, H. M., and A. S. Coolidge, *ibid.*, **1**, 825 (1933).
6. Barker, R. S., R. L. Snow, and Henry Eyring, *ibid.*, **23**, 1686 (1955).
7. Griffing, Virginia, *ibid.*, **23**, 1015 (1955).
8. Hirschfelder, J. O., *ibid.*, **9**, 645 (1941).
9. Coolidge, A. S., and H. M. James, *ibid.*, **2**, 811 (1934).
10. Herschbach, D. R., H. S. Johnston, K. S. Pitzer, and R. E. Powell, *ibid.*, **25**, 736 (1956).
11. Wilson, D. J., and H. S. Johnston *J. Am. Chem. Soc.*, **79**, 29 (1957).
12. Johnston, H. S., W. A. Bonner, and D. J. Wilson, *J. Chem. Phys.*, **26**, 1002 (1956).
13. Pitzer, K. S., *J. Am. Chem. Soc.*, **79**, 1804 (1957).
14. Pauling, Linus, "Nature of the Chemical Bond," p. 164, Cornell University Press, Ithaca, New York (1940).
15. ———, *J. Am. Chem. Soc.*, **69**, 542 (1947).
16. Badger, R. M., *J. Chem. Phys.*, **2**, 128 (1933); **3**, 710 (1934).
17. Wilson, E. B., Jr., J. C. Decius, and P. C. Cross, "Molecular Vibrations," p. 175, McGraw-Hill, New York (1955).
18. Herzberg, Gerhard, p. 193.
19. *Ibid.*, p. 168; Equations (189 to 191; 195 to 200).
20. *a.* Pitzer, K. S., "Quantum Chemistry," pp. 239, 482, 492, Prentice-Hall, New York (1954).
    b. ———, and W. D. Gwinn, *J. Chem. Phys.*, **10**, 428 (1942).
21. Boato, G., G. Careri, A. Cimino, E. Molinari, and G. G. Volpi, *J. Chem. Phys.*, **24**, 783 (1956).
22. Hirschfelder, J. O., and Eugene Wigner, *ibid.*, **7**, 616 (1939).
23. Herzberg, Gerhard, p. 509.
24. Knox, J. H., and A. F. Trotman-Dickinson, *J. Phys. Chem.*, **60**, 1367 (1956).

Presented at A.I.Ch.E. Philadelphia Meeting. Manuscript received June 24, 1958; revision received August 14, 1958; paper accepted August 25, 1958.

The Phase Behavior and Solubility Relations of the Benzene-Water System

CHARLES J. REBERT and WEBSTER B. KAY

The Ohio State University, Columbus, Ohio

In order to contribute to knowledge of the nature of the phase behavior of partially miscible liquid systems, a study of the benzene-water system was undertaken. The pressures at liquid- and vapor-phase boundaries of fifteen mixtures of benzene and water were determined within the temperature range of 200 to 357°C. Along with a complete numerical tabulation, these data are presented graphically as pressure-temperature, pressure-composition, and temperature-composition phase diagrams to show the nature of the boundaries.

Up to the three-phase critical end point, the benzene-water system develops in a manner usually ascribed to a partially miscible system in which the vapor composition at a point of univariance lies intermediate to the two liquid compositions. The three-phase critical end point occurs at 1,364 lb./sq. in. abs. and 268.3°C., and the composition of the critical phase is 25.8 weight % water, with the remaining liquid phase 92.8 weight % water.

The pressure, temperature, and composition of the critical solution end point are deduced as 2,300 lb./sq. in. abs., 306.4°C., and 59 weight % water, respectively. At temperatures between these two critical points the phase behavior is likened to that of a dense gas or fluid dissolved in a liquid. Definite limiting values of temperature and pressure are assignable to this behavior by the extension of the three-phase curve up to the critical solution end point. This extended curve is not a phase boundary, but the temperature and pressure at a given point on the curve represents in a mixture of fixed composition the limit of mutual solubility of the benzene-rich fluid phase and the water-rich phase. At a temperature above or a pressure below the given point the liquid phase begins to vaporize.

Above the critical solution end point the vapor-liquid phase boundaries are like those of a normal binary mixture.

Although the broad principles governing the *P-T-x* relations of partially miscible mixtures were set forth by van der Waals (*16*), van Laar (*9*), Keunen (*8*), and Roozeboom (*12*) in the early part of the present century, few systems exhibiting partial miscibility have been examined in a quantitative fashion over a wide range of temperature, pressure, and composition. Because of this paucity of data, the phase behavior in the region of the liquid-vapor critical state of one of the liquid layers is still greatly a matter of conjecture. In the critical region the compressibility of the liquid approaches that of the vapor, and so the mutual solubility of the liquid layers is greatly influenced by relatively small changes in pressure. In many chemical processes and especially in petroleum processing, where hydrocarbon-water mixtures are encountered, such phase behavior may be of great practical significance. The sparing solubility of oil, gas, and water mixtures, as they are known at the earth's surface, may very well present an entirely different mutual relationship when subject to high underground pressure and temperature.

To obtain a more quantitative picture of the phase behavior of partially miscible systems, the *P-T-x* relations of the benzene-water system have been determined throughout most of its saturated temperature range.

The phase behavior of this system is typical of systems for which the equilibrium vapor composition lies intermediate to the immiscible liquid-layer compositions. Aside from the possible industrial applications of the data, the benzene-water system is an interesting one to study from the point of view of interactions between two molecules representative of nonpolar and polar liquids. The vapor-pressure curves of these compounds intersect at 182°C. At lower temperatures benzene is the more volatile component, whereas at higher temperatures water is more volatile.

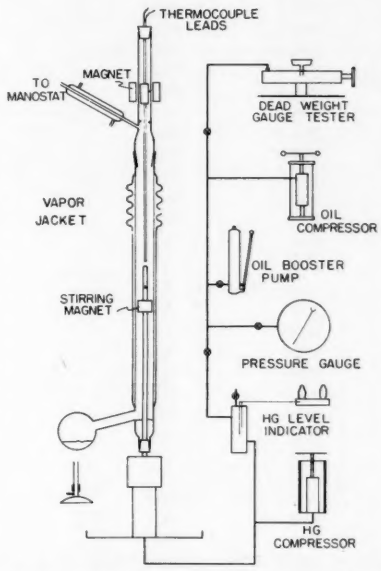

Fig. 1. Schematic diagram of assembled apparatus.

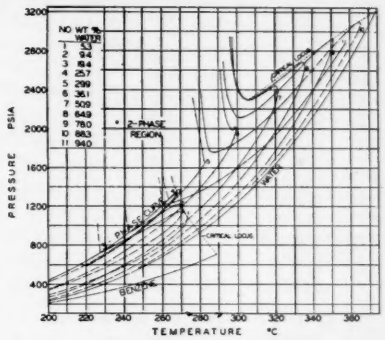

Fig. 2. 2 *P-T-x* space diagram for the benzene-water system.

Scheffer (*13*) has measured the three-phase vapor pressure up to the vaporization critical end point of the benzene-rich layer. Jaeger (*2*) has obtained data on the solubility of benzene in water over an extended temperature range, while others (*14, 1, 3*) have measured the mutual solubility in the vicinity of room temperature and atmospheric pressure.

EXPERIMENTAL METHODS AND APPARATUS

To determine the phase relations in the benzene-water system *P-T* border curves were obtained for fifteen mixtures varying in concentration from nearly pure benzene to nearly pure water. The apparatus employed was a modification of that described by Young (*17*) and Kay (*4*) and is shown schematically in Figure 1. Essentially a small air-free sample of each of the mixtures was confined over mercury, in a quartz capillary tube of 2-mm. bore and 8-mm. O.D. The tube was heated to a constant temperature by the condensing vapor of one of a series of organic liquids or mercury, which was confined in a vacuum-jacketed tube surrounding the capillary tube. The capillary tube was held in a compressor block filled with mercury, and the block in turn was connected to a hydraulic-pressure oil pump used to balance the pressure developed by the sample. The mercury-oil interface was kept at a constant level by means of a mercury-displacement pump and mercury-level indicator. The pressure was measured to within 1-lb./sq. in. by a precision Bourdon type of pressure gauge with a 16-in. diameter dial marked in 5 lb. increments from 0 to 5,000 lb./sq. in. The calibration of the gauge was checked by

Charles J. Rebert is at the University of Southern California, Los Angeles, California.

TABLE 1. THE PRESSURE-TEMPERATURE RELATIONS AT THE PHASE BOUNDARIES OF THE SYSTEM BENZENE-WATER AT EQUAL INTERVALS OF TEMPERATURE

Temperature, °C.	Pressure, lb./sq. in. abs.
Composition: 5.5 wt. % water	
200*	287
210*	351
220*	418
230*	495
240*	582
250*	662
260	807
270	963
273	1055
273.2	1085 *VL-T_m*
273	1100
272.2	1127 *VC*
271	1147
270.3	1150 *VL-F_m*
268	1140
265	1115
260	1060
250	951
240	948
230	745
227.5	720 3p_m
Composition: 9.4 wt. % water	
200*	343
210*	409
220*	482
230*	568
240	673
250	788
260	919
270	1116
271.0	1170 *VL-T_m*
270.5	1190
269.7	1207 *VC*
269.5	1211
269	1217
268.5	1220 *VL-P_m*
268.	1219
265	1193
260	1136
250	1011
242.5	924 3p_m
Composition: 19.4 wt. % water	
180*	290
190*	353
200*	419
210*	505
220*	598
230*	708
240	835
250	981
260	1150
267	1305
267.5	1322
267.8	1354 *VC-T_m*
267	1330
266	1316
265	1300
263.5	1278 3p_m
Composition: 25.7 wt. % water	
200*	417
210*	510
220*	615
230*	732
240*	869
250	1031
260	1212 Azeo
265	1303
266	1320
267	1338
268	1356
268.3	1361 *VC*
Composition: 29.9 wt. % water	
190*	320
200*	395
210*	483
220*	583
230*	698
240*	828
250	985
260	1158
270	1346
280	1572
283.1	1665 *VL-T_m-P_m*
282.8	1670 2*L-T_m*
282.5	1674
282	1710
281	1830
280	1938
277	2275
Composition: 36.1 wt. % water	
200*	348
210*	426
220*	515
230*	618
240*	737
250*	871
260	1020
270	1193
280	1391
290	1632
295	1778
299	1944
299.6	2000 *VL-T_m*
299.5	2015
299.4	2019
299.3	2022
299.2	2024
299.1	2025 *VL-P_m*
298.8	2022
298.6	2018
298.4	2015
298.2	2006
298.0	1998
297.5	1992 2*L-T_m*
297	1997
296	2025
294	2133
292	2405
Composition: 50.9 wt. % water	
210*	331
220*	410
230*	498
240*	601
250*	717
260*	855
270*	1012
280*	1183
290	1382
300	1616
310	1888
320	2240
321.6	2390 *VL-T_m*
321	2439
320.4	2443 *VL-P_m*
320	2441
315	2583
310	2327
306	2302 2*L-T_m*
304	2310
303	2327
300	2429
Composition: 64.9 wt. % water	
220*	363
230*	442
240*	535
250*	642
260*	766
270*	911
280	1073
290*	1249
300	1455
310	1697
320	1972
330	2300
336.2	2650 *VL-T_m*
336.1	2675
335	2685
330	2618
320	2467
310	2327
308	2307
306.4	2301 2*L-T_m*
305	2306
303	2335
300	2460
Composition: 69.9 wt. % water	
336.1	2711 *VC*
Composition: 78.0 wt. % water	
230*	417
240*	500
250*	597
260*	711
270*	840
280*	985
290*	1151
300*	1331
310*	1531
320	1773
330	2057
340	2376
350	2795
351.0	2890 *VL-T_m*
350.4	2920 *VL-P_m*
350.0	2916 *VC*
345	2845
340	2757
330	2552
320	2357
310	2195
305	2136
301.7	2118 2*L-T_m*
300	2125
298	2182
295	2334
293.7	2513
Composition: 88.3 wt. % water	
365	3110 *VC*(est)
335	2497
330	2386
320	2183
310	2011
300	1870
390	1772
287.5	1763 2*L-T_m*
287	1764
286	1770
283	1795
284	1865
282.8	2000
Composition: 94.0 wt. % water	
357	2863
358	2807
350	2667
340	2376
330	2149
320	1932
310	1752
300	1608
290	1475
280	1360
270	1372
265	1240
260.2	1215 3p_m

means of the dead-weight gauge. An iron-constantan thermocouple together with a sensitive potentiometer was used to measure the temperature of the vapor jacket to within 0.05°C. The couple was standardized against the melting point of ice and the condensing temperatures of water, naphthalene, benzophenone, and mercury all at 760 mm. of mercury pressure. Equilibrium between the liquid and vapor phases of the sample was established quickly by the movement of a small steel ball through the sample by means of a series of magnets (Figure 1).

Reagent-grade benzene, which had been dried over phosphorous pentoxide and rectified, and freshly prepared conductivity water were used in the preparation of the mixtures. Small quantities of the pure components were deaerated under high vacuum, and a measured quantity of each component was transferred by molecular distillation to the experimental tube attached to the high vacuum line. The procedure for the preparation of samples has been described elsewhere (*5*). Mixtures of a known composition could be prepared to within 0.002 weight fraction.

The reliability of the apparatus and procedures was checked by a comparison of the measured values of the vapor pressure of the pure components with accepted values from the literature. A summary of the observations showed that the temperature and pressure measurements were accurate to within 0.05°C. and 1 lb./sq. in., respectively.

EXPERIMENTAL RESULTS

The pressure at the liquid- and vapor-phase boundaries of fifteen mixtures of benzene and water were determined within the temperature range from 200° to 357°C. The smoothed data at increments of 10°C. in temperature for twelve of the mixtures are presented in Table 1. More extensive data are available (*10*). Table 2 gives values of the three-phase pressure at increments of 10°C. up to the critical end point temperature. These values are in excellent agreement with those reported by Scheffer (*13*). In addition, pressure-temperature data along the extension of the three-phase curve up to the critical solution point are shown.

Also indicated in these tables are the values of the unique states of each mixture noted as follows: the vaporization critical points (VC), the maximum temperature for the coexistence of vapor and liquid ($VL\text{-}T_m$), the maximum pressure for the coexistence of vapor and liquid ($VL\text{-}P_m$), the maximum three-phase temperature and pressure ($3p_m$), and the maximum temperature for two liquid phases ($2L\text{-}T_m$).

The values in the tables were read from large-scale plots of the experimental data as shown in Figure 2. Because of the limitations of the apparatus, the dew points of the mixtures could not be determined to as low a pressure and tempera-

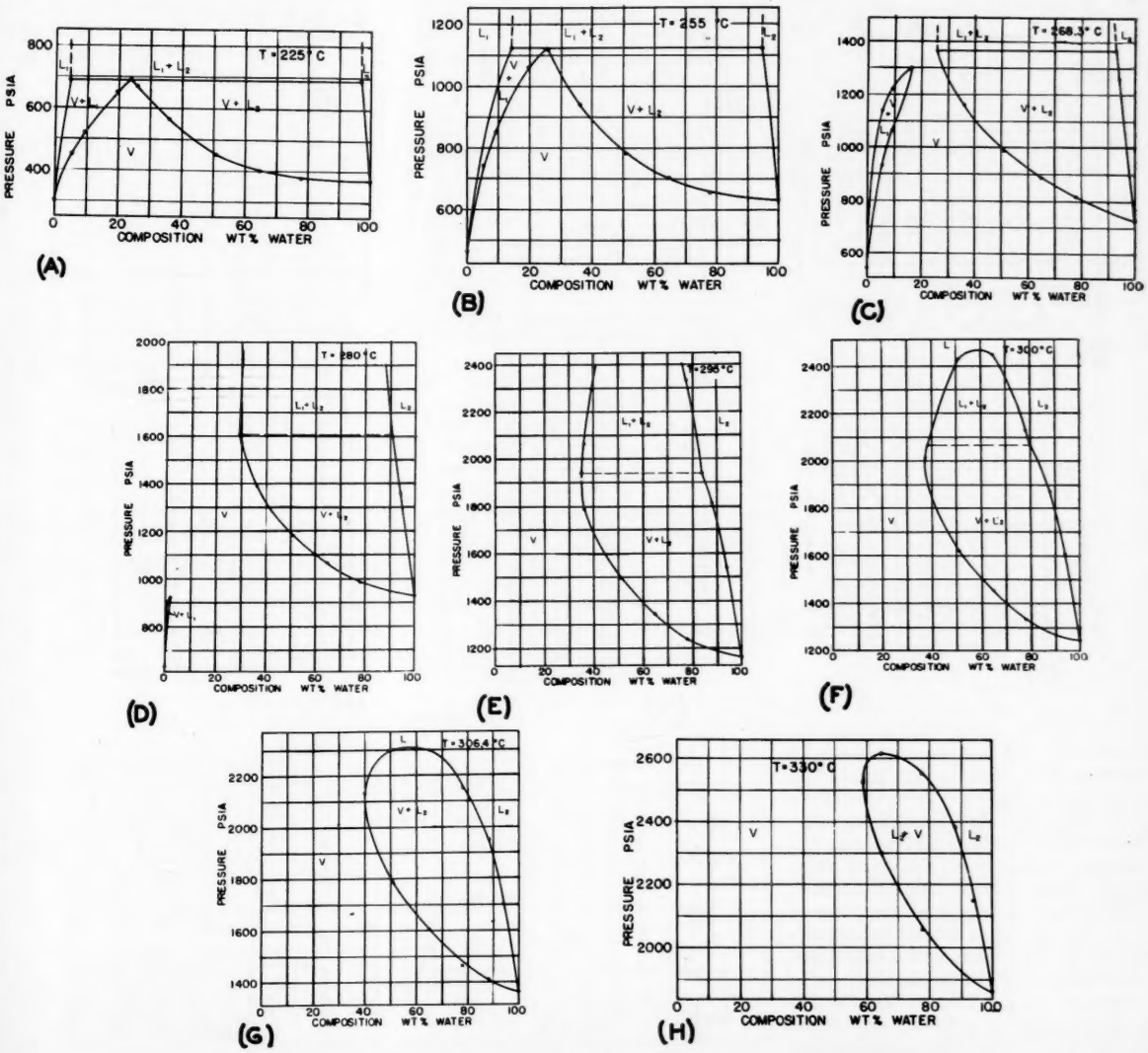

Fig. 3. Pressure-composition isothermal diagrams of the benzene-water system.

ture as desired. However these values were obtained by extrapolation of the measured portion of the curve, by the plotting of the logarithm of the absolute pressure vs. the reciprocal of the absolute temperature, and by the extension of the resulting straight line. The extrapolated curves are shown in Figure 2 by dashed lines, and the extrapolated values are shown in the table by asterisks.

The curves in Figure 2 are the *P-T* border curves of the various mixtures and the vapor-pressure curves of pure benzene and water. The latter curves were constructed with the vapor pressure reported for benzene by Kay and Nevens (*6*) and the vapor pressure of water given by Keenan and Keyes (*7*). These curves together form the *P-T-x* space diagram. The three-phase curve represents the pressure and temperature condition where two liquid phases and a vapor phase coexist in equilibrium; hence, when the pressure or temperature is set, the system is defined. The three-phase curve originates at the solid-liquid phase boundary and terminates in the critical end point. The coordinates of this point are 268.3°C., 1,364 lb./sq. in., and 25.8 weight % water. Immediately above the three-phase curve the system exists as two liquid phases, and below the curve the system is composed of a liquid and a vapor phase. The short, nearly vertical branches for mixtures 5 through 11 (Figure 2), as well as those extending upward from the three-phase curve, represent the phase boundaries separating the region of two liquid phases (to the left of the curve) from a region of a single homogeneous phase (to the right of the curve) for mixtures of the composition indicated. These curves extend into the high-pressure region and presumably are curved so that they intersect the solid-phase boundary at a lower temperature.

The critical locus is not continuous but is separated into two branches by a liquid miscibility gap (*10*). The lower branch of the curve originating in the critical point of benzene has a negative slope and terminates in the critical end point as noted above. The upper branch of the locus, beginning in the critical point of water, ends abruptly at the critical solution point of 306.4°C., 2,300 lb./sq. in., and 59 weight % water. In the miscibility gap between these compositions the phenomenon associated with the *L-V* critical point is observed only for the benzene-rich phase but not for the mixture as a whole.

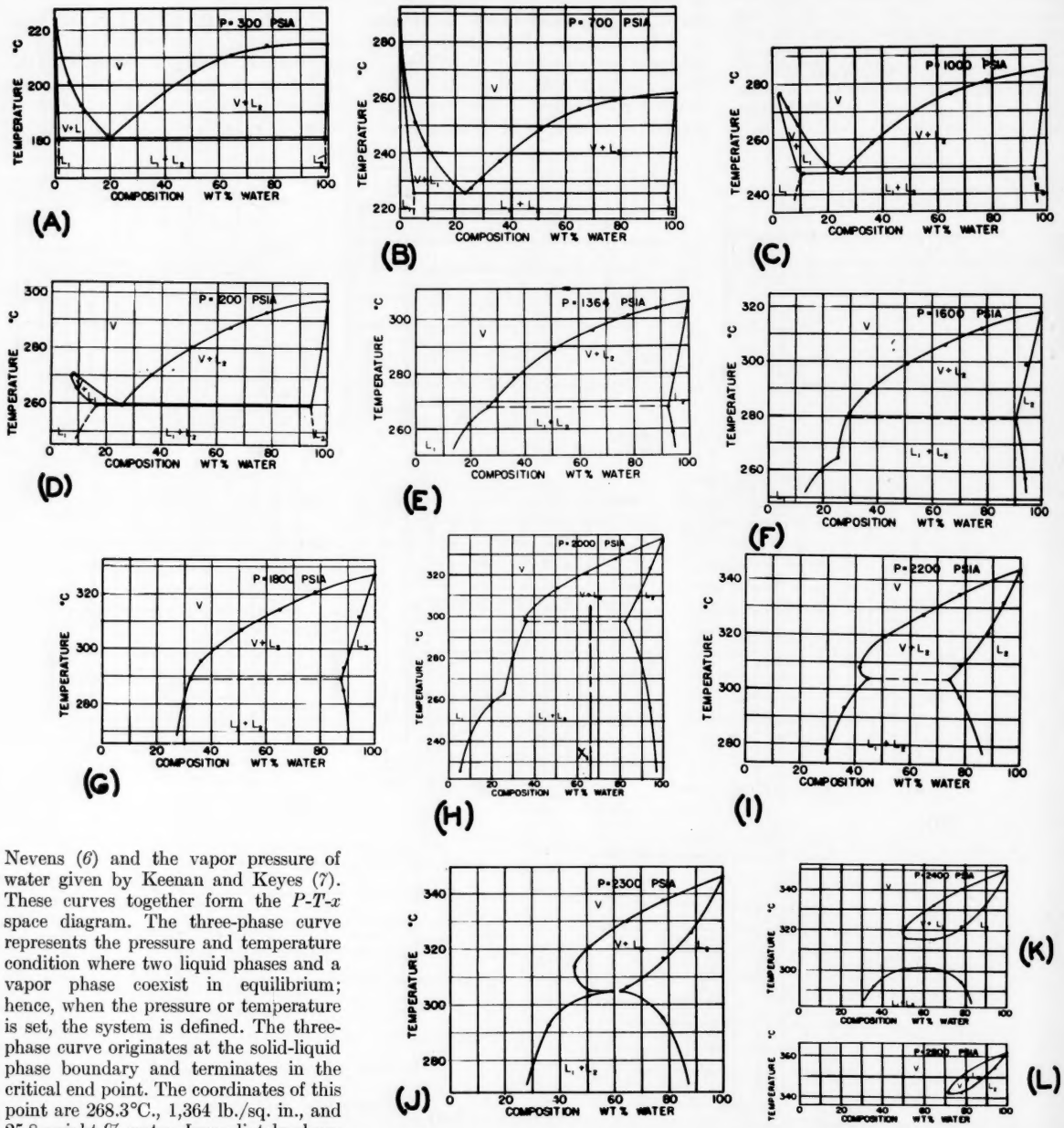

Fig. 4. Temperature-composition isobaric diagrams of the benzene-water system.

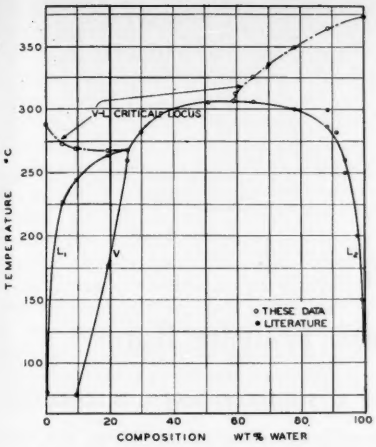

Fig. 5. Temperature-composition diagram for the benzene-water system.

TABLE 2. PRESSURE-TEMPERATURE RELATIONS ALONG THE THREE-PHASE CURVE AND THE EXTENSION OF THE THREE-PHASE CURVE, BENZENE-WATER SYSTEM

Temperature, °C.	Pressure, lb./sq. in. abs.
	Expt.
180	295
190	360
200	438
210	531
220	633
230	752
240	885
250	1038
255	1123
260	1212
265	1307
268.3	1364
270	1404
280	1610
290	1825
300	2070
306.4	2302 ($2L$-T_m)

INTERPRETATION OF THE DATA

From the graphically smoothed data and plots of Figure 2 a series of cross plots was prepared in order to interpret more fully the nature of the phase behavior.

Up to the three-phase critical end point (268.3°C.) the benzene-water system develops in a manner usually ascribed to a partially miscible system in which the vapor composition at a point of univariance lies intermediate to the two liquid compositions. This is clearly shown in the P-x phase diagrams at constant temperature, Figures 3*a*, 3*b*, and 3*c*, and the T-x phase diagrams at constant pressure, Figures 4*a*, *b*, *c*, and *d*. The point of intersection of the vapor curves with the constant-pressure line in each of the P-x diagrams and with the constant-temperature line in each of the T-x diagrams is a heteroazeotropic point (*15*). The three-phase curve is therefore the vapor-pressure curve of the heteroazeotrope or constant-boiling mixture formed by benzene and water. The variation of its composition with temperature is shown by the vapor curve in Figure 5.

The existence of an island in the P-x section (Figures 3*c* and *d*) is the result of the negative slope of the critical-locus curve. Referring to Figure 2, one can see that any isotherm taken in the range of temperatures from the three-phase critical end point to the critical point of pure benzene will have an island.

In the region of the three-phase critical temperature and pressure there can be detected the subtleties of the evolution of the surface to realign itself so as to continue on in another direction. Significantly Figure 5, the solubility diagram, shows the benzene-rich liquid-solubility branch going to the vapor branch abruptly at the three-phase critical end point. There is no smooth, rounded compromise meeting of the two curves. The vapor branch continues directly on above the three-phase critical, having taken on itself the meaning of both branches from which it evolved. Similarly the critical locus curve (Figure 5) goes through a minimum before reaching the three-phase critical to attain a positive slope and be directed toward its ultimate terminal, the critical point of water.

The three-phase curve extended beyond the critical end point temperature (268.3°C.) to the critical solution temperature (306.4°C.) does in effect continue to represent three-phase equilibrium. However the transition of one of the liquid phases to the vapor phase is continuous and accompanied by no volume change at constant temperature and pressure. The extension of the three-phase curve may be considered to represent a metastable three-phase equilibrium. A point on the curve would represent the limit of the solubility of a benzene-rich dense gas or fluid phase and a water-rich liquid phase at a temperature and pressure where the liquid is just beginning to vaporize. However the dense fluid and the vapor form a homogeneous mixture which is identified as a single phase.

When one traces the phase changes of a mixture of composition x_1 in Figure 4*h*, the foregoing interpretation is illustrated. At some low temperature, and a pressure of 2,000 lb./sq. in., the mixture will exist as two liquid phases. These two liquid phases increase mutually in solubility as the temperature is raised to approximately 264°C. With further increase in temperature the benzene-rich phase is no longer identified as a liquid but rather as a dense fluid, and the effect of increased temperature is a continued increase in solubility of the two phases. Upon reaching a temperature of 297°C. these two phases have reached their maximum solubility, which may in a broad sense be called the *limit of solubility* of the gas and liquid. At this temperature the water-rich phase begins to vaporize and the vapor which is formed is completely dissolved in the benzene-rich fluid. An increase in the temperature above 297°C. causes a normal pattern of behavior. In terms of solubility the liquid becomes more soluble in the vapor while the vapor becomes less soluble in the liquid.

Figure 5 outlines completely the solubility relations of the saturated liquids for the system. All mixtures become completely miscible at a temperature of 306.4°C., which corresponds to a pressure of 2.300 lb./sq. in. A mixture containing about 59 weight % water was deduced to be the composition which will be critical at this point. Mixtures which still retain two phases at temperatures and pressures above the critical solution point have phase boundaries like normal binary mixtures, Figures 3(*H*), 4(*K*), and 4(*M*).

LITERATURE CITED

1. Groschuff, E., *Z. Elektrochem.*, **17**, 348 (1911).
2. Jaeger, A. E., *Brennstoff-Chem.*, **4**, 259 (1923).
3. Joris, G. G., and H. S. Taylor, *J. Phys. Chem.*, **16**, 45 (1948).
4. Kay, W. B., *Ind. Eng. Chem.*, **30**, 459 (1938).
5. ———, and W. E. Donham, *Chem. Eng. Sci.*, **5**, 1 (1955).
6. Kay, W. B., and T. D. Nevens, *Chem. Eng. Progr. Symposium Series No.* 3, **48**, 108 (1952).
7. Keenan, J. E., and F. G. Keyes, "Thermodynamic Properties of Steam," p. 28, John Wiley, New York (1936).
8. Kuenen, J. P., "Verdampfung und Verflussigung von Gemisch," Johann Ambrosius Barth, Leipzig (1906).
9. Van Laar, J. J., *Koninkl. Akad. Wetenschap. Amsterdam*, **7**, 517 (1904).
10. Rebert, C. J., and W. B. Kay, Doc. 5911 American Documentation Institute, Photoduplication Service, Library of Congress, Washington 25, D. C., $1.25 for photoprints or 35-mm. microfilm.
11. Ricci, J. E., "The Phase Rule and Heterogeneous Equilibria," p. 65, D. Van Nostrand, New York (1951).
12. Roozeboom, H. W. B., "Die Heterogenen Gleichgewichte vom Standpunkte der Phasenlehre, Part 2, Systeme mit Zwei Flussigen Phasen," Friedrich Vieweg and Sohn, Braunschweig (1918).
13. Scheffer, F. E. C., *Koninkl. Akad. Wetenschap. Amsterdam*, **17**, 834 (1914).
14. Seidell, Atherton, "Solubilities of Inorganic and Organic Compounds," Vol. II, 3rd ed., p. 368, Van Nostrand, New York (1940).
15. Swietoslawski, Wojciech, "Ebulliometric Measurements," p. 46, Reinhold, New York (1945).
16. van der Waals, J. D., and Ph. Kohnstamm, "Lehrbuch der Thermostatik," Part 2, Johann Ambrosius Barth, Leipzig (1927).
17. Young, S., "Stoichiometry," p. 122, Longmans, Green, New York (1918).

Manuscript received August 25, 1958; revision received October 17, 1958; paper accepted October 18, 1958. Paper presented at A.I.Ch.E. Salt Lake City meeting.

Performance of Packed Columns

V. Effect of Solute Concentration on Gas-Phase Mass Transfer Rates

H. L. SHULMAN and L. J. DELANEY

Clarkson College of Technology, Potsdam, New York

In a determination of the effect of solute concentration on gas-phase mass transfer rates carbon tetrachloride was vaporized at three different concentration levels in a short 4.0-in.-diameter column packed with 0.5-in. Raschig rings.

The experimental data indicate that previous mass transfer correlations should be modified to include a term $(P_{BM}/P_T)^{2/3}$ and that the Schmidt number should be evaluated at average film conditions.

The correlation found is suitable for predicting gas-phase mass transfer coefficients which can be combined with effective interfacial areas reported previously to obtain volumetric mass transfer coefficients for any gas-liquid-solute system.

Parts I to III were published in volume 1; part IV appeared in volume 3.

In the previous papers (*4* to *7*) of this series a correlation was developed for the prediction of the gas-phase mass transfer coefficient in packings:

$$j_D = \left[\frac{k_G M_M P_{BM}}{G}\right]\left[\frac{\mu}{\rho D_V}\right]^{2/3} = 1.195\left[\frac{D_P G}{\mu(1-\epsilon)}\right]^{-0.36} \quad (1)$$

This correlation was obtained from experimental work in which several gases and packings were employed at varying temperatures, pressures, and flow rates. As a result it can be said that this correlation has been checked for its ability to predict the effect on the mass transfer coefficient of varying every independent variable which appears in the equation with the exception of that of the mean partial pressure of the inert gas.

For a number of reasons it has been most convenient to do experimental mass transfer work with low solute concentrations, and as a result P_{BM} has always been almost equal to the total pressure on the experimental system. Thus in spite of the enormous amount of experimental mass transfer work which has been done and reported there are very few data available which can be used to check the effect of P_{BM}. Any correlating equation which employs P_{BM} can have it replaced by P_T without any significant effect on the degree of correlation obtained with low solute-concentration data.

The term P_{BM} appears in the equation for the steady state rate of molecular diffusion of one component through a stagnant layer of another gas.

$$N_A = \frac{D_V P_T(\Delta p)}{RTZ\, P_{BM})} \quad (2)$$

As this equation does not describe the rate of mass transfer for physical systems in which turbulent motion of fluids occurs, a simpler empirical approach has been used which employs the gas-phase mass transfer coefficient:

$$N_A = k_G(\Delta p) \quad (3)$$

Unfortunately Equations (2) and (3) have been compared to lead to some false conclusions, as shown in

$$k_G = \frac{D_V P_T}{RTZ\, P_{BM}} \quad (4)$$

Chilton and Colburn (*2*), attempting to correlate mass transfer data by an analogy to work in heat transfer, introduced P_{BM} into the dimensionless group $k_G M_M P_{BM}/G$, which by the methods of dimensional analysis is found to be a function of the Schmidt number $(\mu/\rho D_V)$ and a Reynolds number. It was felt that since P_{BM} is associated with the diffusion coefficient, in relationships such as Equation (2), and diffusion plays a role in the over-all process of mass transfer, the use of P_{BM} was justified. Correlations of mass transfer data for many physical systems of practical importance by means of the Chilton and Colburn relationship have been successful because low solute-concentrations were employed. Under these conditions if P_T had been substituted for P_{BM}, the correlations would have been just as good.

Most correlations of the Chilton and Colburn type have shown that the exponent on the Schmidt number $(\mu/\rho D_V)$ is approximately 2/3 as in Equation (1). This implies that k_G is proportional to $(D_V)^{2/3}$. However the correlations also imply that k_G is inversely proportional to P_{BM}, which does not give the relationship between D_V and P_{BM} as expected from Equation (2) for a region in which molecular diffusion is the rate-controlling mechanism for mass transfer. By analogy with the effect found for D_V one might expect k_G to be inversely proportional to $(P_{BM})^{2/3}$.

If both P_{BM} and P_T are employed, dimensional-analysis methods could yield a modified form of Equation (1) in which the ratio (P_{BM}/P_T) appears as an additional dimensionless group:

$$\left[\frac{k_G M_M P_T}{G}\right]\left[\frac{P_{BM}}{P_T}\right]^n\left[\frac{\mu}{\rho D_V}\right]^{2/3} = 1.195\left[\frac{D_P G}{\mu(1-\epsilon)}\right]^{-0.36} \quad (5)$$

In this equation the exponent n on (P_{BM}/P_T) could be expected to be 2/3 on

Tabular material has been deposited as document 5971 with the American Documentation Institute, Photoduplication Service, Library of Congress, Washington 25, D. C., and may be obtained for $1.25 for photoprints or 35-mm. microfilm.

the basis of the preceding discussion. Regardless of the value of n, this equation will correlate low-solute-concentration data as well as Equation (1).

Two attempts have been made in recent years to obtain reliable gas-phase mass transfer data at high enough solute concentrations to investigate the effect of P_{BM} on the mass transfer coefficient. Cairns and Roper (*1*) employed a wetted-wall column to vaporize water into air at very high humidities. Their mass transfer data scattered badly possibly because they were operating in or near the critical zone by employing Reynolds numbers between 2,390 and 9,095; however they did offer a correlation which shows k_G inversely proportional to $(P_{BM}/P_T)^{0.83}$.

Westkaemper and White (*8*) obtained similar data by vaporizing carbon tetrchloride into an air stream flowing through a duct of rectangular cross section at Reynolds number between 600 and 15,000. By using the data for Reynolds numbers above 2,000 these investigators came to the unusual conclusion that their data could be correlated equally as well by the use of a (P_{BM}/P_T) term raised to the zero or first power. Their equations in rearranged form are

$$\left[\frac{k_G M_M P_T}{G}\right]\left[\frac{P_{BM}}{P_T}\right]^0\left[\frac{\mu}{\rho D_V}\right]^{0.56} = 0.00012\left[\frac{DG}{\mu}\right]^{0.42} \quad (6)$$

and

$$\left[\frac{k_G M_M P_T}{G}\right]\left[\frac{P_{BM}}{P_T}\right]\left[\frac{\mu}{\rho D_V}\right]^{0.56} = 0.0014\left[\frac{DG}{\mu}\right]^{0.08} \quad (7)$$

Both these equations are immediately open to suspicion because they imply that k_G is proportional to the gas rate raised to the 1.42 and 1.08 power, respectively. This is very unusual because extensive experience has shown this power to vary from about 0.60 to 0.83 for mass transfer.

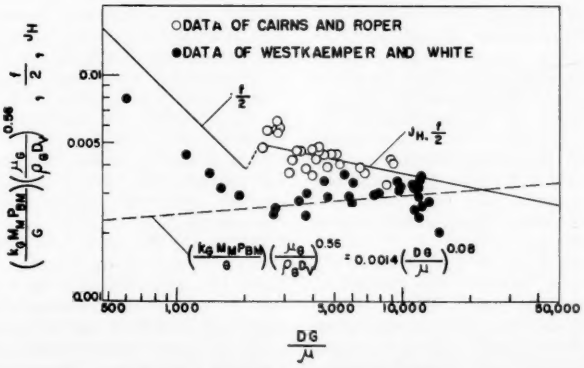

Fig. 1. Comparison of literature data.

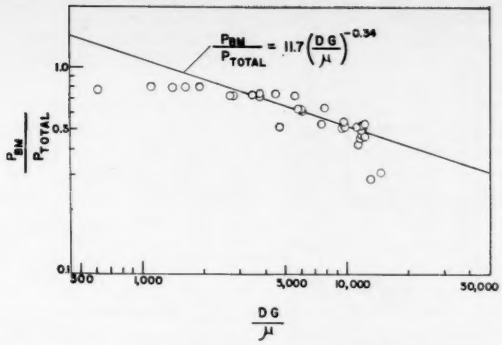

Fig. 2. Data of Westkaemper and White (*8*).

The unusual conclusions reached by these investigations can be explained easily as due to the unfortunate interpretation of a portion of their data and a coincidence in obtaining data in such a manner as to have introduced a relationship between (P_{BM}/P_T) and Reynolds number. These difficulties are shown in Figures 1 and 2. In Figure 1 Equation (7) is compared with the experimental data and a reference line showing the friction factor and the heat transfer factor for smooth round tubes. It can be seen that the data, although somewhat scattered, fall below but in a band parallel to the reference line. Unfortunately the investigators in attempting to obtain a correlation showing the minimum standard deviation ignored the data at low Reynolds numbers and obtained Equation (7). Cairns and Roper's (*1*) data are seen to scatter about the reference line. Figure 2 shows the coincidental relationship between (P_{BM}/P_T) and Reynolds number for the experimental data resulting in

$$\left[\frac{P_{BM}}{P_T}\right] = 11.7\left[\frac{DG}{\mu}\right]^{-0.34} \quad (8)$$

for Reynolds numbers above 2,000. Because of this unfortunate coincidence the data can be correlated just as well by using any power on the (P_{BM}/P_T) term and obtaining the corresponding power on Reynolds number. It can be concluded that the data of Westkaemper and White (*8*) cannot be used to determine the effect of P_{BM} on k_G.

The object of the present work is to determine the effect of P_{BM} on k_G for mass transfer in a packed column. A packed column avoids the difficulties inherent in operating in the ciritical and transition zones, such as encountered in wetted-wall columns. By vaporizing carbon tetrachloride into air streams of three different levels of concentration at varying gas rates one can avoid a coincidental relationship between (P_{BM}/P_T) and Reynolds number. The use of a short packed column results in a small gas-stream concentration change which makes it simple to employ average physical properties to interprete the data. Recycling the liquid carbon tetrachloride, one can adjust operating conditions to provide for little or no liquid temperature change throughout the column. This facilitates the determination of the liquid surface conditions required for the calculation of driving forces.

EQUIPMENT

Figure 3 shows a schematic diagram of the apparatus employed.

The experimental work was done in a Pyrex column 4 in. in diameter and packed with 1.75 in. of 0.5-in. Raschig rings. Air was obtained by means of a blower with a variable speed drive for coarse adjustments. Fine adjustments were made with valves located directly below the rotameters. The liquid rotameter was calibrated for a liquid rate of 3,000 lb./(hr.)(sq. ft.) in the liquid temperature range used. The column was heated with nichrome wire to avoid condensation and to maintain an essentially adiabatic operation.

The liquid receiving tank, a steel tank with a capacity of 5 gal., was located below the column. It was connected directly to a similar constant-head tank located 5 ft. above the top of the column. The liquid was circulated by a gear pump through a filter. An overflow line from the constant head tank to the receiving tank ensured a constant amount of liquid in the overhead tank at all times. The liquid was heated with a 1.5-kw. plate heater located directly

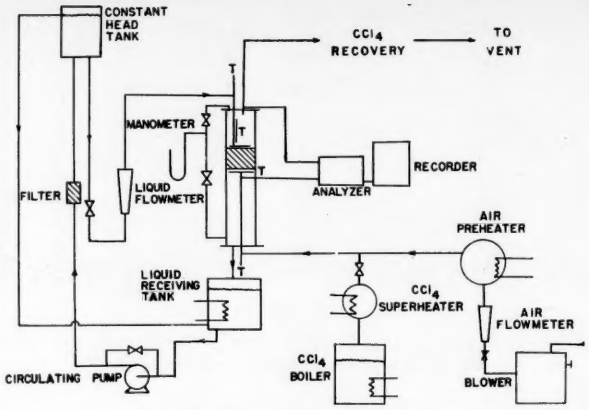

Fig. 3. Diagram of apparatus.

below the receiving tank. The temperature was controlled with a variable transformer used to adjust the power input. The copper lines were insulated with asbestos tape and covered with aluminum foil.

distributor was made of 0.25-in. copper tubing forming a continuous coil of two turns, with fifty holes 0.031 in. in diameter drilled radially along the underside. The temperature of the liquid was measured

for air, and carbon tetrachloride concentration was calculated by difference. The concentration of air was given by comparison of the peak height of pure air with the peak height for the air of the mixtures; because it was found that the width of the air peak was constant, peak heights were used rather than the area under the curve. Peak heights for pure air were reproducible within 0.2%.

PROCEDURE

The chromatographic analyzer required approximately 3 hr. to reach equilibrium, and therefore the analyzer was set well in advance of an actual run. Helium was the carrier gas, and a flow rate was used that gave reproducible peaks for pure air.

When runs were to be made with carbon tetrachloride from the boiler, the power for the boiler was turned on first. Air was then sent through the column. The thermostatic control on the air heater was set at 800°F. to bring the piping and insulation to equilibrium. The jacketed heater on the carbon tetrachloride line was also turned on to superheat the vapor before it was mixed with air. The liquid heater under

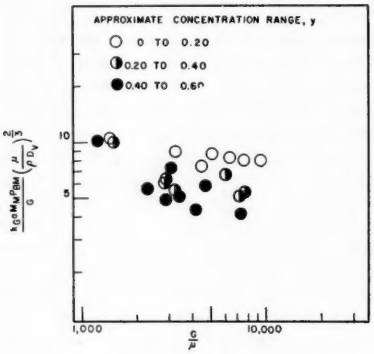

Fig. 4. Experimental data with Schmidt number based on average bulk composition.

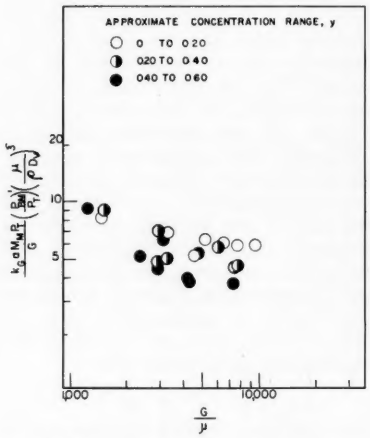

Fig. 5. Correlation of data with Schmidt number based on average film composition and $(P_{BM}/P_T)^1$.

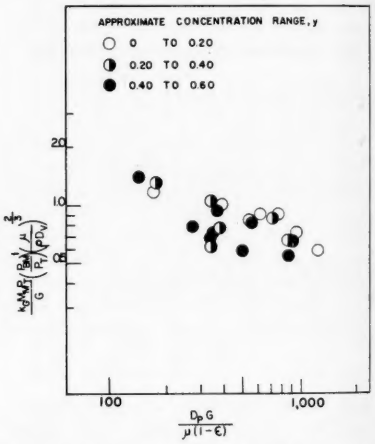

Fig. 6. Correlation of data with Schmidt number based on average film composition and $(P_{BM}/P_T)^1$.

A carbon tetrachloride boiler was used to give gas mixtures of the desired composition. Heat was supplied to the boiler by an immersion heater with the power input controlled by a variable transformer. The carbon tetrachloride vapor was passed through a 2-ft. length of copper tubing covered with a 400-watt jacket type of heater and mixed with air that had been heated to 800°F. The air heater was a 4.5-kw. Chromalox heater equipped with automatic temperature controls.

The heated gases were brought into the base of the column where the temperature was measured with an iron-constantan thermocouple. The gas distributor was a cross made of a brass stock bar $\frac{5}{8}$ in. wide and $\frac{3}{8}$ in. deep. Two grooves were cut along the underside of each arm of the cross, and six 0.125-in. holes were drilled along each groove from the end to the center of the cross, making a total of forty-eight discharge holes.

The liquid entered the top of the column and was discharged directly above the packing to minimize end effects. The liquid

with a thermocouple just before being discharged into the packing; then a portion of the liquid leaving the packing was collected in a shallow trough and the temperature was measured there with a thermocouple which was always immersed in fresh liquid coming from the packing. The temperature of the gas leaving the column was measured with a thermometer placed above the liquid distributor. The carbon tetrachloride recovery system consisted of two double-pipe heat exchangers connected in series. The condensate was returned to the boiler.

Inlet gas samples were taken from the inlet gas line $\frac{1}{2}$ in. below the distributor, and outlet samples were taken as the gas left the column. The samples were drawn through 0.125-in. copper tubing by slight suction, which was kept constant once the runs were started. An analysis was made

the liquid receiver tank was turned on and then the nichrome heating wire on the column. The equipment required about 1 hr. to come to operating conditions.

A series of pure air peaks was then taken to be compared with actual heights taken during runs. Inlet compositions were set by the adjustment of the power input to the boiler following analysis of the inlet stream. When the desired inlet composition was reached, the heated liquid from the constant head tank was started through the column and adjusted to a rate of 3,000 lb./(hr.)(sq. ft.). The system was allowed to run about 15 min. while the liquid temperature was being adjusted so that its temperature remained fairly constant as it passed through the packing.

The analyzer required 6 min. to analyze a sample. To make a given measurement the sample valve was opened to bring the

sample from the top of the column into the analyzer. Temperature and pressure measurements required about 2 min. to be recorded, which was about the time required for the analyzer to produce the analysis for air. The sample line for the inlet concentration was then connected to the analyzer. After the analysis of the top sample for air was complete, the bottom sample had about 3 min. to flush out the sample valve. The inlet stream was then analyzed and the inlet concentration was found to remain constant over a period of time with the same boiler setting. The settings were changed on the boiler and air rate, and the procedure was repeated. Intermittent pure-air samples were taken to make sure that there was no variation in the pure-air peak height.

The high concentration runs were done as the first series, then the medium concentration runs, and finally the low concentration runs. The packing and the distributor were not disturbed once actual runs were being made. Typical experimental data for five runs are presented in Table 1.

and $N_A a$ is obtained from the measured air rate and the analysis of the inlet and outlet streams.

The mass transfer coefficient is calculated from $k_G a$ by estimating a with the methods developed previously (*4* to *7*). Viscosities and diffusivities are calculated by the methods outlined in the text of Hirschfelder, Curtis, and Bird (*3*). The void fraction in the irrigated packing is estimated by methods presented preciously (*4*, *6*, *7*). The reported gas rates are an average of the inlet and outlet rates. Molecular weights and physical properties are determined from an average of the inlet and outlet compositions and temperatures except as otherwise noted. The reported values of P_{BM} are the arithmetic average of the P_{BM} at the inlet and outlet ends of the packed column. The Schmidt number varies rapidly with changing composition but is almost independent of temperature changes. As a result it was evaluated and

concentrations, obtained by difference, were reproducible to within 1% at high concentration and about 2% at low concentrations. As a result it can be estimated that the calculated $k_G a$ values are reproducible to better than 10% at low concentrations and 30% at the very high concentrations where a close approach to equilibrium introduces appreciable uncertainty in the driving forces. The final correlation of the data (Figure 10) shows scatter of the experimental data at the various concentration levels within the limits estimated.

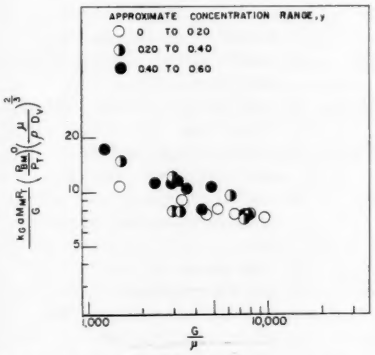

Fig. 7. Correlation of data with Schmidt number based on average film composition and $(P_{BM}/P_T)^0$.

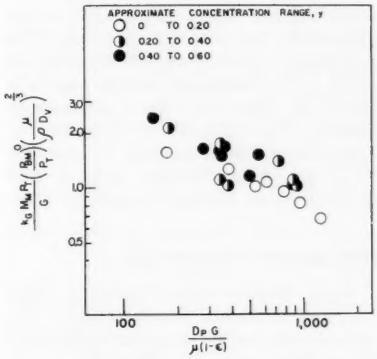

Fig. 8. Correlation of data with Schmidt number based on average film composition and $(P_{BM}/P_T)^0$.

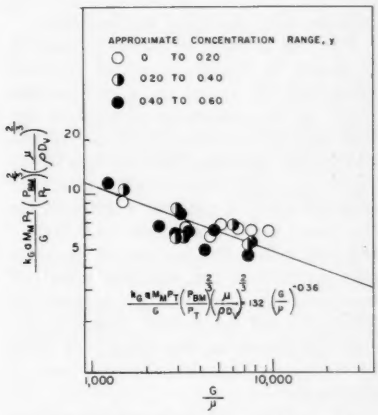

Fig. 9. Correlation of data with Schmidt number based on average film composition and $(P_{BM}/P_T)^{2/3}$.

EXPERIMENTAL RESULTS

An attempt was made to obtain data at three concentration levels with varying gas rates. This was done by introducing gas to the column roughly at the 0, 0.20, and 0.40 mole fraction carbon tetrachloride levels. When one vaporized additional carbon tetrachloride in the column, the outlet concentrations rose approximately 15 to 25 mole % above the inlet concentrations. The highest outlet concentration obtained was 0.616 mole fraction carbon tetrachloride. The data obtained are shown in Figures 4 through 10 with the three different concentration levels indicated. It should be realized that since it was impractical to hold the inlet concentrations constant for each level, the concentration differences between points at the three levels are not uniform and the scatter at any one level may be due in part to concentration differences.

In an attempt to correlate the data to determine the true effect of P_{BM} a problem is encountered which one does have to face at low concentrations or with a system such as air and water. This is the change in physical properties with changes in concentration and

METHODS OF CALCULATION

The volumetric mass transfer coefficient is calculated from

$$k_G a = \frac{(N_A a)}{(\Delta p)_{lm}} \qquad (9)$$

where

$$(\Delta p)_{lm} = \frac{(p_i - p)_1 - (p_i - p)_2}{\ln \dfrac{(p_i - p)_1}{(p_i - p)_2}} \qquad (10)$$

used in two ways, first at the average bulk composition and second at what might be called "film" conditions, that is an average of the inlet, outlet, bulk, and interfacial conditions. The second composition corresponds closely to the value value obtained by the subtraction of P_{BM} from P_T for this work.

The gas rate was read on a rotameter calibrated to within 3%. Air concentrations could be determined to better than 1%. The carbon tetrachloride

Table 1. Typical Experimental Data

Run	1	7	10	17	21
Liquid rate, lb./(hr.)(sq. ft.)	3,000	3,000	3,000	3,000	3,000
Pure-air rate, lb./hr.	4.78	3.41	4.80	1.36	2.38
Mole fraction CCl_4, inlet, y_1	0.360	0.229	0	0.433	0.276
Mole fraction CCl_4, outlet, y_2	0.504	0.359	0.245	0.616	0.454
Liquid temperature, bottom, °C.	57.6	48.2	43.2	62.6	53.2
Liquid temperature, top, °C.	59.4	50.1	45.9	63.6	54.8
Gas temperature, bottom, °C.	144	111	211	175	115
Gas temperature, top, °C.	71	65	63	92	76
Total pressure, atm.	0.973	0.976	1.000	0.988	1.000

In an attempt to correlate the data to determine the true effect of P_{BM} a problem is encountered which one does have to face at low concentrations or with a system such as air and water. This is the change in physical properties with changes in concentration and

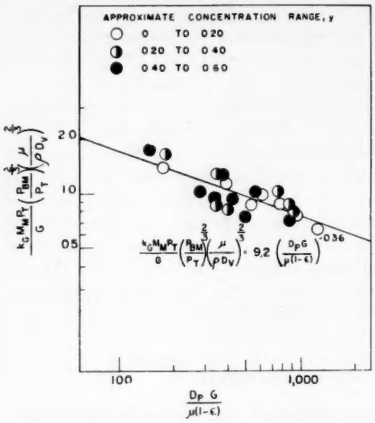

Fig. 10. Correlation of data with Schmidt number based on average film composition and $(P_{BM}/P_T)^{2/3}$.

especially the great variation in Schmidt number with changing concentration.

The first attempt to correlate the data is shown in Figure 4, where physical properties are based on a composition which is the arithmetic average of the inlet and outlet concentrations. It can be seen that the data fall into three bands depending upon concentration level and that the effect of gas rate is different for the three. Further attempts to correlate the date with Schmidt numbers based on average column compositions were not successful because the effect of gas rate found did not agree with Equation (1), and the power on the (P_{BM}/P_T) term as shown in Equation (5) was zero or negative.

All further attempts at correlation employed Schmidt numbers evaluated at average film conditions; that is the inlet, outlet, bulk, and interfacial, concentrations were averaged. Figure 5 shows the data with a $(P_{BM}/P_T)^1$ term used. The points still show an effect of concentration but an effect of gas rate closer to that expected from Equation (1). Since the low concentration runs at the higher gas rates were taken near loading conditions, it was felt that the removal of the effective interfacial area would make it possible to test Equation (5) to find the best power on the (P_{BM}/P_T). This was accomplished by estimating a and ϵ as described under methods of calculation. Figure 6 shows further improvement in correlation by the use of this method, but an effect of concentration is still present. Figures 7 and 8 show attempts with $(P_{BM}/P_T)^0$ employed. Again the proper effect of gas rate is indicated, but the effect of concentration is reversed; that is the low concentration data now fall below the high concentration data. It appears therefore that the best power on (P_{BM}/P_T) lies between zero and one. Several additional trials indicated that the use of $(P_{BM}/P_T)^{2/3}$ would correlate the data to give the effect of gas rate called for by Equations (1) and (5) and eliminate scatter which could be attributed to concentration level. Figures 9 and 10 show the data with $(P_{BM}/P_T)^{2/3}$.

The difference between the coefficient of the equation shown on Figure 10 and that of Equation (5) is probably due to a number of factors, several of which can be shown to predict a higher coefficient for this work. Since a very short column was used, end effects and excellent gas and liquid distribution would tend to provide a much higher coefficient. In addition there is some question as to the reliability of estimating a and ϵ for carbon tetrachloride because it has a density well above that used in developing the methods of predicting these quantities.

Since the effect of gas rate found is identical to that found in previous studies with packings, it is believed that the data are valid for conditions representative of flow patterns in packings and that the effect of P_{BM} can be predicted by the use of $(P_{BM}/P_T)^{2/3}$ in an expression such as Equation (5). The 2/3 power is also in agreement with the effect of D_V found previously, and it is logical to expect the same relationship between P_{BM} and D_V as is found for molecular diffusion to hold for systems where molecular diffusion plays a part in the over-all process of mass transfer.

SUMMARY AND CONCLUSIONS

Mass transfer data including data obtained at three concentration levels indicate that mass transfer coefficients for packings can be correlated by

$$\left[\frac{k_G M_M P_T}{G}\right]\left[\frac{P_{BM}}{P_T}\right]^{2/3}\left[\frac{\mu}{\rho D_V}\right]^{2/3} = 1.195\left[\frac{D_P G}{\mu(1-\epsilon)}\right]^{-0.36} \quad (11)$$

when the Schmidt number is evaluated at average film conditions.

This equation makes it possible to predict a k_G which can be combined with effective interfacial areas reported previously (*4* to *7*) to obtain a $k_G a$ for any desired gas-liquid-solute system for which physical properties are available.

ACKNOWLEDGMENT

The authors wish to acknowledge support of this work under Contract No. AT (30-1)-1463 of the Atomic Energy Commission.

NOTATION

a = effective interfacial area, sq. ft./cu. ft.
D = equivalent diameter or characteristic dimension, ft.
D_P = diameter of sphere possessing the same surface area as a piece of packing, ft.
D_V = diffusivity of solute in gas, sq. ft./hr.
f = friction factor for smooth tubes
G = superficial gas rate, lb./(hr.) (sq. ft.)
j_D = mass transfer factor, defined by Equation (1)
j_H = heat transfer factor for smooth tubes
k_G = gas-phase mass transfer coefficient, lb.-moles/(hr.) (sq. ft.) (atm.)
$k_G a$ = volumetric mass transfer coefficient
M_M = mean molecular weight of gas, lb./lb.-mole
n = exponent on (P_{BM}/P_T) in Equation (5)
N_A = rate of mass transfer, lb.-moles/(hr.) (sq. ft.)
$N_A a$ = lb.-moles of carbon tetrachloride vaporized/hr./cu. ft. of packing
p = partial pressure of carbon tetrachloride in gas, atm.
Δp = solute partial pressure difference, atm.
$(\Delta p)_{lm}$ = logarithmic mean driving force, atm.
P_{BM} = mean partial pressure of inert gas in the gas phase, atm.
p_i = partial pressure of carbon tetrachloride at liquid surface, atm.
P_T = total pressure, atm.
R = gas-law constant
T = absolute temperature, °K.
y = solute mole fraction
Z = diffusion path length, ft.
ϵ = void fraction, cu. ft./cu. ft.
μ = gas viscosity, lb./(hr.) (ft.)
ρ = gas density, lb./cu. ft.

Subscripts

1 = bottom of packing
2 = top of packing

LITERATURE CITED

1. Cairns, R. C., and G. H. Roper, *Chem. Eng. Sci.*, **3**, 97 (1954).
2. Chilton, T. H., and A. P. Colburn, *Ind. Eng. Chem.*, **26**, 1183 (1934).
3. Hirschfelder, J. O., C. F. Curtis, and R. B. Bird, "Molecular Theory of Gases and Liquids," Wiley, New York (1954).
4. Shulman, H. L., C. F. Ullrich, and N. Wells, *A.I.Ch.E. Journal*, **1**, 247 (1955).
5. Shulman, H. L., C. F. Ullrich, A. Z. Proulx, and J. O. Zimmerman, *ibid.*, p. 253.
6. Shulman, H. L., C. F. Ullrich, N. Wells, and A. Z. Proulx, *ibid.*, p. 259.
7. Shulman, H. L., and J. E. Margolis, *ibid.*, **3**, 157 (1957).
8. Westkaemper, L. E., and R. R. White, *ibid.*, p. 69.

Manuscript received August 18, 1958; revision received January 2, 1959; manuscript accepted January 29, 1959.

Multicomponent Distillation on a Large Digital Computer

II. Generalization With Side-Stream Stripping

N. R. AMUNDSON, A. J. PONTINEN, and J. W. TIERNEY

Remington Rand Univac, St. Paul, Minnesota

The problem of multicomponent distillation is considered for a column with an arbitrary number of feed streams and an arbitrary number of side-stream withdrawals. The overheads from the side-stream strippers are admitted to the column, introducing the inert stripping medium into the main column. Provisions are made in the calculations for complete heat balancing, inert injection, and internal reflux cooling. The method of computation is that of a previous paper involving the component-by-component technique. Calculations are made on the main column and give first approximations to the side-stream compositions; stripper calculations are then initiated. An alternating procedure is instituted between the main column and the strippers, the successive iterations continuing until a preassigned accuracy in the desired quantities is reached. An extensive numerical problem is worked.

In a previous paper (*1*) a technique for multicomponent distillation calculations was developed. If the equations of conservation of mass and energy are written around each plate, there are $(m + 1)$ equations, m equations arising from the conservation of each of the m components and one from the heat balance. With $N + 1$ stages in the column it was shown that there are a total of $(N + 1)\ m + N$ equations which must be solved simultaneously under the condition of restraint that temperatures are so chosen that the vapor and liquid mole fractions in each stage total one. It was assumed that the number of plates, feed-plate location, condition of feed, etc., were fixed in advance so that the composition profile through the column might be computed. reflux rate and overhead vapor draw off having been fixed. Design problems such as optimum feed-plate location or number of plates for a given separation were not discussed, since such problems could be solved by the successive application of the above technique with a resultant bracketing of the desired values. In this paper the equations will be written in a more general form to include the effects of side-stream strippers, inert injection, and internal-reflux cooling. A method will be described which should be useful for hydrocarbon distillations in which side streams must be stripped of light components and the overhead from the stripper returned to the column. An extensive numerical example will be discussed.

DEVELOPMENT OF EQUATIONS—MAIN COLUMN

The column shown in Figure 1 is considered with N theoretical stages and a partial condenser, the latter denoted as the zeroth stage and the reboiler the Nth stage. It is assumed that the inert is noncondensible in the column and insoluble in the liquid phase. The inert part of the feed to the jth stage will be treated as an s_j with the remainder F_j. The vapor flow from the jth stage U_j is

$$U_j = V_j + I_j \tag{1}$$

$$Y_j = \sum_{k=0}^{j} (F_k - S_k) \tag{2}$$

must also be defined, and then

$$L_j = Y_j + V_{j+1}$$

The usual mass balance on the ith component is

$$L_{j-1}x_{j-1,i} + U_{j+1}y_{j+1,i} + F_i x_{Fji} - L_j x_{ji} - U_j y_{ji} - S_j x_{ji} = 0 \tag{3}$$

where this equation does not apply to the inert component. With the equilibrium relation $y_{ji} = K_{ji}x_{ji}$, this reduces to

$$(Y_{j-1} + V_j)x_{j-1,i} - (Y_{j-1} + F_j + V_{j+1} + U_j K_{ji})x_{ji} + U_{j+1}K_{j+1,i}x_{j+1,i} = -F_i x_{Fji} \tag{4}$$

This equation holds for all stages including the partial condenser and the reboiler provided one chooses

$$x_{ji} = 0, \quad j < 0, \quad j > N$$

$$U_j = 0, \quad j > N$$

$$Y_{-1} = -V_0$$

$$Y_0 = -V_0$$

Equation (4) is a set of equations which may be written in matrix form:

$$\overline{\overline{M}}_i \bar{X}_i = -\bar{F}_i, \quad i = 1, 2, \cdots, m$$

or, when one inverts $\overline{\overline{M}}_i$,

$$\bar{X}_i = -\overline{\overline{M}}_i^{-1}\bar{F}_i, \quad i = 1, 2, \cdots, m \tag{5}$$

If a_{pq} is an element of $\overline{\overline{M}}_i$, then

$$a_{jj} = -(Y_{j-1} + F_j + V_{j+1} + U_j K_{ji}), \quad 0 \le j \le N$$

$$a_{j,j+1} = U_{j+1}K_{j+1,i} \qquad 0 \le j \le N - 1$$

$$a_{j,j-1} = V_j + Y_{j-1}, \qquad 1 \le j \le N$$

all other elements being zero. The elements of $\bar{x}_i$ are x_{ji}, $j = 0$ to N; $\bar{F}_i$ has components $F_i x_{Fji}$, $j = 0$ to N.

The heat balance around the jth stage gives

$$Q_j + (L_{j-1}h_{j-1} + V_{j+1}H_{j+1} + I_{j+1}H_{s,j+1}) - (L_j h_j + V_j H_j + I_j H_{sj}) + F_j H_{Fj} - S_j h_j + s_j \tilde{H}_{sj} = 0$$

From

$$I_j - I_{j+1} = s_j$$

and

$$Y_j - Y_{j-1} = F_j - S_j$$

it follows that

$$V_j(h_{j-1} - H_j) + V_{j+1}(H_{j+1} - h_j) = -Q_j + Y_{j-1}(h_j - h_{j-1}) + F_j(h_j - H_{Fj}) + I_j(H_{sj} - H_{s,j+1}) + s_j(H_{s,j+1} - \tilde{H}_{sj})$$

or

$$V_j(h_{j-1} - H_j) + V_{j+1}(H_{j+1} - h_j) = -Q_j + Y_{j-1}(h_j - h_{j-1}) + F_j(h_j - H_{Fj}) + I_{j+1}(H_{sj} - H_{s,j+1}) + s_j(H_{sj} - \tilde{H}_{sj})$$

This equation is a set of equations which may be written in matrix form

$$\overline{\overline{H}}\bar{V} = \bar{G}, \qquad \bar{V} = \overline{\overline{H}}^{-1}\bar{G} \tag{6}$$

Neal R. Amundson is with the University of Minnesota, Minneapolis, Minnesota.

Table 1. Data for Illustrative Problem

Component	Equilibrium constant				Vapor enthalpy			Liquid enthalpy		Mole Fraction
	α_i	$\beta_i \times 10$	$\gamma_i \times 10^4$	$\Delta_i \times 10^6$	A_i	$B_i \times 10^2$	$C_i \times 10^4$	a_i	b_i	in feed
C_6	− 22.93	27.42	− 9.64	1.290	9,259	3,125	232	−4,940	45.1	0.11
C_8	− 29.72	37.34	− 4.22	1.761	12,390	4,000	312	−4,800	57.5	0.06
C_9	− 2.631	3.702	− 1.681	0.2828	13,000	4,900	300	−4,250	64.5	0.04
C_{10}	− 1.380	2.125	− 1.040	0.1812	14,400	5,350	350	−3,380	71.4	0.03
C_{11}	− 2.115	2.896	−11.252	0.1841	15,890	5,700	412	−2,660	78.1	0.06
C_{12}	− 1.363	1.864	− 0.811	0.1193	17,650	6,100	450	−1,250	85.0	0.30
C_{13}	− 2.872	3.680	− 1.446	0.1825	18,860	6,650	488	360	91.9	0.07
C_{14}	− 0.950	1.260	− 0.528	0.0723	20,310	7,050	538	2,350	98.8	0.13
C_{15}	− 0.738	0.987	− 0.398	0.0550	22,920	6,250	625	4,700	105.5	0.12
C_{16}	− 0.538	0.722	− 0.300	0.0400	22,800	8,350	550	7,600	112.0	0.08

Number of plates including reboiler = 20 + partial condenser
Side-stream draw off from plate 9
Overhead from side-stream stripper to plate 5
Number of plates in stripper = 6
Feed on plate 15 at 100 moles/unit time
Moles steam in stripper = 5
Side-stream draw-off rate = 35
Overhead vapor rate = 25 (hydrocarbon only)
Reflux ratio = 4
Feed − saturated liquid at 300°F., H_F = 24,769 B.t.u./lb. mole
Steam to stripper superheated to 400°F., H_s = 22,324 B.t.u./lb. mole
$H_s = 18{,}918 + 8.514\,T$ (T in °F.)

where $\tilde{V}$ has as elements V_j, $j = 1$ to N. The elements of $\tilde{G}$ are

$$c_j = -Q_j + Y_{j-1}(h_j - h_{j-1}) + F_j(h_j - H_{Fj}) + I_{j+1}(H_{sj} - H_{s,j+1}) + s_j(H_{sj} - \tilde{H}_{sj}), \qquad j = 1 \text{ to } N$$

and the elements of $\bar{H}$ are b_{pq}, where

$$b_{jj} = h_{j-1} - H_j, \qquad 1 \le j \le N$$

$$b_{j,j+1} = H_{j+1} - h_j, \qquad 1 \le j \le N-1$$

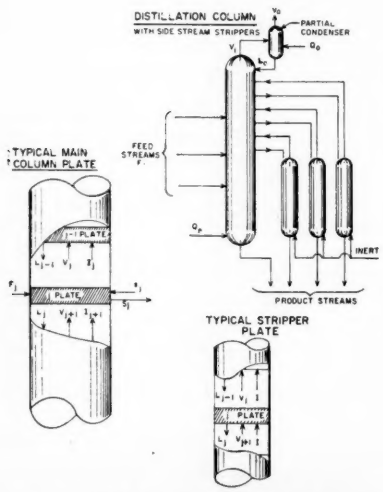

Fig. 1. Diagrammatic sketch of distillation column with side-stream strippers.

all other elements being zero. $\bar{\bar{H}}$ is already in triangular form.

A complete heat balance around the column but excluding the partial condenser gives

$$\begin{aligned} Q_N &= V_1H_1 + I_1H_{s1} - \sum_1^N F_iH_{Fi} + \sum_1^N S_ih_i - \sum_1^N s_i\tilde{H}_{si} - L_0h_0 - \sum_1^{N-1} Q_i \\ &= (R+1)V_0H_1 - RV_0h_0 + I_1H_{s1} - \sum_1^N F_iH_{Fi} + \sum_1^N S_ih_i - \sum_1^N s_i\tilde{H}_{si} - \sum_1^{N-1} Q_i \end{aligned} \tag{7}$$

and Q_N may be eliminated from the enthalpy matrix. Ordinarily all other Q_i's are zero. The heat balance around the partial condenser gives

$$Q_0 = V_0[H_0 - H_1 + R(h_0 - H_1)] \tag{8}$$

Before the method of solution is described, the temperature-correction procedure must be considered. Since V_j represents the noninert vapor and I_j the inert vapor, while y_{ji} is the mole fraction of the ith component in the total vapor U_j, it follows that

$$U_j \sum_i y_{ji} = (V_j + I_j) \sum_i y_{ji} = V_j$$

$$\sum_i y_{ji} = \frac{V_j}{U_j} = g_j$$

where g_j is a number less than 1. In the main column I_j is generally not large compared with V_j, and so g_j is only slightly less than 1. In a side-stream stripper however, where the liquid vaporization is usually not large, g_j may be small, say of the order of one tenth. Thus

$$\sum_i K_{ji}x_{ji} = g_j$$

on each plate. When one uses the first two terms of the Taylor series in the expansion of $\sum_i K_{ji}x_{ji}$ in the temperature,

$$\left(\sum_i K_{ji}x_{ji}\right)_{T_j} = \left(\sum_i K_{ji}x_{ji}\right)_{T_j'} + \left[\frac{\partial \sum_i K_{ji}x_{ji}}{\partial T}\right]_{T_j'} (T_j - T_j')$$

If T_j' is a temperature at which $\sum_i K_{ji}x_{ji}$ is known, then T_j is the temperature at which this same quantity may be approximately computed. If it is assumed that the only necessity for correcting the temperature is that the K_{ji}'s are incorrect, the x_{ji} should be normalized on each tray by division by $\sum_i x_{ji}$. Thus the temperature correction necessary to produce $\sum_i K_{ji}x_{ji} = g_j$ will be

$$T_j - T_j' = \left[g_j \sum_i x_{ji} - \sum_i K_{ji}x_{ji}\right]_{T_j'} \cdot \left[\sum_i x_{ji}\frac{\partial K_{ji}}{\partial T_k}\right]_{T_j'}^{-1} \tag{9}$$

In the computations described in this paper the equilibrium constants used are the ideal-solution constants and hence are independent of composition but dependent upon pressure and temperature. Although there are other rational expressions, it will be assumed here that K_{ji} is a cubic polynomial in T_j with the

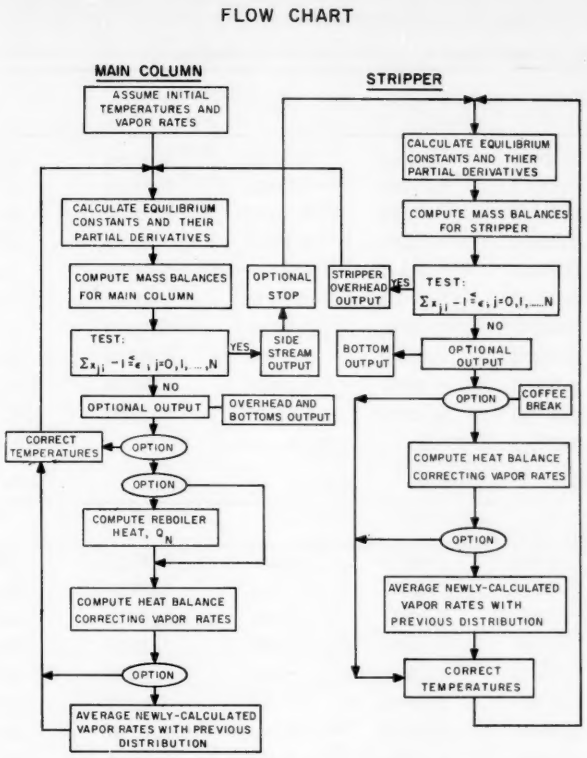

Fig. 2. Simplified flow chart for computer program.

coefficients functions of the pressure. Thus

$$K_{ji} = \alpha_i + \beta_i T_j + \gamma_i T_j^2 + \Delta_i T_j^3$$

$$\frac{\partial K_{ji}}{\partial T_j} = \beta_i + 2\gamma_i T_j + 3\,\Delta_i T_j^2$$

More sophisiticated expressions for the equilibrium constants may be used, such as the one derived from the Benedict-Webb-Rubin equation of state. In this case one may perform the temperature correction as above using the values of the composition from a previous iteration.

SIDE-STREAM STRIPPER ANALYSIS

The equations for the strippers may be obtained from the equations already developed. It will be assumed that the only feeds to the strippers are the side streams from the main column into the top and the inert stripping medium into the bottom. The stripped side stream is the effluent from the bottom, and the vapor overhead, including inert, enters the main column.

If I is the inert rate into the stripper bottom, L_0 is the side stream rate to the top, V_j is the noninert vapor rate from the jth stage, then Equation (4) may be written

$$(L_0 - V_1 + V_i)x_{j-1,i} - (L_0 - V_1 + V_{i+1} + U_iK_{ji})x_{ji} + U_{i+1}K_{j+1,i}x_{j+1,i} = 0$$

for the jth stage. This formula also holds for the top and bottom stages, as x_{0i} is known and $x_{N+1,i} = 0$. It can be written as a set of equations in matrix form:

$$\bar{\bar{S}}_i\bar{X}_i = -\bar{S}_i, \quad \bar{X}_i = -\bar{\bar{S}}_i^{-1}\bar{S}_i \quad (10)$$

where the elements d_{pq} of $\bar{\bar{S}}_i$ are

$$d_{jj} = -(L_0 + V_{i+1} - V_1 + U_iK_{ji}), \qquad 1 \le j \le N$$

$$d_{j,j+1} = U_{j+1}K_{j+1,i}, \qquad 1 \le j \le N-1$$

$$d_{j,j-1} = L_0 + V_j - V_1, \qquad 2 \le j \le N$$

The vector $\bar{S}_i$ has L_0x_{0i} as its first element and zeros elsewhere.

The heat balance around the stripper may be obtained as

$$V_j(h_{j-1} - H_j) + V_{j+1}(H_{j+1} - h_j) = (L_0 - V_1)(h_j - h_{j-1}) + I(H_{sj} - H_{s,j+1}) - Q_j$$

Table 2. Main-Column Calculations—Summarized*

	Initial assumption		Problem 1		Problem 2		Problem 3		Problem 5	
	Temperature, °F.	Vapor	Temperature, °F.	Vapor	Temperature, °F.	Vapor	Temperature, °F.	Vapor	Temperature, °F.	Vapor
P.C.†	200	25	287	25	288	25	263	25	251	25
1	212	125	351	125	351	124.8	347	139.1	333	139.2
2	225	125	368	125	369	137.6	366	163.0	357	164.7
3	237	125	376	125	379	138.9	376	164.8	369	166.8
4	250	125	384	125	386	139.0	383	165.2	376	167.3
5	262	125	389	125	391	139.0	389	165.3	383	167.2
6	275	125	393	125	395	139.1	395	164.0	389	156.9
7	287	125	397	125	398	139.3	399	165.4	393	157.7
8	300	125	400	125	402	139.4	403	165.6	396	157.4
9	312	125	404	125	405	139.3	406	165.5	400	157.1
10	325	125	408	125	409	138.9	410	165.1	403	156.9
11	337	125	412	125	412	138.3	413	164.4	406	156.7
12	350	125	416	125	415	137.7	416	163.7	408	156.3
13	362	125	419	125	419	137.2	420	162.9	410	155.7
14	375	125	423	125	422	136.5	424	161.9	414	154.6
15	387	125	428	125	426	135.4	429	160.4	420	152.7
16	400	125	444	125	442	184.8	443	210.4	432	202.2
17	412	125	451	125	450	197.1	451	222.2	438	212.9
18	425	125	458	125	458	200.7	458	225	444	214.7
19	437	125	467	125	467	203.4	468	226.8	452	215.2
20	450	125	479	125	480	205.4	480	226.9	466	215.0

*Vapor rates are in pound moles per hundred moles of feed of hydrocarbon only.
†Partial condenser.

TABLE 3. FINAL RESULTS, COLUMN AND STRIPPER

Composition of Liquid In Each Stage - hydrocarbon mole fraction

	Partial Condenser Vapor	0	1	2	3	4	5	6
C_6	0.36666	0.06579	0.01362	0.00703	0.00593	0.00550	0.00522	0.00536
C_8	0.19857	0.08868	0.05584	0.03313	0.02164	0.01621	0.01345	0.01225
C_9	0.13104	0.24009	0.13615	0.06636	0.03316	0.01950	0.01407	0.01215
C_{10}	0.09223	0.33986	0.31281	0.22684	0.14478	0.08718	0.05238	0.03471
C_{11}	0.04411	0.24982	0.43508	0.56820	0.62164	0.60328	0.53511	0.46021
C_{12}	0.00151	0.01579	0.04543	0.09663	0.17083	0.26634	0.37762	0.47300
C_{13}	0.00000	0.00000	0.00000	0.00001	0.00004	0.00016	0.00050	0.00085
C_{14}	0.00000	0.00000	0.00000	0.00000	0.00000	0.00001	0.00002	0.00003
C_{15}	0.00000	0.00000	0.00000	0.00000	0.00002	0.00007	0.00019	0.00029
C_{16}	0.00000	0.00000	0.00000	0.00000	0.00000	0.00000	0.00000	0.00000
T_j	-	251.4	337.9	357.3	368.6	376.5	382.6	388.6
V_j	-	25	139.3	164.7	166.8	167.3	167.2	156.9

	7	8	9 Side Stream	10	11	12	13
C_6	0.00518	0.00502	0.00488	0.00475	0.00466	0.00458	0.00450
C_8	0.01114	0.01025	0.00950	0.00887	0.00845	0.00810	0.00773
C_9	0.01100	0.01022	0.00963	0.00914	0.00881	0.00855	0.00829
C_{10}	0.02460	0.01892	0.01569	0.01376	0.01279	0.01218	0.01167
C_{11}	0.37240	0.28396	0.20445	0.13891	0.10041	0.07810	0.06462
C_{12}	0.57238	0.66555	0.74327	0.79776	0.81546	0.80393	0.76537
C_{13}	0.00174	0.00380	0.00829	0.01739	0.03047	0.04820	0.07005
C_{14}	0.00008	0.00023	0.00072	0.00223	0.00553	0.01248	0.02628
C_{15}	0.00056	0.00122	0.00282	0.00650	0.01273	0.02293	0.03890
C_{16}	0.00000	0.00000	0.00000	0.00002	0.00010	0.00048	0.00227
T_j	392.6	396.4	399.9	403.1	405.5	407.8	410.3
V_j	157.7	157.4	157.1	156.9	156.7	156.3	155.7

14	15	16	17	18	19	20

or

$$V_1(h_j - h_{j-1}) + V_j(h_{j-1} - H_j) + V_{j+1}(H_{j+1} - h_j) = L_0(h_j - h_{j-1}) + I(H_{sj} - H_{s,j+1}) - Q_j$$

for any stage. For the bottom stage $V_{N+1} = 0$. In matrix form

$$\bar{\bar{h}}\bar{v} = \bar{g}, \qquad \bar{v} = \bar{\bar{h}}^{-1}\bar{g} \qquad (11)$$

If e_{pq} is an element of $\bar{\bar{h}}$,

$$e_{11} = h_1 - H_1$$

$$e_{jj} = h_{j-1} - H_j, \qquad 2 \le j \le N$$

$$e_{j,j+1} = H_{j+1} - h_j, \qquad 1 \le j \le N-1$$

$$e_{j1} = h_j - h_{j-1}, \qquad 2 \le j \le N$$

The elements of $\bar{v}$ are V_j, $j = 1$ to N; $\bar{g}$ has elements f_p

$$f_j = L_0(h_j - h_{j-1}) + I(H_{sj} - H_{s,j+1}) - Q_j \qquad 1 \le j \le N-1$$

$$f_N = L_0(h_N - h_{N-1}) + I(H_{sN} - H_{sN}) - Q_N, \qquad j = N$$

As in the main column, enthalpies are written as a sum of partial-molar enthalpies and each partial-molar enthalpy may be taken as a cubic in the temperature

$$H_{ji} = A_i + B_iT_j + C_iT_j^2 + D_iT_j^3$$

$$h_{ji} = a_i + b_iT_j + c_iT_j^2 + d_iT_j^3$$

The enthalpy of the inert may usually be calculated when one assumes a constant heat capacity; thus where a difference in enthalpy occurs, the heat capacity is multiplied by the temperature difference.

METHOD OF COMPUTATION

The general method of computation, not including the stripper analysis, was described in the previous paper. The problem to be discussed here is a light-hydrocarbon distillation in which the total number of plates in the main column and the strippers, the feed-stage locations and side-stream draw-off locations and their respective amounts, inert injection in the main column and strippers, pressure, and reflux ratio are specified in advance, and it is desired to obtain the compositions of the top, bottom, and side-stream stripper effluent. Instead of fixing the reflux ratio, one may specify the boil-up heat into the reboiler. It was found that better convergence usually resulted when the reflux ratio was specified. This problem is the analysis problem of distillation as opposed to the synthesis problem. To solve the synthesis problem by this technique it would be necessary to bracket the desired separation by an iterative procedure.

If a temperature distribution is assumed, equilibrium constants may be computed. For the nonheat-balancing problem the vapor rates may be computed directly, and Equations (5) and (9) may be used alternately to obtain the composition of liquid and vapor on each tray. Since the side-stream-stripper over-

TABLE 3. FINAL RESULTS, COLUMN AND STRIPPER (*Continued*)

	Feed Plate						Bottoms
C_6	0.00439	0.00423	0.00027	0.00002	0.00000	0.00000	0.00000
C_8	0.00727	0.00662	0.00101	0.00014	0.00002	0.00000	0.00000
C_9	0.00795	0.00748	0.00194	0.00047	0.00011	0.00002	0.00000
C_{10}	0.01109	0.01030	0.00425	0.00164	0.00059	0.00019	0.00005
C_{11}	0.05536	0.04746	0.03127	0.01899	0.01060	0.00523	0.00211
C_{12}	0.69795	0.59760	0.58804	0.53549	0.44842	0.33169	0.20183
C_{13}	0.09261	0.10729	0.13290	0.15874	0.17704	0.17316	0.13537
C_{14}	0.05123	0.08948	0.10025	0.12210	0.15987	0.21313	0.26061
C_{15}	0.06204	0.09103	0.10163	0.12150	0.15384	0.19806	0.23927
C_{16}	0.00989	0.03837	0.03827	0.04071	0.04933	0.07839	0.16066
T_j	414.0	419.9	432.2	437.6	443.6	452.4	466.0
V_j	154.6	152.7	202.2	212.9	214.7	215.2	215.0

	Vapor Overhead-Stripper	1-S	2-S	3-S	4-S	5-S	6-S Stripper Bottoms
C_6	0.01152	0.00091	0.00022	0.00006	0.00002	0.00001	0.00000
C_8	0.01958	0.00592	0.00449	0.00364	0.00300	0.00240	0.00168
C_9	0.01815	0.00693	0.00572	0.00492	0.00424	0.00356	0.00270
C_{10}	0.02155	0.01360	0.01262	0.01192	0.01126	0.01045	0.00911
C_{11}	0.17466	0.19791	0.19486	0.19259	0.19035	0.18736	0.18072
C_{12}	0.41298	0.76088	0.76784	0.77235	0.77635	0.78107	0.78980
C_{13}	0.00207	0.00887	0.00912	0.00930	0.00948	0.00972	0.01031
C_{14}	0.00014	0.00078	0.00081	0.00083	0.00084	0.00087	0.00092
C_{15}	0.00084	0.00302	0.00311	0.00317	0.00322	0.00330	0.00342
C_{16}	0.00000	0.00000	0.00000	0.00000	0.00000	0.00000	0.00000
T_j	-	377.9	368.2	361.4	355.0	347.3	333.4
V_j	-	9.793	7.225	4.849	3.948	3.142	2.186

head composition is not known at this time, it is assumed to be pure inert. The solution to this problem may then be used as a first approximation for the heat balancing. The order of the iterations here is somewhat arbitrary, but it has been found that a new heat balance need not be made to obtain new vapor rates each time Equations (5) and (9) are iterated. Generally it has been found that the convergence to the final solution is most rapid if Equations (5) and (9) are iterated about three times before new vapor rates are computed from Equation (6).

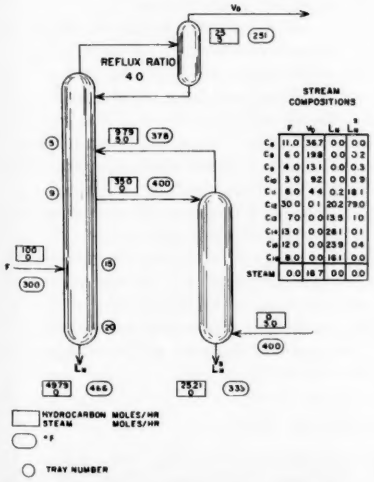

Fig. 3. Schematic diagram showing equilibrium flow rates, temperatures, and compositions for terminal streams in the sample problem.

At this point in the calculation one has a fair idea concerning the side-stream composition from the main column, and the stripper computation may now be instituted. For the strippers vapor rates must be assumed throughout the column. Iterations are then made by the use of Equations (9), (10), and (11). The number of mass-balance iterations between calculations of new vapor rates may be varied to improve the convergence. When the convergence point is reached on the strippers, the main column calculations are reinstituted since the stripper overhead may perturb the previous calculations. It is apparent that the computations are then repeated in an obvious way, iterating between the column and the stripper. Calculations are repeated until the desired degree of accuracy in the pertinent variables is reached. Figure 2 gives a schematic flow chart for the computation.

In an iterative procedure, such as that described here, certain tricks may make the technique converge when otherwise it may converge slowly or not al all. For example the vapor rates calculated from the heat balance may tend to oscillate and thus cause the successive mass-balance iterations to diverge. This may be overcome by using the average of the last two calculated vapor rates as vapor rates. Similar techniques may be used at other points in the computation such as on compositions and temperatures. The convergence of the iterations in these distillation calculations is indeed a delicate and difficult question, for although the methods of this paper have proved satisfactory in the problems considered to date, what seemed like more elegent methods diverged rather badly.

DISCUSSION OF NUMERICAL PROBLEM

A series of numerical problems will now be considered by means of a main column of twenty stages with a side stream drawn from the ninth stage. The overhead from the stream stripper is admitted to the main column in the fifth stage. The final solution is obtained as the result of the solution of a series of five problems. The data are summarized in Table 1.

Problem 1: Main Column Only With Side-Stream Draw Off (No Heat Balancing)

In this problem the vapor rates through the column were held constant at 125 moles with a side-stream draw-off rate at 35 moles. An initial temperature distribution of 200°F. in the partial condenser

and 450°F. in the bottom was assumed with a linear distribution throughout the column. With this assumption the $\sum_i x_{ji}$ varied from a minimum of 0.1112 to a maximum of 1.765 throughout, and $\sum_i K_{ji}x_{ji}$ varied from 0.2112 to 1.772. After five iterations results of sufficient accuracy were obtained. The final temperature and vapor rates are summarized in Table 2.

Problem 2: Main Column Only With Side-Stream Draw Off (Heat Balancing Included)

Complete heat balancing was carried out in this problem. The reflux ratio was held fixed, and Q_N was computed from Equation (7) for insertion into $\bar{G}$. To initiate the solution the results of the previous calculation were used as a first approximation. The mass balancing and heat balancing were alternated, and Q_N was recalculated at each iteration. The average of the last two calculated vapor rates were used in $\overline{\overline{M}}_i$. Temperatures on the plates were not significantly different from those in problem 1, but vapor rates changed substantially below the feed. This is attributed to the fact that the feed was introduced at an unfortunate position, for the feed temperature is at 300°F., which corresponds to a slight subcooling, but the feed tray temperature is 426°F. A rough heat balance at the feed tray indicated that the vapor rates in Table 2 were correct.

Problem 3: Main Column Only With Side-Stream Draw Off and Steam Injection

This problem was no different from problem 2 save that 5 moles of steam was admitted to the column at stage 5. The effects were insignificant except for some changes in composition and temperature at the tower top.

Problem 4: Side-Stream Stripper

By use of the composition of the side stream from problem 3 the stripper computations were initiated. As a first guess the stripper top temperature was taken to be the same as the side-stream plate temperature in the main column. The bottom temperature was assumed to be 450°F., although it was realized that this could not be correct. Vapor rates were assumed to be 6 moles at the bottom and 11 at the top, where these are the total vapor rates. These rates were held fixed for a few iterations on the mass balance. Vapor rates were then calculated after about every third mass-balance calculation. It was essential in these calculations to use the average of the last two calculated vapor rates in the mass balance to ensure convergence. With the latter it was found that the initial guess on vapor rates could be varied quite widely. It is obvious that the lower part of the stripper contains vapor which is mostly inert, and so the compositions may vary appreciably.

Problem 5: Final Solution To Main Column Plus Side-Stream Stripper

With the result of problem 4 the main-column calculations may now be corrected for the effect of the introduction of the stripper overhead to the column. These calculations are repeated to determine what the effect will be on the side-stream composition. If the latter is significantly different, the stripper calculations must be repeated as in problem 4 and successive alterations are made until preassigned accuracy on pertinent variables is obtained. Various modifications of the program may be made here, since it is clear that some variables will not be affected. Table 3 shows the final compositions, temperatures, and vapor rates for both the column and stripper. Vapor rates shown are for the hydrocarbon only. Complete mass balances on each component check. The equilibrium constants were programed as cubics, vapor enthalpies as quadratics, and liquid enthalpies as linear functions of the temperature. The complete program is in floating-point arithmetic. The final mass balance on the system is

Feed to column
= 100 moles hydrocarbon
Vapor overhead
= 25 moles hydrocarbon
Side stream from column
= 35 moles hydrocarbon
Bottom from stripper
= 25.21 moles hydrocarbon
Overhead from stripper
= 9.79 moles hydrocarbon
Bottoms from column
= 49.79 moles hydrocarbon

and the results are shown graphically in Figure 3.

Finally a word should be given on the times required for computation. Problem 1 requires approximately 25 sec. iteration; Problem 2 requires about 5 sec. in addition for each vapor-rate calculation. A full punch out of x_{ji}, $\sum_i x_{ji}$, $\sum_i K_{ji}x_{ji}$, T_j, and V_j for each plate requires 90 sec. for the whole column and 30 sec. on the stripper. In the stripper each cycle requires about 8 sec., 6 sec. on the mass-balance iteration and 2 sec. on the vapor-rate calculation. The total running time for a complete problem, problem 1 through problem 5, involving some 75 cycles on the main column and 26 on the stripper, required about $\frac{1}{2}$ hr. For engineering purposes the total number of iterations may be reduced considerably with a resultant running time of about 10 min. The criterion used in this paper was the sum of the liquid mole fractions on each stage. A 1% check at each stage will be obtained in four or five iterations. An increase in the desired accuracy requires more than a proportional increase in the number of iterations. One tenth of one per cent in the total mole fractions requires of the order of ten iterations.

CONCLUSIONS

A general method of setting up the equations for multicomponent distillation has been presented. A complete machine program has been prepared, and the whole has been applied to a sample problem, with use of side-stream strippers and multiple feeds to the column illustrated. Complete heat and mass balancing is carried out on both the column and strippers, and the technique can be made as accurate as one pleases.

NOTATION

a_{pq} = matrix element of $\overline{\overline{M}}_i$
b_{pq} = matrix element of $\overline{\overline{H}}$
c_p = matrix element of $\bar{G}$
d_{pq} = matrix element of $\overline{\overline{S}}_i$
e_{pq} = matrix element of $\overline{\overline{h}}$
f_p = matrix element of $\bar{g}$
a_i, b_i, c_i, d_i = coefficients in cubic in temperature for h_{ji}
A_i, B_i, C_i, D_i = coefficients in cubic in temperature for H_{ji}
$\alpha_i, \beta_i, \gamma_i, \Delta_i$ = coefficients in cubic in temperature for K_{ji}
F_j = feed rate to the jth stage
$\bar{F}_i$ = feed vector
$\bar{G}$ = feed-enthalpy vector
g_j = ratio of noninert to total vapor rate $- V_jU_j - 1$
h_j = liquid enthalpy in jth stage
h_{ji} = partial molar enthalpy of ith component in jth-stage liquid
H_j = vapor enthalpy in jth stage
H_{ji} = partial molar enthalpy of ith component in the vapor in the jth stage
H_{sj} = partial molar enthalpy of inert in jth-stage vapor
$\bar{H}_{sj}$ = enthalpy of inert injected into jth tage
$\overline{\overline{H}}$ = enthalpy matrix for vapor-rate computations
I_j = inert vapor rate from jth stage (I for stripper)
K_{ji} = equilibrium constant of ith component in jth stage
L_j = liquid overflow from jth stage
$\overline{\overline{M}}_i$ = mass-balance matrix
N = number of stages counting partial condenser as zeroth and reboiler as Nth
Q_j = heat absorbed in the jth stage
Q_N = reboiler heat
R = reflux ratio at top
s_j = inert injection to the jth stage
S_j = side stream draw off from jth stage
T_j = temperature of jth stage
U_j = vapor rate from jth stage
$\bar{v}$ = vector
V_j = noninert vapor rate from jth stage
x_{ji} = mole fraction of ith component in liquid in jth stage
x_{Fji} = mole fraction of ith component in feed to jth stage
$\bar{X}_i$ = composition vector ith component
y_{ji} = mole fraction of ith component in vapor in jth stage
Y_j = sum of feeds minus sum of draw offs from top to jth stage, inclusive

LITERATURE CITED

1. Amundson, Neal R., and Arlene J. Pontinen, *Ind. Eng. Chem.*, **50**, 730 (1958).

Manuscript received June 5, 1958; revision received December 29, 1958; paper accepted December 30, 1958. Paper presented at A.I.Ch.E. Salt Lake City meeting.

Effective Collision Diameters and Correlation of Some Thermodynamic Properties of Solutions

J. M. PRAUSNITZ and P. R. BENSON, University of California, Berkeley, California

Volumetric data on gas mixtures and vapor-phase data for gas-liquid equilibria have been correlated within the framework of the theory of corresponding states. An expression based on the London potential for dispersion forces was used to compute characteristic temperatures for various binary systems, and a correlation was developed relating these temperatures to the polarizabilities, ionization potentials, and critical volumes of the pure components. The correlation shows how the molecular shape of a liquid affects its vapor-phase solubility. With the help of this correlation it is possible to make very good predictions of such gas-liquid equilibria as are required in high-pressure distillation, absorption, and petroleum hydrofining operations.

A study of volumetric data for mixtures of gases at moderate pressures has shown that the properties of gas-phase mixtures can be successfully interpreted within the framework of the theory of corresponding states (*5, 18*). Further it has been shown (*14*) that by extending the theory of corresponding states with techniques based on the theory of intermolecular forces one can make good predictions of fugacities as required in high-pressure phase equilibria and rate processes.

In the work referred to above, a correlation was presented for estimating the parameters required for the calculation of mixture properties. Specifically techniques were given for calculating the second virial coefficient of a mixture, which is given by

$$B_m = \sum_i \sum_j y_i y_j B_{ij} \qquad (1)$$

The second virial coefficient can be calculated from an expression of the form

$$\frac{B_{ij}}{V_{c_{ij}}} = \theta_B\left(\frac{T}{T_{c_{ij}}}, \omega_{ij}\right) \qquad (2)$$

The semiempirical correlations proposed in the earlier work were limited by the scarcity of data for highly asymmetric systems, that is for those systems having one component of low and one of high molecular weight. To overcome this limitation, data were recently obtained on the solubility of several liquids in compressed hydrogen, nitrogen, and carbon dioxide (*16*). These data indicated that the previously proposed correlation could be considerably improved by taking into account the shape as well as the size of the molecules in determining the characteristic temperature of the interaction between dissimilar molecules. The method of correlation described here uses simple mixing rules for the characteristic volume and the characteristic acentric factor. For a binary system containing components 1 and 2

$$V_{c_{12}} = 1/2[V_{c_1} + V_{c_2}] \qquad (3)^*$$

and

$$\omega_{12} = 1/2[\omega_1 + \omega_2] \qquad (4)$$

However the characteristic temperature, which is the most important parameter in the determination of the second virial coefficient, cannot be computed by any simple formula. The temperature characteristic of the interaction between two molecules of different size and/or shape is usually less than the geometric mean of the critical temperatures of the pure components, with the geometric mean as an upper limit. Prausnitz and Gunn (*18*) showed that for some hydrocarbons and related compounds with a common gas the correction which must be applied to the geometric mean is a straight-line function of the critical-volume ratio of the two pure components. However some of the results of recent experimental work (*16*) and of previously published phase-equilibrium data could not be correlated by this method, especially the data for systems containing carbon tetrachloride or *n*-decane. It therefore appeared advisable to consider an alternate method of correlation based on the attraction part of the potential-energy function acting between the dissimilar molecules.

CHARACTERISTIC TEMPERATURES FROM COLLISION DIAMETERS

According to the London theory of dispersion forces (*7*), one can express the potential energy between two molecules 1 and 2 by

$$\Gamma_{12} = -\frac{3\alpha_1\alpha_2 I_1 I_2}{2r^6(I_1 + I_2)} \qquad (5)$$

London's formula can be rewritten in terms of a dimensionless distance:

$$\Gamma_{12} = \epsilon_{12}\left(\frac{\sigma_{12}}{r}\right)^6 \qquad (6)$$

The characteristic energy can be related to the characteristic temperature by

$$\frac{\epsilon_{12}}{k} = \frac{3}{2}\beta T_{c_{12}} \qquad (7)$$

London's formula is strictly valid only for monatomic molecules. However by a suitable choice of parameters the London theory has been applied successfully to the calculation of thermodynamic and transport properties of a variety of polyatomic substances (*7*).

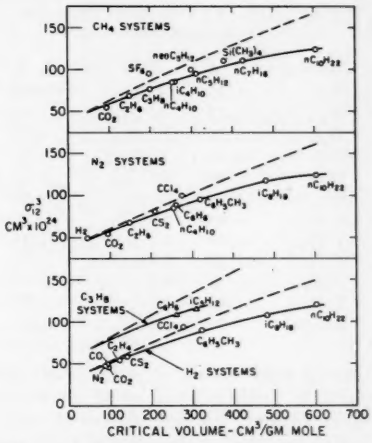

Fig. 1. Collision diameters for binary systems containing methane, nitrogen, hydrogen, and propane.

When one substitutes (6) and (7) into (5),

$$T_{c_{12}} = \frac{\alpha_1\alpha_2 I_1 I_2}{\beta k \sigma_{12}^6 (I_1 + I_2)} \qquad (8)$$

For spherical molecules the characteristic distance of interaction can be related to the characteristic distances for the pure components by

$$\sigma_{12} = \tfrac{1}{2}(\sigma_{11} + \sigma_{22}) \qquad (9)$$

In addition for pure components consisting of spherical molecules the characteristic interaction distance σ_{11} can be related to the critical volume by the empirical relation (*7*)

$$0.75 V_{c_1} = \tfrac{2}{3}\pi N \sigma_{11}^3 \qquad (10)$$

Equation (10) becomes increasingly poor as the molecule becomes more asymmetric.

The constant β in Equation (8) was evaluated by the use of published data for the polarizabilities and ionization potentials of the pure components and by use of characteristic temperatures for binary systems whose components consist of small spherical molecules (*18*). In this calculation the collision diameter σ_{12} was computed by Equations (9) and (10), which are appropriate for small, spherical (or nearly spherical) molecules such as nitrogen, methane, hydrogen, and carbon monoxide. The value of β was found to be 0.744; values of β for pure components

P. R. Benson is with North American Aviation, Canoga Park, California.

*The somewhat more complicated method of obtaining $V_{c_{12}}$ presented earlier (*18*) has not been used in this work.

Table 1. Collision Diameters, Å.

Component	Major axis	Minor axis	Equivalent sphere	Observed from binary data
n-Heptane	13.4	4.36	6.33	5.71
n-Decane	18.8	4.36	7.10	6.17
Carbon tetrachloride	5.47	5.47	5.47	5.48

Table 2. Effective Collision Diameters for Various Molecules Obtained from Binary Data Containing One Small Component

Molecule	σ, Å.	Molecule	σ, Å.
H_2	3.55	iC_4H_{10}	4.91
N_2	3.77	nC_5H_{12}	5.16
H_2S	3.87	iC_5H_{12}	5.25
CO	3.80	$neoC_5H_{12}$	5.37
CO_2	3.68	nC_7H_{16}	5.71
CS_2	4.80	iC_8H_{18}	5.98
CH_4	3.89	$nC_{10}H_{22}$	6.17
C_2H_4	4.10	C_6H_6	5.04
C_2H_6	4.33	$C_6H_5CH_3$	5.38
C_3H_6	4.53	CCl_4	5.48
C_3H_8	4.65	SF_6	5.27
nC_4H_{10}	4.96	$Si(CH_3)_4$	5.67

having small molecules range from 0.70 to 0.79 (*7*). When this value for β was used, binary collision diameters were evaluated for a number of binary systems containing hydrogen, nitrogen, methane, carbon dioxide, hydrogen sulfide, and propane by the use of Equation (8) with values of $T_{c_{12}}$ obtained from previously published volumetric and vapor-liquid equilibria data (*1, 2, 4, 8, 9, 10, 11, 18, 19, 20*). The results of these calculations are shown in Figures 1 and 2, where the cube of the collision diameter is plotted as a function of the critical volume of the second component. The dashed lines are calculated by means of Equation (9) for σ_{12} and Equation (10) for the collision diameter of the second component; thus one assumes the second molecular species to be spherical. To plot the dashed curves for hydrogen, carbon dioxide, and propane, an effective collision diameter σ_{22}* for these molecules was defined by

$$\sigma_{12} = \tfrac{1}{2}(\sigma_{22}^* + \sigma_{11}) \qquad (9a)$$

The effective diameters were calculated from observed collision diameters of these compounds with small, spherical (or nearly spherical) molecules. For carbon dioxide, effective collision diameters with nitrogen, methane, and hydrogen were 3.71, 3.69, and 3.63 Å., respectively.

EFFECT OF MOLECULAR SHAPE

Figures 1 and 2 indicate that the observed collision diameters for binary systems including one small, spherical (or nearly spherical) molecule and one nonspherical molecule are significantly less than those for binary systems containing two spherical molecules. These figures show the interesting result that the points for large molecules having spherical symmetry, such as carbon tetrachloride, sulfur hexafluoride, neopentane, and tetramethyl silane, lie well above the curves for nonspherical molecules.

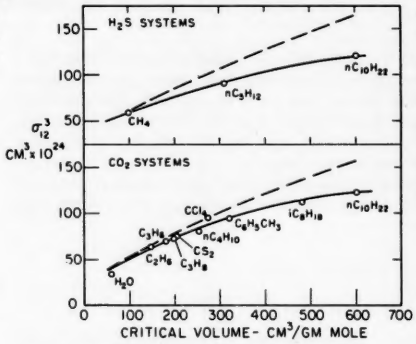

Fig. 2. Collision diameter for binary systems containing hydrogen sulfide and carbon dioxide.

The characteristic temperatures of some of the binary systems containing methane and higher paraffins reported here on the basis of phase-equilibrium data are somewhat larger than those previously reported (*18*) on the basis of vapor-phase compressibility data. The earlier calculations used an indirect method which gives considerably less accurate values for $T_{c_{12}}$ than those which used phase-equilibrium data.

Since only a few substances consist of spherical molecules, Equations (9) and (10) are not generally valid. Most polyatomic molecules could be described more accurately as ellipsoids than as spheres, and it is therefore to be expected that the effective collision diameters of ellipsoidal molecules should lie somewhere between the lengths of their minor and major axes. In a collision between a small spherical molecule and a larger ellipsoidal molecule the spherical molecule would interact mainly with the atoms closest to the point of collision. One might expect therefore that the distance between the colliding spherical molecule and the interacting atoms of the large molecule, that is the collision diameter, should be less than the collision diameter for the same small spherical molecule with a different spherical molecule having the same volume as the ellipsoidal molecule. For example when one considers the collision of a small molecule such as hydrogen with either of two larger molecules of similar size such as *n*-pentane and neopentane, it would appear likely that the collision diameter of hydrogen with *n*-pentane (which is rod-shaped) would be considerably smaller than the collision diameter of hydrogen with neopentane (which is spherical), even though *n*-pentane and neopentane have approximately the same size, as indicated by their critical volumes. It is this effect which is so clearly shown in Figures 1 and 2.

If the assumption is made that a polyatomic molecule is ellipsoidal in shape, the lengths of the two axes can be estimated from the critical volume, bond lengths, and bond angles. To illustrate, measured bond angles and bond lengths reported by Pauling (*13*) were used to calculate the ratio of the length to the width of the molecule for *n*-heptane and *n*-decane. Equating this ratio to the ratio of the lengths of the two axes of an ellipse, and assuming rotation about the major axis, one could calculate the lengths of the axes by means of a modification of Equation (10):

$$0.75 v_{c_1} = \tfrac{2}{3}\pi N \sigma_S^{\,2} \sigma_M \qquad (10a)$$

The results are given in Table 1.

Table 1 shows that for ellipsoidal molecules the collision diameters observed from the data, as expected, lie between the lengths of the minor and the major diameters of the ellipsoids, much closer to the lengths of the minor axes. Also, as indicated in Figures 1 and 2, the observed collision diameters for the ellipsoidal molecules are less than the diameters of spherical molecules having the same size.

Table 2 gives effective collision diameters calculated from published binary data.* These may be used to compute thermodynamic properties of mixtures; for example, to predict the vapor-phase solubility of a liquid in a gas, it is necessary to know only the collision diameter for the pair, the polarizabilities, and the ionization potentials. This information is used to calculate $T_{c_{12}}$, which, together with the generalized function, yields the virial coefficient B_{12}. Once this coefficient is known, the vapor-phase solubility can be found from the thermodynamic equations discussed previously (*16*).

The use of effective collision diameters is not restricted to binary mixtures but, as indicated by Equation (1), may be used for multicomponent mixtures, provided the density is not too high (*14*).

APPLICATIONS

The collision diameters in Table 2 and the correlations shown in Figures 1 and 2 are useful for predicting gas-liquid phase equilibria as may be required in such diffusional operations as high-pressure absorption, distillation, partial condensation, freezing out, etc. The collision diameters are required to determine the characteristic temperature [Equation (8)], which, together with Equations (3) and (4) and the generalized function, determines the cross-virial coefficient B_{12} [Equation (2)], which in turn is required in the phase-equilibrium equations given in reference *16*.

The correlations presented here are useful for the prediction of vapor-phase fugacities

*The effective collision diameters in Table 2 should not be applied to binary mixtures consisting entirely of large molesules, since the values tabulated here were obtained exclusively from binaries containing at least one component which consisted of small spherical molecules.

and hence are of direct applicability in the calculation of the phase-equilibrium behavior of the heavy component in gas-liquid equilibria; however they are not useful for the calculation of the phase-equilibrium behavior of the lighter component whose major correction for nonideality is in the liquid phase. For the light component a different approach must be used (*15, 17*).

One particular application of the ideas developed here is in hydrofining processess in the petroleum industry, where accurate K values for hydrocarbons in the presence of excess hydrogen are needed in process design, for example when one desires to know the equilibrium ratio for n-hexane in hydrogen (a system not used in the correlation presented here) at 340°F. and 100 atm. total pressure.

The collision diameter is obtained by the use of the curve for hydrogen-containing systems. Since the critical volume of n-hexane is 368 cc./g.-mole, $\sigma_{12}^3 = 96 \times 10^{-24}$ cc. The following data are needed for the calculation:

	Hydrogen
(pseudo)V_c	= 47.0 cc./g.-mole
(pseudo)ω	= 0.00
α	= 7.9×10^{-25} cc.
I	= 15.4 e.v.
	n-Hexane
T_c	= 508°K.
ω	= 0.30
α	= 118×10^{-25} cc.
I	= 10.4 e.v.
v^{0L}	= 168 cc./g.-mole
P_1^0	= 10.8 atm.

From Equation (8), $T_{c_{12}} = 98$°K. By using Equations (3) and (4) and tabulated values of θ_B (*14*), one obtains

$$v_{c_{12}} = 208 \text{ cc./g.-mole}$$
$$\omega_{12} = 0.15$$
$$B_{12} = (0.322)(208) = 66.9 \text{ cc./g.-mole}$$

The fugacity of pure liquid n-hexane at 100-atm. pressure is 12.9 atm., and a first estimate of y_1 is calculated with an assumption of ideal behavior and the use of an estimate of x_2, the solubility of hydrogen in the liquid phase (*3*). Since x_2 is small compared to unity, the estimated solubility need not be highly accurate. The second virial coefficient for n-hexane, when one uses tabulated values of θ_B, is −688 cc./g.-mole, and the second virial coefficient for hydrogen is 15 cc./g.-mole from published volumetric data (*6*). The molar volume of the vapor mixture is now calculated from the second virial coefficient of the mixture; it is $v = 369$ cc./g.-mole. Using these quantities, one finds that the vapor-phase fugacity coefficient of n-hexane is 0.627 and that the equilibrium ratio $K_1 = y_1/x_1 = 0.206$.* Using this computed value of K, one finds a new value of y_1, and if necessary the calculation is repeated. Convergence in these calculations is very rapid. Similar calculations were also made at 220°F. and at various pressures; the results are compared with observed data (*12*) in Figure 3, where the equilibrium ratio is plotted as a function of pressure for two temperatures.

The correlations presented in this work may be particularly useful for the calculation of gas-liquid equilibria at lower temperatures, where experimental vapor-phase compositions are very difficult to determine accurately.

*See reference *16* for details of this type of calculation.

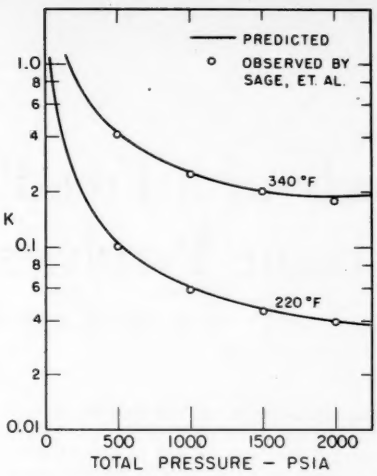

Fig. 3. Equilibrium ratios of hexane in hydrogen at 220 and 340°F.

ACKNOWLEDGMENT

This research was supported in part by a grant from the Petroleum Research Fund administered by the American Chemical Society. Grateful acknowledgment is hereby made to the donors of said fund.

NOTATION

B = second virial coefficient
B_{ij} = second virial coefficient characteristic of interaction between one molecule of species i and one molecule of species j
I = first ionization potential
k = Boltzmann constant
N = Avogadro's number
P = pressure
r = distance between molecules
R = gas constant
T = absolute temperature
$T_{c_{ij}}$ = temperature characteristic of i − j interaction
$T_{c_{12}}$ = characteristic temperature of 1-2 interaction
V = volume
$V_{c_{ij}}$ = volume characteristic of i − j interaction
V_{c_1} = critical volume of pure component 1
v = molar volume
x = mole fraction in liquid phase
y = mole fraction in vapor phase

Greek Letters

α = polarizability
β = a dimensionless constant
ϵ = characteristic energy
ϵ_{12} = energy characteristic of 1-2 interaction
Γ = potential energy
σ = collision diameter
σ_{11} = characteristic interaction distance
σ_{12} = collision diameter characteristic of 1-2 interaction
σ_{22}^* = effective collision diameter
σ_M = major diameter
σ_s = minor diameter
ω = acentric factor
ω_{ij} = acentric factor characteristic of i − j interaction
ω_1 = acentric factor of pure component 1
θ_B = generalized function for the second virial coefficient

Subscripts

c = critical or characteristic
1, 2 = components
m = mixture
M = major
S = minor

Superscripts

L = liquid phase
0 = pure component

LITERATURE CITED

1. Aroyan, H. J., and D. L. Katz, *Ind. Eng. Chem.*, **43**, 185 (1951).
2. Braune, H., and Fritz Strassmann, *Z. physik. Chem., A*, **143**, 225 (1929).
3. Cook, M. W., D. N. Hanson, and B. J. Alder, *J. Chem. Phys.*, 26, 784 (1957).
4. Eucken, Arnold, and F. Bresler, *Z. physik. Chem.*, **134**, 230 (1928).
5. Guggenheim, E. A., and M. L. McGlashan, *Proc. Roy. Soc. (London)*, **A206**, 448 (1951).
6. Hilsenrath, Joseph, ed., "Tables of Thermal Properties of Gases," U. S. Natl. Bur. Standards Circular 564 (1955).
7. Hirschfelder, J. O., C. F. Curtiss, and R. B. Bird, "Molecular Theory of Gases and Liquids," John Wiley, New York, (1954).
8. Krischevsky, I. R., and D. Gamburg, *Acta Physiochim. URSS*, **13**, 362 (1942).
9. Krichevsky, I. R., and R. S. Kalvarskaya, *Acta Physiochim. URSS*, **13**, 49 (1940).
10. Miller, Philip, and B. F. Dodge, *Ind. Eng. Chem.*, **32**, 434 (1940).
11. Nederbragt, G. W., *Appl. Sci. Research*, **A1**, 237 (1948).
12. Nichols, W. B., H. H. Reamer, and B. H. Sage, *A.I.Ch.E. Journal*, **3**, 262 (1957).
13. Pauling, Linus, "The Nature of the Chemical Bond," Chap. 5, Cornell, Ithaca (1948).
14. Prausnitz, J. M., *A.I.Ch.E. Journal*, **5**, No. 1, 3 (1959).
15. *Ibid.*, **4**, No. 3, 269 (1958).
16. ———, and P. R. Benson, *ibid.*, **5**, No. 2, 161(1959).
17. Prausnitz, J. M., K. C. Chao, and W. C. Edmister, paper presented at A. I. Ch. E. meeting Atlantic City (March, 1959).
18. Prausnitz, J. M., and R. D. Gunn, *A.I.Ch.E. Journal*, **4**, No. 4, 430 (1958).
19. Wan, S. W., and B. F. Dodge, *Ind. Eng. Chem.*, **32**, 95 (1940).
20. Wiebe, Richard, and V. L. Gaddy, *J. Am. Chem. Soc.*, **63**, 475 (1941).

Manuscript received September 15, 1958; paper accepted November 10, 1958.

A Computer Study of a Free-Radical Mechanism of Ethane Pyrolysis

R. H. SNOW, R. E. PECK, and C. G. VON FREDERSDORFF

Illinois Institute of Technology, Chicago, Illinois

The pyrolysis of ethane (including the equilibrium behavior and the tendency to form secondary products) has been reproduced by calculations based on a reaction mechanism which includes the reverse of the chain propagating reactions as well as other hitherto neglected elementary reactions. Reverse reactions are important even at low conversion (1%); hence previous investigations of initial reaction rate have doubtful fundamental significance. Values of rate constants used in the calculations were taken mostly from the literature. Consideration was limited to reactions of methyl, ethyl, and hydrogen free radicals with ethane and its primary pyrolysis products. The results can be incorporated into reactor performance calculations to replace empirical reaction rate correlations and thus widen the range of conditions over which the calculations are reliable.

There is much evidence that the pyrolysis of hydrocarbons occurs in steps and that most of the elementary reactions involve free-radical intermediaries. The rate constants of these elementary reactions are fundamental constants in the sense that they have the same value even when the elementary reaction occurs in different systems, for example in the pyrolysis of ethane and of propane. A goal for the technology of pyrolysis of hydrocarbons is the development of the theory to permit making design and performance calculations of reactors based on experimentally determined free-radical reaction-rate constants. The present work represents a step toward that goal.

Means of calculating performance of pyrolysis reactors have been presented by Myers and Watson (*22*), Schutt (*33*), and Snow and Schutt, (*38*). The reaction rates were expressed by means of empirical correlations, and the other aspects of the calculations were based on firm theoretical concepts. In the present work the essential features of the mechanism of ethane pyrolysis have been established, and product distributions have been calculated from theoretically sound expressions. These results can be incorporated into reactor performance calculations to make such calculations valid over a wider range of conditions. The results are also of theoretical interest because they demonstrate certain important but hitherto not understood features of the mechanism of ethane pyrolysis. An understanding of the mechanism even more detailed than that given here is still needed to predict the formation of individual higher hydrocarbons and especially of carbon, which is important because it limits reactor performance.

To include in the study a number of hitherto neglected reactions which proved to be important, it was necessary to apply numerical techniques rather than to solve the equations explicitly. The use of a digital computer was essential for this work, and several computer techniques applicable to such kinetic studies were developed.

EXPERIMENTS ON ETHANE PYROLYSIS

A thorough review of studies of ethane pyrolysis up to 1955 is contained in Steacie's (*41*) monograph, which also reviews investigations of the free-radical reactions involved.

Early workers (*5*, *9*, *18*, *24*, *30*) found that the over-all decomposition is approximately of first order. By extrapolating product distributions to zero conversion Schneider and Frolich (*32*), Hinshelwood and co-workers (*3*), and Silcocks (*36*) showed that the primary products of the pyrolysis are hydrogen, ethylene, and methane. Secondary products are small amounts of acetylene, three- and four-carbon hydrocarbons, higher olefins, aromatic compounds, and carbon. Several investigators have recently determined relatively complete product distributions These studies are listed below:

Reference	Temperature, °K.	Pressure, atm.
36	863	0.7 to 1.2
2a	1023 to 1143	1.0
14	1089	1.0
11	1255	1.0
46	1373	0.04
25	998 to 1148	1.0

Hinshelwood and co-workers (*3*), Travers and Hawkes (*45*), and Silcocks (*36*) have studied the tendency of the pyrolysis to approach the equilibrium

$$C_2H_6 \rightleftharpoons C_2H_4 + H_2 \quad (1)$$

The equilibrium constant for this reaction has been calculated by Kilpatrick and co-workers (*13*), and it appears that the system does tend to approach the equilibrium state defined by this constant. However true equilibrium is never attained because of the occurrence of secondary reactions.

Dintses and Frost (*5*, *6*) derived an empirical expression for the over-all rate as a function of reaction time. The complicated form of this expression suggests that the mechanism must be complex.

Investigations of the pyrolysis of pure samples of secondary products (*14*, *20*, *21*, *31*, *34*, *37*) and of secondary reactions in ethane pyrolysis (*18*, *48*) demonstrate that the primary products, ethylene, hydrogen, and methane, are relatively stable compared with the secondary products, which are three- and four-carbon hydrocarbons. The same conclusion may be reached on thermochemical grounds since hydrogen, ethylene, and methane have bond dissociation energies of over 100 kcal. according to Steacie (*41*), while butene splits into radicals with a dissociation energy of only 60 kcal.

MECHANISM OF ETHANE PYROLYSIS

A free-radical mechanism for ethane pyrolysis was first proposed by Rice and Herzfeld (*28*), who showed that the existence of a free-radical chain can

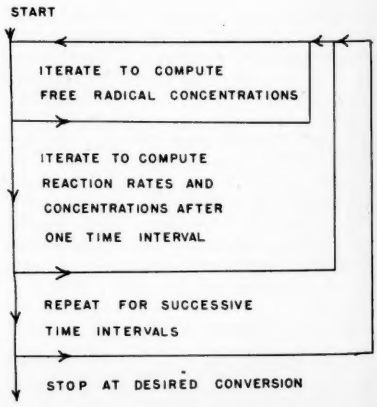
START
ITERATE TO COMPUTE FREE RADICAL CONCENTRATIONS
ITERATE TO COMPUTE REACTION RATES AND CONCENTRATIONS AFTER ONE TIME INTERVAL
REPEAT FOR SUCCESSIVE TIME INTERVALS
STOP AT DESIRED CONVERSION

Fig. 1. Computer program scheme.

R. H. Snow is with the Armour Research Foundation of Illinois Institute of Technology, Chicago, Illinois.

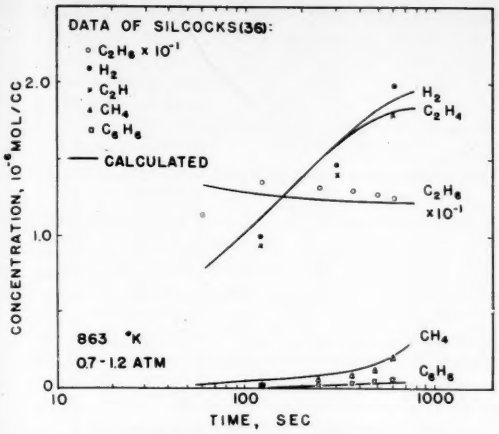

Fig. 2. Calculated and experimental products from ethane pyrolysis.

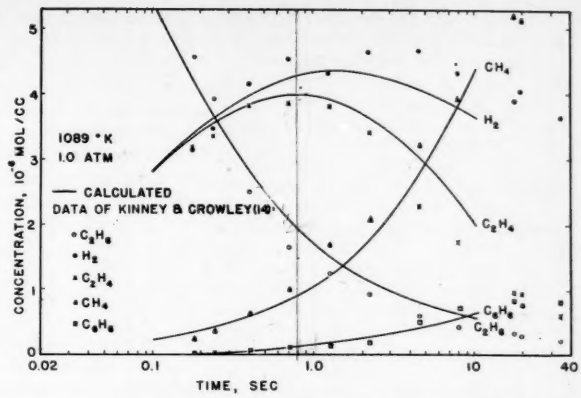

Fig. 3. Calculated and experimental products from ethane pyrolysis.

result in an over-all rate having a lower activation energy than the energy of scisson of ethane into radicals, and they thus succeeded in explaining a puzzling experimental fact. The best estimate of the carbon-carbon bond dissociation energy in ethane is 86 kcal., according to Steacie (*41*), and the activation energy for the scission reaction (2) cannot be less than this value,

$$C_2H_6 \rightleftharpoons 2\,CH_3 \qquad (2)$$

An Arrhenius plot of the reported values of the over-all rate constants for ethane pyrolysis is consistent with a value between 70 and 72 kcal. (*42, 38*). Hence it is necessary to postulate the existence of such a chain mechanism or alternatively to assume the occurrence of some radical initiating reaction with a lower activation energy.

Free-radical mechanisms for ethane pyrolysis have also been proposed by Küchler and Thiele (*15*), Storch and Kassel (43), and Steacie (*41*). None of these mechanisms fit the experimental data quantitatively, although they explain certain trends in the data. The qualitative agreement of these mechanisms, together with certain other evidence, indicates that the true mechanism does involve free radicals and is complex. Other evidence that ethane pyrolysis involves free radicals is provided by experiments in which the pyrolysis is inhibited by nitric oxide and olefins (*37, 39, 45*). Rice and Dooley (*26*) detected methyl radicals in the pyrolysis of ethane by means of chemical detectors. Eltenton (*8*) detected both methyl and ethyl radicals, with a mass spectrometer. The ortho-para hydrogen conversion measurements of Patat and Sachsse (*30, 31*) indicate that atomic hydrogen is involved.

Radicals other than ethyl, methyl, and hydrogen have not been directly detected in pyrolyzing ethane (*41*). Hinshelwood and co-workers (*3*) have proposed that the methylene radical may be an intermediary. Methylene radical has been detected from decomposing diazomethane (*26, 27*) and from ketene (*23*) but not from pyrolyzing hydrocarbons (*26*). Pearson, Purcel, and Saigh (*23*) suggested that methylene radicals may form and may react too rapidly to be detected, but this is merely speculation. Although unsaturated radicals may play a role in ethane pyrolysis, it is not feasible to analyze a mechanism including their reactions since there are insufficient data concerning the pertinent reaction rates. The results of the present work indicate that for a first approximation they may be neglected.

Hinshelwood and co-workers (*40, 44*) have shown that large amounts of nitric oxide do not produce as great an inhibitory effect as would be predicted on the basis of any reasonable free-radical mechanism. They (*44*) concluded that a direct molecular split of ethane by reaction (1) is involved in addition to a free-radical chain. But Rice and Varnerin (*29*) studied the products of isotope-exchange reactions in ethane pyrolysis and concluded that the molecular split does not occur. Steacie (*41*) has reviewed other conflicting evidence. The only safe conclusion to be drawn from this controversy is that the mechanism of inhibition by nitric oxide is not fully understood.

Silcocks (*36*) has proposed molecular reactions to account for the formation of secondary products in ethane pyrolysis and has cited experimental attempts to inhibit the formation of secondary products as evidence that the secondary reactions are essentially molecular. In view of the lack of understanding of the role of nitric oxide in the secondary reactions this evidence is questionable. Nor does his own kinetic analysis of the secondary reactions answer the question, since his results are based on the assumption that free radicals play only a minor role.

ANALYSIS OF A FREE-RADICAL MECHANISM OF ETHANE PYROLYSIS

This analysis was limited to reactions of ethyl, methyl, and hydrogen radicals and of ethane, ethylene, hydrogen, and methane. The reactions to be considered were selected in a systematic way by means of Steacie's (*41*) classification, which includes molecule scission, radical transfer, addition of radicals and molecules, and radical recombination.

Of the reactions included in the above categories those requiring three-body collisions, such as the recombination of hydrogen atoms or hydrogen and methyl radicals, were neglected. Scission of ethane to give hydrogen atoms was neglected, since the activation energy for this reaction is at least 98 kcal., while that of the competing reaction (2) is only 86 kcal. (*41*). The dissociation reactions of methane, ethylene, and hydrogen were neglected, since the bond dissociation energies for these compounds appear to be much higher than the dissociation energy for ethane, according to Steacie (*41*). The remaining reactions considered in the mechanism are

$$C_2H_6 \rightleftharpoons 2\,CH_3 \qquad (2)$$

$$CH_3 + C_2H_6 \rightleftharpoons CH_4 + C_2H_5 \qquad (3)$$

$$H_2 + CH_3 \rightleftharpoons H + CH_4 \qquad (4)$$

$$C_2H_5 \rightleftharpoons C_2H_4 + H \qquad (5)$$

$$H + C_2H_6 \rightleftharpoons H_2 + C_2H_5 \qquad (6)$$

$$H + C_2H_5 \rightarrow C_2H_6 \qquad (7)$$

$$CH_3 + C_2H_5 \rightarrow C_3H_8 \qquad (8)$$

$$\left.\begin{aligned} 2C_2H_5 &\rightarrow C_4H_{10} \\ &\rightarrow C_2H_4 + C_2H_6 \end{aligned}\right\} \qquad (9)$$

This mechanism is similar to that of Rice and Herzfeld (*28*) but includes additional important reactions, especially the reverse ones.

Two other reactions, (10) and (11), were included but later had to be eliminated to make calculated product distributions agree with experimental ones. This subject is discussed later.

$$CH_3 + C_2H_4 \rightarrow C_3H_7 \qquad (10)$$

$$C_2H_5 + C_2H_4 \rightarrow C_4H_9 \qquad (11)$$

The secondary products C_3H_8 and C_4H_{10} result from reactions (8) and (9). These substances actually react further

TABLE 1. RATE CONSTANTS AS FUNCTIONS OF TEMPERATURE

$$k_i = A_i e^{-E_i/RT}$$

	Reaction	Rate constants from literature: Frequency factor, A_i	Rate constants from literature: Activation energy, E_i	Literature source of: Activation energy	Literature source of: Frequency factor	Rate constants used in calculations: Frequency factor, A_i	Rate constants used in calculations: Activation energy, E_i
2	$C_2H_6 \rightleftharpoons 2CH_3$	1×10^{17}	86,000	Bond strength(41)	Entropy calculation(47)	6.3×10^{16}	86,000
2′		7×10^{13}	0	Experiment(10)	Experiment(10)	7×10^{13}	0
3	$CH_3 + C_2H_6 \rightleftharpoons CH_4 + C_2H_5$	2×10^{11}	10,400	Experiment(48)	Experiment(48)	2.5×10^{11}	10,800
3′		1×10^{13}	13,000	Thermochemical(41)	Assumed	1×10^{11}	13,200
4	$CH_3 + H_2 \rightleftharpoons CH_4 + H$	2×10^{11}	9,200	Experiment(47)	Experiment(16)	1.9×10^{11}	9,500
4′		1×10^{9}	4,500	Experiment(41)	Experiment(41)	1.1×10^{9}	4,700
5	$C_2H_5 \rightleftharpoons C_2H_4 + H$	3×10^{14}	39,500	Experiment(2)	Entropy calculation(47)	5.3×10^{14}	40,800
5′		2×10^{13}	4,000	Experiment(4)	Experiment(4, 19)	5.4×10^{13}	5,400
6	$H + C_2H_6 \rightleftharpoons H_2 + C_2H_5$	3.4×10^{12}	7,000	Experiment(1)	Experiment(1)	3.8×10^{12}	7,000
6′		1×10^{11}	11,400	Experiment(41)	Estimate(41)	1.8×10^{12}	11,400
7	$H + C_2H_5 \rightarrow C_2H_6$	7×10^{13}	0	Analogy with 2′	Analogy with 2′	7×10^{13}	0
8	$CH_3 + C_2H_5 \rightarrow C_3H_8$	7×10^{13}	0	Analogy with 2′	Analogy with 2′	7×10^{13}	0
9	$2C_2H_5 \rightarrow C_4H_{10}$	6×10^{13}	0	Experiment(12)	Experiment(12)	7×10^{13}	0
	$\rightarrow C_2H_4 + C_2H_6$	1×10^{13}	0	Experiment(35)	Experiment(35)		

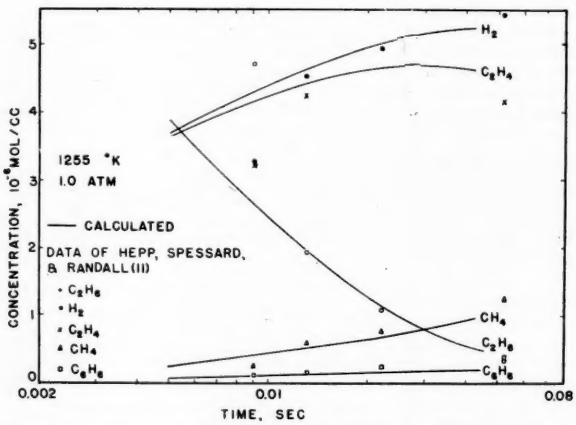

Fig. 4. Calculated and experimental products from ethane pyrolysis.

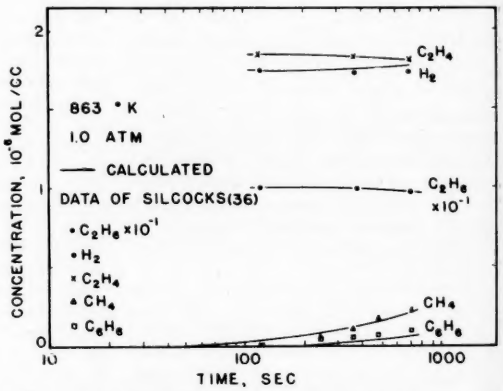

Fig. 5. Calculated and experimental products from an equilibrium mixture of ethane, ethylene, and hydrogen.

to give methane, higher hydrocarbons, and perhaps hydrogen. The amount of methane formed by secondary reactions was made to depend on a parameter which could be varied to fit the pyrolysis data. The mechanism does not predict the individual higher hydrocarbons formed. The average molecular weight and carbon-hydrogen ratio of the higher hydrocarbons depend on the conversion and the temperature and pressure, but as a crude approximation their average properties are like benzene (33). The formation of methane, higher hydrocarbons expressed as benzene, and hydrogen is given by the stoichiometric reactions (8a) and (9a):

$$CH_3 + C_2H_5 \rightarrow C_3H_8 \rightarrow X\,CH_4 + (1/2 - X/6)\,C_6H_6 + (5/2 - 3X/2)\,H_2 \qquad (8a)$$

$$2C_2H_5 \rightarrow C_4H_{10} \rightarrow 2X\,CH_4 + (2/3 - X/3)\,C_6H_6 + (1 - X)\,H_2 \qquad (9a)$$

To calculate the rates of reactions and hence the product distributions expressions giving the free-radical concentrations are needed. It is known and was confirmed by later calculations that the concentrations of free radicals are small compared with the concentrations of molecular species and that therefore the net rate of formation of radicals is small compared with the rate of formation of other compounds. Therefore the usual procedure was used, in which the net rate of formation from reactions (2) to (9) of each radical was equated to zero, and the resulting expressions were solved for the free radical concentrations. The following expressions were obtained:

$$(CH_3) = \frac{D}{4k_2'}\left[-1 + \sqrt{1 + \frac{8k_2'[2k_2\,(C_2H_6) + k_3'\,(C_2H_5)(CH_4) + k_4'\,(H)(CH_4)]}{D^2}}\right] \qquad (a)$$

where

$$D = k_3\,(C_2H_6) + k_8\,(C_2H_5) + k_4\,(H_2)$$

$$(C_2H_5) = \frac{E}{4k_9}\left[-1 + \sqrt{1 + \frac{8k_9[k_3\,(CH_3)(C_2H_6) + k_4\,(H_2)(CH_3) - k_4'\,(H)(CH_4)]}{E^2}}\right] \qquad (b)$$

where

$$E = k_3'\,(CH_4) + k_8\,(CH_3) + 2k_7\,(H)$$

$$(H) = \frac{k_5 + k_6'\,(H_2)(C_2H_5) + k_4\,(H_2)(CH_3)}{k_5'\,(C_2H_4) + k_6\,(C_2H_6) + k_4'\,(CH_4) + k_7\,(C_2H_5)} \qquad (c)$$

At this point in the derivation the values of free-radical concentrations are usually substituted into the expressions for the formation rates of the products; these rate expressions are then solved explicitly. In some cases drastic simplifying assumptions were formerly made to solve the rate expressions. The simplifications required for ethane pyrolysis have been discussed by Steacie (*41*); they destroy essential features of the mechanism. Simplifying assumptions were not made in this work. Instead the rate expressions were solved numerically by a trial procedure, with a digital computer.

This change of method dictated by the inherent complexity of ethane pyrolysis required some change in conventional ways of thought. For example order of reaction with respect to pressure or concentration of a reactant is ordinarily defined by the form of an explicit rate expression. With simple systems experimental evidence that the rate is of a certain order has been used to establish that the rate expression has the corresponding form; with systems as complicated as ethane pyrolysis an accurate rate expression cannot be written in explicit form, and therefore the order of reaction cannot be predicted in the usual way. In the case of ethane experimental evidence indicates that the over-all reaction is approximately of first order, but on the other hand the complexity of the proposed mechanism suggests that the order may vary with conditions. Instead of using the order of reaction concept in cases as complicated as ethane one can always compute incremental changes in reaction rates with respect to any variable at point values of temperature, pressure, and conversion.

CALCULATION OF PRODUCT DISTRIBUTIONS

To calculate a product distribution a step-by-step trial-and-error integration is carried out. An IBM 650 digital computer was programed for these calculations. Figure 1 is a simplified block diagram showing the steps in the calculation. In the first loop Equations (a), (b), and (c) are solved for (CH_3), (C_2H_5), and (H), iterating until the results converge to within six significant figures.

With the free-radical concentrations obtained in this way, the rates of the individual reactions are calculated in the second loop. The over-all rates of formation of each product due to all the reactions in the mechanism are calculated from stoichiometric relations. By multiplying these over-all rates by a small interval of time one obtains the change in concentration of each component. Then new arithmetic averages of the values of (C_2H_6), (C_2H_4), (H_2), and (CH_4) at either end of the time interval are computed. The free-radical concentrations and the reaction rates are then calculated anew, and this procedure is repeated until it is determined that that the first six significant figures of successive values of (C_2H_6) are the same.

The concentrations of all components are computed at the end of the time interval for a static system. For a flow system at essentially constant pressure these results are corrected for the stoichiometric expansion of the gases by the multiplication of the concentrations by the ratio $\sum_i C_{0i}/C_t$. The computer then proceeds to the third loop, where a new interval of time is taken for the next step in the calculation. The whole procedure is repeated until the desired conversion is reached. The calculation of each product distribution by the computer requires from 2 to 4 hr.

FITTING RATE CONSTANTS TO EXPERIMENTAL DATA

The main objective of this work was to establish that the proposed mechanism is consistent with experimental data and with the results of other investigators. For this purpose product distributions were calculated based on the kinetics of this mechanism and compared with experimental product distributions. The rate constants used in these calculations were chosen to lie within the uncertainties of values previously determined by other investigators from studies of numerous reacting systems. These values and their literature sources are listed in Table 1. Considerable uncertainty exists concerning the true values of some of these rate constants. It was therefore necessary to establish some of the rate constants more exactly by finding the values which resulted in the best fit of calculated and experimental product distributions. Since product distributions were available at a number of widely spaced temperatures, these experimental data provided more than enough quantitative restrictions to fix the values of certain rate constants.

Special experiments are often designed to test selectively the form of the rate expressions when the rate expressions can be solved explicitly. For example the concentrations of the reactants are varied separately or in other special ways. The value of each rate constant is then found by a least-squares fit of the data from such experiments.

This procedure cannot be used in the present case because separate terms in the rate expressions cannot be identified solely with particular variables. Therefore an unconventional treatment is necessary. In this work the rate constants were established by the following trial procedure: A trial set of rate constants for a particular temperature is chosen based on the work of previous investigators. A product distribution is then calculated as described above. The calculated product distribution is compared with an experimental product distribution from the literature. If it does not agree, the rate constants are changed in a systematic way, and a new product distribution is calculated. The process is repeated until the calculated product distribution agrees with the experimental one. To aid in selecting new trial values of rate constants, provision is made in the computer program to calculate at several levels of conversion the incremental changes in product distribution resulting from incremental changes in rate constants. New trial values of rate constants are then estimated based on the incremental changes in product distributions, and a new product distribution is computed.

To determine rate constants as functions of temperature, separate sets of such constants are determined for experimental product distributions corresponding to different temperatures. An additional requirement imposed is that the temperature dependence of the rate constants conform to Arrhenius functions.

This trial-and-error procedure for determining rate constants is as rigorous as the conventional procedures, since in both procedures the results are based on measurements of product distribution or on measurements of special aspects of product distributions.

The results are listed in Table 1. Some calculated product distributions are shown in Figures 2 to 5. The solid lines represent computed product distributions, while the points represent experimental data from the literature. Each figure corresponds to a particular temperature and pressure. It may be seen that no trend exists over different temperatures in the deviations of calculated results from experimental results. The temperatures range from 863° to 1,255°K. at about 1 atm. A calculated product distribution also agrees with an incomplete product distribution determined by Tropsch and Egloff (*46*) at 1,373°K. and 0.04 atm.

Certain inconsistencies are evident within each set of experimental data. Pyrolysis product distributions at these temperatures are extremely difficult to measure, the greatest uncertainty resulting from uncertainty of true gas temperature. A simple calculation shows that an error of a factor of 2 in the primary reaction rate could for example result from an error of 25°K. in the

Table 2. List of Reactions Which are Important Under Various Conditions

Data, Ref.	Temperature, °K.	Pressure, atm.	Reactions						
(*36*)	863	1	2	3 (4)	5 5′	6 6′			9
(*25*)	998	1	2	3 (4)	5 5′	6 6′		8	9
(*14*)	1089	1	2(2′)	(3) 4	5 5′	6 6′		8	9
(*11*)	1255	1	2 2′	(3) 4	5 5′	6 6′	(7)	8	(9)
(*46*)	1373	0.04	2 2′	3 4	5 5′	6 6′	7	8	

measurement of the true-average pyrolysis temperature. The calculated results agree with the data within 10 %. The experimental data are a little more precise than this but not more accurate. To use the present results as the basis for design of pyrolysis-reactor coils it would be necessary to compare data from a commercial pyrolysis coil with a product distribution computed from the proposed mechanism for the varying temperatures

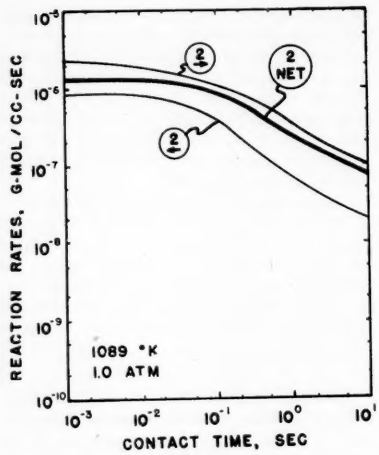

Fig. 6. Forward, reverse, and net rates of initiating reaction.

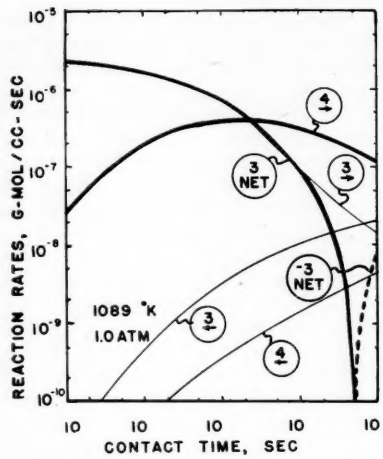

Fig. 7. Forward, reverse, and net rates of radical transfer reactions.

and pressures of such a coil. Snow and Schutt (*38*) have described a method for making such a comparison. Any slight discrepancy could then be corrected by correcting the frequency factors of the pertinent rate constants.

The rate constants given in the last column of Table 1 are those which resulted in the best fit of calculated product distributions with the laboraroty pyrolysis data shown in Figures 2 to 5. Some of these rate constants are believed to be more accurate than previously determined values, especially the frequency factors for reactions 2, 3′, 5, and 6′ and the activation energy for reaction 2.

DISCUSSION OF KINETICS OF ETHANE PYROLYSIS

The mechanism includes a number of competing reactions; those found to be important under various conditions of temperature and pressure are listed in Table 2. The exact relationships depend of course on the conversion. The reactions listed in parentheses are of minor importance. Reactions 3′ and 4′ are not important under any of these conditions. The rates are compared in detail for one set of conditions in Figures 6 to 9.

Of particular importance is the finding that reactions 5′ and 6′ are important at very low conversions. These are the reverse of the chain-carrying reactions. The following are approximate results for all conditions studied:

Conversion, %	Rate of 6′/rate of 6, %
0.5	10
1	20
5	55

Hinshelwood and co-workers (*3*) and Steacie and Shane (*42*) measured the rate of ethane disappearance at 5 to 10 % conversion, extrapolated the rate to zero conversion, and identified the result with the forward rate alone. It now appears that the reverse rate was high at these conversions, and the extrapolation was of doubtful validity*.

The net reactions 5 − 5′ and 6 − 6′ actually reverse at higher conversions for the conditions of Figures 3 and 4, and ethylene and hydrogen begin to disappear to form secondary products. The calculations quantitatively account for this interplay of equilibrium behavior with continual occurrence of secondary reactions. They reproduce even a product distribution for an equilibrium mixture of ethane. ethylene, and hydrogen given in Figure 5. This mechanism is valid for such mixtures due to higher stability of ethylene and hydrogen than that of ethane. Even when present in larger amounts than ethane they do not split as much and do not produce appreciable amounts of free radicals, which would affect the pyrolysis rate. The same would not be true of the pyrolysis of higher hydrocarbons, whose primary reaction products are not highly stable.

An attempt was made to include reactions (10) and (11) in the mechanism It was assumed that the C_3H_7 and C_4H_9 react further to give a mixture of higher hydrocarbons and methane. Rate constants for these reactions were assumed to equal $10^{11} \exp(-7{,}000/RT)$. This is a reasonable value, since Mandelcorn and Steacie (*17*) found the activation energy of (10) to be 7 kcal., and similar reactions are known to have similar activation energies. With these assumptions it was found that the rates of Reactions (10) and (11) are too high, and calculated product distributions did not agree with experiment. The rate constants would have to be smaller by several orders of magnitude, but it is not reasonable to expect this to be true. It is believed that this difficulty arises because Reactions (10) and (11) may not be included without also including other important reactions of the radicals C_3H_7 and C_4H_9. In particular, calculations based on values of the rate constants (*2*, *7*, *47*) indicate that the reverse of reactions (10) and (11) are more important than other reactions of these radicals; hence the net rates could be much less than the forward rates.

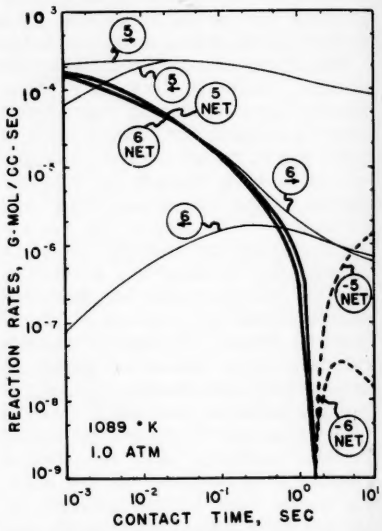

Fig. 8. Forward, reverse, and net rates of chain-propagating reactions.

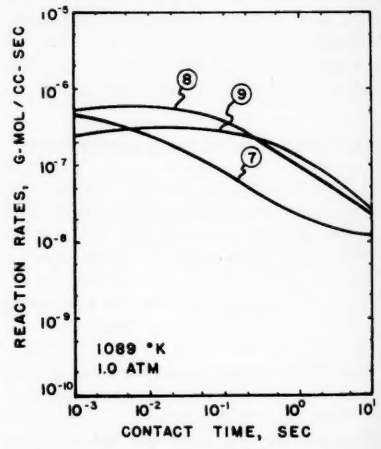

Fig. 9. Rates of terminating reactions.

These reactions and other reactions of secondary products could affect the concentrations of methyl, ethyl, and hydrogen free radicals and thus affect

*Two possible approaches to investigations of reaction kinetics are designing experiments for simplicity of interpretation, by attempting, for example, to measure a reaction rate at zero conversion, and carrying out the most complete mathematical analysis permitted by available knowledge for a given experiment. This example indicates that many kinetic problems, including some which were once thought simple, are actually so complicated that both methods should be used insofar as is feasible. One objective of the present work was to further develop the second method.

the primary pyrolysis rate. No reasonable number of elementary reactions can completely characterize a hydrocarbon pyrolysis mechanism, since the number of secondary products and radicals which can react is large. However the mechanism studied fits the available pyrolysis data from 863° to 1,373°K. up to relatively high conversions (20 to 85%), for which the concentrations of secondary products become equal to the concentration of unreacted ethane, and exhibits rate constants which agree with previously determined values. It is therefore believed that if all important reactions of secondary products are included, the rate constants needed to fit the pyrolysis data would differ from those given here by not more than twofold. For example in this work it was found that about half the methane is produced direct from ethane by reactions (3) and (4). The other half therefore results from secondary reactions, and probably exclusively from scissions of molecules or radicals to produce methyl radical. This additional methyl radical may again react via (3) or (4) to give methane and at the same time initiate primary reaction chains. If the amount of methane measures this effect, then it may be expected that rate constants for the primary part of the pyrolysis should be lower by a factor of 2.

As was previously explained, the production of methane from secondary products was empirically accounted for by means of a stoichiometric factor, X. The required variation of X with temperature to best fit the pyrolysis data is given in Table 3.

Table 3. Variation of Stoichiometric Factor with Temperature

Temperature, °K.	Data identification	Stoichiometric factor, X
863	L—Fig. 2	0.5
1089	D—Fig. 3	0.85
1255	E—Fig. 4	0.95

It would be desirable to include more reactions in order to calculate the amounts of individual higher hydrocarbons formed and eventually to calculate the amount of coke formed, since this is a problem of major industrial importance. It is not at present feasible to make a more complete study because the rate constants of the additional reactions are not known. They cannot be determined solely by fitting pyrolysis data because there are so many possible reactions that pyrolysis data alone would not provide enough quantitative restrictions. Further experimental work on simpler hydrocarbon reaction systems needs to be done to determine these rate constants.

ACKNOWLEDGMENT

The authors wish to thank Armour Research Foundation for providing the use of an IBM 650 digital computer and for supporting part of the work. This article is based on a Ph.D. thesis in the Department of Chemical Engineering, Illinois Institute of Technology, Chicago, Illinois.

NOTATION

A_i = frequency factor, same units as k_i
(A) = concentration of substance A, g-mole/cc.
C = concentration, g.-mole/cc.
C_i = concentration of component in product
C_{0i} = concentration in feed
E_i = activation energy, cal./g.-mole
k_i = rate constant of the ith reaction, 1/sec. for a first-order reaction or cc./g. mole-sec. for a second-order reaction
k_i' = rate constant of the reverse of the ith reaction, 1/sec. or cc./g. mole-sec.
X = parameter, stoichiometric factor

LITERATURE CITED

1. Berlie, M. R., and D. J. Leroy, *J. Chem. Phys.*, **20**, 200 (1952).
2. Bywater, S. E., and E. W. R. Steacie, *ibid.*, **19**, 172, 319, 326 (1951).
2a. Calderbank, P. H., and V. P. Hovnanian, *Ind. Chemist*, **33**, 557 (1957).
3. Danby, C. J., B. C. Spall, F. J. Stubbs, and C. N. Hinshelwood, *Proc. Roy. Soc.* (*London*), **A218**, 450 (1953).
4. Darwent, B. B., and Robert Roberts, *Discussions Faraday Soc.*, **14**, 55 (1953).
5. Dintses, A. I., *Compt. rend. acad. sci. U.S.S.R.*, **2**, 153 (1933).
6. ———, and A. V. Frost, *J. Gen. Chem. U.S.S.R.*, **3**, 747 (1933); *Compt. rend. acad. sci. U.S.S.R.*, **3**, 510 (1934).
7. Durham, R. W., G. R. Martin, and H. C. Sutton, *Nature*, **164**, 1052 (1949).
8. Eltenton, G. C., *J. Chem. Phys.*, **10**, 403 (1942); **15**, 455 (1947).
9. Frey, F. E., and D. F. Smith, *Ind. Eng. Chem.*, **20**, 948 (1928).
10. Gomer, Robert, and G. B. Kistiakowski, *J. Chem. Phys.*, **19**, 85 (1951).
11. Hepp, H. J., F. P. Spessard, and J. H. Randall, *Ind. Eng. Chem.*, **41**, 2531 (1949).
12. Ivin, K. J., and E. W. R. Steacie, *Proc. Roy. Soc.* (*London*), **A208**, 25 (1951).
13. Kilpatrick, J. E., E. J. Prosen, K. S. Pitzer, and F. D. Rossini, *Research Paper U.S. Bureau of Standards No. 1722* (1946).
14. Kinney, R. E., and D. J. Crowley, *Ind. Eng. Chem.*, **46**, 258 (1954).
15. Küchler, L., and Heinrich Thiele, *Z. physik. Chem.*, **B42**, 359 (1939).
16. Majury, T. G., and E. W. R. Steacie, *Can. J. Chem.*, **30**, 800 (1952); *Discussions Faraday Soc.*, **14**, 45 (1953).
17. Mandelcorn, L., and E. W. R. Steacie, *Can. J. Chem.*, **32**, 474 (1954).
18. Marek, L. F., and W. B. McCluer, *Ind. Eng. Chem.*, **23**, 878 (1931).
19. Melville, H. W., and J. C. Robb, *Proc. Roy. Soc.* (*London*), **A196**, 494 (1949).
20. Molera, M. J., and F. J. Stubbs, *J. Chem. Soc.*, 381 (1952).
21. Murphy, M. T., and A. C. Duggan, *J. Am. Chem. Soc.*, **71**, 3347 (1949).
22. Myers, P. S., and K. M. Watson, *Natl. Petrol. News*, **38**, R388 (May 1, 1946); R439 (June 5, 1946).
23. Pearson, T. G., R. H. Purcell, and G. S. Saigh, *J. Chem. Soc.*, 409 (1938).
24. Pease, R. N., *J. Am. Chem. Soc.*, **50**, 1779 (1928).
25. Potalovskii, L., and A. Atal'yan, *Petrol Engr.*, **10**, 40 (July, 1939).
26. Rice, F. O., and M. D. Dooley, *J. Am. Chem. Soc.*, **55**, 4245 (1933); **56**, 2747 (1934).
27. ———, and A. L. Glazebrook, *ibid.*, p. 2381.
28. ———, and K. F. Herzfeld, *ibid.*, p. 284.
29. ———, and R. E. Varnerin, *ibid.*, **76**, 324 (1954).
30. Sachsse, Hans, *Z. physik. Chem.*, **B31**, 79 (1935); **B31**, 87 (1935).
31. ———, and Franz Patat, *Z. Electrochem.*, **41**, 493 (1935).
32. Schneider, Valerie, and P. K. Frolich, *Ind. Eng. Chem.*, **23**, 1405 (1931).
33. Schutt, H. C., *Chem. Eng. Progr.*, **43**, 103 (1947).
34. Sehon, A. H., and Michael Szwarc, *Proc. Roy. Soc.* (*London*), **A202**, 263 (1950).
35. Shepp, Allan, and K. O. Kutsche, *J. Chem. Phys.*, **26**, 1020 (1957).
36. Silcocks, C. G., *Proc. Roy. Soc.* (*London*), **A233**, 465 (1956).
37. Smith, J. R. E., and C. N. Hinshelwood, *ibid.*, **A180**, 237 (1942).
38. Snow, R. H., and H. C. Schutt, *Chem. Eng. Progr.*, **53**, 133M (1957).
39. Spall, B. S., F. J. Stubbs, and C. N. Hinshelwood, *Proc. Roy. Soc.* (*London*), **A218**, 439 (1953).
40. Staveley, L. A. K., and C. N. Hinshelwood, *Nature*, **137**, 29 (1936); *Proc. Roy. Soc.* (*London*), **A154**, 335 (1936); **A159**, 192 (1937); *J. Chem. Soc.*, 812 (1936).
41. Steacie, E. W. R., "Atomic and Free Radical Reactions," 2 ed., Vol. I, II, Reinhold, New York (1954).
42. ———, and Gerald Shane, *Can. J. Res.*, **B18**, 203 (1940).
43. Storch, H. H., and L. S. Kassel, *J. Am. Chem. Soc.*, **59**, 1240 (1937).
44. Stubbs, F. J., K. U. Ingold, B. S. Spall, C. J. Danby, and C. N. Hinshelwood, *Proc. Roy. Soc.* (*London*), **A200**, 458 (1950); **A201**, 18 (1950); **A203**, 486 (1950); **A214**, 20 (1952).
45. Travers, M. W., and J. A. Hawkes, *Trans. Faraday Soc.*, **35**, 864 (1939).
46. Tropsch, Hans, and Gustav Egloff, *Ind. Eng. Chem.*, **27**, 1063 (1935).
47. Trotman-Dickenson, A. F., *J. Chem. Phys.*, **21**, 211 (1953).
48. ———, J. R. Birchard, and E. W. R. Steacie, *J. Chem. Phys.*, **19**, 163 (1951).

An appendix to this paper has been deposited as Document No. 5970 with the American Documentation Institute, Photoduplication Service, Library of Congress, Washington 25, D. C. and may be obtained for $2.50 for photoprints or $1.75 for 35-mm. microfilm. It contains calculated product-distribution tables including rates of individual reactions at various conversions, a discussion of the mathematics of the computations, and a description of the computer program.

Manuscript received September 17, 1958; revision received January 27, 1959; paper accepted January 29, 1959. Paper presented at A.I.Ch.E. Salt Lake City meeting.

Particulate Fluidization and Sedimentation of Spheres

A. L. LOEFFLER, JR., and B. F. RUTH

Iowa State College, Ames, Iowa

Particulate fluidization and sedimentation data were taken over the Reynolds number range of 0.005 to 1,800 by means of glass spheres in both water and ethylene glycol. Porosities for each series of measurements varied from about 0.50 to 0.91 and larger. The closely sized samples of spheres used were obtained by grinding between glass plates. The data for Reynolds numbers up to about 0.5 are in excellent agreement with the laminar theory of Ruth and the porosity function from Ruth's theory gave a satisfactory correlation of all the data, both laminar and turbulent.

The problem of the motion of a cloud of solid particles through a fluid has been treated theoretically by a number of investigators. Thus for the case where the concentration of solids is very small, solutions to the problem have been obtained by Einstein (*4*), Kermack *et al.* (*9*), Burgers (*2*), and others, For engineering applications, however, the more difficult problem of concentrated beds of particles moving in fluids is of greater importance than the limiting case of dilute beds. Sedimentation and fluidization, perhaps the two most common examples of this kind of motion, may be either particulate or aggregative, depending upon whether the particles appear to be evenly dispersed and moving independently or unevenly dispersed and moving in groups.

Steinour (*17*) experimentally studied the sedimentation of fine-pearl tapioca particles in the laminar range and found that for porosities up to 0.80 the results could be correlated by a modified form of the equation of Kozeny (*10*); namely

$$u = \frac{\epsilon^3}{(1-\epsilon)} \frac{D^2(\delta - \rho)g}{36k\mu} \qquad (1)$$

Brinkman (*1*) modified Darcy's equation for flow through a compacted bed to apply to flow through an expanded bed and obtained the equation

$$u = \frac{V}{1 + \dfrac{D}{2\sqrt{p}} + \dfrac{D^2}{12p}} \qquad (2)$$

where

$$p = \frac{D^2}{72}\left[3 + \frac{4}{(1-\epsilon)} - 3\left(\frac{8}{1-\epsilon} - 3\right)^{\frac{1}{2}}\right] \qquad (3)$$

Verschoor (*19*) obtained experimental data in the laminar range which agree with Brinkman's theory, but the validity of the comparison is doubtful since the particles used were highly nonspherical.

Lewis *et al.* (*11*) studied the fluidization of glass spheres and found that their results could be best correlated by

$$u = V\epsilon^{4.65} \qquad (4)$$

The data of reference *11*, however, were all for $Re > 0.1$ and hence not strictly laminar. Richardson and Zaki (*14*) examined theoretically the laminar sedimentation of particles arranged in adjacent horizontal layers so as to offer minimum flow resistance and found that Equation (4) was an approximation of their theoretical results. Jottrand (*8*) studied fluidization of nonspherical particles (crushed sand) in water in the laminar regime, mostly at porosities above 0.70. He concluded that Equation (4) is valid only for aggregative fluidization and that when the fluidization is particulate the correct equation is

$$u = V\epsilon^{5.6} \qquad (5)$$

The effect of particle shape upon Jottrand's data cannot be completely evaluated at this time.

Ruth (*16*) derived an equation describing laminar fluidization and sedimentation. This equation, in the limit of infinite bed expansion, extrapolates to Stokes's law and for porosities approaching those of compacted beds becomes almost identical to the Kozeny equation. Ruth's analysis will be presented in more detail in a later section.

Hawksley (*7*), utilizing a viscosity expression formulated by Vand (*18*), presented the equation for the settling of a suspension as

$$u = \epsilon^2 \exp\left[\frac{-2.5(1-\epsilon)}{1 - \dfrac{39}{64}(1-\epsilon)}\right] V \qquad (6)$$

Hanratty and Bandukwala (*5*) reported a large number of fluidization and sedimentation tests and found that Equation (6) correlated the laminar data well.

In view of the lack of complete experimental verification of any existing theory, it was decided that additional carefully taken experimental data were needed. The present paper describes the resulting experimental work and compares representative data with some of the previously mentioned theories and experiments. The complete experimental work is described in reference *12*.

One question which has received but little attention in the past is the relation between fluidization and sedimentation. Hawksley considered that sedimentation was adequately described by his theory but that fluidization was a much more complex process. The fluidization and sedimentation data of reference *5*, however, are identical when plotted for instance as ϵ against Re. Happel and Brenner (*6*) have recently shown theoretically that circulation of particles throughout a bed results in a decrease in the pressure drop through the bed. Since circulation occurs to a greater extent in fluidization than in sedimentation, this result can be interpreted as meaning that the flow resistance of a particle bed is less in fluidization than in sedimentation. It is hoped that the data presented herein will shed some light upon this problem too.

EXPERIMENTAL

Preparation of Sphere Samples

Inasmuch as serious doubt can arise in determining the correct average diameter of a sample of spheres if the size variation is large, considerable effort was made to obtain very closely sized sphere samples.

First the spheres were separated by screening with Tyler screens varying successively in aperture ratio by $1:\sqrt[4]{2}$. The spheres of each sample were then rolled down a slightly inclined glass plate, and those which rolled to one side or refused to roll were discarded.

A portion of the sample was then ground between two flat glass plates, with the aid of carborundum compound, until a uniform diameter was reached. The grinding apparatus employed four such sets of glass plates, with the top plates being mechanically moved in eccentric fashion over the lower stationary plates. Various numbers of 5-lb. lead weights could be placed on the top plates to control grinding speed. Carborundum finishing compound grade A280-V8-WS was used in all cases except for the two smallest size spheres ground, 35 and 48 mesh, for which Carborundum finishing compound grade AA440-V7-WS was used. Estimates of grinding progress were made by periodically removing a number of spheres from between the plates and measuring them. Periodic reversal and replacement of the glass plates were necessary because of wear. Experimental difficulties in grinding increased with decreasing sphere size, and grinding was not attempted for spheres smaller than 48 mesh.

Next the individual samples were fluidized, and the spheres at the top of the bed

A. L. Loeffler, Jr., is now at Lewis Research Center of the National Aeronautics and Space Administration, Cleveland, Ohio. The late B. F. Ruth was at Iowa State College, Ames, Iowa.

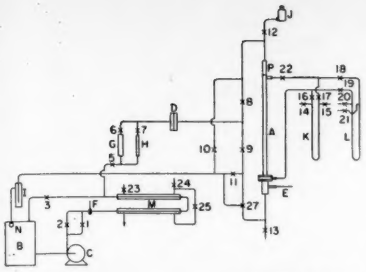
A - GLASS COLUMN
B - 55 GAL WATER RESERVOIR
C - CENTRIFUGAL PUMP
D - FILTER
E, F - THERMOMETERS
G, H - ROTAMETERS
I - SPHERE TRAP
J - WOULFF BOTTLE
K, L - MANOMETERS
M - COOLER SUPPLIED WITH TAP WATER
N - BAG FILTER
P - HOSE CONNECTION
1-27 VALVES

Fig. 1. Apparatus used for studies with water.

were slowly siphoned off with a glass tube and discarded, until a fairly sharp top interface was obtained at greater than 95% porosity. This removed particles that had been damaged in grinding or that contained large air bubbles.

Sphere Measurement

Size determinations for both ground and unground samples were then made. To obtain a correct average about 200 randomly selected spheres from each sample were measured. For diameters of 28 mesh and larger, ordinary micrometer calipers were employed; for the smaller spheres a filar micrometer was used.

The size variation for each sample of ground spheres was less than 5% as compared with almost 20% before grinding. The scale of surface roughness for the ground spheres was negligible compared with the sphere diameter.

Density Measurements

Liquid-density measurements were taken in a 25-ml. specific gravity bottle at 25°C. The density of the glycol at 25°C. was 1.110 g./cc. Density measurements of the spheres were obtained by first weighing the specific gravity bottle empty, next filling it about two thirds full of spheres and weighing, and finally filling it with water at 25°C. and again weighing. From these three weighings, the density of water at 25°C., and the volume of the specific gravity bottle at 25°C., the density of the glass spheres was computed.

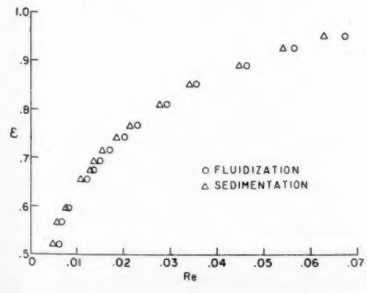

Fig. 2. Comparison of fluidization and sedimentation data for ground 48-mesh spheres in glycol.

Viscosity Measurements

Viscosity-temperature values for liquids used in this work were obtained with a precision viscosimeter, a constant-temperature bath, and a pump to circulate the bath water through the viscosimeter.

Free-fall Velocity Determination

Free-fall velocities in water were measured in a 4-in.-diameter, 5 ft. long thermally insulated Pyrex column. It was necessary to introduce the spheres at the center of the top cross section to prevent wall effect.

Free-fall velocity data for spheres in ethylene glycol were taken in a 1,000-ml. graduate cylinder of 6.1-cm. I. D.

Runs with Distilled Water

The small glass column employed for runs with distilled water was 2.603 cm. in diameter and 110 cm. long. Pressure taps were located at the top and in the flange assembly at the bottom. Both mercury and water manometers were available for pressure-drop measurements, but these data are not included in this paper. A 1/10°C.-thermometer was located immediately below the column for accurate temperature measurement.

Figure 1 shows a diagram of the over-all apparatus. As set up, it can be used for making permeability studies by passing liquid down through the column but these studies also are not included in this paper. Distilled water from a 55-gal. stainless steel drum B was pumped by C through a cooler M, the purpose of which was to remove pumping heat. A gate and a needle valve, 1 and 2, provided accurate flow control. Next the water passed through a pair of rotameters, G and H, and on through an Orlon cloth filter D. From the filter the water flowed through valves 9 and 27 into the bottom of the column and then passed up through the column, through valve 10, and back into the reservoir B. For fluidization and sedimentation work valves 8 and 11 were kept closed, while valves 9 and 10 were open. To prevent troublesome rust sediment from clogging the screen bed support, all piping and valves between the Orlon filter and the column were of stainless steel, aluminum, and brass.

To save time and to obtain fluidization and sedimentation data at the same porosities, it was ultimately decided to take sedimentation data immediately after the bed height, manometer reading, flow rate, and temperature were read for the fluidization run. This was done by turning the two-way stopcock 27 to stop the liquid flow to the column and simultaneously starting a stop watch. The time required for the top interface of the bed to pass various measured marks on the column was noted.

For use with larger particles a column 120 cm. long and 5.508 cm. in diameter was used. Operation with this column was similar to that of the smaller one, except that no pressure-drop measurements were made and flow rates were determined from the weight of effluent collected in a measured time.

Runs with Ethylene Glycol

The fluidization apparatus, not shown, for use with ethylene glycol was similar in principle to the water apparatus. For small particles and hence small flow rates the test section used was 115 cm. long and 2.477 cm. in diameter. A 5-cm.-diameter glass tube, for thermal insulation, surrounded the test section. The bed support was of cloth. A 1/10°C. thermometer was installed directly before the column. A Sigmamotor pump was used to pump the glycol from a 5-gal. reservoir to a constant-head tank provided with overflow line and located about 7 ft. above the top of the column. Rough flow rates were taken with a rotameter, but exact flow measurements were made in volumetrically calibrated collection tubes. The experimental procedure was essentially the same as with the water apparatus.

For the larger particles a 120-cm.-long, 5.508-cm.-diameter column was used. Operation was the same as just described, except that the constant-head tank provided insufficient flow and the solution was pumped directly to the column by means of a small centrifugal pump.

Since ethylene glycol is hygroscopic, the specific gravity of the liquid used was periodically checked to ensure that it had not changed from its original value.

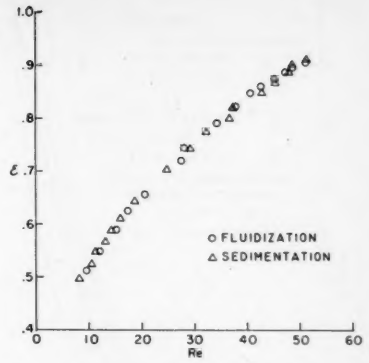

Fig. 3. Comparison of fluidization and sedimentation data for 28-mesh spheres in water.

RUTH'S THEORY

Since the theory of Ruth has not yet been published, it is developed in some

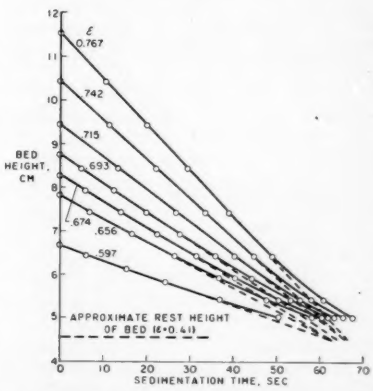

Fig. 4. Bed height against sedimentation time for ground 48-mesh spheres in glycol.

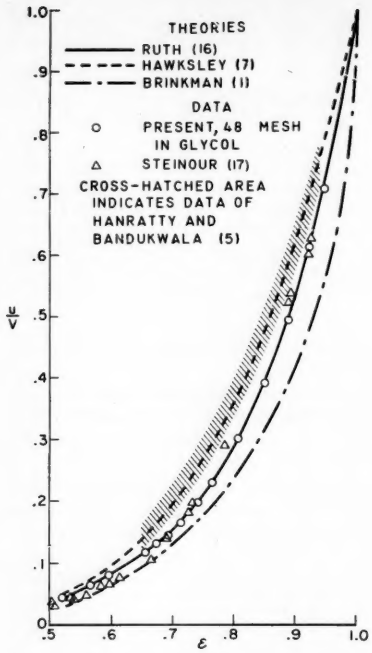

Fig. 5. General comparison of existing data and theories for the laminar regime.

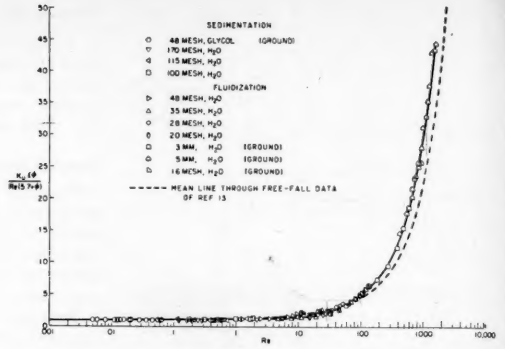

Fig. 6. Single-line correlation of present data over the entire Reynolds number range.

detail in this section. For purposes of brevity the original derivation (*16*) has been slightly modified.

The well-known drag force for the very slow motion of a sphere was given by Stokes as

$$F = 3\pi\mu u D \tag{7}$$

A more general expression for the resistance force, for the case where more than one particle is present, can be written as

$$F = f(\epsilon)\cdot 3\pi\mu u D \tag{8}$$

The limiting conditions on f are

$$\left.\begin{aligned} \epsilon \to 1.0: &\quad f(\epsilon) \to 1.0 \\ \epsilon \to \sim 0.48: &\quad f(\epsilon) \to \frac{2k(1-\epsilon)}{\epsilon^3} \end{aligned}\right\} \tag{9}$$

The first of these conditions is obtained by a consideration of Stokes's law, Equation (7). The second is obtained by comparison of Equation (8) with the equation derived by Kozeny for the case of compacted beds of spheres. The quantity k is a constant which must be determined experimentally. A suitable expression for $f(\epsilon)$ is

$$f(\epsilon) = \frac{1}{\epsilon} + \frac{2k(1-\epsilon)}{\epsilon^3} \tag{10}$$

This expression identically satisfies the first of limiting conditions (9) and for not too small k approximates the second very closely. Since at any rate Kozeny's equation is not an exact solution, there is no reason to demand exact agreement with it in the compacted-bed porosity range.

If the only body force acting upon the spheres is the force of gravity, then the force to be resisted by the drag force is

$$F = \frac{\pi D^3}{6}(\delta - \rho)g \tag{11}$$

Equating the drag and buoyancy forces as given by Equations (8) and (11) respectively and making use of Equation (10) for $f(\epsilon)$, one obtains the following equation:

$$u = \frac{1}{\left[\frac{1}{\epsilon} + \frac{2k(1-\epsilon)}{\epsilon^3}\right]} \cdot \frac{D^2(\delta - \rho)g}{18\mu} \tag{12}$$

If a new quantity φ is defined as

$$\varphi = \frac{\epsilon^2}{(1-\epsilon)} \tag{13}$$

then Equation (12) may be rewritten as

$$u = \left[\frac{\epsilon\varphi}{2k+\varphi}\right] \cdot \frac{D^2(\delta - \rho)g}{18\mu} \tag{14}$$

It may be noted that Equation (14) may also be written as

$$\frac{u}{V} = \frac{\epsilon\varphi}{2k+\varphi} \tag{15}$$

Equation (14) can be rearranged to

$$\frac{K_u}{Re}\left[\frac{\epsilon\varphi}{2k+\varphi}\right] = 1 \tag{16}$$

where

$$K_u \equiv \frac{gD^3(\delta - \rho)\rho}{18\mu^2} \tag{17}$$

and

$$Re \equiv \frac{Du\rho}{\mu} \tag{18}$$

RESULTS AND DISCUSSION

General Considerations

The nominal sphere sizes, diameters, densities, and the comparison of experimental free-fall velocities with the experimental data of Pettyjohn and Christiansen (*13*) for the spheres used in these studies are given in Table 1. The agreement for the free-fall velocities is seen to be good.

Except in the case of the 3- and 5-mm. spheres for which the top interface of the bed oscillated somewhat at the higher porosities, the beds fluidized quite evenly and uniformly. The top interface of the fluidized bed was easily distinguishable for the porosity range covered in this investigation.

To compare the processes of fluidization and sedimentation, the data have been plotted as ϵ against Re for two different sphere-liquid combinations in Figures 2 and 3. If the two processes

Table 1. Properties of Spheres

Nominal sphere size	D, cm.	δ, g./cc.	Deviation of experimental free-fall velocity from that predicted by ref. *13*, %
20 mesh	0.09029	2.629	−2.66
28 mesh	0.06586	2.630	−1.21
35 mesh	0.04590	2.667	−1.21
48 mesh	0.03445	2.671	−5.08
100 mesh	0.01645	2.582	−1.37
115 mesh	0.01399	2.587	−6.38
170 mesh	0.01015	2.575	0.89
16 mesh, ground	0.09769	2.656	−2.80 (in glycol)
48 mesh, ground	0.02872	2.671	2.14 (in glycol)
3mm., ground	0.3360	2.572	
5mm., ground	0.5056	2.514	

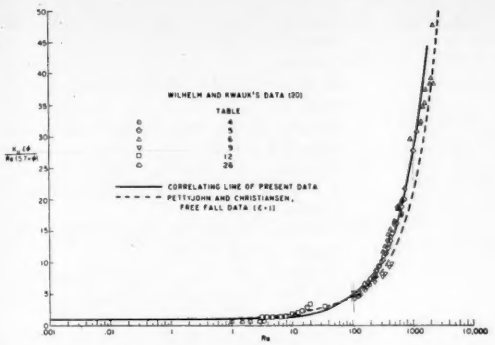

Fig. 7. Comparison of correlating line for present data with the data of Wilhelm and Kwauk (19).

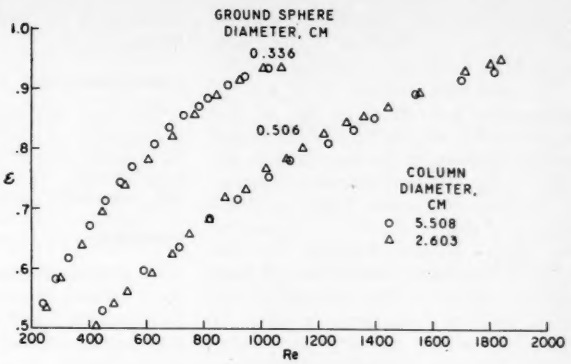

Fig. 8. Study of wall effect.

were identical, it would be expected that the data for each figure would fall upon a single curve. However a close scrutiny reveals that generally for the same porosity the Reynolds number is slightly less for the case of sedimentation; that is the flow resistance of the sedimenting bed is greater than that of the fluidized bed. This trend was also noticed for considerable other data not presented here. This finding appears to be in qualitative agreement with the previously mentioned theoretical results of reference *6*. The difference between the fluidization and sedimentation data appears to decrease somewhat for higher Reynolds numbers; thus the difference in Figure 3 is less than that in Figure 2. The effect does not appear large enough to make possible quantitative conclusions at this time.

Generally plots of bed height against sedimentation time were straight lines, demonstrating uniform beds and lack of interparticle forces. However a slight curvature was noted for large times during the sedimentation of the ground 48-mesh spheres in glycol, as shown in Figure 4. This curvature could conceivably be caused by the particles taking on an electrical charge and was neglected in the computation of sedimentation velocities, as shown by the dotted lines.

Laminar Correlation

The only data of the present investigation which are completely in the laminar regime of flow are those for the ground 48-mesh spheres in glycol. These data are plotted as u/V against ϵ in Figure 5, where they are compared with the theory of Ruth, Equation (15), for $k = 2.85$. The agreement is seen to be very good. The Stokes's velocity used in obtaining u/V was calculated separately for each run, with the proper temperature used.

The fact that the value of the Kozeny constant k is just over half that of about 5.0 recommended for compacted beds [for example Carman (*3*)] leads to the belief that the particles have rearranged themselves in such a way as to approximately halve the resistance of the bed in the flow direction. This conclusion appears to have been reached also in references *7* and *14*.

In Figure 5 the present data are compared also to a number of theories and the data of references *5* and *17*. The data of reference *17* are seen to be in reasonably close agreement with the present data. Data from the literature for nonspherical particles are not included, since the effect of particle shape is not yet understood.

The correlation given by Equation (4), as reported by references *11* and *14*, is not plotted in Figure 5 but agrees very closely with the theoretical line of reference *7*.

Correlation of All Data

Since the porosity function described by Ruth was successful in correlating the laminar data, it was decided to employ the same porosity function in trying to correlate the turbulent data too. This was done by plotting $\epsilon\varphi/(5.7+\varphi)\cdot K_u/Re$ against Re as shown in Figure 6, where k has been taken throughout as 2.85.* The small differences between fluidization and sedimentation as evidenced by Figures 2 and 3 have been neglected for the purposes of this plot, and both types of data are plotted. At the higher Reynolds numbers fluidization data only are shown because sedimentation data in this range were relatively inaccurate. Conversely at very low Reynolds numbers the fluidization data were the least accurate. It is seen that the data give a satisfactory single-line correlation. The porosity range of the data presented is 0.48 to 0.96. The scatter of the data in Figure 6 in the neighborhood of $Re = 10$ to 40 could conceivably be caused by a transition from laminar to turbulent tube flow.

For the laminar and near-laminar regime it can be seen from Equation (16) that the value of the ordinate of Figure 6 should be equal to 1. This is nicely verified by the fact that the ordinate is approximately 1 up to a Reynolds number of about 0.5.

The free-fall ($\epsilon = 1$) data of Pettyjohn and Christiansen are approximated by the dotted line in Figure 6. If the Reynolds number effect for a fluidized bed were similar to that of a free-falling sphere, it would be expected that the present data would fall along the dotted line. That they do not fall exactly along it is not surprising, since the flow patterns for the two cases are obviously not identical. The correlating line drawn through the data should be of practical interest in most fluidization and sedimentation work, however, since it is valid over the porosity range of 0.48 to 0.96.

It is quite important to notice that the data for the ground and unground spheres all fall along the same correlating line in Figure 6. Since the size variation within the ground sphere samples is less than 5%, while that in the unground is less than 20%, it would appear that the samples of spheres used in the present investigation are uniform for all practical purposes; that is, there is no uncertainty as to the effective diameter characterizing each sample.

For comparison purposes the correlating line of the present data, as determined in Figure 6, is compared in Figure 7 with data obtained by Wilhelm and Kwauk (*20*). The data chosen from reference *20* are those for fluidization of spherical particles by water. Although the scatter here is considerably more than in Figure 6, a mean line through the data would not deviate greatly from the correlating line obtained from Figure 6.

Richardson and Zaki (*15*) reported laminar and turbulent data indicating a logarithmic relationship between u and ϵ (for constant temperature) with the slope a function of the terminal-velocity Reynolds number and equal to 4.65 for the laminar regime. The latter case, as given by Equation (4), does not represent the present data as well as the theory of

*Tabular material has been deposited as document No. 5974 with the American Documentation Institute, Photoduplication Service, Library of Congress, Washington 25, D. C., and may be obtained for $1.25 for photoprints or 35-mm. microfilm.

Ruth, as previously mentioned. However all the data do show an approximate logarithmic relationship between u and ϵ.

To determine whether there was an appreciable wall effect in any of the data it was decided to fluidize the largest spheres employed in the investigation, the 0.336 and 0.506-cm.-diameter spheres, in a column of diameter 2.603 cm. Comparison of these data with the data for the same spheres fluidized in the 5.508-cm.-diameter column should then give a measure of the maximum wall effect. Such a comparison is made in Figure 8, where porosity is plotted against Reynolds number, and it is concluded that wall effect is negligible.

SUMMARY

A careful experimental study, over a wide Reynolds number range from 0.005 to 1,800, was made of fluidization and sedimentation of glass spheres, with both water and ethylene glycol used. Porosities varied from about 0.50 to 0.91 and larger. Closely sized and spherical particles were obtained by grinding the particles between glass plates. For Reynolds numbers up to about 0.5 the data are in very good agreement with the laminar theory of Ruth, while the porosity function from Ruth's theory gave a satisfactory correlation for all the data, both laminar and turbulent. There were small but consistent differences between the fluidization and sedimentation data which indicated that for an expanded bed of given porosity more flow resistance is experienced in sedimentation than in fluidization.

ACKNOWLEDGMENT

This work was made possible by use of the facilities of the Ames Laboratory of the Atomic Energy Commission at Iowa State College. Invaluable assistance was also provided by Alden F. Presler.

NOTATION

D = particle diameter
D_c = column diameter
f = undetermined function of porosity
g = acceleration of gravity
K_u = function of particle and fluid properties, Reynolds number evalualted for Stokes's velocity [Equation (18)]
k = constant
p = permeability coefficient
u = fluidization velocity based on empty column cross section, or absolute velocity of top interface of bed in sedimentation
V = Stokes's velocity
ϵ = volume fraction of voids
μ = fluid viscosity
ρ = fluid density
δ = particle density

LITERATURE CITED

1. Brinkman, H. C., *Research*, **2**, 190 (1949).
2. Burgers, J. M., *Proc. Koninkl. Ned. Akad. Wetenschap*, **45**, 9, 126 (1942).
3. Carman, P. C., "Flow of Gases Through Porous Media," p. 13, Academic Press, New York (1956).
4. Einstein, Albert, *Ann. Phys.*, **19**, 286 (1906); **34**, 591 (1911).
5. Hanratty, T. J., and Abdemannan Bandukwala, *A.I.Ch.E. Journal*, **3**, 293 (1957).
6. Happel, John, and Howard Brenner, *ibid.*, 506 (1957).
7. Hawksley, P. G. W., "Some Aspects of Fluid Flow," p. 114, Edward Arnold, London (1951).
8. Jottrand, René, *J. Appl. Chem.*, **2**, Suppl. 1, S17 (1952).
9. Kermack, W. O., A. G. M'Kendrick, and Eric Ponder, *Proc. Roy. Soc. Edinburgh*, **44**, 170 (1928–9).
10. Kozeny, Josef, *Sitzber. Akad. Wiss. Wien., Math.-naturw. Kl.*, **136**, 271 (1927).
11. Lewis, W. K., E. R. Gilliland, and W. C. Bauer, *Ind. Eng. Chem.*, **41**, 1104 (1949).
12. Loeffler, A. L., Jr., Ph.D. thesis, Iowa State College, Ames, Iowa (1953).
13. Pettyjohn, E. S., and E. B. Christiansen, *Chem. Eng. Progr.*, **44**, 157 (1948).
14. Richardson, J. F., and W. N. Zaki, *Chem. Eng. Sci.*, **3**, 65 (1954).
15. ———, *Trans. Inst. Chem. Engrs. (London)*, **32**, 35 (1954).
16. Ruth, B. F., unpublished lecture notes, Iowa State College, Ames, Iowa (Summer, 1951).
17. Steinour, Harold, *Ind. Eng. Chem.*, **36**, 618 (1944).
18. Vand, Vladimir, *J. Phys. Coll. Chem.*, **52**, 277 (1948).
19. Verschoor, H., *App. Sci. Research*, **A2**, 155 (1950).
20. Wilhelm, R. H., and Mooson Kwauk, *Chem. Eng. Progr.*, **44**, 201 (1948).

Manuscript received August 14, 1958; revision received March 9, 1959; paper accepted March 10, 1959

Effect of Liquid on Interparticle Forces in Gas-fluidized Beds

HARRY W. PARKER and WILLIAM F. STEVENS

Northwestern University, Evanston, Illinois

In an investigation of the behavior of an air-fluidized bed of glass spheres under varying interparticle forces, the results obtained are explained by hypothesizing the coexistence of particulate and aggregative fluidization. As interparticle forces are increased, a greater portion of the particles are in aggregative fluidization, resulting in a decrease in bed height. In this study water added to the fluidizing air increased the interparticle forces. Up to 0.5 mass % water was used, with a fluidized bed of glass spheres 0.013 to 0.035 in. in diameter. The resulting decrease in bed height has been correlated by means of a theoretical equation for the increase in interparticle forces due to the added water.

The widely differing natures of liquid- and gas-fluidized beds were observed in early laboratory fluidization experiments and received the names *particulate* and *aggregative* fluidization respectively (*11*). It has been suggested that the cause of aggregative fluidization is the attraction of individual particles for each other, usually termed *inter-particle forces*. The need for further information concerning interparticle forces has been indicated by several authors. Gamson has stated that a shape factor is needed to correlate particle heat and mass transfer data taken in aggregative fluidization with similar data from particulately fluidized beds and fixed beds (*3*). Workers who have studied heat transfer from surfaces in contact with the fluidized bed have also suggested that the attraction of particles for each other may be a factor in the correlation of heat transfer data (*1, 10*).

Interparticle forces may be divided into two groups, those due directly to the motion of fluid through the solids, and those forces not directly caused by the flowing fluid. The first class of forces are due to two causes: Bernoulli forces and the tendency of a flowing fluid to seek the path of least resistance. The latter phenomenon is very well described by

H. W. Parker is with Phillips Petroleum Company, Bartlesville, Oklahoma.

Morse (7). The most common forces involved in the second group are electrostatic. In practically all laboratory studies attempts are made to minimize electrostatic forces. Some other possible forces in this group are the magnetic attraction of particles for each other and surface forces resulting in sticking together of the particles owing to liquid on their surfaces. The latter one was chosen for study in this paper.

LIQUIDS AND FLUIDIZED BEDS

The behavior of small amounts of liquid in a gas-fluidized bed has not been studied extensively. Meissner and Mickley have used a fluidized bed to remove mists from gas streams; however they state only that nonporous particles had a life of only a few minutes before liquid adhering to the particles stuck them together and fluidization stopped (6). The commercial realization of fluid coking has made practical application of liquid injection into a gas-fluidized bed, but there is little information as to the behavior of the fluidized bed. United States patent 2,567,959 has been issued for a fluidized-bed evaporator.

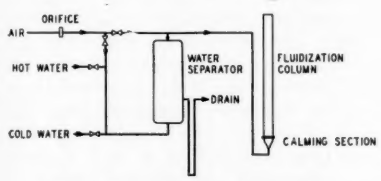

Fig. 1. Flow diagram of apparatus.

From the appearance of a gas-fluidized bed with liquid in it and a consideration of the forces involved, the action of interparticle forces caused by a liquid on the surface of the particles appears to be comparable to that resulting from forces due to other sources. It has been observed that the particles in dense-phase fluidization are in actual contact with each other (5, 3). Since the particles are in contact with each other, whether they are held together by a liquid film or other forces is not of great significance, provided that the forces are of the same order of magnitude.

For particulate fluidization to exist, the particles must be separated enough from each other so that interparticle forces are negligible; otherwise the particles would be attracted together, and aggregative fluidization would result. The type of interparticle forces present is not therefore important. It is realized that a liquid film on particles is not an effective interparticle force until the particles have actually touched, in contrast to other interparticle forces which act more or less continuously. However the very rapid decrease in attraction between particles as separation increases for other interparticle forces should allow the assumption of similarity for exploratory study.

Both particulate and aggregative fluidization may occur at the same time, resulting in dense- and light-phase fluidization. As interparticle forces are increased, a greater portion of the particles are in aggregative fluidization, resulting in a decrease in bed height. In the following section an equation is derived relating moisture content to bed height.

DERIVATION OF EQUATION RELATING BED HEIGHT TO MOISTURE CONTENT OF THE BED

For this derivation a hypothetical fluidized bed in which the interparticle forces may be varied independently of other conditions will be considered. When interparticle forces are negligible, particulate fluidization results. If the interparticle forces are sufficiently large, aggregative fluidization results. The difference in height between the fluidized bed in entirely particulate fluidization and entirely aggregative fluidization is proportional to the additional bed volume involved in particulate fluidization. The fraction of this excess bed volume occupied by the bed at a given set of conditions represents the fraction of particles in particulate fluidization.

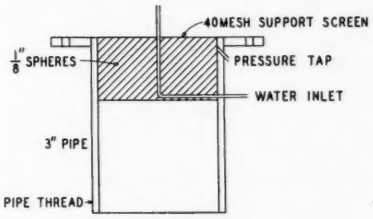

Fig. 1*a*. Calming section.

Fraction of particles in particulate fluidization

$$= \frac{h - h_m}{h_p - h_m} \qquad (1)$$

One minus the right-hand quantity in this equation is the fraction of particles in aggregative fluidization. This assumes that the average bulk density of the two phases is independent of interparticle forces.

Equation (2) expresses in the least complex manner a relationship between the rate of particle aggregation and the fraction of particles in the particulate phase. The proportionality factor K_a is a function of the fluid, particle properties, and fluid velocity. The rate of particle aggregation is not however affected by the small quantities of water added during this study. At a maximum, 0.5 mass % water was added, and usually the addition was less than 0.1 mass %. This small amount of liquid on the particles cannot affect a fluidized bed until the particles have come in contact with each other.

Rate of aggregation

$$= K_a \frac{h - h_m}{h_p - h_m} \qquad (2)$$

A similar equation may be written for the rate of separation of particles from the aggregated phase, where the fraction aggregated is represented by one minus the fraction in the dispersed phase.

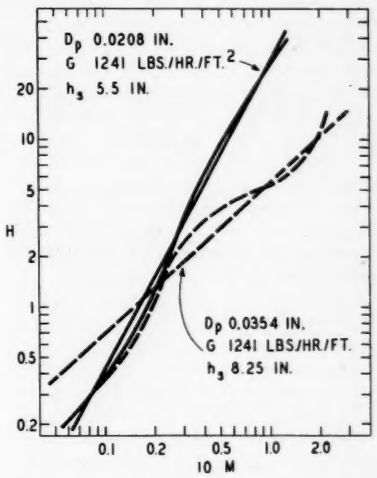

Fig. 2. *H* vs. *M*.

Rate of separation

$$= K_s\left(1 - \frac{h - h_m}{h_p - h_m}\right) \qquad (3)$$

In this case the proportionality factor is a function of moisture content. The forces holding the particles together, in this investigation, are the sum of two parts: those forces which are already present in the dry bed and the added forces due to the presence of water. Since the only quantity changed during a run was the amount of water present, the proportionality factor may be expressed in terms of constants as

$$K_s = \frac{K_1}{K_2 + f(M)} \qquad (4)$$

Equation (4) assumes that the dry interparticle forces and those due to the addition of water do not interact. The increase of interparticle forces due to added moisture content will be assumed to have the following relation:

$$f(M) = K_3 M^b \qquad (5)$$

Since the rates of agglomeration and separation are equal, Equations (2) and (3) are equal to each other and in com-

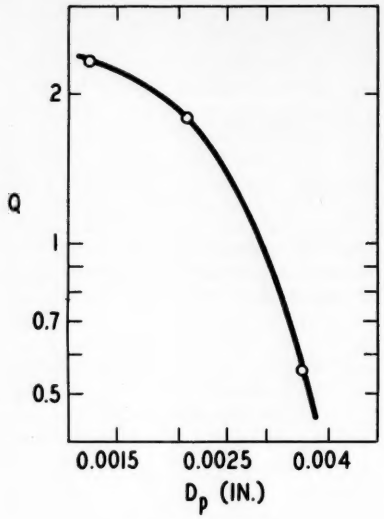

Fig. 3. Q vs. D_p.

bination with Equations (4) and (5) will give Equation (6):

$$K_a \frac{h - h_m}{h_p - h_m} = \frac{K_1}{K_2 + K_3 M^b} \cdot \left(1 - \frac{h - h_m}{h_p - h_m}\right) \tag{6}$$

This equation may be further simplified by algebraic manipulation and combination of constants to Equation (7):

$$\frac{h_p - h}{h - h_m} = K_4 + K_5 M^b \tag{7}$$

The term on the left side of Equation (7) may be expanded as follows to consider the height of a dry bed:

$$\frac{h_p - h}{h - h_m} = \frac{h_p - h_d}{h - h_m} + \frac{h_d - h}{h - h_m} \tag{8}$$

Equation (8) substituted into Equation (7) provides Equation (9).

$$\frac{h_p - h_d}{h - h_m} + \frac{h_d - h}{h - h_m} = K_4 + K_5 M^b \tag{9}$$

When the fluidized bed is dry, Equation (9) reduces to Equation (10).

$$\frac{h_p - h_d}{h_d - h_m} = K_4 \tag{10}$$

Equation (10) is substituted into Equation (9) to eliminate h_p.

$$\frac{K_4(h_d - h_m)}{h - h_m} + \frac{h_d - h}{h - h_m} = K_4 + K_5 M^b \tag{11}$$

Further manipulation and rearrangement following the steps shown below result in the final equation, (17).

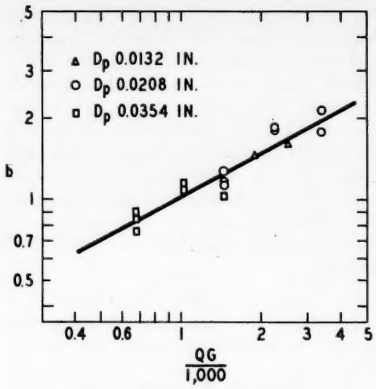

Fig. 4. b vs. $QG/1{,}000$.

$$\frac{h_d - h}{h - h_m} = K_4\left(1 - \frac{h_d - h_m}{h - h_m}\right) + K_5 M^b \tag{12}$$

$$\frac{h_d - h}{h - h_m} = K_4\left(\frac{h - h_d}{h - h_m}\right) + K_5 M^b \tag{13}$$

$$(K_4 + 1)\left(\frac{h_d - h}{h - h_m}\right) = K_5 M^b \tag{14}$$

$$\frac{h_d - h}{h - h_m} = K M^b \tag{15}$$

$$\frac{h_d - h}{h - h_m} \equiv H \tag{16}$$

$$H = K M^b \tag{17}$$

EXPERIMENTAL OPERATIONS

Figure 1 shows a sketch of the apparatus. The fluidization column was a 5-ft. length of 3-in. commercial Pyrex glass pipe. A detailed sketch of the calming section is also shown in Figure 1. It was necessary to both saturate the air used with water and to control its temperature, by injecting a mixture of hot and cold water into the air line and providing a tank for the air to separate from the water (Figure 1). The air entering the fluidization column was saturated with water and was slightly above room temperature. Cooling of this air by the surroundings offset warming of the air by passage through the fluidized bed and thus minimized drying of the bed.

The range of variables used is indicated in Table 1. A weighed quantity of particles (Superior Crystal Beads supplied by B. F. Drakenfield and Company) was charged to the apparatus and the desired air rate set. Distilled water could be added to the fluidized bed when nesessary by means of a metering pump, as shown in Figure 1. When the bed appeared in steady operation, its height was measured and a sample of particles taken. Samples taken simultaneously at various depths of the fluidized bed showed that no vertical moisture gradient existed. Samples of about 100 g. were required owing to the small moisture content. The quantity of water was determined by difference after the sample had been dried in an oven.

There was no large change in pressure drop across the fluidized bed as water was added, except with small particles and large amounts of liquid. In this case sufficient particles stuck to the wall of the apparatus to reduce the pressure drop appreciably. This difficulty was eliminated in taking data by tapping the side of the column, when necessary, to free the stuck particles. Moisture definitely increases the gas flow rate required for minimum fluidization and aids the formation of stable channels at lower velocities. Attempts to study these phenomena were not successful, because under some conditions the bed could alternate between stable channels and proper fluidization. To study this situation the moisture content of the bed would have to remain constant for a considerable period of time to determine its most usual mode of behavior.

ANALYSIS OF DATA

The following steps were taken in the evaluation of the constants in Equation (17). The experimental data were plotted on rectangular coordinates as mass percentage of moisture vs. bed height, and a curve which best fitted the points was drawn and transferred to logarithmic coordinates H vs. M, where M equals the analyzed mass percentage moisture minus 0.008. The subtractive term was an average residual moisture content in the fluidized bed. This residual moisture was present even when unsaturated air was used. When new beads were used, this term was smaller, but it soon reached this value after a few hours of operation. These used beads had a yellowish color which was insoluble in water or ether. Perhaps it was small adhering rust particles, which could have retained some moisture.

In an evaluation of H the measured height of the dry bed was used, but h_m needed to be found by trial and error, since it is approached asymptotically. The criterion used for the selection of h_m was the approach to a straight line of the plot of H vs. M on logarithmic coordinates. A straight line was drawn which best fitted the resulting curve, the slope and intercept of which gave values of b and K. Examples are given in Figure 2. This transfer of experimental data to logarithmic coordinates is shown as the curved lines in Figure 2. A straight line was then drawn which best fitted the curved line, the slope and intercept of which gave values of b and K. Table 2 presents the constants obtained in this manner. Equations for b and K as a function of particle diameter and air rate are

$$K = 185(100\ D_p)^{-2.68}$$

$$b = 1.02\left(Q\,\frac{G}{100}\right)^{0.54}$$

Q is presented graphically in Figure 3. These equations are compared with experimental values of b and K in Figures 4 and 5. Using these correlations and experimental values of h_d and h_m, one

Table 1. Properties of Materials Used

Material	Size no.	D_p, in.	Particle density, lb./cu.ft.	G_{mf}, lb./hr./sq. ft.
Glass spheres	3	0.0354	159	380
	7	0.0208	162	161
	10	0.0132	160	78.2

may plot Equation (17) on the original data. Figures 6 and 7 are examples of this. A reasonable correlation can be prepared for h_d and h_m, as shown in Figures 8 and 9, but owing to subtractive terms in the original equation it was desirable to use

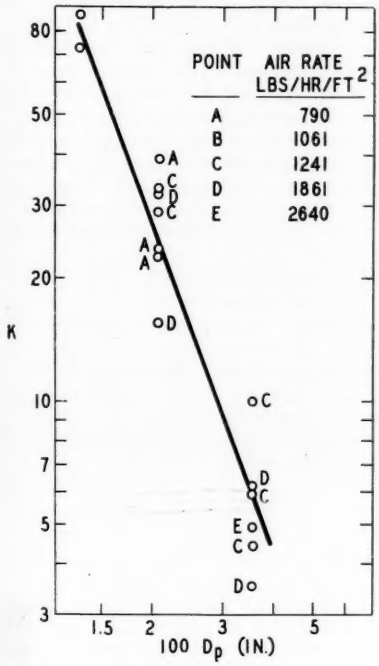

Fig. 5. K vs. D_p.

experimental values of h_m and h_d in the preparation of Figures 6 and 7. Figure 9 also includes portions of two runs of Lewis, Gilliland, and Bauer (*4*), which fall within the range of variables studied in this paper. The correlations of Figures 8 and 9 should not be used outside the range of data shown. More complex correlations such as those used by Lewis (*4*) are necessary for wider ranges of data.

The ranges of variables employed in this study are presented in Table 1. The upper particle diameter was limited because larger glass spheres of the type used were not available. The lower limit was caused by the fact that the water on appreciably smaller particles makes fluidization impossible. The maximum bed height and air rates were controlled by the tendency of particles to be carried out of the system by entrainment. Fifteen different combinations of bed height, air rate, and particle size were run, over the possible ranges of moisture content, to give the original data on which the correlation is based (*8*). The equation constants are listed in Table 2.

The main reason for the scatter of the experimental data and the resultant scatter of points used in the correlation is the difficulty of measuring the fluidized bed height accurately. In this study it was done visually, since height had to be measured and a sample of the bed taken in a short period of time, owing to a slow drift in moisture content in the bed. At low moisture contents measurement of the water concentration also became a factor, resulting in scatter of the experimental data. Comparison of the experimental points and the curves drawn according to the theoretical Equation (17) is shown in Figures 6 and 7. For the four lines shown the average deviation of the data points is $\pm 7.7\%$. For the top line in Figure 6, obviously the worst of the cases presented, the average deviation is $\pm 14.5\%$. These data, typical of those obtained in the study, indicate reasonable agreement between experiment and theory, in view of the experimental difficulties encountered.

PROPOSED CRITERION FOR THE EXISTENCE OF AGGREGATIVE OR PARTICULATE FLUIDIZATION

Wilhelm and Kwauk have shown that Froude numbers $U_{mf}^2/(D_p g)$ greater than 1 result in aggregative fluidization and less than 1 in particulate fluidization, for the range of their variables. They mention however that this criterion would predict particulate fluidization for small particles in gas systems, which they demonstrate did not happen (*11*).

Since the velocity in the Froude number above is taken as being the velocity required for minimum fluidization, this criterion does not consider the type of fluidization to be a function of bed expansion. A fluidized bed of puffed rice which was aggregatively fluidized at low velocities became particulate at higher velocities, resulting in about a hundredfold bed expansion. For this case the Froude number was about 1.6. Aggregative fluidization becoming particulate in a liquid system was also noticed by Richardson and Zaki (*9*), who used ¼-in. steel spheres, cylinders, and cubes.

The Froude number was not intended to be used as a criterion for the type of fluidization when artificial interparticle forces are applied, and as discussed above is not applicable to all other cases of fluidization. The equations developed in this paper may give a basis for the prediction of a predominance of aggregative or particulate fluidization, in a particular case.

$$\frac{h - h_m}{h_p - h_m} = \frac{K_1}{K_a(K_2 + K_3 M^b)} \cdot \left(1 - \frac{h - h_m}{h_p - h_m}\right) \qquad (6)$$

As shown in the derivation, the quantity on the left side represents the fraction of particles in particulate fluidization and that in parentheses on the right side represents the fraction of particles in aggregative fluidization. The quantities

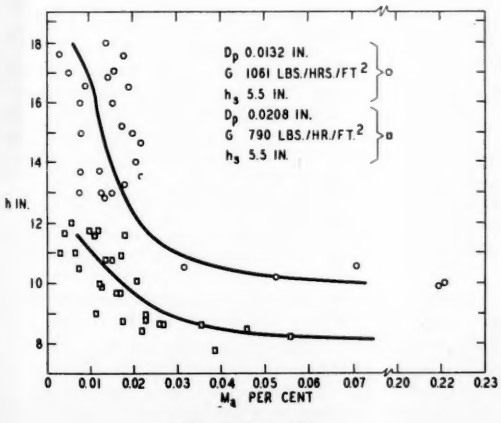

Fig. 6. h vs. M_a.

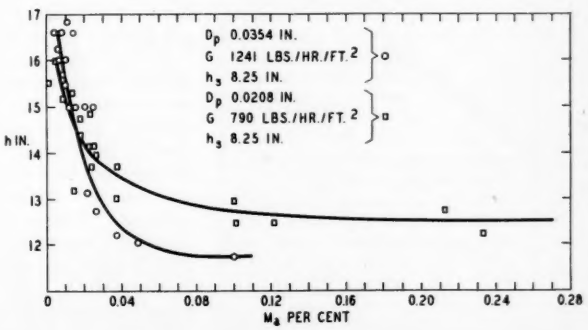

Fig. 7. h vs. M_a.

Table 2. Summary of Equation Constants

D_d, in.	G, lb./(hr.)(sq. ft.)	h_s, in.	h_m/h_s	h_d/h_s	b	K
0.0132	790	5.5	1.64	2.91	1.415	88.0
0.0132	1,061	5.5	1.82	3.27	1.6	75.0
0.0208	790	2.75	1.51	2.18	1.27	39.0
0.0208	790	5.5	1.44	2.09	1.14	23.5
0.0208	790	8.25	1.40	2.00	1.17	22.5
0.0208	1,241	2.75	1.87	3.18	1.83	33.0
0.0208	1,241	5.5	1.81	3.00	1.83	29.0
0.0208	1,861	2.75	2.18	4.73	2.14	32.0
0.0208	1,861	5.5	2.38	3.82	1.79	15.5
0.0354	1,241	2.75	1.49	2.18	0.76	10.0
0.0354	1,241	5.5	1.56	2.18	0.84	4.4
0.0354	1,241	8.25	1.49	1.94	0.91	5.9
0.0354	1,861	2.75	1.78	3.24	1.15	6.2
0.0354	1,861	5.5	2.00	3.04	1.07	3.5
0.0354	2,640	5.5	2.45	3.68	1.028	4.9

not in parentheses on the right side may be considered, as a group, to be analogous to a chemical equilibrium constant. When this equilibrium constant is very large, particulate fluidization results, and when it is small, aggregative fluidization is predominant. In this study only the portion of the equilibrium constant involving the moisture content was studied.

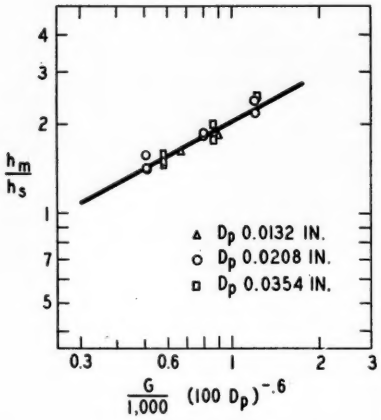

Fig. 8. $\frac{h_m}{h_s}$ vs. $\frac{G}{1{,}000}(100\ D_p)^{-0.6}$.

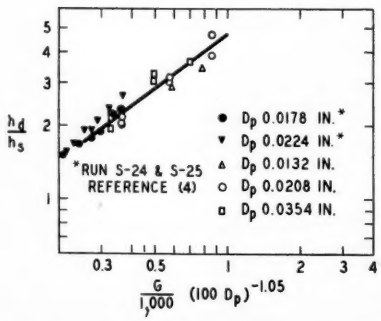

Fig. 9. $\frac{h_d}{h_s}$ vs. $\frac{G}{1{,}000}(100\ D_p)^{-1.05}$.

CONCLUSIONS AND RECOMMENDATIONS

The equation proposed in this paper relating bed height to liquid content has been shown to correspond to the experimental data. However the scatter of the data and the nature of the derivation made accurate quantitative results difficult to obtain.

The results which were obtained indicate that the height of a fluidized bed is little influenced by further additions of liquid after a initial small quantity has been added. Therefore if a maximum amount of liquid in a fluidized bed is desired, conditions should be selected to allow operation on the nearly horizontal portions of the height-vs.-moisture curve (Figures 6 and 7). Here other limiting factors concerning liquid in a fluidized bed, such as particles sticking to the wall or liquid being entrained out of the system by the gas stream, would occur.

A criterion has been suggested to indicate the predominance of either aggregative or particulate fluidization; however with the data available it was not possible to develop it completely.

Further study involving the independent variation of interparticle forces should aid in the extension of these concepts. By the addition of liquid to a gas-fluidized bed interparticle forces may be increased only in a system where they are already appreciable. A desirable extension of this work would involve increasing interparticle forces sufficiently from a negligible value, as in particulate fluidization, to cause predominately aggregative fluidization. One way of doing this would be by using particles which could be magnetized in a liquid system.

ACKNOWLEDGMENT

The authors wish to express their thanks to the National Science Foundation for the fellowship under which the work for this paper was carried out.

NOTATION

- b = experimentally determined exponent in Equation (17)
- D_p = average diameter of particles fluidized, in.
- G = mass rate of air flow, lb./(hr.)(sq. ft.)
- G_{mf} = mass rate of air flow for minimum fluidization, lb./(hr.)(sq. ft.)
- H = by definition $(h_d - h)/(h - h_m)$
- h = height of fluidized bed, in.
- h_d = height of dry fluidized bed, in.
- h_m = height of bed when in complete aggregative fluidization, in.
- h_p = height of bed when entirely in particulate fluidization, in.
- h_s = height of settled bed, in.
- K = experimentally determined constant in Equation (17); when it is used with any subscript, a proportionality factor used in derivation of Equation (17)
- M = mass percentage of water added to fluidized bed
- M_a = mass percentage of water analyzed in fluidized bed
- Q = graphical function of D_p used to express b in terms of G and D_p in Figure 3
- U_{mf} = velocity for minimum fluidization, ft./sec.

LITERATURE CITED

1. Dow, W. M., and Max Jakob, *Chem. Eng. Progr.*, **47**, 637 (1951).
2. Ergun, Sabri, and A. A. Orning, *Ind. Eng. Chem.*, **41**, 1179 (1949).
3. Gamson, B. W., *Chem. Eng. Progr.*, **47**, 19 (1951).
4. Lewis, W. K., E. R. Gilliland, and W. C. Bauer, *Ind. Chem.*, **41**, 1104 (1949).
5. Mickley, H. S., and D. F. Fairbanks, *A.I.Ch.E. Journal*, **1**, 374 (1955).
6. Missner, H. P., and H. S. Mickley, *Ind. Eng. Chem.*, **41**, 1238 (1949).
7. Morse, R. D., *ibid.*, 1117 (1949).
8. Parker, H. W., Ph.D. thesis, Northwestern Univ., Evanston, Illinois (1956).
9. Richardson, J. F., and W. N. Zaki, *Trans. Inst. Chem. Engrs. (London)*, **32**, 33 (1954).
10. Van Heerden, C., A. P. P. Nobel, and D. W. Krevelen, *Ind. Eng. Chem.*, **45**, 1237 (1953).
11. Wilhelm, R. H., and Mooson Kwauk, *Chem. Eng. Progr.*, **44**, 201 (1948).

Manuscript received December 3, 1957; revision received October 6, 1958; paper accepted November 24, 1958. Paper presented at A.I.Ch.E. Chicago meeting.

Formation of Gas Bubbles at Submerged Orifices

W. B. HAYES, III, B. W. HARDY, and C. D. HOLLAND

Agricultural and Mechanical College of Texas, College Station, Texas

The formation of air bubbles at constant pressure at submerged orifices was investigated for several liquids. The frequency of formation of the bubbles was determined by the use of a stroboscope, and the rate of gas flow was measured with conventional rotameters. Several orifices having diameters ranging from 0.0794 to 0.397 cm. were employed, and the gas flow rate was varied from about 0.1 cc. (at standard conditions)/sec. to about 150 cc./sec. It was found that the formation of bubbles could be correlated with the physical variables of the system by the application of Newton's second law of motion to the bubble at the instant just prior to its release from the orifice.

Gas, as a dispersed phase, plays a significant role in numerous physical and chemical processes. This is reflected by the attention given in the literature to the formation of gas bubbles at capillary tubes, orifices, and other devices submerged beneath liquid surfaces (*1*, *2*, *4*, *5*, *6*). In the experiments described herein the bubbles were formed at approximately constant pressure within the gas chamber (Figure 1) by passing air through orifices each of which was submerged in several liquids in turn. Correlation of the physical variables involved was achieved through the application of Newton's second law of motion.

It has been established that at very low rates of air flow the size of the bubble is nearly independent of the flow rate and is determined primarily by the orifice diameter, the surface tension, and the liquid density. At higher or intermediate rates of gas flow the size of the bubble becomes dependent upon the rate of gas flow through the orifice, as shown by Davidson *et al.* (*1*). At very high rates of gas flow Leibson *et al.* (*6*) demonstrated that the apparent jet of air issuing from the orifice is actually a series of closely spaced, irregular bubbles which undergo further separation upon rising through the liquid.

The influence of the volume of the gas chamber (Figure 2) and other physical dimensions of the apparatus on the formation of bubbles has been pointed out by Hughes *et al.* (*4*), who also observed that the effect of the chamber volume was not considered in the treatment of many of the data in the literature. Davidson *et al.* (*1*) demonstrated that as long as the volume of the gas chamber was less than a critical size it did not affect the formation of bubbles. For a given orifice diameter and gas flow rate the volume of the bubbles formed increased as the chamber volume was increased until approximately constant pressure within the gas chamber was approached. Most of the experiments reported in the literature were carried out with both capillary tubes and relatively small gas-chamber volumes; however in some instances Davidson (*1*) and Leibson (*6*) did use chamber volumes large enough to insure the formation at constant pressure within the gas chamber.

Since the majority of the bubble type of contactors employed in industrial applications operate at constant gas-chamber pressure and since such data are scarce, this investigation was undertaken.

EXPERIMENTAL

Experimental Apparatus

The equipment employed to collect the data used in the correlations consisted of the following major items: a column 10 in. in diameter and 72 in. long, an orifice holder 2 in. in diameter and 22 in. long, three rotameters, a Strobotac and Strobolux attachment, two manometers 60 in. long, six orifice plates, a wet-test gas meter, and two pressure regulators.

Figure 3 is a schematic flow diagram of the equipment. The pressure of the air entering the column through the orifice holder, located at the bottom of the column, was measured with respect to atmospheric pressure with a 60-in. manometer in which water was used as the fluid. Gas temperatures were measured with dial thermometers, and a mercury-filled glass thermometer was used to measure the temperature of the liquid, which could be read to within 0.1°C. The orifice plates employed to obtain the data used in the correlations shown herein were made of stainless steel plate 0.318 cm. thick. The diameters of the orifices were 0.0794, 0.159, 0.238, 0.318, 0.397, and 0.635 cm. The orifice holder, shown in Figure 1, was constructed from a section of stainless steel tubing. The rotameters used to measure the rates of gas flow were calibrated by with a wet-test meter.

Physical Properties of the Liquids

The interfacial tensions of the liquids with respect to air were measured with a Du Nouy direct-reading tensiometer, the viscosities were determined with a Stormer viscosimeter, and densities of the liquids were measured with a Westphal balance. The experimental values so obtained were in good agreement with those in the literature. These results are given in reference *3* and are also on file.* The correlations, Equations (27) and (28), were based on the results of 504 experiments. In all of them either pure liquids or mixtures of pure liquids which wet the orifice were employed, and the chamber volume was held constant at 1,322 cc. A wide variation in the viscosity of the liquid phase was obtained by the use of aqueous solutions of glycerine. Other liquids employed in this series of experiments were kerosene and isopropyl alcohol. In seventy-three other experiments the viscosity of the liquid phase was altered by the use of silicone additives. A chamber volume of 1,322 cc. was also employed in these runs. The effect of the geometry of the chamber volume on the formation of bubbles was investigated in a series of forty-one experiments. Throughout the entire investigation air was used as the gas phase.

Operation of Equipment

Prior to the initiation of a series of experiments the orifice holder was placed under pressure to prevent liquid from flowing into it. The column was then filled with liquid to a height of 6 in. above the level of the orifice. After the liquid level had been properly adjusted, the rotameter was set to give the desired gas-flow rate. At low rates of gas flow the frequency of formation of the bubbles was determined by visual inspection; at the higher rates of gas flow the frequency of formation was measured by a Stroboscope.

The data for the rate of formation of bubbles were taken at normal flow rates, or gas-flow rates above which a continuous stream of gas issues from an orifice. At gas-flow rates higher than the normal flow rates the bubble formation was not uniform and could not be determined with a stroboscope.

Experiments 232 through 243 and 561 through 575 were made under identical operational conditions. In a comparison of these data a smooth curve (frequency as a function of the gas-flow rate) was determined by the method of the least squares for each set of results. The average deviation of the experimental values with respect to the corresponding calculated values was 3 % for each set of results. The frequencies given by the smooth curve representing experiments 561 through 575 were on the average (taken over the range of flow rates employed in the two sets of

*Tabular material has been deposited as document No. 5969 with the American Documentation Institute, Photoduplication Service, Library of Congress, Washington 25, D. C., and may be obtained for $3.75 for photoprints or $2.00 for 35-mm. microfilm.

experiments) 4% below those given by the smooth curve for runs 232 through 243. Also the data from both sets of experiments were used to determine a single smooth curve for which an average deviation of 5% was obtained.

The room temperature was maintained at approximately 25°C. throughout the course of the investigation.

Description of Bubble Formation

Two types of bubble formation occurred. At low rates of gas flow the volume of the bubble remained relatively constant, but the frequency of formation increased as the gas-flow rate was increased. At the higher rates of gas flow the frequency of formation of the bubbles remained relatively constant, but the volume of the bubble increased as the flow rate was increased.

At low flow rates the bubbles formed singly at the orifice with a given time interval between the formation of each bubble. However as the flow rate was increased, the bubbles began to form in pairs; that is, two bubbles would appear to form simultaneously, a given time interval would elapse, and then two more bubbles would form. As the flow rate was increased further, the bubbles formed in groups of three, four, or five. Again a group would form, a given time interval would elapse, and another group would form. The time interval of course depended on the number of bubbles in the group and the rate of gas flow. This multiple bubble formation was not always reproducible. Experimental conditions that would yield groups of four might when repeated yield groups of three. In the computation of the volumes of the bubbles, however, it was assumed that they formed singly with equal time intervals between the formation of each bubble. On this basis it was found that with a given set of experimental conditions the calculated volumes of the bubbles were the same regardless of the number of bubbles in the group. Additional increases in the gas rate resulted in the formation of single bubbles at equal time intervals. This regular bubble formation continued, as the gas rate was increased, until irregular bubble formation occurred at higher flow rates, at which it was impossible to obtain quantitative data with a stroboscope.

EFFECTS OF VARIOUS DIMENSIONS OF THE APPARATUS ON THE FORMATION OF BUBBLES

The purpose of the experiments discussed in this section was to establish the approximate range over which the geometry of the apparatus could be altered without any significant deviations from the results upon which the correlations were based. Most of the geometrical quantities discussed here have been investigated with systems having zero chamber volume, although in some instances larger volumes were employed.

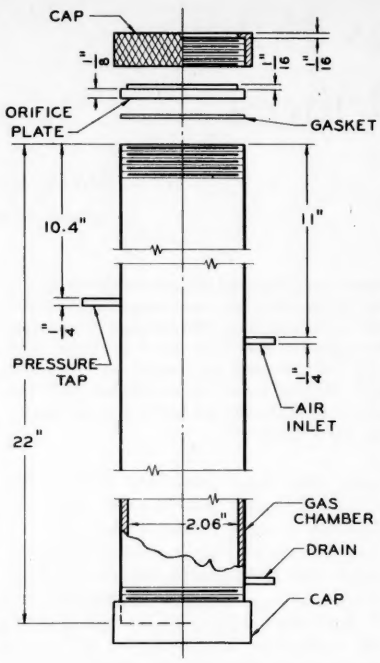

Fig. 1. Orifice holder

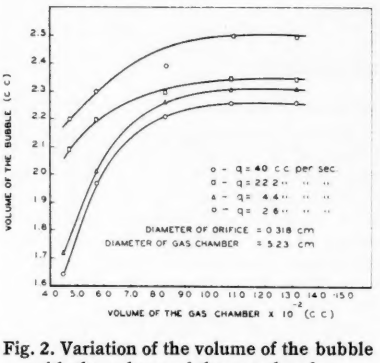
VOLUME OF THE BUBBLE (C C)
VOLUME OF THE GAS CHAMBER X 10⁻² (C C)
o - q = 40 C C per sec
o - q = 22 2 " "
Δ - q = 4 4 " "
o - q = 2 6 " "
DIAMETER OF ORIFICE = 0.318 cm
DIAMETER OF GAS CHAMBER = 5.23 cm

Fig. 2. Variation of the volume of the bubble with the volume of the gas chamber.

Except as noted, the experiments discussed below were performed at the following conditions: (*a*) the orifices were submerged beneath 15.2 cm. of water (*b*) the volume of the gas chamber was 1,322 cc., (*c*) the internal diameter of the gas chamber was 5.23 cm., (*d*) the thickness of the orifice plates was 0.318 cm., and (*e*) air was used in all the experiments.

The height of liquid above the orifice plate was varied from 45.7 to approximately 2.54 cm. Over the range of heights investigated the formation of bubbles appeared to be independent of the height of liquid, provided the height of liquid was greater than approximately two bubble diameters. This result is in agreement with the findings of Davidson *et al.* (*1*).

In another set of experiments the effect of the volume of the gas chamber on the formation of bubbles was investigated. In these experiments (Figure 2) the diameter of the gas chamber was held constant at 5.23 cm., and its volume was varied by partially filling it with water. For the experimental conditions stated it is evident that the formation of bubbles is independent of the chamber volume, provided that the latter is greater than about 800 cc. This result is in agreement with the concepts developed by Hughes (*4*).

As the diameter of the gas chamber is decreased, the diameter of the orifice is approached in the limit, where the formation of bubbles is said to occur at zero gas-chamber volume. In contrast, the data used in the correlations given in a subsequent section were obtained at the condition of "infinite" gas-chamber volume (or constant pressure within the gas chamber). For the experiments performed, the effect of the diameter of the gas chamber was insignificant in the formation of bubbles, provided that the ratio of the internal diameter of the gas chamber to that of the orifice was equal to or greater than 4.5. Actually the lower limit lies between 1.0 and 4.5, since the results of experiments performed at the limit stated, $D_c = 1.43$ cm., $D_0 = 0.318$ cm., were in agreement with those obtained with an orifice diameter of 0.318 cm. and gas chamber diameters of 2.69, 5.23, and 10.3 cm.

The effect of the thickness of the orifice plate on the formation of bubbles was also investigated. It should be pointed out that as the thickness of the orifice plate is increased indefinitely, the condition of zero chamber volume is approached in the limit. Capillary tubes were used as orifice plates in those experiments where plate thickness greater than 0.318 cm. were employed. These tubes were attached to a gas chamber having a volume of 1,322 cc. For the flow rates (corresponding to the region of relatively constant frequency) employed, the effect of the thickness of the orifice plate on the formation of bubbles became significant at thicknesses equal to or greater than 100 orifices diameters, in agreement with the results of Hughes (*4*). Orifices having diameters of 0.318 and approximately 0.635 cm. were used in this set of experiments. If a lower limit of the ratio of the plate thickness to the orifice diameter exists, it appears to lie below 0.5 (obtained with an orifice diameter of 0.318 cm. and a plate thickness of 0.159 cm.). The results corresponding to the latter ratio were in agreement with those obtained when both a plate thickness and an orifice diameter of 0.318 cm. were employed.

DEVELOPMENT OF EQUATIONS

The analysis of the formation of bubbles at submerged orifices is concerned with the forces acting on the surface of the bubble, as would be seen

by a stationary observer located at any point exterior to the bubble. The various forces acting were related through the application of Newton's second law of motion.

In the following analysis of this process the actual bubble was replaced by one of equal mass, which moved with the average vertical-component velocity and had the same forces acting on it as those which acted on the actual bubble.

First the center of a spherical bubble is considered fixed and the bubble allowed to expand equally in all directions. Then

$$\frac{dV}{dt} = q \tag{1}$$

Furthermore

$$\frac{dV}{dt} = \frac{dV}{dD}\frac{dD}{dt} = \pi D^2 \frac{dr}{dt} \tag{2}$$

For convenience

$$v_n = \frac{dr}{dt} = \frac{q}{\pi D^2} \tag{3}$$

The growth of a spherical bubble at a submerged orifice may be represented as shown in Figure 4. To obtain the velocity of a point on the surface of a bubble at any instant during its formation, it is convenient to think of a given growth process of a bubble at an orifice as being composed of two steps: first, that the center of a given bubble is fixed and that the bubble experiences an expansion in unit time such that its radius is increased by an amount v_n, and, second, that each point on the surface of the bubble so formed is displaced vertically by an amount v_n in unit time. The vector representation of this two-step growth process is shown in Figure 5. The subscripts 1 and 2 of the vectors $\mathbf{v}_{n_1}$ and $\mathbf{v}_{n_2}$ denote the steps just mentioned. The velocity $\mathbf{v}_R$ of any given point on the surface of the bubble is of course the vector sum of $\mathbf{v}_{n_1}$ and $\mathbf{v}_{n_2}$, as indicated in Figure 5. Thus

$$\mathbf{v}_R = \mathbf{v}_{n_1} + \mathbf{v}_{n_2} \tag{4}$$

The magnitude of the vertical component of $\mathbf{v}_R$ is given by the dot product $\mathbf{v}_R \cdot \mathbf{j}$, as

$$\mathbf{v}_R \cdot \mathbf{j} = \mathbf{v}_{n_1} \cdot \mathbf{j} + \mathbf{v}_{n_2} \cdot \mathbf{j} = v_y \tag{5}$$

By definition of the dot product

$$v_y = (v_{n_1})(1)\cos\left(\frac{\pi}{2} - \alpha\right) + (v_{n_2})(1)\cos(0) \tag{6}$$

and

$$v_y = v_{n_1}\cos\left(\frac{\pi}{2} - \alpha\right) + v_{n_2} \tag{7}$$

Since

$$\sin\alpha = \cos\left(\frac{\pi}{2} - \alpha\right) \tag{8}$$

and since $v_{n_1} = v_{n_2} = v_n$, Equation (7) may be written as

$$v_y = v_n(1 + \sin\alpha) \tag{9}$$

Examination of Equation (9) shows that v_y is symmetrical about the vertical axis of the bubble. Thus the average of v_y over a circle containing the vertical axis as a diameter is equal to the average of v_y over the entire surface. Then

$$v(2\pi r) = \int_0^{2\pi} v_y r \, d\alpha \tag{10}$$

When the expression for v_y as a function of α [Equation (9)] is substituted in the preceding expression, one obtains upon integration

$$v = v_n \tag{11}$$

where v_n is of course defined by Equation (3).

The formation of a bubble at a submerged orifice is a variable-mass type of problem. Pars (*8*) has shown that when to a body of mass which is moving with the instantaneous velocity v (relative to a fixed observer), mass traveling with the velocity v_0 (relative to a fixed observer) is added at the rate dm/dt, one must include the force v_0 (dm/dt) in the application of Newton's second law of motion. In addition to this force, a bubble is also acted upon by the following forces during its formation: the net bouyancy force $gV\Delta\rho$ and the excess pressure force $(\pi D_0^2/4)$ $(p_i - p)$, the surface tension force $\pi D_0\sigma$, the drag force, and the force required to overcome the inertia of the fluid surrounding the bubble. For a bubble moving with the instantaneous velocity, the latter force is given by m' (dv/dt). Thus when the actual bubble is replaced by one moving with the instantaneous velocity and with the same set of forces acting on its external surface and when the vertical direction is taken as positive, one obtains by application of Newton's second law

$$v_0\frac{dm}{dt} + gV\,\Delta\rho + \frac{\pi D_0^2}{4}(p_i - p) - \pi D_0\sigma - F - m'\frac{dv}{dt} = \frac{d(mv)}{dt} \tag{12}$$

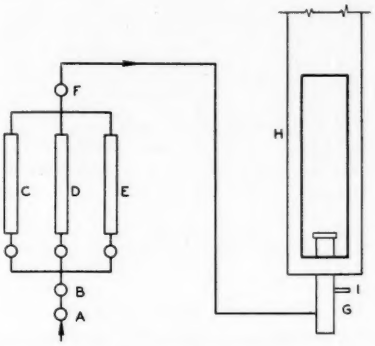

Fig. 3. Flow diagram of equipment: A—air inlet; B—pressure regulators; C, D, E—rotameters; F—¼-in. needle valve; G—orifice holder; H—column; I—connection for open-end manometer.

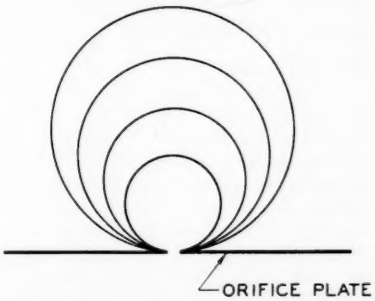

Fig. 4. Formation of a spherical bubble at a submerged orifice.

The pressure in the liquid at the level of the orifice is slightly less than the pressure of the gas at the top edge of the orifice because of the effect of surface tension. When the net buoyancy force is taken to be $gV\Delta\rho$, it is implied that the pressure, p, instead of the actual pressure, p_i, acts over the area of the bubble immediately above the orifice. In accordance with the treatment of Hughes *et al.* (*4*), the excess pressure force was included to account for the error in the expression for the net bouyancy force. The fact that a pressure slightly greater than p_i is required for the gas to flow from the top of the orifice to the various parts of an expanding bubble is neglected in the present treatment. Since the diameter of the orifice was always small as compared with that of the bubble, the excessive pressure force was relatively small. Because of the large chamber volumes employed, the pressure within the chamber was approximately constant and the well-known relationship

$$p_i - p = \frac{4\sigma}{D} \tag{13}$$

was employed for the evaluation of the excessive pressure force at the instant just prior to the release of the bubble from the orifice. Prandtl (*9*) has given an informative derivation of this relationship. It should also be pointed out that in the calculation of q the pressure within the gas chamber was employed, because in all experiments the pressure drops across the orifice were less than 1 in. of water.

Other terms in Equation (12) may be evaluated also at the instant just prior to the release of the bubble. When the first member of the left-hand side of

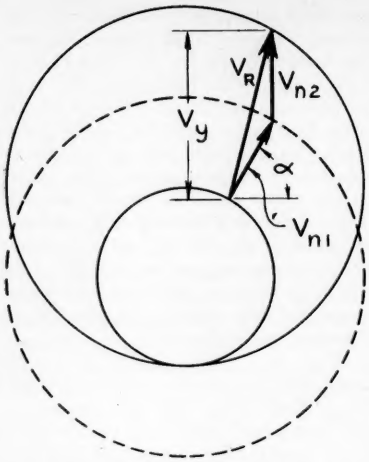

Fig. 5. Velocity of a point on the surface of a bubble during formation.

Equation (12) is transposed to the right-hand side, the latter becomes

$$\frac{d(mv)}{dt} - v_0\frac{dm}{dt} = m\left(\frac{dv}{dD}\right)\left(\frac{dD}{dt}\right) + (v - v_0)\frac{dm}{dt} \tag{14}$$

Substitution of $2v$ for dD/dt and $q\rho_g$ for dm/dt in Equation (14) yields

$$\frac{d(mv)}{dt} - v_0\frac{dm}{dt} = (2mv)\left(\frac{dv}{dD}\right) + (v - v_0)(q\rho_g) \tag{15}$$

Since $v = q/\pi D^2$, $dv/dD = (-2q)/(\pi D^3)$, $v_0 = (4q)/(\pi D_0^2)$, and $m = V\rho_g$, it is readily shown that the above expression reduces to

$$\frac{d(mv)}{dt} - v_0\frac{dm}{dt} = -\frac{4q^2\rho_g}{\pi D_0^2}\cdot\left[1 - \frac{1}{12}\left(\frac{D_0}{D}\right)^2\right] \tag{16}$$

The total drag force was expressed in terms of the drag coefficient as

$$F = \frac{c_D\rho_L v^2 A_f}{2} \tag{17}$$

When the the assumption of spherical bubbles is made, the representative area may be replaced by $\pi D^2/4$. Since $v = q/\pi D^2$, the drag force is readily stated in terms of the Froude number, the drag coefficient, and the volume of the bubble; that is,

$$F = \frac{c_D\rho_L v^2 A_f}{2} = \left(\frac{c_D\rho_L}{2}\right)\left(\frac{q^2}{\pi^2 D^4}\right)\left(\frac{\pi D^2}{4}\right) \tag{18}$$

$$F = \frac{3g\rho_L c_D N_{Fr} V}{4}$$

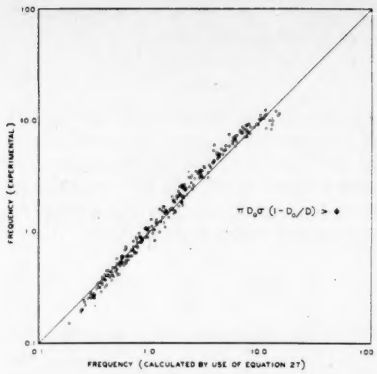

Fig. 6. Comparison of experimental and calculated values of the frequency of bubble formation.

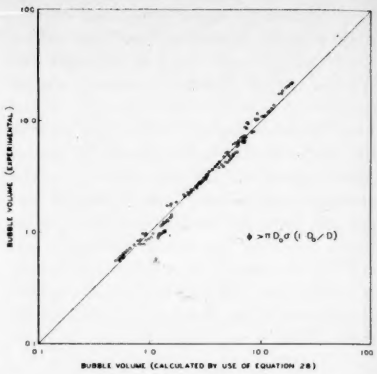

Fig. 7. Comparison of experimental and calculated values of the bubble volume.

where the Froude number is defined by

$$N_{Fr} = \frac{v^2}{Dg} = \frac{q^2}{\pi^2 D^5 g} \tag{19}$$

In the consideration of the last term on the left-hand side of Equation (12) Streeter (*10*) has shown that in the case of irrotational motion m' equals one half of the mass of the displaced fluid. Although in the present case the flow was not irrotational, m' was taken proportional to the mass of the displaced fluid. Thus

$$m'\frac{dv}{dt} = \rho_L V\chi\left(\frac{dv}{dt}\right) = \rho_L V\chi\left(\frac{dv}{dD}\right)\left(\frac{dD}{dt}\right) \tag{20}$$

When the derivatives appearing in the right-hand member are evaluated as outlined previously in the treatment of Equation (14), one obtains

$$m'\frac{dv}{dt} = \rho_L V\chi\left(\frac{-2q}{\pi D^3}\right)\left(\frac{2q}{\pi D^2}\right) = -4\rho_L g\chi N_{Fr} V \tag{21}$$

For irrotational motion the quantity χ is of course equal to $\frac{1}{2}$, but since it was not irrotational, the quantity χ and the drag coefficient were correlated as a power function of the appropriate dimensionless groups.

When the results given by Equations (13), (16), (18), (21) are substituted in Equation (12), it reduces to

$$V\,\Delta\rho_g(1 - \psi) = \pi D_0\sigma\left(1 - \frac{D_0}{D}\right) - \phi \tag{22}$$

The symbols ψ and ϕ, introduced for convenience, have the following definitions:

$$\psi = \left(\frac{3\rho_L}{4\,\Delta\rho}\right)(N_{Fr})\left[c_D - \frac{16}{3}\chi\right] \tag{23}$$

$$\phi = \frac{4q^2\rho_g}{\pi D_0^2}\left[1 - \left(\frac{1}{12}\right)\left(\frac{D_0}{D}\right)^2\right] \tag{24}$$

The use of Equation (22) in the correlation of the experimental results follows.

CORRELATIONS

The variables contained in Equation (22) were evaluated at the instant just prior to the release of the bubble from the orifice. Since the drag coefficient is a function of the Reynolds number, Equation (23) demonstrates that ψ is a function of both the Froude and Reynolds numbers. Because of the relative magnitudes of the terms constituting Equation (22), the direct solution for and correlation of $(c_D - 16/3\ \chi)$ proved impractical; instead the positive difference of $(1 - \psi)$ was correlated.

Since the diameter of the bubble was always considerably greater than the diameter of the orifice, the expression for ϕ reduces to $(4q^2\rho_g)/(\pi D_0^2)$, which is the time rate of change of momentum of the gas added to the bubble at the instant just prior to its release from the orifice. In effecting a correlation, the data were divided into two groups. The first group consisted of the runs for which $\pi D_0\sigma(1 - D_0/D) > \phi$; that is, the net-surface tension force was greater than the time rate of change of the momentum of the gas added to the bubble. In the actual classification of the runs the complete expression for ϕ [given by Equation (24)] was employed.

The experimental value for the positive difference of $(1 - \psi)$ was obtained indirectly by the experimental determination of the remaining terms of Equation (22). For each set of data the absolute value of $(1 - \psi)$ was correlated as a power function of the Froude number, the Reynolds number, and the ratio D_0/D as

$$|(1 - \psi)| = K(N_{Re})^a(N_{Fr})^b\left(\frac{D_0}{D}\right)^c \tag{25}$$

where

$$N_{Re} = \frac{Dv\rho_L}{\mu_L} = \frac{q\rho_L}{\pi D\mu_L} = \frac{q^{2/3}f^{1/3}\rho_L}{\pi^{2/3}6^{1/3}\mu_L} \tag{26}$$

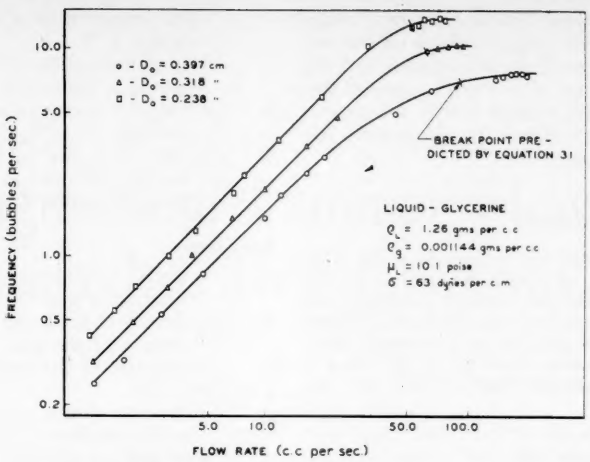

Fig. 8. Prediction of the division of the two ranges of bubble formation.

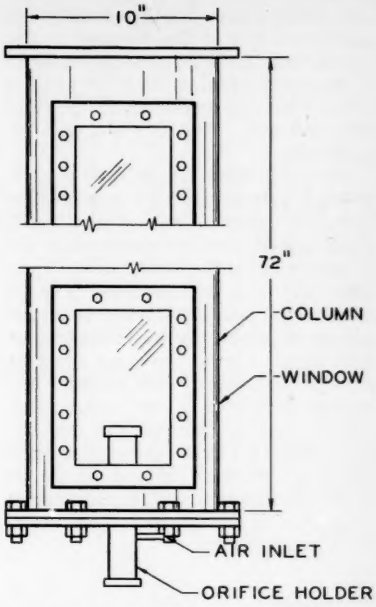

Fig. 9. Experimental column.

For those runs for which $\pi D_0\sigma\ (1 - D_0/D) > \phi$, the volume of the bubble varied little with the gas-flow rate, but the frequency of bubble formation changed appreciably with the gas-flow rate. In the upper range of flow rates [for which $\phi > \pi D_0\sigma\ (1 - D_0/D)$] the situation just described was reversed. In view of these physical considerations the frequency of bubble formation was selected as the dependent variable for those experiments where $\pi D_0\sigma\ (1 - D_0/D) > \phi$. For the range of flow rates in which $\phi > \pi D_0\sigma\ (1 - D_0/D)$, the volume of the bubble was taken as the dependent variable.

When Equation (22) is solved for V, one obtains V as a function of V, since $(1 - \psi)$ is also a function of V. Similarly, since $V = q/f$, Equation (22) may be solved for the frequency as a function of the frequency. For those data in the range $\pi D_0\sigma\ (1 - D_0/D) > \phi$, the best correlation for the calculation of the frequencies (or bubble volumes) was obtained by the use of the expression obtained by solving Equations (22) and (25) for f as a function of the other variables. Actually the diameter of the bubble was left in the expression for ϕ, since the latter was relatively insensitive to the bubble diameter. The following correlation was obtained. For $\pi D_0\sigma\ (1 - D_0/D) > \phi$

$$f = \frac{7.56 \times 10^{-3}}{\bar{N}_{Re}^{\ 3}} (\bar{N}_{Fr}\bar{N}_{Re}^{-5})^{-0.172} \cdot (Nq\bar{N}_{Re}^{\ 3})^{0.525} \left[\frac{D_0\bar{N}_{Re}^{\ -1}}{\left(\frac{6q}{\pi}\right)^{1/3}}\right]^{-0.697} \quad (27)$$

where

$$\bar{N}_{Fr} = N_{Fr}f^{-5/3} = \frac{q^{1/3}}{g\pi^{1/3}\,6^{\,5/3}}$$

= modified Froude number

$$\bar{N}_{Re} = N_{Re}f^{-1/3} = \frac{q^{2/3}\rho_L}{\pi^{2/3}6^{1/3}\mu_L}$$

= modified Reynolds number

$$N = \left|\frac{\pi}{6}\left(\frac{\Delta\rho g}{\pi\ D_0\sigma(1 - D_0/D) - \phi}\right)\right|$$

Those data falling in the variable volume range were correlated in a similar manner by solving Equations (22) and (25) for the volume of the bubble as a function of the other variables. Again the diameter of the bubble was left in the expression for ϕ because the latter was relatively insensitive to this diameter. The correlation for these data follows. For $\phi > \pi D_0\sigma\ (1 - D_0/D)$

$$V = \frac{23.4}{N} (N_{Fr}'N^{5/3})^{0.463} \cdot (N_{Re}'N^{1/3})^{-0.0764} (D_0N^{1/3})^{0.712} \quad (28)$$

where

$$N_{Fr}' = N_{Fr}\ D^5$$

$$N_{Re}' = N_{Re}\ D$$

Equations (27) and (28) apply for the case of infinite chamber volume. The constants and exponents in Equations (27) and (28) were determined by the method of the least squares through the use of a digital computer. The average percentage deviations of the calculated values of f and V [as given by Equations (27) and (28)] from the experimental values were 16 and 10 repectively. The corresponding correlation coefficients were 0.998 and 0.988. Graphs of the experimental values of f and V vs. the values calculated by the use of Equations (27) and (28) are shown in Figures 6 and 7. The significance of each of the groups in these equations was shown by the determination of the correlation coefficient and the average percentage deviation when each of the terms shown in the equation was omitted and the others were retained. When each of the groups containing the modified Froude number, the term (Nq), and the diameter of the orifice was omitted from Equation (27) and the others were retained, the correlation coefficients were 0.994, 0.994, and 0.997, respectively, and the corresponding average percentage deviations were 3×10^8, 44, and 1.4×10^9. Similarly, omission of the groups containing the modified Froude number, the modified Reynolds number, the diameter of the orifice, and the retention of all the other groups in Equation (28) gave the following correlation coefficients: 0.976, 0.965, and 0.984 respectively. The corresponding average percentage deviations were 69, 16, and 11. Thus all the terms shown in Equation (27) are required in order to represent adequately the experimental results. In the process of correlating the data, a surface-tension number [defined in the same manner as the one used by Hughes *et al.* (4)] was used together with those groups shown in Equations (27) and (28), and the average percentage deviations were only about 1% better than those given by Equations (27) and (28).

It is to be observed that little accuracy was lost when the term containing the diameter of the orifice was omitted in the correlation of the data for the upper region of the flow rates. In view of this the correlation is included.

For $\phi > \pi D_0\sigma\ (1 - D_0/D)$

$$V = \frac{5.94}{N} (N_{Fr}'N^{5/3})^{0.748} \cdot (N_{Re}'N^{1/3})^{-0.0637} \quad (29)$$

It should also be mentioned that when stated in terms of the diameter of the bubble, the average percentage deviations of the experimental values of D from the values calculated by the use of Equations (27) and (28) were 5.0 and 3.0 respectively.

Some experiments were performed in which a silicone additive was used to alter the surface tension of the liquid. Those results were not employed in the determination of the constants for Equations (27) and (28) because in some instances (7) such liquid mixtures do not appear to exhibit the characteristics of pure liquids having the same apparent physical properties. The average percentage deviations of the experimental value of the dependent variable from the value calculated by the use of Equations (27) and (28) were 25 and 30 % respectively. The relatively poor agreement lends further support to the characteristics just discussed.

DISCUSSION

A comparison of the volumes of the bubbles obtained in the present work with those of other workers who employed essentially zero chamber volumes shows that at similar operating conditions the volumes of the bubbles obtained by the use of the system described herein (operation was at constant pressure within the gas chamber, or infinite gas-chamber volume) were always larger. The equations stated by Hughes *et al.* (4) and given the numbers 19, 20, 23 and 24 did not correlate the data obtained by the authors nearly so well as did Equations (27) and (28), perhaps because of the large gas-chamber volumes employed in the present work.

The theoretical treatment of the formation of bubbles led to a description of the two regions of bubble formation as well as a physical explanation for the division of the two regions. As discussed previously, at low gas-flow rates the surface-tension force was greater than than the time rate of change of the momentum of the gas entering the bubble, while at the higher rates of gas flow the order of magnitude of the two forces was reversed. Furthermore, according to the theory developed for the case of infinite chamber volume, the division of the two regions occurred when there was an equality between the two forces, namely

$$\pi D_0 \sigma (1 - D_0/D) \cong \frac{4q^2 \rho_g}{\pi D_0^2} \qquad (30)$$

or

$$q = \frac{\pi}{2} \sqrt{\frac{D_0^3 \sigma (1 - D_0/D)}{\rho_g}} \qquad (31)$$

In Figure 8 the experimental results as well as the predicted division of the two ranges are shown. Although there is no sharp division between the lower range of relatively constant bubble volume and variable frequency of formation and the upper range of relatively constant frequency and variable bubble volume, the division predicted by Equation (31) appears adequate.

ACKNOWLEDGMENT

This work was supported by the E. I. du Pont de Nemours and Company, Humble Oil and Refining Company, and The Texas Engineering Experiment Station. This aid is gratefully acknowledged. Helpful suggestions offered by D. M. Vestal of the Experiment Station are also appreciated.

NOTATION

A_f = representative area of the bubble, $\pi D^2/4$ for spheres; L^2
c_D = drag coefficient, dimensionless
D = diameter of the bubble (assumed to have a spherical shape), L
D_0 = diameter of the orifice, L
F = drag force, the sum of the vertical components of the viscous and form drag forces, ML/T^2
f = frequency of bubble formation
g = acceleration of gravity, L/T^2
g_c = conversion factor, ML/T^2F
$\mathbf{j}$ = unit vector in the vertical direction, dimensionless
L = thickness of the orifice plate in the direction of flow, L
m = mass of the bubble at any time, t; M
m' = mass term for the displaced fluid, M
N = a term defined below Equation (27), L^{-3}
N_{Fr} = Froude number defined by Equation (19), dimensionless
N_{Re} = Reynolds number defined by Equation (26), dimensionless
p = pressure in the liquid at the level of the top of the orifice, M/LT^2
p_i = static pressure of the gas stream at the level of the exit side of the orifice plate, M/LT^2
q = volumetric rate of gas flow evaluated at the conditions at the top of the orifice, (because of the small pressure drops involved the pressure was taken equal to that of the gas chamber in the calculation of q), L^3/T
t = time, T
v = average of the vertical component of velocity over the surface of the bubble, L/T
$\mathbf{v}_{n_1}, \mathbf{v}_{n_2}$ = vectors having the magnitude v_n given by Equation (4) and directions indicated in Figure 5, L/T
$\mathbf{v}_R$ = velocity vector of any point on the surface of a bubble during its formation at a submerged orifice, L/T
v_y = magnitude of the vertical component of the velocity v_R, L/T
v_0 = velocity at which the gas flows through the orifice, L/T
V = volume of the bubble at the instant just prior to its release from the orifice, L^3

Greek Letters

α = angle used in the vector diagram (Figure 5), radians
$\Delta\rho$ = density of the liquid minus the density of the gas, M/L^3
μ_L = viscosity of the liquid, M/LT
π = 3.1416
ρ_g = density of the gas evaluated at the temperature and pressure of the gas chamber, M/L^3
ρ_L = density of the liquid in which the orifice plate was submerged, M/L^3
σ = interfacial tension of the liquid with respect to air, M/T^2
ϕ = a variable which was approximately equal to the time rate of change of the momentum of the gas entering the bubble, defined by Equation (24), ML/T^2
χ = a function defined by Equation (20), dimensionless
ψ = a function defined by Equation (23), dimensionless

Mathematical Symbols

$|x|$ = absolute value of x

LITERATURE CITED

1. Davidson, Leon, and Edwin H. Amick, Jr., *A.I.Ch.E. Journal*, **2**, No. 3, 337 (1956).
2. Eversole, W. G., G. H. Wagner, and Eunice Stackhouse, *Ind. Eng. Chem.*, **33**, 1459 (1941).
3. Hayes, William B., III, dissertation, Agricultural and Mechanical College of Texas, College Station, Texas (May, 1958).
4. Hughes, R. R., A. E. Handlos, H. D. Evans, and R. L. Maycock, *Chem. Engr. Progr.*, **51**, No. 12, 557 (1955).
5. Leibson, Irving, E. G. Holcomb, A. G. Cacoso, and J. J. Jacmic, *A.I.Ch.E. Journal*, **2**, No. 3, 296 (1956).
6. *Ibid.*, **2**, No. 3, 300 (1956).
7. Pattle, R. E., *Trans. Inst. Chem. Engrs. (London)*, **28**, 32 (1950).
8. Pars, L. A., "Introduction to Dynamics," pp. 162 to 165, Cambridge University Press, Cambridge, England (1953).
9. Prandtl, Ludwig, "Essentials of Fluid Dynamics, Authorized translation, pp. 26 to 30, Hafner Publishing Company, New York (1952).
10. Streeter, V. L., "Fluid Dynamics," pp. 64 to 67, McGraw-Hill, New York (1948).

Manuscript received July 7, 1958; revision received December 29, 1958; paper accepted December 30, 1958.

Longitudinal Laminar Flow Between Cylinders Arranged in Regular Array

E. M. SPARROW and A. L. LOEFFLER, JR.

National Aeronautics and Space Administration, Lewis Research Center, Cleveland, Ohio

An analytical solution has been obtained for the longitudinal fully developed laminar flow between cylinders arranged in triangular or square array. Numerical results for the pressure drop and the friction factor are given over a wide range of spacing-to-diameter ratios. For large spacings the results can be represented by a single expression independent of the type of array. Plots are also given of velocity distributions and of the variation of the local shear stress around the periphery of a cylinder.

The increasing complexity of heat transfer and process situations which involve fluid flow has demanded the frequent use of flow passages of unusual geometrical configuration. The present investigation is concerned with one such novel configuration, namely the longitudinal flow between solid cylindrical rods which are arranged in regular array. A schematic diagram of the situation under study is shown in Figure 1. The rods may be located either in triangular or square array. The flow will be taken to be laminar and fully developed.

The aim of this analysis is to determine the pressure drop, shear stress, and velocity-distribution characteristics of the system. The starting point of this study is the basic law of momentum conservation. The resulting differential equation has been solved in an approximate, but almost exact, manner by the use of truncated trigonometric series. Results are obtained over a wide range of porosity values for both the triangular and square arrays. Heat transfer has not been considered.

The configuration under investigation has potential application in compact heat exchangers for nuclear reactors and other situations. Further the results should also be of interest in the theory of flow through unconsolidated porous beds (*1a*, *2a*).

The only related analytical work known to the authors is that of Emersleben (*3*), who considered only the square array. His rather involved solution, based on complex zeta functions, appears to be valid only at high porosities. Experiments covering a porosity range of 0.093 to 0.984 have been made by Sullivan (*4*) using parallel-oriented fibers, most of the tests being for fibers in random array. These previous investigations will be compared with the present theory in a later section.

ANALYSIS

The Governing Equation and Its General Solution

The physical principle which governs the velocity distribution in a (isothermal) flowing fluid is conservation of momentum. To translate this physical law into mathematical terms, cylindrical coordinates will be used. The derivation is facilitated by Figure 2. The conservation principle requires that under steady state conditions the net change of momentum must equal the net forces. However for fully developed flow the net momentum flux is zero (no accelerations), and hence the forces must sum to zero. The forces involved in the problem are those of pressure and viscosity, and these must be in balance. Therefore

$$\left[\left(p + \frac{dp}{dz}\,dz\right) - p\right] r\,d\theta\,dr = \mu\left[\frac{\partial}{\partial r}\left(\frac{\partial u}{\partial r}\,r\,d\theta\,dz\right)dr + \frac{\partial}{\partial \theta}\left(\frac{1}{r}\frac{\partial u}{\partial \theta}\,dr\,dz\right)d\theta\right] \tag{1}$$

When one rearranges, the governing equation for the velocity as a function of the coordinates r and θ is obtained:

$$\frac{\partial^2 u}{\partial r^2} + \frac{1}{r}\frac{\partial u}{\partial r} + \frac{1}{r^2}\frac{\partial^2 u}{\partial \theta^2} = \frac{1}{\mu}\frac{dp}{dz} \tag{2}$$

where the pressure gradient dp/dz is a negative constant. This partial differential equation is frequently called Poisson's equation.

It is not difficult to write a solution of this equation, but subsequently one must face the more challenging task of fitting the solution to the particular boundary conditions of specific problems. The general solution is dealt with here, leaving specific flow situations to later sections.

In approaching Equation (2) it is convenient to introduce a reduced velocity defined by

$$u^* = u - \frac{r^2}{4}\left(\frac{1}{\mu}\frac{dp}{dz}\right) \tag{3}$$

By substitution into Equation (2) one finds that u^* must obey

$$\frac{\partial^2 u^*}{\partial r^2} + \frac{1}{r}\frac{\partial u^*}{\partial r} + \frac{1}{r^2}\frac{\partial^2 u^*}{\partial \theta^2} = 0 \tag{4}$$

which is the well-known Laplace equation. The general solution of Equation (4) may be taken from numerous books on advanced calculus. Therefore

$$u^* = A + B\ln r + \sum_{k=1}^{l}(C_k r^k + D_k r^{-k})\cdot(E_k\cos k\theta + F_k \sin k\theta) \tag{5}$$

where k takes on integral values to ensure that the velocity is single valued, that is that the velocity computed at a location (r, θ) is identical to that computed at $(r, \theta + 2\pi)$. The constants A, B, etc., in Equation (5) are to be determined from the boundary conditions, as are the number of terms of the series.

Thus a general solution for the velocity is obtained by the combining of Equations (3) and (5) which yields

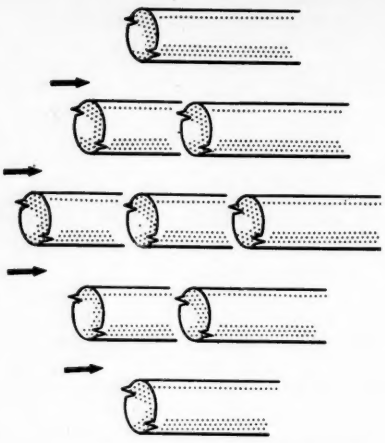

Fig. 1. Schematic of flow configuration.

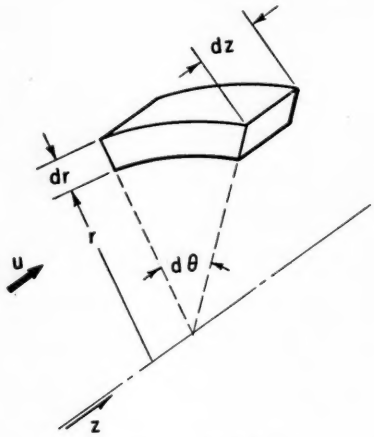

Fig. 2. Control volume for deriving momentum equation.

$$u = A + B \ln r - \frac{r^2}{4}\left(-\frac{1}{\mu}\frac{dp}{dz}\right) + \sum_{k=1}^{l} (C_k r^k + D_k r^{-k}) \cdot (E_k \cos k\theta + F_k \sin k\theta) \qquad (6)$$

Now one may turn to the problem of specializing this solution to flow parallel to cylindrical rods in regular array.

Cylinders in Triangular Array

Consideration is first given to flow between cylinders arranged on centers which form the vertices of equilateral triangles. An end view of the arrangement is shown in Figure 3. From the symmetry of the situation it is easily seen that attention need be focused on only the cross-hatched element in the left-hand sketch. An enlarged view is shown at the right, on which has been noted the boundary conditions and dimensional nomenclature. The condition $\partial u/\partial n = 0$ is the expression of the symmetry property, while the condition that $u = 0$ at the inner boundary stems from the no-slip requirement of viscous flow.

Table 1. Listings of Δ_j and δ_j for Various Spacing Ratios

(a) Values of Δ_j.

s/r_0	Δ_1	Δ_2	Δ_3	Δ_4	Δ_5	Δ_6	Δ_7
4.0	−0.0505	−0.0008	0.0000	→			
2.0	−0.0505	−0.0008	0.0000	→			
1.5	−0.0502	−0.0007	0.0000	→			
1.2	−0.0469	0.0007	0.0002	0.0000	→		
1.1	−0.0416	0.0028	0.0004	0.0000	→		
1.05	−0.0368	0.0043	0.0003	−0.0001	0.0000	→	
1.04	−0.0357	0.0046	0.0002	−0.0001	0.0000	→	
1.03	−0.0345	0.0049	0.0002	−0.0001	0.0000	→	
1.02	−0.0332	0.0051	0.0000	−0.0001	0.0000	→	
1.01	−0.0319	0.0052	−0.0001	−0.0002	0.0000	→	
1.00	−0.0305	0.0053	−0.0003	−0.0002	0.0000	→	

(b) Values of δ_j

s/r_0	δ_1	δ_2	δ_3	δ_4	δ_5	δ_6	δ_7
4.0	−0.1253	−0.0106	−0.0006	0.0000	→		
2.0	−0.1250	−0.0105	−0.0006	0.0000	→		
1.5	−0.1225	−0.0091	−0.0002	0.0000	→		
1.2	−0.1104	−0.0024	−0.0015	0.0003	0.0001	0.0000	→
1.1	−0.0987	0.0036	0.0029	0.0005	0.0000	→	
1.05	−0.0904	0.0073	0.0032	0.0002	−0.0001	0.0000	→

One may now proceed to apply the boundary conditions to determine the constants of Equation (6). Starting with the simplest conditions, one requires first that $\partial u/\partial n = \partial u/\partial\theta = 0$ at $\theta = 0$ deg. and at $\theta = 30$ deg. From the first of these it follows that since $\cos 0 \neq 0$, then

$$F_k \equiv 0 \qquad (7a)$$

while from the second one finds that

$$k = 6, 12, 18\cdots \qquad (7b)$$

to guarantee that $\sin k\pi/6 = 0$. Next imposing the condition that $u = 0$ at $r = r_0$ one gets

$$D_k = -C_k r_0^{2k},$$

$$A = -B \ln r_0 + \frac{r_0^2}{4}\left(-\frac{1}{\mu}\frac{dp}{dz}\right) \qquad (7c)$$

Further it is required that the total drag force exerted on the fluid by the solid rod be balanced by the net pressure force acting over the entire cross section of the typical element (Figure 3b); that is

$$\int_0^{\pi/6} \mu\left(\frac{\partial u}{\partial r}\right)_{r=r_0} r_0\, d\theta = \int_0^{\pi/6}\int_{r_0}^{s/\cos\theta} \left(\frac{dp}{dz}\right) r\, dr\, d\theta \qquad (8)$$

The evaluation of this over-all force balance from Equation (6) yields

$$B = \frac{\sqrt{3}}{\pi} s^2\left(-\frac{1}{\mu}\frac{dp}{dz}\right) \qquad (7d)$$

Before going on to the final boundary condition the findings of the previous paragraph are brought together, and Equation (6) becomes

$$u = \frac{\sqrt{3}}{\pi} s^2\left(-\frac{1}{\mu}\frac{dp}{dz}\right)\ln\frac{r}{r_0} - \frac{1}{4}\left(-\frac{1}{\mu}\frac{dp}{dz}\right)(r^2 - r_0^2) + \sum_{j=1}^{l} G_j\left(r^{6j} - \frac{r_0^{12j}}{r^{6j}}\right)\cos 6j\theta \qquad (9)$$

where $G_j \equiv C_j E_j$. There still remains the task of determining the G_j, and at one's disposal is the condition that $\partial u/\partial n = 0$ on the right-hand boundary of Figure 3b, on which $r = s/\cos\theta$. It is convenient to make use of the identity

$$\frac{\partial u}{\partial x} = \frac{\partial u}{\partial r}\cos\theta - \frac{\partial u}{\partial\theta}\frac{\sin\theta}{r}$$

where one may associate x with n on the boundary under consideration. Introducing Equation (9) and setting $\partial u/\partial n = 0$ when $r = s/\cos\theta$, one finds after rearrangement

$$\sum_{j=1}^{l} \Delta_j (\cos\theta)^{1-6j}\left[\cos(6j-1)\theta + \left(\frac{r_0\cos\theta}{s}\right)^{12j}\cos(6j+1)\theta\right] + \frac{\sqrt{3}}{\pi}\cos^2\theta - \frac{1}{2} = 0 \qquad (7e)$$

where

$$\Delta_j = G_j \frac{6j\, s^{6j}}{\left(-\frac{1}{\mu}\frac{dp}{dz}\right)s^2} \qquad (7f)$$

Equation (7e) provides a means for determining the Δ_j(that is G_j). The first thought for attacking this equation would be to apply the techniques of Fourier series. Such an approach, if possible, would provide an infinite set of Δ_j while satisfying Equation (7e) at all points along the boundary (that is all $0° \leq \theta \leq 30°$). Unfortunately the nature of Equation (7e) precludes the use of

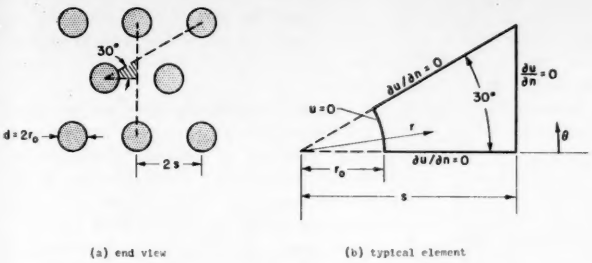

Fig. 3. Diagram of equilateral triangular array.

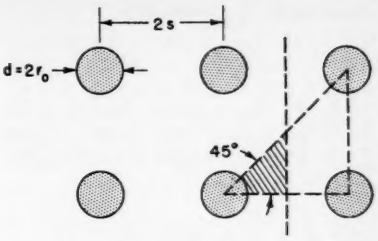

Fig. 4. Diagram of square array.

Fourier analysis, and some other approach must be found for solving for the Δ_j.

The method used here is to apply Equations (7*e*) at a finite number of points along the boundary. Suppose for example that one successively evaluates Equation (7*e*) at six values of θ between 0 and 30°. This will provide six equations. If one truncates the series after six terms (that is $l = 6$), then there are sufficient simultaneous equations to evaluate the coefficients $\Delta_1, \Delta_2 \cdots \Delta_6$. This procedure may now be repeated with the use of seven boundary points and seven series coefficients, and so forth. The sets of coefficients Δ_j from these repeated calculations were compared. It was immediately seen that adding additional terms to the series did not significantly affect the numerical values of the first few coefficients. Further it was found that only these first coefficients are important in the computation of the shear stress and velocity distribution. In view of these favorable circumstances the method presented here for determining the Δ_j appears quite adequate.

Numerical values of Δ_j, computed as outlined above, have been listed in Table 1. Inasmuch as the ratio s/r_0 (half spacing to rod radius) appears in Equations (7*e*), so does it appear as a parameter of Table 1. It is noted that for large spacings (that is large s/r_0) the Δ_j are little affected by increases of spacing, as might have been expected since s/r_0 is raised to a large negative power in Equation (7*e*). The tabulation is given to four decimal places because this is sufficient for the shear stress and velocity computations.*

So with the determination of the Δ_j (that is, G_j) one may return to Equation (9) and state that the velocity distribution for the triangular array is now available. In a later section the authors will make use of this velocity solution to compute several quantities of engineering interest. But first they will solve for the velocity distribution associated with flow between rods in square array.

Cylinders in Square Array

An end view of the configuration for flow between cylinders in square array is shown schematically in Figure 4. Because of symmetry considerations attention is confined to the cross-hatched element of the sketch. This element has essentially the same form as that shown in Figure 3*b*, except that now the opening angle is 45 deg. rather than 30 deg. as before.

The velocity solution as given by Equations (6) applies, and one now has to find the constants A, B, $\cdots$ appropriate to the square array. The procedure is identical to that followed in the preceding section for the triangular array. From the conditions that $\partial u/\partial n = \partial u/\partial\theta = 0$ at $\theta = 0$ deg. and $\theta = 45$ deg., there is obtained, respectively

$$F_k \equiv 0 \qquad (10a)$$

and

$$k = 4, 8, 12 \cdots \qquad (10b)$$

Imposing the requirement that $u = 0$ at $r = r_0$ gives

$$D_k = -C_k {r_0}^{2k},$$

$$A = -B \ln r_0 + \frac{{r_0}^2}{4}\left(-\frac{1}{\mu}\frac{dp}{dz}\right) \qquad (10c)$$

while the over-all force balance between net pressure and wall shear, Equation (8) with $\pi/6$ replaced by $\pi/4$, provides the following value of B:

$$B = \frac{2}{\pi} s^2 \left(-\frac{1}{\mu}\frac{dp}{dz}\right) \qquad (10d)$$

Introducing these findings into (6) results in the following equation for the velocity:

$$u = \frac{2}{\pi} s^2 \left(-\frac{1}{\mu}\frac{dp}{dz}\right) \ln \frac{r}{r_0} - \frac{1}{4}\left(-\frac{1}{\mu}\frac{dp}{dz}\right)(r^2 - {r_0}^2) + \sum_{i=1}^{l} G_i \left(r^{4j} - \frac{{r_0}^{8j}}{r^{4j}}\right) \cos 4j\theta \qquad (11)$$

where the G_j $(= C_j E_j)$ still remain to be determined. The condition that $\partial u/\partial n = 0$ on the right-hand boundary of Figure 3*b*, on which $r = s/\cos\theta$, may be used. The procedure for determining the G_j follows along the lines previously discussed. For several values of θ between

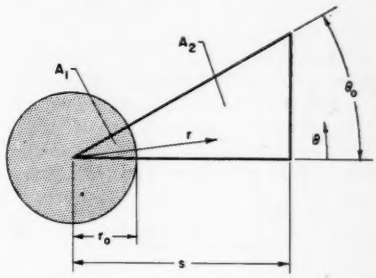

Fig. 5. Diagram for pressure-drop and friction-factor derivation.

0 and 45 deg. one successively applies the condition of zero normal derivative; that is

$$\sum_{j=1}^{l} \delta_j (\cos\theta)^{1-4j}\left[\cos(4j-1)\theta + \left(\frac{r_0 \cos\theta}{s}\right)^{8j} \cos(4j+1)\theta\right] + \frac{2\cos^2\theta}{\pi} - \frac{1}{2} = 0 \qquad (12a)$$

where

$$\delta_j = G_j \frac{4j\, s^{4j}}{\left(-\frac{1}{\mu}\frac{dp}{dz}\right)s^2} \qquad (12b)$$

The result is l simultaneous equations for $\delta_1, \delta_2 \cdots \delta_l$. Sufficient terms are retained in the series to assure good accuracy in shear-stress and velocity-distribution calculations. Numerical values of the δ_j obtained in this manner are listed in Table 1 as a function of s/r_0.

So with the determination of the δ_j (that is G_j) the velocity solution for the square array, Equation (11), can be regarded as known, and one can pass on to the presentation of results of engineering interest.

RESULTS

Attention will first be focused on the pressure drop-flow relationship, which is generally the result of greatest practical importance. Then this information will be rephrased in terms of the friction factor and Reynolds number. Finally plots will be given of velocity contours and also of the distribution of the wall shear stress around the periphery of a rod.

*Additional figures were used in satisfying Equation (7*e*).

Pressure-Drop–Flow Relationship

First the volume rate of flow Q which may be calculated by integrating the velocity over the flow area is introduced. As before, only a typical element of the flow configuration need be used (Figure 5). In terms of symbols given there the integral for Q becomes

$$Q = \int\int_{A_2} ur\,dr\,d\theta = \int_0^{\theta_0}\int_{r_0}^{s/\cos\theta} ur\,dr\,d\theta \tag{13}$$

In evaluating Equation (13) one introduces u from either Equations (9) or (11) depending whether a triangular or square array is being considered. As is shown in the Appendix the end result of inserting the velocity expressions takes the form

$$Q = \left(-\frac{dp}{dz}\right)\frac{r_0^4}{\mu}\cdot\text{function}\,(s/r_0) \tag{14}$$

or

$$-\frac{dp}{dz} = \frac{Q\mu}{r_0^4}\cdot\frac{1}{\text{function}\,(s/r_0)} \tag{14a}$$

The function of s/r_0 is different for each array and has been computed by the use of the integrals given in the Appendix.

Before numerical results are discussed, an important fact may be drawn from Equation (14a): for a given array with fixed-rod diameter and spacing (that is, fixed configuration) the pressure drop is directly proportional to flow rate. This finding is in accord with previous laminar-flow analyses.

As a final prelude to presenting the pressure-drop results, the authors chose to replace the ratio s/r_0 by the more general variable, the porosity, which is the fraction of the total cross section available to flow. In terms of Figure 5 one may write

$$\epsilon \equiv \frac{A_2}{A_1 + A_2} = 1 - \frac{\theta_0}{(s/r_0)^2\tan\theta_0} \tag{15}$$

where the facts that $(A_1 + A_2)$ is a right triangle and A_1 is a circular sector have been used in deriving the last expression. For the triangular array, $\theta_0 = 30$ deg., and

$$\epsilon = 1 - \frac{\sqrt{3}\pi}{6(s/r_0)^2} \tag{15a}$$

while for the square array, $\theta_0 = 45$ deg., and

$$\epsilon = 1 - \frac{\pi}{4(s/r_0)^2} \tag{15b}$$

With these expressions, plus the evaluated integrals of the Appendix, one is able to plot the pressure-drop–flow relationship as a function of porosity on Figure 6. There are several aspects of the curves worthy of discussion. First it is seen that for the same flow, r_0 and ϵ, the triangular array gives rise to a higher pressure drop. This might have been intuitively expected because each rod in the triangular array is surrounded by more neighbors and hence feels more flow disturbance than does a rod in the square array.

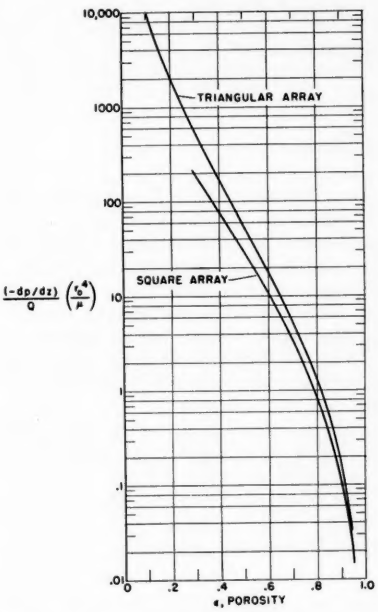

Fig. 6. Pressure-drop–flow parameter as a function of porosity.

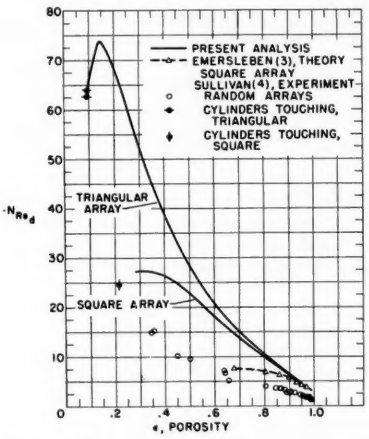

Fig. 7. Friction factor–Reynolds number as a function of porosity.

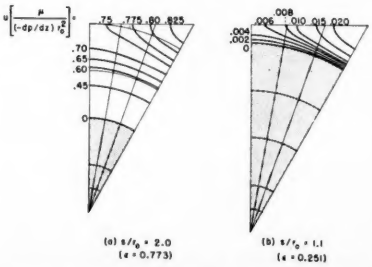

Fig. 8. Representative velocity contour lines for equilateral triangular array.

It would appear that the two curves of the figure have generally the same shape, with possibly a growing deviation at smaller values of ϵ. Consideration of the system suggests that, except for large spacings (large ϵ), similar flow performance need not necessarily be expected from the different arrays. At large spacings, where there is little effect of neighboring rods, the flow passages of the two arrays are almost geometrically similar. But at small spacings the flow passages of the two arrays are very different indeed. For the case of cylinders touching ($s/r_0 = 1$) the passages of the square array are curvilinear squares, and those of the triangular array are curvilinear triangles. One would have no reason to expect that at small spacings the curves for the two arrays should be identical in form. (These observations will have even greater meaning when the friction-factor curves are given.)

That the curves of Figure 6 should give increasing ordinate values with decreasing porosity is intuitively reasonable. If the flow and rod radius are regarded as fixed, and the porosity is decreased, this will give rise to an increase in flow velocity and a decrease in passage dimensions. Both these effects would be expected to contribute to an increase in pressure drop, and this is in accord with the findings of Figure 6.

The rod radius is used here as a characteristic dimension because it can be easily measured and identified in an experiment or application. The equivalent diameter, $\equiv \epsilon d/(1 - \epsilon)$, was also considered but not used because it is physically somewhat obscure in the present instance and did not assist in correlating the results.

Friction-Factor–Reynolds-Number Relationship

The pressure-drop information may be rephrased into a friction-factor–Reynolds-number relationship. To begin, the definition of the friction factor is

$$f \equiv \bar{\tau}\Big/\frac{\rho\bar{u}^2}{2} \tag{16}$$

The shear stress may be related to the pressure drop, dp/dz. When one refers to Figure 5, a force balance yields

$$\bar{\tau}\cdot r_0\theta_0\,dz = -dp\cdot A_2, \quad \text{or} \quad \bar{\tau} = -\frac{(dp/dz)A_2}{r_0\theta_0} \tag{17}$$

With this Equation (16) becomes

$$f = -\frac{2(dp/dz)A_2}{r_0\theta_0\rho\bar{u}^2} \tag{16a}$$

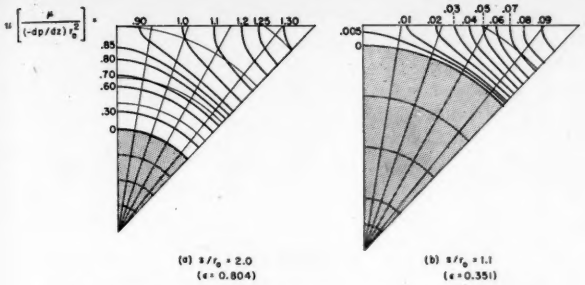

Fig. 9. Representative velocity contour lines for square array.

and, after further rearrangement

$$f \cdot N_{Re_d} = \left[\frac{r_0^4}{Q\mu}\left(-\frac{dp}{dz}\right)\right]\left[\frac{4A_2^2}{\theta_0 r_0^4}\right] \quad (16b)$$

where N_{Re_d} is based on the rod diameter $d(= 2r_0)$ and is given by

$$N_{Re_d} = \frac{d\bar{u}\rho}{\mu}$$

In writing Equation (16*b*) the authors have used the fact that $\bar{u} = Q/A_2$.

The first bracket of Equation (16*b*) is the pressure-drop–flow ratio, which for a given array has been previously shown to depend only on the porosity. The second bracket is purely geometrical. When one uses the definition of ϵ, Equation (15), in conjunction with the geometry of Figure 5, it is easy to show that for a given array the second bracket also is a function of porosity alone.

The friction-factor–Reynolds-number relationship has been computed for each array from Equation (16*b*), and the results are plotted on Figure 7 as a function of porosity. The curve representing the triangular array lies higher than that for the square array, but intuitive interpretation is not easy because, in addition to the pressure drop, complicated geometrical factors enter into the friction factor. For low porosities it would appear that the curves for the two arrays are not completely similar in shape, but, as previously discussed, similarity is not to be expected in the low-porosity range.

For high values of porosity it is possible to find a very accurate analytical representation of the friction-factor results. Under these conditions, where the rods are relatively wide apart, the velocity distribution around any one rod depends very little on the angular position. So the velocity can be accurately represented by the first two terms of Equations (9) and (11). The friction-factor–Reynolds-number relationship corresponding to both these abbreviated velocity expressions is

$$f \cdot N_{Re_d} = \frac{8(1-\epsilon^*)^2}{2\epsilon^* - \ln \epsilon^* - (\epsilon^*)^2/2 - 1.5} \quad (18)$$

where $\epsilon^* = 1 - \epsilon$.

By the comparison of the predictions of this relation with Figure 7 (which is based on the more complete velocity solution) it is found that Equation (18) is an excellent representation of the results for the conditions

$\epsilon > 0.80$, triangular array

$\epsilon > 0.90$, square array

In addition to the curves of the present analysis, Figure 7 also includes the results of related work. The analysis of Emersleben, represented by the triangles* and the dashed line, was carried out for the square array with complex zeta functions used. The nature of his solution is such that it can be valid only for large values of ϵ, but heretofore the actual range of validity has not been known. Inspection of Figure 7 shows that Emersleben's results are in close agreement with those of the current work for $\epsilon > 0.9$, and this may be taken to define the limit of validity of his analysis.

Sullivan's experiments were carried out with parallel-oriented filaments of goat's wool, blond hair, Chinese hair, glass wool, copper wire, and segments of drill rod. Each of these materials was used separately. The tests utilizing the drill rods corresponded to the situation of cylinders touching, and the associated data points are shown as black circles in Figure 7. For the triangular array these data are in excellent agreement with the present predictions and thereby provide support for the theory. For the square array the theory was not carried out for the situation of cylinders touching because of the relatively slower convergence of the truncated series. However inspection of Figure 7 leads to the belief that good agreement would also be obtained for this case. For the other tests (aside from those with the drill rods) the filaments were inserted in a tube in an array which was presumably random. Hence the experimental conditions corresponded to neither of the two regular arrays studied here. The data, shown as open circles in Figure 7, generally fall below the analytical curves. It is especially interesting that the data continue to fall substantially lower than

*The points shown on Figure 7 are those reported by Carman (*2*).

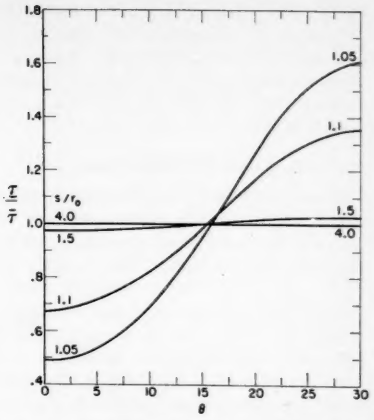

Fig. 10. Local wall shear-stress distribution for equilateral triangular array.

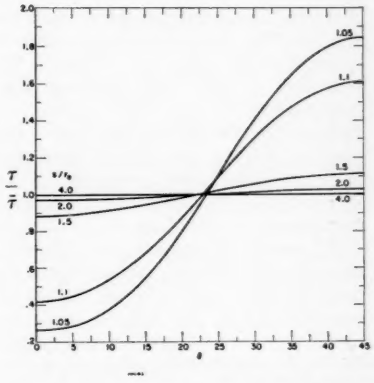

Fig. 11. Local wall shear-stress distribution for square array.

theory even for $\epsilon > 0.9$, where the relatively large spacing essentially removes the effect of rod orientation. This suggests the possibility of a shortcoming in the experimental apparatus, the most likely of which would be that the cylindrical filaments were not tightly packed against the wall of the bounding tube. Such an occurrence would lead to relatively large, open flow areas near walls and a consequent decrease in pressure drop and friction factor.

Velocity Contours

The distribution of the velocity may also be of some interest. The authors have confined themselves to representative situations, selecting results for a spacing ratio s/r_0 of 1.1 to represent close packings and those for a ratio 2.0 to represent open packings. Dimensionless velocity contours (lines of constant velocity) are plotted on Figure 8 for the triangular array for a typical flow element. Inspection of Figure 8*a* (relatively large spacing) reveals that the velocity contours are essentially circular for a sizable region near the rod surface, an indication that the neighboring rods have little effect there. In Figure 8*b*,

where the spacing has decreased, the influence of the neighbors extends to regions very near the rod surface. Similar findings may be observed on the velocity contours of Figures 9*a* and *b* for the square array.

Variation of Local Wall Shear Stress

Since the velocity distribution around a rod varies with angular position, so also will the local shear stress exerted by the wall on the fluid. The manner in which the shear stress varies is shown respectively on Figures 10 and 11 for the triangular and square arrays. Using symmetry considerations as before one need consider only the typical elements which are shown cross hatched in Figures 3 and 4.

The curves of Figures 10 and 11 graphically illustrate the role of neighboring rods on the flow pattern around a given rod. For large spacings, for example $s/r_0 = 4.0$, the local shear stress is essentially a constant around the periphery of the rod, showing that neighbors have little effect on the flow pattern. As the spacing decreases, the angular dependence of the local-wall shear stress increases, testifying to the increasing asymmetry of the flow due to interference of neighbors.

As would be expected on physical grounds the highest shear stress is associated with the location of highest velocities ($\theta = 30$ and 45 deg., respectively), and the smallest shear stress is at the location of lowest velocity ($\theta = 0$ deg.).

CONCLUDING REMARKS

In the investigation reported here the analytical procedure based on truncated trigonometric series has been applied to symmetrical arrays such as the square and the equilateral triangle. However the same methods can be applied with no essential modification to unsymmetrical arrangements, examples of which are the rectangular and the isosceles triangular with various apex angles.

APPENDIX

Integration to Compute Flow Rate

Equation (13) is the integral for the volume flow. For purposes of illustration attention is focused on the square array; the result for triangular array will be given later.

The expression for the velocity for the square array is given by Equation (11). The G_j are related to the tabulated constants δ_j (Table 1) by

$$G_j = \delta_j \frac{(-dp/dz)s^2}{4j\mu s^{4j}} \qquad \text{(A1)}$$

For purpose of integration the dimensionless variable

$$\zeta = r/r_0 \qquad \text{(A2)}$$

is introduced. Then substituting Equations (11), (A1), and (A2) into the flow-rate integral (13), one gets

$$Q = \left(-\frac{dp}{dz}\right)\frac{r_0^4}{\mu}\left\{\int_0^{\pi/4}\int_1^{s/r_0\cos\theta} \cdot\left[\frac{2}{\pi}\left(\frac{s}{r_0}\right)^2 \ln\zeta - \frac{1}{4}(\zeta^2-1) + \sum_{j=1}^{l}\frac{\delta_j(r_0/s)^{4j-2}}{4j} \cdot(\zeta^{4j} - \zeta^{-8j})\cos 4j\theta\right]\zeta\, d\zeta\, d\theta\right\} \qquad \text{(A3)}$$

where $\theta_0 = \pi/4$ has been introduced for the square array. Inspection of the contents of the brace shows that the only parameter is the ratio (s/r_0), ζ being a dummy integration variable. So the assertion of Equation (14) is shown to be correct.

The integrals appearing in Equation (A3) can be carried out in a straightforward way, giving

$$\frac{Q\mu}{(-dp/dz)r_0^4} = \left(\frac{s}{r_0}\right)^4 \cdot\left[\frac{1}{2\pi}\left(2\ln\frac{s}{r_0} + \ln 2 - 3\right) + \frac{1}{6}\right] + \left(\frac{s}{r_0}\right)^4 \sum_{j=1}^{l}\frac{\delta_j}{4j} \cdot\left[\frac{\Lambda_j}{4j+2} + \left(\frac{r_0}{s}\right)^{8j}\frac{\beta_j}{4j-2}\right] + \frac{1}{4}\left(\frac{s}{r_0}\right)^2 - \frac{\pi}{64} \qquad \text{(A4)}$$

where

$$\Lambda_j = \int_0^{\pi/4}\frac{\cos 4j\theta}{(\cos\theta)^{4j+2}}\,d\theta,$$

$$\beta_j = \int_0^{\pi/4}\frac{\cos 4j\theta}{(\cos\theta)^{2-4j}}\,d\theta$$

The definite integrals represented by Λ_j and β_j were computed numerically by the Kutta-Runge method.

For the triangular array the authors proceed as above, with the exception that the velocity is taken from Equation (9) with

$$G_j = \Delta_j \frac{(-dp/dz)s^2}{6j\mu s^{6j}} \qquad \text{(A5)}$$

The final result for the flow rate for the triangular array is

$$\frac{Q\mu}{(-dp/dz)r_0^4} = \left(\frac{s}{r_0}\right)^4\left[\frac{1}{2\pi}\left(\ln\frac{s}{r_0} - \ln\cos 30^0 - \frac{3}{2}\right) + \frac{13\sqrt{3}}{216}\right] + \left(\frac{s}{r_0}\right)^4 \sum_{j=1}^{l}\frac{\Delta_j}{6j} \cdot\left[\frac{\Omega_j}{6j+2} + \left(\frac{r_0}{s}\right)^{12j}\frac{\chi_j}{6j-2}\right] + \frac{\sqrt{3}}{12}\left(\frac{s}{r_0}\right)^2 - \frac{\pi}{96} \qquad \text{(A6)}$$

where

$$\Omega_j = \int_0^{\pi/6}\frac{\cos 6j\theta}{(\cos\theta)^{6j+2}}\,d\theta,$$

$$\chi_j = \int_0^{\pi/6}\frac{\cos 6j\theta}{(\cos\theta)^{2-6j}}\,d\theta$$

NOTATION

A,B,C,D,E,F,G = constants in velocity solution
A_1 = solid area normal to flow direction
A_2 = flow area
d = cylinder diameter, $2r_0$
f = friction factor, $2\bar{\tau}/\rho\bar{u}^2$
n = direction of the normal
N_{Re} = Reynolds number, $d\bar{u}\rho/\mu$
p = static pressure
Q = volumetric rate of flow through typical element (See Figures 3*a* and 4.)
r = radial coordinate measured from center of cylinder
r_0 = cylinder radius
s = half spacing between cylinders
u = velocity in $+z$ direction
u^* = reduced velocity defined by Equation (3)
$\bar{u}$ = mean velocity
z = longitudinal coordinate

Greek Symbols

δ_j = constants defined by Equation (12*b*)
Δ_j = constants defined by Equation (7*f*)
ϵ = porosity, $A_2/(A_1 + A_2)$
ϵ^* = solidity, $1 - \epsilon$
ρ = fluid density
θ = angular coordinate
θ_0 = angle subtended by flow element
τ = shear stress at cylinder wall
$\bar{\tau}$ = average shear stress
μ = fluid viscosity

LITERATURE CITED

1. Hawksley, P. G. W., "The Effect of Concentration on the Settling of Suspensions and Flow through Porous Media: Some Aspects of Fluid Flow," pp. 114 to 135, Edward Arnold and Co., London (1951).
1a. *Ibid.* p. 132.
2. Carman, P. C., Flow of Gases through Porous Media," Butterworth Science Publishers, London (1956).
2a. *Ibid.*, pp. 26–28.
3. Emersleben, Otto, *Physik.* Z., Bd. 26, 601 (1925).
4. Sullivan, R. R., *J. Appl. Phys.*, **13**, 725 (1942).

Manuscript received October 27, 1958; paper accepted January 21, 1959.

Some Aspects of Fluid Mechanics in Chemical Engineering

B. H. SAGE

California Institute of Technology, Pasadena, California

The prediction of the transfers of momentum, energy, and material is of ever-pressing concern to the engineer interested in process design. Recently developed facts concerning the transport of momentum which are of particular use in predicting transfers of energy and material are reviewed, as well as the background of thermodynamics associated with transport processes. The more elemental relationships pertaining to thermal and material transfer in flowing streams are considered, and some of the interrelations of the transport processes are presented.

Processes of interest in chemical engineering include the transfers of momentum, energy, and material. The science of fluid mechanics is primarily concerned with the transfer of momentum in fluid systems. Momentum by nature is a vector quantity; as a result, its proper evaluation involves more complicated mathematical concepts than are encountered in the study of transfers of the scalar quantities, energy and material. In the first third of this century the chemical engineer was concerned chiefly with the application of macroscopic concepts to the prediction of momentum, energy, and material transport in fluid systems. Such interest led to the extensive application of the principles of dimensional analysis (*20*) and to a corollary, widespread use of dimensionless parameters in the correlation of experimental data. These treatments for the most part did not take into account the intensity or scale of turbulence as it influences each of the several transport processes.

With the development of the airplane and consequent rapid advances in the science of fluid mechanics, it was found advantageous to consider momentum transport at a point in the fluid. The work of Horace Lamb and Theodore von Kármán are examples of the early application of the conservation of mass and momentum to the prediction of velocity as a function of the spatial coordinates of fluid systems. Application of such concepts of fluid mechanics, together with the conservations of energy and of matter, to the prediction of energy and material transport in fluid systems was first made by men outside the chemical engineering profession. Most chemical engineers were content until recently to consider all transport phenomena in their macroscopic aspect and treated in a simple manner the variation in molecular properties of a fluid in a conduit with respect to position at a section. These assumptions were usually adequate for the design of equipment used in the accomplishment of physical processes such as fractionation and distillation. Macroscopic methods were applicable also to the design of equipment in which fluids approached physicochemical equilibrium, or in which the approach to chemical equilibrium was sufficiently slow as to be of a time scale different from that associated with the transport processes involved.

Such macroscopic concepts, however, are inadequate for dealing with many processes of widespread and increasing interest, such as jet propulsion and industrial processes in which the exchange between the kinetic energy of a flowing stream and the internal energy of the fluid is large. It has been recognized that in fluids flowing through the nozzles of gas turbines and rocket motors (*26*) deviations from physicochemical equilibrium are often encountered. These deviations are of such a magnitude as to suggest that the process of exchange between internal and kinetic energy within a nozzle or similar device might be used to freeze chemical reactions. Such rapid changes in thermodynamic state have been applied to the manufacture of nitric oxide (*9*) and acetylene (*2, 4*), where the rapid change in internal energy is effected by thermal transfer to solid or liquid phases. It is probable that rapid cooling may be employed to advantage in the manufacture of a variety of other chemical compounds. The prediction of the momentum of reacting fluids as a function of spatial position will, it seems, be of increasing importance to the chemical engineering profession.

This discussion will outline briefly the interrelation of momentum, energy, and material transfer in fluid systems and treat briefly the effect of the level of turbulence upon such transfers. All the following equations are based on the dimensions of force, length, and time, which when taken with temperature serve as the undefined concepts sufficient to describe the phenomena. For convenience, energy is expressed in conventional units, but density has the dimensions pounds seconds squared per foot^4 and specific weight the dimensions pounds per cubic foot. The equations for the sake of simplicity apply to momentum transport in one dimension, unless otherwise noted.

TRANSFER OF MOMENTUM

In a prediction of the transfer of momentum in fluid systems an understanding of the pertinent variables is necessary. Knowledge of these variables, velocity and specific weight, as a function of the spatial coordinates of the system is sufficient to define the local values of the momentum flux. The momentum flux in the x direction can be described by

$$\mathring{M}_x = \frac{\mathring{m}_x u_x}{g} = \frac{\sigma u_x^2}{g} \qquad (1)$$

It is essential that it be possible to apply

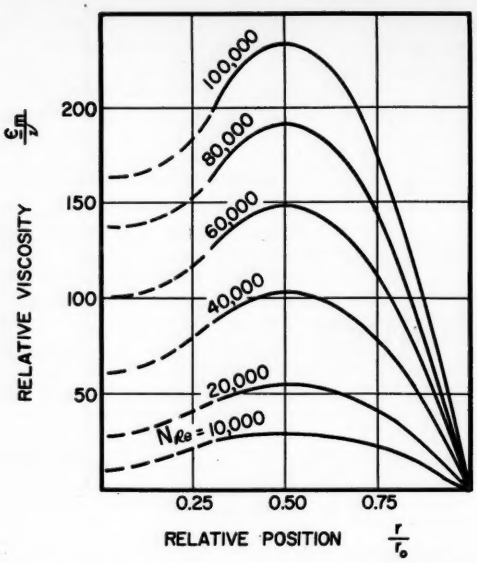

Fig. 1. Variation in eddy viscosity with position and Reynolds number for shear flow in a circular conduit.

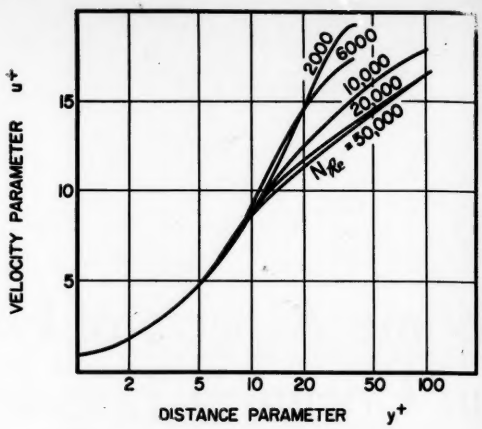

Fig. 2. Effect of distance parameter upon velocity parameter in shear flow.

to the flowing system the equation of continuity, which can be expressed for one-dimensional flow as

$$\left(\frac{\partial \sigma}{\partial \theta}\right)_x = -\left(\frac{\partial \mathring{m}_x}{\partial x}\right) = -\frac{\partial(\sigma u_x)}{\partial x} \qquad (2)$$

The subsonic flow of fluids can be described by two typical kinds of flow, laminar and turbulent. In laminar flow the velocity gradients are related to the viscosity of a Newtonian fluid by

$$\frac{du}{dy} = \frac{\tau_{yx}}{\eta} = \frac{\tau_{yx} g}{\sigma \nu} \qquad (3)$$

In this case the viscosity, which is a molecular property of the fluid, is solely a function of the thermodynamic state of a Newtonian fluid and can be determined from a knowledge of the temperature, pressure, and composition.

Transition to turbulent flow occurs when velocities increase for a given set of physical boundaries and instabilities appear. Turbulent flow can be characterized as a statistical phenomenon in which the situation at any point is random with respect to time. Application of the basic equations of fluid mechanics to turbulent flow is not very useful, except in unusually simple situations. For this reason there has been some interest in a macroscopic measure of the effects of turbulence. This involves the concept of eddy viscosity (*14*).

$$\epsilon_m = \frac{g \tau_{yx}}{\sigma\left(\frac{du_x}{dy}\right)} - \nu \qquad (4)$$

Equation (4) is different from Equation (3) because the total viscosity is the sum of the kinematic viscosity and the eddy viscosity.

$$\epsilon_m = \epsilon_m + \nu \qquad (5)$$

The eddy viscosity is a function not only of the state of the fluid but of the condition of flow at and in the vicinity of the point in question. Furthermore the eddy viscosity may not be isotropic.

One of the difficult problems associated with turbulence is the prediction of its rate of growth and decay under particular boundary conditions. This problem adds greatly to the complexity of predicting the flow pattern and the transport characteristics in turbulent flow. In addition the artificially induced turbulence associated with turbulence bars and grids in shear flow materially influences values of the eddy viscosity.

Variations in the relative viscosity ϵ_m/ν in steady, uniform, turbulent shear flow of fluids in circular conduits have been shown to be a function of the position in the channel and the Reynolds number of the flow (*24*). Such variations are illustrated in Figure 1. From experimental measurements of velocity distributions and pressure gradients values of the relative viscosity as a function of position in flow between parallel plates have been established (*23*). The velocity distribution in the turbulent boundary flow at Reynolds numbers above 20,000 can be conveniently related to the velocity parameter defined by

$$u^+ = \frac{u_x}{\sqrt{\frac{(\tau_{yx})_0 g}{\sigma}}} = K_3 + \frac{1}{K_2} \ln (y^+) = 5.5 + \frac{1}{0.4} \ln (y^+) \qquad (6)$$

The symbol $(\tau_{yx})_0$ refers to the shear at the wall of the circular conduit. It has been found that, contrary to the simple considerations of the principles of similarity (*13*), the velocity parameter u^+ is not a single-valued function of the distance parameter y^+ at transition Reynolds numbers. In this region the relationship varies decidedly with the Reynolds number (Figure 2).

The relationship between the Fanning friction factor and the position in the channel and the total viscosity ϵ_m for Reynolds numbers above 20,000 for flow between parallel plates (*7*) is given by:

$$\frac{\epsilon_m}{\nu} = \frac{\epsilon_m + \nu}{\nu} = \frac{l}{l_0} \cosh^2 \cdot \left\{0.0695 \frac{l_0 - l}{\nu} U \sqrt{\frac{f}{2}}\right\} \qquad (7)$$

for $y^+ < 27$

and

$$\frac{\epsilon_m}{\nu} = 0.4 \frac{U}{\nu} \sqrt{\frac{f}{2}} \left(\frac{l}{l_0}\right)(l_0 - l)$$

for $y^+ > 27$ to $\frac{l}{l_0} < 0.66$

The first of the expressions is applicable only in the boundary flow, whereas the second may be used throughout all but the central third of the channel.

At the present time it is difficult to predict the influence of turbulence upon nonuniform boundary flow. Application of the Blasius equation (*3*) permits ready evaluation of the velocity as a function of distance from the wall in the case of potential flow in the main stream for a flat plate. Such an approach has been expanded to include the boundary flow for cylinders (*10, 22*) and spheres (*10*). The predicted velocity distributions in the boundary flow about a 2-in. cylinder and a 2-in. sphere for an air stream velocity of 10 ft./sec. are depicted in Figures 3 and 4. The normal distance from the surface to lines of

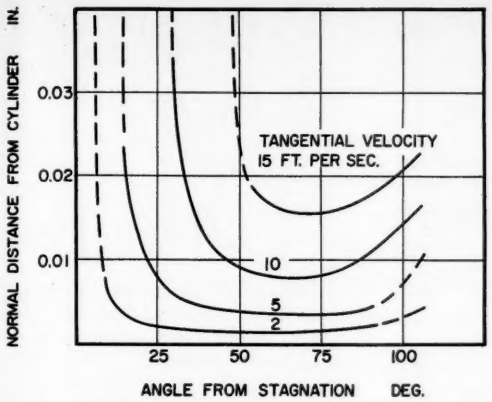

Fig. 3. Estimated velocity distribution in boundary flow about a cylinder.

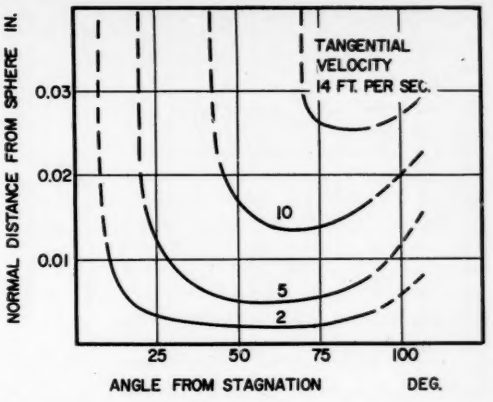

Fig. 4. Estimated velocity distribution in boundary flow about a sphere.

constant velocity is shown in the diagrams as a function of the angle measured from stagnation.

Experimental data illustrating the effect of position upon the velocity in the wake of a cylinder are shown in Figure 5 for a Reynolds number of 4,440 and a gross air velocity of 45 ft./sec. (*1*). The marked complexity in the flow patterns is evident, and furthermore the flow in the wake is distinctly turbulent. Near the point of separation of the boundary flows, as described by Equation (7), there exist regions in which vortex streets are shed from the cylinder. The existence of these vortex streets introduces periodic disturbances in the flow pattern in the wake which are of much lower frequency than the perturbations associated with the turbulent flow. It is obvious that as the scale or intensity of turbulence is increased, numerous inroads into the laminar boundary flows about cylinders and spheres are to be expected. Significant increases in the thermal and material transfer have been found to result from modifications in the level of turbulence (*5, 21*).

THERMODYNAMICS

Many of the concepts of thermodynamics, particularly those relating to the first law, are of importance in the application of fluid mechanics to problems of chemical engineering. The energy transfers to a system may be limited to heat, defined as thermal flux at the boundary, and work, defined as mechanical transfers at the boundary of the system. The defining relations for heat and work are given by

$$\underline{q} = -\int_0^{\theta}\int_0^{A} k\left(\frac{\partial T}{\partial z}\right) d\theta\, dA = m[C_p\, dT + l_p\, dP] + \sum_1^n \lambda_k\, dm_k - \underline{j} \tag{8}$$

$$\underline{w} = P\, d\underline{V} - P_a V_a\, dm - \underline{j} = mP\left[\left(\frac{\partial V}{\partial T}\right)_{P,n} dT + \left(\frac{\partial V}{\partial P}\right)_{T,n} dP\right] + \sum_1^n P\bar{V}_k\, dm_k - P_a V_a\, dm - \underline{j} \tag{9}$$

The coefficient λ_k is the coefficient of the differential change in weight of component k. It may be evaluated by methods described later in the discussion. The quantity $\underline{j}$ is an infinitesimal that takes into account the mechanical irreversibility associated with changes in total volume of the system. It is considered to be associated with the boundaries. The conservation of energy may be written as

$$d\underline{E} = \underline{q} - \underline{w} + E_a\, dm = \underline{q} - \underline{w} + \sum_1^n \bar{E}_{ka}\, dm_k \tag{10}$$

The basic expression for the first law of thermodynamics is

$$d\underline{E} = m\left[\left(\frac{\partial E}{\partial T}\right)_{P,n} dT + \left(\frac{\partial E}{\partial P}\right)_{T,n} dP\right] + \sum_1^n \bar{E}_k\, dm_k \tag{11}$$

The foregoing expressions apply to multicomponent systems of variable weight. A combination of Equations (8) to (11) gives a useful expression relating the change in state of a system to the energy transfers across its boundary:

$$\begin{aligned} d\underline{E} &= m\left[\left(\frac{\partial E}{\partial T}\right)_{P,n} dT + \left(\frac{\partial E}{\partial P}\right)_{T,n} dP\right] + \sum_1^n \bar{E}_k\, dm_k \\ &= m[C_p\, dT + l_p\, dP] + \sum_1^n \lambda_k\, dm_k - mP\left[\left(\frac{\partial V}{\partial T}\right)_{P,n} dT + \left(\frac{\partial V}{\partial P}\right)_{T,n} dP\right] - \sum_1^n (P\bar{V}_k - P_a\bar{V}_{ka})\, dm_k + \sum_1^n \bar{E}_{ka}\, dm_k \end{aligned} \tag{12}$$

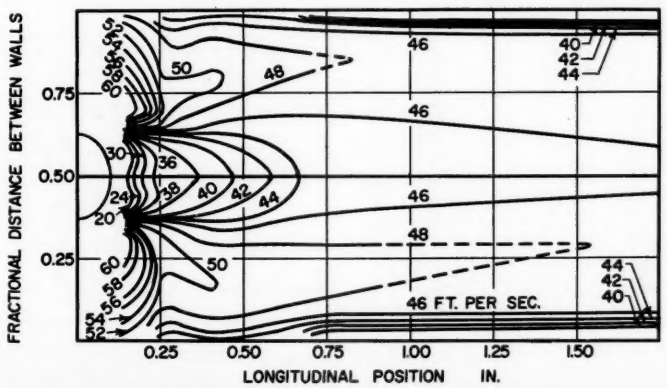

Fig. 5. Variation in velocity throughout the wake of a cylinder.

Equating coefficients one gets

$$m\left(\frac{\partial E}{\partial T}\right)_{P,n} = \left(\frac{\partial E}{\partial T}\right)_{P,m} = m\left[C_p - P\left(\frac{\partial V}{\partial T}\right)_{P,n}\right] \quad (13)$$

$$m\left(\frac{\partial E}{\partial P}\right)_{T,n} = \left(\frac{\partial E}{\partial P}\right)_{T,m} = m\left[l_p - P\left(\frac{\partial V}{\partial P}\right)_{T,n}\right] \quad (14)$$

and with the defining relationship for the partial enthalpy there results

$$\bar{E}_k - \bar{E}_{ka} = \lambda_k - (P\bar{V}_k - P_a\bar{V}_{ka}) \quad (15)$$

$$\lambda_k = \bar{H}_k - \bar{H}_{ka} \quad (16)$$

$$C_p = \left(\frac{\partial E}{\partial T}\right)_{P,n} + P\left(\frac{\partial V}{\partial T}\right)_{P,n} = \left(\frac{\partial H}{\partial T}\right)_{P,n} \quad (17)$$

$$l_p = \left(\frac{\partial E}{\partial P}\right)_{T,n} + P\left(\frac{\partial V}{\partial P}\right)_{T,n} = -T\left(\frac{\partial V}{\partial T}\right)_{P,n} \quad (18)$$

Equation (16) and the first equalities of Equations (17) and (18) serve as defining relations for the coefficients of change in weight, pressure, and temperature. The second equality of Equation (18) results from application of the test for exactness to relations involving both the first and second laws. Equation (8) serves as a direct and simple means of evaluating the thermal transfers to a system. The corresponding expressions for the second law, when one assumes an identity between the thermodynamic temperature and the absolute temperature, are

$$d\underline{S} = \frac{\underline{q} + \underline{j}}{T} - \frac{1}{T}\sum_1^n \lambda_k\, dm_k + \sum_1^n \bar{S}_{ka}\, dm_k \quad (19)$$

$$d\underline{S} = m\left[\left(\frac{\partial S}{\partial T}\right)_{P,n} dT + \left(\frac{\partial S}{\partial P}\right)_{T,n} dP\right] + \sum_1^n \bar{S}_k\, dm_k \quad (20)$$

The following coefficients may be defined in terms of the second law. The corresponding first-law evaluations are included.

$$C_p = T\left(\frac{\partial S}{\partial T}\right)_{P,n} dT = \left(\frac{\partial H}{\partial T}\right)_{P,n} \quad (21)$$

$$l_p = T\left(\frac{\partial S}{\partial P}\right)_{T,n} = -T\left(\frac{\partial V}{\partial T}\right)_{P,n} \quad (22)$$

$$\bar{S}_k = \left(\frac{\partial \underline{S}}{\partial m_k}\right)_{T,P,m_i} \quad (23)$$

The second equalities in Equations (21) and (22) are derived from simultaneous application of the first and second laws or from the first law alone. There is no expression for the coefficient for the change in entropy with respect to composition. There exists no equivalent to the conservation of energy, and a combination of Equations (19) and (20) does not lead to anything as useful as Equation (12).

From some of the concepts of irreversible thermodynamics it may be readily shown that the existence of shear, transfer of energy, and the transfer of material each results in an entropy source

$$\overset{\circ}{\sigma}_{S,V} = \frac{1}{T}\cdot\tau\cdot\left(\frac{\partial u}{\partial y}\right) = \frac{\eta}{T}\left(\frac{\partial u}{\partial y}\right)^2 = J_x X_x \quad (24)$$

$$\overset{\circ}{\sigma}_{S,V} = -\frac{\overset{\circ}{q}}{T}\left(\frac{\partial \ln T}{\partial x}\right) = k\left(\frac{\partial \ln T}{\partial x}\right)^2 = J_x X_x = \left[k\left(\frac{\partial \ln T}{\partial x}\right)\right]\left[\frac{\partial \ln T}{\partial x}\right] \quad (25)$$

$$\overset{\circ}{\sigma}_{S,V} = -\sum_1^n \frac{\overset{\circ}{m}_k}{T}\left(\frac{\partial \mu_k}{\partial x}\right)_{T,P} = \sum_1^n \frac{D_{\mu,k}}{T}\left(\frac{\partial \mu_k}{\partial x}\right)^2 = \sum_1^n J_{x,k}X_{x,k} = -\sum_1^n [\overset{\circ}{m}_k]\left[\frac{1}{T}\left(\frac{\partial \mu_x}{\partial x}\right)_{T,P}\right] \quad (26)$$

These expressions are limited to a steady uniform one-dimensional transfer of momentum, energy, and material under nonturbulent conditions. The third equality of the first line of Equation (26), $\sum_1^n (D_{\mu,k}/T)\,(\partial\mu_k/\partial x)^2$, involves a frame of reference moving with a velocity equal to that of the system. It may be readily shown that the velocity of the system does not in itself contribute to the entropy production. The dissipative functions of Equations (24) through (26) indicate some of the ways by which the entropy of a system is increased as a result of momentum, thermal, and material transfers. The Onsager reciprocity relationships afford a simple linear approximation to the interrelation between fluxes, and these relationships can be employed with confidence at states near equilibrium but are not thought to apply with accuracy at steady states remote from equilibrium. Furthermore the concepts of irreversible thermodynamics have not been extended yet to transient processes and therefore are not directly applicable to local turbulent transport or to reaction kinetics in a turbulently flowing medium.

THERMAL TRANSFER

The macroscopic aspects of thermal transfer are well known and are not reviewed in this discussion. The prediction of convective thermal transfer from a macroscopic standpoint has not been so satisfactory as the prediction of the transport of momentum. In the case of molecular transport and in situations involving laminar flow the basic concepts of thermal transfer are well established and can be applied within the limits of

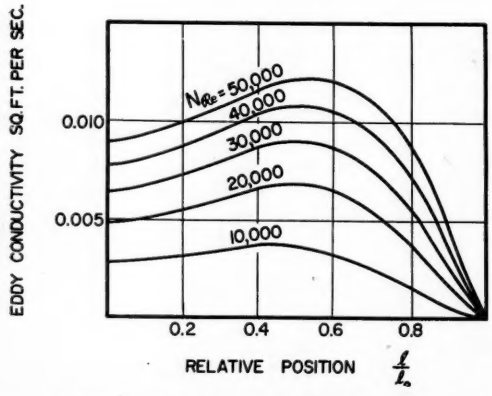

Fig. 6. Variation of eddy conductivity with position and Reynolds number for flow between parallel plates.

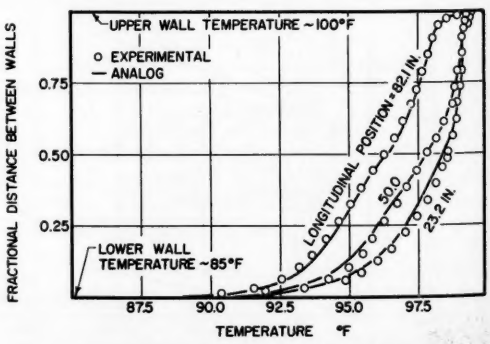

Fig. 7. Temperature distribution in turbulent flow between parallel plates for a gross velocity of 30 ft./sec.

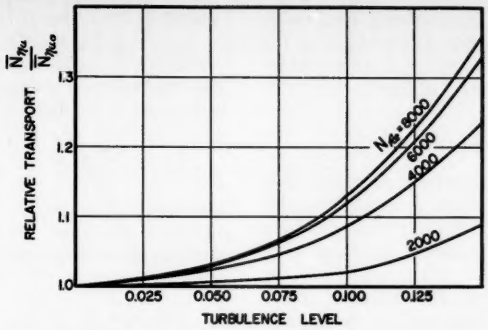

Fig. 8. Effect of turbulence level upon macroscopic thermal transfer.

the solution of the applicable differential equation.

The following equations represent approximations of the actual situation and neglect the differences between the normal-stress tensor and the pressure. For many purposes they prove to be a useful approximation, but care should be exercised in their application to situations where marked divergences between the pressure and the normal-stress tensor exist. In one-dimensional transport with laminar flow the transport of energy at a section may be described by

$$\mathring{\mathcal{E}} = \mathring{m}\left(H + h + \frac{u^2}{2g}\right) - k\left(\frac{\partial t}{\partial x}\right) \quad (27)$$

If potential and kinetic energy are neglected, Equation (27) reduces to

$$\mathring{\mathcal{E}} = \mathring{m}H - k\left(\frac{\partial t}{\partial x}\right) = \sigma u H - k\,\frac{\partial t}{\partial x} \quad (28)$$

The conservation of energy may be written in the following form if the thermal conductivity is considered a constant:

$$\frac{\partial \sigma \mathcal{E}}{\partial \theta} = -\frac{\partial(\sigma u H)}{\partial x} + k\,\frac{\partial^2 t}{\partial x^2} \quad (29)$$

If thermal transfer by diffusion takes place in two dimensions, Equation (29) may be written for steady, uniform, laminar flow in one dimension as

$$k\left(\frac{\partial^2 t}{\partial y^2}\right) = -k\left(\frac{\partial^2 t}{\partial x^2}\right) + \sigma u_x \frac{\partial H}{\partial x} \quad (30)$$

As a matter of interest the exact form of Equation (30) may be shown to be

$$\sigma u_x \frac{\partial H}{\partial x} - u_x \frac{\partial P}{\partial x} = k\left[\frac{\partial^2 t}{\partial x^2} + \frac{\partial^2 t}{\partial y^2}\right] + \Phi \quad (31)$$

It should be noted that Equation (31) contains the dissipation function Φ and the term $-u_x\,(\partial P/\partial x)$, which in part compensate each other; thus their omission from Equation (30) does not introduce as large an error as would the omission of only one of the terms. In many situations it is advantageous to consider the internal energy rather than the enthalpy, particularly when marked digression between the normal-stress tensor and the pressure exists.

Equation (30) assumes the following form for cases in which the fluid follows the equation of state of a perfect gas or of a liquid in which the enthalpy is only a function of temperature:

$$k\left(\frac{\partial^2 t}{\partial y^2}\right) = -k\left(\frac{\partial^2 t}{\partial x^2}\right) + \sigma u_x C_p \frac{\partial t}{\partial x} \quad (32)$$

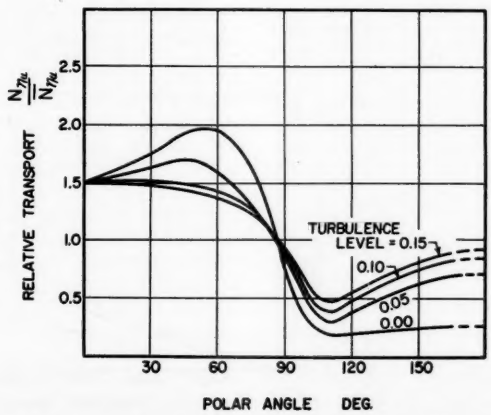

Fig. 9. Effect of turbulence level upon local thermal transfer at an air velocity of 16 ft./sec.

In Equation (32), it is assumed that the transfer of momentum in the system is both steady and uniform.

In the case of turbulent flow use of only the molecular properties of the fluid to describe its local thermal-transport characteristics is not sufficient, and it is necessary to consider eddy conductivity. Figure 6 shows the variation in eddy conductivity with position and Reynolds number during steady uniform flow between parallel plates. The eddy conductivity possesses the same dimensions as the thermometric conductivity and the kinematic viscosity. For turbulent conditions of flow Equation (32) can be rewritten as

$$\frac{\partial}{\partial y}\left[(\epsilon_c)_y \frac{\partial t}{\partial y}\right] = -\frac{\partial}{\partial x}\left[(\epsilon_c)_x\left(\frac{\partial t}{\partial x}\right)\right] + u_x \frac{\partial t}{\partial x} \quad (33)$$

In Equation (33) it was not assumed that the eddy conductivity was isotropic, and if the Reynolds analogy possesses even qualitative significance, the recent work by Laufer (*16*) would indicate that the eddy conductivity may differ significantly in the longitudinal and normal modes. The importance of the difference between the longitudinal and transverse values of the eddy conductivity is probably of greatest magnitude in the transition region of the boundary flow. In any consideration of the local conditions in turbulent flow the nature of the fluctuations in temperature with time at a given point in the flowing stream becomes important. It is beyond the scope of this paper to discuss the interrelations of the local fluctuations in temperature and velocity. Nevertheless the influence of turbulence upon the transport is in a large measure influenced by the relative magnitudes of these two fluctuations.

Figure 7 illustrates an application of Equation (33) to the prediction of temperature distribution in two-dimensional turbulent flow between parallel plates. In this instance the temperature along one boundary undergoes an abrupt change from 100° to 85°F. and effects a marked change in the temperature distribution within the stream.

If Equation (30) is written for the two-dimensional laminar flow of a reacting system, the following equation is obtained:

$$\frac{\partial \sigma \mathcal{E}}{\partial \theta} = \mathring{r}\sigma(\Delta E_c) - \frac{\partial(\sigma u_x H)}{\partial x} + k\,\frac{\partial^2 t}{\partial x^2} - \frac{\partial(\sigma u_y H)}{\partial y} + k\,\frac{\partial^2 t}{\partial y^2} \quad (34)$$

In Equation (34) the reaction rate per unit weight of system $\mathring{r}$ is markedly a function of the state of the system, and its evaluation may not be a simple matter.

Effect of Level of Turbulence

The foregoing discussion is related to thermal transfer in shear flow. Recently the influence of level of turbulence upon thermal and material transport has been investigated, and studies have been made by Sherwood (*19*), Kestin (*15*), Sato (*21*), Short (*25*), and Brown (*5*).

Level of turbulence in the x direction can be conveniently defined as

$$\alpha_r = \frac{\sqrt{\overline{u_{xf}^2}}}{U} \tag{35}$$

In most situations the turbulence is not isotropic. Figure 8 shows the influence of level of turbulence upon thermal transfer from a 0.5-in. silver sphere. It is apparent that the effect is not nearly so great at the lower Reynolds numbers as at the higher ones. The ordinate in Figure 8 is the ratio of the average Nusselt number for the entire sphere at the indicated level of turbulence and at constant Reynolds number to the same Nusselt number at zero level of turbulence. In some instances there is as much as 40% increase in the thermal transfer with an increase in the level of turbulence to 0.15. The variation in the local transport around a sphere has been studied by Cary (*6*), Lautman and Droege (*17*), and Hsu (*11*). In Figure 9 the ordinate is the ratio of the local Nusselt number to the average Nusselt number for the entire sphere for the conditions of flow in question. The data shown in Figure 9 were obtained with a 0.5-in. silver sphere and at an air velocity of 16 ft./sec. It is apparent that there exists a nearly fivefold variation in the local Nusselt number with variation in the angle from 0 to 180 deg. as measured from stagnation. It is not clear from the experimental data available whether or not the local transport is in fact a continuous function or whether at the point of separation there exists a discontinuous increase in the Nusselt number. The location of the discontinuity, if it exists, is undoubtedly a statistical function of time.

MATERIAL TRANSPORT

In considering material transport it is necessary to take into account the molecular transport resulting from diffusion and the gross transport resulting from the velocity of the phase relative to the frame of reference. The transport of one component by diffusion can be directly related to the concentration gradient of that component and the Fick diffusion coefficient, if the influence of other fields, such as temperature and the gradients of other components, is neglected. To make the presentation relatively straightforward, the influence of other fields is neglected in the following discussion. As a matter of interest the variation in the Fick diffusion coefficient of methane with the molecular weight of various paraffinic stagnant components is shown in Figure 10. A nearly thirtyfold variation in the Fick diffusion coefficient occurs in passing from a stagnant component, such as propane, to a relatively heavy oil.

Laminar Flow

The material transport of component k can be established from

$$\mathring{m}_{k,x} = \sigma_k u - D_{Fk}\frac{\partial \sigma_k}{\partial x} \tag{36}$$

From the conservation of material as applied to component k there follows, when D_{Fk} is assumed to be a constant,

$$\frac{\partial \sigma_k}{\partial \theta} = -\frac{\partial \mathring{m}_k}{\partial x} = -\frac{\partial \sigma_k u}{\partial x} + D_{Fk}\frac{\partial^2 \sigma_k}{\partial x^2} \tag{37}$$

Equations (36) and (37) are restricted to the one-dimensional transport of component k. In the case of the steady state transport of component k in two dimensions it follows that

$$\frac{\partial \mathring{m}_{kx}}{\partial x} = -\frac{\partial \mathring{m}_{ky}}{\partial y} \tag{38}$$

Combining Equations (37) and (38), neglecting all gross motions in the y direction other than those introduced by diffusion, and remembering that

$$\sum_1^n D_{Fk}\left(\frac{\partial \sigma_k}{\partial x}\right) = 0,$$

one gets

$$\mathring{m}_{ky} = -\left(1 + \frac{\sigma_k}{\sigma_i}\right) D_{Fk}\left(\frac{\partial \sigma_k}{\partial y}\right) - \frac{\sigma_k}{\sigma_i} D_{Fi}\frac{\partial \sigma_i}{\partial x} - \frac{\sigma_k}{\sigma_i} D_{Fk}\frac{\partial \sigma_k}{\partial x} \tag{39}$$

The last two terms in Equation (39) arise from consideration of two-dimensional diffusion. When one neglects those two terms, a combination of Equation (39) with Equations (36) and (38) results for steady conditions in

$$\frac{\partial \sigma_k u}{\partial x} - D_{Fk}\left(\frac{\partial^2 \sigma_k}{\partial x^2}\right) = D_{Fk}\frac{\partial}{\partial y}\left[\left(1 + \frac{\sigma_k}{\sigma_i}\right)\left(\frac{\partial \sigma_k}{\partial y}\right)\right] \tag{40}$$

Equation (40) may be solved by a number of the standard methods for solution of partial differential equations, for example that proposed by Longwell (*18*). Some simplifications are usually required.

Turbulent Flow

In the case of turbulent flow the total diffusivity is substituted for the Fick diffusion coefficient, and Equation (40) becomes

$$\frac{\partial \sigma_k u}{\partial x} - \frac{\partial}{\partial x}\left[(\epsilon_{dk})_x \frac{\partial \sigma_k}{\partial x}\right] = \frac{\partial}{\partial y}\left[(\epsilon_{dk})_y\left(1 + \frac{\sigma_k}{\sigma_i}\right)\left(\frac{\partial \sigma_k}{\partial y}\right)\right] \tag{41}$$

In this instance, since the total eddy diffusivity is distinctly a function of

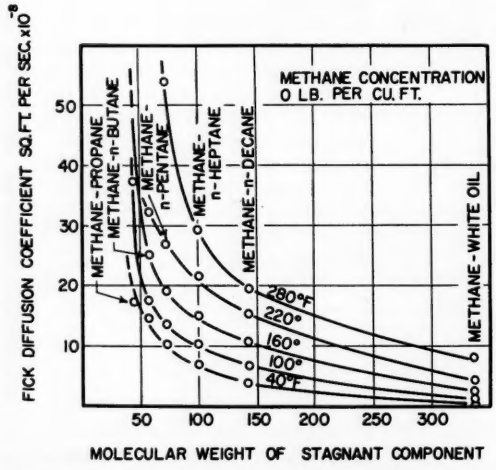

Fig. 10. Variation in Fick diffusion coefficient for methane with molecular weight of the paraffinic stagnant component.

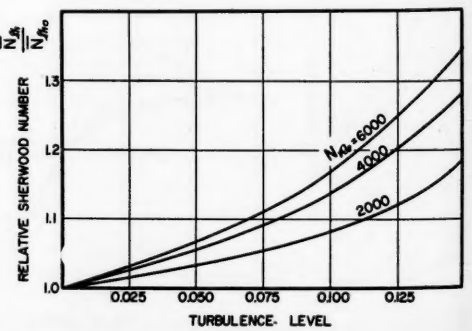

Fig. 11. Effect of level of turbulence upon macroscopic material transfer.

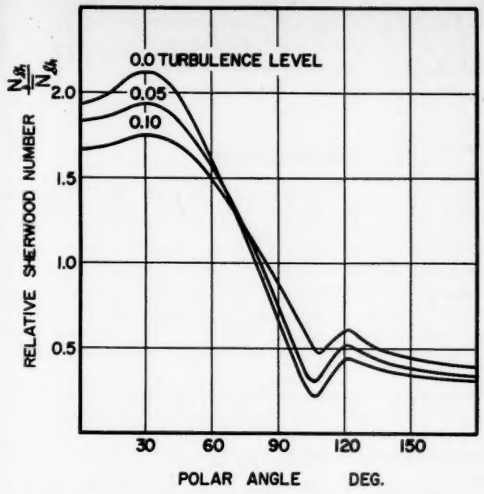

Fig. 12. Effect of level of turbulence upon local material transfer at an air velocity of 16 ft./sec.

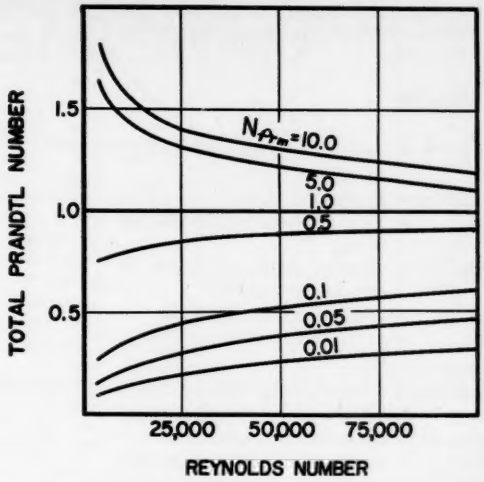

Fig. 13. Effect of Reynolds number upon total Prandtl number.

position in the flowing stream and may not be isotropic, it has been kept within the partial differential rather than being removed from it, as was done in the case of the Fick diffusion coefficient in Equation (40). It is apparent that if the variation in velocity with respect to the x direction is neglected, Equation (41) is analogous to Equation (33).

Effect of Level of Turbulence

From the earlier consideration of the influence of level of turbulence as defined by Equation (35), material transport would be expected to be markedly influenced by the level of turbulence. Figure 11 illustrates the variation in the average Sherwood number with level of turbulence for several different Reynolds numbers. Again it is seen that there is approximately a 35 % increase in the material transfer with an increase in the level of turbulence to about 0.15; again the effect is much more pronounced at the higher Reynolds numbers. The data for Figure 11 are based upon evaporation from 0.5-in. porous spheres (*5*).

The corresponding local material transport from spheres as determined from the local thermal transfer to the surface is presented in Figure 12. There exists nearly a fivefold variation in the local transport with polar angle measured from the stagnation point. The influence of the level of turbulence upon the distribution of material transport is significant. Again it is possible that there is a discontinuous change in the rate of material transfer at the point of separation, and the polar angle corresponding to this separation probably varies statistically with respect to time. The values shown in Figure 12 do not take into account the thermal conduction within the sphere which may have influenced the results slightly. It should be recognized that there exist significant local fluctuations in the concentration of the diffusing component in turbulent flow. The interrelation of these fluctuations with the local fluctuations in velocity is a complicated matter and is not fully understood at present. It is beyond the scope of this paper to consider the nature of these fluctuations, although they undoubtedly control the effectiveness of turbulent transport.

Analogies between Momentum, Thermal, and Material Transport

The conventional Reynolds analogy assumes that transport in turbulent flow is identical for momentum, internal energy, and material. From this assumption it follows that

$$\epsilon_m = \epsilon_e = \epsilon_d \tag{42}$$

In this situation the total viscosity, conductivity, and diffusivity are related to the kinematic viscosity, thermometric conductivity, and Fick diffusion coefficient by

$$\mathfrak{e}_m = \epsilon_m + \nu \tag{43}$$

$$\mathfrak{e}_e = \epsilon_e + \mathrm{K} \tag{44}$$

$$(\mathfrak{e}_d)_k = (\epsilon_d)_k + D_{Fk} \tag{45}$$

Recently Corcoran and Sage (*8*), utilizing some of the ideas of Jenkins (*12*), showed that there is a relatively small variation in the total Prandtl number with Reynolds number. With this in view it might be possible to describe another type of limiting analogy:

$$\phi\left(N_{Re}, \frac{r}{r_0}\right) \approx \frac{(\mathfrak{e}_m)_y}{\nu} = \frac{(\epsilon_m)_y + \nu}{\nu}$$

$$\approx \frac{(\mathfrak{e}_e)_y}{\mathrm{K}} = \frac{(\epsilon_e)_y + \mathrm{K}}{\mathrm{K}} \tag{46}$$

$$\approx \left|^n_1 \frac{(\mathfrak{e}_d)_k}{D_{Fk}} = \left|^n_1 \frac{(\epsilon_d)_k + D_{Fk}}{D_{Fk}}\right.\right.$$

The function of Reynolds number and position in the stream is the same as that shown in Figure 1. Equation (46) is equivalent to the assumption that the turbulent Prandtl and Schmidt numbers are identical with the molecular Prandtl and Schmidt numbers and that in the end all transport is dependent upon molecular processes. It is well known that the Reynolds analogy is not true, and it is equally probable that the analogy set forth by Equation (46) is not true. At relatively low Reynolds numbers, however, and for fluids which possess Prandtl numbers that are not far different from unity, it is probable that Equation (46), which is the equivalent of

$$\underline{N}_{Pr} = N_{Pr} \tag{47}$$

$$\underline{N}_{Sc} = N_{Sc} \tag{48}$$

is as descriptive of the actual situation as the conventional Reynolds analogy. On the basis of Jenkin's theory, modified by recent experimental data, the effect of Reynolds number upon the total Prandtl number is indicated in Figure 13. As a first order of approximation it may be assumed that the same values apply to the total Schmidt number.

ACKNOWLEDGMENT

The assistance of P. A. Longwell and R. A. S. Brown in reviewing the manuscript is appreciated. The figures were

prepared by Virginia Berry, and Ann Hansen contributed to preparation of the manuscript.

NOTATION

A = area, sq. ft.
C_p = isobaric heat capacity, B.t.u./(lb.)(°R.)
cosh = hyperbolic cosine
D_F = Fick diffusion coefficient, sq. ft./sec.
D_μ = diffusion coefficient based on chemical potentials
E = internal energy, B.t.u./lb.
$\bar{E}$ = partial internal energy, B.t.u./lb.
$\underline{E}$ = total internal energy, B.t.u.
$\mathcal{E}$ = kinetic and internal energy, B.t.u./lb.
$\overset{\circ}{\mathcal{E}}$ = energy flux, B.t.u./(sq. ft.)(sec.)
f = Fanning friction factor
g = acceleration due to gravity, ft./sec.^{2}
H = enthalpy, B.t.u./lb.
$\bar{H}$ = partial enthalpy, B.t.u./lb.
h = height, ft.
J = a flux
$\underline{j}$ = total friction, B.t.u.
K_2, K_3 = constants
k = thermal conductivity, B.t.u./(sec.)(ft.)(°F.)
l = distance from center of channel, ft. or in.
l_0 = distance from center to wall, ft. or in.
ln = natural logarithm
l_p = latent heat of pressure change, (B.t.u./lb.)/(lb./sq. in.)
$\overset{\circ}{M}$ = momentum flux, lb./sq. ft.
m = weight of material, lb.
$\overset{\circ}{m}$ = weight rate of flow, lb./(sq. ft.)(sec.)
$\underline{N}_{Nu}$ = Nusselt number
$\underline{\underline{N}}_{Nu}$ = space-average Nusselt number
N_{Nu0} = space-average Nusselt number at zero turbulence level
N_{Pr} = Prandtl number
$\underline{N}_{Pr}$ = total Prandtl number
N_{Prm} = molecular Prandtl number
N_{Re} = Reynolds number
N_{Sc} = Schmidt number
$\underline{N}_{Sc}$ = total Schmidt number
$\underline{N}_{Sh}$ = Sherwood number
$\underline{\underline{N}}_{Sh}$ = space-average Sherwood number
$\underline{\underline{N}}_{Sh0}$ = space-average Sherwood number at zero turbulence level
n = nth value or index
n = weight fraction
P = pressure, lb./sq. in.
$\underline{q}$ = total heat, B.t.u.
$\overset{\circ}{q}$ = local thermal flux, B.t.u./(sq. ft.)(sec.)
$\overset{\circ}{r}$ = reaction rate, sec.$^{-1}$
r = radial distance, ft. or in.
r_0 = radius of conduit, ft. or in.
S = entropy, B.t.u./(lb.)(°R.)
$\bar{S}$ = partial entropy, B.t.u./(lb.)(°R.)
$\underline{S}$ = total entropy, B.t.u./°R.
T = absolute temperature, °R.
t = temperature, °F.
U = gross velocity, ft./sec.
u = point velocity, ft./sec.
u^+ = velocity parameter,

$$u^+ = u/\sqrt{g(\tau_{yx})_0/\sigma}$$

$\tilde{u}_{xf}$ = mean fluctuating velocity in the x direction, ft./sec.
V = volume, cu. ft./lb.
$\bar{V}$ = partial volume, cu.ft./lb.
$\underline{V}$ = total volume, cu. ft.
$\underline{w}$ = total work, B.t.u.
X = a potential
x = downstream distance along axis of flow, ft. or in.
y = distance normal to axis of flow, ft. or in.
y_d = vertical distance from wall, ft. or in.
y^+ = distance parameter,

$$y^+ = (y_d/\nu)\sqrt{(g/\sigma)(\tau_{yx})_0}$$

z = distance normal to boundary

Greek Letters

α_τ = turbulence level
Δ = difference
ΔE_c = change in internal energy resulting from a chemical reaction, B.t.u./lb.
ϵ_e = eddy conductivity, sq. ft./sec.
ϵ_ε = total conductivity, sq. ft./sec.
ϵ_d = eddy diffusivity, sq. ft./sec.
ϵ_δ = total diffusivity, sq. ft./sec.
ϵ_m = eddy viscosity, sq. ft./sec.
ϵ_μ = total viscosity, sq. ft./sec.
η = absolute viscosity, (lb.)/(sec.)/sq. ft.
θ = time, sec.
K = thermometric conductivity, sq. ft./sec.
λ = defined in Equation (16)
μ = chemical potential, B.t.u./lb.
ν = kinematic viscosity, sq. ft./sec.
σ = specific weight, lb./cu. ft.
σ = concentration, lb./cu. ft.
$\overset{\circ}{\sigma}$ = rate of entropy production
τ = shear, lb./sq. ft.
Φ = dissipation function
$\phi(\ )$ = function of

Subscripts

a = material added
i = ith property or index
j = component j
k = component k
m = weight
n = weight fraction
o = reference
P = pressure
S = entropy
T = temperature
V = volume
x = in x direction
y = in y direction

LITERATURE CITED

1. Billman, G. W., D. M. Mason, and B. H. Sage, *Chem. Eng. Progr.*, **46**, 625 (1950).
2. Bixler, G. H., and C. W. Coberly, *Ind. Eng. Chem.*, **45**, 2596 (1953).
3. Blasius, Heinrich, *Natl. Advisory Comm. Aeronaut., Tech. Mem. No. 1256* (1950).
4. Bogart, M. J. P., and R. H. Dodd, *Chem. Eng. Progr.*, **50**, 372 (1954).
5. Brown, R. A. S., Kazuhiko Sato, and B. H. Sage, *Ind. Eng. Chem., Chem. Eng. Data Series*, **3**, 263 (1958).
6. Cary, J. R., *Trans. Am. Soc. Mech. Engrs.*, **75**, 483 (1953).
7. Corcoran, W. H., J. B. Opfell, and B. H. Sage, *Momentum Transfer in Fluids*, Academic Press, New York (1956).
8. Corcoran, W. H., and B. H. Sage, *A.I.Ch.E. Journal*, **2**, 251 (1956).
9. Daniels, Farrington, J. I. Slaughter, and W. G. Hendrickson, *The Chemistry of the Oxides of Nitrogen*, Symposium sponsored by the Office of Ordnance Research, Chicago, Illinois (September 3 and 4, 1953).
10. Frössling, Nils, *Natl. Advisory Comm. Aeronaut., Tech., Mem.* 1432 (1958).
11. Hsu, N. T., Kazuhiko Sato, and B. H. Sage, *Ind. Eng. Chem.*, **46**, 870 (1954).
12. Jenkins, Rodman, Ph.D. thesis, Calif. Inst. Technol., Pasadena (1950).
13. Kármán, Th. von, *Nachr. Ges. Wiss. Gottingen, Math.-physik. Kl., Fachgruppen* (1930).
14. ——— *Trans. Am. Soc. Mech. Engrs.*, **61**, 705 (1939).
15. Kestin, Joseph, and P. F. Maeder, *Natl. Advisory Comm. Aeronaut., Tech. Note 4018* (1957).
16. Laufer, John, *ibid., Tech. Note 2954* (1953).
17. Lautman, L. G., and W. C. Droege, *Air Materiel Command*, Serial No. *AIRL* A 6118, 50-15-3 (1950).
18. Longwell, P. A., *A.I.Ch.E. Journal*, **3**, 353 (1957).
19. Maisel, D. S., and T. K. Sherwood, *Chem. Eng. Progr.*, **46**, 172 (1950).
20. Rouse, Hunter, "Fluid Mechanics for Hydraulic Engineers," McGraw-Hill, New York (1938).
21. Sato, Kazuhiko, and B. H. Sage, *Trans. Am. Soc. Mech. Engrs.*, **80**, 1380 (1958).
22. Schlichting, Hermann, "Boundary Layer Theory," translated by J. Kestin, McGraw-Hill, New York (1955).
23. Schlinger, W. G., V. J. Berry, J. L. Mason, and B. H. Sage, *Ind. Eng. Chem.*, **45**, 662 (1953).
24. Schlinger, W. G., and B. H. Sage, *ibid.*, **45**, 2636 (1953).
25. Short, W. W., and B. H. Sage, *J. Appl. Mechanics*, to be published.
26. Wimpress, R. N., "Internal Ballistics of Solid Fuel Rockets," McGraw-Hill, New York (1950).

Manuscript received August 14, 1958; revision received December 9, 1958; paper accepted December 11, 1958. Presented at A.I.Ch.E. Philadelphia meeting.

Diffusion-controlled Chemical Reactions

H. L. TOOR and S. H. CHIANG

Carnegie Institute of Technology, Pittsburgh, Pennsylvania

Transformations are obtained which reduce the system of differential equations for certain types of diffusion-controlled reactions to the equation for pure diffusion.

Simple relationships between the diffusion rate with and without reactions are presented for reversible unimolecular reactions, certain types of reversible bimolecular reactions, and irreversible reactions between species with equal diffusivities. It is shown that these relationships are independent of geometry, hydrodynamics, or boundary conditions, and so the mass transfer coefficient in the presence of reactions can be obtained from the coefficient in the absence of reactions without an explicit knowledge of the mass transfer mechanism.

The reaction factor for irreversible reactions with equal diffusivities, obtained by others for specific mass transfer mechanisms, is found to be quite general and essentially independent of the mechanism.

Some data on the absorption of sulfur dioxide in a laminar water jet is considered.

The theory of simultaneous diffusion and chemical reaction is basic to the study of mass transfer in reacting systems. Although many systems are difficult to handle analytically, even when the reactions are rapid relative to the diffusion, a number can be considerably simplified by reducing them to pure diffusion problems. It will be shown that this reduction is possible for certain classes of reactions and that in these cases the effect of the chemical reaction on the transfer rate may be obtained even though the pure diffusion problem is too complicated to handle analytically.

A combination of a differential material balance with Fick's law gives the equation for pure diffusion in an isothermal system (*2*):

$$\frac{DC_1^0}{D\theta} = D_1^0 \nabla^2 C_1^0 \qquad (1)$$

The diffusion coefficient is assumed constant, and the substantial derivative is used in this and subsequent equations to account for any bulk motion superimposed on the system. If bulk motion is present, the term *diffusion-controlled reactions* is used in a somewhat general sense to include diffusion-convection controlled reactions as well. The system is taken to be dilute enough so that the hydrodynamic velocities are independent of the diffusion, and it is assumed that there is no convection across the boundaries. Solutions of Equation (1) with the appropriate boundary conditions give the concentration profile of the diffusing species, which, upon application of Fick's first law at the system boundary

$$N_{1B}^0 = -D_1^0 (\nabla C_1^0)_B \qquad (2)$$

yields the rate of transfer across the boundary.

If the flow is turbulent, the equations can be considered to apply at every instant of time, and the solutions give the instantaneous concentration and flux. Although many of the conclusions given below are valid for turbulent flow, this paper is concerned specifically with a stagnant fluid or laminar flow.

Equations (1) and (2) with the boundary conditions fix the diffusion rate and also yield the mass transfer coefficient. The two simplest solutions, which are used as models for mass transfer in systems such as packed towers (*7*), are the semi infinite slab solution (penetration model)

$$N_{1B}^0 = \sqrt{\frac{D_1^0}{\pi\theta}} (C_{1I}^0 - C_{10}^0) \qquad (3)$$

and the steady state solution (film model)

$$N_{1B}^0 = \frac{D_1^0}{L} (C_{1I}^0 - C_{1II}^0) \qquad (4)$$

When a chemical reaction takes place, Equation (1), with a source or sink term to account for the reaction, applies to each molecular species in turn,

$$\frac{DC_i}{D\theta} = D_i \nabla^2 C_i + r_i, \qquad i = 1, 2, \cdots n. \qquad (5)$$

and there are n equations for n species. The diffusion flux for each species is given by Fick's law, since the system is dilute enough so that there are no diffusional interactions:

$$N_i = -D_i \nabla C_i \qquad (6)$$

In the presence of convection this is the flux with respect to the local bulk-fluid velocity.

REVERSIBLE REACTIONS

To determine the relationship among the concentrations of reversibly reacting species in a diffusion controlled system, it is necessary to examine the rate equation for reversible reactions. This can be written for species 1 as

$$-r_1 = k_f \Delta_1 \qquad (7)$$

where Δ_1 depends upon the mechanism of the reaction. For first-order reactions in both directions, for example,

$$\Delta_1 = \left(C_1 - \frac{C_2}{K}\right) \qquad (8)$$

It will be seen later that the form of Δ_1 is not important here, but the important characteristic is that when Δ_1 is zero, local chemical equilibrium exists whatever the order of the reactions.

Now if a number of diffusion-reaction systems which differ only in their values of k_f are examined, it is seen that at low values of k_f, Δ_1 will not generally be zero. However if k_f is allowed to increase without limit by the consideration of systems with larger and larger values of k_f, Equation (7) shows that the reaction rate will also increase without limit unless Δ_1 approaches zero. But the reaction rate cannot increase without limit, since it will be limited at any point by the finite rate of supply and removal of reacting species to the region of the point. Consequently as k_f gets large, Δ_1 must approach zero as the reactions become diffusion controlled, and local chemical equilibrium is approached at all points in the system. Equation (7) is then indeterminate, and the reaction rate must be obtained from the diffusion equations. [See Equation (20) for example.]

Thus in general a diffusion-controlled reversible reaction system can be defined as one in which local chemical equilibrium exists at all points. Strictly this demands infinite reaction velocity constants, but for any system there is some finite value of k_f which is large enough to render negligible the error caused by the assumption of local equilibrium. Reactions in which k_f is equal to or greater than this value are considered to be rapid reactions. As long as the reactions are rapid, it is not necessary to restrict k_f, but it is assumed in the subsequent work that the equilibrium constants are true constants.

For rapid irreversible reactions the analogue of the above result is the well-known fact that the reaction must take place at a surface (*15*).

REVERSIBLE UNIMOLECULAR REACTIONS

An isothermal system with a dilute solute will be considered. Species 1 is diffusing in the solvent which is stagnant or in laminar flow, and it reacts rapidly and reversibly to form species 2. Species 2 is not immobilized and is free to diffuse. The reactions are unimolecular or psuedo-unimolecular

$$1 \rightleftarrows 2$$

S. H. Chiang is with Linde Company, Tonawanda, New York.

so the equilibrium constant K is given by

$$K = \frac{C_2}{C_1} \tag{9}$$

Since the reaction is rapid, local chemical equilibrium exists at all points; therefore C_1 and C_2 are always in a constant ratio, and the diffusion and reaction rates are both controlled by the diffusion. If it it assumed that any intermediate reactions are much more rapid than the first and last steps and that the amount of the intermediate species present at any time is negligible, $r_1 + r_2 = 0$. (It is shown that these qualifications are unnecessary if the intermediate reactions are unimolecular). If the first two equations of (5) are added together, since $r_1 + r_2 = 0$, the reaction terms are eliminated and

$$\frac{D(C_1 + C_2)}{D\theta} = D_1\nabla^2 C_1 + D_2\nabla^2 C_2 \tag{10}$$

This simplifies with the aid of Equation (9) to

$$\frac{DC_1}{D\theta} = \left(\frac{D_1 + KD_2}{1 + K}\right)\nabla^2 C_1 = D_e\nabla^2 C_1 \tag{11}$$

Comparison of Equation (11) with Equation (1) shows that species 1 diffuses as if there were no chemical reaction, but its effective diffusivity is given by

$$D_e = \frac{D_1 + KD_2}{1 + K} = \frac{C_1D_1 + C_2D_2}{C_1 + C_2} \tag{12}$$

and the effective diffusivity is the concentration weighted, mean diffusivity. Since D_1, D_2, and K were assumed to be constants, D_e is also a constant, independent of concentration, and is a true diffusivity for the system. [If species 2 is immobilized, D_2 is zero and the result given by Crank (*5*) is obtained. If the reaction is irreversible, $K = \infty$ and $D_e = D_2$; only species 2 exists inside the system.]

Although it is tempting to visualize the complex $1 \rightleftarrows 2$ as diffusing as a unit, this is not generally the case, for a comparison of Equations (11) and (5) shows that

$$r_1 = -r_2 = -\frac{K}{1 + K}(D_1 - D_2)\nabla^2 C_1 \tag{13}$$

Thus if the diffusivities are not equal, the reaction continues throughout the system and varies from point to point (unless $\nabla^2 C_1 = 0$). This is a direct consequence of the diffusivity difference which tends to eliminate local equilibrium and which must be balanced by the reaction which restores the equilibrium. The direction of the reaction depends upon the relative magnitude of the diffusion coefficients (it will shortly be shown that the sign of $\nabla^2 C_1$ is unaffected by the reaction) so with $\nabla^2 C_1$ positive species 1 is removed by the reaction when $D_1 > D_2$, but when $D_2 > D_1$, species 1 is formed by the reaction.

When $D_1 = D_2$, the rate of reaction is zero. After local chemical equilibrium is reached at the boundaries of the system, the complex $1 \rightleftarrows 2$ does diffuse as a unit, since as far as diffusion is concerned 1 and 2 are the same species if their diffusivities in the solvent are equal.

Equation (11) can be written in another form by noting that the concentration of species 1 is linearly related to the total concentration of diffusing species:

$$C_t = C_1 + C_2 = (K + 1)C_1 \tag{14}$$

Therefore

$$\frac{DC_t}{D\theta} = D_e\nabla^2 C_t \tag{15}$$

If there are a series of reactions of the form

$$1 \rightleftarrows 2 \rightleftarrows 3$$

or any combination of reactions of this type, then $\sum_{i=1}^{n} r_i = 0$, and by the same procedure as before it can be shown that Equations (11) and (15) hold if the effective diffusivity is defined as

$$D_e = \sum_{i=1}^{n} K_iD_i \Big/ \sum_{i=1}^{n} K_i \tag{16}$$

where the equilibrium constants K_i are defined by

$$K_i = \frac{C_i}{C_1} \tag{17}$$

and C_t is

$$C_t = \sum_{i=1}^{n} C_i = C_1 \sum_{i=1}^{n} K_i \tag{18}$$

Equations (17) and (18) show that the C_i are linearly related to C_t by

$$C_i = \frac{K_i}{\sum_{j=1}^{n} K_j} C_t \tag{19}$$

The equilibrium constants defined by Equation (17) are not necessarily the normal chemical equilibrium constants but are combinations of them which depend upon the reaction scheme.

The rate of reaction of species i is given by

$$r_i = -\frac{\sum_{j=1}^{n} K_j(D_i - D_j)}{\sum_{j=1}^{n} K_j}\nabla^2 C_i \tag{20}$$

or alternately

$$r_i = -\frac{K_i \sum_{j=1}^{n} K_j(D_i - D_j)}{\left(\sum_{j=1}^{n} K_j\right)^2}\nabla^2 C_t \tag{21}$$

Again the reaction rate in the system is zero only when all the diffusivities are equal, and the direction of the reaction depends upon the relative magnitudes of the diffusivities and the equilibrium constants. The total diffusion flux of solute is obtained by the summing of Equation (6) over all species;

$$N_t = \sum_{i=1}^{n} N_i = -\sum_{i=1}^{n} D_i\nabla C_i \tag{22}$$

which from Equation (16) and (19) becomes

$$N_t = -D_e\nabla C_t \tag{23}$$

If this equation is applied on the inner side of the system boundary, it gives the rate at which species 1 crosses the boundary, while inside the system it gives the rate of diffusion of species 1 in all forms with respect to the local bulk velocity. At the boundary then with no ambiguity

$$N_{1B} = -D_e(\nabla C_t)_B \tag{24}$$

Equations (15) and (24) are mathematically identical to the pure diffusion Equations (1) and (2), since D_e is constant, and if the boundary conditions have the same form, the two solutions will be identical when the following transformations are carried out:

$$D_1^{\,0} \rightarrow D_e \qquad C_1^{\,0} \rightarrow C_t \qquad N_{1B}^{\,0} \rightarrow N_{1B} \tag{25}$$

These transformations are only of immediate use if the boundary conditions on C_t can be obtained without the necessity of an explicit knowledge of the behavior of each species. When the reacting phase is contacted by another phase containing species 1, and there is no interfacial resistance, the interfacial concentration of species 1 is fixed by the physical equilibrium relationship between 1 in the external phase and the reacting phase. But C_1 and C_t are related by the reaction equilibria [Equation (18)], and so C_{tI} is also fixed by the equilibria. Since the phase equilibrium relationship is usually reported in terms of the total amount of species 1 present in the reacting phase at complete equilibrium, C_{tI} is the normal equilibrium value.

Generally the concentration of only one species can be fixed at a boundary; the others are then set by the chemical equilibrium relationships. If the reaction products are volatile, the external composition adjacent to the interface must adjust to satisfy the solubility relationship for each species.

For example if a pure gas is absorbed

in a layer of stagnant liquid in which it reacts by one or more rapid unimolecular reactions, the instantaneous absorption rate is obtained by applying Equation (25) to (3):

$$N_{1B} = \sqrt{\frac{D_e}{\pi\theta}}\,(C_{tI} - C_{t0}) \qquad (26)$$

and the transformation of Equation (4) gives the steady state solution

$$N_{1B} = \frac{D_e}{L}\,(C_{tI} - C_{tII}) \qquad (27)$$

Since equations of the above type are used to measure diffusivities, what is measured is D_e as defined by Equation (16), and since D_e is a constant (within the limitations of the previous assumptions), it may be used in all the solutions to Fick's law for pure physical absorption. Consequently diffusion with rapid reversible (or irreversible) unimolecular reactions may be treated as a pure diffusion problem by ignoring the reaction altogether, since the diffusivity and solubility data will already contain the effects of the reaction.

However if the diffusivity has not been experimentally determined and must be estimated from one of the correlations, Equation (16) should be used to determine the effect of the reaction on the diffusivity.

Although the above analysis has focused on diffusion rate, it can be seen that the reduced concentration profiles of total solute are identical to the profiles which would be obtained in a nonreacting system. The concentration profile for each species is then obtained from Equation (19), and the local rate of reaction then follows from Equation (20) or (21). Since the functional form of $\nabla^2 C_i$ and $\nabla^2 C_t$ are fixed by the boundary conditions and hydrodynamics, the rate and direction of the reactions are set by the relationships among the diffusion coefficients and equilibrium constants.

Finally since the transformations given by Equation (25) do not depend upon hydrodynamics, geometry, or boundary conditions, the mass transfer rate in the presence of rapid unimolecular reactions can be obtained from the rate in the absence of reactions by means of Equation (25), even in such complex systems as packed columns. [Equation (25) applies directly to the various types of mixing models considered by Danckwerts (*7*) for packed columns, but if the reactions are first order, it is easy to show that the result is valid even if the flow is turbulent.]

The simplifications which occur with unimolecular reactions arise because of the simple relationship among concentrations and cannot be expected to be general. However certain types of bimolecular reactions can be reduced to simple forms by an approach similar to the one above.

REVERSIBLE BIMOLECULAR REACTIONS

Diffusion with the bimolecular reactions

$$1 + 2 \rightleftarrows 3 + 4$$

is described by Equation (5) with

$$r_1 = r_2 = -r_3 = -r_4 \qquad (28)$$

When the reactions are rapid enough so that local chemical equilibrium exists at all points, the concentrations are related by

$$K = \frac{C_3 C_4}{C_1 C_2} \qquad (29)$$

It is convenient in this case to add the first and third equations of (5), and with Equation (28)

$$\frac{D(C_1 + C_3)}{D\theta} = D_1\nabla^2 C_1 + D_3\nabla^2 C_3 \qquad (30)$$

$$C_t = C_1 + C_3 \qquad (31)$$

is defined. At this point it should be noticed that the effective diffusivity for the total solute as defined by Equation (23) is given by

$$D_e = \frac{\nabla(D_1 C_1 + D_3 C_3)}{\nabla(C_1 + C_3)} \qquad (32)$$

so even if C_t were fixed at the system boundaries, the transfer of total solute could not be treated as a purely diffusional problem, since the effective diffusivity would be a function of the concentration gradients. Only when the diffusivities of species 1 and 3 are equal does Equation (30) reduce to the simple form of Equation (15). It still does not follow that the problem can be treated as pure diffusion, for if the concentration of species 1 is held constant at the system boundaries, Equation (29) shows that C_t is not fixed.

To fix C_t one must assume that species 3 and 4 are initially at zero concentration or present in equal amounts and that $D_3 = D_4$, so $C_3 = C_4$ at all points during the process. This also gives C_t a clear physical meaning, for it can now be interpreted as the total concentration of species 1 in all forms at any point. Further it is necessary to reduce the forward reaction to psuedo first order by the assumption that species 2 is present in large excess. Then Equation (29) becomes

$$C_3 = \sqrt{KC_2C_1} = \sqrt{K'C_1} \qquad (33)$$

and

$$C_t = C_1 + \sqrt{K'C_1} \qquad (34)$$

Under these conditions C_t is a function only of C_1, so the relationship between C_t at the system boundary and the concentration of species 1 in an external phase is the normal equilibrium relationship for total solute. Finally it is seen that the rate of transfer of total solute is given by Equation (23).

Thus this reaction problem is reduced to the equivalent pure-diffusion problem, and the mathematical solutions for the two cases are related by the transformations (25) with $D_e = D_1 = D_3 = D_4$. The rate of diffusion of total solute, or species 1 at the boundary, then follows the equations for pure diffusion if the total solute concentration at the boundaries is used in the integrated rate equations. These results are only valid when species 3 and 4 are initially present in equal amounts, species 2 is in large excess, and $D_1 = D_3 = D_4$. Generally the effective diffusivity may vary from D_1 to D_3, and the interfacial concentration of total solute will vary with time and depend upon the conditions of the experiment as well as the relationship among the diffusivities.

IRREVERSIBLE REACTIONS

Diffusion with the rapid irreversible reaction

$$a1 + b2 \rightarrow \text{products}$$

is discussed by Sherwood and Pigford (*15*) in terms of the film and penetration models for the case $a = b$.

Previous methods of analysis have treated the diffusion-reaction equations for each species as a system of partial differential equations to be solved simultaneously. The mathematics are quite complex, and only a few special cases have been solved. It will be shown by a modification of the method used in the preceding sections that very general solutions may easily be obtained for the special case of equal diffusivities.

The defining equations are given by (5) but here

$$r_1 + \frac{a}{b}\,r_2 = 0 \qquad (35)$$

Multiplying the first equation of (5) by b and the second by a, letting $D_2 = D_1$, and substracting one from the other removes the reaction term and yields

$$\frac{DC_t'}{D\theta} = D_1\,\nabla^2 C_t' \qquad (36)$$

where

$$C_t' = bC_1 - aC_2 \qquad (37)$$

Although C_t' satisfies Equation (36), even for a slow reaction, generally the boundary conditions and the relationship between N_t' and N_1 cannot be obtained without a direct solution of the separate diffusion-reaction equations.

When the reaction is rapid and irreversible, at no point can there be both species 1 and 2 present, and so C_t' at some points equals bC_1 and at others equals $-aC_2$. As this is also true at the system boundaries, there is no difficulty in fixing the boundary concentrations.

For convenience one defines

$$N_i' = -D_1 \nabla C_i' \qquad (38)$$

which from Equations (37) and (6) reduces to

$$N_i' = bN_1 - aN_2 \qquad (39)$$

At a boundary where the concentration of species 1 is fixed, no species 2 can be present, so at this boundary

$$N_{iB}' = bN_{1B} = -D_1(\nabla C_i')_B \qquad (40)$$

By the comparison of Equations (36) and (40) with the pure diffusion equations it is seen that the transfer rate with the reaction is obtained from the rate without reaction by the following transformations:

$$\begin{aligned} C_1^0 &\rightarrow C_i' \\ N_{1B}^0 &\rightarrow bN_{1B} \\ D_1^0 &\rightarrow D_1 \end{aligned} \qquad (41)$$

These equations are quite useful; in addition to yielding explicit solutions when the pure diffusion problem can be solved, they also allow a quantitative determination of the effect of the reaction on the mass transfer coefficient for cases where the pure diffusion problem is intractable.

The penetration solution follows immediately by the application of the above transformations to Equation (3). For a slab which initially has a constant composition of species 2, $C_{i0}' = -aC_{20}$, and if the interface is saturated with species 1 at time zero, $C_{iB}' = bC_{1I}$. The rate of transfer of species 1 across the interface is then

$$N_{1B} = \sqrt{\frac{D_1}{\pi\theta}}\left(1 + \frac{a}{b}\frac{C_{20}}{C_{1I}}\right)C_{1I} \qquad (42)$$

which for $a = b$ is the solution obtained by Danckwerts (*6*) by a direct solution of the equations for each species.

If a plane at a distance L from the interface is held at the composition C_{2II}, then the steady state solution obtained by the application of the transformations (41) to Equation (4) gives

$$N_{1B} = \frac{D_1}{L}\left(1 + \frac{a}{b}\frac{C_{2II}}{C_{1I}}\right)C_{1I} \qquad (43)$$

and for $a = b$ this is Hatta's solution (*10*).

Since C_1 is zero at time zero and at plane II, the bracketed term in both of the equations above is a correction factor which accounts for the effect of the chemical reaction on the rate, the reaction factor. If $C_{2II} = C_{20}$, then for both the penetration and film mechanisms

$$k = k^0\left(1 + \frac{a}{b}\frac{C_{20}}{C_{1I}}\right) \qquad (44)$$

This equation is considerably more general than Equations (42) and (43). It holds for example if the transfer mechanism is neither a pure penetration type nor a pure film type but a combination of both such as film penetration (*16*), and it is valid even in the presence of externally imposed convection.

Friedlander and Litt (*8*) recently obtained Equation (44) by direct integration of the separate diffusion equations for a laminar boundary layer on a flat plate, and they suggested that the same reaction factor be used as a first approximation for geometries where the diffusion problem cannot be solved. The present approach allows a direct proof of the validity of this assumption, for it will be shown that the reaction factor does not depend upon geometry.

A laminar boundary layer with a geometry such that the following boundary conditions may be applied in the case of pure diffusion will be considered.

$$\begin{aligned} x = 0, &\quad C_1^0 = C_{1m}^0 \\ y = 0, &\quad C_1^0 = C_{1I}^0 \\ y = L, &\quad C_1^0 = C_{1m}^0 \end{aligned} \qquad (45)$$

where L may be infinite. By the use of dimensionless units the solution to the pure diffusion problem, Equations (1) and (2) with the above boundary conditions, may readily be shown to have the form

$$N_1 = k^0(C_{1I}^0 - C_{1m}^0) \qquad (46)$$

where k^0 depends upon the geometry and is a function of position.

If the concentration of species 1 at the wall is C_{1I} and species 1 reacts with species 2, which initially is evenly distributed theoughout the fluid, the transformations (41) as in the previous cases immediately yield Equation (44) as the solution to the problem under consideration. Thus the reaction factor $[1 + (a/b)\ (C_{20}/C_{1I})]$ applies to any laminar boundary layer (even if the normal boundary layer assumptions do not hold) when the boundary conditions (45) apply, and it can be used to correct empirical mass transfer coefficients for the effect of an irreversible reaction.

Friedlander and Litt also obtained the reaction factor for the flat plate when the diffusivities are not equal, and since the transformations (41) do not apply under these circumstances, it is likely that the reaction factor will have different forms for other geometries.

The first equation of (41) transforms the equation for the concentration profile in the absence of reaction to the profile for C_i' in the presence of the reaction. Generally it will be possible to obtain the separate concentration profiles for both species 1 and 2 from the C_i' profile in the following manner.

Since the two species will meet and react at surface moving in time, on one side of the surface only species 1 will exist and on the other side only species 2; at the surface itself C_1 and C_2 will be zero. Consequently on one side C_i' reduces to bC_1, and on the other side it reduces to $-aC_2$; the equation for the reaction surface can be determined by setting C_i' equal to zero in the equation for the C_i' profile. If so desired, the flux profile for each species can then be explicitly determined by the application of Equation (6) to each of the separate concentration profiles.

For example boundary conditions of the type considered earlier lead to solutions of the form

$$\frac{C_1^0 - C_{10}^0}{C_{1I}^0 - C_{10}^0} = f(\vec{r}, \theta) \qquad (47)$$

where $f(\vec{r}, \theta)$ depends upon geometry and hydrodynamics; in the boundary-layer problem f does not depend upon θ, and C_{10} is C_{1m}.

Equation (47) transforms by (41) to

$$\frac{C_i' - C_{i0}'}{C_{iI}' - C_{i0}'} = f(\vec{r}, \theta) \qquad (48)$$

when $D_1 = D_1^0$ is assumed for simplicity. The reaction takes place on the surface at which $C_i = 0$, and so from Equations (48) and (37)

$$\frac{1}{\frac{b}{a}\frac{C_{1I}}{C_{20}} + 1} = f(\vec{r}, \theta) \qquad (49)$$

and this equation can be solved for the reaction surface as a function of time. On the side of the surface where only species 1 exists, Equation (48) yields

$$\frac{C_1 + \frac{a}{b}C_{20}}{C_{1I} + \frac{a}{b}C_{20}} = f(\vec{r}, \theta) \qquad (50)$$

and on the other side where only species 2 exists

$$\frac{C_{20} - C_2}{C_{20} + \frac{b}{a}C_{1I}} = f(\vec{r}, \theta) \qquad (51)$$

The separate concentration profiles are now completely defined.

ABSORPTION OF SULFUR DIOXIDE BY WATER

Sulfur dioxide reacts with water as follows:

$$SO_2 + H_2O \rightleftarrows H_2SO_3 \rightleftarrows HSO_3^- + H^+$$

$$1 + 2 \rightleftarrows 3 \rightleftarrows 4 + 5$$

There is evidence that all these forms are present at equilibrium, and although the equilibrium amounts of ionized and total unionized species are known, the amounts of sulfur dioxide and sulfurous acid present are not known (*11*).

If the reactions are assumed to be rapid, then in the absorption of sulfur dioxide by water the following equi-

libria exist at all points during the diffusion process.

$$K_\alpha = \frac{C_3}{C_1 C_2} \tag{52}$$

$$K_\beta = \frac{C_4 C_5}{C_3} \tag{53}$$

As discussed earlier, equilibria of these types generally will not reduce the diffusion equations to the form corresponding to pure diffusion. In fact if the above equilibria are not qualified, the effective diffusivity is a variable, and the interfacial concentration of total solute depends upon the concentration profiles of all species even when there is equilibrium between the sulfur dioxide gas and the liquid solution at the interface.

However if the sulfur dioxide concentration is not too large, then the water concentration may be taken as constant in Equation (52). Furthermore if the solution is not too dilute, the major part of the H^+ is produced by the dissociation reaction, and so HSO_3^- and H^+ are produced at the same rate. As ionic forces will keep the two species from separating in order to preserve local electrical neutrality, it can be assumed that $C_4 = C_5$ at all points. Equation (53) then reduces to

$$\frac{C_4^2}{C_3} = K_\beta \tag{54}$$

The total solute concentration is, from Equations (52) and (54),

$$C_t = C_1 + C_3 + C_4$$

$$= C_1\left(1 + C_2 K_\alpha + \sqrt{\frac{C_2 K_\alpha K_\beta}{C_1}}\right) \tag{55}$$

and Equation (55) shows that with C_2 constant C_t is a function only of C_1. Consequently the equilibrium relationship between sulfur dioxide gas and unreacted sulfur dioxide fixes the total solute concentration at the interface. However unless all the diffusivities are equal, which is unlikely, or the amount of HSO_3^- is negligible, the effective diffusion coefficient will be a variable.

Even if the ionized sulfurous acid is assumed to have the same diffusivity as the unionized form, the effective diffusivity should not be constant, for the ratio of total sulfurous acid in both forms to dissolved sulfur dioxide will vary with total concentration.

In solutions saturated at 1 atm. sulfur dioxide partial pressure at room temperature about 10% of the total sulfur dioxide in solution is ionized, and the percentage ionized increases as the total sulfur dioxide concentration decreases, so that at 10% of saturation about 30% is ionized (*13*).

Lynn *et al.* (*12*) have measured the rate of absorption of sulfur dioxide into water flowing down the outside of a rod. These data have been extended by the absorption of pure sulfur dioxide into a laminar water jet, which is in rodlike flow (*4*), by a technique described in an earlier paper (*14*). In Figure 1 the average rate of absorption over the jet is plotted against $1/\sqrt{\theta}$, and the range of Lynn's data is also shown. The absorption rate follows the reciprocal square-root time dependence over the full 300-fold range of contact time, and the data extrapolate to zero at infinite contact time.

Since the mean absorption rate is twice the point rate, Equation (26) indicates that the effective diffusivity is a constant and the interfacial resistance is negligible. This constant effective diffusivity would result if the ionization reaction were so slow that this reaction did not occur over the range of contact time studied, for the hydrolysis step is psuedo first order, and it was shown above that this leads to a constant effective diffusivity. However Lynn (*12*) showed independently that the entire sequence of reactions reaches completion in less than 0.1 sec. and concluded that all the reactions must rapidly reach equilibrium. If this is the case the present data indicate that the reactions must be completed in less than 0.003 sec.

Another possible explanation of the constant diffusivity is that the high ionization which takes place at the dilute end of the concentration profile has little effect on the diffusion rate, and since only 10% of the total sulfur dioxide is ionized near the saturated jet surface, this small effect may be negligible.

In any case the rate measurements allow determination of the effective diffusivity. The jet surface temperature is estimated to be 1°C. higher than the surrounding temperature of 22.2°C. (*4*), and at 23.2°C. the total solubility of sulfur dioxide in water is 1.42×10^{-3} g. moles/cc. (*13*). This solubility is considered to be reliable and is within ± 2% of two other independent measurements (*1, 3*).

By the use of the time average of Equation (26) it is found that the straight line through the data corresponds to an effective diffusivity of 1.54×10^{-5} sq. cm./sec. When corrected to 20°C. by the Stokes-Einstein equation the measured value is 1.41×10^{-5}, compared with Lynn's measurement (*12*) of 1.46×10^{-5} and Groothuis and Kramers' (*9*) value of 1.40×10^{-5}.

As mentioned earlier, in the estimation of the diffusivity of a solute in a solvent with which it reacts the various molecular species present should be taken into account. If the ionized sulfurous acid is assumed to have the same diffusivity as the unionized portion, then only sulfur dioxide and sulfurous acid need be considered. Table 1 gives the values calculated from Wilke's correlation (17) at 20°C.

Table 1. Diffusivities at 20°C. in Water

	SO_2	H_2SO_3	Experimental
$D \times 10^5$, sq. cm./sec.	1.46	1.17	1.41

Since the average deviation of Wilke's correlation is 6% and there are other uncertainties as well, no definite conclusions can be drawn from these figures; if they are accepted at their face value they indicate that most of the unionized material is in the form of sulfur dioxide rather than sulfurous acid.

ACKNOWLEDGMENT

This work was carried out with the financial support of the National Science Foundation.

NOTATION

a, b	= stoichiometric coefficients
C_i	= concentration of species i
C_t	= total solute concentration
C_t'	= concentration of total solute defined by Equation (37)

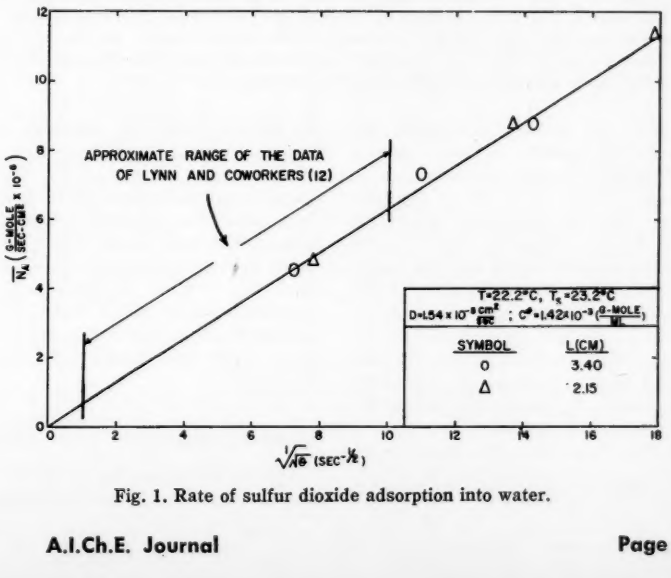

Fig. 1. Rate of sulfur dioxide adsorption into water.

D_e = effective diffusivity
D_i = diffusivity of species i
f = functional symbol
k = local mass transfer coefficient
k_f = forward reaction-velocity constant
K, K_a, K_s = equilibrium constants
K_i = modified equilibrium constants defined by Equation (17)
K' = effective equilibrium constant defined by Equation (33)
L = film thickness, jet length in Figure (1)
n = number of species
N_i = flux of species i
N_t = flux of total solute
N_t' = flux defined by Equation (38)
r_i = volumetric rate of production of species i by reaction
$\vec{r}$ = position vector
x, y = generalized position coordinates
Δ = displacement from chemical equilibrium
θ = time
∇ = gradient
∇^2 = Laplacian operator
$D/D\theta$ = substantial derivative

Subscripts

B = boundary
i, j = indices taking on values 1, 2, ... n.
m = main stream
0 = time zero
I = boundary I
II = boundary II

Superscript

^{0} = absence of reaction

LITERATURE CITED

1. Beuschlein, W. L., and L. O. Simenson, *J. Am. Chem. Soc.*, **62**, 610 (1940).
2. Bird, R. Byron, "Advances in Chemical Engineering," Vol. I, Academic Press, New York (1956).
3. Campbell, W. B., and O. Maass, *Can. J. Research*, **2**, 42, (1930).
4. Chiang, S. H., Ph.D. thesis, Carnegie Inst. Technol., Pittsburgh, Pennsylvania (1958).
5. Crank, John, "The Mathematics of Diffusion," Oxford Univ. Press, Oxford, England (1956).
6. Danckwerts, P. V., *Trans. Faraday Soc.*, **46**, 300 (1950).
7. ———, *A.I.Ch.E. Journal*, **1**, 456 (1955).
8. Friedlander, S. K., and M. Litt, *Chem. Eng. Sci.*, **7**, 229 (1958).
9. Groothuis, H., and H. Kramers, *ibid.*, **4**, 17 (1955).
10. Hatta, S., *Technol. Repts. Tohoku Imp. Univ.*, **8**, 1 (1928–1929).
11. Johnstone, H. F., and P. W. Leppla, *J. Am. Chem. Soc.*, **56**, 2233 (1934).
12. Lynn, Scott, J. R. Straatemeier, and H. Kramers, *Chem. Eng. Sci.*, **4**, 49 (1955).
13. Morgan, O. M., and O. Maass, *Can. J. Research*, **5**, 162 (1931).
14. Raimondi, Pietro, and H. L. Toor, *A.I.Ch.E. Journal*, **5**, 86 (1959).
15. Sherwood, T. K., and R. L. Pigford, "Absorption and Extraction," 2 ed., McGraw-Hill, New York (1952).
16. Toor, H. L., and J. M. Marchello, *A.I.Ch.E. Journal*, **4**, 97 (1958).
17. Wilke, C. R., *Chem. Eng. Progr.*, **45**, 218 (1949).

Manuscript received September 24, 1958; revision received February 5, 1959; paper accepted February 20, 1959. Paper presented at A.I.Ch.E. Cincinnati meeting.

Mechanism of Drying Thick Porous Bodies During the Falling-Rate Period

II. A Hygroscopic Material

J. R. BELL and A. H. NISSAN

The University of Leeds, Leeds, England

A further analysis of the second falling-rate period in the drying of thick highly porous textile structures is made, this time in the case of drying wool, special attention being paid to the adsorbed water held by the wool in the air-dry region. As the solid-to-void ratio is low, the quantities of adsorbed water are small and have little effect on the general equilibrium. Values of thermal conductivity are calculated for wet wool.

In part 1 (*1*) experimental results were given for the heating and air drying of two thick highly porous textile structures. Extremes were chosen in a Terylene (British form of a polyester fiber) net fabric of open structure and a woolen flannel of close structure and the results compared for the two materials. It was found that despite the difference in structure a similar equilibrium between heat transfer inward and vapor diffusion outward was established at a constant pseudo-wet-bulb temperature during the second falling rate period.

A further important difference between the fabrics, which was neglected in the first treatment, is the hygroscopic nature of the wool, whereby some 30% of bound water is in equilibrium with the fibers when the surrounding atmosphere is saturated with water vapor. In this paper the data given previously for the wool are further analyzed with the adsorbed water taken into account. Values of the apparent thermal conductivity of the wet porous solid are also calculated.

A. H. Nissan is with the Rensselaer Polytechnic Institute, Troy, New York.

WATER DISTRIBUTION IN WOOL BOBBIN

The woolen cloth, being wound on a spindle, formed an annular package just over 1 in. thick of about 3-in. O.D. and 6-in. long. The hot air flowed parallel to the outer surface, and thermocouples situated at each succeeding $\frac{1}{8}$ in. in depth and also just below the surface thickness of cloth provided a record of the temperature distribution during the drying cycle. Weighing gave the total weight of water held by the package as drying proceeded.

The General Distribution Deduced from the Temperature Record

In Figure 1 the curves showing the temperatures at the different depths are reproduced. In the case of Terylene it was shown that when the temperature registered by a thermocouple embedded in the cloth rises from the pseudo-wet-bulb temperature level, the material outside the position of the thermocouple is dry and the material within is wet. In other words, as the thermocouple is left

in the dry region by the retreating water surface, the temperature rises sharply. In the case of the wool it is assumed that this temperature rise of the thermocouples marks the passing of a boundary within which there is pore water and the maximum quantity of adsorbed water associated with the wool. Outside the boundary the layers will be termed *air-dry*.* The liquid-water boundary is considered to be of uniform cylindrical shape, whereas in practice it will be irregular owing to slight inconsistencies in the material.

The time at which the water surface passed each thermocouple was noted from Figure 1, and hence the position of the water surface was noted with respect to time plotted in Figure 2. It is interesting to note from this figure that the water surface appears to leave the fabric surface just after the end of the first falling rate period. Thus the drying out of the surface could coincide with the linearity in agreement with the classical concept.

An average weight of free-water content per unit volume appertaining within the water surface can be calculated from the total weight of water and the radius of the water surface at any time. Such values are plotted in Figure 3.

The rapid fall of over-all free-water content (assumed uniform throughout the wet portion of the bobbin) during the constant-rate period represents the diminution of the water content through the flow of water to the surface. This is followed by a period of transition to the new equilibrium conditions when the temperature of the free water is rising from the wet bulb to the pseudo-wet-bulb temperature, after which the average free-water content appears to remain constant with time.

*The air-dry layer is one which is free from liquid water but which has a regain (% moisture content - dry basis) dictated by the local humidity of the air in the pores of the layer.

The Distribution of Adsorbed Water in the Falling-Rate Period

Although one cannot be certain that the limiting equilibrium between the amount of bound water and the vapor atmosphere in the pores is always reached, it is reasonable to assume that this is so and to obtain the amounts of adsorbed water from the appropriate desorption curve. King and Cassie (*2*) have deduced that the time to establish equilibrium conditions at the fiber is very short; it is the movement of vapor and changing temperature conditions which prolong the process. In the second falling rate period conditions are changing very slowly, and one might expect equilibrium conditions to be reached. McCready and McCabe (*3*) assumed this to be so in their analysis of the drying of slabs of paper pulp.

The amount of adsorbed water in a layer thus depends on the vapor pressure appertaining, which in turn depends on how the vapor concentration gradient varies between the water surface and the air stream. Use is made here of the analogy between temperature gradient and concentration gradient. In Figure 4 the temperature gradients are shown to be linear, and the assumption is therefore made that the concentration gradients are linear as well.

For particular times the values of p/T representing concentrations were calculated for each $\frac{1}{8}$-in.-thick layer by proportion from the gradient $(p_w/T_w - p_a/T_a)$; thus the mean partial vapor pressures and relative humidities for each layer were evaluated. Speakman's desorption data (*4, 5*) were used to give the moisture regain for each value of relative humidity. In this manner the moisture content of each of the $\frac{1}{8}$-in. layers outside the water boundary was calculated at a number of different times in the second falling-rate period.

Table 1 gives the calculated values at times $t = 500$ and 800 min. along with the results of some experimental determinations. The latter were obtained at a later date, when the bobbin was cut up so that it might consist of a central portion and eight $\frac{1}{8}$-in.-thick layers which could be unwrapped and weighed after the bobbin had been dried for the appropriate time under similar experimental conditions.

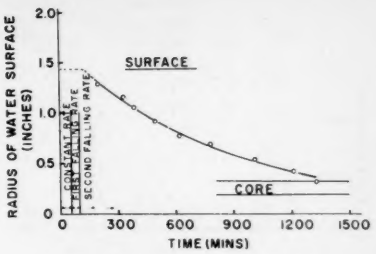

Fig. 2. Water radius vs. time.

There is good agreement between calculated and experimental values, which supports the many assumptions made in the calculations. The fact that the saturated vapor pressure increases rapidly with temperature means that the relative humidity falls off quickly with increased distance from the water surface. This and the sigmoid nature of the desorption curve produce the rapid fall off in the quantities of adsorbed water in the succeeding layers from the water surface; that is, most of it lies in the $\frac{1}{4}$ in. adjacent to the water boundary.

When one subtracts the adsorbed water in the air-dry region from the total water, the sloping dotted line in Figure 3 is produced, showing that the average free-water content within the boundary gradually decreases, a fact which is borne out by the experimental values. This presumably means that there is some form of water movement to the water surface. The experimental values also show that the free-water content is not constant throughout but increases slightly with increasing depth.

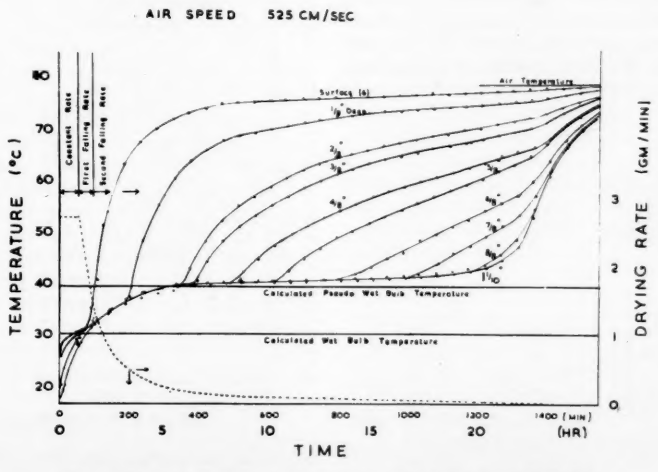

Fig. 1. Temperature vs, time at various depths in wool bobbin.

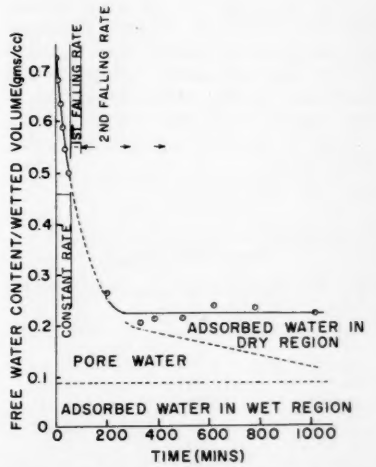

Fig. 3. Wetted-volume free-water content vs. time.

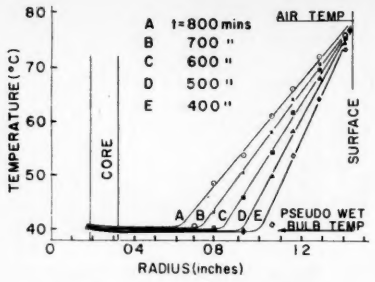

Fig. 4. Temperature vs. radius.

HEAT CONDUCTION

Heat transfer in the drying-wool bobbin is studied, the bound water being taken into account as required. The method used in Part I of dividing the bobbin into $\frac{1}{8}$-in.-thick annuli and considering steady state conditions to apply for 5-min. intervals is again employed.

The Total Heat Transfer

Use is made of the drying-rate curve and temperature record (Figure 1) to calculate the total heat received by the bobbin from the air stream.

$$q = hA_s(\Theta_a - \Theta_s) = \frac{dX}{dt}\lambda$$

+ sensible heat to wool, water, vapor, and heat of adsorption.*

From this formula the heat transfer coefficient may be calculated, and Figure 5 represents the variation of h with time. The first term on the right-hand side of Equation (1) is the dominant one, representing some 95% of the total heat.

There appears to be a significant fall in h during the first falling-rate period. The final tailing off of the plotted points is probably due to the high error in measuring the small temperature difference $(\Theta_a - \Theta_s)$; a very slight overestimate of Θ would produce such a fall off.

If it is possible to rely on a thermocouple just below the surface as a measure of surface temperature, then Figure 5 means that the heat transfer to the bobbin is greater when the surface is wet than when it is dry. Coplan (7) has attributed the fact that a hairy surface dries slower than a smooth one, which is borne out by the present work, to some modification (thickening) of the boundary layer as a result of the protruding hairs. Thus when a wool surface is dry the degree of hairiness would be increased and cause reduction of heat transfer.

*Data reported by Hedges (6) were used to obtain this small quantity of heat.

Table 2. Values of $k \times 10^4$ c.g.s. Centigrade Units

Time, min.	Average free-water content, gm./cc. of wetted fabric	Average k, annuli 2–7 inclusive
10–15	0.670	10.1
15–20	0.645	9.6
20–25	0.620	8.6
25–30	0.595	8.4
30–35	0.570	7.3
35–40	0.545	7.3
40–45	0.525	7.6
45–50	0.500	6.5

Table 1. Values of Percentage Regain to Nearest 1% in Successive $\frac{1}{8}$-in. Thick Layers From the Surface

Layer	1	2	3	4	5	6	7	8
Experimental values								
At critical moisture content	124	175	186	199	208	212	210	209
At end of first falling-rate period	85	118	125	131	135	140	131	165
			Air-dry			Wet		
At t = 500 min.								
Calculated	4	7	10	22		61 (average)		
Experimental	3	5	8	20	58	70	77	82
			Air-dry				Wet	
At t = 800 min.								
Calculated	3	5	7	9	12	23	49 (average)	
Experimental	2	2	4	6	9	18	54	62

k for Wet Wool

The first 50 min. of the temperature record, representing the heating of the wet wool, has been used, in the manner already described in Part I for the dry material, to give values of k for the $\frac{1}{8}$-in.-wide annuli; that is

$$\frac{\left[\begin{matrix}\text{rate of heat}\\ \text{entering}\end{matrix}\right] + \left[\begin{matrix}\text{rate of heat}\\ \text{leaving}\end{matrix}\right]}{2} = (k \text{ annulus}) \times \left[\begin{matrix}\text{mean area}\\ \text{of annulus}\end{matrix}\right] \times \left[\begin{matrix}\text{temperature gradient}\\ \text{across annulus}\end{matrix}\right] \quad (2)$$

The rate of heat leaving an annulus is compounded from the rate of supply of sensible heat to water and wool contained in the enclosed portion of the bobbin. When one uses the average free-water content value from Figure 3, it is assumed that the water distribution is uniform throughout the wet material. Adsorbed and pore water are considered identical so far as uptake of sensible heat is concerned, the wool and water being dealt with separately. Wahba and Nashed (8) from their experiments with cellulose suggest that the specific heat of adsorbed water may be higher than for ordinary water.

The complete results are given in Table 2. Values for the outermost and innermost annuli are omitted from the final-average values. In the case of the former these tend to be low, possibly because there may be less water in the layer; in the case of the latter a high error can be present in measuring the small amount of heat passing through the annulus. Another value which might be added to Table 1 is the value when the wool is in equilibrium with tunnel humidity, that is, when the free-water content is zero. The value previously reported from a dry wool experiment was $k = 1.07 \times 10^{-4}$ c.g.s. centigrade units.

Calculating k for fibers packing into a space between two concentric cylinders, Schuhmeister (9) assumed that they were distributed uniformly in all directions or, for the purposes of calculation, that $\frac{1}{3}$ were plane slabs parallel to the direction of heat flow and $\frac{2}{3}$ were slabs at right

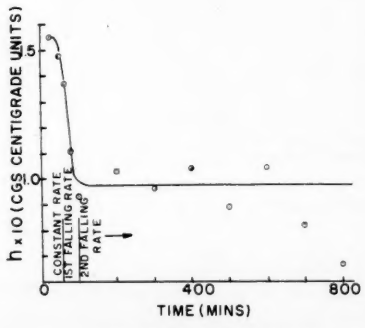

Fig. 5. h vs. time.

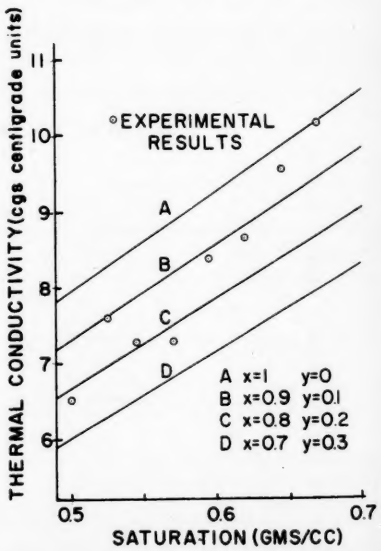

Fig. 6. k vs. average free-water content for wet wool.

angles to the direction of heat flow. On these assumptions

$$k_m = \tfrac{1}{3}(k_1v_1 + k_2v_2) + \tfrac{2}{3}\left(\frac{k_1k_2}{k_1v_2 + k_2v_1}\right) \quad (3)$$

Using k for wool fiber as 4.6×10^{-4} and k for air at the average experimental temperature as 0.661×10^{-4}, one gets

$$k_m \times 10^4 = 0.53 + 0.55 = 1.08$$

Thus the experimental value in the dry case fits this formula. If the formula is extended to three components, it becomes

$$k_m \times 10^4 = x(k_1v_1 + k_2v_2 + k_3v_3) + y\left(\frac{k_1k_2k_3}{k_2k_3v_1 + k_1k_3v_2 + k_1k_2v_3}\right) \quad (4)$$

where the mixture is represented by comparison with an arrangement of x parts where conductors are in parallel and y parts where they are in series. In Figure 6 the experimental values are compared. A value of $k = 7.0 \times 10^{-4}$ is used for saturated wool fiber and values appropriate to the average temperature for the rest of the water and air. It can be seen that when the wool is very wet the system giving the closest agreement is the one where all the conductors are in parallel. One might expect the dominant conduction of the water to tend to produce the parallel case as all the pores are filled. At the lower end of the experimental range of saturation the line representing $x = 0.8$ $y = 0.2$ gives better agreement.

k for Air-Dry Layers

Values were calculated for the quantities of adsorbed water in the various annuli at times 300, 400 ··· 900 min. after the method given previously. The amount in an annulus at 500 min. minus that at 700 min. would give the loss of adsorbed water in 200 min., the rate of loss of water being taken as that applying at $t = 600$ min. In this manner rates of evaporation of adsorbed water were calculated for $t = 400, 500 \cdots 800$ min.; for example at $t = 800$ min. the rates in grams per minute were 0.0003 (outer annulus), 0.0008, 0.001, 0.002, 0.005, 0.008, and at the water surface 0.043, making a total rate of drying of 0.06 g./min. Thus some 90% of the evaporation takes place within ¼ in. from the pore-water surface. Allowance was made for the latent heat and heat of adsorption required by the rate of evaporation, as well as for the sensible heat to the water present, in the case of each layer when the k value was calculated for a particular layer. The temperature gradient, the same for all layers, came directly from Figure 4.

Table 3 sets out the results for the five times considered. The k values are compared with the appropriate average regains for the layers. There is a fair amount of scatter in these results; the correlation coefficient is only 0.436, but the regression line to give the best value of k, in terms of R^*, is

$$k \times 10^4 = 1.30 + 0.011\,R^* \quad (5)$$

Thus when the regain increases from 2 to 20%, k increases from 1.32 to 1.52, an increase of 0.20. Baxter (*10*) reports an increase from 1.10 to 1.25, an increase of 0.15, when the bulk density is 0.335 g./cc. compared with 0.283 g./cc. in the present case. Thus the variation with regain is reasonable, though the absolute values are high.

Nevertheless the agreement is sufficient to indicate that the general approach, involving the calculated distribution of adsorbed water, fits the experimental data.

Table 3. Value of $k \times 10^4$ c.g.s. Centigrade Units

	t = 400 min.		500 min.		600 min.		700 min.		800 min.	
Annulus	Regain %	k,	Regain %	k,	Regain %	k,	Regain %	k,	Regain %	k,
1 (Outer)	4.0	1.66	3.5	1.34	3.4	1.39	3.3	1.19	3.2	1.00
2	9.5	1.67	6.6	1.44	5.8	1.53	5.3	1.29	5.0	1.08
3	22.7	1.58	10.4	1.46	8.3	1.63	7.3	1.41	6.7	1.18
4			22.1	1.35	12.1	1.68	9.9	1.52	8.8	1.29
5					23.4	1.58	14.8	1.54	12.2	1.38
6							25.0	1.48	23.1	1.42

CONCLUSION

The basic theory of the second falling-rate period indicates that a balance between heat transfer to and water vapor diffusing from the retreating water surface establishes equilibrium at the pseudo-wet-bulb temperature. If the textile adsorbs water, most of the evaporation of the adsorbed water takes place close to the boundary of the pore water, so that the over-all balance remains.

The theory in its present stage is still descriptive. It could be used to predict the second falling-rate curve only if some further knowledge is available as to the variation of the free-water content with time and depth. It is also necessary to find whether the pseudo-wet-bulb temperature appears with systems other than textile fibers or whether it is specific to these systems alone.

Current work along these lines is aimed at establishing further the generality of the pseudo-wet-bulb temperature and at deriving exact quantitative evaluation of the rate of drying during the falling rate period.

NOTATION

A_s = area of bobbin surface, sq. cm.
h = surface heat transfer coefficient, cal. cm.$^{-2}$ sec.$^{-1}$ (°C.)$^{-1}$
k = thermal conductivity coefficient, cal. cm.$^{-1}$ sec.$^{-1}$ (°C.)$^{-1}$
k_m = thermal conductivity coefficient of mixture, cal. cm.$^{-1}$ sec.$^{-1}$ (°C.)$^{-1}$
k_1 = thermal conductivity coefficient of first component, cal. cm.$^{-1}$ sec.$^{-1}$ (°C.)$^{-1}$
k_2 = thermal conductivity coefficient of second component, cal. cm.$^{-1}$ sec.$^{-1}$ (°C.)$^{-1}$
k_3 = thermal conductivity coefficient of third component, cal. cm.$^{-1}$ sec.$^{-1}$ (°C.)$^{-1}$
p = vapor pressure, mm. Hg.
p_a = vapor pressure in air stream, mm. Hg.
p_w = vapor pressure at water surface, mm. Hg.
q = rate of flow of heat, cal. sec.$^{-1}$
r = radius of water surface, cm.
R = radius of bobbin surface, cm.
R^* = regain, dimensionless (gm. gm.$^{-1}$)
t = time, sec.
T = absolute temperature, ° abs.
T_a = absolute temperature of air stream, ° abs.
T_w = absolute temperature of water surface, ° abs.
v_1 = volume of first component, cc.
v_2 = volume of second component, cc.
v_3 = volume of third component, cc.
X = free-water content of bobbin, g.
E = void fraction, dimensionless (cc. cm.$^{-3}$)
Θ_a = temperature of air stream, °C.
Θ_s = temperature of bobbin surface, °C.
Θ_w = temperature of water surface, °C.
λ = latent heat of evaporation, cal. g.$^{-1}$

LITERATURE CITED

1. Nissan, A. H., W. G. Kay, and J. R. Bell, *A.I.Ch.E. Journal*, **5**, No. 1, 103 (1959).
2. King, G., and A. B. D. Cassie, *Trans. Faraday Soc.*, **36**, 445, (1940).
3. McReady, D. W., and W. L. McCabe, *Trans. Am. Inst. Chem. Engrs.* **29**, 131 (1933).
4. Speakman, J. B., *Trans. Faraday Soc.*, **25**, 92 (1929).
5. ———, and C. A. Cooper, *J. Text. Inst.*, **27**, T183 (1936).
6. Hedges, J. J., *Trans. Faraday Soc.*, **22**, 178 (1926).
7. Coplan, M. J., *Text. Res. J.*, **23**, 897 (1953).
8. Wahba, Maurice, and Shawky Nashed, *Nature*, **166**, 998 (1950).
9. Schuhmeister, *Ber. K. Akad. Wien., Math.-Naturw. Kl.*, **76**, 283 (1877).
10. Baxter, S., *Proc. Phys. Soc. (London)*, **58**, 105 (1946).

Manuscript received May 20, 1958; revision received November 26, 1958; paper accepted November 28, 1958.

Initiation of the Homogeneous *n*-Butane Oxidation

J. F. SKRIVAN and H. E. HOELSCHER

The Johns Hopkins University, Baltimore, Maryland

Initiation of the oxidation of hydrocarbons, an important part of many flame systems' remains largely unsolved. This paper reports a study of the oxidation of butane under conditions that yield information on the homogeneous initiation reactions.

A sequential reaction mechanism is proposed involving activation of an oxygen molecule followed by attack on a butane. This leads to rate equations which accurately describe the observed butane decomposition rates. Activation energies have been calculated from experimental data with this equation and are found to check values obtained from the literature and from theoretical considerations.

The tentative initiation mechanism is used to explain the existence of three classes of products in the exit gases: hydrocarbons other than butene, butene, and oxygenated products.

Under some operating conditions periodic cool flame phenomena are observed, and their effect on the course of the reaction has been explained.

Although considerable progress has been made in the field of low-temperature hydrocarbon oxidation, kinetic data which could be used as a basis for the formulation of reaction mechanisms are lacking. Methane and formaldehyde, the two simplest members of their respective series, have been studied extensively, and their oxidation reaction kinetics has been clarified by Norrish and his co-workers (*10*). However for hydrocarbons above methane only a few systematic kinetic studies have been made, and virtually no information is available for hydrocarbons above heptane. The large number of reaction products, their isolation, identification, and quantitative analysis have without the use of expensive mass spectrographic techniques presented a considerable barrier to the characterization of the oxidation reaction. Although the development of gas chromatography as an analytical device has given a powerful new tool to investigators in this field, nevertheless the myriad chemical reactions occurring simultaneously in the oxidation of even such apparently simple molecules as ethane prohibits the writing of any single rate equation descriptive of the entire process. An excellent review article by Tipper (*14*) points up the complexity of the problem.

There are at least three different regions of interest: a precool-flame region in which slow, partial oxidation occurs, usually accompanied by a faint luminescence; the cool flame region, evidenced by higher rates of partial oxidation, usually characterized by periodic pressure fluctuations which correspond to the alternate formation and extinction of cool flames; and two-stage ignition, leading to complete reaction. The last of these is always preceded by a single cool flame. Which of the above phenomena is realized in a given experiment depends on the pressure, temperature, concentration, and reactor geometry.

By far the large majority of partial-oxidation studies have been performed in batch systems in which reaction rates are followed by a measurement of pressure increase, and quenching of the reaction is accomplished by removing the system from its oven and plunging it into a cold bath. There are, however, several advantages of flow system over batch systems for partial oxidation studies. In addition to their obvious manipulatory advantages, flow systems are capable of yielding much larger quantities of product for analysis and are far more flexible to operate. Flow systems have been used by King, Sandler, and Strom (*8*), Kovijman (*9*), Garner and Petty (*6*), Frank and Blackham (*5*), Quon, Dalla Lana, and Govier (*11*), and others. Stable (nonperiodic) cool flames have been obtained in flow systems of the proper configuration by Boord and associates (*2*) and Williams, Johnson, and Carhart (*15*).

The effect of surface on the partial oxidation of hydrocarbons is particularly difficult to characterize. The nature and state of the surface and surface-to-volume ratio often play important roles in the reaction. Surface is generally acknowledged to have an inhibitory effect on the reaction by free radical destruction. Although free radicals can be destroyed and initiated both homogeneously and heterogeneously, surface destruction is more efficient than gas-phase destruction. Hence an increase in surface to volume ratio should yield a decreased reaction rate. This has been observed experimentally. However surface initiation is known to play an important role in many partial oxidation reactions (*13*). One of the goals of this research was to attempt clarification of this point.

The paper then reports results from a kinetic investigation of the initiation of normal-butane oxidation in a flow reactor. As will become evident, wall effects were proved negligible, and only the homogeneous reaction was studied. Normal butane was chosen because less attention has been paid to it than to any normal hydrocarbon in the C_1 to C_5 range and because it is the logical precursor to an understanding of the combustion of higher hydrocarbons which may be of more practical interest. The latter arises because butane is the first member of the series having both primary and secondary carbon atoms adjacent to the points of most probable attack.

EXPERIMENTAL PROGRAM: EQUIPMENT

The equipment used in this project consisted of the normal sequence of reaction system and analytical apparatus. The reactor is shown diagrammatically in Figure 1. A mixture of oxygen and normal butane of better than 99.5% purity was fed to the reactor through standard flow regulation and metering devices. Gas pressure at all flow meters and in the reactor was measured manometrically, and temperatures were measured throughout the apparatus by iron-constantan, glass-insulated thermocouples. Surface temperatures were measured at the inlet to the reactor, at the axial center of the reactor, and at the reactor outlet (Figure 1). All temperatures were recorded continuously. The reactor and gas preheaters were surrounded by a high-temperature oven providing the primary heat source.

The reactor consisted of three parts. The first was a packed inlet section, the second the reactor proper, the third a packed outlet section. The packing was random chips and turnings of stainless steel washed with acetone and dried overnight at 110°C. It was supported by a stainless steel screen. The conical inlet and outlet sections served two purposes. They served as smooth enlarging and reducing sections, thus eliminating any large stagnant areas upstream or downstream to the reaction zone, and they provided effective heat transfer sections.

Product gases were led to a cold-finger type of condenser. Liquid product was collected in standard 0°C, cold traps,

J. F. Skrivan is with the American Cyanamid Company, Stamford, Connecticut.

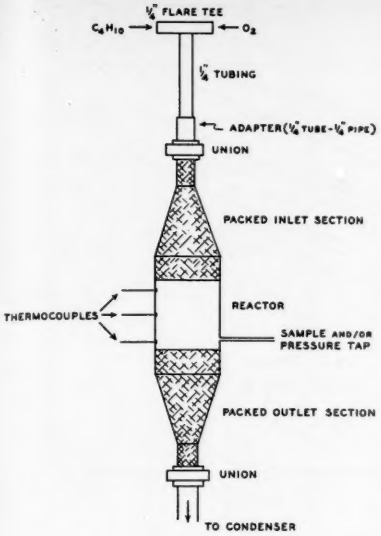

Fig. 1. Reactor assembly.

and the uncondensed gases were sampled in conventional gas-collecting bulbs.

For analysis a gas chromatographic unit was constructed. Helium of 99.99% minimum purity was used as a carrier gas. Details of the construction, operation, and use of this device as well as of the complete experimental apparatus are available (*12*).

Because of the large number of products present in the exit gases, five separate columns were used for the analysis. All columns were made of ¼-in. copper tubing and were packed tightly by use of an electric vibrator. The following columns were used:

1. Column 1, 7 ft. of 30 to 60–mesh type 5A molecular sieve, was used for analysis of hydrogen, oxygen, nitrogen, methane, and carbon monoxide.

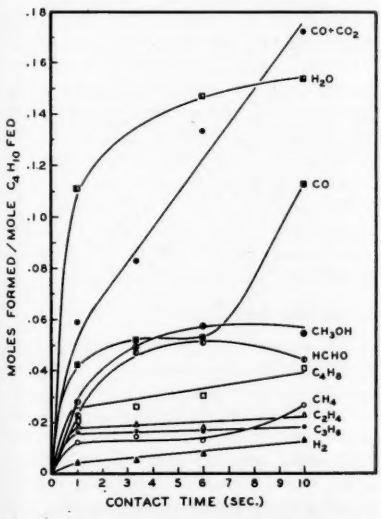

Fig. 2. Sample product distribution; moles of product formed vs. contact time at 350°C., 20% initial oxygen concentration.

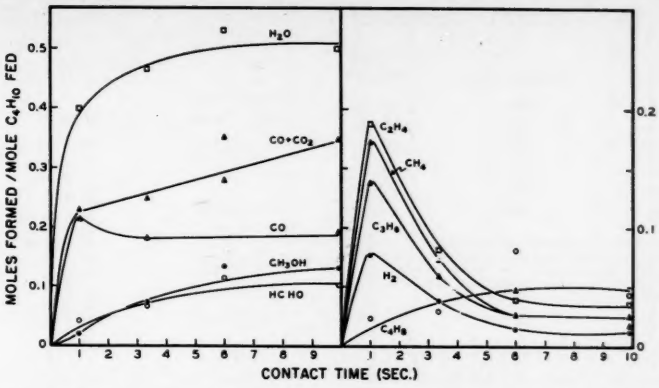

Fig. 3. Sample product distribution; moles of product formed vs. contact time at 350°C., 40% initial oxygen concentration.

2. Column 2, 4 ft. of 80-mesh activated charcoal, was used for analysis for methane, ethylene, and ethane. This column could also be used for carbon dioxide but was not nearly so sensitive for this as was column 3.

3. Column 3, 3½ ft. of 40 to 60–mesh silica gel, was used for analysis of carbon dioxide.

4. Column 4, 3 ft. of 20-mesh activated alumina, was used for analysis of ethylene, propane, acetylene, propylene, butane, and the butylenes.

5. Column 5 was 10 ft. in length, 4 ft. of which were packed with di-*n*-octyl phthalate supported on 60 to 100–mesh acid-washed celite, and the remaining 6 ft. consisted of celite impregnated with glycerol. The packing of each section was prepared by contacting 35 wt. % of the liquid with 65 wt. % celite in an acetone slurry. The acetone was subsequently removed by overnight oven drying at 110°C. Column 5 was used for analysis of the liquid product (aldehydes, alcohols, ketones, and water).

The chromatographic columns and the thermal-conductivity cell were enclosed in a constant-temperature oven, with heat supplied by nichrome-resistance wire coils mounted on the inner surface of the oven. Temperatures in excess of 200°C. were obtainable and were measured at the center of the oven. Temperature control was effected by standard devices.

EXPERIMENTAL PROGRAM: PROCEDURE

After preliminary start-up operations had been completed, a reaction was initiated and the reaction temperature was adjusted to the desired value. The system was allowed to equilibrate and was operated continuously for 2 hr. before any product was collected. The duration of any single run was usually determined by the rate of liquid-product formation, 2 cc. being required for all analyses. If more than one run was made in any given day, 2 hr. was allowed for the system to reequilibrate at the new conditions.

Preliminary experimentation established that reaction temperatures from 275° to 350°C., contact times between 1 and 10 sec., and from 20 to 40% inlet oxygen concentrations would be suitable for the purposes of this work. To randomize errors throughout the program an experimental sequence was set up in which the runs were made in random order. To obtain information regarding the reproducibility of the work, a set of check runs was superimposed on the random series. Complete details of the experimental work and the results obtained are, again, available in reference *12*.

The preliminary work also served to prove the absence of surface effects. For this purpose the entire reactor assembly was packed with stainless steel chips and turnings. The reactor temperature was adjusted to 335°C., and the reactor was fed with a 30% oxygen–to–70% butane mixture at a rate such that the contact time was 7 sec. Over 7½ hr. of operation no measurable reaction of any kind was found. After the detailed experimental program had been completed, a check on this was made with the conditions under which the highest reaction rate had been observed. At a temperature of 350°C., 40% initial oxygen concentration, and 1.09 sec. contact time no reaction was observed in 2 hr. of operation with the completely packed

Table 1. Typical Product Distribution
Run conditions: temperature = 300°C., contact time = 3.35 sec., initial oxygen concentration = 40%

Constituent	Total moles exit reactor × 10^3
H_2	3.61
O_2	72.1
CH_4	9.61
CO	84.1
C_2H_4	14.7
C_2H_6	0.37
CO_2	16.5
C_3H_8	0.05
C_3H_6	14.0
C_4H_8	17.5
C_4H_{10}	299.0
HCHO	37.0
CH_3CHO	3.56
$(CH_3)_2CO$	1.28
CH_3OH	30.0
H_2O	161.0
Acid	2.58

Butane conversion, oxygen conversion, material balances, mole fractions, etc., may be calculated from these data.

Table 2. Material Balance

Run (12)	Carbon balance	Oxygen balance
24	100.9	99.6
25	102.1	97.6
26	100.0	97.9
47	105.8	92.9
48	93.0	98.0
49	98.1	97.5

The data are reported as percentage of reactant fed which was accounted for in the exit stream. For the carbon and oxygen the mean balances yield 100.0 and 97.4% respectively, and the coefficients of variation are 3.63 and 2.13.

reactor. The reactor temperature was then gradually increased. At 420°C. a reaction was obtained. This reaction was characterized by a very low carbon monoxide formation, approximately 2.5% of the methane-formation and approximately $\frac{1}{3}$ of the hydrogen-formation rates previously observed. This reaction was sustained as the reactor temperature was decreased below 420°C., but the rate dropped off very sharply. At 370°C. the reaction was again below the detectable level. Since the maximum operating temperature throughout this work was 350°C., it is evident that reaction in the inlet packed section may be ignored in this study.

To study the quenching action of the packed outlet section, samples were taken directly from the reactor and compared with those removed from the condenser outlet. The samples from the reactor were removed at a rate slower than the flow rate in order to avoid sucking of gas back from the packed section. There was no detectable difference between the concentrations of products in the sample taken just prior to the packed section and in those taken from the condenser.

RESULTS

A typical list of products obtained at one set of operation conditions is shown in Table 1. Forty-nine experimental runs were made, approximately half at 20% inlet oxygen concentration (the remainder being normal butane) and approximately half at 40% inlet oxygen concentration. Contact time was varied between 1 and 10 sec. and the temperature between 275° and 350°C. All product analyses were obtained by means of gas chromatography with the exception of analyses for acid, formaldehyde, and peroxide in the liquid, which were made chemically. The absence of peroxides in the products is interesting but easily explained by the configuration of the reactor and condenser system; peroxides are known to be unstable and to decompose on the walls of a reactor or on other surfaces.

Figures 2 and 3, which illustrate typical product distributions as a function of contact time, formed the basis for the kinetic analysis which was made. Complete material balances were made for six of the runs; the results are shown in Table 2. A reproducibility study was made on five of the runs. Statistical analysis of the results indicated that all deviations from the mean were random, and the standard deviation for all constituents varied between 0.50 and 2.06.

Table 3 presents a sample of the experimental data which formed the basis for the conclusions presented in this paper. Similar tables were obtained for each run and are available (*12*). These data were correlated graphically by the preparation of plots of product distribution as a function of contact time. Because of the configuration of the reactor and condenser system, the presence of peroxides in more than trace quantities is not to be expected. Chemical analysis of the liquid product indicated an average peroxide concentration of 0.5% based on the liquid product.

It will be noted that the data from runs using 40% initial oxygen concentration show a maximum in the conversion-contact time curve which is not observed in the 20% data. This peak was due to periodic cool-flame formation which manifested itself by strong pressure fluctuations and marked increases in the cracking reactions leading to the formation of unusually large amounts of hydrogen, methane, ethylene, and propylene. The final conversion rate at high contact time in this 40% data is approximately double that observed in the 20% data.

ANALYSIS OF THE RESULTS

Wall Effect

As previously noted, surface was shown to have an inhibitory effect on the over-all oxidation reaction. To estimate the effect of surface in the unpacked reactor (the effect of any quenching at the wall), it was necessary to calculate a range of effectiveness of the wall. The *range of effectiveness* may be defined as that distance from the wall at which the probability of a free radical-wall collision (and subsequent destruction) is equal to the probability of a radical-molecule collision (leading to chain continuation). When one assumes a free radical at distance δ from the wall, and when one assumes that in its next move it moves toward the wall, the ratio of the probability of a collision with the wall to that of a collision with another molecule may be calculated (as a function of δ) and set equal to unity. For $T_R = 600$°K., a typical reactor temperature, and with $r_m = 4 \times 10^{-8}$ cm., such a calculation yields $\delta \cong 4.06 \times 10^{-6}$ cm. Hence the range of effectiveness of the wall extends approximately 10^{-6} cm. into the reactor. The authors have assumed in this calculation that all collisions between free radicals and surface or molecules are effective. Even if the wall collisions are 1,000 times as effective as homogeneous collisions, δ is only $\approx 10^{-3}$ cm. Thus the volume bounded by δ is negligible by comparison with the total reactor volume, and the wall effect in the homogeneous section may be neglected.

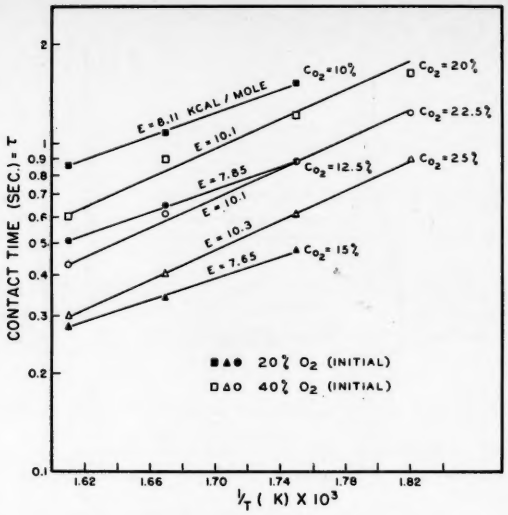

Fig. 4. Estimation of activation energy from

$$\log \tau = \log \left[\frac{\rho}{A} \int_0^{x_A} \frac{dx_A}{\prod_i^i (C_i^{\,i})} \right] + E/2.3RT.$$

Temperature Gradient

To employ the surface temperature measured at the axial center of the reactor in subsequent calculations of the activation energy, it is necessary to show that this temperature is an adequate representation of the true reactor temperature. Since it was not feasible to obtain a radial temperature profile experimentally, this gradient was calculated for the most drastic conditions (that is, run 34, in which the maximum heat generation

Table 3. Sample Data Sheet—Run 26

Initial oxygen concentration = 39.9%, reactor temperature = 299°C. (572°K.) contact time = 3.34 sec., room temperature = 29°C.

Constituent	Mole oxygen	Reacted carbon, %	Mole %	Moles formed/ mole C_4H_{10} fed
H_2			0.47	0.0094
O_2	0.144		9.39	
N_2				
CH_4		2.75	1.25	0.0249
CO	0.084	24.1	10.9	0.218
$CH_4(c)$				
C_2H_4		8.39	1.91	0.0381
C_2H_6		0.21	0.048	0.00096
CO_2	0.033	4.72	2.15	0.0427
$C_2H_4(Al_2O_3)$				
C_3H_8		0.04	0.007	0.00013
C_3H_6		16.0	1.82	0.0362
C_4H_8		20.0	2.28	0.0454
C_4H_{10}			38.9	
HCHO	0.037	10.6	4.81	0.0959
CH_3CHO	0.0036	2.04	0.463	0.0092
$(CH_3)_2CO$	0.0013	1.10	0.167	0.0033
CH_3OH	0.030	8.56	3.90	0.0777
H_2O	0.161		20.9	0.417
*Acid	0.0052	1.48	0.336	0.0067
Totals	0.499			

Rate of liquid product formation = 4.28 g./hr.; 5.35 g. total
Moles O_2 fed = 0.255
Moles C_4H_{10} fed = 0.386; moles carbon fed = 1.544 = C
Total mass fed = 30.57 g.
$R_1 = 1.65$
$R_2 = 0.925$
$R_3 = CO_2/C_2H_4 = 1.12$

$T_i = 28.3/224 \times 273/302 \times 0.465\ N_i = 0.0531\ N_i$

Material Balances:
Oxygen 97.9%
Carbon 100%
Conversions:
Oxygen 71.7%
Butane 22.7%
% C_4H_{10} to: oxygenated products 11.9%

per unit volume per unit time was obtained).

Assuming radial symmetry and no axial gradient, one can solve the heat transfer equation with a heat-generation term. Assuming that half the butane reacts (all going to carbon dioxide and water), one obtains a generation rate of 0.00125 cal./(cc.) (sec.) This is undoubtedly much higher than the values realized during the experimentation. An average value of the thermal conductivity was estimated to be 1.03×10^{-4} cal./(sec.) (cm. °C.), and a maximum temperature difference between reactor center and wall was calculated to be 6.9°C. The axial temperature gradient, as measured by surface thermocouples, was found to be 2°C./cm. Since the length of the reactor is 3 cm., this represents a 6°C. maximum variation in temperature under the worst possible conditions. Thus the assumption of an isothermal reactor is justified, and the reaction temperature (as measured by a center axial-wall thermocouple) is subject to an uncertainty of approximately 6°C. This represents a temperature variation of less than 2% on the Kelvin scale.

Preliminary Estimate of Over-all Activation Energy

In order to postulate a set of initiation reactions which would lead to a rate equation to be tested against the experimental data, some information concerning the energies of the reaction was required. An estimate of the over-all activation energy was made as follows. In a flow reactor

$$r\,dV = F\,dX_A \qquad (1)$$

when one rearranges and integrates, with

$$r = \frac{dC_B}{dt} = -k[\prod_i^j (C_i^j)] \qquad (2)$$

where dC_B/dt = rate of consumption of butane, $\pi^i\ C_i^j$ = the product of all of the molecular concentrations upon which the rate depends, raised to the appropriate power j, and with

$$F = \rho Q \qquad (3)$$

one obtains

$$\frac{V}{\rho Q} = \frac{1}{k}\int_0^{X_A} \frac{dX_A}{\prod_i^j C_i^j} \qquad (4)$$

But

$$\frac{V}{Q} = \tau$$

= contact time based on inlet flow rates. Then

$$\frac{\tau}{\rho} = \frac{1}{k}\int_0^{X_A} \frac{dX_A}{\prod_i^j C_i^j} \qquad (5)$$

Taking the logarithm of each side and substituting the Arrhenius form for k, one obtains after slight rearrangement

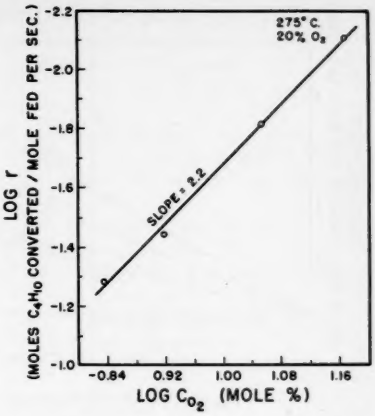

Fig. 5. Test of second-order oxygen dependence (20% oxygen data).

$$\ln \tau = \ln\left[\frac{\rho}{A}\int_0^{X_A} \frac{dX_A}{\prod_i^j C_i^j}\right] + \frac{E}{RT} \qquad (6)$$

Since butane is present in large excess, oxygen is the limiting reactant and to a first approximation will be the major term in $\pi^i\ C_i^j$. At constant oxygen concentration the second log term will be approximately constant, and a plot of $\ln \tau$ vs $(1/T)$ should yield an activation energy. At very low contact times, conversions are small and the oxygen concentration does not change radically through the reactor. Plots of outlet oxygen concentration as a function of contact time were made, and from these curves for each value of oxygen concentration values of τ and T were taken and plotted as log τ vs. $(1/T)$. These results are shown in Figure 4 for both 40 and 20% initial oxygen concentrations. Activation energies between 7.7 and 10.3 kcal./mole were obtained.

Initiation Reaction

With a knowledge of the approximate activation energy, obtained in the previous section, some tentative statements can be made regarding the nature of the controlling step or steps in the partial oxidation reaction. Over-all activation energies in the range of 8 to 10 kcal./mole could indicate either a diffusion-controlled step or a low-energy gas phase or wall activation. Since the reaction has been shown to be surface inhibited, a diffusion or activation involving the wall can play no part in the activation process. This leaves the possibility of a low-energy gas-phase bond-activation step, involving either O_2/C_4H_{10}, C_4H_{10}/C_4H_{10}, or O_2/O_2 collisions.

Of the three possible types of initiating collisions the oxygen-butane and the butane-butane collisions may be eliminated from consideration due to the number of degrees of freedom involved. The energy transferred by the collision is dissipated among these many degrees of freedom, and as a result no one of the

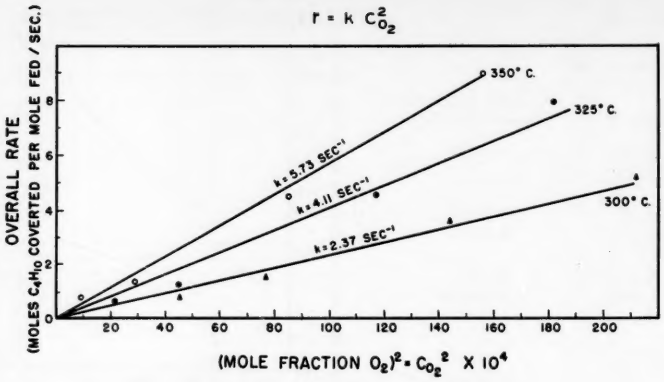

Fig. 6. Test of rate equation (20% oxygen data).

bonds is likely to undergo activation. However in an oxygen-oxygen collision only one bond is available for activation in each of the two participating molecules. The following tentative mechanism, descriptive of the initiation process, may now be written

$$O_2 + O_2 \underset{k_{-1}}{\overset{k_1}{\rightleftarrows}} O_2^* + O_2 \qquad (7)^*$$

$$O_2 + A \underset{k_{-2}}{\overset{k_2}{\rightleftarrows}} O_2^* + A \qquad (8)$$

$$O_2^* + C_4H_{10} \xrightarrow{k_3} C_4H_9\cdot + HO_2 \qquad (9)$$

Equation (7) represents a collisional activation-deactivation process resulting in the formation of excited oxygen molecules. Equation (8) indicates that the activation and deactivation could also involve another species A, where A may be any other molecule present with the exception of O_2 and O_2^*. Equation (9) is the free radical initiation step. The rate of O_2^* formation is then

$$\frac{dC_{O_2^*}}{dt} = k_1 C_{O_2}{}^2 + k_2 C_{O_2} C_A - k_{-1} C_{O_2^*} C_{O_2} - k_{-2} C_{O_2^*} C_A - k_3 C_B C_{O_2^*} \qquad (10)$$

*Bleakney (1) has recently reported the relaxation time for excited oxygen to be approximately 10^{-5} sec. under the conditions of this work. Since the collision frequency is many orders of magnitude greater than this, the proposed mechanism involving vibrationally excited oxygen molecules appears not to be unreasonable from this point of view.

when one makes the steady state assumption for the active species

$$\frac{dC_{O_2^*}}{dt} = 0 \qquad (11)$$

and

$$C_{O_2^*} = \frac{k_1 C_{O_2}{}^2 + k_2 C_{O_2} C_A}{k_{-1} C_{O_2} + k_{-2} C_A + k_3 C_B} \qquad (12)$$

Since butane is present in large excess, $C_A \approx C_B$, and

$$C_{O_2^*} = \frac{k_1 C_{O_2}{}^2 + k_2 C_{O_2} C_B}{k_{-1} C_{O_2} + k_{-2} C_B + k_3 C_B} \qquad (13)$$

It seems reasonable to assume that $k_2 C_{O_2} C_B$ is much smaller than $k_1 C_{O_2}{}^2$, and similarly that $k_{-2} C_B \ll k_{-1} C_{O_2}$. Hence

$$C_{O_2^*} \cong \frac{k_1 C_{O_2}{}^2}{k_{-1} C_{O_2} + k_3 C_B} \qquad (14)$$

The rate of butane conversion from (9) is

$$\frac{dC_B}{dt} = -k_3 C_{O_2^*} C_B = -\frac{k_3 k_1 C_B C_{O_2}{}^2}{k_{-1} C_{O_2} + k_3 C_B} \qquad (15)$$

An approximate second-order oxygen dependence, confirmed in the next section, indicates that the term $k_{-1} C_{O_2}$ must be negligible in comparison with $k_3 C_B$ and that for subsequent development and testing the following over-all rate equation may be used:

$$\frac{dC_B}{dt} = -k_1 C_{O_2}{}^2 \qquad (16)$$

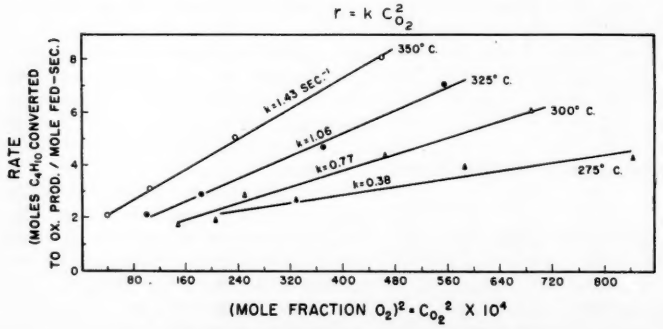

Fig. 8. Test of rate equation (40% oxygen data).

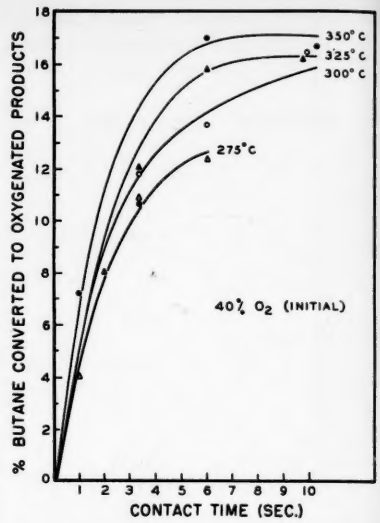

Fig. 7. Conversion to oxygenated products (40% oxygen data).

Test of Rate Equation

The validity of Equation (16) was tested by the experimental data. Figure 5 shows a check of the second-order dependence on oxygen concentration. A plot of log r vs. log C_{O_2} should have a slope of 2 if the proposed rate equation is correct. The rates were obtained from the butane conversion-contact time curves. At a given contact time the rate was measured graphically, and the corresponding value of oxygen concentration at this contact time was used to prepare

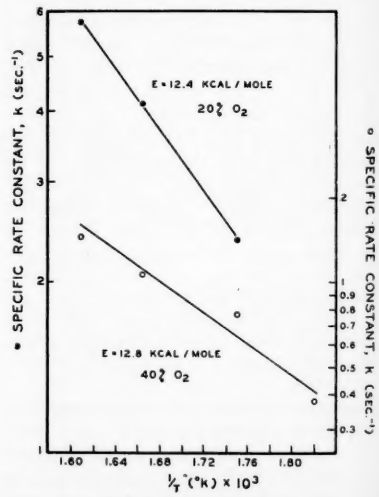

Fig. 9. Arrhenius plot.

Figure 5. A slope of 2.2 was obtained in excellent agreement with the proposed second-order oxygen dependence.

The entire rate equation was next tested for constancy of the specific rate constant. To satisfy the rate equation, plots of rate of butane conversion vs. $C_{O_2}{}^2$ must be linear and pass through the origin. Rates were obtained by graphical differentiation of the data. These data are plotted for the 20% oxygen runs in Figure 6. The results are in definite agreement with the rate equation.

As has previously been noted, cool-flame formation was observed in some of the runs made at 40% initial oxygen concentration. The innate unsteadiness of this periodic phenomenon precludes the direct use of the proposed rate equation for this data. However some interesting information can be obtained by a modification of the rate term itself. If, instead of over-all butane conversion, butane converted only to oxygenated products is plotted against contact time, a smooth curve is obtained (Figure 7). Bearing in mind that the rates obtained from this data are of different significance than the rates used previously one may make a similar type of analysis (Figure 8). In Figure 8 the rate of conversion to oxygenated products only is plotted against $C_{O_2}{}^2$. The linearity of these plots confirms the validity of the rate equation and indicates that the initiation mechanism is probably the same as for the 20% runs.

Values of k were obtained from the slopes of the lines shown in Figures 7 and 8. The over-all energy of activation of the process was then determined from plots of log k vs. $1/T$ (Figure 9). The values obtained for E_A are in good agreement with those estimated in the previous section.

The postulate of an activated oxygen molecule resulting from an oxygen-oxygen collision seems to be in agreement with the over-all activation energies obtained. The energy E_1 required for a transition from the oxygen ground state to the first vibrational level is 4.6 kcal./mole, and 10 kcal./mole is required for the second (7). Excitation to the second or third level then seems necessary for this process.

Over-all Reaction

Over twenty products of the partial oxidation of n-butane were observed; there are no doubt traces of many more. To set up a reaction sequence which not only leads to all the observed products but also agrees with the distributions obtained experimentally is an insurmountable task at this time. Many of the products react further, and it is not feasible to specify completely the interrelations of these products with the reactants, radicals, and other products involved. A partial list of reactions which probably occur has been prepared (12).

Three general types of products have been found: butenes, cracking reaction products, and oxygenated products. The reactions leading to the formation of each of the classes depend either directly or indirectly on the fate of the butyl radical. Butene formation by hydrogen abstraction from the butyl radical seems most probable. The butyl-peroxide radical formed by oxygen addition to the butyl radical leads to the oxygenated products. Decomposition of the butyl radical leads to formation of cracking products. Reactions of the types suggested are validated in the literature (3, 4).

CONCLUSIONS

1. An initiation step for the homogeneous butane oxidation involving activated oxygen molecules resulting from oxygen-oxygen collisions has been proposed. A rate equation involving a second-order oxygen dependence was derived and confirmed by testing against experimental data. The initiation step was shown to be the same for both cool-flame and noncool-flame regions.

2. Activation energies resulting from the use of the derived rate expression are in agreement with those obtained by other techniques and were comparable with those found in other investigations.

3. The products and product distributions obtained indicated that the butyl radical is a critical intermediate in the partial oxidation process studied. The types of products obtained and their relative importance depend in large measure on the fate of this radical.

ACKNOWLEDGMENT

The authors wish to express their gratitude to the Heyden-Newport Chemical Corporation whose financial assistance permitted initiation of this project. J. F. Skrivan held the American Cyanamid Fellowship in the Department of Chemical Engineering during his last year of work. For this award both authors are grateful.

The interest and suggestions of W. C. Bastian and J. W. Gryder were also helpful and are hereby acknowledged.

NOTATION

A	= Arrhenius frequency factor, sec.$^{-1}$
A	= symbol for a gas-phase constituent
cc.	= size of sample analyzed
C	= total moles carbon fed
C_B	= butane mole fraction
C_i	= mole fraction of i
C_{O_2}	= mole fraction of oxygen
$C_{O_2}{}^*$	= mole fraction of activated oxygen molecules
C_P	= specific heat, cal./(g. mole) (°K.)
E_A	= apparent activation energy, kcal./mole
E	= activation energy, kcal./mole
F	= feed rate, mass per unit time
k	= specific reaction rate constant, sec.$^{-1}$
$M.W.$	= molecular weight
N_i	= cc.^{i}/10cc. total exit gas
Q	= inlet flow rate, cc./sec.
R	= gas constant, cal./(mole) (°C.)
R	= gas-phase concentration ratio
r	= reaction rate, moles/(mole feed) (sec.)
r_m	= molecular radius, cm.
T	= temperature, °K.
T_i	= total moles i leaving reactor during run
T_R	= reactor temperature, °K.
T_W	= wall temperature
V	= reactor volume, cc.
X_A	= moles of A converted per unit mass of feed

Greek Letters

δ	= range of effectiveness of the wall, cm.
ν	= molecular concentration, molecules/cc.
ρ	= gas density, g./cc.
τ	= contact time based on inlet flow rate, sec.

LITERATURE CITED

1. Bleakney, Walker, *Proc. Conf. Chem. Aeronaut.*, Cambridge, Massachusetts (1956).
2. Boord, Cecil E., *Armed Services Technical Information Agency*, AD 50173 (1954).
3. Byrko, V. M., K. E. Krughyakova, and A. F. Lukovnikov, *Doklady Akad. Nauk SSSR*, **6**, 1093 (1936).
4. Dobvinskaya, A. A., and M. B. Neiman, *ibid.*, **58**, 1969 (1947).
5. Frank, C. E., and A. U. Blackham, *Natl. Advisory Comm. Aeronaut., Tech. Note* 2958 (1953).
6. Garner, F. H., and D. S. Petty, *Trans. Faraday Soc.*, **47**, 877, 844 (1951).
7. Herzberg, Gerhard, "Molecular Spectra and Molecular Structure," D. Van Nostrand, New York (1950).
8. King, R. O., S. Sandler, and R. Strom, *Nature*, **180**, 335 (1957).
9. Kovijman, P. L., *Rec. Trav. Chem.*, **66**, 5 (1947).
10. Norrish, R. G. W., "Cinetique et Mechanisme des Reactions D'Inflammation et de Combustion en Phase Gazeuse," *Centre natl. recherche sci.*, p. 16 (1948).
11. Quon, D., I Dalla Lana, and G. W. Govier, *Can. J. Chem.*, **32**, 880 (1954).
12. Skrivan, J. F., dissertation, Johns Hopkins Univ., Baltimore, Maryland (November, 1958).
13. Taylor, C. F. H., E. S. Taylor, J. D. Livingood, W. A. Russel, and W. A. Leary, *Soc. Automotive Engrs.*, **4**, 232 (1950).
14. Tipper, C. F. H., *Quarterly Rev.* (*London*), 313 (1957).
15. Williams, K. G., J. E. Johnson, and H. W. Carhart, *Natl. Res. Lab. Report 4249* (1953).

Manuscript received November 25, 1958; revision received February 23, 1959; paper accepted February 25, 1959. Paper presented at A.I.Ch.E. Atlantic City meeting.

Experimental Foundations of Chemical Engineering

R. R. WHITE and S. W. CHURCHILL

University of Michigan, Ann Arbor, Michigan

Fundamental knowledge consists of understanding not only the models which correlate and rationalized observations but also the quantity and quality of the observations. The degree of correlation attempted should be consistent with this quantity and quality.

The scientist correlates and rationalizes observations primarily to broaden his general understanding of the physical universe, and his efforts at correlation are more often than not a way of speculating on the future experiments which should be undertaken to test his concepts. For this purpose he is often satisfied with accuracy to one order of magnitude. The engineer, faced with the design and operation of expensive equipment, is almost always interested in a much higher accuracy in his correlations.

Virtually all existing data in the rate processes are forced into rationalizations based upon either potential-difference or potential-gradient models. The application of these models to systems of even relatively simple geometry gives rise to mathematical complexity beyond present analytic ability. Even so, our ability to measure and observe seems to be far below our ability to analyze. These two models have been used effectively in chemical engineering in the past and have served to organize a great deal of information in the rate processes. Present research efforts appear to be directed primarily toward filling in gaps in available data and in refining the application of the models. We seem to suffer from a lack of models to test and a lack of data designed to test critically the existing models. There is relatively little exploratory research in chemical engineering as compared, for example, to physics.

When one views chemical engineering as a chain extending from economics, markets, mechanical design, process design, and process development to process research, the uncertainties inherent in some of the links easily involve variances of 50 to 80%. Under these circumstances it would appear that the present orientation of research is distributed much too heavily toward refinement of existing ideas and not nearly enough toward exploration.

The observations made by scientists and engineers form the basis of chemical engineering. These observations are collected in a concise form as correlations and rationalized in terms of models or mechanisms, which are referred to as *hypotheses*, *theories*, and *laws*.

It is natural that the consideration of engineering problems is focused on theories. In today's explosive production of engineering data the pressure on the engineer to follow the patterns of thought and technique suggested by existing theory is almost irresistible; thus it is ironic that in a time of "plenty," with respect to engineering accomplishment, the phenomenological bases of chemical engineering seem to be increasingly ignored.

Typical of this tendency is the fact that publication of original data has largely been abandoned in favor of deposition in such repositories as the American Documentation Institute or in the original research records, which are relatively inaccessible. As a result present knowledge, as represented by the literature, has the appearance of correlation resting upon correlation, theory upon theory, and the data presented consist of a few graphs greatly reduced in scale, with only a few major coordinate lines. It is becoming more and more usual to accept the general statements and conclusions of the authors because of the time and trouble involved in obtaining the data necessary to test alternate correlations or even to appraise the quantity or quality of the expreimental work.

While the editors of technical publications justify the omission of experimental data on the grounds of cost, it is the profession that must be blamed. Obviously the profession as a whole values the literature more as a record of theory than as a repository of data.

The rationalization of data in terms of models and mechanisms is of paramount importance in scientific and technological development. However in the absence of an understanding of the quantity and quality of the data being rationalized, rationalization becomes meaningless speculation. The Greeks of ancient times were superb philosophers but poor scientists and engineers because they did not wish to be bothered with experimental measurements. As Alfred North Whitehead stated, "There are these hard and irreducible things we call facts; you hear them, you smell them, you see them, you taste them and you feel them, directly or by instrumental extension. Without them you may think indefinitely and have nothing." An understanding of the phenomenological bases of the rate processes is overwhelmingly important in developing the judgment that is crucial in engineering. It seems fitting, therefore, that this paper, as part of a symposium on fundamentals discusses in a general way the kinds of observations with which chemical engineers are concerned, the implications of the rate concepts which are used to summarize these observations, and the requirements and experience which are peculiar to chemical engineering.

DESCRIPTION OF RATE PROCESSES

There are two principal aspects to the rate processes, the phenomenological and the theoretical. The phenomenological aspect is concerned primarily with identification of the phenomenon under consideration. The need for identification does not arise from thin air but from highly practical considerations. We wish to rationalize the performance of heat or mass exchangers, or we wish to say

something about time and the composition of a reacting system, etc. Therefore, we attempt to define processes in such a way that the definition will be useful either for comparing processes under different conditions or for designing equipment in which processes are carried out. Isaac Newton encountered these same problems with respect to velocity and solved them by devising the calculus. The general definition of rate processes

$$r = \frac{1}{L}\frac{dS}{d\theta} \qquad (1)$$

Where r is the change in some quantity S per unit time θ per unit extent of the system L, is essentially the expression devised by Newton. When applied to heat transfer, r is the heat flux density expressed in British thermal units per hour per square foot, S is energy in British thermal units, and L is the area through which the energy is transferred; when applied to mass transfer, S is the mass of some component transferred per unit time through the area L. For a homogeneous chemical reaction S is the mass of some species produced per unit time per unit volume L, etc. The sign of the derivative is usually chosen to yield a positive rate.

The rate of a steady state process can alternatively be written as

$$r = \frac{ds}{dL} \qquad (2)$$

where s is the flux of some quantity and L is again the extent of the system. The rate in each case has the same dimensions as in the corresponding unsteady state process. For heat transfer s is the heat flux in British thermal units per hour, and L is again the area through which the the heat is transferred. For mass transfer s is the component flux in mass per unit time and L is the area through which the component is transferred. For a chemical reaction s is the mass flux of some species and L is the volume of the system.

All these particular definitions incorporate a time rate of change of a property or quantity per unit extent of the system and, explicitly or implicity, an indication of the direction of the change.

DETERMINATION OF THE RATE

A definition is essentially a set of instructions as to what to measure in order to determine a rate. Thus in transient heat transfer one must measure the enthalpy or energy of a given system and time or its equivalent. In mass transfer and chemical reactions the mass of a particular species in a chosen system must be measured as a function of time. In steady state heat transfer the heat flux must be measured as a function of area, etc.

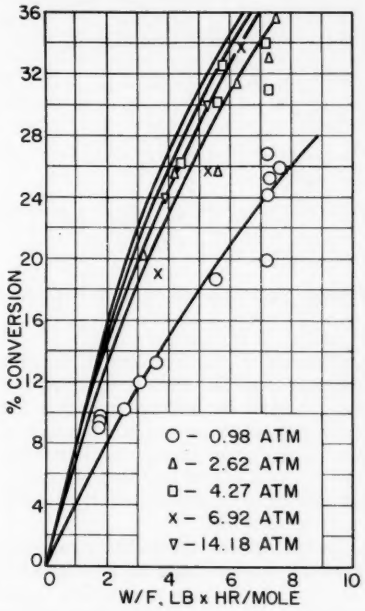

Fig. 1. Conversion as a function of space time.

While the basic concepts of the calculus with respect to the limiting process represented by the derivative is taught to, and apparently understood by, most engineering students when presented in the frame of reference of mathematics, it appears to be rather easy to forget these concepts in an engineering frame of reference. One is likely to forget that rate is a concept and that instantaneous or point rates of any kind are very difficult if not impossible to measure directly. Ordinarily one can obtain data from which average rates can be computed over finite intervals of time or over finite areas or volumes, but one is then forced to smoothing or some other interpretative process in order to deduce or estimate instantaneous or point rates. Basically the problem is one of numerical differentiation or smoothing of integral data. Whenever integral data are numerically differentiated, errors or irreproducibilities of the integral data are exaggerated by approximately one order of magnitude. Thus integral data which are precise to 10% commonly yield values of average rates which are precise only to 50 to 90%.

PROCESS CALCULATIONS

The use of measured rates in process design involves precisely the same mental operations as the definitions or measurements, since the process calculation is in a sense a hypothetical or mental experiment. This is illustrated by rewriting the definition in the form of Equation (3), which indicates how one would calculate the size of batch equipment required to transport a certain amount of heat or mass in a certain time.

$$A = \frac{\int -\frac{dS}{r}}{\int d\theta} \qquad (3)$$

A similar integral

$$A = \int \frac{ds}{r} \qquad (4)$$

arises for steady state heat or mass transfer.

The most important consequence of

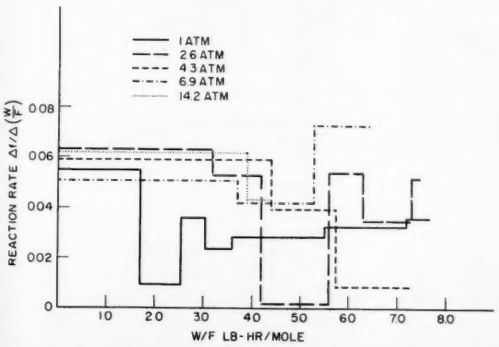

Fig. 2. Average rates for space-time increments.

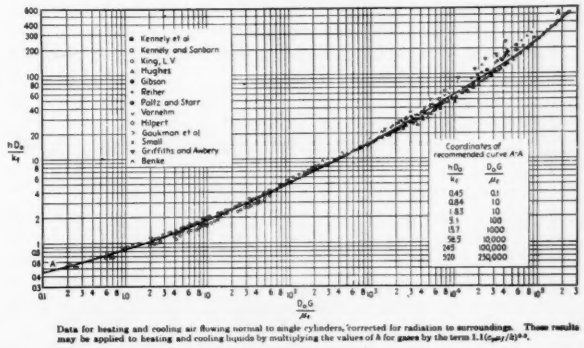

Fig. 3. Original correlation for convection between a gas stream and a cylinder (5).

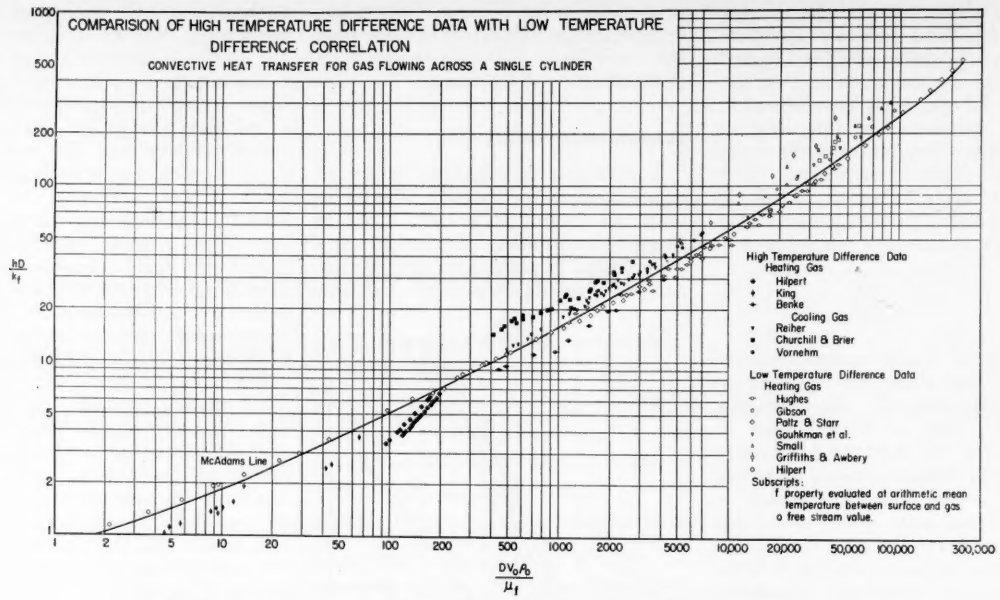

Fig. 4. Corrected correlation for convection between a gas stream and a cylinder (*1*).

Equations (3) and (4) is that in order to carry out the indicated integration, it is necessary to know the rate at which the process occurs as a function of the properties undergoing change. In the case of heat transfer this property is enthalpy or energy; in the case of mass transfer or chemical reaction it is composition.

CORRELATION

The primary purpose of correlation is to provide convenient and compact summaries of the relationship between the rate and the environment. This is the practical reason that scientists and engineers devote so much attention to the correlation of experimental facts and to the postulation of theories which provide models for the economical summary of the facts.

Generalization of rate data means that a set of measurements of a change can be associated with a description of the environment in which the change occurred. If a relationship between a rate of change and the environment can be expressed with a reasonable economy of words or other symbols, a correlation results that simply an assumed cause-and-effect relationship between variables. The scope in relatively limited.

If the statement covers a somewhat limited field of knowledge, we say we have a *theory*, which is a picture invented to classify as far as possible but not necessarily completely the knowledge of a group of events and further to describe speculative results of observations yet to be made.

When a very large number of observa-

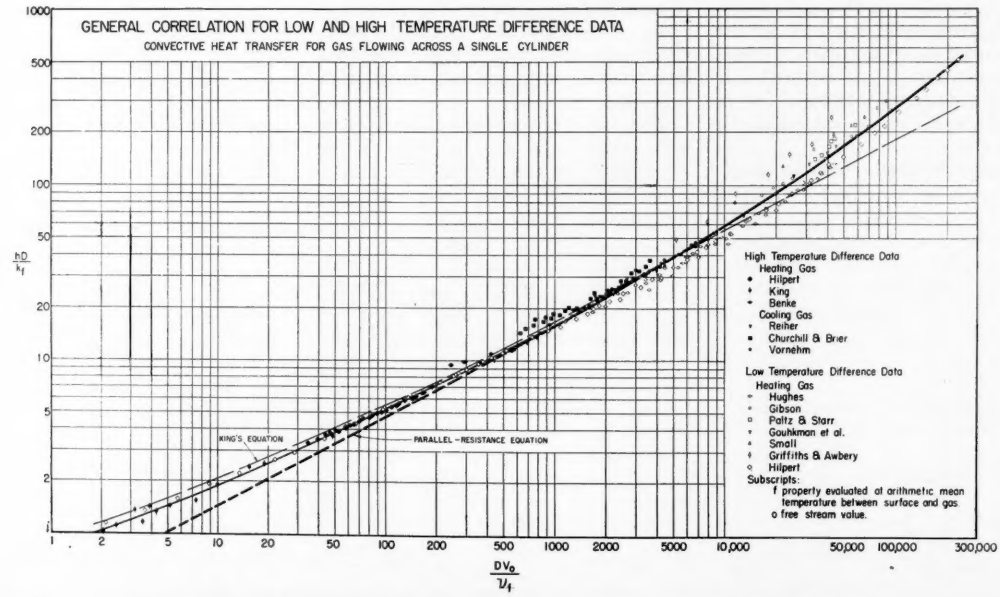

Fig. 5. Modified correlation for convection between a gas stream and a cylinder (*1*).

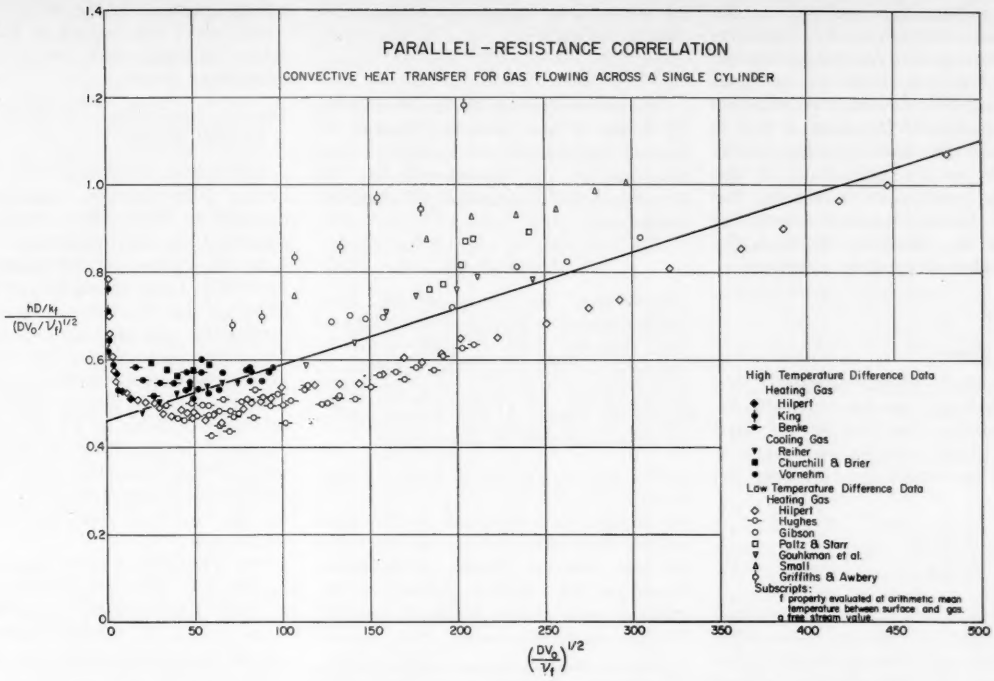

Fig. 6. Parallel-resistance correlation for convection between a gas stream and a cylinder (*1*).

tions show reproducible behavior, we may be able to make a general statement. If virtually no exception is found in our collective experience, and if the statement covers a relatively wide field of knowledge, it is then called *law* or *principle*. The statement of the first law of thermodynamics, "matter and energy cannot be created or destroyed," is an example. A law is useful because it describes in brief but complete form a very large body of knowledge. Obviously *correlations* lead to *theories*, which in turn lead to *laws*.

ILLUSTRATIONS OF THE CORRELATION PROBLEM

Chemical Kinetics

Integral vs. differential representations

Much of the previous discussion is illustrated by the data Figure 1 relating conversion to space velocity at a number of pressures for a catalytic decomposition. The reaction was of the type

$$A \rightleftharpoons R + S \qquad (5)$$

with no identifiable side reactions.

The curves in Figure 1 are based upon a correlation of the form

$$r = \frac{k\left[p_A - \frac{p_R p_S}{K}\right]}{1 + K_A p_A + K_R p_R} \qquad (6)$$

and the summary of the paper from which the data are reproduced states, "It has been shown that a single site surface reaction is the controlling mechanism. . . "

The rate of reaction is defined by

$$r = -\frac{dn}{dW} = -\frac{d(^n/F)}{d(^W/F)} = \frac{df}{d(^W/F)} \qquad (7)$$

This definition indicates that the basic rate information consists of average rates.

$$r_{avg} = \frac{\Delta f}{d(^W/F)} \qquad (8)$$

These values of the average rate over finite steps of $^W/F$ are shown in Figure 2, the preparation of the data for which conversions at virtually the same value of $^W/F$ were averaged.

The values of Figure 2 are the only known rates and constitute the raw material for correlation. They scatter widely and are typical of the data available from this type of experiment. The data, in fact, scatter so much that reasonably good correlations could be made on a zero-order basis, that is a straight horizontal line to represent all of the values, a somewhat better correlation on the basis of a simple first, second-order-reversible reaction, and perhaps a better correlation by Equation (6) as proposed by the experimenter. While the data can be represented adequately by Equation (6), there is a real question as to whether so complex a correlation is justified. It seems obvious that the reliability of the previously quoted conclusion as to mechanism is extremely dubious. The real point is that the presentation of the experimental results in the form of Figure 1 and Equation (6) without tabulation of the experimental data and without showing the rate values in Figure 2 may be extremely misleading not only to the scientist but especially to the perhaps less sophisticated practicing engineer.

There seems to be a strong psychological resistance to the differential treatment of data, particular on the part of those who have labored long, hard hours in the laboratory obtaining the data. The inconsistencies, errors, and uncertainties which the differential treatment brings to light constitute "bad news" to the experimenter, who, being human, wishes to view the results of his work in the most favorable light, as contrasted with the engineer, who in designing equipment wants to know the worst, since his design must allow for the uncertainties so that he may guarantee successful operation of the equipment. This conflict in viewpoint between the engineer and the laboratory is never ending and often difficult to resolve.

Over Correlation

The elucidation of the absolute-reaction-rate theory (*2*) and the presentation by Hougen and Watson of this material in parctical form (*3*) has promoted a considerable volume of research and has led to the presentation of fairly extensive sets of chemical reaction-rate data for gas-solid systems. The correlations involve as many as five parametric constants. It was only recently pointed out (*6*) that many of these data can be expressed by simple two-constant kinetic relationships as well as by the multi-

constant relationships reported by the investigators themselves. The improvement in the degree of correlation through the use of several additional constants is often negligible as compared with the intrinsic scatter of the data, and it is rather clear that little meaning can be attributed to the magnitude of the adsorption equilibrium constants, the frequency factor, apparent energy of activation, etc., obtained by fitting the data to such multiconstant equations.

Heat Transfer

Improper Model

Unrecognized shortcomings in the models used may also be responsible for poor correlation. For example, the usual definition of heat transfer coefficients for a double-pipe exchanger involves the relation

$$r = -\frac{d(wC_p t)}{dA} = h(t - t_i) \qquad (9)$$

This model, which ignores longitudinal transport due to eddy or back-mixing mechanisms, provides satisfactory correlations of h in fluid dynamic regimes which approximate piston flow. When the same definition is applied to contacting equipment, such as packed towers and fluidized beds where extensive back-mixing may occur, difficulty is encountered in obtaining general correlations of the transfer coefficients so defined. Present investigation of back-mixing by means of response techniques may soon make it possible to obtain more satisfactory results when models which allow for back-mixing effects separately are used, as by

$$k_E \frac{d^2t}{dz^2} - GC_p \frac{dt}{dz} = h(t - t_i) \qquad (10)$$

Misinterpretation of Data

The data for heat transfer to a gas flowing normal to a single cylinder provide an excellent example of the danger of the acceptance of correlations without examination of the raw data, as well as of the inhibiting effect of traditional models. The correlation for this system included in McAdams (*5*) is shown in Figure 3. It appears to be an excellent one. However examination of the raw data in the original references (mostly in German) revealed (*1*) that some of these points were transferred directly to Figure 3 without conversion of the physical properties from those used by the different authors to those in Figure 3. A corrected plot is shown in Figure 4. Unfortunately the ratio of the temperature of the surface to the temperature of the gas is now revealed to be a parameter. This error or its equivalent has been made in many other books on heat transfer. The parametric effect indicated in Figure 4 can be minimized by the use of $DV_0\rho_f/\mu_f$ as the abcissa instead of $DV_0\rho_0/\mu_f$ as shown in Figure 5.

Inhibitions

The curves through the data in Figures 3, 4, and 5 have definite curvature in log-log coordinates, an indication that they cannot be represented by the favorite type of equation of chemical engineers:

$$Nu = A\,Re^n \qquad (11)$$

Nevertheless this equation has been recommended by almost all textbooks on heat transfer, with a whole series of values of n and A being given for different ranges of Re, such as those given in the legend of Figure 3. The representation of these same data by the equation

$$Nu = A\sqrt{Re} + B\,Re \qquad (12)$$

which can be rationalized on the basis of the summation of the contributions of heat transfer through a boundary layer on the forward portion of the cylinder and purely turbulent transfer through the wake on the rear portion, is illustrated in Figure 6. At first glance this is a poor correlation, but the coordinates here are linear instead of logarithmic and absolute deviations rather than percentage deviations are observable; the straight line in Figure 6 when replotted in logarithmic coordinates in Figure 5 appears to be a good representation except at low Re in logarithmic coordinates as shown in Figure 5. Re-examination of the points in Figure 5 for low Re indicates that they were all obtained at a sufficiently high Δt so that natural convection may have led to higher transfer rates than forced convection, and the appearance of Figure 5 in the literature immediately produced correspondence from two investigators who had obtained data for low Δt's which agreed with the dotted line but which were not published because of failure to agree with McAdam's well-established curve.

Integral Correlations as Tests of Differential Models

Misleading conclusions are frequently drawn from integral correlations as opposed to differential correlations as suggested by the following examples. King (*4*) derived an expression for the local rate of convection to a cylinder by utilizing the theoretical flow pattern derived for potential (nonviscous) flow. The over-all rate obtained by integrating his expression is in reasonable agreement with the data in Figure 5, giving considerable credence to his expression for the local rates. However subsequently obtained experimental data for local rates reveal (Figure 7) that the agreement for the over-all coefficient was only fortuitous.

The differential energy balance resulting from an expression of heat transfer in fully developed turbulent flow in a pipe in terms of effective conductivities can be integrated formally to yield

$$\frac{hD}{k} = \frac{2}{\displaystyle\int_0^1 \frac{V}{V_m}\left[\int_{r/a}^1 \frac{k}{k_E}\left[\frac{\displaystyle\int_0^{r/a} \frac{V}{V_m}\frac{\partial t}{\partial z}\,d\left(\frac{r}{a}\right)^2}{\displaystyle\int_0^1 \frac{V}{V_m}\frac{\partial t}{\partial z}\,d\left(\frac{r}{a}\right)^2}\right] d\left(\frac{r}{a}\right)\right] d\left(\frac{r}{a}\right)^2} \qquad (13)$$

This triple integration is a very effective smoothing operation, and as might be expected hD/k proves to be quite insensitive to the velocity and eddy conductivity disturbances assumed in the various theoretical expressions which have been obtained by Von Karman, Martinelli, Lyon, Poppendick, etc., who integrated this equation by making various idealizations. hD/k therefore is not a sensitive characterization of heat transfer rate data. This fact is also apparent from the observation that hD/k approaches an asymptotic value in, say, ten pipe diameters while the temperature profile in the fluid is still developing thirty pipe diameters later.

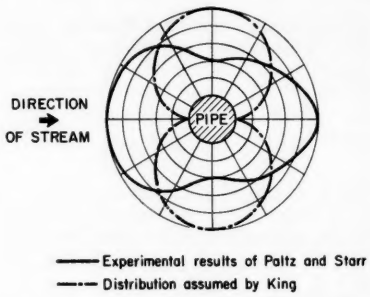

Fig. 7. Local rates of heat transfer between a gas stream and a cylinder (*5*).

Momentum Transfer

The differential momentum balances for a fluid, called the Navier-Stokes equations, have a great deal of gamevalue accuring from their complexity and virtual insolubility. However these equations and in particular the viscous stress terms which are derived on the basis of an assumed analogy between the shear and normal stress in a fluid and the stresses in a deformed plastic solid have not been tested experimentally. The system of momentum, energy, and material-balance equations if reducible to a single equation would contain high-order derivatives of the velocity. A critical test would therefore require

instantaneous velocity-distribution data that would stand four or more differentiations, more precise data than have been obtained to date. The Navier-Stokes equations therefore consist of a more complex model for correlation than there are data to justify. Agreement between between experimental data and integral results obtained by analytical or numerical integration of the Navier-Stokes equations is subject to the same possibility of coincidence and the same problem of lack of sensitivity as illustrated above and cannot provide a critical test of the differential representation.

Simultaneous Heat and Mass Transfer

The Wet-Bulb Temperature

The problem of simultaneous heat and mass transfer through the same phase will be considered. Perhaps the simplest illustration of such a case is the so-called "wet-bulb temperature." If the wet-bulb process is described by a potential-difference model, the rate of heat transfer from the gas to the wick may be expressed as

$$q = hA(t - t_w) \qquad (14)$$

and the rate of component transfer from the wick to the gas as

$$r = k_g A(p_w - p) \qquad (15)$$

At dynamic equilibrium the energy received by the wick from the gas must be equal to the latent heat of vaporization of the liquid at the wick temperature. Therefore

$$hA[t - t_w] = k_g MA\lambda[p_w - p] \qquad (16)$$

which may be rearranged to give the so-called "wet-bulb depression" the difference between the dry- and wet-bulb temperatures:

$$t - t_w = \frac{k_g M\lambda}{h}[p_w - p] \qquad (17)$$

Equation (17) has been reasonably successful as a correlation model for wet-bulb behavior. The values of h/k_g evaluated from wet-bulb measurements agree reasonably well with values calculated from the j-factor concept. While the use of wet-bulb thermometers is quite old, the amount of data available is surprisingly small and limited almost entirely to air systems. It is instructive to inquire somewhat more deeply into the correlation of such data, since they are closely related to other processes, particularly evaporation and drying. Because the data are limited and are well correlated by Equation (14), we cannot expect better correlation, but perhaps only a better insight into the mechanism of the transfer processes.

The logic by which Equation (17) was derived dodges a point which illustrates the basic difficulty of the potential-difference model. The heat transfer coefficient in Equation (17) was defined in terms of the energy received by the wick from the gas. Obviously at equilibrium the heat transfer rate must equal the component transfer rate times the latent heat of vaporization of the liquid at the wet-bulb temperature, since the vaporized liquid leaves the interface at the wet-bulb temperature. However the vaporized liquid as it diffuses and mixes with the gas stream comes to the temperature of the gas streams, so that the total enthalpy change involved is $\lambda + C_p(t - t_w)$.

The question therefore arises as to whether the heat transfer coefficient should be defined to include just the energy received by the wick or the total enthalpy. The reason for the question is of course that one would like to measure the heat transfer coefficient between air and a cylinder having the same geometry as the wick in the absence of component transfer and apply the coefficient to the performance of wet-bulb thermometers.

The only answer that can be given today is that heat transfer in the presence of component transfer is a different phenomenon from heat transfer in the absence of component transfer, and therefore there is no common meaning for the heat transfer coefficient. It is known that when the component transfer rate is small, the difference in the meaning of heat transfer coefficients is negligible compared with experimental error. However the potential-difference model remains uncomfortable.

These questions can be partially alleviated by the use of a potential-gradient model for the wet-bulb phenomena instead of the potential-difference model. Consider a flat plane of infinite extent with countercurrent heat and component transfer by diffusion across a differential element dy at a distance y measured normal to the plane.

Under steady conditions there is no accumulation of enthalpy in the differential element due either to the temperature gradient or to the flow of enthalpy accompanying the flow of mass. Expressing this energy balance mathematically, one obtains

$$k\frac{d^2t}{dy^2} = GC_p\frac{dt}{dy} \qquad (18)$$

At the interface, where $y = 0$, $t = t$ and $k(dt/dy)_{y=0} = G\lambda$. Integrating equation (18) yields

$$\ln\left[1 + \frac{C_p}{\lambda}(t - t_w)\right] = \frac{GC_p y}{k} \qquad (19)$$

Equation (19) is somewhat disturbing in that as y approaches ∞, t also approaches ∞. This raises again the incompatibility of the potential-gradient and the potential-difference model. Obviously a heat transfer coefficient based upon the difference between a bulk value of t and a surface temperature t_w must be related to some finite value of y. The normal impulse is to say that the bulk value of t is some value far removed from the surface, but this implies the selection of some arbitrary and large value of y according to Equation (19). Perhaps it is not necessary to reconcile this difficulty in matching what may be unmatchable models. One evaluates w in Equation (19) as a function of partial pressure so as to obtain a relation for the wet-bulb phenomena. If one follows a similar procedure in evaluating the mass transfer equation,

$$G = \frac{\rho D_f}{y}\ln\frac{P - p}{P - p_w} \qquad (20)$$

Combining Equations (19) and (20) to eliminate G gives the wet-bulb relationship

$$t - t_w = \frac{\lambda}{C_p}\left[\left(\frac{P - p}{P - p_w}\right)^{\rho D_f C_p/k} - 1\right] \qquad (21)$$

Equation (21) correlates the available wet-bulb data as readily as Equation (17). However the comparison suggests a number of experiments designed to test the new model. A large factor is the ratio of λ/C_p in Equation (21), which suggests an experiment to test whether the heat capacity of the vaporized liquid indicated by Equation (21) is important. Experiments in the hydrogen–carbon tetrachloride system with large values of p approaching P should therefore be interesting.

It is natural for the engineer to fall into a typical trap and to assume that because Equation (21) is a more "mathematical" model it is a better one. Only data can decide this. The use of Equation (21) for the data now available in the literature would represent overcorrelation, even though successful.

The basic difficulty with the potential-difference models is further illustrated by consideration of simultaneous heat and mass transfer in a gas-liquid contactor, such as a dehumidifier. The mass balance around a differential section is

$$dL = G\,dH \qquad (22)$$

and the mass transport relationship is

$$G\,dH = k_g aM_r(p_i - p)\,dZ \qquad (23)$$

Similarly the enthalpy balance around the differential section is

$$G\{s\,dt + [\lambda_r + C_v(t - t_r) - C_l(t_i - t_r)]\,dH\} = LC_l\,dt_l \qquad (24)$$

A flux balance around the interface of the differential section may be made by equating the rate of heat transfer through the gas and liquid phases to the interface and the enthalpy requirement for vaporizing the material at the interface, leading to

$$h_v a(t - t_i) + h_l a(t_l - t_i) = k_g aM_r(p_i - p)\lambda_i \qquad (25)$$

There is now a need for additional heat transfer relationships, and it is customary in the literature to write

$$-Gs\,dt = h_v a(t - t_i)\,dZ \qquad (26)$$

$$LC_l\,dt = h_l a(t - t_i)\,dZ \qquad (27)$$

Equations (23, 26, and 27) are substituted into (25),

$$G[s\,dt + \lambda_i\,dH] = LC_l\,dt_l \qquad (28)$$

is obtained and comparison of Equation (28) with Equation (24) requires that

$$\lambda_r + C_v(t - t_r) - C_l(t_l - t_r) = \lambda_i \qquad (29)$$

Equation (29) leads to

$$t - t_i = \frac{t - t_l}{1 - C_v/C_l} \qquad (30)$$

since $0 < C_v/C_l > 1$, $t_i - t > t_l - t$; $t_i > t_l$ always. This cannot apply in a cooling tower with hot water and and cold dry gas.

Thus Equations (25) through (27) are basically incompatible. This results from the fact that while we can conceive of the right-hand side of Equations (26) and (27) as being the energy transferred to the interface, we cannot identify such heat in the enthalpy balance, since the enthalpy of the gas is a function both of temperature and composition and the entahlpy of the liquid is a function of its flow rate and its temperature. Arbitrarily segregating the so-called "sensible" heat part of the enthalpy change as indicated in Equations (26) and (27) is not operationally sound.

Thus if Equations (26) and (27) are used, we are in the impossible position of having to repeal the second law of thermodynamics as expressed by Equation (24) or to discard the concept of the flux balance as expressed by Equation (25). This constitutes a basic defect in the model, and while in the air-water system the defect is unimportant because the heat capacities are small as compared with the latent heat of vaporization, the defect may become very serious in other systems, such as hydrogen–carbon tetrachloride. Furthermore the defects may be serious when similar procedures are applied to the treatment of heat and mass transfer in catalytic reactors, where not only heat transfer but multicomponent mass transfer across the fluid phase are present. No satisfactory rationalization or model has been suggested to take care of this difficulty.

CONCLUSIONS

All the foregoing suggests that in chemical engineering we are still infants in treating adequately the complex problems encountered even in relatively simple processes. The profession suffers from a lack of data that will stand differentiation so as to give raw materials which are actual values of rates. Furthermore it suffers conceptually in that essentially all existing data and ideas are forced into two models, the potential-difference and the potential-gradient models. The potential-difference models contain basic defects when applied in complex transport systems involving both heat and mass transfer; the potential-gradient models suffer because in their application to flow systems they lead to nonlinear, second-order, partial-differential equations which are extremely difficult to handle mathematically and which place extreme requirements on the precision of the data which is necessary to evaluate the various terms. We tend to overcorrelate the data because we do not appreciate the intrinsic defects of the available rate information. This all suggests that the field of chemical engineering is still wide open for precise and careful expreimentation on relatively simple systems to provide the foundation for experimental evidence which by and large is still missing. One is reminded of the words of Mark Twain, who wrote in "Life on the Mississippi,"

> In the space of one hundred and seventy-six years the lower Mississippi has shortened itself two hundred and forty-two miles. That is an average of a trifle over one mile and a third per year. Therefore, any calm person, who is not blind or idiotic, can see that in the Old Oolitic Silurian Period, just a million years ago next November, the lower Mississippi River was upward of one million, three hundred thousand miles long, and stuck out over the Gulf of Mexico like a fishing rod. And by the same token any person can see that seven hundred and forty-two years from now the lower Mississippi will be only a mile and three-quarters long, and Cairo and New Orleans will have joined their streets together, and be plodding comfortably along under a single mayor and a mutual board of aldermen. There is something fascinating about science. One gets such wholesale returns of conjecture out of such a trifling investment of fact.

NOTATION

A = area; also a constant
a = radius of pipe; also surface area of packing per unit volume
B = a constant
C = heat capacity
D = diameter
D_f = diffusivity
D_0 = cylinder diameter
dy = differential element
F = feed rate
f = fractional conversion
G = mass velocity
H = humidity
h = heat transfer coefficient
K = equilibrium constant
k = reaction-rate constant; also thermal conductivity
k_E = effective conductivity
k_g = mass transfer coefficient
L = extent of the system, usually area or volume; also liquid mass velocity
M = molecule weight
$Nu = hD/k$, Nusselt number
n = molal flux; also an exponent
P = pressure
p = partial pressure
q = heat flux
$Re = D\rho V/\mu$, Reynolds' number
r = general symbol for a rate; also radius
S = general symbol for a quantity
s = general symbol for the flux of a quantity; also humid heat
t = temperature
t_w = surface temperature
V = velocity
W = mass of catalyst
w = mass flux
y = distance from surface
Z = height
z = axial distance

Greek Letters

λ = latent heat of vaporization
μ = viscosity
ρ = density
ν = kinematic viscosity
θ = time

Subscripts

$A, R, S,$ = components A, R, S
f = film
i = interface
l = liquid
m = mean
0 = free stream
p = constant pressure
r = reference
v = vapor
w = wet bulb; also wall

LITERATURE CITED

1. Douglas, W. J. M., and S. W. Churchill, *Chem. Eng. Progr. Symp. Series No. 18*, **52**, 23 (1956).
2. Glasstone, Samuel, K. J. Laidler, and Henry Eyring, "The Theory of Rate Processes," McGraw-Hill, New York (1941).
3. Hougen, O. A., and K. M. Watson, "Chemical Process Principles, Wiley, New York (1947).
4. King, L. V., *Trans. Roy. Soc. (London)*, **A214**, 373 (1914).
5. McAdams, W. H., "Heat Transmission," 2 ed., McGraw-Hill, New York (1942).
6. Weller, Sol, *A.I.Ch.E. Journal*, **2**, 59 (1956).

Manuscript received August 14, 1958; revision received December 10, 1958; paper accepted December 11, 1958. Paper presented at A.I.Ch.E. Philadelphia meeting.

Vinyl Chloride from Acetylene and Hydrogen Chloride: Catalytic-Rate Studies

R. D. WESSELHOFT, J. M. WOODS, and J. M. SMITH

Purdue University, Lafayette, Indiana

The reaction rate of gaseous acetylene and hydrogen chloride was studied experimentally on a mercuric chloride–activated carbon catalyst at pressures from 1 to 4 atm. and temperatures of 167°, 212°, and 257°F. The measurements were made in a differential reactor packed with mercuric chloride impregnated on activated carbon, the data being taken to obtain the separate effect of the partial pressure of each of the components on the rate.

The results indicated that hydrogen chloride was strongly adsorbed on the catalyst and that vinyl chloride was also adsorbed to a significant extent. A rate equation, which well represented the data, was developed from the following postulates: (*a*) acetylene is adsorbed on the catalyst on one type of site, (*b*) hydrogen chloride and vinyl chloride are adsorbed on a different kind of site, (*c*) the formation of vinyl chloride occurs by reaction of adsorbed acetylene and adsorbed hydrogen chloride, and (*d*) the rates of adsorption and desorption are fast compared with the formation rate of vinyl chloride.

Vinyl chloride is produced commercially by the hydrochlorination of acetylene with anhydrous hydrogen chloride or by the chlorination of ethylene. The availability of low-cost acetylene from natural gas has increased the significance of the first method. In it acetylene and hydrogen chloride in the gas phase are passed over a solid catalyst carrier containing mercuric chloride. While the commercial process (*1, 2, 3*) has been in operation for some time, suitable rate data for studying the kinetics of the reaction are lacking.

Wakano and Shenichi (*13*) proposed an empirical expression of the exponential form for the rate

$$r = C p_A^{\,a} p_H^{\,h} e^{-B/RT} \qquad (1)$$

in which the values of a, h, B, and C, depended upon the operating conditions. Lynn and Kobe (*8*) presented data showing the effect of impurities in the acetylene feed and variations in catalyst preparations on the product obtained. The reaction product was identified as pure vinyl chloride. Conversions were measured as a function of space velocity, but accurate rate data could not be deduced from the measurements.

A number of laboratory investigations have been carried out in fluidized beds (*4, 5, 11, 15*) over limited ranges of conditions and with varying precision. Because of these limitations substantial conclusions regarding a rate equation could not be reached.

The chief objective of the present study was to obtain reliable rate data for the mercuric chloride–catalyst reaction over a range of pressure and composition. Because of the uncertainties in interpretation introduced by back-mixing in fluidized beds, a fixed-bed, differential type of reactor was used. The total catalyst bed of about 22 in. was diluted to a ratio of approximately one part of catalyst (mercuric chloride impregnated on activated carbon) to sixteen parts of inert packing (porcelain). This arrangement resulted in conversions from 2 to 3%, based upon total feed, and reduced the temperature gradients in the bed to a few degrees (maximum radial temperature difference = 6°F.). No evidence of by-product formation (dichloroethane) was found in operating at these conditions.

R. D. Wesselhoft is with the Humble Oil and Refining Company, Baytown, Texas, and J. M. Smith is at Northwestern University, Evanston, Illinois.

EXPERIMENTAL WORK

There were three main parts to the experimental equipment used to obtain rate measurements: gas purification and metering system, the reactor system, and the product gas-analysis system. Figure 1 shows a schematic diagram of the reactor and product gas-analysis system.

Feed gases from commercial cylinders were purified and dried to minimize catalyst poisoning and corrosion. The feed rates of acetylene, hydrogen chloride, and vinyl chloride were controlled with needle valves augmented with constant-differential pressure flow meters. Steel-encased glass capillary meters were used in the flow measurement. Wherever either hydrogen chloride or vinyl chloride was present, the connecting lines were constructed of ¼-in. Hastelloy-B tubing to resist corrosion. A nitrogen feed was provided for purging the system.

The acetylene was purified by passage through water, a ferric chloride solution (an aqueous solution containing 5% ferric chloride, 0.5% mercuric chloride, and 1% acetic acid), and a silica-gel column before metering. Traces of moisture were removed from the hydrogen chloride and nitrogen by scrubbing with concentrated sulfuric acid and from the vinyl chloride by passage through a column of silica gel.

The reactor (Figure 2) was fabricated of standard 1-in. stainless steel pipe with a length of 36-in. Heat transfer oil was circulated through a jacket surrounding the central section, 22-in. long. The reactor wall temperature was held constant to within 0.25°F. Temperatures within the reactor were measured with seven thermocouples at fixed positions in an axial well of ⅛-in. stainless steel hypodermic tubing. The well extended the entire length of the reactor. The end sections of the reactor were packed with glass beads and heated electrically to minimize thermal gradients. Preliminary studies (*9*) indicated that one part of catalyst (by volume) in sixteen parts of inert packing minimized the combined uncertainty due to temperature and composition effects. Initial tests showed that the inert material, 6- to 8-mesh crushed porcelain, had no catalytic activity. The catalyst bed contained 9.08 g. of catalyst particles and 285 cc. of inert material.

A diaphragm type of back-pressure regulator at the outlet from the reactor permitted operation at any pressure up to 60 lb./sq. in. gauge over the entire range of flow rates. The gases were metered with a precision rotameter and then scrubbed in a water-spray column before venting. A soap-bubble meter, especially constructed for corrosion resistance, was inserted after the rotameter and used to calibrate all flow meters in place

Product gas analysis was based upon a comparison of the thermal conductivity of a small portion of the feed gases with a small portion of the product gases by the use of a thermistor type of thermal-conductivity cell. Flow rates to the cell were held at fixed known values. This procedure gave greater precision than the use of a single reference gas for two reasons: the cell was used to detect directly the difference in thermal conductivity due to reaction, and the effect of small errors in

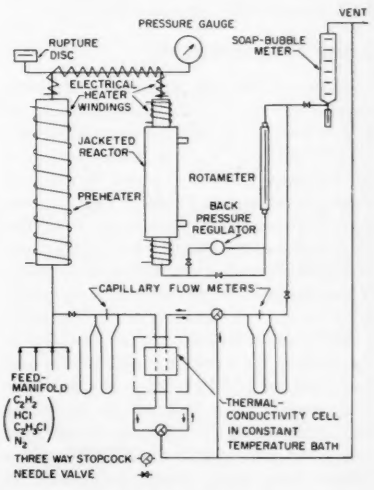

Fig. 1. Flow diagram.

setting the relative flow rates of the feed gases was almost completely canceled.

In the use of thermal-conductivity measurements for a three-component system the mole fractions of the components must be interrelated in a known manner. In the present investigation the ratio of acetylene to hydrogen chloride in the feed gas could be set, and the molal composition of the product gases was related to the feed by the stoichiometry of the reaction. To determine this information, the cell had to be calibrated for various ratios of the reactants and various conversions. This was accomplished by preparing known mixtures of the three components. In the calibration procedure the cell imbalance [difference in cell electromotive force when the feed gas was passed through both sides of the cell and when the product gas (synthetic sample) was passed through the sample side] was measured under constant current conditions. From this information calibration curves were prepared giving the mole fraction of vinyl chloride in the product stream as a function of the imbalance and the feed-gas composition.

The acetylene used in these experiments was a commercial grade. Besides the acetone solvent, the principal impurities were phosphine, arsine, ammonia, and hydrogen sulfide. The hydrogen chloride was 99.8% pure; air was the principal contaminant, although traces of carbon dioxide, benzene, and chlorobenzene were present. Vinyl chloride contained 0.1% each of polymer and water vapor. The monomer was inhibited by 1,000 p.p.m. of phenol.

Mercuric chloride, 8.7% by weight of the total mass, was deposited on granular activated carbon. A 6- to 8-mesh size with an average particle diameter of 0.00833 ft. was used. The fresh catalyst had a total area of 868 sq.m./g.; this had dropped to 130 sq.m./g. at the end of the experiments. The bulk density of the active catalyst particles (undiluted) was 25 lb./cu. ft.; the external surface per unit volume, 504 sq. ft./cu. ft.; and the external void fraction, approximately 30%.

Because of the potential explosion hazard of acetylene, high surface-volume ratios were maintained in all lines and vessels. Extensive data on the conditions and hazards of acetylene decomposition have been presented by Sargent (*10*).

RANGE OF MEASUREMENTS

Most of the rate measurements were carried out at 212°F., although data at a few feed compositions were obtained at 167° and 257°F. The partial pressures of reactant gases for which runs were made are shown in Table 1. The pressure combinations were chosen so that the feed ratios corresponding to the thermal-conductivity-cell calibrations were used. The total pressure varied from 1 to 4 atm. Flow rates were chosen for each feed composition so as to give the best precision in evaluating the average reaction rate and temperature and in reading the flow-rate manometers. The order of the runs was randomized, and duplicate runs were made for each condition at 212°F., since these data were most important in analyzing the kinetics of the reaction.

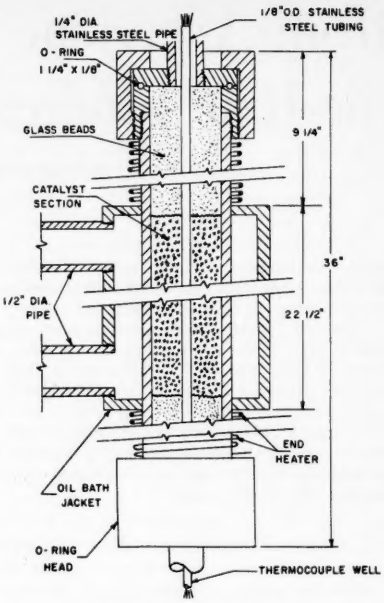

Fig. 2. Reactor details.

CALCULATION OF RESULTS

To have the data in a form suitable for interpretation it was necessary to convert the measured conversion to vinyl chloride in each run to a rate at a known temperature and composition. Because of variations in catalyst activity with on-stream time, the treatment of the measured conversions included correction to a standard activity.

Before the corrections were carried out to a point rate at a standard activity, the importance of diffusion had to be estimated. When one used the procedures of Hougen and Yang (*7*) and measured rate data, it was found that the partial pressure difference between the bulk gas and catalyst surface was about 10^{-4} atm. An estimate of the effectiveness factor from the reaction rate, pore volume, particle size, and diffusivity data following the procedures of Smith (*12*) gave a value greater than 0.99 under the worst conditions. Under these circumstances it was supposed that neither external nor internal diffusion resistances were significant in the overall reaction. Thus the bulk-gas partial pressures could be substituted for the values at the catalyst surface in the kinetic interpretation.

Table 1. Experimental Design

Temperature = 212°F (no vinyl chloride in feed)

P_A (atm) \ P_H (atm)	0.5	0.66	1.0	1.33	2.0	2.66	3.0
0.5	xx		xx		xx		
0.66		xx		xx		xx	
1.0	xx		xxx		xx		xx
1.33		xx		xxx		xxx	
2.0	xx		xx		xx		
2.66		xx		xx			
3.0			xx				

Temperature = 167°F and 257°F

P_A (atm) \ P_H (atm)	0.5	2.0
0.5	x	x
2.0	x	x

Temperature = 212°F (with vinyl chloride in feed)

P_A and P_H \ P_{VC}	0.25	0.5	0.75	1.0	1.5
0.25		x			
0.375	x		x		
0.5				x	
0.75		x			xx
1.125			x		

x = indicates one run

The conversion for each run was used to evaluate an average rate for the differential reactor by

$$r = \frac{\Delta x'}{W/F} \qquad (2)$$

Corrections for the significant variation of catalyst activity with time (the rate, at the same conditions, decreased to one-third the initial value from the initial to final run) were made by alternating standard runs with data runs. The conditions for the standard run were a feed of 50 mole % acetylene and 50 mole % hydrogen chloride, total feed rate of 0.06 cu. ft./min. (at standard temperature and pressure) total pressure of 1 atm. and a reactor temperature of 212°F. A standard conversion curve of x' vs. W/F was prepared by varying the feed rate while maintaining the other standard conditions constant. This curve and the results for the alternating standard runs were employed to obtain a corrected value of W/F for each run. Then assuming that the activity of the catalyst was directly proportional to the rate, one obtains the corrected rate by

$$r_{corr} = r\left[\frac{(W/F)_{corr}}{(W/F)_{actual}}\right]_{const\ \Delta x'} \qquad (3)$$

The rate evaluated from Equation (3) is an average value for the varying compositions in different parts of the differential reactor. To place these results on the basis set forth in the experimental design, each rate was corrected to a zero-conversion value, that is the rate corresponding to conditions at the inlet to the reactor. Since the conversions were low in all cases, these corrections were likewise small. They were made by using the approximate values from Equation (3) to determine the variation in rate with partial pressures of each of the components, acetylene, hydrogen chloride, and vinyl chloride. Knowing these individual gradients and the average conversion in the bed, one could correct the average rate to a zero-conversion value.

Similarly the average rate from Equation (3) represents the combined result of the temperature variations with position in the reactor. The method of correction of all runs to a single temperature must be approximate without

multiple temperature measurements in the bed. Preliminary work (*14*) indicated the thermocouple readings in the well, and the adjacent gas temperature agreed within 1°F. Also the radial gradients were small, and most of the resistance to heat transfer in the bed is probably near the wall. Hence the measured temperatures in the thermocouple well were assumed to be the same as the bulk mean-radial temperature.

The axial temperature changes in the bed were somewhat larger. Whereas a maximum change of 15°F. was obtained at the highest operating temperature, most of these changes were about 6°F. An average gas temperature was calculated from the values determined at the six axial positions in the thermocouple well.

Once the average gas temperature was obtained for each run, the rate was corrected to one of the reference temperatures (167°, 212° or 257°F.) by the Arrhenius equation. The approximate activation energy (determined from the data at different temperatures) used for this correction was 12,400 B.t.u./lb. mole. The Arrhenius plot was based upon catalyst-surface temperatures rather than gas temperatures. These surface temperatures were estimated from the heat (−71,500 B.t.u./lb. mole) and rate of reaction and a dimensionless correlation (*6*) of heat transfer coefficient between the fluid and solid particles in a packed bed. This difference became very significant at 257°F. The rate measurements in the vicinity of 212°F. were referred to the average gas temperature rather than to the estimated surface value because of the uncertainties in the latter temperatures.

The resultant values of the rate and temperature along with the initial composition are shown in Table 2.* Both initial rates (no vinyl chloride) and values for vinyl chloride in the feed are shown. Complete data for each run are also available (*14*). The results are represented graphically by the indicated experimental points in Figures 3 to 6. Figures 3 and 4 show initial rates; Figures 5 and 6, the effect of vinyl chloride.

PRECISION OF RESULTS

The primary sources of error in the rate data are the measurements of flow rates, the assignment of an average temperature for the gas in the reactor and for the catalyst particles, and the variation in catalyst activity.

Errors in flow-rate measurements affected the results in several ways: in the calibration of the thermal conductivity cell, in the value of W/F assigned

*Complete tabular material has been deposited as document No. 5973 with the American Documentation Institute, Photoduplication Service, Library of Congress, Washington 25, D. C., and may be obtained for $1.25 for photoprints or for 35-mm. microfilm.

Table 2. Table of Results

Run	P_A	P_H	Experimental Rate	Calculated Rate	Deviation	Percent Deviation
260	0.5	0.5	0.0130	0.0120	−0.0010	−7.7
304	1.0	0.5	0.0200	0.0202	0.0002	1.0
383	1.0	0.5	0.0195	0.0202	0.0007	3.6
327	2.0	0.5	0.0275	0.0308	0.0033	12.0
371	2.0	0.5	0.0290	0.0308	0.0018	6.2
300	0.66	0.66	0.0175	0.0169	−0.0006	−3.4
373	0.66	0.66	0.0174	0.0169	−0.0005	−2.9
321	1.33	0.66	0.0260	0.0273	0.0013	5.0
356	1.33	0.66	0.0266	0.0273	0.0007	2.6
341	2.66	0.66	0.0378	0.0396	0.0018	4.7
370	2.66	0.66	0.0384	0.0396	0.0012	3.1
302	0.5	1.0	0.0154	0.0152	−0.0002	−1.3
362	0.5	1.0	0.0152	0.0152	0.0000	0.0
310	1.0	1.0	0.0261	0.0257	−0.0004	−1.5
317	1.0	1.0	0.0250	0.0257	0.0007	2.8
364	1.0	1.0	0.0251	0.0257	0.0006	2.4
331	2.0	1.0	0.0400	0.0391	−0.0009	−2.2
360	2.0	1.0	0.0400	0.0391	−0.0009	−2.2
336	3.0	1.0	0.0496	0.0470	−0.0026	−5.2
387	3.0	1.0	0.0484	0.0470	−0.0014	−2.9
319	0.66	1.33	0.0201	0.0205	0.0004	2.0
385	0.66	1.33	0.0201	0.0205	0.0004	2.0
347	1.33	1.33	0.0333	0.0333	0.0000	0.0
368	1.33	1.33	0.0312	0.0333	0.0021	6.7
391	1.33	1.33	0.0333	0.0333	0.0000	0.0
350	2.66	1.33	0.0490	0.0483	−0.0007	−1.4
377	2.66	1.33	0.0503	0.0483	−0.0020	−4.0
392	2.66	1.33	0.0501	0.0483	−0.0018	−3.6
325	0.5	2.0	0.0184	0.0176	−0.0008	−4.3
354	0.5	2.0	0.0175	0.0176	0.0001	0.5
329	1.0	2.0	0.0290	0.0297	0.0007	2.4
358	1.0	2.0	0.0291	0.0297	0.0006	2.0
338	2.0	2.0	0.0450	0.0452	0.0002	0.4
389	2.0	2.0	0.0458	0.0452	−0.0006	−1.1
343	0.66	2.66	0.0222	0.0230	0.0008	3.6
366	0.66	2.66	0.0223	0.0230	0.0007	3.1
344	1.33	2.66	0.0340	0.0373	0.0033	9.7
375	1.33	2.66	0.0364	0.0373	0.0009	2.5

TABLE 2. (CONTINUED)

RUN	P_A	P_H	EXPERIMENTAL RATE	CALCULATED RATE	DEVIATION	PERCENT DEVIATION
352	1.33	2.66	0.0351	0.0373	0.0022	6.2
334	1.0	3.0	0.0297	0.0314	0.0017	5.7
379	1.0	3.0	0.0309	0.0314	0.0005	1.6
						3.3
412	0.5	0.5	0.00684	0.00633	-0.0005	-7.5
413	2.0	0.5	0.0158	0.0152	-0.0006	-3.8
415	0.5	2.0	0.00935	0.00913	-0.0002	-2.3
416	2.0	2.0	0.0203	0.0221	0.0017	8.4
						5.5
418	0.5	0.5	0.0235	0.0216	-0.0019	-8.1
420	2.0	0.5	0.0590	0.0572	-0.0018	-3.0
421	0.5	2.0	0.0350	0.0322	-0.0028	-8.0
423	2.0	2.0	0.0800	0.0850	0.0050	6.2
						6.3
398	0.25	0.5	0.0030	0.0021	-0.0009	-30
400	0.375	0.25	0.0067	0.0056	-0.0011	-16.5
403	0.375	0.75	0.0043	0.0034	-0.0009	-21
405	0.5	1.0	0.0065	0.0046	-0.0019	-29
396	0.75	0.5	0.0117	0.0119	0.0002	1.7
407	0.75	1.5	0.0065	0.0067	0.0002	3.8
410	0.75	1.5	0.0068	0.0067	-0.0001	-1.2
409	1.125	0.75	0.0162	0.0169	0.0007	4.3
						13.7
						5.7

Temperature = 212°F (without vinyl chloride in the feed).

Temperature = 167°F. (without vinyl chloride in the feed).

Temperature = 257°F. (without vinyl chloride in the feed).

Temperature = 212°F. (with vinyl chloride in the feed).

to a run, and in determining the composition of the feed gas. Analysis of magnitudes of flow-rate fluctuations indicated that maximum errors of a few per cent were possible from this source.

Temperatures were read to $\pm\frac{1}{2}$°F. on the recorder, which was calibrated to the same accuracy. Since the maximum radial-temperature difference between the oil (in the jacket) temperature and that in the center of the reactor was 6°F., it was believed that the average gas temperature was accurate within 2°F. Estimates of the temperature difference between gas and catalyst surface should be accurate to ±2°F. The total temperature error of ±4°F. suggests a maximum error in rate of about 5%.

The variation in catalyst activity with time was taken into account by alternating runs at standard conditions, as already described. While the variations in activity were large, there were indications that the correction method adequately accounted for the possible errors. The repeat runs made at different times, and hence different activities, were in good agreement after correction for activity variations. This is evident from Table 2, for example, by comparing runs 304 and 383, 327 and 371, 300 and 373, etc. (The runs were numbered in sequence so that the difference in two numbers is a measure of the time interval between the two runs.)

The summing of all the errors indicates a maximum error in reaction rate of 10 to 15%. At most conditions the error would be less than this maximum. The scatter in the data, as seen in Figure 3 for example, is well within the maximum predicted error.

KINETICS OF THE REACTION

The determination of a mechanism for most gas-solid reactions from over-all rate measurements is virtually impossible. The hydrochlorination of acetylene is no exception. Information on adsorption rates of reactants and products on the catalyst at reaction conditions, as well as identification of intermediate products, is necessary before conclusions about the mechanism can be stated. Over-all rate data can be used only to test rate equations determined from likely postulates about the mechanism of the reaction and to reject those which are incompatible.

From the data as plotted in Figure 3 it is seen that the initial rate (no vinyl chloride present) increased with partial pressure of hydrogen chloride at low values of p_H and then became constant at higher partial pressures. This behavior suggests that hydrogen chloride is strongly adsorbed, filling most of the active sites available to it at relatively low partial pressures. In contrast, Figure 4 indicates that the rate increases with p_A over the whole range of partial pressures of acetylene. The curves in Figure 4 are evidence that acetylene is less strongly adsorbed than hydrogen chloride, if it is adsorbed. If both acetylene and hydrogen chloride are adsorbed on the same types of sites, and reaction occurs between the adsorption compounds, the rate would be expected to pass through a maximum and ultimately to decrease with continually increasing partial pressures of hydrogen chloride. Thus the more strongly adsorbed hydrogen chloride would displace acetylene from the active sites. This would result in fewer adjacent pairs of adsorbed hydrogen chloride and acetylene and a lower rate, particularly if the surface reaction between adsorption compounds were a relatively slow step in the over-all reaction. The data (Figure 3) did not show this maximum in rate. This behavior and the chemical dissimilarity between acetylene and hydrogen chloride suggest that the two components, if adsorbed, reside on different types of sites.

The effect of vinyl chloride on the rate is shown directly in Figure 5 and as a parameter in Figure 6. Since the reaction is essentially irreversible at the conditions studied (equilibrium constant = 10^8 at 212°F.), the decrease in rate with the partial pressure of vinyl chloride suggests that this component is adsorbed and occupies active sites on the catalyst. Other evidence is available

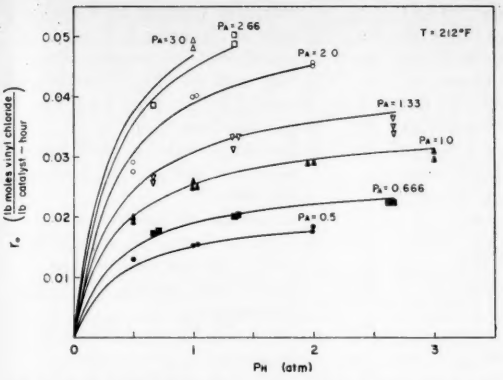

Fig. 3. Effect of hydrochloric acid partial pressure on initial rate.

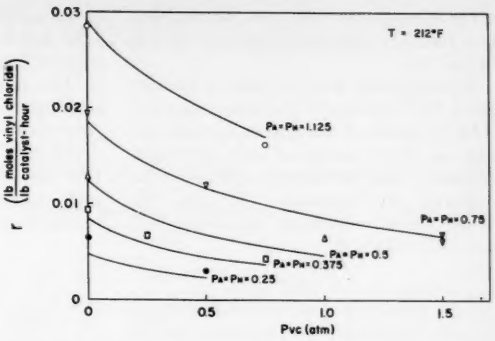

Fig. 5. Effect of vinyl chloride partial pressure on rate.

indicating the vinyl chloride is adsorbed. Frescoln (*4*) found that this component produced channeling and slugging in a fluidized catalyst bed. In an adsorption apparatus he noted that vinyl-chloride adsorption was irreversible, and he theorized that short-chain polymers formed on the catalyst.

On the basis of this information a rate equation, which agrees well with the experimental data, can be derived. It is supposed that all three components are adsorbed, acetylene on one type of site and hydrogen chloride and vinyl chloride on another. The reactions may be written

$$A + S_1 \underset{k_2}{\overset{k_1}{\rightleftharpoons}} A : S_1 \qquad (4)$$

$$H + S_2 \underset{k_4}{\overset{k_3}{\rightleftharpoons}} H : S_2 \qquad (5)$$

$$VC + S_2 \underset{k_7}{\overset{k_6}{\rightleftharpoons}} VC : S_2 \qquad (6)$$

The reaction to form vinyl chloride is postulated to occur by interaction between adsorbed acetylene ($A : S_1$) and adsorbed hydrogen chloride ($H : S_2$) on adjacent sites; that is

$$A : S_1 + H : S_2 \overset{k_5}{\rightarrow} VC + S_1 + S_2$$

If the fraction of the sites of type 1 occupied by acetylene is θ_{A1} and the fraction of type-2 sites occupied by hydrogen chloride is θ_{H2}, the rate may be written

$$r = k_5\theta_{A_1}\theta_{H_2} \qquad (7)$$

At steady state conditions the fraction of the surface occupied by the three components will not change with time. Hence the net rate of formation of each of the three adsorption compounds may be set equal to zero. Thus for acetylene, when one follows Langmuir's formulation of rates of adsorption,

$$k_1p_A(1 - \theta_{A1}) - k_2\theta_{A1} - k_5\theta_{A1}\theta_{H2} = 0 \qquad (8)$$

Similar equations for hydorgen chloride and vinyl chloride are

$$k_3p_H(1 - \theta_{VC2} - \theta_{H2}) - k_4\theta_{H2} - k_5\theta_{A1}\theta_{H2} = 0 \qquad (9)$$

$$k_6p_{VC}(1 - \theta_{VC2} - \theta_{H2}) - k_7\theta_{VC2} = 0 \qquad (10)$$

In these expressions $(1 - \theta_{A1})$ is the fraction of type-1 sites which are vacant, and $(1 - \theta_{H2} - \theta_{VC2})$ is the fraction vacant of sites of type 2. Equations (8) through (10) can be solved for θ_A, θ_{H2}, and θ_{VC2}. The expression for θ_{H2} is

$$\theta_{H2} = \frac{k_3k_7p_H}{k_3k_7p_H + (k_7 + k_6p_{VC})\left[k_4 + \dfrac{k_5k_1p_A}{k_1p_A + k_2 + k_5\theta_{H2}}\right]} \qquad (11)$$

and in terms of θ_{H2}

$$\theta_{A1} = \frac{k_1p_A}{k_1p_A + k_2 + k_5\theta_{H2}} \qquad (12)$$

These two expressions can be adapted to explicit equations for θ_{A1} and θ_{H2} and substituted in Equation (7) to give an equation for the rate of reaction in terms of the partial pressures and constants (at a given temperature). However the result is too complex to be useful.

Simplifications are possible if one makes assumptions regarding the relative magnitudes of some of the reaction rates. It is evident that many sets of assumptions may be made, each leading to a final rate equation which will contain

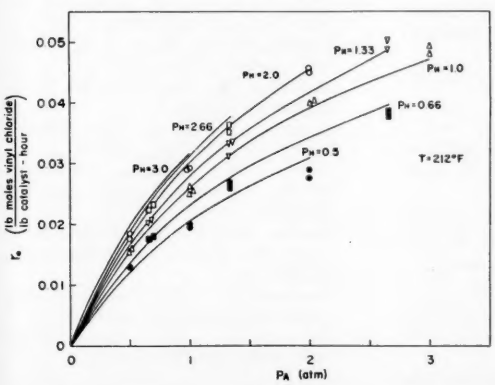

Fig. 4. Effect of acetylene partial pressure on initial rate.

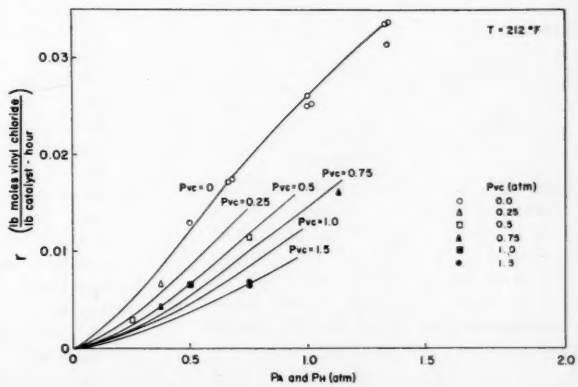

Fig. 6. Effect of hydrochloric acid and acetylene partial pressure on rate.

several constants. One set which leads to a result in agreement with the data is as follows.

It is supposed that the rate of reaction given by Equation (7) is slow compared with the rates of desorption and adsorption of both acetylene and hydrogen chloride. Then the term $k_5\theta_{A1}\theta_{H2}$ can be neglected in Equations (8) and (9). Under these restrictions Equations (11) and (12) reduce to

$$\theta_{H2} = \frac{k_3k_7p_H}{k_3k_7p_H + k_4k_7 + k_4k_6p_{VC}} \qquad (13)$$

$$= \frac{\frac{k_3}{k_4}p_H}{1 + \frac{k_3}{k_4}p_H + \frac{k_6}{k_7}p_{VC}}$$

and

$$\theta_{A1} = \frac{k_1p_A}{k_1p_A + k_2} = \frac{\frac{k_1}{k_2}p_A}{\frac{k_1}{k_2}p_A + 1} \qquad (14)$$

Substituting these quantities in Equation (7) gives the following equation for the rates:

$$r = \frac{Cp_Ap_H}{(1 + K_Hp_H + K_{VC}p_{VC})(1 + K_Ap_A)} \qquad (15)$$

where

$$C = k_5 \times \frac{k_1}{k_2} \times \frac{k_3}{k_4} \qquad K_H = \frac{k_3}{k_4},$$

$$K_A = \frac{k_1}{k_2}, \qquad K_{VC} = \frac{k_6}{k_7}$$

The constants C, K_H, and K_A in Equation (15) were determined first, with the initial rate data given in Table 2 used. The numerical values were obtained by an iterative procedure, with one of the constants changed at a time and the agreement of the rate data with Equation (15) evaluated (with $p_{VC} = 0$). The values which gave the minimum absolute deviation are

$$C = 0.14, \qquad K_H = 2.67, \qquad K_A = 0.46 \qquad (16)$$

K_{VC} was determined by relating the rate data with vinyl chloride and the initial rate. Thus the ratio obtained from Equation (15) is

$$\frac{r_0}{r} = \frac{1 + K_Hp_H + K_{VC}p_{VC}}{1 + K_Hp_H} \qquad (17)$$

$$= 1 + \frac{K_{VC}p_{VC}}{1 + K_Hp_H}$$

A plot of r_0/r vs. p_{VC}, at constant partial pressures of hydrogen chloride, gave a series of straight lines whose slope was equal to $K_{VC}/(1 + K_Hp_H)$. The slope of these lines was plotted vs. the reciprocal of $1 + K_Hp_H$. The slope of the least-mean-square line fitted to the points gave

$$K_{VC} = 3.8 \qquad (18)$$

The rates from Equation (15) predicted by means of the numerical values of the constants from Equations (16) and (18) are shown by the solid lines in Figures 3 to 6 and numerically in Table 2. The absolute deviation between experimental and calculated rates (all the runs being employed) averaged 3.3% at 212°F. and increased to 5.5 and 6.3% at 167° and 257°F. where only a few runs were made. The values used for the constants at 167° and 257°F. are

	167°F.	257°F.
C	0.08	0.232
K_H	2.9	2.5
K_A	0.58	0.40

It is apparent that Equation (15) closely follows the data within the range of conditions studied. However extrapolation of the equation beyond these conditions may lead to considerably larger errors.

As mentioned earlier, previous investigations (*4, 5, 11, 15*) of the kinetics of the reaction did not result in quantitative rate measurements. Hence numerical comparison with these studies is not possible.

Based upon different postulates for the mechanism, other rate equations can be derived which would agree as well with the data. Hence the results for Equation (15) cannot be cited as conclusive evidence for the postulates. However the mechanism of rapid adsorption and desorption of the components, and a slow conversion to vinyl chloride by interaction of adsorbed acetylene and hydrogen chloride, does predict rates in agreement with the data.

ACKNOWLEDGMENT

This work was supported by a grant from the National Science Foundation.

NOTATION

- A = acetylene in chemical equations
- ΔE = thermal-conductivity-cell imbalance, emf.
- C = over-all rate of reaction constant [Equation (15)], lb. moles of vinyl chloride/(lb. of catalyst)(hr.)
- E_A = activation energy, B.t.u./lb. mole
- F = flow rate, cu. ft./min.
- H = hydrogen in chemical equations
- ΔH_R = heat of reaction, B.t.u./lb. mole
- k = reaction-rate constant
- K = ratio of forward and reverse reaction-rate constants for adsorption reactions; adsorption equilibrum constant, atm.$^{-1}$
- p = partial pressure, atm. (defined as total pressure times mole fraction)
- r = reaction rate, lb. moles/(hr.)(lb. of catalyst)
- r_{corr} = rate of reaction corrected to a standard catalyst activity [used only in Equation (3)]
- r_0 = initial rate of reaction, that is rate with no vinyl chloride present
- R = gas constant
- R_0 = reactants ratio in feed, moles acetylene per mole of hydrogen chloride
- s = active site on catalyst
- S = entropy, B.t.u./(lb. mole)(°R.)
- S_1 = active catalyst sites of type 1
- S_2 = active catalyst sites of type 2
- T = temperature, °R.
- VC = vinyl chloride in chemical equations.
- W = mass of catalyst (including carrier)
- W/F = reciprocal space velocity, (lb. of catalyst)(hr.)/lb. mole
- x' = conversion of acetylene based upon total feed, moles of acetylene converted per mole of feed
- y = mole fraction
- θ = fraction of catalyst sites
- $\Delta x'$ = conversion

Subscripts

- A = acetylene
- H = hydrogen chloride
- VC = vinyl chloride
- 1 = adsorption site type 1
- 2 = adsorption site type 2

LITERATURE CITED

1. Boesler, Johannes, Ernst Eberhardt, Wilhelm Sandhass, and Robert Stadler, U. S. patent 2,265,509 (Dec. 9, 1941).
2. Bralley, J. A., U. S. patent 2,436,711 (Feb. 24, 1948).
3. Carter, A. S., and G. A. Cain, *FIAT Final Rept. 988*, p. 10, Office Tech. Services, U. S. Dept. of Commerce, Washington, D. C. (April 1947).
4. Frescoln, L. O., Ph.D. thesis, Case Inst. Technol., Cleveland, Ohio (1951).
5. Geiger, M. G., Ph.D. thesis, Purdue University, Lafayette, Ind. (1954).
6. Hougen, O. A., B. W. Gamson, and George Thodos, *Trans. Am. Inst. Chem. Engrs.*, **39**, 1 (1943).
7. Hougen, O. A., and K. H. Yang, *Chem. Eng. Progr.*, **46**, 146 (1950).
8. Lynn, R. E., and K. A. Kobe, *Ind. Eng. Chem.*, **46**, 633 (1954).
9. Reerink, Herman, M. S. thesis, Purdue Univ., Lafayette, Ind. (1957).
10. Sargent, H. B., *Chem. Eng.*, **64**, No. 2, 25 (1957).
11. Sheng, P. H., M. S. thesis, Purdue Univ., Lafayette, Ind. (1957).
12. Smith, J. M., "Chemical Engineering Kinetics," pp. 265ff., McGraw-Hill, New York (1956).
13. Wakano, Seiji, and Kondo Sin-ichi, *J. Chem. Soc., Japan, Ind. Chem. Sect.*, **57**, 909 (1954).
14. Wesselhoft, R. D., Ph.D. thesis, Purdue Univ., Lafayette, Ind. (1958).
15. Wortman, F. G., M. S., thesis, Purdue Univ., Lafayette, Ind. (1955).

Manuscript received September 15, 1958; revision received December 17, 1958; paper accepted January 5, 1959.

Thermal Conductivity of Diatomic Gases: Liquid and Gaseous States

CHARLES A. SCHAEFER and GEORGE THODOS

The Technological Institute, Northwestern University, Evanston, Illinois

After an extensive literature survey the experimental thermal-conductivity data for twelve diatomic gases were utilized to produce an accurate and expedient means of predicting values over extensive ranges of temperature and pressure. Plotting values of k^* against T_R on logarithmic coordinates produced similarities pointing to the existence of corresponding states behavior for this family of substances with the exception of hydrogen. Because hydrogen cannot be included in a correlation generalized for the diatomic gases, it has been eliminated from this study. Based on atmospheric pressure data, ratios of $k^*/k^*_{T_c}$ produced a unique relationship with reduced temperature. To include the effect of pressure, residual thermal conductivities were correlated with density for nitrogen and oxygen, the only substances for which high-pressure data exist. These relationships enabled the determination of the thermal conductivity at the critical point. When the value $k_c = 8.55 \times 10^{-5}$ cal./sec. cm. °K. for nitrogen was used, an extensive reduced thermal-conductivity correlation was constructed against reduced temperature for parameters of constant reduced pressure. This chart, extending to reduced pressures of 100 and to reduced temperatures of 85, is recommended for the diatomic gases in their gaseous and liquid states.

The developed correlation reproduces experimental nitrogen data to within 1.39%. For the other diatomic gases experimental agreement extends from 1.00 to 3.20%. Such agreement indicates that this correlation is more reliable for the diatomic gases than are other generalized plots presented in the literature.

Present technological advances continue to depend upon progress in understanding the fundamentals of mass and energy transfer; consequently, more careful scrutiny of these operations has stimulated an increasing interest in transport properties. An accurate but simple means of predicting coefficients of diffusion, thermal conductivity, and viscosity is needed to meet the demands of current engineering practice. Besides proving useful in practical applications, a reliable method of determination will be of value in testing and extending modern theories associated with transport phenomena.

Although the use of experimental data is most desirable, such direct values are limited to a few substances. Furthermore, even for the more common substances difficulties inherent in obtaining experimental thermal conductivities restrict the majority of values to the low-pressure region. Where experimental data are lacking, theoretical and empirical equations have been presented (*12, 23, 31, 56*). For accurate usage these are limited in application to the conditions of temperature and pressure for which they have been developed; furthermore, the nature of these expressions makes them inconvenient for expedient usage. Hence, graphical correlations would be desirable, but certain of these (*9*) are too limited to be useful over wide ranges of temperature and pressure. Other methods (*19*) are too generalized to be accurate for specific substances. To overcome these limitations, thermal-conductivity and viscosity correlations have been developed from experimental data specific to families of substances (*7, 42, 48, 51*). Such treatment permits the prediction of accurate values over wide ranges of temperature and pressure for both the gaseous and liquid states. As a continuation of these studies, the available experimental data for the thermal con-

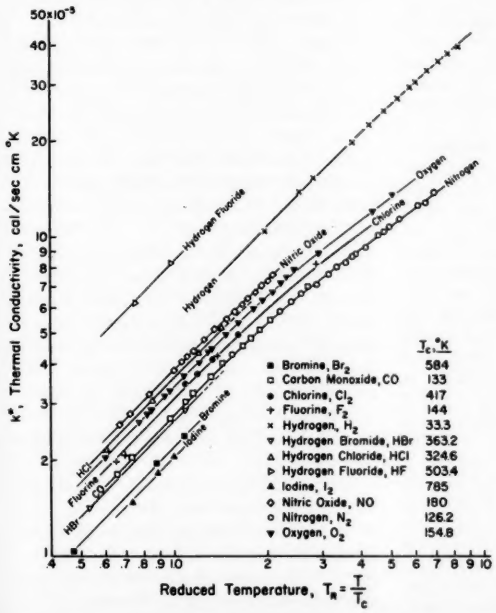

Fig. 1 Thermal conductivity-temperature relationships of diatomic gases at atmospheric pressure.

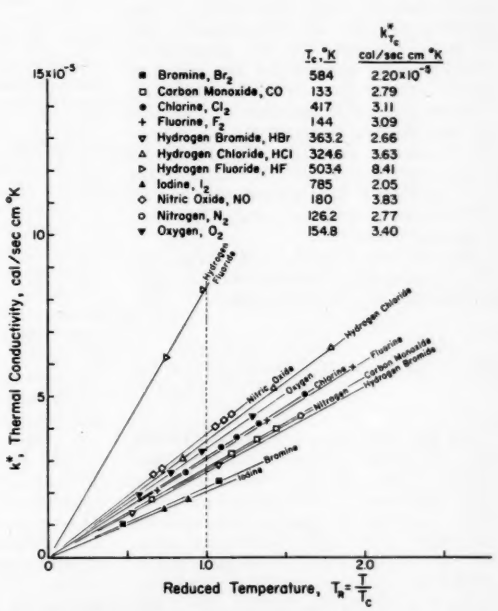

Fig. 2. Thermal conductivity-temperature relationships of diatomic gases at atmospheric pressure.

TABLE 1. COMPARISON OF EXPERIMENTAL THERMAL CONDUCTIVITIES WITH VALUES OBTAINED FROM REDUCED STATE CORRELATION AND RANGE INVESTIGATED

		Deviation, %		Range investigated		
	z_c	This investigation	Owens and Thodos (*42*)	T_R	P_R	References
Bromine	0.3065	1.31	—	0.47–1.88	0.0008–0.0013	*15,17*
Carbon monoxide	0.2943	1.04	2.4	0.59–2.83	0.0003–0.0290	*2,6,11,14,20,21,28,29*
Chlorine	0.2758	2.76	5.6	0.48–1.62	0.0009–0.0131	*14,15*
Fluorine	—	3.12	—	0.65–6.94	0.0017–0.0060	*15,17*
Hydrogen bromide	—	1.98	—	0.26–1.60	0.0020–0.0039	*15*
Hydrogen chloride	0.2656	1.13	3.4	0.61–1.78	0.0034–0.0042	*15*
Hydrogen fluoride	—	1.15	—	0.53–1.56	0.0007–0.0070	*16,18*
Iodine	—	1.93	—	0.57–0.88	0.0006–0.0020	*15*
Nitric oxide	0.2513	1.00	1.00	0.67–2.09	0.0156	*2,14,27,28*
Nitrogen	0.2915	1.39	2.6	0.51–8.50	0.0001–74.1	*2,4,5,6,11,13,14,15, 20,21,22,24,26,30, 32,33,34,36,37,39, 41,43,45,46,49,53, 54,55,58,59,60,61, 63,64*
Oxygen	0.2935	1.67	2.7	0.43–5.08	0.0003–1.93	*2,4,5,11,13,14,18, 20,21,22,27,28,29, 33,40,44,53,58,62, 63,65*

ductivity of diatomic gases have been compiled for the purpose of developing a reduced-state correlation (*47*). This correlation is generalized for the diatomic gases and extends over temperatures ranging from $T_R = 0.3$ to $T_R = 85$ and pressures extending up to $P_R = 100$.

PREVIOUS CORRELATING PROCEDURES

Early attempts at predicting transport properties were based on kinetic theory considerations. Maxwell (*38*) showed the consequences of treating molecules as point centers of forces which vary inversely as the fifth power of the distance between them. Chapman (*8*), assuming only spherical molecules, derived a thermal-conductivity expression which was limited by the accuracy of values for heat capacity and viscosity. Eucken (*13, 14*) proposed a relationship to account for the effect of internal energy in polyatomic molecules.

Sutherland (*57*) proposed an equation for the thermal conductivity at atmospheric pressure as an explicit function of temperature, and Enskog (*12*) and Keyes (*31*) developed the Sutherland type of relationships based on data in limited temperature intervals.

Hirschfelder, Curtiss, and Bird (*23*) present a first approximation to the thermal conductivity of monatomic gases:

$$[k]_1 = 19.89 \times 10^{-5} \frac{\sqrt{T/M}}{\sigma^2 \Omega^{(2,2)*}[T_N]} \quad (1)$$

For the inert gases Owens and Thodos (*42*) found good agreement between experimental values and the results obtained with Equation (1). For polyatomic molecules Equation (1) must be corrected for the transfer of energy between translational and internal degrees of freedom. The correction factor to be applied to Equation (1) is $1 + \{2/5(\rho D/\mu)[(2/3)(C_v/R) - 1]\}$. For the restricted condition of $\rho D/\mu = 1$ this factor reduces to the Eucken correction, and the modified form of Equation (1) for polyatomic gases becomes

$$[k_1]^{\text{Eucken}} = \left[\frac{4}{15}\frac{C_v}{R} + \frac{3}{5}\right][k_1] \quad (2)$$

An attempt to predict thermal conductivity at higher pressures follows from the theory of Enskog (*12*). For a gas composed of molecules that are mutually attracting rigid spheres, Enskog presents a power-series function in density to relate the thermal conductivity at high pressures to that at low pressures. A simpler power-series type of expansion has been used by Michels and Botzen (*39*) to account for pressure effects at isothermal conditions.

The correlating methods discussed possess certain serious limitations. The application of their equations must be confined to the temperature range for which they have been developed, and the majority of these expressions are restricted to moderate pressures. Furthermore these equations are not expedient to use, since the refinements which have increased their accuracy limit their ease of application.

Comings and Nathan (*9*) present a simple graphical correlation for the prediction of thermal conductivity for gases at high pressures, which was developed by the use of viscosity and PVT-data for nitrogen, argon, and methane in the Enskog equation. Calculated thermal-conductivity ratios k/k^* were plotted against reduced pressure with parameters of constant reduced temperature. Although later modified and extended by Lenoir, Junk, and Comings (*37*), the final correlation is limited to temperatures between $T_R = 1.0$ and 3.0 and pressures of $P_R < 7.0$.

A more extensive correlation was developed by Gamson (*19*). This represents an initial attempt toward generalization by means of the concept of k_R. This correlation extends to temperatures of $T_R = 10$ and pressures of $P_R = 30$; however no consideration is given to the liquid state. Owing to an overgeneralized approach embodying data for twenty-seven gases, the correlation is claimed to be reliable to within only 15%.

Owens and Thodos (*42*) have developed a reduced-state correlation for the liquid and gaseous states based solely on experimental data for the inert gases. By restricting their method of approach to a family of similar substances, they presented a final correlation that was capable of reproducing the experimental data to within 2%. In view of these improved results, an analogous approach has been adopted for the investigation of the diatomic gases.

CORRELATION OF DATA

An extensive literature survey was undertaken to compile the available thermal-conductivity data of the diatomic gases. The ranges of temperature and pressure and sources of experimental data are presented in Table 1.

Based only upon the atmospheric data, Figure 1 presents a log-log plot of experimental values of k^* as a function of reduced temperature $T_R = T/T_c$. This figure also indicates the twelve gases considered in this study. The notable characteristic of this plot is the parallelism exhibited by the relationships of the various gases. An exception to this is noted for hydrogen at higher temperatures. As postulated from kinetic theory, the behavior of corresponding states should apply to a family of substances possessing molecules of similar shapes and having the same intermolecular-force relationships. The parallelism noted suggests that the behavior of corresponding states should apply to diatomic gases with the exception of hydrogen. An explanation for this anomalous behavior has been advanced in terms of quantum deviations by de Boer and Bird (*10*). For the hydrogen data to conform with those of the other diatomic gases, an adjustment of the critical constants has been utilized by previous investigators. Owing to their empirical nature, these adjustments vary between

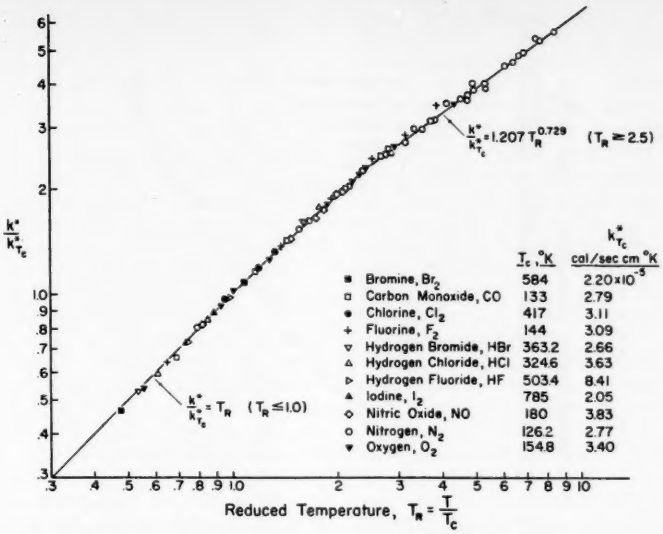
$\frac{k^*}{k_{T_c}^*}$
$\frac{k^*}{k_{T_c}^*} = 1.207\,T_R^{0.729}$ $(T_R \geq 2.5)$
$\frac{k^*}{k_{T_c}^*} = T_R$ $(T_R \leq 1.0)$
Reduced Temperature, $T_R = \frac{T}{T_c}$
$k_{T_c}^*$ cal/sec cm °K
Bromine, Br_2 584 2.20×10⁻⁵
Carbon Monoxide, CO 133 2.79
Chlorine, Cl_2 417 3.11
Fluorine, F_2 144 3.09
Hydrogen Bromide, HBr 363.2 2.66
Hydrogen Chloride, HCl 324.6 3.63
Hydrogen Fluoride, HF 503.4 8.41
Iodine, I_2 785 2.05
Nitric Oxide, NO 180 3.83
Nitrogen, N_2 126.2 2.77
Oxygen, O_2 154.8 3.40

Fig. 3. Ratio of thermal conductivity-temperature relationship for diatomic gases at atmospheric pressure.

investigators and are applicable in limited ranges of temperature and pressure. A more direct and reliable approach is to consider the properties of hydrogen separately from those of the diatomic gases (*48*); consequently, hydrogen has been eliminated from further consideration in these studies.

The similarity of the relationships shown in Figure 1 suggests the representation of these curves by an equation of the form

$$\log k^* = n \log T_R + \log H \qquad (3)$$

For the boundary condition of $T_R = 1$, k^* equals $k_{T_c}{}^*$. Thus Equation (3) becomes

$$\log \frac{k^*}{k_{T_c}{}^*} = n \log T_R \qquad (4)$$

Equation (4) indicates that a unique relationship exists for the diatomic gases when the ratio $k^*/k_{T_c}{}^*$ is related to T_R. This requires a knowledge of $k_{T_c}{}^*$ values specific to each substance.

To obtain $k_{T_c}{}^*$ values more accurately than could be obtained from Figure 1, advantage is taken of the linearity that exists at low temperatures, when k^* is related to temperature on rectilinear coordinates. Therefore the low-temperature thermal-conductivity data for these gases are plotted in Figure 2 as a function of T_R. The values of $k_{T_c}{}^*$ along with the critical temperatures are presented in Figure 2.

An attempt to correlate $k_{T_c}{}^*$ values as a function of molecular weight and the critical values T_c, P_c, and z_c has been made. These studies indicate that $k_{T_c}{}^*$ is independent of z_c. Trial-and-error procedures using the critical constants resulted in the expression

$$k_{T_c}{}^* = 3.05 \times 10^{-5} \frac{P_c^{9/16}}{M^{1/2} T_c^{1/5}} \qquad (5)$$

Equation (5) is specific to diatomic gases and reliable to 3.4%.

The $k_{T_c}{}^*$ values from Figure 2 and the experimental k^* values were used to calculate ratios of $k^*/k_{T_c}{}^*$, which were plotted against reduced temperature to produce the curve of Figure 3. This unique relationship for the diatomic gases is defined by Equation (4). The relationship is linear below $T_R = 1.0$ and above $T_R = 2.5$ and can be expressed as

$$\frac{k^*}{k_{T_c}{}^*} = T_R \qquad (T_R \leq 1.0) \qquad (6)$$

$$\frac{k^*}{k_{T_c}{}^*} = 1.207 T_R^{0.729} \qquad (T_R \geq 2.5) \qquad (7)$$

The correlations presented in Figures 1, 2, and 3 can be used to account for the variation in thermal conductivity with temperature at atmospheric pressure. Sherratt and Griffiths (*50*) state that thermal conductivity is independent of pressure from 1 atm. down to 5 cm. of mercury. Spencer-Gregory and Marshall (*52*, *53*) indicate that the lower limit is between 0.49 and 1.1 cm. of mercury. For pressures above 1 atm. thermal conductivity is dependent not only on temperature but also on pressure.

While extensive data are available at 1 atm., experimental values at higher pressures are limited owing to inherent difficulties in obtaining such values. Of the eleven gases considered in this study nitrogen and oxygen are the only ones for which sufficient data exist to permit the development of a correlation over extensive conditions of temperature and pressure. Even for nitrogen and oxygen too many high-pressure data are lacking to permit this development by direct cross-plotting techniques.

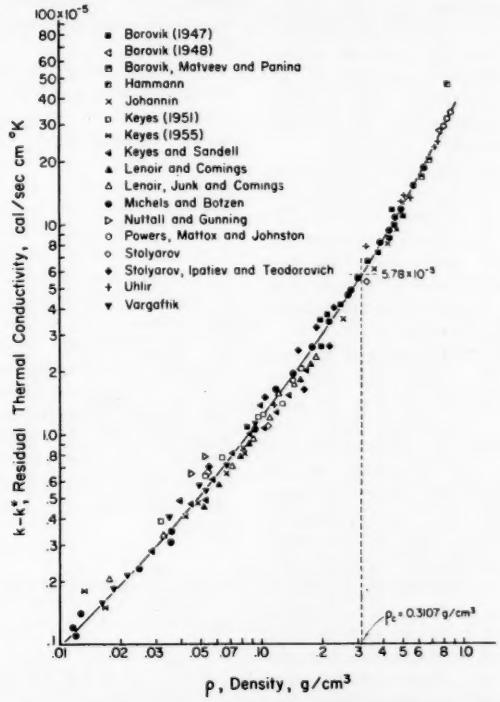

Fig. 4. Residual thermal-conductivity–density relationship for nitrogen in the liquid and gaseous states.

To handle the high-pressure data presently available, use was made of an extension to the method of Abas-Zade (*1*). His correlations, developed from the consideration of functions of invariant quantities, relate thermal conductivity to density and suggest correlating the residual thermal conductivity $k - k^*$ with the density to cover the liquid and gaseous states. Thermal conductivities at atmospheric pressure were substracted from high-pressure thermal conductivities at the same temperature and plotted against density to produce the relationship presented in Figure 4 for nitrogen and Figure 5 for oxygen. The advantage of these correlations is twofold. First is the ability to bring together as a continuous curve the high-pressure gaseous data (*25, 26, 39*) and the low-temperature liquid data (*43, 59*); secondly, the thermal conductivity at any condition of temperature and pressure can be obtained from a knowledge of ρ and k^*. In particular k_c can be evaluated.

When one uses in Figure 4 a value of $\rho_c = 0.3107$ g./cc. (*35*) for the critical density of nitrogen, the residual thermal conductivity at the critical point becomes $k_c - k_{T_c}^* = 5.78 \times 10^{-5}$ cal./sec. cm. °K. Adding to this value $k_{T_c}^* = 2.77 \times 10^{-5}$ cal./sec. cm. °K., one can determine the critical thermal conductivity to be 8.55×10^{-5} cal./sec. cm. °K. Likewise when one uses in Figure 5 a value of $\rho_c = 0.430$ g./cc. (*51*) for the critical density of oxygen, the residual thermal conductivity at the critical point becomes $k_c - k_{T_c}^* = 7.00 \times 10^{-5}$ cal./sec. cm. °K. Adding to this value $k_{T_c}^* = 3.40 \times 10^{-5}$ cal./sec. cm. °K., one can determine the critical thermal conductivity to be 10.40×10^{-5} cal./sec. cm. °K. These critical values permit the construction of reduced thermal-conductivity correlations.

The liquid and high-pressure–gaseous experimental data are more plentiful for nitrogen than for oxygen; moreover, the nitrogen data are considered more reliable. Therefore preference has been given to this substance for the development of a reduced-state correlation applicable to the diatomic gases.

The division of atmospheric thermal conductivities by k_c enabled the construction of the base isobar, $P_R \approx 0$. For pressures above 1 atm. densities at specific conditions of temperature and pressure were used to obtain residual thermal conductivities $k - k^*$ from Figure 4. Values of k^* at the specified temperatures were added to these residuals to produce thermal conductivities corresponding to the density conditions of temperature and pressure. Dividing these values of k by k_c, one obtained reduced thermal conductivities for pressures above 1 atm. These reduced values of k_R were plotted against reduced temperature for parameters of constant reduced pressure. The final correlation

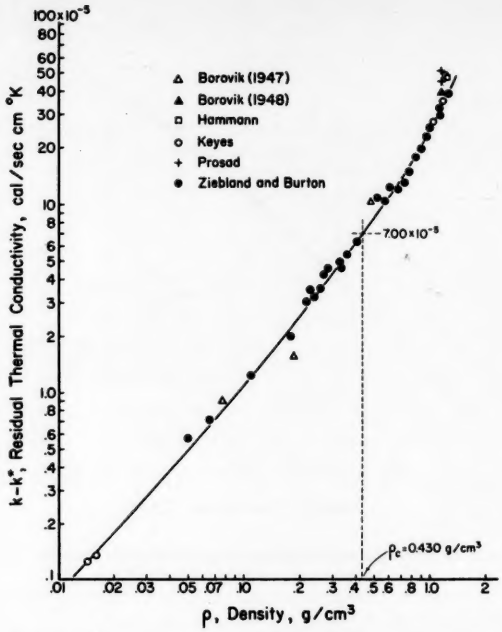

Fig. 5. Residual thermal-conductivity–density relationship for oxygen in the liquid and gaseous states.

is presented in Figure 6. It extends from the high-temperature gaseous region, through the critical point, and into the liquid state. This correlation, based only on experimental nitrogen data, enables the determination of reduced thermal conductivities for diatomic gases from atmospheric pressure to $P_R = 100$ and for temperatures up to $T_R = 85$.

To obtain absolute thermal conductivities requires a critical value for each substance. Since experimental data are limited to atmospheric pressure for the diatomic gases other than nitrogen and oxygen, correlations similar to Figures 4 and 5 cannot be developed. Hence k_c cannot be established from experimental data in a manner similar to that used for nitrogen and oxygen. Instead critical thermal conductivities can be obtained by the division of k_R values from Figure 6 into experimental values which are available only at atmospheric pressure.

A more rigorous approach is based on the concept of corresponding states as postulated by the parallel curves of Figure 1. The analytical expression for these relationships is given by Equation (3). Substracting log k_c from both sides yields

$$\log \frac{k^*}{k_c} = n \log T_R + \log \frac{H}{k_c} \qquad (8)$$

or

$$\log \frac{k^*}{k_c} = n \log T_R + \log \frac{1}{A} \qquad (9)$$

As before, at $T_R = 1.0$, $k^* = k_{T_c}^*$, and therefore

$$\frac{k_{T_c}^*}{k_c} = \frac{1}{A} \qquad (10)$$

or

$$k_c = A k_{T_c}^* \qquad (11)$$

With the use of the values $k_c = 8.55 \times 10^{-5}$ cal./sec. cm. °K. and $k_{T_c}^* = 2.77 \times 10^{-5}$ cal./sec. cm. °K., the ratio $k_c/k_{T_c}^* = 3.087$ was calculated for nitrogen. Likewise with the use of the values $k_c = 10.4 \times 10^{-5}$ cal./sec. cm. °K. and $k_{T_c}^* = 3.40 \times 10^{-5}$ cal./sec. cm. °K., the ratio $k_c/k_{T_c}^* = 3.059$ was calculated for oxygen. The close agreement of these two results validates the use of Equation (11) to calculate values of k_c for the other diatomic substances. Since Figure 6 has been developed from nitrogen data, the value of $A = 3.087$ was selected; it is in contrast to the value of 2.60 proposed by Gamson (*19*) for the twenty-seven gases included in that study. From this value in Equation (11) and the values of $k_{T_c}^*$ obtained from Figure 2, critical thermal conductivities were calculated for the other diatomic gases. These values are presented in Figure 6 along with the critical temperatures and pressures.

DISCUSSION OF RESULTS

The reduced-state correlation presented in Figure 6 has been recommended for the prediction of thermal conductivities for the diatomic gases in the gaseous and liquid states. Its utility depends upon the consistency with which it reproduces experimental data. To be

useful, it must be reliable in determining thermal conductivities not only for nitrogen, for which it was developed, but also for the other diatomic gases for which it is recommended. Accordingly thermal conductivities at the experimental conditions of temperature and pressure have been calculated by means of this correlation for purposes of comparison with the experimental data.

Consideration of one hundred fifty nitrogen values representing the available ranges of temperature and pressure produced agreement to within 1.39%. The causes for the average deviation lie in the experimental measurements as well as in the techniques utilized to construct the final correlation. Inherent difficulties are encountered at high pressures. This is evidenced by the lack of accurate data over extensive ranges of temperature and pressure. Even at atmospheric pressure and 273°K. the usually reliable data of Keyes (*30, 32, 34*) are found to disagree within themselves by as much as 2.95%.

In an attempt to produce a reliable correlation, consideration has been given to all the available nitrogen data. Other than the elimination of those investigators whose data were obviously out of line from the general trends, no discrimination has been made. Such elimination is justified by the fact that deviations of 30% were found for the data of Hammann (*22*) and 7.9% for those of Borovik *et al.* (*4, 5, 6*).

To test the usefulness of Figure 6 as a correlation generalized for the diatomic gases, comparisons with available experimental data have been made in a manner similar to that employed for nitrogen. Agreement to within 1.67% was obtained for oxygen in the gaseous state. While this deviation is not large, it does not include the liquid data of Hammann (*22*) and Ziebland and Burton (*65*). Their results deviate by 6.03 and 16.95% respectively. Disagreement of this magnitude was also encountered in viscosity studies (*7*) and, as pointed out by Bird (*3*), can be explained as the result of paramagnetic effects associated with liquid oxygen.

The results of comparing values calculted from Figure 6 with experimental data for the remaining diatomic gases considered in this study are summarized in Table 1, which also presents the deviations for nitrogen and oxygen and those obtained by use of the inert gas correlation of Owens and Thodos (*62*). It is to be noted that except for nitrogen and oxygen these deviations are for the gaseous data available only at atmospheric pressure. The extent of liquid data is limited to the values reported by Borovik, Matveev, and Panina (*6*) for carbon monoxide; their results were found to agree to within 3.30%. From the results of the comparisons presented for the eleven gases considered in this study, it can be concluded that Figure 6 not only reproduces the experimental nitrogen data from which it was developed but is also reliable as a generalized correlation for the other diatomic gases. This is valid provided these substances do not possess anomalous behavior as encountered for liquid oxygen.

As indicated early in this study, hydrogen deviated from a corresponding-states behavior; hence it cannot be included in the generalized reduced state correlation of Figure 6. Consideration has been given to z_c as a possible parameter for correlating $k_c/k_{T_c}{}^*$ ratios. Because high-pressure thermal-conductivity data are available for hydrogen (*48*), values of k_c and $k_{T_c}{}^*$ were obtained in a manner analogous to that used for nitrogen and oxygen. These values as well as z_c and the product $k_c/k_{T_c}{}^* z_c$ for these three gases are as follows:

	$k_{T_c}{}^*$	k_c	$k_c/k_{T_c}{}^*$	z_c	$k_c/k_{T_c}{}^* z_c$
Hydrogen	5.40×10^{-5}	15.9×10^{-5}	2.944	0.3045	0.8964
Nitrogen	2.77	8.55	3.087	0.2915	0.8999
Oxygen	3.40	10.4	3.059	0.2935	0.8978

If these substances adhere strictly to the behavior of corresponding states, values for the ratio $k_c/k_{Tc}{}^*$ should be identical, as postulated from Equation (11), but they are not. Multiplying these ratios by their respective critical compressibility factors, one can produce values which are essentially the same. From the average of these values, the following relationship is proposed:

$$\frac{k_c}{k_{T_c}{}^*} z_c = 0.8980 \qquad (12)$$

This equation is recommended to account for deviations from the behavior of corresponding states for the diatomic gases.

Since values of k_c for the other diatomic gases have been calculated from Equation (11) with $A = 3.087$ resulting from $k_c/k_{T_c}{}^*$ for nitrogen, it would be meaningless to use these values in Equation (12). Hence until more direct means become available for obtaining k_c values from experimental data the validity of Equation (12) cannot be tested rigorously.

ACKNOWLEDGMENT

Grateful acknowledgment is extended to the Dow Chemical Company for the financial assistance which made this study possible.

NOTATION

A = constant, k_c/H
C_v = heat capacity at constant volume
H = constant
k = thermal conductivity, cal./sec. cm. °K.
k^* = thermal conductivity at moderate pressures (1 atm.), cal./sec. cm. °K.
k_c = critical thermal conductivity, cal./sec. cm. °K.
k_R = reduced thermal conductivity, k/k_c
$k_{T_c}{}^*$ = thermal conductivity at the critical temperature and atmospheric pressure, cal./sec. cm. °K.
M = molecular weight
n = exponent, $\varphi(T_R)$
P = pressure, atm.
P_c = critical pressure, atm.
P_R = reduced pressure, P/P_c
R = gas constant
T = absolute temperature, °K.
T_c = critical temperature, °K.
T_N = normalized temperature, $T/(\epsilon/\kappa)$
T_R = reduced temperature, T/T_c
z_c = critical compressibility factor

Greek Letters

ϵ = maximum energy of attraction of two molecules for the Lennard-Jones potential function, erg.
κ = Boltzmann constant, 1.3805×10^{-16} ergs/°K.
ρ = density, g./cc.
ρ_c = critical density, g./cc.
σ = collision diameter for the Lennard-Jones potential function, Å.
$\Omega^{(2,2)*}[T_N]$ = collision integral for Lennard-Jones potential function

LITERATURE CITED

1. Abas-Zade, A. K., *Zhur. Eksptl. i Teoret. Fiz.*, **23**, 60 (1952).
2. Andrussow, Léonide, *J. chim. phys.*, **52**, 295 (1955).
3. Bird, R. B., private communication.
4. Borovik, E., *Zhur. Eksptl. i Teoret. Fiz.*, **17**, 328 (1947).
5. *Ibid.*, **18**, 48 (1948).
6. ———, A. Matveev, and E. Panina, *J. Tech. Phys.* (*U.S.S.R.*), **10**, 988 (1940).
7. Brebach, W. J., *Ind. Eng. Chem.*, **50**, 1095 (1958).
8. Chapman, S., *Phil. Trans. Roy. Soc.* (*London*), **A211**, 433 (1912).
9. Comings, E. W., and M. F. Nathan, *Ind. Eng. Chem.*, **39**, 964 (1947).
10. de Boer, H. G. J., and R. B. Bird, *Phys. Rev.*, **83**, 1259 (1951).
11. Dickins, B. G., *Proc. Roy. Soc.* (*London*), **A143**, 517 (1934).
12. Enskog, David, *Kgl. Svenska Vetenskapsakad. Handl.*, **63**, No. 4 (1921).
13. Eucken, A., *Phys. Z.*, **12**, 1101 (1911).
14. *Ibid.*, **14**, 324 (1913).
15. Franck, E. U., *Z. Elektrochem.*, **55**, 636 (1951).
16. ———, and W. Spalthoff, *Naturw.*, **40**, 580 (1953).
17. ———, *Z. Elektrochem.*, **58**, 374 (1954).
18. Franck, E. U., and E. Wicke, *Z. Elektrochem.*, **55**, 643 (1951).
19. Gamson, B. W., *Chem. Eng. Progr.*, **45**, 154 (1949).

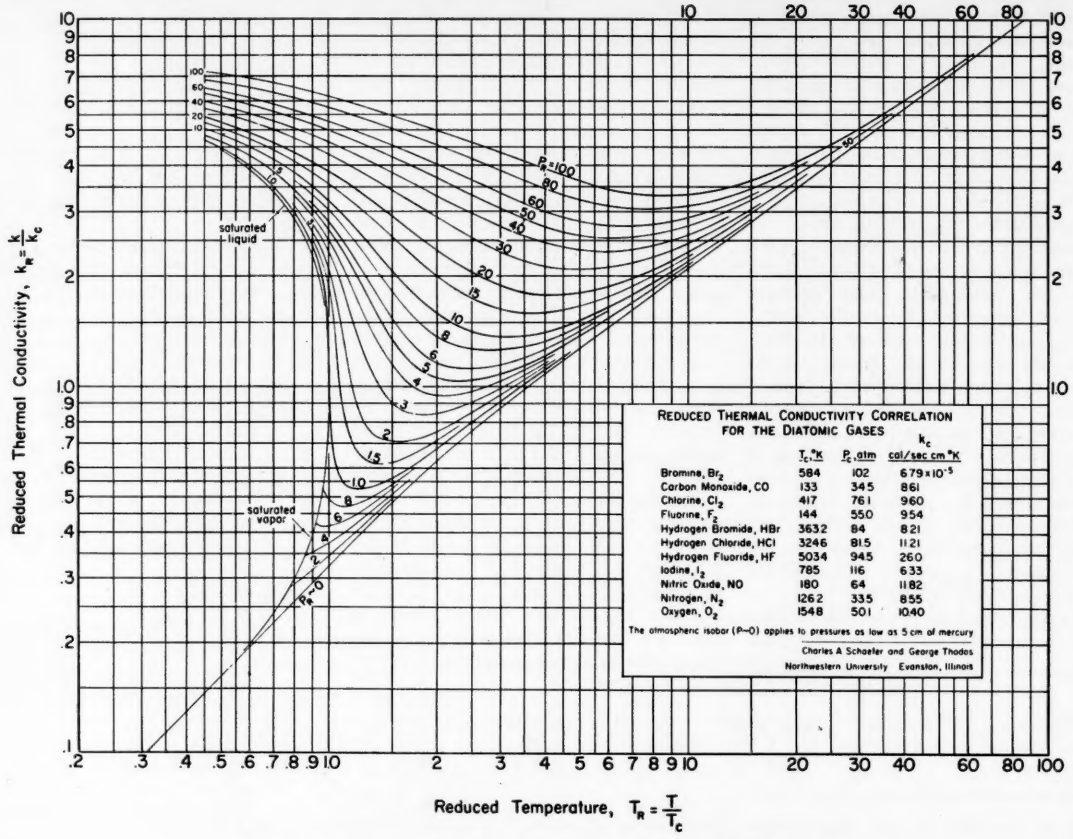
Reduced Thermal Conductivity, $k_R = \frac{k}{k_c}$
Reduced Temperature, $T_R = \frac{T}{T_c}$
saturated liquid
saturated vapor
P_R=100
80
60
50
40
30
20
15
10
8
6
5
4
3
2
1.5
1.0
REDUCED THERMAL CONDUCTIVITY CORRELATION FOR THE DIATOMIC GASES

	T_c, °K	P_c, atm	k_c cal/sec cm °K
Bromine, Br_2	584	102	679×10^{-5}
Carbon Monoxide, CO	133	345	861
Chlorine, Cl_2	417	761	960
Fluorine, F_2	144	550	954
Hydrogen Bromide, HBr	3632	84	821
Hydrogen Chloride, HCl	3246	815	1121
Hydrogen Fluoride, HF	5034	945	260
Iodine, I_2	785	116	633
Nitric Oxide, NO	180	64	1182
Nitrogen, N_2	1262	335	855
Oxygen, O_2	1548	501	1040

The atmospheric isobar (P=0) applies to pressures as low as 5 cm of mercury

Charles A Schaefer and George Thodos
Northwestern University Evanston, Illinois

Fig. 6. Reduced thermal-conductivity correlation for the diatomic gases.

20. Godridge, A. M., *Bull. Brit. Coal Utilisation Research Assoc.*, **18**, 1 (1954).
21. Gruss, H., and H. Schmick, *Wiss. Veröffentl. Siemens-Konzern*, **7**, 202 (1928).
22. Hammann, Günther, *Ann. Physik* (5), **32**, 593 (1938).
23. Hirschfelder, J. O., C. F. Curtiss, and R. B. Bird, "Molecular Theory of Gases and Liquids," p. 534, John Wiley, New York (1954).
24. Ibbs, T. L., and A. A. Hirst, *Proc. Roy. Soc.* (*London*), **A123**, 134 (1929).
25. Johannin, Pierre, "Experimental Determination of the Thermal Conductivity of Nitrogen at High Pressures and Elevated Temperatures," presented by The Institution of Mechanical Engineers and The International Union of Pure and Applied Chemistry, London, (July 10–12, 1957).
26. ———, private communication.
27. Johnston, A. I., and Chen-jung Huang, *Chem. Eng.*, **61**, 204 (1954).
28. Johnston, H. L., and E. R. Grilly, *J. Chem. Phys.* **14**, 233 (1946).
29. Kannuluik, W. G., and L. H. Martin, *Proc. Roy. Soc.* (*London*), **A144**, 496 (1934).
30. Keyes, F. G., *Trans. Am. Soc. Mech. Engrs.*, **73**, 597 (1951).
31. Keyes, F. G., *U. S. Navy and U. S. Air Force Project Squid Tech. Rep.* 37 (April 1, 1952).
32. ———, *Trans. Am. Soc. Mech. Engrs.*, **74**, 1303 (1952).
33. *Ibid.*, **77**, 1395 (1955).
34. ———, and D. J. Sandell, Jr., *Trans. Am. Soc. Mech. Engrs.*, **72**, 767 (1950).
35. Kobe, K. A., and R. E. Lynn, Jr., *Chem. Revs.*, **52**, 117 (1953).
36. Lenoir, J. M., and E. W. Comings, *Chem. Eng. Progr.*, **47**, 223 (1951).
37. ———, and W. A. Junk, *ibid.*, **49**, 539 (1953).
38. Maxwell, J. C., "Collected Works," vol. 2, p. 23 (1866).
39. Michels, A., and A. Botzen, *Physica*, **19**, 585 (1953).
40. Northdurft, Walter, *Ann. Physik* (**5**), **28**, 137 (1937).
41. Nuttall, R. L., and D. C. Gunnings, *J. Research Natl. Bur. Standards*, **58**, 271 (1957).
42. Owens, E. J., and George Thodos, *A.I.Ch.E. Journal*, **3**, 454 (1957).
43. Powers, R. W., R. W. Mattox, and H. L. Johnston, *J. Am. Chem. Soc.*, **76**, 5968 (1954).
44. Prosad, S., *Brit. J. Appl. Phys.*, **3**, 58 (1952).
45. Rothman, A. J., *U.S. Atomic Energy Comm. Tech. Inform. Service*, UCRL-2339 (1953).
46. Rothman, A. J., and L. A. Bromley, *Ind. Eng. Chem.*, **47**, 899 (1955).
47. Schaefer, C. A., M. S. thesis, Northwestern Univ., Evanston, Illinois (1957).
48. ———, and George Thodos *Ind. Eng. Chem.*, **50**, 1585 (1958).
49. Schottky, W. F., *Z. Elektrochem.*, **56**, 889 (1952).
50. Sherratt, G. G., and Ezer Griffiths, *Phil. Mag.* (7), **27**, 68 (1939).
51. Shimotake, Hiroshi, and George Thodos, *A.I.Ch.E. Journal*, **4**, 257 (1958).
52. Spencer-Gregory, H., and S. Marshall, *Proc. Roy. Soc.* (*London*), **A114**, 354 (1927).
53. *Ibid.*, **A118**, 594 (1928).
54. Stolyarov, E. A., *Zhur. Fiz. Khim.*, **24**, 279 (1950).
55. V. V. Ipatiev, and V. P. Teodorovich, *ibid.*, 166 (1950).
56. Stops, D. W., *Nature*, **164**, 966 (1949).
57. Sutherland, William, *Phil. Mag.* (5), **36**, 507 (1893).
58. Todd, G. W., *Proc. Roy. Soc.* (*London*), **A83**, 19 (1909).
59. Uhlir, Arthur, Jr., *J. Chem. Phys.*, **20**, 463 (1952).
60. Vargaftik, N. B., *Tech. Phys.* (*U.S.S.R.*), **4**, 341 (1937).
61. Vargaftik, N. B., and O. N. Oleshchuk, *Izvest. Vsesoyuz. Teplotekh. Inst. im Feliksa Dzerzhinskogo*, **15**, 7 (1946).
62. Wassiljewa, Alexandra, *Physik. Z.*, **5**, 737 (1904).
63. Weber, S., *Ann. Physik* (**4**), **54**, 437 (1917).
64. Wilner, T., and G. Borelius, *ibid.* (5), **4**, 316 (1930).
65. Ziebland, H., and J. T. A. Burton, *Brit. J. Appl. Phys.*, **6**, 416 (1955).

Manuscript received May 21, 1958; revision received December 8, 1958; paper accepted December 9, 1958.

Ion Exchange Kinetics for Systems of Nonlinear Equilibrium Relationships

CHI TIEN and GEORGE THODOS

The Technological Institute, Northwestern University, Evanston, Illinois

Mathematical relationships based on material balance and rate equations have been derived for the study of ion exchange kinetics in a fixed-bed operation. Numerical techniques for the solution of the systems possessing equilibrium relationships of the Freundlich-adsorption isotherm type have been developed, and numerical results have been obtained with the use of a digital computer. The resulting numerical solutions have been found to be dependent on parameters involving time, position, and the relative resistances of the liquid and resin phases. The numerical solutions are presented in both tabular and graphical forms.

Ion exchange operations are becoming increasingly important and find considerable utility in processes associated with the removal of undesirable constituents or the concentration and recovery of valuable components present in trace amounts in solutions. The design of equipment capable of performing a specific separation depends primarily on the prediction of the concentration history of effluent solutions.

The work of Du Domaine, Swain, and Hougen (*3*) presents results which make possible the prediction of the performance of the softening of water through a zeolite bed. Their mathematical analysis has been based on a particular rate-controlling step and therefore proves valuable for the solution of problems limited to this type of mechanism. Hougen and Dodge (*8*) studied the drying of air through a bed of silica gel. A more general case was presented later by Thomas (*12*), who considered a second-order reversible reaction as the rate-controlling step. Subsequent work by Hiester and Vermeulen (*6*) has shown that a certain type of adsorption mechanism can be considered equivalent to that of a second-order chemical reaction. Boyd, Meyers, and Adamson (*1, 2*) considered the rate-controlling mechanism to be the diffusion through the liquid film. Similar work has been carried out by Hagerty (*4*), assuming a Freundlich as well as a Langmuir equilibrium relationship. Later studies by Lapidus and Amundson (*9*) deal with the significance of longitudinal diffusion for the case of a first-order reaction. Perhaps the most rigorous treatment is presented by Rosen (*11*), who considers the resistances of both the liquid and solid phases for systems exhibiting a simple, linear equilibrium relationship.

Since the work of Rosen presents a rather restricted equilibrium relationship, the object of this investigation is to solve the general case for which the equilibrium relationship is of a nonlinear nature. Analytical solutions for this type of problem are quite improbable, and consequently numerical methods have been used. The numerical results to this problem have been made possible through the use of the Univac 1103 and are presented in both tabular and graphical forms.

DEVELOPMENT OF MATHEMATICAL EQUATIONS

The most common ion exchange operation involves the removal of a solute from a solution on solid resins. For a flow system this is accomplished by passing the solution through a bed of resin particles. During the operation the solute is continuously removed until the resin phase reaches equilibrium with the influent stream. For this process the kinetic behavior is determined by the rate-controlling mechanism. Three commonly encountered mechanisms are (1) transfer of solute from solution to resin surface, (2) adsorption of solute at solid surface, and (3) diffusion of adsorbed solute through the resin. Any possible combination of these mechanisms defines the kinetic behavior of the system. In cases when the adsorption step is rapid in comparison with the other steps, it can be disregarded in the subsequent kinetic treatment. Under these conditions the kinetics will be controlled by the combination of steps (1) and (3). The transfer of mass across the liquid film and consequent diffusion within the particle are affected by the existence of concentration gradients in the liquid and solid phases. The physical picture is presented diagrammatically in Figure 1.

The following assumptions have been made in this investigation: (1) constant liquid-film resistance during operation, (2) constant diffusion coefficient of solute through resin, (3) insignificant longitudinal diffusion, (4) presence of only linear flow through resin bed, (5) uniform bed porosity, (6) no radial variation of concentration in liquid and solid phases, and (7) perfect spherical particles of uniform size. With these assumptions the equation of continuity can be written as

$$uC\,dt - u\left[C + \frac{\partial C}{\partial z}\,dz\right]dt - \frac{\partial q}{\partial t}\,\rho\,dz\,dt = \frac{\partial C}{\partial t}\,\varphi\,dz\,dt$$

$$\frac{u}{\varphi}\frac{\partial C}{\partial z} + \frac{\partial C}{\partial t} = -\frac{\rho}{\varphi}\frac{\partial q}{\partial t} \qquad (1)$$

The rate equation considered from the liquid side can be expressed as

$$\frac{\partial q}{\partial t} = k_l[C - C_s] \qquad (2)$$

The adsorption of the solute on the resin establishes a concentration gradient which in turn causes the diffusion of the solute toward the center. Consequently the concentration of solute will vary radially inside the particle. The following expressions will relate q_i, q_s, and q:

$$q(t, z) = \frac{3}{b^3}\int_0^b q_i(t, z, r)r^2\,dr \qquad (3)$$

$$q_s(t, z) = q_i(t, z, b) \qquad (4)$$

At the beginning of the operation q_i, q_s, and q are zero and eventually

*Chi Tien is at Assumption University of Windsor, Windsor, Ontario, Canada.

become identical when the particle reaches equilibrium with the influent solution. When this condition prevails, diffusion into the particle ceases.

It is obvious the q_i should be a solution of the following diffusion equation:

$$\frac{\partial q_i}{\partial t} = D\nabla^2 q_i = \frac{D}{r^2}\left[r^2 \frac{\partial q_i}{\partial r}\right] \qquad (5)$$

with the following initial condition:

$$q_i = 0 \quad \text{for} \quad z \geq 0$$

$$0 < r < b \quad \text{when} \quad t \leq (\varphi/u)z$$

where the quantity $(\varphi/u)z$ represents the time required for the liquid front to reach a particular position in the bed, and the following boundary condition:

$$q_i = q_s(z, t) \quad \text{when} \quad r = b$$

The solution of Equation (5) together with its initial and boundary conditions can be obtained by Duhamel's principle (7)

$$q_i = \int_0^\tau q_s(z, \lambda)\, \frac{\partial}{\partial \tau} H(r, \tau - \lambda)\, d\lambda \qquad (6)$$

where

$$\tau = t - \frac{\varphi}{u} z$$

The function $H(r, \tau)$ is the solution of Equations (5) when the surface concentration is unity. For $\tau > 0$, $H(r, \tau)$ can be represented by

$$H(r, \tau) = 1 - 2 \cdot \sum_{n=1}^{\infty} \frac{(-1)^{n+1}}{\frac{n\pi}{b} r} e^{-D(n\pi/b)^2 \tau} \sin \frac{n\pi}{b} r \qquad (7)$$

Differentiating Equation (7) with respect to τ and substituting into Equation (6) one obtains q_i by integration. This expression is then substituted into Equation (3) to obtain

$$q(z, r) = \frac{6D}{b^2} \cdot \sum_{n=1}^{\infty} \int_0^\tau q_s(z, \lambda)\, e^{-D(n\pi/b)^2(\tau-\lambda)} \cdot d\lambda \qquad (8)$$

When one differentiates Equation (8) with Leibnitz's rule and integrates by parts,

$$\frac{\partial}{\partial \tau} q(z, \tau) = \frac{6D}{b^2} \cdot \sum_{n=1}^{\infty} \int_0^\tau \frac{\partial q_s}{\partial \lambda} e^{-D(n\pi/b)^2(\tau-\lambda)} \cdot d\lambda \qquad (9)$$

Equations (1), (2), and (9) describe the situations existing in the column, the liquid phase, and the resin phase respectively. An additional equation relating the physical picture at the liquid-solid interface is required for the complete description of this problem.

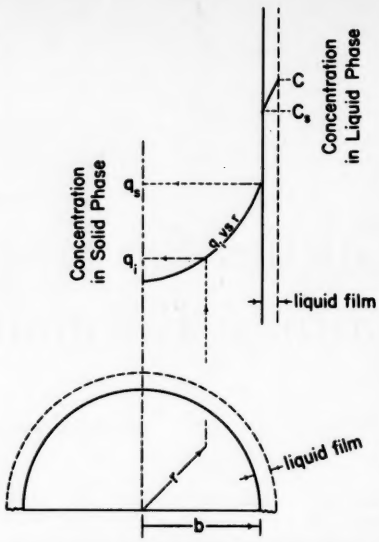

Fig. 1. Concentration gradients around and within a resin particle.

A logical assumption is to consider the existence of equilibrium condition at the interface. For the majority of cases experimental evidence indicates that a Freundlich type of adsorption isotherm could be used to approximate the equilibrium relationship

$$q_s = AC_s^a \qquad (10)$$

With this stipulation and the transformation $\xi = (\rho/u)z$ the fixed-bed operation can be described in terms of the following four equations:

$$\frac{\partial C}{\partial \xi} + \frac{\partial q}{\partial \tau} = 0 \qquad (1)$$

$$\frac{\partial q}{\partial \tau} = k_l[C - C_s] \qquad (2)$$

$$\frac{\partial}{\partial \tau} q(z, \tau) = \frac{6D}{b^2} \cdot \sum_{n=1}^{\infty} \int_0^\tau \frac{\partial q_s}{\partial \lambda} e^{-D(n\pi/b)^2(\tau-\lambda)} \cdot d\lambda \qquad (9)$$

$$q_s = AC_s^a \qquad (10)$$

where $\xi = (\rho/u)z$ and $\tau = t - (\varphi/u)z$

and the following initial and boundary conditions exist:

$$\left.\begin{aligned} C &= 0 \\ q &= 0 \\ C_s &= 0 \\ q_s &= 0 \end{aligned}\right\} \quad \text{for} \quad \xi \geq 0, \qquad \tau < 0$$

$$C = C_0 \quad \text{at} \quad \xi = 0, \qquad \tau \geq 0$$

ADAPTATION OF EQUATIONS FOR NUMERICAL TREATMENT

Equations (1), (2), (9), and (10) contain the four unknown quantities, q, q_s, C, and C_s, the most pertinent being C.

By a process of elimination and substitution a single integral-differential equation containing C alone can be developed to be

$$\frac{\partial C}{\partial \xi} = -\frac{6D}{b^2} \cdot \sum_{n=1}^{\infty} \int_0^\tau aA\left[C + \frac{1}{k_l}\frac{\partial C}{\partial \xi}\right]^{a-1} \cdot \left[\frac{\partial C}{\partial \lambda} + \frac{\partial^2 C}{\partial \lambda \partial \xi}\right] e^{-D(n\pi/b)^2(\tau-\lambda)} \cdot d\lambda \qquad (11)$$

The solution of Equation (11) is the answer to the problem sought in this investigation. However an analytical solution is not available except for the special case $a = 1$, which corresponds to the linear system. In view of this situation, numerical methods must be utilized to obtain the corresponding solutions.

To facilitate the subsequent calculations, it becomes necessary to approximate the infinite series (*13*), which appears under the integral sign of Equation (9) with the following closed-form expression:

$$\sum_{n=1}^{\infty} e^{-D(n\pi/b)^2(\tau-\lambda)} \approx \frac{b}{2\sqrt{\pi D(\tau - \lambda)}} - \frac{1}{2} \qquad (12)$$

For the simplification of the numerical calculations the following transformations have been introduced:

$$\alpha = \frac{C}{C_0}\left[\frac{C_0 b^2 k_l}{4\pi q_{\max} D}\right]^{1/1-a} \qquad (13)$$

$$\beta = \frac{q}{q_{\max}}\left[\frac{C_0 b^2 k_l}{4\pi q_{\max} D}\right]^{a/1-a} \qquad (14)$$

$$x = k_l \xi = k_l \frac{\rho}{u} z \qquad (15)$$

$$\vartheta = \frac{4\pi D}{b^2}\tau = \frac{4\pi D}{b^2}\left[t - \frac{\varphi}{u} z\right] \qquad (16)$$

and

$$q_{\max} = AC_0^a \qquad (17)$$

Substituting Equations (13,) (14), (15), and (16) into Equations (1), (2), (9), and (10), one gets

$$\frac{\partial \alpha}{\partial x} + \frac{\partial \beta}{\partial \vartheta} = 0 \qquad (18)$$

$$\frac{\partial \beta}{\partial \vartheta} = (\alpha - \alpha_s) \qquad (19)$$

$$\frac{\partial \beta}{\partial \vartheta} = \frac{3}{2\pi} \int_0^\vartheta \frac{\partial \beta_s}{\partial \lambda} \cdot \left[\frac{1}{\sqrt{\vartheta - \lambda}} - \frac{1}{2}\right] d\lambda \qquad (20)$$

$$\beta_s = \alpha_s{}^a \tag{21}$$

with the following initial and boundary conditions:

$$\left.\begin{aligned}\alpha &= 0\\ \alpha_s &= 0\\ \beta &= 0\\ \beta_s &= 0\end{aligned}\right\} \quad x \geq 0, \qquad \vartheta < 0$$

$$\alpha = \alpha_0 \quad \text{at} \quad x = 0, \qquad \vartheta \geq 0$$

Approximate solutions of differential equations can be obtained by evaluating the derivatives and integrating numerically by means of the resulting difference equation. To formulate the corresponding difference equations for Equations (18), (19), (20), and (21) a net of mesh-widths of Δx and $\Delta\vartheta$ is established. When the subscript i is used for x and superscript j for ϑ,

$$\frac{\alpha_{i+1}{}^j - \alpha_i{}^j}{\Delta x} = -\frac{\beta_i{}^{j+1} - \beta_i{}^j}{\Delta\vartheta} \tag{22}$$

$$\frac{\beta_i{}^{j+1} - \beta_i{}^j}{\Delta\vartheta} = \alpha_i{}^j - \alpha_{s_i}{}^j \tag{23}$$

$$\frac{\beta_i{}^{j+1} - \beta_i{}^j}{\Delta\vartheta} = \frac{3}{2\pi}\int_0^{(j+1)\Delta\vartheta} \frac{\partial\beta_{s_i}}{\partial\lambda} \cdot\left[\frac{1}{\sqrt{(j+1)\,\Delta\vartheta - \lambda}} - \frac{1}{2}\right] d\lambda \tag{24}$$

$$\beta_{s_i}{}^j = (\alpha_{s_i}{}^j)^a \tag{25}$$

There are numerous ways to approximate these derivatives. It is more logical to approximate dy/dx by $(y_{i+1} - y_{i-1})/2\Delta x$. However for this particular case a reiterative type of calculation has to be used if the derivatives are to be approximated in this manner. This procedure would complicate the numerical calculations, and for this reason approximations as expressed in Equations (22) and (23) are used.

Combining Equations (22) and (23) one gets

$$\alpha_{i+1}{}^j - \alpha_i{}^j = (\alpha_{s_i}{}^j - \alpha_i{}^j)\,\Delta x$$

or

$$\alpha_{i+1}{}^j = \alpha_i{}^j + (\alpha_{s_i}{}^j - \alpha_i{}^j)\,\Delta x \tag{26}$$

The integral of Equation (24) can be rewritten as

$$\int_0^{(j+1)\Delta\vartheta} \frac{\partial\beta_{s_i}}{\partial\lambda} \cdot\left[\frac{1}{\sqrt{(j+1)\,\Delta\vartheta - \lambda}} - \frac{1}{2}\right] d\lambda = \sum_{k=0}^{j}\left(\frac{\partial\beta_s}{\partial\vartheta}\right)_i^{k+\frac{1}{2}} (2\sqrt{\Delta\vartheta}) \cdot[\sqrt{(j+1) - k} - \sqrt{(j+1) - (k+1)}] - \tfrac{1}{2}\beta_{s_i}{}^{j+1} \tag{27}$$

When one makes the approximation that

$$\left(\frac{\partial\beta_s}{\partial\vartheta}\right)_i^{k+\frac{1}{2}} \approx \frac{\beta_{s_i}{}^{k+1} - \beta_{s_i}{}^k}{\Delta\vartheta}$$

Equation (27) becomes

$$\int_0^{(j+1)\Delta\vartheta} \left(\frac{\partial\beta_s}{\partial\lambda}\right)_i \cdot\left[\frac{1}{\sqrt{(j+1)\,\Delta\vartheta - \lambda}} - \frac{1}{2}\right] d\lambda = \sum_{k=0}^{j}\left(\frac{\beta_{s_i}{}^{k+1} - \beta_{s_i}{}^k}{\Delta\vartheta}\right)(2\sqrt{\Delta\vartheta}) \cdot[\sqrt{(j+1) - k} - \sqrt{j-k}] - \tfrac{1}{2}\beta_{s_i}{}^{j+1} \tag{28}$$

When one rearranges the infinite series, Equation (28) becomes

$$\sum_{k=0}^{j}(\beta_{s_i}{}^{k+1} - \beta_{s_i}{}^k) \cdot[\sqrt{(j+1) - k} - \sqrt{j-k}] = \beta_{s_i}{}^{j+1} + \sum_{k=1}^{j}\beta_{s_i}{}^k \cdot[\sqrt{j - (k-2)} - 2\sqrt{j-(k-1)} + \sqrt{j-k}] \tag{29}*$$

The substitution of Equation (29) into Equation (28) produces

$$\int_0^{(j+1)\Delta\vartheta} \frac{\partial\beta_{s_i}}{\partial\lambda} \cdot\left[\frac{1}{\sqrt{(j+1)\,\Delta\vartheta - \lambda}} - \frac{1}{2}\right] d\lambda = \frac{2}{\sqrt{\Delta\vartheta}}\beta_{s_i}{}^{j+1} + \frac{2}{\sqrt{\Delta\vartheta}} \cdot\sum_{k=1}^{j}\beta_{s_i}{}^k[\sqrt{j-(k-2)} - 2\sqrt{j-(k-1)} + \sqrt{j-k}] - \tfrac{1}{2}\beta_{s_i}{}^{j+1} \tag{30}$$

Substituting Equation (30) into Equation (24) one obtains

$$\frac{\beta_i{}^{j+1} - \beta_i{}^j}{\Delta\vartheta} = \beta_{s_i}{}^{j+1} \cdot\left(\frac{3}{\pi\sqrt{\Delta\vartheta}} - \frac{3}{4\pi}\right) + \frac{3}{\pi\sqrt{\Delta\vartheta}} \cdot\sum_{k=1}^{j}\beta_{s_i}{}^k[\sqrt{j-(k-2)} - 2\sqrt{j-(k-1)} + \sqrt{j-k}] \tag{31}$$

The combination of Equation (31) with Equation (23) yields

$$\beta_{s_i}{}^{j+1} = C_1[(\alpha_i{}^j - \alpha_{s_i}{}^j) + C_2\sum_{k=1}^{j}K_{j-(k-1)}\beta_{s_i}{}^k] \tag{32}$$

$$\frac{1}{C_1} = \left(\frac{3}{\pi\sqrt{\Delta\vartheta}} - \frac{3}{4\pi}\right)$$

$$C_2 \qquad \frac{3}{\pi\sqrt{\Delta\vartheta}}$$

and

$$K_{j-(k-1)} = -\sqrt{j-(k-2)} + 2\sqrt{j-(k-1)} - \sqrt{j-k}$$

Equations (32), (26), and (25), together with the proper initial and boundary conditions, constitute the basis for the following numerical calculations:

$$\beta_{s_i}{}^{j+1} = C_1[(\alpha_i{}^j - \alpha_{s_i}{}^j) + C_2\sum_{k=1}^{j}K_{j-(k-1)}\beta_{s_i}{}^k] \tag{32}$$

$$\alpha_{i+1}{}^j = \alpha_i{}^j + (\alpha_{s_i}{}^j - \alpha_i{}^j)\,\Delta x \tag{26}$$

$$\beta_s = \alpha_s{}^a \tag{25}$$

$$\left.\begin{aligned}\alpha &= 0\\ \alpha_s &= 0\\ \beta_s &= 0\end{aligned}\right\} \quad \text{at} \quad x \geq 0, \qquad \vartheta \leq 0$$

$$\alpha = \alpha_0 \quad \text{at} \quad x = 0, \qquad \vartheta > 0$$

In accordance with the definition of α, it can be shown that the ratio of the effluent to the influent concentrations C/C_0 is the same as α/α_0. From Equations (32), (26), and (25) it is obvious that for particular values of a, α is a function of x, ϑ, and α_0. The procedure for numerical calculations is summarized as follows:

(1) β_s and α_s are calculated along the ϑ axis for $j = 1, 2, 3, \cdots n$ with Equations (32) and (25).

(2) With the information obtained from step 1, values of α for $x = (i+1)\Delta x$ and $j = 1, 2, 3, \cdots n$ can be computed through the use of Equation (26).

(3) Values of β_s and α_s are succesively computed by repeating step 1 for $x = (i+1)\Delta x$ and $j = 1, 2, 3 \cdots n$.

(4) Step 2 is repeated. Values of α are found for $x = (i+1)\Delta x$ and $j = 1, 2, 3 \cdots n$.

By repeating this procedure, values of α corresponding to particular values of α_0 and a, any value of x and ϑ can be computed.

SELECTION OF INCREMENTS Δx and $\Delta\vartheta$

The accuracy of the numerical calculations is obviously dependent on the magnitude of the increments Δx and $\Delta\vartheta$. The smaller the size of the increments, the more accurate will be the results. However more calculations will be needed to find the value of α for a definite value

*Tabular material has been deposited as document No. 5976 with the American Documentation Institute, Photoduplication Service, Library of Congress, Washington 25, D. C., and may be obtained for $1.25 for photoprints or 35-mm. microfilm.

of x and ϑ. Consequently the selection of these increments becomes a compromise of these opposing factors.

When Equation (26) and the physical situation that $\alpha \geq 0$ are considered, the maximum value of Δx becomes

$$\Delta x < \frac{\alpha_i^{\,j} - \alpha_{i+1}^{\,j}}{\alpha_i^{\,j} - \alpha_{s_i}^{\,j}} < \frac{\alpha_i^{\,j}}{\alpha_i^{\,j} - \alpha_{s_i}^{\,j}} \quad (33)$$

The value of $\Delta\vartheta$ has to meet the physical reality imposed on this problem. The criterion is developed as follows.

Equation (32) will be considered:

$$\beta_{s_i}^{\,j+1} = C_1[(\alpha_i^{\,j} - \alpha_{s_i}^{\,j}) + C_2 \sum_{k=1}^{j} K_{j-(k-1)}\beta_{s_i}^{\,k}]$$

$$\text{for} \quad i = 0 \quad \text{and} \quad j = 0$$

$$\beta_{s_0}^{\,1} = C_1[\alpha_0^{\,0} - \alpha_{s_0}^{\,0}]$$

but $\alpha_{S_0}^{\,0} = 0$, and therefore

$$\beta_{s_0}^{\,1} = C_1\alpha_0^{\,0} = C_1\alpha_0$$

However

$$\beta_{s_i}^{\,j} \leq \beta_{\max} = (\alpha_{\max})^a = \alpha_0^{\,a}$$

Therefore

$$C_1\alpha_0 < \alpha_0^{\,a}$$

or

$$C_1 < \frac{1}{\alpha_0^{\,1-a}}$$

since by definition

$$C_1 = \frac{1}{\frac{3}{\pi\sqrt{\Delta\vartheta}} - \frac{3}{4\pi}} \approx \frac{\pi\sqrt{\Delta\vartheta}}{3}$$

for small values of $\Delta\vartheta$.

This gives

$$\frac{\pi\sqrt{\Delta\vartheta}}{3} < \frac{1}{\alpha_0^{\,1-a}}$$

or

$$\Delta\vartheta < \left(\frac{3}{\pi}\right)^2\left(\frac{1}{\alpha_0^{\,1-a}}\right)^2$$

For example if $a = \frac{1}{2}$ and $\alpha_0 = 1{,}000$

$$\Delta\vartheta < \left(\frac{3}{\pi}\right)^2\left(\frac{1}{1{,}000}\right) = \frac{1}{1{,}097}$$

Another stipulation required by the physical condition of the system is that the numerical value of β_s has to be equal to, or greater than, its preceding value, or that

$$\beta_{s_i}^{\,m+1} \geq \beta_{s_i}^{\,m}$$

or

$$\beta_{s_i}^{\,m+1} - \beta_{s_i}^{\,m} \geq 0$$

and

TABLE 1. NUMERICAL VALUES OF CONCENTRATION RATIOS FOR SYSTEMS HAVING NONLINEAR EQUILIBRIUM RELATIONSHIPS

for $\alpha_0 = 1{,}000$ and $a = \frac{1}{2}$

where $\alpha_0 = \left[\frac{C_0 b^2 k_l}{4\pi q_{\max} D}\right]^{1/1-a}$, $q_{\max} = AC_0^{\,a}$, $x = k_l \frac{\rho}{u} z$ and $\vartheta = \frac{4\pi D}{b^2}\left[t - \frac{\varphi}{u} z\right]$

$\vartheta \times 2^{13}$	C/C_0	$\vartheta \times 2^{13}$	C/C_0	$\vartheta \times 2^{13}$	C/C_0
$x = 1$		$x = 3$		$x = 5$	
1	0.62267	1	0.06727	11	0.00203
11	0.71875	11	0.21612	21	0.02529
21	0.76662	21	0.32565	41	0.13709
41	0.81761	41	0.45978	61	0.24319
81	0.86430	81	0.59273	81	0.32380
161	0.90261	161	0.70603	161	0.50633
321	0.93196	321	0.79419	321	0.65343
641	0.95359	641	0.85952	641	0.76340
821	0.95978	821	0.87824	821	0.79494
$x = 7$		$x = 9$		$x = 11$	
41	0.00128	81	0.00040	161	0.00495
61	0.02632	101	0.00777	181	0.01919
81	0.08579	141	0.07297	221	0.07256
121	0.21088	201	0.19618	301	0.18964
201	0.37606	361	0.40073	441	0.33496
401	0.56465	541	0.51975	581	0.42895
821	0.70959	821	0.62199	821	0.53202
$x = 13$		$x = 17$		$x = 21$	
221	0.00100	421	0.00189	701	0.00747
241	0.00547	441	0.00567	721	0.01316
281	0.03330	481	0.02251	741	0.02049
341	0.10076	541	0.06338	761	0.02914
441	0.20684	601	0.10859	781	0.03873
601	0.32963	701	0.17823	801	0.04886
821	0.43964	821	0.24837	821	0.05957

See footnote page 375

$$\beta_{s_i}^{\,m} = C_1[(\alpha_i^{\,m-1} - \alpha_{s_i}^{\,m-1}) - C_2(K_1\beta_{s_i}^{\,m-1} + K_2\beta_{s_i}^{\,m-2} + \cdots + K_{m-1}\beta_{s_i}^{\,1})]$$

$$\beta_{s_i}^{\,m+1} = C_1[(\alpha_i^{\,m} - \alpha_{s_i}^{\,m}) - C_2(K_1\beta_{s_i}^{\,m} + K_2\beta_{s_i}^{\,m-1} + \cdots + K_m\beta_{s_i}^{\,1})]$$

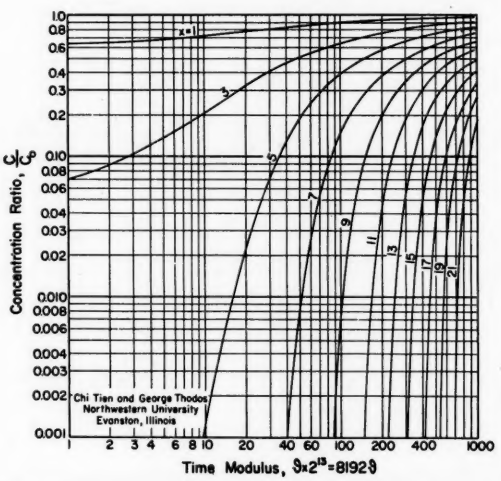

Fig. 2. Concentration- position-time relationship for the case $\alpha_0 = 1{,}000$ and $a = \frac{1}{2}$: $\alpha_0 = \left[\frac{C_0 b^2 k_l}{4\pi q_{\max} D}\right]^{1/1-a}$, $q_{\max} = AC_0^{\,a}$, $x = k_l \frac{\rho}{u} z$, and $\vartheta = \frac{4\pi D}{b^2}\left[t - \frac{\varphi}{u} z\right]$.

TABLE 2. NUMERICAL VALUES OF CONCENTRATION RATIOS FOR SYSTEMS HAVING NONLINEAR EQUILIBRIUM RELATIONSHIPS

for $\alpha_0 = 100$ and $a = \frac{1}{2}$

where $\alpha_0 = \left[\frac{C_0 b^2 k_l}{4\pi q_{max} D}\right]^{1/1-a}$, $q_{max} = AC_0{}^a$, $x = k_l \frac{\rho}{u} z$ and $\vartheta = \frac{4\pi D}{b^2}\left[t - \frac{\varphi}{u} z\right]$

$\vartheta \times 2^9$	C/C_0	$\vartheta \times 2^9$	C/C_0	$\vartheta \times 2^9$	C/C_0
$x = 1$		$x = 3$		$x = 5$	
1	0.71036	1	0.20214	1	0.00117
11	0.79039	11	0.38638	11	0.05975
31	0.85409	31	0.56013	21	0.17182
61	0.89398	61	0.67657	41	0.34332
101	0.91968	101	0.75359	101	0.57882
301	0.96151	301	0.88095	301	0.79496
501	0.97524	501	0.92307	501	0.86697
821	0.98578	821	0.95544	821	0.92233
$x = 7$		$x = 9$		$x = 11$	
21	0.00365	41	0.00057	71	0.00037
31	0.03598	51	0.00854	81	0.00421
41	0.09736	61	0.03482	101	0.04252
61	0.22279	81	0.12105	141	0.17521
101	0.39524	121	0.27982	201	0.33414
301	0.70290	301	0.60425	361	0.56462
501	0.80654	501	0.74140	601	0.72384
821	0.88621	821	0.84686	821	0.80407
$x = 15$		$x = 21$		$x = 29$	
161	0.00200	321	0.00125	621	0.01138
181	0.01854	341	0.00905	641	0.02632
201	0.05496	361	0.02792	661	0.04601
301	0.26564	401	0.08565	681	0.06821
441	0.45686	501	0.23354	701	0.09144
641	0.61635	701	0.44291	761	0.16076
821	0.70732	821	0.53073	821	0.22512

See footnote page 375.

This gives the following inequality:

$$-(\alpha_{s_i}{}^m - \alpha_{s_i}{}^{m-1}) + (\alpha_i{}^m - \alpha_i{}^{m-1}) + C_2[K_1(\beta_{s_i}{}^m - \beta_{s_i}{}^{m-1}) + K_2(\beta_{s_i}{}^{m-1} - \beta_{s_i}{}^{m-2}) + \cdots + K_{m-1}(\beta_{s_i}{}^2 - \beta_{s_i}{}^1) + K_m\beta_{s_i}{}^1] \geq 0$$

Therefore

$$C_2 \geq \frac{\alpha_{s_i}{}^m - \alpha_{s_i}{}^{m-1}}{K_1\Delta_m + K_2\Delta_{m-1} + \cdots + K_m\Delta_1}$$

where

$$\Delta_m = \beta_{s_i}{}^m - \beta_{s_i}{}^{m-1}$$

$$\Delta_{m-1} = \beta_{s_i}{}^{m-1} - \beta_{s_i}{}^{m-2}$$

and

$$C_2 = \frac{3}{\pi(\Delta\vartheta)^{\frac{1}{2}}}$$

$$(\Delta\vartheta)^{\frac{1}{2}} \leq \frac{3}{\pi} \cdot \frac{K_1\Delta_m + K_2\Delta_{m-1} + \cdots + K_m\Delta_1}{\alpha_{s_i}{}^m - \alpha_{s_i}{}^{m-1}}$$

This requirement would be met, if

$$(\Delta\vartheta)^{\frac{1}{2}} = \frac{3}{\pi}\Delta_m \frac{\sum_{i=1}^{m} K_i}{\alpha_{s_i}{}^m - \alpha_{s_i}{}^{m-1}}$$

since

$$\Delta_m \leq \Delta_{m-1} \leq \Delta_{m-2}$$

If m is a relatively large number

$$\sum_{i=1}^{m} K_i \approx 1$$

and the following condition is obtained:

$$(\Delta\vartheta)^{\frac{1}{2}} \leq \frac{3}{\pi}\frac{\Delta_m}{\alpha_{s_i}{}^m - \alpha_{s_i}{}^{m-1}} = \frac{3}{\pi}\frac{\beta_{s_i}{}^m - \beta_{s_i}{}^{m-1}}{\alpha_{s_i}{}^m - \alpha_{s_i}{}^{m-1}} \quad (35)$$

For the case $a = \frac{1}{2}$ and $\alpha_0 = 1{,}000$

$$\beta_s = \alpha_s{}^{\frac{1}{2}} \quad \text{or} \quad \alpha_s = \beta_s{}^2$$

$$\alpha_{s_i}{}^m - \alpha_{s_i}{}^{m-1} = (\beta_{s_i}{}^m)^2 - (\beta_{s_i}{}^{m-1})^2 = (\beta_{s_i}{}^m + \beta_{s_i}{}^{m-1})(\beta_{s_i}{}^m - \beta_{s_i}{}^{m-1})$$

When one substitutes into Equation (35)

$$(\Delta\vartheta)^{\frac{1}{2}} \leq \frac{3}{\pi}\frac{1}{\beta_{s_i}{}^m + \beta_{s_i}{}^{m-1}} \leq \frac{3}{2\pi\beta_{max}}$$

$$\Delta\vartheta \leq \left(\frac{3}{2\pi}\right)^2 \frac{1}{\beta_{max}{}^2} = \left(\frac{3}{2\pi}\right)^2 \frac{1}{\alpha_{max}} = \left(\frac{3}{2\pi}\right)^2 \frac{1}{\alpha_0} = \left(\frac{3}{2\pi}\right)^2 \frac{1}{1{,}000} = \frac{1}{4{,}410}$$

The latter case is obviously more stringent. At the beginning it was thought that this requirement might be too restrictive. Trial calculations were made with $\Delta\vartheta$ satisfying the first requirement, and the results were compared with those satisfying both requirements. It was found that these numerical values agreed for low values of x, however, as x increased, the resulting values of α

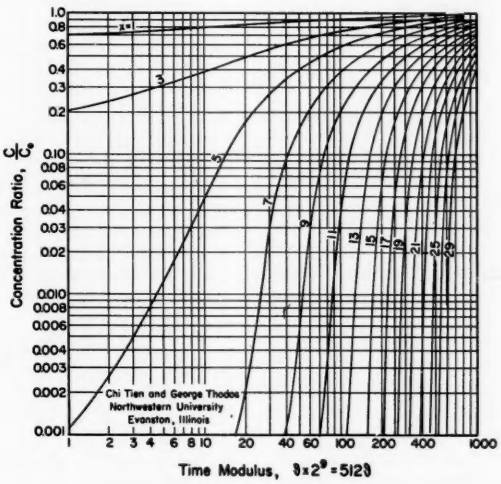

Fig. 3. Concentration-position-time relationships for the case $\alpha_0 = 100$ and $a = \frac{1}{2}$: $\alpha_0 = \left[\frac{C_0 b^2 k_l}{4\pi q_{max} D}\right]^{1/1-a}$, $q_{max} = AC_0{}^a$, $x = k_l \frac{\rho}{u} z$, and $\vartheta = \frac{4\pi D}{b^2}\left[t - \frac{\varphi}{u} z\right]$.

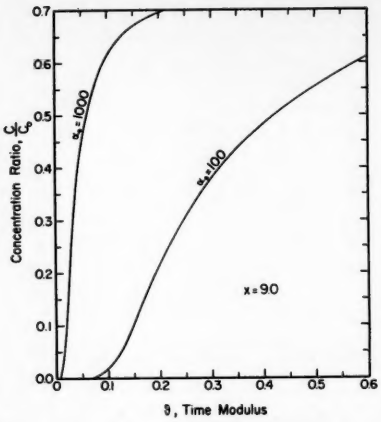

Fig. 4. Effect of α_0 on concentration ratio.

were found to oscillate, a situation similar to that reported by O'Brien (*10*). For this reason the subsequent calculations were restricted to values of $\Delta\vartheta$, satisfying Equation (35).

DISCUSSION OF RESULTS

Numerical calculations were carried out with a digital computer. The coding was based on Equations (32), (26), and (25), and computations were made according to the procedure already outlined. Two cases have been worked for $a = \frac{1}{2}$, one for $\alpha_0 = 1{,}000$ and the other for $\alpha_0 = 100$. The increments used for the case $\alpha_0 = 1{,}000$ are $\Delta\vartheta = 2^{-13}$ and $\Delta x = 1$, whereas for the second case, $\alpha_0 = 100$, the increments are $\Delta\vartheta = 2^{-9}$ and $\Delta x = 1$. All these increments satisfy the requirements of Equations (33) and (35).

The extent of x, which was to be reached for $\alpha_0 = 1{,}000$, was limited to $x = 23$, whereas for $\alpha_0 = 100$, $x = 29$. This restriction was due to the limited storage space on the magnetic core and drum of the computer. It is possible to use the magnetic tape of the machine for additional storage space and thus make it possible to reach higher values of x. This however would reduce the speed of calculation appreciably. Even with the present setup the machine time used for each case was approximately 3 hr.

Numerical values of the concentration ratio C/C_0 for each case are presented both in tabular and graphical form for selected values of x and ϑ. These results appear in Tables 1 and 2 and Figures 2 and 3 for $a = \frac{1}{2}$ and the cases $\alpha_0 = 1{,}000$ and $\alpha_0 = 100$. The accuracy of these computations is accurate to eight decimal places for the case of $\alpha_0 = 1{,}000$ and nine decimal places for $\alpha_0 = 100$. The effect of α_0 is presented in Figure 4, where the concentration ratio C/C_0 is plotted against the time modulus $\vartheta = (4\pi D)/b^2[t - (\varphi/u)z]$ corresponding to the position modulus $x = k_l(\rho/u)z$.

Although the results of this study present solutions for the cases $\alpha_0 = 1{,}000$ and $\alpha_0 = 100$, when both the liquid film resistance and that of diffusion through the solid are significant, it is interesting to point out that $\alpha_0 = 0$ corresponds to the case when the liquid phase is governing and $\alpha_0 = \infty$ for the corresponding case when diffusion through the solid controls.

The plots of Figures 2 and 3 can be used to predict the concentration history of a fluid subjected to ion exchange operations provided that the equilibrium relationship of the system satisfies the Freundlich-adsorption isotherm for the case $a = \frac{1}{2}$. The effect of a and α_0 cannot be stated exactly from the present computational results. Therefore in the absence of further computations it is difficult to state quantitatively that the effect of the exponent a on the breakthrough curve should be generalized beyond $a = \frac{1}{2}$. Further work for different values of a is necessary to clarify this point; this could be conducted by the use of the same basic equations developed in this investigation with slight coding modifications. When results for sufficient cases have been computed, it is very likely that these numerical values could be approximated with some of the known functions in terms of the three parameters and the exponent a. This method has been shown in the resent work of Helfferich and Plesset (*5*).

ACKNOWLEDGMENT

The authors wish to express their gratitude to the Remington-Rand Univac Division of Sperry Rand Corporation, St. Paul, Minnesota, and in particular to L. F. Stutzman and J. W. Tierney for providing the computing facilities that made this work possible.

NOTATION

a = exponent in the equilibrium relationship [Equation (10)]
b = radius of particle, cm.
C = concentration of solution, milliequivalents/cc.
C_0 = concentration of influent solution, milliequivalents/cc.
C_s = concentration of solution at surface of particle, milliequivalents/cc.
D = diffusion coefficient in resin phase, sq. cm./sec.
k_l = mass transfer coefficient for liquid film, milliequivalents/(sec.)(g. of dry resin)(miliequivalents/cc.)
q = average concentration in resin, milliequivalents/g. of dry resin
q_i = point concentration in resin, milliequivalents/g. of dry resin
q_{max} = concentration in resin phase in equilibrium with influent solution, milliequivalents/g. of dry resin
q_s = concentration on resin surface, miliequivalents/g. of dry resin
t = time, sec.
u = superficial velocity of solution, cm./sec.
x = position parameter, $k_l(\rho/u)z$
z = bed height, cm.

Greek Letters

α = concentration parameter for liquid phase,

$$\frac{C}{C_0}\left[\frac{C_0 b^2 k_l}{4\pi q_{max} D}\right]^{1/1-a}$$

α_0 = initial concentration parameter for liquid phase,

$$\left[\frac{C_0 b^2 k_l}{4\pi q_{max} D}\right]^{1/1-a}$$

β = concentration parameter for resin phase [Equation (14)]
ϑ = time parameter, $(4\pi D/b^2)[t - (\varphi/u)z]$
ξ = $(\rho/u)z$
ρ = bulk density of resin, g. of dry resin/cc.
τ = $t - (\varphi/u)z$
φ = porosity of bed, external void volume/total volume, dimensionless

LITERATURE CITED

1. Boyd, G. E., L. S. Meyers, Jr., and A. W. Adamson, *J. Am. Chem. Soc.*, **69**, 2836 (1947).
2. *Ibid.*, 2849.
3. Domaine, John Du, R. L. Swain, and O. A. Hougen, *Ind. Eng. Chem.*, **35**, 546 (1943).
4. Hagerty, P. F., "Numerical Solution for the Non-Linear Transient Behavior of Stationary Beds," N.S.F. Report, Univ. of Pennsylvania, Philadelphia, Penn. (1957).
5. Helfferich, F., and M. S. Plesset, *J. Chem. Phys.*, **28**, 418 (1958).
6. Hiester, N. K., and Theodore Vermeulen, *Chem. Eng. Progr.*, **48**, 506 (1952).
7. Hildebrand, F. D., "Advanced Calculus for Engineers," p. 445, Prentice-Hall, Englewood Cliffs, New Jersey (1948).
8. Hougen, O. A., and F. W. Dodge, "Drying of Gases," prepared for NDRC of OSRD (June 30, 1941); Office of Technical Services, PB 2301, U. S. Department of Commerce (1946).
9. Lapidus, Leon, and N. R. Amundson, *J. Phys. Chem.*, **56**, 948 (1952).
10. O'Brien, G. G., M. A. Hyman, and Sidney Kaplan, *J. Math. Phys.*, **29**, 223 (1951).
11. Rosen, J. B., *J. Chem. Phys.*, **20**, 387 (1952).
12. Thomas, H. C., *J. Am. Chem. Soc.*, **66**, 1664 (1944).
13. Tien, Chi, Ph.D. thesis, Northwestern Univ., Evanston, Ill. (1958).

Manuscript received August 14, 1958; revision received January 9, 1959; paper accepted January 9, 1959. Paper presented at A.I.Ch.E. Cincinnati Meeting.

Theory of Solvent Extraction of Phosphoric and Hydrochloric Acids

W. H. SEATON and C. J. GEANKOPLIS

The Ohio State University, Columbus, Ohio

Mixtures of hydrochloric and phosphoric acids were extracted from aqueous solution by organic solvents in a study to advance the theories of solvent extraction.

Four solvents, t-amyl alcohol, n-butanol, cyclohexanol, and 2-hydroxyethyl, n-hexyl ether, were found to give high distribution coefficients of 0.1 to 0.5 for both acids. In studies using the ether type of solvent an increase of the *p*H of the aqueous phase from 0 to 10 reduced the distribution ratio of phosphoric acid by a factor of 1,100.

The substitution of hydriodic acid for hydrochloric caused a 42% increase in the *K* of phosphoric acid, which could indicate the importance of internal pressure of the additive in extraction. Measurements of activity coefficients of the hydrochloric acid in aqueous solution showed only a 1% increase in its activity coefficient with addition of large amounts of phosphoric acid. This could not be sufficient to cause up to a 40% increase in the distribution coefficient of the hydrochloric acid with the addition of the phosphoric acid.

In extraction of inorganic acids from aqueous solutions little has been published concerning the effects of such properties as *p*H, activity coefficient, and internal pressure on the distribution coefficients of acids between organic solvents and water. A few qualitative observations have been reported (*9, 23*) on the extraction of acids by control of *p*H. The effects of activity coefficients on the distribution coefficients of inorganic acids have been discussed by various investigators (*4, 17, 18*), but little actual data are available. Hildebrand and others (*8, 13*) have shown the role of internal pressure in extraction.

For the study of some of these factors in extraction a four-component system containing water, an organic solvent, and two solutes was used. Phosphoric acid was used as one solute, since very little is known about its extraction and its compounds are becoming increasingly important; hydrochloric acid was chosen as the second solute, to be used with phosphoric acid, because extraction of hydrochloric acid solutions has been extensively studied (*2, 13, 14, 19, 22*). Also, activity coefficients for hydrochloric acid are available (*6, 16, 18, 21*) for finding its effect on extraction of phosphoric acid and for comparisons between this research and that of others.

The choice of organic solvent was determined by an evaluation of different types of solvents. *N*-butanol, cyclohexanol, and 2-hydroxyethyl *n*-hexyl ether (2-HEHE) were found to be the best solvents for extraction of both hydrochloric and phosphoric acids. Quantitative equilibrium-extraction data were obtained on three complex systems containing water and hydrochloric and phosphoric acids, and each of the above three solvents.

More detailed studies were made with 2-HEHE as a solvent, and the effects of temperature, concentration, *p*H, solubility parameter, and the activity coefficient of hydrochloric acid as affected by phosphoric acid were studied.

THEORY

Distribution Coefficients and pH

In solvent extraction one is usually interested in the fraction of total solute in the organic phase as compared with that in the aqueous phase, regardless of the mode of dissociation, association, or interaction of the solute with other molecules. This is defined as

$$K = C_0/C_w \qquad (1)$$

This distribution ratio may not be constant, since the distribution law (*5*) is applicable only to the molecular species common to both phases. Hence the K will be affected by ionization, association, etc. The relationship between these factors can be derived for various cases.

1. *No association of the acid in the organic phase and ionization in the aqueous phase:*

For a monobasic acid HA, Golumbic (*7*) derived

$$K = K^1_{HA}/(1 + B_1/[H^+]_w) \qquad (2)$$

If $[H^+]_w \ll B_1$,

$$\log K = \log K^1_{HA} - \log B_1 - p\mathrm{H} \qquad (3)$$

Hence a plot of log K vs. *p*H should have a slope of -1. Golumbic (*7*) showed that this held for extraction of phenols. If $[H^+]_w \gg B_1$, log K is constant and independent of *p*H.

For a dibasic acid H_2A

$$K = K^1_{H_2A}/(1 + B_1/[H^+]_w + B_1B_2/[H^+]_w^2) \qquad (4)$$

A plot of log K vs. *p*H should have a slope of -2 to 0 depending on the *p*H range.

2. *Association of the acid in the organic phase and ionization in the aqueous phase:*

For HA when one uses a derivation similar to Golumbic's (*7*)

$$n(\mathrm{HA})_0 \leftrightarrows ((\mathrm{HA})_n)_0 \qquad (5)$$

$$K = K^1_{HA}\,(1 + nK_a[\mathrm{HA}]_0^{n-1})/(1 + B_1/[H^+]_w) \qquad (6)$$

Hence K depends on the concentration of HA as well as on *p*H. If $[H^+]_w \ll B_1$ and a very slight amount of association occurs, the slope of log K vs. *p*H is approximately -1.

For H_2A

$$K = K^1_{H_2A}\,(1 + nK_a[H_2A]_0^{n-1})/(1 + B_1/[H^+]_w + B_1B_2/[H^+]_w^2) \qquad (7)$$

Irving and coworkers (*10*), Tribalat (*23*), and Glasstone (*5*) also derived equations for other special cases.

W. H. Seaton is with the Tennessee Eastman Company, Kingsport Tennessee.

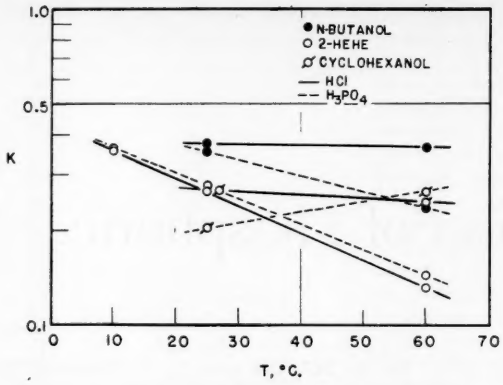

Fig. 1. Effect of temperature on distribution ratios.

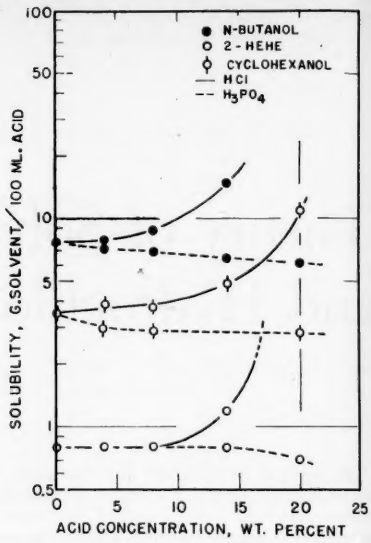

Fig. 3. Solubility of solvents in aqueous acids at 25°C.

Solubility Parameters and Extraction

Hildebrand (*8*) states that two liquids will be immiscible when their internal pressures are sufficiently different so that the molecules of one liquid may force out those of another. Using the thermodynamic equation of state and the fact that the energy of vaporization is equal to the internal pressure, he defines a solubility parameter,

$$\delta = \left(\frac{\Delta H - RT}{V}\right)^{\frac{1}{2}} \qquad (8)$$

Hildebrand derives theoretically most of the thermodynamic properties of solutions using δ values.

Hence an organic solvent which is highly selective for the solute should have a value similar to that of the solute. Highly polar ionic compounds tend to have high δ values; for water the δ value is 23.4. Most paraffinic hydrocarbons have values of 6 to 9 and organic solvents values of 7 to 14. Irving and coworkers (*10*) report that the extraction of dithizone from water by organic solvents decreases in the order chloroform (δ = 9.3), *o*-dichlorobenzene (9.9), chlorobenzene (9.5), benzene (9.2), toluene (8.9), carbon tetrachloride (8.6), cyclohexane (8.2), and hexane (7.3). Since dithizone should have a high δ value of approximately 9 to 10, solvents of high δ values should favor the extraction as shown above.

The δ values could be used to screen solvents in a preliminary way for extraction of a given solute. However chemical interactions, such as hydrogen bonding, association, complex formation, etc., may appreciably affect the extraction, and so solubility parameters may not always be valid criteria of extraction.

Activity Coefficients and Extraction

Garwin and Hixson (*4*) found that certain inorganic additives enhanced, while others hindered, the extraction of aqueous cobalt-chloride solutions by organic solvents. They observed that the additive enhanced the extraction when its activity coefficient increased with concentration in a manner similar to the cobalt salt, and when its activity coefficient decreased, the additive had no effect or hindered the extraction. Schlea (*17*) in the extraction of cobalt sulfate found contradicting effects of activity coefficients of the additives. However activity coefficients of the solute have not been measured when both the solute and additive are present in the solution in order to find the actual effect of the additive on the activity coefficient of the solute.

The true distribution coefficient of a solute is a constant and is equal thermodynamically to its activity in the organic over its activity in the aqueous phase (*5*):

$$K_t = a_0/a_w = \gamma_0 C_0/\gamma_w C_w = (\gamma_0/\gamma_w)K$$

Increasing the activity coefficient of the solute in the water phase with an additive should decrease its concentration and increase the distribution ratio. Glasstone (*5*) also shows that the ratio of the saturation solubilities of the pure solute in the two layers is approximately equal to K. Hence a compound which is slightly soluble in the organic phase will have a low K value.

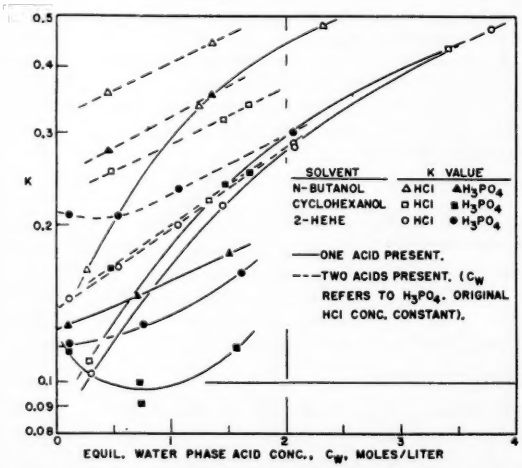

Fig. 2. Effect of concentration on distribution ratios at 25.0°C.

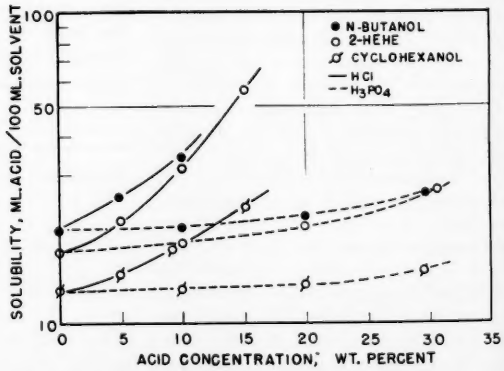

Fig. 4. Solubility of acid solutions in solvents at 25.0°C.

TABLE 1. DISTRIBUTION-RATIO DATA FOR VARIOUS SOLVENTS AT 25.00 ± 0.05°C.
(Each acid equilibrated separately)

Solvent	Acid	Concentrations, mole/liter C_o	C_w	Distribution ratio K	Solubility parameter δ
t-Amyl alcohol	HCl	0.4971	1.178	0.4218	
t-Amyl alcohol	H_3PO_4	0.1127	0.6837	0.1648	
n-Butanol	HCl	0.4201	1.241	0.3386	11.3
n-Butanol	H_3PO_4	0.1036	0.7085	0.1462	
Cyclohexanol	HCl	0.3037	1.332	0.2280	11.1
Cyclohexanol	H_3PO_4	0.0663	0.7307	0.0908	
2-Hydroxyethyl, *n*-hexyl ether	HCl	0.3152	1.45	0.2173	9.6
2-Hydroxyethyl, *n*-hexyl ether	H_3PO_4	0.0987	0.7624	0.1294	
Octylene glycol	HCl	0.2661	1.327	0.2007	
Octylene glycol	H_3PO_4	0.0510	0.7564	0.0674	
Cyclopentanone	HCl	0.1217	0.8705	0.1398	10.2
Cyclopentanone	H_3PO_4	0.1110	0.4680	0.2371	
iso-Amyl alcohol	HCl	0.1811	1.396	0.1297	
iso-Amyl alcohol	H_3PO_4	0.0351	0.7450	0.0471	
n-Amyl alcohol	HCl	0.1752	1.422	0.1230	10.7
n-Amyl alcohol	H_3PO_4	0.0355	0.7438	0.0478	
2-Hydroxyethyl, phenyl ether	HCl	0.1252	1.512	0.0828	
2-Hydroxyethyl, phenyl ether	H_3PO_4	0.0330	0.7532	0.0437	
n-Hexyl alcohol	HCl	0.1119	1.473	0.0760	10.4
n-Hexyl alcohol	H_3PO_4	0.0237	0.7589	0.0312	
Benzyl alcohol	HCl	0.0947	1.479	0.0640	11.7
Benzyl alcohol	H_3PO_4	0.0200	0.7581	0.0264	
Tri-*n*-butyl phosphate	HCl	0.0893	1.525	0.0586	
Tri-*n*-butyl phosphate	H_3PO_4	0.0816	0.710	0.1149	
n-Octanol	HCl			0.0417	10.0
2-Ethyl-1-butanol	HCl	0.0573	1.487	0.0385	
2-Ethyl-1-butanol	H_3PO_4	0.0112	0.7513	0.0149	
o-Chlorophenol	HCl	0.0227	1.669	0.0136	
o-Chlorophenol	H_3PO_4	0.0042	0.8522	0.0050	
Isophorone	HCl	0.0103	1.530	0.0067	9.2
n-Butyl ether	HCl	0.0010	1.498	0.0007	7.6
n-Butyl ether	H_3PO_4	0.00002	0.7385	0.00003	
Tri-perfluorobutyl amine	HCl	0.0009	1.503	0.0006	
Tri-perfluorobutyl amine	H_3PO_4	0.0000	0.7411	0.0000	
Acetophenone	HCl	0.0005	1.517	0.0003	10.2
Acetophenone	H_3PO_4	0.0004	0.751	0.0005	
Ethylene glycol dibutyl ether	HCl	0.0004	1.512	0.003	
Ethylene glycol dibutyl ether	H_3PO_4	0.0000	0.7430	0.000	
Thiophene	HCl	0.0003	1.499	0.0002	9.6
Thiophene	H_3PO_4	0.0000	0.7370	0.0000	
Methyl isobutyl ketone	HCl	0.0002	1.548	0.0001	8.4
Methyl isobutyl ketone	H_3PO_4	0.0002	0.7402	0.0003	
Chloroform	HCl	0.00008	1.487	0.00005	9.3
Chloroform	H_3PO_4	0.00005	0.7344	0.00007	
4-Heptanone	HCl	0.00005	1.509	0.00003	8.3
Carbon tetrachloride	HCl	0.00002	1.509	0.00001	8.6
Carbon tetrachloride	H_3PO_4	0.00005	0.7449	0.00007	
n-Hexyl ether	HCl	0.000	1.506	0.0000	7.5
n-Hexyl ether	H_3PO_4	0.0025	0.7386	0.0034	
1-Pentanethiol	HCl	0.0000	1.506	0.0000	
1-Pentanethiol	H_3PO_4	0.0003	0.7433	0.0004	

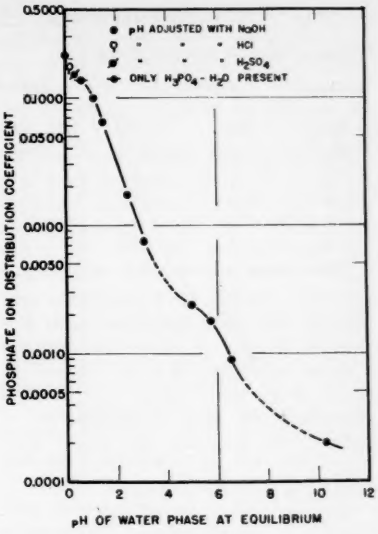
pH ADJUSTED WITH NaOH
" " " HCl
" " " H_2SO_4
ONLY H_3PO_4 - H_2O PRESENT
PHOSPHATE ION DISTRIBUTION COEFFICIENT
pH OF WATER PHASE AT EQUILIBRIUM

Fig. 5. Distribution ratio of phosphate vs. hydrogen ion concentration at 25.0°C.

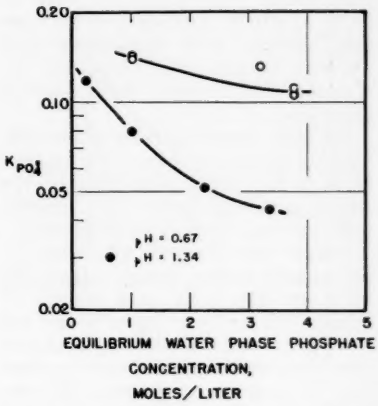

Fig. 6. Phosphate distribution ratio vs. phosphate concentration at constant hydrogen ion concentration values (25.0°C).

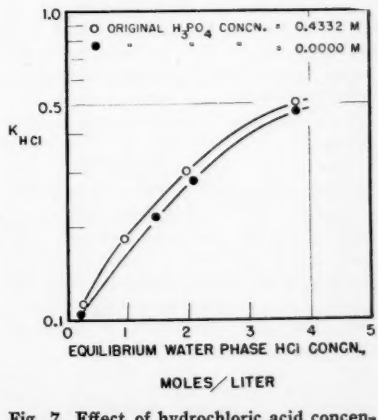

Fig. 7. Effect of hydrochloric acid concentration on distribution ratio of hydrochloric acid in phosphoric acid solutions at 25.0°C.

EXPERIMENTAL METHODS

When hydrochloric acid was alone in the aqueous solution, it was analyzed by titration with 0.1 to 0.5 *N* sodium hydroxide solutions. When in the organic phase, distilled water was added and the two-phase layer was titrated with sodium hydroxide solutions. Phosphoric acid alone in the aqueous solution was titrated by means of glass and calomel electrodes to a *p*H of 9.2 according to the method of Dijksman (*3*). Thymol blue was used in some cases. Both methods gave results to ±0.5%. Analysis of the organic phase was carried out as above after the addition of distilled water.

Several methods of analyzing mixtures containing both hydrochloric and phosphoric acids in solution were tried and discarded; two methods were employed. When the ratio of moles of hydrochloric acid to moles of phosphoric acid was in the range of 1/5 to 20/1, the sample was titrated to a phenolphthalein end point which gave total moles of sodium chloride and sodium phosphate, dibasic (*20*). Then the total chlorides were determined by the addition of excess silver nitrate solution and back titration by the Volhard procedure (*11*). The maximum deviation when knowns were used was −1.3% for hydrochloric acid and −2.1% for phosphoric acid; the average devia-

Table 2. Influence of H_3PO_4 on Activity Coefficient of HCl at 25.0°C. in Aqueous Solution

Nominal original concentrations			Equilibrium compositions			Molal activity*-coefficient of HCl		
HCl side	H_3PO_4 side		HCl side	HCl-H_3PO_4 side				
HCl, wt %	HCl, wt %	H_3PO_4, wt %	HCl concentration, moles/liter	HCl concentration, moles/liter	H_3PO_4 concentration, moles/liter	Actual, (γ_1)	Corresponding to HCl molality in HCl-H_3PO_4 solution, (γ_2)	γ_1/γ_2
2	2	5	0.698	0.6831	0.5276	0.773	0.773	1.000
5	5	1	1.397	1.400	0.1073	0.884	0.885	0.999
5	5	5	1.459	1.398	0.5130	0.896	0.892	1.004
5	5	10	1.478	1.365	1.108	0.899	0.891	1.009

*From data of Robinson and Stokes.

tion was ±0.6% for hydrochloric acid and ±1.0% for phosophoric acid. For extreme ranges of moles hydrochloric acid to phosphoric acid of 1.4/100 to 41/1, or in basic solution, a method depending on silver precipitation of hydrochloric acid and phosphoric acid was developed and used (*20*). Similar accuracies were also obtained.

The equilibrium extractions were performed in glass-stoppered Erlenmeyer flasks sealed on the outside by rubber stalls. Fifty- to one hundred-milliliter samples of aqueous phase and organic solvent were added to the flasks, which were totally immersed in the bath at 25.00 ± 0.05°C. and agitated by magnetic stirrers. After equilibration and settling, samples were pipetted for chemical analysis and density determinations.

Solubility determinations of the solvent in the aqueous phase or the aqueous phase in the solvent were made by the titration of one phase with another until a permanent turbidity appeared.

Activity measurements were made by an isopiestic method similar to that used by others (*15*). An aqueous solution of hydrochloric acid was placed in one leg of a glass container and hydrochloric acid–phosphoric acid solution in another leg. The only contact between the two legs of the container was through the vapor space. Three identical samples were placed in a constant-temperature bath. The first sample was analyzed after 10 days and the second 6 days later. These samples always checked; hence equilibrium was reached in 10 days. Only the hydrochloric acid and the water were able to migrate in the vapor space. Analyses showed that no phosphoric acid ever reached the hydrochloric acid side. Details are given elsewhere (*20*).

The main solvent was 2-HEHE, known as *n*-hexyl Cellosolve. The solvent was redistilled, and the portion boiling at 95.5°C. at 11 mm. was retained with only 2% boiling below 95.5°C. and 2% over 95.5°C. The hydrochloric acid and phosphoric acid used were reagent grade. Other solvents were research grade or the purest obtainable.

DISCUSSION OF SOLVENT SEARCH

The experimental data using various solvents (Table 1) show that, as found by Crittenden and Hixson (*2*), alcohols are the best solvents for extracting hydrochloric acid; however, ketones and ethers show some ability to extract it. Those solvents which are best for hydrochloric acid are also best for phosphoric acid extraction. The K_{HCl} is greater than the $K_{H_3PO_4}$ for the same solvent. Cyclopentanone is an exception, but unfortunately this solvent is excessively soluble in the aqueous phase. The two solvents 2-hydroxyethyl *n*-hexyl ether and 2-hydroxyethyl phenyl ether were also studied, since each compound includes functional groups of the alcohol and the ether.

Generally in a given family or homologous series of solvents the higher the solubility parameter, δ, the higher the extraction. The high distribution ratios for the 2-HEHE with respect to its δ value may be due to the oxonium type of complex. For all the alcohols the $K_{HCl}/K_{H_3PO_4}$ was approximately constant at 2.55 ± 0.2.

Four solvents, *t*-amyl alcohol, *n*-butanol, cyclohexanol, and 2-HEHE, which gave the highest distribution ratios, were selected for further study at different temperatures. At 60°C. and in contact with acidic solutions *t*-amyl alcohol decomposed and was eliminated from further study. The temperature data are tabulated elsewhere (*1*) and are plotted in Figure 1. The hydrochloric and phosphoric acids were equilibrated together. In all cases the K values decreased somewhat with increasing temperature except for the K_{HCl} with cyclohexanol. The separation factor $K_{HCl}/K_{H_3PO_4}$ changed greatly with temperature for *n*-butanol and cyclohexanol and, this fact could be used to separate hydrochloric from phosphoric acid.

The effects of concentration of hydrochloric or phosphoric acid on the distribution ratio were investigated, and the data, which are given elsewhere (*1*), are plotted in Figure 2. In all cases except one (phosphoric acid and cyclohexanol) the distribution ratio increased with increasing concentration. For phosphoric acid alone the $K_{H_3PO_4}$ values seem to approach the same value for all three solvents at dilute concentrations. It is apparent from the mixed-acid curves that each acid increases the distribution ratio of the other acid by an average of approximately 50%. The highest K values were obtained with *n*-butanol.

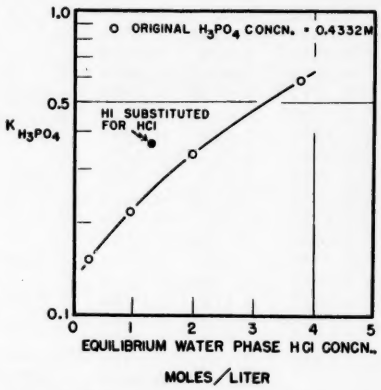

Fig. 8. Effect of hydrochloric acid concentration on distribution ratio of phosphoric acid in phosphoric acid solutions at 25.0°C.

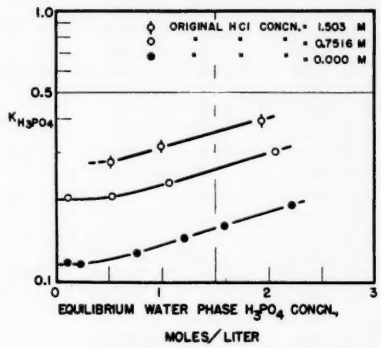

Fig. 9. Effect of phosphoric acid concentration on distribution ratio of phosphoric acid in hydrochloric acid solutions at 25.0°C.

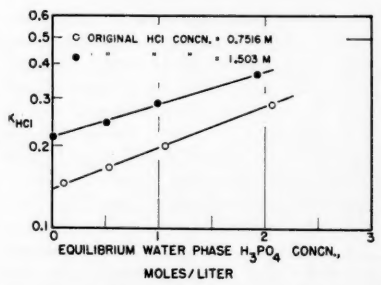

Fig. 10. Effect of phosphoric acid concentration on distribution ratio of hydrochloric acid in hydrochloric acid solutions at 25.0°C.

Solubilities of the solvents in the aqueous acid phase (Figure 3) and of the aqueous acid phase in the solvents (Figure 4) were studied. All solvents became completely miscible in the aqueous phase (Figure 3) at approximately 15 to 20 wt. % hydrochloric acid. The presence of phosphoric acid in the aqueous phase decreased all the solubilities slightly. The solvent 2-HEHE showed a small solubility of less than 1%. The solubilities of the aqueous solutions in the solvents (Figure 4) are quite high and all over 12%. The solubilities of the solvents in the aqueous acids (Figure 3) are much less and well below 10% in most cases. This would increase the internal pressure of the organic layer and cause a greater distribution coefficient of the acid (*2*). For the solvent 2-HEHE the increase of water solubility in the organic solvent phase due to the increase in acid concentration can only partially explain the increase in the K value. The solvent n-butanol was not considered for further research because of its excessive miscibility with aqueous solutions. Since cylcohexanol has a very high viscosity, it was decided to select 2-hydroxyethel n-hexyl ether as the solvent for further studies.

EXTRACTION WITH 2-HYDROXYETHYL *N*-HEXYL ETHER

Effect of pH

Hydrochloric acid has a great effect on increasing the $K_{H_3PO_4}$. This may be due to the hydrochloric acid lowering the internal pressure of the aqueous solution, the raising of the internal pressure of the organic by the solubility of water in the organic, or to the importance of pH. It seems that pH should play an important part in the extraction of a partly ionized acid like phosphoric acid as shown in Equations (2) to (7). To obtain the pH plot in Figure 5, a 1.003M phosphoric acid solution containing suitable amounts of sodium hydroxide or hydrochloric acid was equilibrated with 2-HEHE and the pH and concentrations determined. The data are tabulated elsewhere (*1*).

The pH does have a large effect on the distribution of the phosphate, since increasing the pH from 0 to 10 causes the distribution coefficient of the phosphate to drop by a factor of 1,100. This could offer a means of removing the phosphate from the solvent in an extraction porcess. The plot also shows that the pH is important to the distribution of phosphate even in the region where essentially all the phosphate is present as phosphoric acid. The acid ionization constants for phosphoric acid are $B_1 = 7.5 \times 10^{-3}$, $B_2 = 6.2 \times 10^{-8}$, $B_3 = 4.8 \times 10^{-13}$ (*12*).

The average slope of the log K vs. pH line in the region of 0 to 6 pH is approximately -0.4. For a pH range of about 3 to 6 and no association of the acid in the organic phase, the slope should be -1 to -2 as given by Equations (3) and (4). This may indicate association of phosphoric acid in the organic phase. Others (*10*) also indicate appreciable association for hydrochloric acid in similar solvents.

Data obtained by varying the phosphoric acid concentration while keeping the pH constant with addition of sodium hydroxide are plotted in Figure 6 and tabulated elsewhere (*1*). As the phosphate concentration increases at constant pH, the distribution ratio decreases. Equations (6) and (7) show that at constant pH the distribution coefficient should vary with concentration only if association occurs.

Effect of Concentration and Internaal Pressure

Additional data on the four-component system water, hydrochloric acid, phosphoric acid, 2-hydroxyethel n-hexyl ether, which were obtained, are tabulated elsewhere (*1*) and are plotted in Figures 7 to 10. These show that the K_{HCl} as well as the $K_{H_3PO_4}$ are increased by the increase in concentration of hydrochloric acid in the aqueous phase or by the increase of phosphoric acid in this phase. This helps support the theory that since the hydrochloric acid lowers the internal pressure of water, it diminishes the advantage of water for the solutes. Hence the organic solvent is able to share in a greater amount of the solute.

Reburn and Shearer (*13*) reported that hydriodic acid has a greater ability to lower the internal pressure of water than has hydrochloric acid. Hence a higher $K_{H_3PO_4}$ would be obtained for phosphoric acid if it were extracted in the presence of hydriodic instead of hydrochloric acid. This experiment was performed, and the data point plotted in Figure 8 shows that substitution of hydriodic acid for hydrochloric acid resulted in a 42% imcrease in the $K_{H_3PO_4}$. However since the activity coefficient of hydriodic acid in pure water is about 22% higher than that of hydrochloric acid at the same concentrations (*16*), this could be a contributing factor.

Effect of Activity Coefficients

The data on the effect of the presence of phosphoric acid on the activity coefficient of hydrochloric acid in aqueous solution are given in Table 2. The data show that the presence of approximately 1 to 10% phosphoric acid in aqueous solutions containing 2 to 5% hydrochloric acid raises the activity coefficient of the hydrochloric acid a maximum of only 0.9%. However in an aqueous solution of 2.8% hydrochloric acid (Figure 3) the presence of 1% phosphoric acid raises the K_{HCl} about 4%, and the presence of 10% phosphoric acid raises the K_{HCl} by 40%. Also in an aqueous solution of hydrochloric acid containing from 2 to 5% hydrochloric acid (Figure 7) the presence of about 4% phosphoric acid raised the K_{HCl} by an average of 13%.

Equation (9) shows that the K value is directly proportional to the activity coefficient. It appears inconceivable that a 0.9% increase in activity coefficient of the hydrochloric acid can increase the distribution coefficient by up to 40%. Hence the changes in internal pressure of the water or other factors are causing the increase in distribution coefficient. This small raising of the activity coefficient of hydrochloric acid by the addition of phosphoric acid is in contrast to the increase of 43% in the activity coefficient of hydrochloric acid having a concentration of 10% in aqueous solutions, when 10% sulfuric acid is added as reported by others (*18*). The data of Garwin and Hixson (*4*) and Schlea (*17*) do not answer this question of the effect of activity coefficient on K, since the activity coefficients of the solute were not measured when both solute and additive are present. In their discussions these investigators used the activity coefficients of the additives when the additives were alone in the aqueous solutions.

ACKNOWLEDGMENT

Grateful acknowledgment is made to the Eastman Kodak Company and to the Shell Oil Company for their fellowships which aided in this work.

NOTATION

a = molal activity of hydrochloric acid

a_0 = activity of solute in organic phase

a_w = activity of solute in aqueous phase

B = Brönsted dissociation contant

C_0 = equilibrium concentration of total solute in organic phase, g. mole/liter

C_w = equilibrium concentration of total solute in aqueous phase, g. mole/liter

ΔH = latent heat of vaporization at 25°C., cal./g. mole

2-HEHE = 2-hydroxyethyl n-hexyl ether

$[HA]_0$ = concentration in organic phase of molecular HA

K = C_0/C_w = distribution ratio of total solute

K^1 = distribution ratio of molecular solute

K_a = association constant of molecular HA or H_2A

K^1_{HA} = constant, distribution ratio of unionized, molecular HA in both phases

$K_t = a_0/a_w$ = true thermodynamic distribution ratio

n = number of molecules associating
R = gas constant
T = temperature, °K.
V = molar volume of the liquid, ml./g. mole
δ = solubility parameter

$$= \left(\frac{\Delta H - RT}{V}\right)^{1/2}$$

γ = molal activity coefficient of hydrochloric acid
γ_w = activity coefficient of solute in water phase

LITERATURE CITED

1. Geankoplis, C. J., and W. H. Seaton, *Doc.* 5978 A.D.I. Auxiliary Publications Project, Washington, D. C.; $1.25 for photoprints or 35-mm. microfilm.
2. Crittenden, E. D., and A. N. Hixson, *Ind. Eng. Chem.*, **46**, 265 (1954).
3. Dijksman, J. C. W., *Rec. trav. chim.*, **68**, 57 (1949).
4. Garwin, Leo, and A. N. Hixson, *Ind. Eng. Chem.*, **41**, 2298 (1949).
5. Glasstone, Samuel, "Textbook of Physical Chemistry," 2 ed., p. 736, D. Van Nostrand, New York (1946).
6. Glueckauf, E., *Nature*, **163**, 414 (1949).
7. Golumbic, C., M. Orchin, and S. Weller, *J. Am. Chem. Soc.*, **71**, 2624 (1949).
8. Hildebrand, J. H., and R. L. Scott, "The solubility of Electrolytes," 3 ed., p. 425, Reinhold, New York (1950).
9. Irving, H. M., and D. Phil., *Quarterly Rev. (London)*, **5**, 200 (1951).
10. Irving, H. M., F. J. C. Rossatti, and R. J. P. Williams, *J. Chem. Soc.*, **1955**, 1906 (1955).
11. Kolthoff, I. M., and E. B. Sandell, "Textbook of Quantitative Inorganic Analysis," p. 543, Macmillan, New York (1936).
12. Lange, N. A., "Handbook of Chemistry," 9 ed., p. 1201, Handbook Publishers, Sandusky, Ohio (1956).
13. Reburn, W. T., and W. N. Shearer, *J. Am. Chem. Soc.*, **55**, 1774 (1933).
14. Robinson, R. A., and R. C. Selkirk, *J. Chem. Soc.*, **70**, 1460 (1948).
15. Robinson, R. A., and D. A. Sinclair, *J. Am. Chem. Soc.*, **56**, 1830 (1934).
16. Robinson, R. A., R. H. Stokes, *Trans. Faraday Soc.*, **45**, 612 (1949).
17. Schlea, C. S., Ph.D. dissertation, Ohio State Univ., Columbus, Ohio (1955).
18. Schmid, H., A. Mashka, and H. Breit, *Z. Elektrochem.*, **55**, 384 (1951).
19. Schreinemakers, F. A. H., and J. L. M. Bos, *Z. physik. Chem.*, **79**, 551 (1912).
20. Seaton, W. H., Ph.D. dissertation, Ohio State Univ., Columbus, Ohio (1958).
21. Shedlovsky, Theodore, *J. Am. Chem. Soc.*, **72**, 3680 (1950).
22. Smith, E. L., and J. E. Page, *J. Soc, Chem. Ind.*, **67**, 48 (1948).
23. Tribalat, S., *Ann. Chim. (Paris)*, **8**. 642 (1953).

Manuscript received August 20, 1958; revision received February 23, 1959; paper accepted February 24, 1959.

Continuous Stirred Tank Reactors:

Designs for Maximum Conversions of Raw Material to Desired Product. Homogeneous Reactions

P. J. TRAMBOUZE and EDGAR L. PIRET

University of Minnesota, Minneapolis, Minnesota

It is shown in a series of illustrative examples how the conversion efficiency of many reactions can be markedly affected by the type of reactor used, even though the temperatures, catalyst, and basic kinetics are already fixed by the chemistry of the process.

For such purpose graphical and analytic criteria are developed which permit the selection of a continuous stirred tank or tubular reactor system to obtain the most advantageous conversion of raw material to desired product. When a continuous stirred tank reactor process is preferable, the optimum number of reactor stages for maximum conversion is one. An example is given of a case where a combination of a continuous stirred tank and a tubular reactor is advantageous.

A new graphical method of reactor design for simple or complex reactions is also introduced. This method utilizes continuous stirred tank reactor data directly rather than batch data or kinetics analyses.

Reactions are classified according to the kinetic and stoichiometric characteristics which determine the allowable design procedures and the differences in the composition paths occurring in batch, tubular, or continuous stirred tank reactors.

The mathematical analysis of continuous stirred tank reactor systems for complex reactions leads to a set of difference equations. For cases of zero- or first-order reactions these are readily solved as illustrated in examples, even when several independent components influence the reaction kinetics.

Even when identical feed compositions are used, the concentrations of the chemical components flowing from any one reactor of a continuous stirred tank reactor system may or may not be the same as the concentration obtainable from a batch process or from a tubular reactor design. Consequently in many cases the engineer can markedly improve the conversion efficiency of an important reaction by selecting the proper type and arrangement of reactor system. The possibility of effecting a gain, however, depends upon the characteristics of the reaction.

From the stoichiometric viewpoint a

P. J. Trambouze is with Institut Francais du Petrole, Rueil-Malmaison, France, and Edgar L. Piret is at the American Embassy, Paris France.

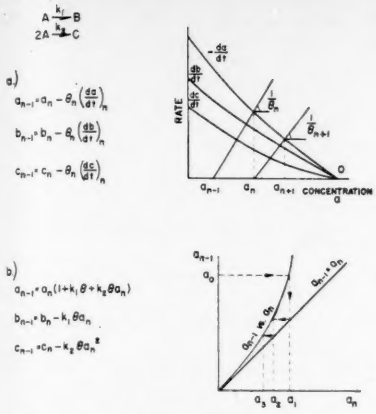

Fig. 1. Design procedures for kinetically simple reactions.

reaction is called *simple* if the evolution of the system can be represented by a single stoichiometric equation (*1*). In other cases the reaction is *stoichiometrically complex.*

From the point of view of kinetics a reaction system is called *simple* if its instantaneous rate depends on the concentration of only one component; it is called *complex* in other cases. A stoichiometrically simple reaction is always kinetically simple, but not vice versa.

It will be seen that the stoichiometric classification of a reaction determines whether or not the conversion can be affected by the choice of reactor type, that is tubular or batch reactor vs. continuous stirred tank reactor. On the other hand the kinetic classification determines whether or not certain convenient procedures may be used in the design of continuous stirred tank reactor processes (Table 1).

For a clear delineation of the areas of application of the several methods, previously published theory on the design of continuous stirred tank reactor systems for homogeneous reactions will first be briefly summarized and also extended.

KINETICALLY SIMPLE REACTIONS

Graphical and algebraic design methods are applicable. In a simple graphical procedure which requires only the availability of batch data giving the concentrations of the components of interest as a function of time, the rates of reaction are obtained by graphical or numerical differentiation of these data. The rates are then plotted as shown in Figure 1a (*7*). The example is for the kinetically simple but stoichiometrically complex reaction

$$\left\{\begin{matrix} A \xrightarrow{k_1} B \\ 2A \xrightarrow{k_2} C \end{matrix}\right\}$$

When one assumes constant volumetric flow rate and adequate mixing, the material balances lead to the three equations shown. The intersections of the rate curves with the straight line of slope $1/\theta_n$, drawn from the feed concentration a_{n-1}, provides the rates of reaction in the n^{th} reactor. These rates with the known feed compositions a_{n-1}, b_{n-1}, c_{n-1} and holding time θ_{n-1} allow by the use of the material balances, for example

$$a_{n-1} = a_n - \theta_n(da/dt)_{a=a_n},$$

the calculation of the desired reactor effluent concentrations a_n, b_n, c_n. The process can be repeated stage by stage for systems of reactors of equal or unequal volumes by simply drawing from each subsequent feed composition shown on the axis the straight lines of slope θ_n, θ_{n+1}, θ_{n+2}, etc.

If the reaction rate constants are known, however, algebraic procedures or the graphical technique illustrated in Figure 1b can be used (*6*). Again material balances lead to the three equations shown in the example. In this case insertion of arbitrary values of a_n into the first equation conveniently allows the plotting of the a_n vs. a_{n-1} curve; then since the effluent of a reactor is the feed to the next reactor in the chain, the step-by-step procedure illustrated provides the concentration of a in each reactor of the chain. Substitution of feed concentrations b_{n-1}, c_{n-1} and of the concentration a_n into the second and third equations allows the calculation of the concentrations of b_n, c_n in the n^{th} reactor, and so on down the chain. In this case equal-volume reactors have been assumed. This graphical technique (or a trial-and-error algebraic solution) is applicable even when, as illustrated above, the difference equations are nonlinear. Analytical solutions for linear systems will be illustrated later.

KINETICALLY COMPLEX REACTIONS

The methods mentioned above are not applicable to kinetically complex reactions, in which their use will lead to error.

Graphical Methods

Batch data known. A graphical design method for complex reactions recently developed is convenient and does not require knowledge of the reaction-velocity constants but directly uses batch-composition—vs.—time data (*1*). In this method the batch-composition paths are plotted on a concentration space representation (Figure 4a). If the product given by a continuous stirred tank reactor stage has the composition (P), then, since the instantaneous conversion rates are proportional to the direction cosines of the tangents to the batch curves, the possible compositions of the feeds to this stage at this point will be on a line going through the product-composition point and drawn tangent to the batch-composition path.

The method is applicable when only two and at most three independent components affect the rate of formation of the products of interest and is especially suitable when recycles or side streams are used. If the holding times in each stage are to be equal, a trial-and-error procedure is required.

Continuous stirred tank reactor data known. It is of interest for design purposes to carry out kinetic investigations in the laboratory by the use of a continuous stirred tank reactor rather than batch methods. In this case the effluent compositions from a single stage continuous stirred tank reactor using various feed compositions F_1, F_2 ··· etc., and different holding times are conveniently plotted as shown in Figure 2a or on rectangular coordinates. On such a chart a straight line which joins a feed-composition point and any one of its continuous stirred tank reactor product

TABLE 1

Classification		Definition	Typical stoichiometric and kinetic equations	Consequences
Stoichiometry	Simple	Single reaction	$A + B \rightarrow C$ $-da/dt = -db/dt = dc/dt = kab$	Tubular and continuous stirred tank reactor composition paths* are identical.
	Complex	Several reactions	$A + B \rightarrow C$ $A + C \rightarrow D$ $-da/dt = kab + k_1ac$ $-db/dt = kab$	Tubular and continuous stirred tank reactor composition paths are different
Kinetics	Simple	Rate depending on only one component	$A \rightarrow B + C$ $2A \rightarrow D$ $-da/dt = ka + k_1a^2.$	Continuous stirred tank reactor design methods of Figure 1 are applicable.
	Complex	Rate depending on more than one component	$A + B \rightarrow C$ $A \rightarrow D$ $-da/dt = kab + k_1a$	Continuous stirred tank reactor design methods of Figure 1 are *not* applicable.

*By the composition path of a reaction is meant the evolution of the concentrations of the components of interest with respect to time or length in the case of a batch or a tubular reactor in plug flow or with respect to the holding time in a continuous stirred tank reactor.

composition points is tangent at its intersection with the curve to a batch composition path (dotted curve on Figure 2b).

The performance of a continuous stirred tank reactor chain can be readily predicted from the triangular plot as follows. The feed to the first stage is assumed to be F_1 and its product P_1 (Figure 2c). A straight line drawn through P_1 and for example F_2 will intersect at P_2 the continuous stirred tank reactor composition path beginning at F_2. P_2 will then be the product of a second stage, of which the feed is P_1. The straight line $F_2P_1P_2$, it will be noted, is tangent at P_2 to some batch-composition path (dotted curve). Hence as seen before, the feed composition of the continuous stirred tank reactor stage giving the product P_2 can be any point on this tangent line, and thus P_1 may be this feed. The construction can be continued in the same way for other stages. The holding time in each stage can be conveniently found by the addition of a time grid, as illustrated by the θ_1', θ_2' curves shown in Figure 2c. The holding time of the first stage is directly given by the time grid for the single-stage operations, that is $\theta_1' - \theta_1$. The holding time of the second stage is obtained as follows.

From the chart:

θ_2': holding time of a single stage giving the product P_2 from the feed F_2

a_1: concentration of component A in the product P_1

a_2: concentration of component A in the product P_2

a_2^0: concentration of component A in the single stage feed F_2.

From the relation $(da/dt)_{P_2}\theta_2' = a_2 - a_2^0$ the rate of reaction (da/dt) at P_2 can be calculated. Then the holding time of the second stage is obtained from

$$\theta_2 = \frac{a_2 - a_1}{\left(\frac{da}{dt}\right)_{P_2}}$$

The use of several reactors in series affords a means of determining whether components other than A, B, C affect the kinetics and need be considered. Generally interpolation will be required for the synthesis of single-stage curves when data obtained from a multistage laboratory unit are used.

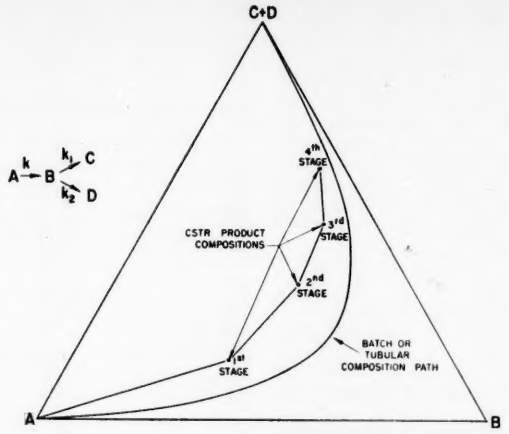

Fig. 3. Results of analytical solution for continuous stirred tank reactor design (illustration 1).

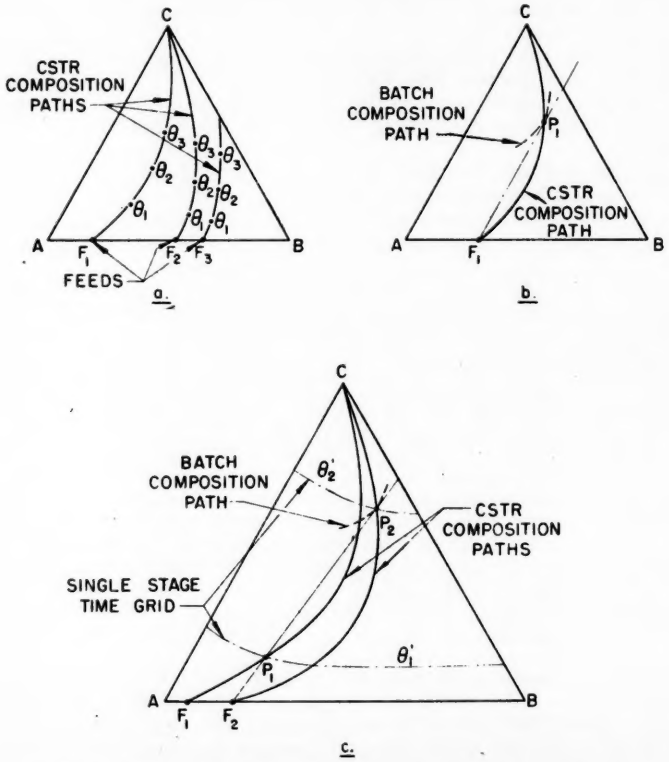

Fig. 2. Design procedure for complex reactions, single-stage, continuous stirred tank reactor composition paths used.

Analytical Method

The reaction rate constants must be known.

The algebraic procedures of reference (*6*) can be used, and the design equations for a variety of complex as well as simple reactions have been tabulated. The algebraic procedures, which for complex reactions are always step by step and frequently require trial-and-error solutions become more tedious as the number of stages increases. In such cases the analytical methods which follow are advantageous.

The design of a tubular reactor for complex reactions leads to a set of first-order differential equations. Similarly, the continuous stirred tank reactor systems design for such reactions requires the solution of a set of first-order difference equations. If all the reactions involved are chemically of zero or first order (for example $da/dt = k$ or $da/dt = k_1a + k_2b$), the problem can easily be solved analytically, since the difference equations in the set are then linear and have *constant* coefficients if the holding times are the same in each stage. The mathematical treatment of such equations is well known (*10, 11*).

Illustration 1

$$A \xrightarrow{k} B \begin{matrix} \xrightarrow{k_1} C \\ \xrightarrow{k_2} D \end{matrix}$$

This case will illustrate that the optimum number of stages required to obtain the maximum concentration of desired product (for fixed operating conditions, for example, given feed composition and fixed nominal holding time) can be immediately calculated from the analytical relations. In this illustration the reactions are assumed to be of order one.

If the holding time, in each stage is the same, and $k\theta = \alpha$; $k_1\theta = \beta$; $k_2\theta = \gamma$, then the material balances are

$$a_{n-1} = a_n(1 + \alpha) \qquad (1a)$$

$$b_{n-1} = b_n(1 + \beta + \gamma) - \alpha a_n \qquad (1b)$$

$$c_{n-1} = c_n - \beta b_n \qquad (1c)$$

$$d_{n-1} = d_n - \gamma b_n \qquad (1d)$$

The solutions are, if $\beta + \gamma \neq \alpha$,

$$a_n = \frac{G_2}{\alpha}(\beta + \gamma - \alpha)\rho_2^{\,n} \qquad (2a)$$

$$b_n = G_1\rho_1^{\,n} + G_2\rho_2^{\,n} \qquad (2b)$$

$$c_n = \frac{\beta G_1}{1 - 1/\rho_1}\rho_1^{\,n} + \frac{\beta G_2}{1 - 1/\rho_2}\rho_2^{\,n} + G_3 \qquad (2c)$$

$$d_n = \frac{\gamma G_1}{1 - 1/\rho_1}\rho_1^{\,n} + \frac{\gamma G_2}{1 - 1/\rho_2}\rho_2^{\,n} + G_4 \qquad (2d)$$

where

$$\rho_1 = \frac{1}{1 + \beta + \gamma} \quad \text{and} \quad \rho_2 = \frac{1}{1 + \alpha}$$

If the feed is pure A at concentration a_0 in an inert solvent so that $b_0 = c_0 = d_0 = 0$, the constants G_1, G_2, G_3, and G_4 are determined by

$$G_1 = -G_2 = \frac{-\alpha a_0}{\beta + \gamma - \alpha}$$

$$G_3 = \beta G_1\left(\frac{1}{1 - 1/\rho_2} - \frac{1}{1 - 1/\rho_1}\right)$$

$$G_4 = \gamma G_1\left(\frac{1}{1 - 1/\rho_2} - \frac{1}{1 - 1/\rho_1}\right)$$

If, however, $\beta + \gamma = \alpha$, then $\rho_1 = \rho_2 = 1/(1 + \alpha) = \rho$, and the solutions, again for $b_0 = c_0 = d_0 = 0$, are

$$a_n = a_0\rho^n \qquad (3a)$$

$$b_n = \frac{\alpha a_0}{1 + \alpha} n\rho^n \qquad (3b)$$

$$c_n = \left(-\frac{\beta}{\alpha}a_0 - \frac{\beta}{1 + \alpha}a_0 n\right)\rho^n + \frac{\beta}{\alpha}a_0 \qquad (3c)$$

$$d_n = \left(-\frac{\gamma}{\alpha}a_0 - \frac{\gamma}{1 + \alpha}a_0 n\right)\rho^n + \frac{\gamma}{\alpha}a_0 \qquad (3d)$$

The value of n to obtain a maximum concentration of B for a fixed-stage holding time can be found by differentiating (2b) with respect to n, so that if $\beta + \gamma \neq \alpha$, at the maximum

$$(\rho_1/\rho_2)^n = \frac{\log \rho_2}{\log \rho_1} \qquad (4)$$

Similarly, if $\beta + \gamma = \alpha$,

$$n = \frac{1}{\log_e (1 + \alpha)} \qquad (5)$$

As a numerical example, $k = 0.1$, $k_1 = 0.02$, $k_2 = 0.02$, and $a_0 = 1$. Two equal-volume reactors in series are to be used, and a value of the holding time is desired which will give the maximum concentration of B in the product. Since $k \neq k_1 + k_2$, relation (4) may be used, and solving for $n = 2$ (θ being the variable) one obtains the value $\theta = 10$. Then $\rho_1 = 0.71$, $\rho_2 = 0.5$ and $G_1 = 0.166$, $G_2 = -0.166$.

When one substitutes into Equations (2), the concentrations of A and B in a four-stage continuous stirred tank reactor chain are

$$b_0 = 0 \qquad a_0 = 1$$

$$b_1 = 0.35 \qquad a_1 = 0.5$$

$$b_2 = 0.41 \qquad a_2 = 0.25$$

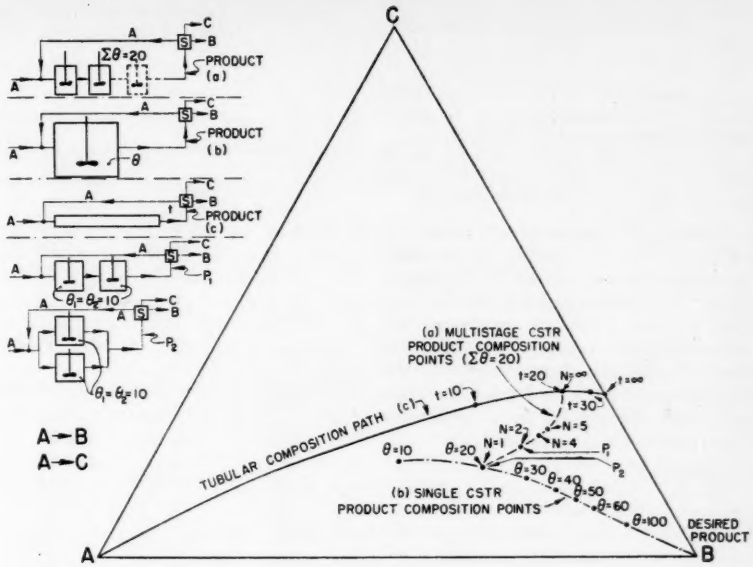

Fig. 5. Comparison of tubular and continuous stirred tank performances. The reaction $A \rightarrow C$ is second order.

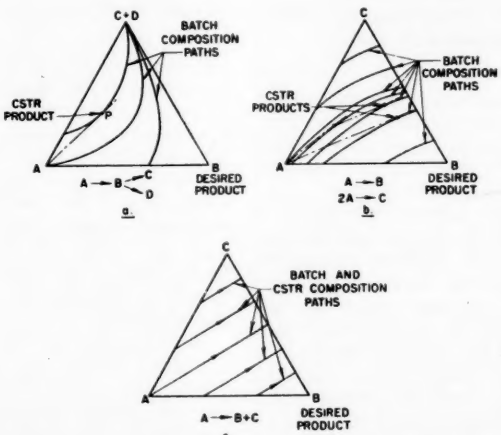

Fig. 4. Reactor-systems selection for optimum conversion based on batch-composition paths: (*a*) tubular reactor preferable, (*b*) continuous stirred tank reactor preferable, (*c*) either system.

$$b_3 = 0.39 \qquad a_3 = 0.12$$

$$b_4 = 0.31 \qquad a_4 = 0.06$$

The maximum tabulated concentration of B occurs, as required, at $n = 2$. These results are represented by Figure 3.

This particular illustration will be of interest in a subsequent paper for a process wherein solvent streams are introduced.

If among the reactions some are chemically of second or higher order, then nonlinear difference equations will appear on the set of material balances. When in the nonlinear difference equations only one variable is present, each of these can be easily solved graphically by the procedure indicated in Figure 1b. Then the remaining set of linear difference equations is solved analytically.

Illustration 2

$$A \xrightarrow[k_2]{k} B \underset{k_2}{\overset{k_1}{\rightleftarrows}} C$$

$$A \xrightarrow[k_3]{} D$$

In this example the rate of formation of D is expressed by $dd/dt = k_3a^2$.

$$a_{n-1} = a_n(1 + k\theta + k_3\theta a_n) \qquad (6a)$$

$$b_{n-1} = b_n(1 + k_1\theta) - k_2\theta c_n - k\theta a_n \qquad (6b)$$

$$c_{n-1} = c_n(1 + k_2\theta) - k_1\theta b_n \qquad (6c)$$

$$d_{n-1} = d_n - k_3\theta a_n^2 \qquad (6d)$$

Equation (6a) is nonlinear, but since only one variable appears, it can be solved graphically for a_n. Then d_n is determined directly from (6d).

Letting $\alpha = k\theta$, $\beta = k_1\theta$, $\gamma = k_2\theta$, $\delta = k_3\theta$, one obtains from (6b) and (6c)

$$(1 + \beta + \gamma)c_n - (2 + \beta + \gamma)c_{n-1} + c_{n-2} = \alpha\beta a_n \qquad (7)$$

The solution of the homogeneous equation is readily obtained as before:

$$c_n = G_1 + G_2\rho^n$$

where

$$\rho = \frac{1}{1 + \beta + \gamma}$$

The general solution of (7) can be written directly as

$$c_n = G_1 + G_2\rho^n + \sum_{p=0}^{n} \alpha_{p,n}a_p \qquad (8)$$

By substituting (8) into (6) one finds the following relations between the $\alpha_{p,n}$:

$$\alpha_{p,n-2} - K\alpha_{p,n-1} + H\alpha_{p,n} = 0 \quad \text{for} \quad 0 \le p < n$$

where $K = 2 + \beta + \gamma$ and $H = 1 + \beta + \gamma$

$$\alpha_{n,n} = \frac{\alpha\beta}{H} \quad \text{for} \quad n = p$$

and

$$\alpha_{p,n} = 0 \quad \text{for} \quad p < 0 \quad \text{or} \quad p > n$$

Then

$$\alpha_{n-1,n} = \frac{K\alpha\beta}{H^2}$$

$$\alpha_{n-2,n} = \frac{\alpha\beta}{H^3}K[K^2 - H]$$

$$\alpha_{n-3,n} = \frac{\alpha\beta}{H^4}K[K^2 - 2H] \quad \text{etc.}$$

By the substitution of (8) into (6c)

$$\beta b_n = \gamma G_1 - \beta G_2\rho^n + \sum_{p=0}^{n} [(1 + \gamma)\alpha_{p,n} - \alpha_{p,n-1}]a_p \qquad (9)$$

COMPARISON OF THE CONVERSION EFFICIENCY OF TUBULAR REACTORS AND CONTINUOUS STIRRED TANK REACTOR SYSTEMS

A reaction is considered in which operating temperature, catalyst concentration, feed composition, and basic kinetics are fixed by the chemistry of the process and for which a suitable tubular or continuous stirred tank reactor design is sought. Before the tubular and continuous stirred tank reactors for several cases are compared, however, it is desirable to define a measure of the efficiency of the process. If, for example, compounds A and B are the starting materials of one or several reactions in a process giving various products, among which C and D are desired, an over-all stoichiometric equation may be written:

$$\alpha A + \beta B \rightarrow \gamma C + \delta D + \text{waste product} \qquad (10)$$

Table 2. Product Compositions and Conversions for Several Continuous Stirred Tank Reactor Systems and for a Tubular Reactor

$$A \rightarrow B$$
$$A \rightarrow C$$

The rate equations are $db/dt = ka$ and $dc/dt = ka$..

a. Multistage Continuous Stirred Tank Reactor—Total holding time constant, $\Sigma\theta = 20$

	Product composition a	b	c	Conversion per pass	Over-all conversion
$N = 1$	0.28	0.56	0.16	0.56	0.77 ← P_2
2	0.19	0.60	0.21	0.60	0.74 ← P_1
4	0.15	0.625	0.225	0.625	0.73
5	0.13	0.63	0.24	0.63	0.72
∞*	0.070	0.62	0.31	0.62	0.66

*or tubular reactor in plug flow or batch process

b. Single Continuous Stirred Tank Reactor with variable holding time ($N = 1$)

$\theta = 10$	0.41	0.41	0.18	0.41	0.70
20	0.28	0.56	0.16	0.56	0.77 ← P_2
30	0.21	0.64	0.15	0.64	0.81
40	0.175	0.70	0.125	0.70	0.84
50	0.15	0.74	0.11	0.74	0.87
60	0.13	0.78	0.09	0.78	0.90
100	0.085	0.85	0.065	0.85	0.93
∞	0	1.00	0.00	1.00	1.00

c. Tubular reactor or batch process

$t = 10$	0.23	0.48	0.29	0.48	0.62
20	0.070	0.62	0.31	0.62	0.66
30	0.020	0.670	0.31	0.67	0.685
∞	0.00	0.69	0.31	0.69	0.69

The over-all stoichiometric coefficients and may or may not be constant and are generally dependent upon the conditions of operation.

If the values of compounds A, B, C, and D are respectively V_A, V_B, V_C, and V_D (dollars/mole for instance), an economic efficiency may be defined by

$$E = \frac{\frac{a_0F}{\alpha}(\gamma v_C + \delta v_D)}{\frac{a_0F}{\alpha}(\alpha v_A + \beta v_B) + (\text{H.C.})} = \frac{\gamma v_C + \delta v_D}{\alpha v_A + \beta v_B + \frac{\alpha}{a_0F}(\text{H.C.})} \qquad (11)$$

Since for stoichiometrically simple reactions the coefficients are constant, then for a given temperature the use of a tubular or a continuous stirred tank reactor system will affect the value of E, only as the hourly charges differ. On the other hand if the reaction is stoichiometrically complex, the coefficients, as explained before, can also be influenced by the choice of the type of reactor, and, as will be seen, this can markedly affect the value of E.

For simplicity in the following it is considered that in the reaction $\alpha A = \beta B +$ waste, where B is the desired product, the hourly charges are small compared with the value of the starting material; then from (*11*)

$$E = \frac{v_B\beta}{v_A\alpha} = \frac{v_B}{v_A}f \qquad (12)$$

The conversion in such a case can be taken as the basis of comparison between various processes.

If a stoichiometrically complex reaction is considered (for instance the cases *a* and *b* of Figure 4), it can be seen that since a straight line cannot be drawn from the same feed tangent to the batch or tubular path (*1*), a continuous stirred tank reactor system cannot give the same product as a tubular reactor operating in plug flow with the same feed. However the composition paths of stoichiometrically simple reactions, carried out in idealized tubular or a single stage continuous stirred tank reactor, will be straight lines on such a diagram (Figure 4c) and will coincide, so that either system can be used to obtain the same products and conversion when the same feed composition is used. The continuous stirred tank reactor volume will be larger for the same hourly production.

If B is the desired product in the case of Figure 4, the tubular reactor has an advantage over the continuous stirred tank reactor system in case *a*, but in case *b* the continuous stirred tank reactor system will give a better yield of B than the tubular reactor. MacMullin (*9*), Corrigan (*2*), and Denbigh (*3, 4, 5*) have given industrially important examples of such effects.

A general rule can be used to determine whether a tubular or continuous stirred tank reactor system will give the higher conversion efficiency for a particular reaction. The continuous stirred tank reactor system will be better if the concavity of the batch-composition paths is turned toward the desired product-representation point, that is point B. On the other hand if the convexity is turned toward B, the tubular reactor will be preferable.

The analytical and general expressions of these conditions are as follows: for any values of a, b, and c where $\partial^2 b/\partial a^2 < 0$, the tubular reactor is preferable (case *a*). For any values of a, b, and c where $\partial^2 b/\partial a^2 > 0$, the continuous stirred tank reactor system is superior (case *b*).

If, for any values of a, b, and c, $\partial^2 b/\partial a^2 = 0$, the composition paths are straight lines and the two types of reactors will give the same conversion, when the same feed composition is used (case *c*).

If $\partial^2 b/\partial a^2$ is positive in a certain range of values of a, b, and c and negative in another range, a combination of a tubular reactor and continuous stirred tank reactor system may be envisaged, the point of change of design being preferably at $\partial^2 b/\partial a^2 = 0$.

In Figure 4b, it appears that the maximum conversion of A to B for the same feed composition will be obtained when the continuous stirred tank reactor product-composition point is as distant as possible from the batch-composition path. This occurs when only one reactor stage is used. If more than one continuous stirred tank reactor stage is used, then for the same consumption of A less desired product B will be obtained.

The above condition may be understood from another point of view; $-\partial b/\partial a$ is the instantaneous conversion f_i, and as a simple case this is only dependent on a. If $\partial^2 b/\partial a^2 > 0$, f_i is increasing when a decreases, and then

$$f_{C\,STR} = \frac{1}{a_0 - a_N} \sum_{i=1}^{N} f_i \cdot \Delta a_i$$

will be larger than

$$f_{tub.} = \frac{1}{a_0 - a(t)} \int_0^t f_i a \, dt,$$

where

$$a(t) = a_N$$

Furthermore f_{CSTR} will be maximum (for the same values of a_0 and a_N) When $N = 1$, that is when the system uses only one reactor stage.

In some instances of course the volume of the single reactor required to drive a reaction to near completion may be so large that the economic balance, which includes hourly charges, Equation (11), will indicate the use of reactor series even for cases where $\partial^2 b/\partial a^2 > 0$. The over-all economic optimum arrangement of number and sizes of reactors must be determined for each specific case.

As the number of reactors to be used in series is increased, the continuous stirred tank reactor product composition approaches (but does not coincide with) that of the tubular reactor. In reactions where a tubular design produces the highest conversion, a continuous stirred tank reactor design may nevertheless be imposed by other considerations, for example if a high agitation level, independent of flow rates, is required to increase heat transfer rates or to maintain a suspension of heavy particles or liquid- or gas-phase droplets. In such cases the continuous stirred tank reactor system should be multistage to approach the optimum conversion as closely as needed.

In the case of stoichiometrically simple reactions, for which idealized tubular reactors operating in plug flow and continuous stirred tank reactors systems can give the same conversion, the choice of the type of reactor will depend only upon the hourly charges [Equations (*11*)]. The tubular reactor has a higher volumetric efficiency, since it operates at higher mean concentration levels than a continuous stirred tank reactors system (*4, 8*); however agitation requirements, stability, or other considerations also enter into the choice.

Illustration 3

This illustration shows the marked effect on conversion which can be arrived at by an engineering design of a reactor assembly.

The envisaged reaction is

$$A \overset{k}{\underset{k_1}{\nearrow\!\searrow}} \begin{matrix} B & (\text{order } n) \\ C & (\text{order } m) \end{matrix}$$

the desired product being B.

$$\frac{db}{dt} = ka^n \quad \text{and} \quad -\frac{da}{dt} = ka^n + k_1 a^m$$

Then

$$\frac{\partial b}{\partial a} = -\frac{ka^n}{ka^n + k_1 a^m}$$

and

$$\frac{\partial^2 b}{\partial a^2} = \frac{kk_1 a^{m+n-1}(m-n)}{(ka^n + k_1 a^m)^2}$$

If

$$m > n, \; \partial^2 b/\partial a^2 > 0,$$

the continuous stirred tank reactor system will be superior.

If

$$m < n, \; \partial^2 b/\partial a^2 < 0,$$

the tubular reactor will be the more efficient.

As a numerical example, $n = 1$, $m = 2$, with $k = k_1 = 0.1$ and $a_0 = 1$; $b_0 = c_0 = 0$.

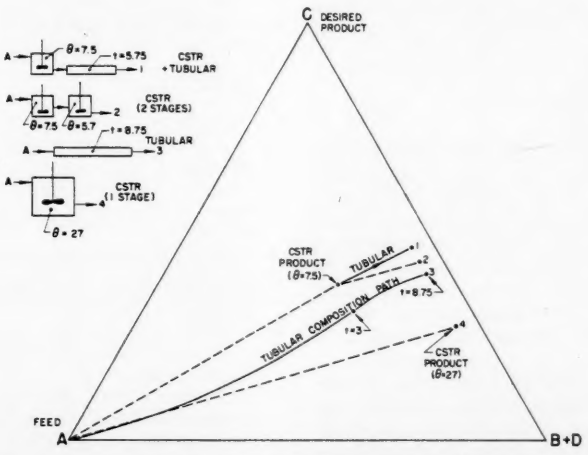

Fig. 6. Combined continuous stirred tank reactor and tubular design for maximum conversion.

Table 2 and Figure 5 compare the performances of a tubular reactor and of a continuous stirred tank reactor system (with the same feed of pure A and inert solvent) with various numbers of stages, holding times, and reactor arrangements. For each case the over-all conversion is calculated on the assumption of a complete recycle of component A present in the reaction product. It is apparent that for this case the continuous stirred tank reactor system is markedly superior in conversion efficiency over a tubular reactor and that furthermore for a given total holding time the single stage continuous stirred tank reactor gives the highest conversion. The limiting conversion for large holding times indeed approaches 1.00 for a single continuous stirred tank reactor system but is only 0.69 for a tubular reactor. Thus it is seen in this example how by proper design of a reactor system a reaction can advantageously be forced in a desired direction.

Illustration 4

The following is a case of a batch-composition path having a double curvature. Taking the reaction

$$A \xrightarrow{k} B \quad \text{zero order}$$

$$\searrow_{k_1} C \quad \text{first order}$$

$$\searrow_{k_2} D \quad \text{second order}$$

where C is the desired product and A the starting material, one has the relations

$$-\frac{da}{dt} = k + k_1 a + k_2 a^2$$

$$\frac{dc}{dt} = k_1 a$$

Then

$$\frac{\partial^2 c}{\partial a^2} = \frac{k_1 a(k_1 + 2k_2 a) - k_1(k + k_1 a + k_2 a^2)}{(k + k_1 a + k_2 a^2)^2}$$

This quantity is $= 0$ when $a^2 = k/k_2$

> 0 when $a^2 > k/k_2$

< 0 when $a^2 < k/k_2$

As a numerical example, $k = 0.025$, $k_1 = 0.2$ and $k_2 = 0.4$, $a_0 = 1$, $b_0 = c_0 = d_0 = 0$

$$\frac{\partial^2 c}{\partial a^2} = 0 \quad \text{when} \quad a = 0.25$$

$$> 0 \quad \text{when} \quad a > 0.25$$

$$< 0 \quad \text{when} \quad a < 0.25$$

The design possibilities shown in Figure 6 are one continuous stirred tank reactor stage followed by a tubular reactor, two continuous stirred tank reactors stages, tubular reactor, or single stage continuous stirred tank reactor. The conversions which are obtained, when the same utilization of A is assumed, are $f_1 = 0.49$, $f_2 = 0.45$, $f_3 = 0.42$, and $f_4 = 0.29$. It is seen that the combination of a continuous stirred tank reactor stage and a tubular reactor gives the highest conversion to C and hence is the design having maximum conversion efficiency.

The case of two compounds of value in the feed A and B and two desired products C and D will now be briefly considered. The efficiency of such a process is defined by Equation (11). By differentiating (11) with respect to a and considering the hourly costs to be small enough to be neglected, one has the relation

$$\frac{\partial E}{\partial a} = \frac{(v_A + \beta/\alpha v_B)\left[v_C \frac{\partial(\gamma/\alpha)}{\partial a} + v_D \frac{\partial(\delta/\alpha)}{\partial a}\right] - \left(\frac{\gamma}{\alpha} v_C + \frac{\delta}{\alpha} v_D\right) \frac{\partial(\beta/\alpha)}{\partial a} v_B}{\left(v_A + \frac{\beta}{\alpha} v_B\right)^2}$$

in which appear the conversions of A to C, that is γ/α, of A to D, that is δ/α and also β/α, the ratio of the moles of the components disappearing by reaction.

Whenever E increases when a decreases, that is if $\partial E/\partial a < 0$, the continuous stirred tank reactor system will be superior. On the other hand if $\partial E/\partial a > 0$, a tubular reactor will be more efficient.

More generally a chemical process ($\sum \nu_i Ai = \sum \mu_i Pi +$ waste) the efficiency of which has been defined(for example by $E = \sum \mu_i v_{Pi} / \sum \nu_i v_{Ai}$) will be considered. If in the range of concentration of the components which are of interest from either a kinetic or cost viewpoint, the efficiency increases as the reaction advances, a continuous stirred tank reactor process (with only one stage) will be the more efficient design. On the other hand wherever along the reaction path E decreases as the reaction proceeds, the tubular reactor will give the higher efficiency. It is clear that even when the temperature, catalyst, and basic kinetics have been fixed by the chemistry of the process, considerable gains in conversion efficiency may accrue from the proper application by the engineer of the techniques of reactor systems design such as described herein. Obviously all costs of separation and recirculation or side stream units, if used, must be included in the economic analysis.

Reactor-systems engineering encompasses the selection of the type, size, and arrangement of the reactors and of the separation, recirculation, and control system considered as a whole. It also is concerned with operating conditions such as temperature, pressure, catalyst concentration, etc. Numerical examples have been given here to illustrate some of the effects which can be achieved by the selection of the type and arrangement of reactors used.

ACKNOWLEDGMENT

The appointment of P. J. Trambouze was supported by International Cooperation Administration under a program administered by the National Academy of Sciences.

NOTATION

A, B, C, D	= compounds A, B, C, D
a, b, c, d	= molar concentrations of compounds A, B, C, D
a_0	= molar concentration of A in feed to system
E	= economic efficiency
F	= volumetric rate of flow
f	= conversion (mole/mole)
$(H.C.)$	= hourly charges on entire production unit, including recirculation costs, amortization, labor, burden rates, and costs of any separation process in the system
k	= specific reaction velocity constant
N	= number of reactor stages operated in series
t	= time
V	= vessel volume occupied by reaction medium
v	= market value
$\alpha, \beta, \gamma, \delta$	= stoichiometric coefficients or constants
$\theta = V/F$	= nominal holding time

Subscripts

A, B, C, D	= components A, B, C, D
n	= n^{th} reactor stage
0	= feed to the system (initial conditions)

LITERATURE CITED

1. Bilous, Olegh, and E. L. Piret, *A.I.Ch.E. Journal*, **1**, 480 (1955).
2. Corrigan, T. E., and E. F. Young, *Chem. Eng.*, 201 (March, 1956).
3. Denbigh, K. G., *Trans. Faraday Soc.*, **40**, 352 (1944).
4. ———, *J. Applied Chem.*, **1**, No. 5, 227 (1951).
5. ———, *Petrol Refiner*, 271 (Sept., 1957).
6. Eldridge, J. W., and E. L. Piret, *Chem. Eng. Progr.*, **46**, 290 (1950).
7. Jones, R. W., *Chem. Eng. Progr.*: **47**, 46 (1951).
8. Leclerc, V. R., *Chem. Eng. Sci.*, **2**, 213 (1953).
9. McMullin, R. B., *Chem. Eng. Progr.*, **44**, 183 (1948).
10. Milne-Thomson, L. M., "The Calculus of Finite Differences," Macmillan, London (1933).
11. Richardson, C. H., "An Introduction to the Calculus of Finite Differences, Van Nostrand, New York (1953).

Manuscript received August 27, 1958; revision received February 22, 1959; paper accepted February 27, 1959.

Studies of the Cation Exchange System Fe^{+++}-H^{+}

I. Equilibrium Studies

R. C. VASISHTH and M. M. DAVID

University of Washington, Seattle, Washington

Equilibrium data are presented for the exchange of Fe^{+++} and H^{+} on a sulfonated polystyrene exchanger. The data cover solution concentrations from 0.05 *N* to 2 *N* in total cation for solutions having either nitrate or perchlorate ion as the common anion. The nitrate system shows irregular behavior because of complex ion formation, but for composition where such behavior is absent the equilibrium data can be correlated by equations based on the law of mass action. Equilibrium compositions for the perchlorate system can be correlated over the entire range studied by a single equation based on the law of mass action. Methods based on the law of mass action are presented for correlating or predicting equilibrium compositions for both systems.

Equilibrium studies with cation exchange materials are important for increasing the understanding of the fundamental nature of these exchange materials. Equilibrium investigations have yielded valuable information about the mechanism of ion exchange (*2, 7, 16*), the selectivity of the resin for various cations as a function of solution composition (*5, 8*), and the properties of the ions in contact with the exchange material, such as hydrated radii (*2, 7*), activity coefficients (*3, 4, 6, 13*), and complex-ion formation (*10, 19*). Equilibrium data are also necessary for the study and interpretation of ion exchange rate data, and from a practical viewpoint equilibrium studies aid in understanding and predicting the performance of industrial ion exchange units. Despite the importance of ion exchange equilibrium data, relatively few studies covering a wide range of compositions and concentrations have been reported. Most of the available comprehensive studies deal with uniunivalent exchange (for example, *11, 14, 18*), a few are available for diunivalent exchange (*1, 5, 16*), but none have previously been presented for monotrivalent exchange. Accordingly the equilibrium data for the cation exchange system Fe^{+++} — H^{+}, which were obtained preliminary to a study of the kinetics of this system, are presented in this paper.

EXPERIMENTAL PROCEDURE

A previous ion exchange study (*12*) had indicated that ferric ions in nitric acid solutions are essentially noncomplexing over the concentrations ranges used in that study, and nitrate was initially selected for the common anion in the present study. Subsequent experimental work revealed large amounts of complexing with the nitrate ion, an undesirable feature for rate studies, and so additional equilibrium studies were carried out with perchlorate as the common anion. The latter anion did not exhibit complexing with the iron.

Analytical grade ferric nitrate, ferric perchlorate, nitric acid, and perchloric acid were used to prepare the necessary solutions. Nitrate solutions were aged at least 6 hr. before use to prevent erratic results. The cation resin employed was Dowex-50, X-8, 20- to 50-mesh particle size, a cation exchange resin extensively used in industry. The cation resin was preconditioned by three preliminary saturation-regeneration cycles, and the moisture content of the resin was obtained by drying samples at 105°C. for 24 hr. The resin-exchange capacity was determined by passing a solution of barium chloride through a weighed amount of the resin in hydrogen form and titrating the effluent with standardized sodium hydroxide solution. The barium was then eluted from the bed and measured gravimetrically. The capacity as determined by these methods was 5.2 meq./g. of dry hydrogen-form resin.

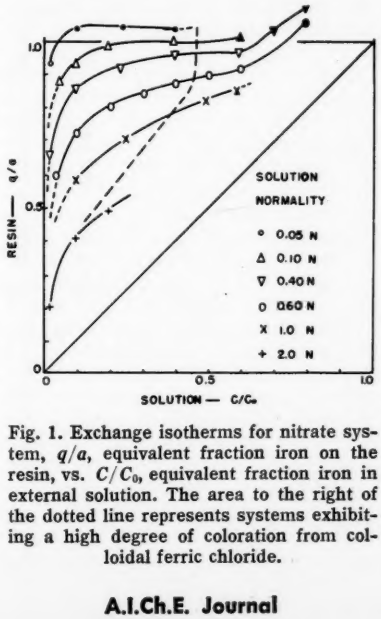

Fig. 1. Exchange isotherms for nitrate system, q/a, equivalent fraction iron on the resin, vs. C/C_0, equivalent fraction iron in external solution. The area to the right of the dotted line represents systems exhibiting a high degree of coloration from colloidal ferric chloride.

The equilibrium data were obtained with small beds of exchange material through which equilibrating solutions were passed. Each bed consisted of approximately 1 g. of exchange material supported on a sintered-glass filter mounted in 12-mm. glass tubing. The ends of the glass tubing above the bed and below the filter were drawn to permit ready attachment to Tygon tubing. Another sintered-glass filter was mounted upstream of the bed section to serve as a filter for the equilibrating solution and to prevent loss of resin during preliminary steps of the runs. Tygon tubing was used to connect the bed to reservoirs containing the various solutions needed.

For an equilibrium measurement 2 to 4 liters of solution of accurately known composition was passed through the bed at 5 to 10 ml./min. These conditions were found by preliminary work to be overgenerous for attainment of equilibrium. After passage of the equilibrating solution the glass tube containing the resin bed was detached from the system, and most of the excess solution remaining between the resin particles in the bed was removed by passing air through the bed. The remainder was removed by centrifuging for 5 min. at 2,000 rev./min., these conditions also having been determined by exploratory study. The tube and resin were weighed, the resin was washed with 100 ml. of distilled water to remove the solution from within the resin pores, and the wash water was analyzed for iron content. One liter of 3 to 4 *N* acid was then passed through the bed at a low flow rate and the effluent analyzed for iron content. After the washing the bed was ready for reuse. All runs were at room temperature.

In most runs the resin was initially in the hydrogen form; however in a few runs the resin was started in the iron form, and these gave results identical to those obtained by approaching equilibrium from the hydrogen side. In some runs with nitrate as the common anion hydrochloric acid rather than nitric acid was used as the regenerant solution, so that nitrate complexes present on the resin at equilibrium might be measured.

Both iron and nitrate ion were determined colorimetrically, with potassium thiocyanate and brucine used respectively.

The data obtained with this procedure permitted computation of the amount of iron present on the resin and the amount of solution present in the pores of the resin, as well as an estimate of the amount of iron present in the pore solution.

R. C. Vasishth is with Reichhold Chemicals, Inc. Seattle, Washington.

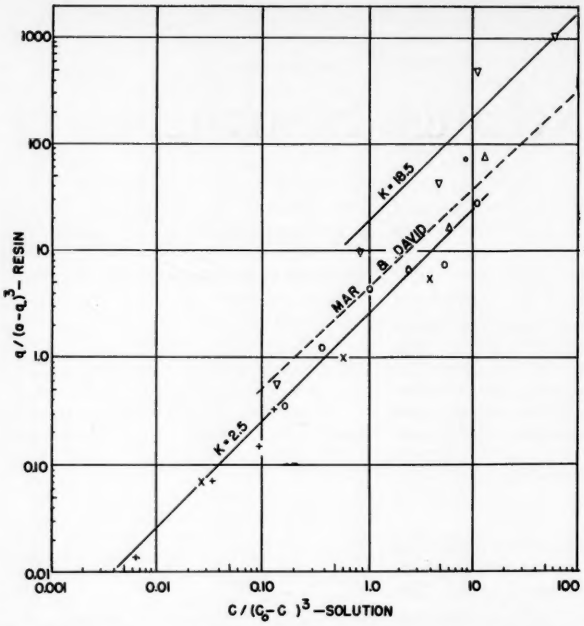

Fig. 2. Nitrate system equilibrium data plotted according to Equation (3); symbols are the same as in Figure 1.

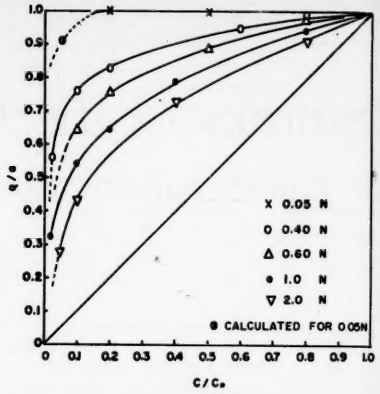

Fig. 4. Exchange isotherms for perchlorate system.

EQUILIBRIUM RESULTS WITH NITRATE AS THE COMMON ANION

The equilibrium data obtained when the nitrate ion was used as the common anion are shown in Figure 1.* In this figure q/a, the milliequivalents of iron per gram of resin (when one assumes all iron on the resin to be trivalent) divided by the total milliequivalent capacity per gram of resin, is plotted vs. C/C_0, the equivalent fraction of iron in the equilibrating solution. Since only negligible amounts of iron were found in the pore solution (see discussion below), the ordinate represents both total iron content and the chemically exchanged iron content of the resin. As is to be expected for trimonovalent exchange (*2*, *8*), the results in Figure 1 show that the equilibrium on the resin is highly favorable for iron take-up. Most of the data fall on normally shaped ion exchange isotherms, but at low solution concentrations and/or high iron-to-hydrogen ratios in the solution, the curves show abnormal behavior characteristized either by q/a larger than 1 or a sudden upturn in the equilibrium curve. (Points on these portions of the curves are shown in solid symbols.) The equilibrium curves for the 1.0 N and 2.0 N solutions were obtained only for the C/C_0 values shown, as at higher C/C_0's plugging of the sintered-glass filter by colloidal ferric hydroxide was encountered.

The exchange of trivalent iron in solution for hydrogen on an ion exchange resin may be represented by the equation

$$Fe^{+++} + 3\ HR \rightleftharpoons FeR_3 + 3\ H^+ \quad (1)$$

By application of the law of mass action the equilibrium constant for this system may be defined by

$$K = \frac{[FeR_3][H^+]^3}{[Fe^{+++}][HR]^3} \quad (2)$$

wherein the terms in brackets represent activities of the components. If the necessary data were available, these activities could be replaced in terms of concentrations and activity coefficients, but since activity coefficients are lacking for ferric salts in either ordinary solutions or in ion exchange resins, it is

*A complete tabulation of original data and computed results is given in the Ph.D. thesis of R. C. Vasishth, University of Washington, Seattle, Washington.

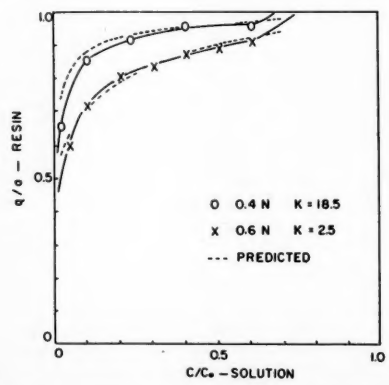

Fig. 3. Prediction of exchange isotherms for the nitrate system.

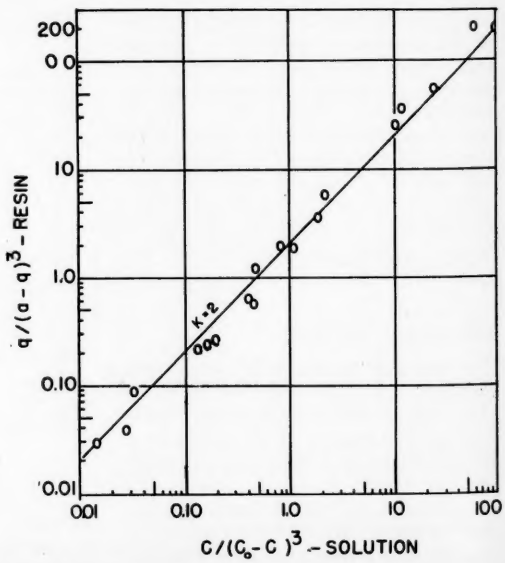

Fig. 5. Perchlorate system equilibrium data plotted according to Equation (3).

Table 1. Results of Equilibrium Studies for the System $Fe^{+++} - H^+$ with Perchlorate as the Common Anion

Run number	C_0 milliequivalents	C/C_0	q/a	K	Calculated q/a ($K = 2.0$)	% Dev.
1	0.4	0.2	0.83	2.65	0.815	+1.84
2	0.6	0.2	0.755	1.71	0.765	−1.3
3	1.0	0.1	0.545	1.57	0.576	−5.38
4	1.0	0.4	0.798	2.02	0.795	+0.37
5	1.0	0.8	0.943	2.01	0.941	+0.21
6	2.0	0.4	0.72	2.6	0.70	+2.86
7	2.0	0.05	0.273	1.815	0.276	−1.08

necessary to approximate Equation (2) with Equation (3), wherein the activities are approximated by concentrations

$$\frac{q}{(a-q)^3} = K\frac{C}{(C_0-C)^3} \qquad (3)$$

where C_0 is the total solution normality and C is the iron normality in solution.

The equilibrium data from the normally-shaped portions of the curves in Figure 1 are replotted in Figure 2 in accordance with Equation (3). Data from Mar and David (*12*) are also included in this plot and agree well with the data of the present studies. From Equation (3), the data should determine a straight line on the log-log plot, with a slope of unity. The value of K determined from the intercept of this line is 6. However the data tend to cluster into two groups, one above and one below the single line; most of the points lying above represent dilute solutions and solutions containing large proportions of iron to hydrogen. If these points are considered separately, they indicate a value of K of 18.5, and the remaining points have a value of K of 2.5. Lines corresponding to these K values are shown on Figure 2. The higher value of K for the one group of points may simply reflect changes in activity coefficients, or it may result in part from complex formation, as discussed later.

Predicted equilibrium-resin compositions determined by the use of the values of K listed above are compared in Figure 3 with experimentally determined values. For solutions 0.1 to 0.4 N the equilibria are represented well by the K value of 18.5. For more concentrated solutions the value of $K = 2.5$ provides good agreement. Thus most of the equilibrium data for the nitrate system may be adequately correlated by equations based on the law of mass action.

The abnormally high iron take-up on the resin in equilibrium with very dilute solutions or solutions containing large iron-to-hydrogen ratios presumably could result from either physical adsorption of colloidal ferric hydroxide or from the exchange of iron present in lower valence complexes, such as $Fe(NO_3)^{++}$, $Fe(OH)^{++}$, $Fe(NO_3)_2^+$, etc. Almost all ferric solutions are hydrolyzed to some extent, and in the present study those solutions with C/C_0's to the right of the dashed line on Figure 1 contained sufficient colloidal ferric hydroxide to exhibit a high degree of coloration from this source. Ferric ions also have a tendency to form complexes with most anions, and available data for ferric nitrate (*17*) and ferric chloride (*15*) solutions indicate the probability of a high degree of nitrate complexing in the concentration ranges where unusually high iron take-up on the resin was noted. Other data (*9*) indicate that appreciable quantities of $Fe(OH)^{++}$ might be present in the solutions. Color effects in the solutions and on the resin militated for the presence of complex ions in the system and against the adsorption of colloidal ferric hydroxide. Subsequent studies with hydrochloric acid used as regenerant showed that for cases where high resin capacity for iron existed, sufficient nitrate ion also existed in the resin phase (as part of the exchanged ions) to account for the major portion of the increased resin capacity. Hence nitrate complexes undoubtedly are responsible for much of the abnormal behavior of the equilibrium for this system.

EQUILIBRIUM RESULTS WITH PERCHLORATE AS THE COMMON ANION

The presence of complexes in the ferric nitrate solutions made these solutions undesirable for use in ion exchange rate studies, and accordingly a ferric system without complexing was sought. Several workers (*15, 19*) have reported that the degree of complexing in dilute ferric perchlorate solutions is almost negligible, even at low hydrogen ion concentrations, and a few test runs indicated that this was also true at higher concentrations. Equilibrium data were then obtained for $Fe^{+++} - H^+$ exchange with perchlorate as the common anion. Figure 4 presents the results. The equilibrium isotherms are normal in shape, and no abnormally high take-up of iron on the cation exchange resin was observed.

As with the nitrate system, only negligible amounts of iron were detected in the solution contained in the pores of the resin particles. This situation might result from further take up of iron on the resin during the washing step, since during this step the resin is effectively in contact with a very dilute solution, but the results are in striking contrast to the pore solution compositions reported in studies of $Cu^{++} - Na^+$ exchange on the same type of resin (*16*). From a practical viewpoint it is immaterial whether the iron is completely exchanged onto the resin initially or whether part of the iron remains within the pores until the washing step and is then exchanged onto the resin.

The data for the perchlorate system were plotted in accordance with Equation (3), as shown on Figure 5, and show very little scatter on this plot as compared with the nitrate system. The value of K obtained from the graph is 2, and typical calculated values of equilibrium resin compositions with this value of K used are compared in Table 1 with experimentally measured resin compositions. The average deviation between experimental and computed values is only 2.5%, and hence K of 2 may be recommended for use for design calculations with this system.

That Equation (3) correlates the equilibrium data so well for the perchlorate system is somewhat surprising in view of the variations of the activity coefficients which might be expected for the components of the system.

LITERATURE CITED

1. Bauman, W. C., J. R. Skidmore, and R. H. Osmun, *Ind. Eng. Chem.*, **40**, 1350 (1948).
2. Boyd, G. E., J. Schubert, and A. W. Adamson, *J. Am. Chem. Soc.*, **69**, 2818 (1947).
3. Davis, C. W., and G. D. Yeoman, *Trans. Faraday Soc.*, **49**, 975 (1953).
4. Duncan, J. F., and B. A. J. Lister, *Discussions Faraday Soc.*, **7**, 104 (1949).
5. Gregor, H. P., O. R. Abolafia, and M. H. Gottlieb, *J. Phys. Chem.*, **58**, 984 (1954).
6. ———, and M. H. Gottlieb, *J. Am. Chem. Soc.*, **75**, 3539 (1953).
7. Gregor, H. P., *ibid.*, **73**, 642 (1951).
8. Kressman, T. R. E., and J. A. Kitchener, *J. Chem. Soc.*, **71**, 1190, 1201, 1208 (1949).
9. Lamb, A. B., and A. G. Jacques, *J. Am. Chem. Soc.*, **60**, 977, 1215 (1938).
10. Lister, A. J., "Ion Exchange and its Applications," p. 112, (Society Chemical Industry, London (1954).
11. Lowen, W. K., W. J. Argersinger, Jr., R. W. Stoenner, A. W. Davidson, and D. N. Hume, *J. Am. Chem. Soc.*, **73**, 2666 (1951).
12. Mar, B. W., and M. M. David, *A.I.Ch.E. Journal*, **2**, No. 3, 381 (1956).
13. Meyer, N. J., W. J. Argersinger, and A. W. Davidson, *J. Am. Chem. Soc.*, **79**, 1024 (1957).
14. Pepper, K. W., *J. Appl. Chem.*, **1**, 124 (1951).
15. Rabinowitch, Eugene, and W. H. Stockmayer, *J. Am. Chem. Soc.*, **64**, 335 (1942).
16. Subba Rao, H. C., and M. M. David, *A.I.Ch.E. Journal*, **3**, No. 2, 187 (1957).
17. Sykes, K. W., *J. Chem. Soc.*, 124 (1952).
18. Whitcombe, J. A., J. T. Banchero, and R. R. White, *Chem. Eng. Progr. Symposium Ser. No. 14*, **50**, 73 (1954).
19. Whiteker, R. A., and Norman Davidson, *J. Am. Chem. Soc.*, **75**, 3081 (1953).

II. Rate Studies in Concentrated Solutions

Fixed-bed kinetic studies were made for Fe^{+++} – H^+ exchange, with perchlorate as the anion, covering concentrations from 0.5 *N* to 2.0 *N* in total cation, flow rates of 5 ml./min. sq. cm. to 45 ml./min. sq. cm. bed depth of 25 to 60 cm., and average resin particle diameters of 0.28 and 0.56 mm. The results are correlated on the assumption of internal diffusion as the rate-controlling step and an essentially irreversible equilibrium.

The exchange of ions between the liquid and resin phases in an ion exchange system can be interpreted, and subsequently predicted for design purposes, in terms of well-established mass transfer principles. Thus the three fundamental principles governing cation exchange are conservation of mass, as expressed by a material balance; the law of mass action, represented by the equilibrium relationships between ions in solution and on the resin phase; and the rate of mass transfer between the liquid and resin phases. Although considerable attention has been given in recent years to the elucidation and application of these principles for ion exchange processes, especially from a theoretical viewpoint, large areas exist for which experimental studies are lacking to verify proposed theories and equations or to provide the data needed to use available theory for design of commercial units. One such area is polyvalent—univalent cation exchange at high concentrations. Part I has presented the equilibrium relationships for a system of this type, the Fe^{+++} – H^+ exchange. The present paper deals with rate studies in fixed beds for this same system, at solution concentrations from 0.5 to 2.0 *N* in Fe^{+++} content.

PERTINENT THEORY

Fixed beds were employed in the present study both because this experimental method appeared to be best adapted to working with concentrated solutions of the type under study and because the majority of commercial ion exchange operations employ fixed-bed units, or moving-bed units to which fixed-bed theory is applicable (*1, 9*). In fixed-bed studies the concentrations of the exchanging ions in the effluent from the bed are related to operating variables such as the entering solution composition and concentration, the mass flow rate through the bed, the bed size, and the exchange-material particle size. If possible, the effluent concentration is related to these variables by an equation termed the *breakthrough* equation. Breakthrough equations are obtained by the combination of the proper equations for the fundamental principles governing ion exchange, as listed above, into a partial differential equation defining the ion exchange process in a differential length of the bed. This differential equation is then solved with the boundary conditions conforming to the operating variables of the particular system under consideration. An exact generalized breakthrough equation covering all possible cases of fixed-bed ion exchange is not feasible, partly because of the wide variety of equilibria encountered in ion exchange. Another factor rendering generalization difficult is that the rate of exchange in fixed beds may be controlled by diffusion of any of the exchanging ions through the liquid film surrounding the resin particle, through the solution within the pores of the resin particle (internal diffusion), or by a combination of these two diffusional processes (*3*). An approximate generalized solution, based on various simplifying assumptions, has recently been presented graphically (*5*), but in the present study it was found more convenient to employ breakthrough equations specifically applicable to the system being studied.

As discussed in Part I, the equilibrium for the Fe^{+++} – H^+ exchange is such that the exchange of iron onto the resin is always highly favored. Previous studies have also indicated that, with the concentrated solutions being employed in the present study, diffusion within the pores of the resin would be the rate-controlling step in the exchange process (*3*). For the similar conditions of irreversible equilibria, internal diffusion rate controlling, Vermeulen (*11*) has shown that at a given instant the exchange of ions in a fixed bed occurs within a fairly small length of the bed. This exchanging zone, once formed, then moves down the bed at a constant rate and with constant thickness. In the exchange zone the surface of the resin particles becomes and remains saturated with the incoming ion as soon as solution containing this ion reaches a particle (material-balance conditions permitting). Thereafter transfer of incoming ions to the particle is limited by the rate at which ions can diffuse within the pores of the particle, a process defined by Fick's second law. By replacing the exact series solution of Fick's second law (*2, 3*) by a satisfactory empirical equation, Vermeulen (*11*) obtained the following breakthrough equation:

$$C/C_0 = (1 - \exp -[\theta - \Sigma + 0.614])^{\frac{1}{2}} \qquad (1)$$

Data conforming to this equation should produce a straight line when plotted as $\log [1 - (C/C_0)^2]$ vs. ΔY. The slope of the line is the internal mass transfer coefficient.

The internal mass transfer coefficient is defined as $k_p s = (4\pi^2 D_s)/(d_p^2)$. Generally it has been assumed that D_s, which is the proportionality constant in Fick's second law is a function only of the cations being exchanged* and of temperature (*3*). Hence for a given isothermal ion exchange system $k_p s$ is a function only of resin particle size.

The formation of the constant-pattern exchange zone upon which Equation (1) is based requires a certain minimum bed length corresponding to $\Sigma = 4$. For beds shorter than this minimum required length the material-balance equation becomes more complicated and so therefore does the breakthrough equation. For this situation Vermuelen (*11*) has employed an empirical approximation to replace the exact solution to the differential equation formed from the material balance, equilibria, and rate relationships. The solution is presented as generalized breakthrough curves relating the effluent concentration to Σ and θ. These curves may be used for matching with experimental curves to determine whether the experimental data conform to the breakthrough equation. The internal diffusion transfer coefficient may then be evaluated from the curve parameters when correspondence is found.

EXPERIMENTAL PROCEDURE

Ferric perchlorate solutions prepared from a reagent-grade chemical were used as the exhausting solutions, since a previous study (Part I) had found that iron complexes were essentially completely absent in such solutions. Therefore exchange of only a single iron-containing ion, Fe^{+++}, occurs. Most regenerations were made with 2*N* hydrochloric acid. Dowex-50, *X* – 8 was employed. The resin was back washed to remove fines and was pretreated and tested for capacity and water content as described previously.

Experimental runs were made by passing solutions of known compositions into beds of ion exchange material at controlled flow rates. The beds were mounted in 1.13-mm. I.D. Pyrex glass tubes. The upper end of each tube was closed with a sintered-glass disk, and the lower end of the bed was

*More recent studies indicate that D_s should also be a function of resin composition (*6,7*), although no evidence of this was found in the present study.

TABLE 1. CALCULATED VALUES OF $K_p s$

Run	C_0, meq./ml.	Flow rate, ml./(min.) (sq. cm.)	Bed depth, cm.	Σ found by curve matching	$K_p s$ (1/hr.) calculated	Σ calculated for $K_p s$ = 33
1–5	Preliminary runs					
6	1	5	25.5	—	26	4.06
7	1.0	14.8	25.5	1.5	36.6	1.35
8	1.0	26.5	25.5	0.85	36.4	0.77
9	1.0	45	25.5	0.6	46.0	0.45
10	1.25	15	25.5	1.0	30.5	1.08
11	2.0	15	25.5	0.71	34.6	0.628
12	2.0	14	45.5	0.8	20.0	1.33
13	1.15	15	45.5	2.0	28.2	2.33
14	0.51	14	25.5	3.0	35.0	2.83
15*	0.81	15	25.5	—	124	
16	0.51	15	45.5	—	33	4.90
17	0.51	24	61	—	33	4.2
18	0.4	15	61	—	33	7.7

*This run was made with 50- to 100-mesh-size resin particles.

supported by a glass-wool plug, which also served as a distributor. To minimize mixing within the solution after passage through the bed, the entire space between the glass-wool plug and sintered glass was filled with resin, and the effluent line above the bed was held to a minimum volume. To minimize mixing between the incoming solution and the water initially present in the bed from previous washings, all runs were made upflow, and the free volume between the individual feed lines and the bottom of the bed was held to a minimum. Because of the sintered-glass disk at the top of the bed, upflow runs could be made at high velocities without fluidizing the bed. In the preparation and use of the bed care was taken to ensure the absence of any entrapped air. Solutions were led to and from the bed through Tygon tubing and glass fittings, and the flow rate was controlled at the outlet. All effluent from the bed was collected in small samples, either manually or by use of a mechanically rotated collection table. The samples were subsequently analyzed for iron content colorimetrically, with potassium thiocyanate as the reagent.

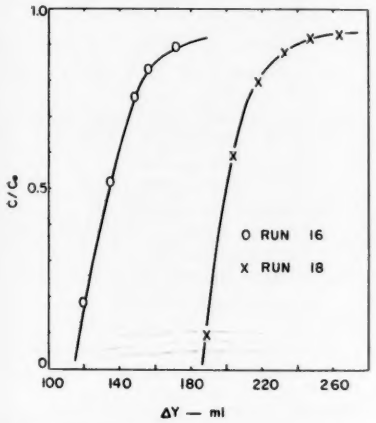

Fig. 1. Typical breakthrough curves for long beds; C/C_0, ratio of effluent to influent iron concentration, vs. ΔY, the effluent from bed (corrected for bed holdup).

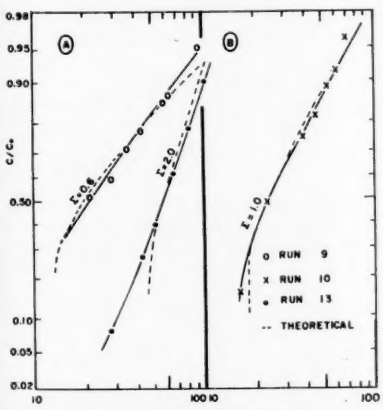

Fig. 2. Example of curve matching with generalized graphical solution of Vermeulen.

Following saturation of the bed with iron, the bed was washed, regenerated until the effluent gave no test for iron, and rewashed until the wash-water effluent was neutral to litmus paper. Washings and regenerations were also performed upflow.

Three different bed lengths, 25.5, 45.5, and 61 cm. were used. Flow rates ranged from 5 ml./min.-sq. cm. to 45 ml./min.-sq. cm. Influent exhaustion solutions were from 0.5 to 2.0 N in Fe^{+++}. Most runs were made with 20- to 50-mesh resin particles, but in one run 50- to 100-mesh particles were used. All runs were at approximately 24°C. A summary of the operating conditions in the various runs is included in Table 1.*

RESULTS

Typical breakthrough curves for the takeup of iron are shown in Figures 1 and 5. The trailing upper ends of the curves are characteristic of breakthrough curves when internal diffusion is the rate-controlling step. The lower ends of the curves should start almost vertically if rate-affecting factors other than internal diffusion were completely absent. The formation of constant pattern conditions may be noted by comparing the curves for runs 16 and 18, which differed only in bed lengths used.

For runs in which Σ was less than 4, the breakthrough curves were compared with curves on the generalized plot presented by Vermeulen (Figure 2). The plot is made on semilog probability paper. As shown in Figure 2, matching was usually obtained for C/C_0 values greater than approximately 0.2, so that the upper 80% of the curves matched. Values of $k_p s$ were then determined from the values of Σ for the matching curves. These values are given in Table 1, and it may be noted that for the same particle size of resin the values of $k_p s$ show only moderate variation in view of the curve-matching method employed.

The data from typical runs in which $\Sigma \geqq 4$ were plotted as log $[1 - (C/C_0)^2]$ vs. ΔY and as demanded by Equation (1) provided straight lines as shown in Figure 3. The values of $k_p s$ given by the slopes of these lines are also listed in Table 1 and show very good agreement among themselves and with $k_p s$'s computed by the curve-matching method.

DISCUSSION

In runs 6 through 9 the flow rate was varied, while other operating variables were held constant. In all but one of the subsequent runs (run 17) the flow rate was maintained constant, while either the entering solution was varied in iron content (0.5 N to 2.0 N) or the bed size was changed (25.5 to 61 cm.) Despite the ninefold velocity change and the above-listed changes in other variables, the experimental data for all but the very first portion of the breakthrough curves could be interpretated on the assumption that the only resistance to mass transfer is within the solid phase and that the equilibrium is essentially irreversible, as is indicated by the constancy of the $k_p s$ values for the 20- to 50-mesh-size beds. To test further the conclusion that internal diffusion was the rate-controlling step, resin particles of 50- to 100-mesh size were used in run 15. For solid diffusion as the rate-controlling step $k_p s$ should vary inversely as the square of the particle diameter (3). Average particle sizes for the 20- to 50-mesh- and the 50- to 100-mesh-size beds were found by particle-size measurements to be 0.56 and 0.28 mm. respectively. For these particle sizes and a $k_p s$ of 33 for the 20- to 50-mesh-size particles, the predicted value of $k_p s$ for the 50- to 100-mesh-size particles is 132. The experimentally determined value was 124, which is in very good agreement with the predicted value. An approximate value of D_s can be calculated from this equation for the average resin-particle diameter of 0.056 cm. and a $k_p s$ of 33 1/hr. (9.16×10^{-3} 1/sec.). The calculated value of D_s is 7.6×10^{-7} sq. cm./sec. The self-diffusion coefficients

*A complete tabulation of original data and results is available in the Ph.D. thesis of R. C. Vasishth, University of Washington, Seattle, Washington, Seattle, (1958).

of some trivalent ions reported are Y^{+++} 9 × 10^{-9} sq cm./sec. (*10*) and Ce^{+++} 9.4 × 10^{-9} sq. cm./sec. (*4*). These are considerably smaller than the values calculated for the present studies. However Selke (*8*) has reported that for cations replacing H^+ the values of interdiffusion coefficients are considerably higher than the self diffusion coefficients, probably because of the very high diffusivity of the hydrogen ions.

The failure of the first portions of the experimental breakthrough curves to show the vertical rise at $C/C_0 = 0$, called for by theoretical considerations when internal diffusion is rate controlling, could be caused by either longitudinal mixing within the bed or by liquid-film resistance to mass transfer being important during the early part of the breakthrough. The latter might be anticipated because of the low concentration of iron in solution during this portion of the breakthrough (*3, 5*). However attempts to correlate the data from the first parts of runs 6 through 9 on the basis of a liquid-film rate-controlling mechanism (*5*) were unsuccessful. To test the effects of longitudinal mixing within the bed, two runs were made in which a 1*N* iron solution was passed in the same manner as in ordinary exhaustion runs through a bed already saturated with iron. The results are shown in Figure 4. Although the width of the breakthrough curves for these two runs is narrow compared with ordinary exhaustion runs, the longitudinal mixing effects are sufficient to prevent formation of the vertical breakthrough curve which should be present for these runs with no longitudinal mixing in the bed.

The equations presented by Vermeulen are based on a completely irreversible equilibrium. The equilibrium data for Fe^{+++} — H^+ exchange at the concentrations used in the present study (see Part I) show that while the take-up of iron on the resin is highly favored, the equilibrium is not completely irreversible. However, when the equilibrium is as favorable as it is for iron take-up in the present system, for practical purposes the equilibrium may be treated as irreversible (*5*).

CONCLUSIONS

The match between the experimental breakthrough curves and theoretically predicted breakthrough curves and the consistency of the $k_p s$ values found for the experimental runs both support the conclusion that the ion exchange rate under the conditions of the present study is controlled by the diffusion rate within the pores of the resin particles. Although the flow rates used in the study ranged only from 1.23 to 11.1 g./(min.)(sq. ft.) of bed cross section, and the flow rates used industrially in ion exchange beds are often higher than these, higher flow rates should tend only to accentuate the rate-controlling importance of diffusion within the particles (*3, 8*).

Back calculations also support the conclusion that the equations proposed by Vermeulen, equations based on internal diffusion being rate controlling and an irreversible equilibrium, represent well the major portion of the breakthrough curve for the system studied. Use of these equation with $k_p s$ = 33 to

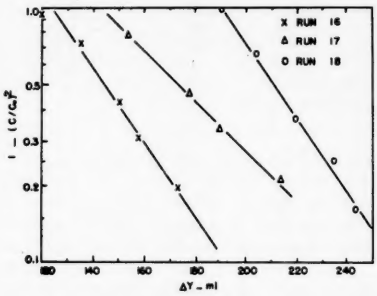

Fig. 3. Breakthrough data for long beds plotted according to Equation (1).

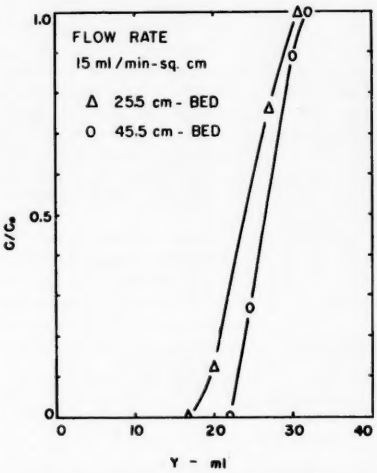

Fig. 4. Effects of longitudinal mixing on breakthrough curves.

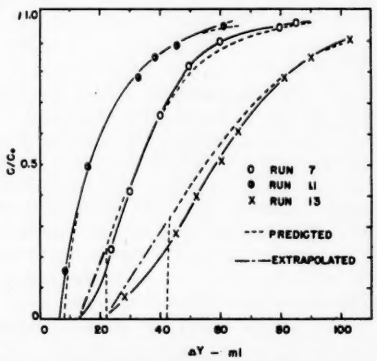

Fig. 5. Comparison of experimental and predicted breakthrough curves.

back calculate some of the breakthrough curves from the present study is shown in Figure 5. Although the equations do not predict the first portion of the breakthrough curve because of longitudinal mixing effects within the bed, it was found that a reasonable approximation of this part of the curve could be obtained by the extrapolation of the breakthrough curve above C/C_0 of 0.2 on down to C/C_0 of 0. Accordingly it is felt that the equations can be used to predict breakthrough curves and to design commercial ion exchange units for the system studied or for similar systems for which the necessary basic data are available.

NOTATION

- a = resin capacity, meq./g. dry hydrogen-form resin
- C = concentration in effluent solution of the ion exchanging onto the resin, meq. iron/ml.
- C_0 = concentration in entering solution of the ion exchanging onto the resin meq. iron/ml.
- d_p = mean diameter of the resin particles, cm.
- D_s = effective diffusivity of the exchanging ions in the resin phase, sq. cm./hr.
- $k_p s$ = internal diffusion transfer coefficient = $(4\pi^2 D_s)/d_p^2$, 1/hr.
- K = equilibrium constant
- q = resin composition, meq. iron/g. dry hydrogen-form resin
- R = flow rate through the bed, ml./hr.
- v = volume of bed, ml.
- ΔY = volume throughput corrected for the bed holdup, ml.
- θ = $(k_p s\ \Delta Y)/R$, dimensionless
- ρ = superficial resin density, g./ml.
- Σ = $(k_p s a \rho v)/C_0 R$, dimensionless

LITERATURE CITED

1. Arehart, T. A., J. C. Bresee, C. W. Hancher, and S. H. Jury, *Chem. Eng. Progr.*, **52**, No. 9, 353 (1956).
2. Barrer, R. M., "Diffusion In and Through Solids," p. 29, University Press, Cambridge, England (1941).
3. Boyd, G. E., A. W. Adamson, and L. S. Myers, Jr., *J. Am. Chem. Soc.*, **69**, 2836 (1947).
4. *Ibid.*, **72**, 4807 (1950).
5. Hiester, N. K., S. B. Radding, R. L. Nelson, and Theodore Vermeulen, *A.I.Ch.E. Journal*, **2**, No. 3, 404 (1956).
6. Mar, W. A., and M. M. David, *ibid.*, p. 381 (1956).
7. Schlogl, R., and F. Helferich, *J. Chem. Phys.*, **26**, No. 1, 5 (1957).
8. Selke, W. A., Y. Bard, A. D. Pasternak, and S. K. Aditya, *A.I.Ch.E. Journal*, **2**, 468 (1956).
9. Selke, W. A., *Chem. Eng. Progr.*, **53**, No. 12, 601 (1957).
10. Soldano, B. A., *Ann. N. Y. Acad. Sci.*, **57**, 116 (1953).
11. Vermeulen, Theodore, *Ind. Eng. Chem.*, **45**, 1664 (1953).

Manuscript received June 30, 1958; revision received February 16, 1959; paper accepted March 25, 1959. Paper presented at A.I.Ch.E. Salt Lake City Meeting.

Fluid Dynamics and Diffusion Calculations for Laminar Liquid Jets

L. E. SCRIVEN and R. L. PIGFORD

University of Delaware, Newark, Delaware

In connection with a study of the mechanism of gas absorption the problem arose of predicting absorption rates into laminar liquid jets. A solution to the problem is presented in this paper, which provides an example of the application of fluid dynamics to the analysis of mass transfer in a complex flow system.

The water jets considered here issued from circular nozzles of about 1.5-mm diameter, flowed intact downward through an atmosphere of solute gas at average velocities of from 75 to 550 cm./sec. over distances of 1 to 15 cm., and were collected in a receiver slightly larger in diameter than the nozzles. Equations describing the liquid flow near the jet surface are deduced from measurements of jet diameter and analogy to related flow situations. When one uses these equations, absorption rates are predicted from unsteady state diffusion theory with the assumption of interfacial equilibrium. The predicted rates for carbon dioxide at 25°C are in close agreement with experimental determinations over the observed range of contact time of the liquid with gas, namely 0.003 to 0.04 sec.

Laminar liquid jets possess several attractive advantages over other types of apparatus for fundamental studies of the mechanism of gas absorption. To obtain a valid experimental test of unsteady state diffusion theory in a flow system, it is imperative that the fluid dynamics of the system be known accurately. The area of contact between gas and liquid must be known, and furthermore the nominal time of exposure of liquid to gas should be of the order of 0.001 to 1 sec., since exposure times of these magnitudes are encountered in most contacting equipment of practical interest. If there is departure from equilibrium at the interface, the effect of an interfacial resistance on absorption rates is likely to be greater the shorter the period of exposure of liquid to gas, simply because the shorter the contact time the smaller the bulk-phase diffusional resistance to mass transfer.

Bubbles of gas rising through liquid are manifestly unsuitable, for the flow regime in the vicinity of the bubble surface is not well understood (*1*) and probably is strongly influenced by the presence of traces of surface-active contaminants (*9*). Falling droplets of liquid likewise suffer the considerable shortcoming of poorly understood fluid dynamics (*10*). A well-behaved moving film of liquid satisfies the requirements, except that end effects at the points at which the film is brought into and out of contact with the gas seem unavoidable, although they may be minimized to a certain extent through apparatus design and experimental technique. Unfortunately the fluid dynamics of the oft-employed wetted-wall column is usually complicated by rippling, which may be either the cause or an indication of mixing within the falling liquid film (*19*). Rippling can be greatly decreased by the addition of small amounts of surface-active agents to the liquid feed or altogether eliminated by reducing the length of the column sufficiently. However the first practice raises new uncertainties on account of possible interaction between solute and surfactant, while the second promotes the end effects to major importance (*11*). Recently the idea of carrying a liquid film on a moving solid surface has been put to use by Danckwerts and Kennedy (*3*) in their novel rotating-drum apparatus, which appears to be nearly free of appreciable end effects for most operating conditions.

Laminar liquid jets, which have been utilized in surface tension studies for many years (*14*), are well suited for absorption measurements. By employing long, fast-moving jets the end effects at the nozzle and the collection device can be reduced to insignificance, but the influences of viscous drag in the nozzle and gravitational acceleration on flow and absorption must be assessed, as they are herein. Previous investigators (*4, 5, 13, 18*) have overlooked these complications, with the exception of Cullen and Davidson (*2*), who discussed qualitatively the influence of gravity insofar as it affects the axial velocity distribution and who evidently succeeded by judicious nozzle design in greatly reducing the influence of viscosity. Contact area can be evaluated readily from measurements of jet diameter. A particular advantage of jets is the wide range of liquid contact times which can be achieved with them, down to a few milli-seconds or even less.

APPARATUS

Detailed descriptions have been given elsewhere of the gas-absorption apparatus in which the jets of interest here were produced (*16, 17*). In brief, a jet of water issued from a circular nozzle about 1.5-mm. I.D. flowed intact downward at an average velocity of from 75 to 550 cm./sec. over a distance of 1 to 15 cm. and was collected in a glass capillary receiver about 2 mm. I.D. The receiver and a nozzle are shown in Figure 1. Between the nozzle and receiver the surface of the jet was exposed to an atmosphere of solute gas confined within a glass chamber. The apparatus was similar to that used by Matsuyama (*13*), Manogue (*12*), and Eipper (*6*).

It was possible to collect the entire jet in the receiver for prolonged periods of operation without entraining any gas bubbles in the liquid, provided the nozzle and receiver were accurately aligned, the resistance to flow downstream of the receiver was carefully adjusted, and strong vibrations were eliminated. Operating

L. E. Scriven is with the Shell Development Company, Emeryville, California.

troubles, when they occurred, seemed to arise from occasional small fluctuations in the liquid feed rate.

FLUID DYNAMICS

Diameter Measurements

As the first step in analyzing the fluid dynamics of the jet, measurements were made with a Gaertner traveling microscope of the jet diameter vs. length across three diameters 60 deg. apart. Measurements made at two flow rates have been plotted in Figure 2.

From these was inferred the velocity distribution. It was assumed that the velocity within the core of the jet issuing from the nozzle was uniform and that outside the core there existed an annular boundary layer in which the velocity was reduced, in consequence of the frictional drag exerted by the inside surface of the nozzle. It was supposed that after the jet left the nozzle, momentum interchange between the core and boundary layer would have produced a substantially flat velocity profile beyond some not-too-distant downstream point. By assuming that the velocity distribution within the boundary layer at the nozzle could be adequately represented by a cubic equation, one gets

$$\frac{U}{U_\infty} = \frac{3}{2}\left(\frac{Y}{\delta}\right) - \frac{1}{2}\left(\frac{Y}{\delta}\right)^3, \qquad 0 \le Y \le \delta \tag{1}$$

$$\frac{U}{U_\infty} = 1, \qquad \delta \le Y \le R_0 \tag{2}$$

and writing mass and momentum balances between the face of the nozzle and a downstream point corresponding to a flat velocity profile (Figure 3), one obtains the following approximate expression relating boundary-layer thickness to the measured diameters:

$$b \equiv \frac{\delta}{R_0} = 2.094\left[\left(\frac{R_0}{R}\right)^2 - 1 - \frac{\pi^2 g_L R_0^{\,4} X}{4q^2}\left(\frac{R_0 + R}{R_0}\right)^2\right] \tag{3}$$

The length of flat plate oriented parallel to the direction of flow which would be required to produce a boundary layer of thickness, if one assumes a cubic velocity distribution, is given by (*15*):

$$l = \left(\frac{13}{280}\right)\frac{U_\infty}{\nu}\,\delta^2 \tag{4}$$

Values of b and l calculated from the data presented in Figure 2 are given in Table 1; it is apparent from the near constancy of b that the velocity profiles within the jets were indeed very nearly flat after 5 cm. or less of travel. This conclusion is borne out by a further est of the data. Downstream from the nozzle in a vertical jet the velocity profile becomes nearly flat, the principal force acting is gravity, and the variation of velocity with jet length is given to a close approximation by [see the discussion of Equation (9)]

$$U = \sqrt{U_0^2 + 2g_L X} \tag{5}$$

TABLE 1

Flow, q, cc./sec.	Distance, X, cm.	Diameter, D, cm.	$b \equiv \delta/R_0$	Average length, l, cm.
5.02	0	0.1543		
	5	0.1454	0.103	
	10	0.1419	0.098	0.088
	15	0.1385	0.098	
2.58	0	0.1546		
	3	0.1406	0.114	
	5	0.1362	0.095	0.043
	7	0.1320	0.099	

From this expression and the equation of continuity it follows that

$$\frac{D}{D_0} = \left(1 + \frac{\pi^2 g_L D_0^{\,4} X}{8q^2}\right)^{-\frac{1}{4}} \tag{6}$$

The agreement of observed variations of diameter with the behavior predicted by Equation (6) is quite good at downstream distances beyond 2.5 cm. (broken curves in Figure 2).

In passing it should be pointed out that the calculated values of boundary-layer thickness do provide confirmation of the laminar character of the flow in the emerging jet. The Reynolds number based on boundary-layer thickness $U_\infty\delta/\nu$ varies from 100 to 250 for the jets. In contrast the analogous critical Reynolds number for flow over a flat plate is in the range 1,500 to 7,000 (*15*); furthermore the stability of laminar flow is increased in the presence of a favorable pressure gradient as obtained with the nozzle design employed in the present work.

Surface Velocity

To predict absorption rates it is necessary to know the velocity distribution in the liquid at and close to the surface of the jet. For the relatively short contact times of interest in connection with the present study, the penetration depth of the diffusing molecules is very small compared with the jet diameter; therefore detailed knowledge of the flow within the interior of the jet is not required.

Since the boundary-layer thickness at the nozzle, as calculated above, amounted to only one tenth of the nozzle radius, it seemed reasonable to assume that (*a*) the core velocity remained unchanged by momentum exchange with the boundary layer and (*b*) the annular boundary layer could be treated as two dimensional. In addition it was assumed that (*c*) the drag of the surrounding gas on the surface of the jet was negligible, (*d*) the minor complication arising from the small rate of change of diameter with length was also negligible, and (*e*) gravitational acceleration was absent. Except in the region close to the nozzle, where gravitational forces were small compared with viscous shear, the last assumption is a gross oversimplification, as is shown below. But with it the problem of analyzing the velocity distribution in the neighborhood of the jet surface became identical with the problem of calculating the velocity distribution in a laminar wake behind an infinitely thin, flat plate oriented parallel to the direction of flow, as depicted in Figure 3, a problem solved many years ago by Goldstein (*7, 8*). The analogy between the laminar jet and Goldstein's problem was pointed out by Rideal and Sutherland (*14*).

For velocities close to the trailing edge of the flat plate Goldstein used three terms of a series solution obtained by continuation of the classical Blasius solution for a flat plate; for velocities far downstream he obtained first and second approximations to an asymptotic solution:

$$\frac{U_s}{U_\infty} = 1.2262\xi(1 - 0.9631\xi^3 + 2.2068\xi^6) = a_1\xi(1 - a_2\xi^3 + a_3\xi^6), \qquad \xi \equiv \left(\frac{X}{4l}\right)^{\frac{1}{3}}; \quad \frac{X}{4l} \le 0.0486 \tag{7}$$

$$\frac{U_s}{U_\infty} = 1 - \frac{0.1873}{\sqrt{x}} - \frac{0.0176}{x} = 1 - \frac{a_4}{\sqrt{x}} - \frac{a_5}{x}, \qquad x \equiv \frac{X}{4l} + 0.13; \quad \frac{X}{4l} \ge 0.125 \tag{8}$$

Figure 4 reproduces Goldstein's complete curve for surface velocity (velocity downstream in the plane of the flat plate).

At distances downstream of the nozzle of more than about 2.5 cm. the velocity profiles within the jets were very nearly flat, and the flow, insofar as it affected jet diameter, could be approximated by the free-fall Equation (5). In the downstream portions of the jets, then, gravitational effects were far from negligible as assumed in (*e*) above, and in fact they predominated in these regions. Thus another estimate of the liquid velocity in the neighborhood of the jet surface is given by

$$\frac{U_s}{U_0} = \sqrt{1 + \frac{2g_L X}{U_0^2}} \tag{9}$$

Precisely speaking, Equation (9) assumes a strictly one-dimensional flow, although the very slight taper of the

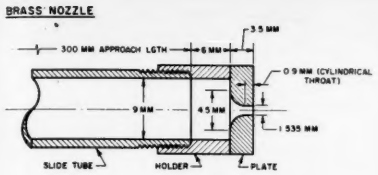

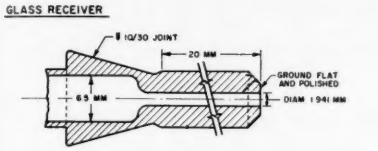

Fig. 1 Jet nozzle and receiver.

jets showed that the flow was in fact two dimensional. Because of the small influence of viscosity and the very nearly uniform jet cross section, however, the assumption of strictly one-dimensional flow neglecting $\partial U/\partial Y$ is felt to yield a very good approximation for U_s far downstream of the nozzle.

From the surface velocity one can easily obtain the component of velocity normal to the surface at small depths beneath the liquid surface. Continuity of an incompressible liquid in two-dimensional flow requires that

$$\frac{\partial U}{\partial X} + \frac{\partial V}{\partial Y} = 0 \qquad (10)$$

But

$$dV = \frac{\partial V}{\partial X}\,dX + \frac{\partial V}{\partial Y}\,dY \qquad (11)$$

$$= \frac{\partial V}{\partial X}\,dX - \frac{\partial U}{\partial X}\,dY \qquad (12)$$

$$\int_{X,0}^{X,Y} dV = -\int_0^Y \frac{\partial U}{\partial X}\,dY = -\frac{d}{dX}\int_0^Y U\,dY \qquad (13)$$

Also $V(X, 0) = 0$, and furthermore $U \cong U_s$ is nearly independent of Y in the vicinity of the surface; hence

$$V \cong -Y\frac{dU_s}{dX} \qquad (14)$$

ABSORPTION

Diffusion Equation

The absorption of a slightly soluble, nonreacting gas is governed by the equation for ordinary diffusion in a binary system, with constant diffusivity and mass density:

$$\frac{\partial C}{\partial t} + (\mathbf{v}\cdot\nabla)C = \mathfrak{D}\nabla^2 C \qquad (15)$$

In the jets the penetration depth of the absorbed molecules was much smaller than the jet diameter; consequently the absorbing liquid can be regarded as semi-infinite and its surface as planar. Except in a very small region near the jet surface at the nozzle, diffusion in the axial direction was negligible in comparison with convective transport. Absorption measurements with the jets were made during steady state operation. Under all these conditions Equation (15) simplifies to

$$U\frac{\partial C}{\partial X} + V\frac{\partial C}{\partial Y} = \mathfrak{D}\frac{\partial^2 C}{\partial Y^2} \qquad (16)$$

Furthermore $\partial U/\partial Y$ was very nearly zero at the jet surface (the adjoining gas exerted negligible drag upon the liquid surface) and beneath to a large depth as compared with the penetration depth (*16*); hence U can be replaced by the surface velocity and V can be expressed in terms of U_s by means of Equation (14):

$$U_s\frac{\partial C}{\partial X} - Y\frac{dU_s}{dX}\frac{\partial C}{\partial Y} = \mathfrak{D}\frac{\partial^2 C}{\partial Y^2} \qquad (17)$$

Two boundary conditions appropriate to the problem are

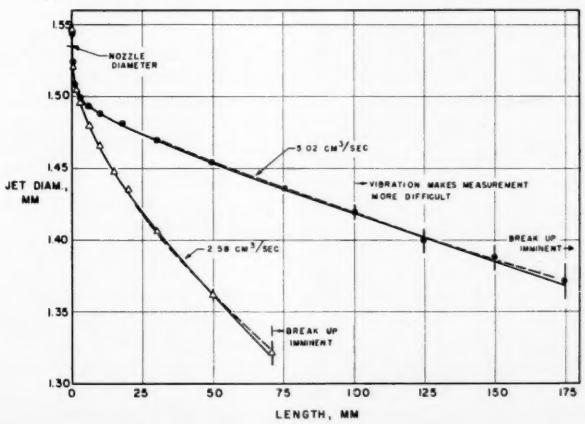

Fig. 2. Jet diameter for 1.535-mm. I. D. paraffin-coated nozzle.

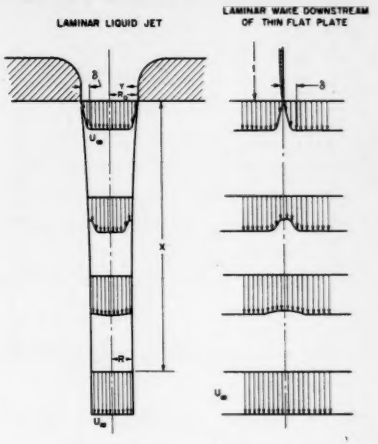

Fig. 3. Velocity Distributions.

$$C(0, Y) = C(X, \infty) = C_0 \qquad (18a, b)$$

If interfacial equilibrium is assumed and heat effects at the interface and gas-phase diffusional resistance are negligible, the third boundary condition is

$$C(X, 0) = C_s \qquad (19)$$

To find a solution of this boundary value problem, one tries the transformation $C(X, Y) = C(\eta)$, where

$$\eta = Yf(X) \qquad (20)$$

Equation (17) then becomes

$$\left(\frac{U_s}{f^3}\frac{df}{dX} - \frac{1}{f^2}\frac{dU_s}{dX}\right)\eta\frac{dC}{d\eta} = \mathfrak{D}\frac{d^2C}{d\eta^2} \qquad (21)$$

If $f(X)$ satisfies

$$\frac{U_s}{f^3}\frac{df}{dX} - \frac{1}{f^2}\frac{dU_s}{dX} = -2\mathfrak{D} \qquad (22)$$

then Equation (21) simplifies to

$$-2\eta\frac{dC}{d\eta} = \frac{d^2C}{d\eta^2} \qquad (23)$$

which, integrated once, gives

$$\frac{dC}{d\eta} = Ae^{-\eta^2} \qquad (24)$$

A second integration, with Equation (18), yields

$$C = C_0 + A\int_\infty^\eta e^{-z^2}\,dz \qquad (25)$$

The remaining constant of integration is evaluated by means of Equation (19); thus

$$\frac{C - C_0}{C_s - C_0} = \frac{2}{\sqrt{\pi}}\int_\eta^\infty e^{-z^2}\,dz = \operatorname{erfc}(\eta) \qquad (26)$$

This is the desired solution provided that $f(X)$ satisfies Equation (22), a

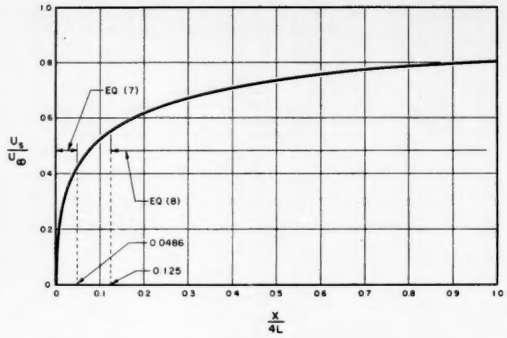

Fig. 4. Surface velocity after Goldstein (*7, 8*).

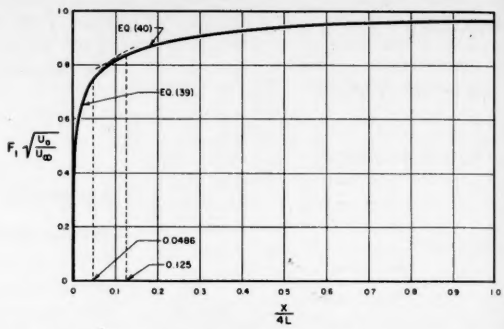

Fig. 5. Effect of nozzle drag on local absorption rate.

Bernoulli equation, the solution of which is

$$f(X) = \frac{U_s(X)}{\sqrt{B + 4\mathfrak{D}\int U_s(X)\,dX}} \tag{27}$$

Hence for any given surface velocity the reduced coordinate η is given by

$$\eta = \frac{YU_s(X)}{\sqrt{B + \mathfrak{D}\int U_s(X)\,dX}} \tag{28}$$

The constant B is evaluated by means of Equation (18*a*), which requires that $\eta(X, Y) \to \infty$ in the limit as $X \to 0$, or else through some other boundary condition in X.

Local absorption rate, rather than the concentration distribution given by Equation (26), is required for absorption predictions:

$$N = -\mathfrak{D}\left(\frac{\partial C}{\partial Y}\right)_{Y=0} = \frac{2}{\sqrt{\pi}}(C_e - C_0)\,\mathfrak{D}f(X) \tag{29}$$

For an idealized jet throughout which velocity is constant (equal to $U_0 = 4q/\pi D_0^2$) it follows from Equations (27) and (29) that

$$N_* = \frac{1}{\sqrt{\pi}}(C_e - C_0)\sqrt{\frac{\mathfrak{D}U_0}{X}} \tag{30}$$

It is convenient to refer absorption rate to this rate for an ideal jet; the ratio is

$$\frac{N}{N_*} = 2f\sqrt{\frac{\mathfrak{D}X}{U_0}} = \frac{2U_s(X)}{\sqrt{U_0\left[B + 4\mathfrak{D}\int U_s(X)\,dX\right]}} \tag{31}$$

Finally the total absorption rate of solute gas by a jet of length h is obtained by integration over jet length:

$$\phi = \int_0^h \pi D(X)N(X)\,dX \tag{32}$$

For an ideal jet the diameter as well as velocity is constant; hence

$$\phi_* = 2(C_e - C_0)\,D_0\sqrt{\pi\,\mathfrak{D}U_0 h} = 4(C_e - C_0)\sqrt{\mathfrak{D}qh} \tag{33}$$

Approximate Solution for Absorption Rate

An exact prediction of absorption rate requires accurate knowledge of the velocity distribution near the surface of a jet affected simultaneously by viscous drag in the nozzle and by gravitational acceleration. The combined effect is not accurately known; however the separate effects can be assessed from the estimates of surface velocity provided by Equations (7) to (9) and can then be combined to give a fairly accurate prediction of absorption rate. The method of combination can be explained as follows.

On the basis of Equations (7), (8), (9), and (31) the functional dependence of local absorption rate can be written as

$$\frac{N}{N_*} = F(\mathfrak{D}, U_0, U_\infty, 4l, g_L, X) \tag{34}$$

Purely dimensional considerations lead immediately to a more fruitful, functional relationship in terms of dimensionless variables:

$$\frac{N}{N_*} = F\left(\frac{U_0X}{\mathfrak{D}}, \frac{U_\infty}{U_0}, \frac{4l}{X}, \frac{g_LX}{U_0^2}\right) = F(\mathfrak{N}_P, \mathfrak{N}_u, \mathfrak{N}_l, \mathfrak{N}_F) \tag{35}$$

If the first two dimensionless groups are regarded as fixed parameters in the problem, expansion of Equation (35) in a Maclaurin series yields

$$\frac{N}{N_*} = F(0,0) + \mathfrak{N}_l\left(\frac{\partial F}{\partial \mathfrak{N}_l}\right)_{0,0} + \mathfrak{N}_F\left(\frac{\partial F}{\partial \mathfrak{N}_F}\right)_{0,0} + \frac{\mathfrak{N}_l^2}{2}\left(\frac{\partial^2 F}{\partial \mathfrak{N}_l^2}\right)_{0,0} + \mathfrak{N}_l\mathfrak{N}_F\left(\frac{\partial^2 F}{\partial \mathfrak{N}_l\,\partial \mathfrak{N}_F}\right)_{0,0} + \frac{\mathfrak{N}_F^2}{2}\left(\frac{\partial^2 F}{\partial \mathfrak{N}_F^2}\right)_{0,0} \tag{36}$$

Now the local absorption rate must approach that into an ideal jet as viscous drag in the nozzle and gravitational acceleration approach zero; therefore $F(0, 0)$ is unity. After evaluation at $\mathfrak{N}_l = \mathfrak{N}_F = 0$, the various partial derivatives may be replaced by constants, say α_1, β_1, γ_{11}, etc., giving

$$\frac{N}{N_*} = -1 + (1 + \alpha_1\mathfrak{N}_l + \alpha_2\mathfrak{N}_l^2 + \cdots) + (1 + \beta_1\mathfrak{N}_F + \beta_2\mathfrak{N}_F^2 + \cdots) + \gamma_{11}\mathfrak{N}_l\mathfrak{N}_F + \cdots \text{ (higher-order interaction terms)} \tag{37}$$

Here the first series may be identified with jet operation in a vanishingly small gravitational field, that is with $F_1 = F(\mathfrak{N}_l, 0)$, and the second series may be identified with operation in the absence of nozzle drag, that is with $F_2 = F(0, \mathfrak{N}_F)$. It then follows (provided certain mathematical conditions are satisfied) that for sufficiently small values of the nozzle drag and Froude numbers the local absorption rate is given to a good approximation by

$$\frac{N}{N_*} = -1 + F_1\left(\frac{4l}{X}\right) + F_2\left(\frac{g_LX}{U_0^2}\right) \tag{38}$$

where first- and higher- order interaction terms have been neglected.

The functions F_1 and F_2 are obtained from the estimates of surface velocity and from Equation (31). From Equation (7)

$$F_1 = \sqrt{\frac{4a_1U_\infty\xi}{3U_0}}\cdot\frac{1 - a_2\xi^3 + a_3\xi^6}{\sqrt{1 - \frac{4a_2\xi^3}{7} + \frac{2a_3\xi^6}{5}}} \tag{39}$$

$$\xi = \left(\frac{X}{4l}\right)^{\frac{1}{2}}; \qquad \frac{X}{4l} \le 0.0486$$

TABLE 2.

X, cm.	$\mathfrak{N}_l$	F_1, Equation (39) or (40)	$\mathfrak{N}_F$	F_2, Equation (42)	N/N_*, Equation (38)	D/D_0	ϕ/ϕ_*	h, cm.
$D_0 = 0.1535$ cm., $U_0 = 271$ cm./sec., $4l = 0.352$ cm., $U_\infty = 292$ cm./sec.								
0.01	35.2	0.720	0.00013	1.000	0.720	1.000	0.545	0.01
0.1	3.52	0.937	0.00133	1.001	0.938	0.982	0.786	0.1
1	0.352	1.026	0.0133	1.010	1.036	0.968	0.916	1
10	0.0352	1.038	0.133	1.091	1.129	0.924	0.988	10
$D_0 = 0.1535$ cm., $U_0 = 145$ cm./sec., $4l = 0.172$ cm., $U_\infty = 150$ cm./sec.								
0.005	34.4	0.710	0.00047	1.000	0.710	1.000	0.545	0.005
0.05	3.44	0.923	0.00467	1.001	0.924	0.987	0.762	0.05
0.5	0.344	1.009	0.0467	1.017	1.026	0.966	0.911	0.5
5	0.0344	1.019	0.467	1.149	1.168	0.889	0.993	5

where the constant B of Equation (31) has been taken as zero in accordance with Equation (18a). From Equation (8)

$$F_1 = \sqrt{\frac{U_\infty}{U_0}} \frac{1 - \frac{a_4}{\sqrt{x}} - \frac{a_5}{x}}{\sqrt{1 - \left(\frac{4l}{X}\right)(2a_4\sqrt{x} + a_5 \ln x - 0.0956)}} \qquad (40)$$

$$x = \frac{X}{4l} + 0.13; \qquad \frac{X}{4l} \geq 0.125$$

where B has been set equal to 0.0956 ($16l\ \mathfrak{D}U_\infty$) to give a smooth transition from Equation (39) in the region $0.0486 < X/4l < 0.125$ (Figure 5). From Equation (9)

$$F_2 = \sqrt{\left(\frac{3g_L X}{U_0^2}\right) \frac{[1 + (2g_L X/U_0^2)]}{[1 + (2g_L X/U_0^2)]^{\frac{3}{2}} - 1}} \qquad (41)$$

$$= \sqrt{\frac{1 + (2g_L X/U_0^2)}{1 + \frac{(2g_L X/U_0^2)}{4} - \frac{(2g_L X/U_0^2)^2}{24} + \cdots}} \qquad (42)$$

The calculation of the parameters l and U_0 has already been described. The core velocity within the emerging jet was evaluated from the average velocity, the assumed form of the velocity distribution in the boundary layer, and the inferred boundary-layer thickness at the nozzle by means of

$$U_\infty = \frac{U_0}{1 - \frac{3b}{4} - \frac{b^2}{5}} \qquad (43)$$

Comparison with Experimental Results

By the use of the foregoing equations absorption rates at 25°C. of carbon dioxide into several laminar water jets were predicted. The diffusivity of carbon dioxide in water at 25°C. was taken as 1.97×10^{-5} sq. cm./sec., and the solubility at the same temperature and 760 mm. Hg partial pressure was taken as 3.39×10^{-5} g.-mole/cc. The initial concentration, was assumed to be zero, the water having been carefully stripped of dissolved gas before use (*16*).

The order of magnitude of the adjustments to the reference local-absorption rate is indicated in Table 2, in which representative values are listed for jets produced with a 1.535-mm. I.D. brass nozzle at flow rates of 5 and 2.6 cc./sec. Equation (32) with Equation (38) was integrated numerically to arrive at the predicted total absorption rates plotted as full curves in Figure 6. The predicted absorption rates for an ideal jet, according to Equation (33), are plotted for comparison as broken lines.

Experimentally determined absorption rates for nominal contact times ranging from 0.003 to 0.04 sec. are also plotted in Figure 6. Details of the experimental procedure have been reported elsewhere (*16, 17*). In brief, feed and effluent water samples were drawn with the apparatus operating at steady state. Due precaution was taken to prevent transfer of carbon dioxide to or from the samples. Analysis for dissolved carbon dioxide depended upon the precipitation in basic solution of carbonate ion as barium carbonate, followed by back titration of excess hydroxyl ion with standard acid to the carbonate-bicarbonate end point. Both the precision and accuracy of the analysis were found to be about 0.4 p.p.m.; the range of concentrations analyzed in the effluent water was 10 to 44 p.p.m. That the reproducibility of replicate runs was, with few exceptions, excellent can be seen from the data. The agreement of experimental and predicted absorption rates is very good.

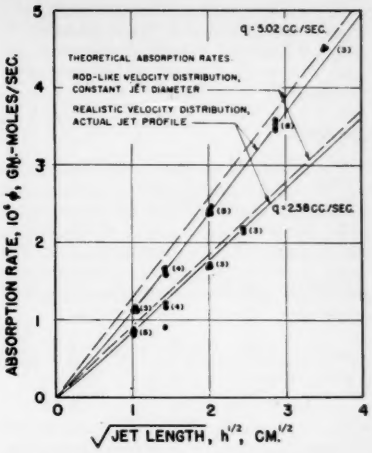

Fig. 6. Carbon dioxide absorption into water.

DISCUSSION

The experimental and predicted absorption rates agree closely, but this fact alone verifies neither the approximate solution of the diffusion equation from which the predictions arise nor the particular set of boundary conditions used to obtain that solution. Before any conclusion is drawn, it is necessary to consider the extent to which the approximate solution may deviate from the exact solution. In over-all absorption rate the former leads to predictions differing from those based on the assumption of an ideal jet by no more than 10%. Such deviation may be regarded as a first perturbation to the ideal-jet absorption rate, caused by the disturbing influences of viscous drag in the nozzle and gravitational acceleration. Now the principal part of the unknown second perturbation is proportional to the product of the already small disturbing influences [Equations (37) and (38)] and may reasonably be expected to be about 1% of the ideal-jet prediction; the higher-order perturbations should be proportionately smaller. It is therefore quite unlikely that the predictions based on the approximate solution are more than 2 or 3% in error, even under the conditions of the lowest absorption rates measured, for which the deviation from ideal-jet behavior was greatest.

Thus the data substantiate the physical model underlying the theoretical predictions; in particular, they confirm the validity of the asumption of thermodynamic equilibrium between gaseous and liquid phases everywhere on the jet surface [Equation (19)]. This matter has been discussed in detail by the authors in an earlier paper (*17*).

ACKNOWLEDGMENT

Thanks are due M. M. Wendel and Stanley Corrsin for helpful discussions of portions of this work and W. J. Baur for

assistance with some of the measurements. The investigation was made possible in part by National Science Foundation and Shell Fellowship Committee fellowships received by L. E. Scriven.

APPENDIX

The nature of the problem of absorption into an accelerating liquid flow is illustrated by a simple example. For a two-dimensional flow directed toward a sink at the origin and bounded by free streamlines at the acute angles $\pm\ \theta_0$ in polar coordinates the potential and stream functions are, respectively,

$$\Phi = R_0 U_0 \ln R$$

$$\Psi = R_0 U_0 \theta$$

where U_0 is the radial velocity at distance R_0 from the origin. Such a flow corresponds to a two-dimensional liquid jet in a certain body force field. If one considers absorption along the free streamlines between R_0 and R, $0 \ll R < R_0$, the appropriate diffusion problem is

$$U\frac{\partial C}{\partial R} = \mathfrak{D}\left(\frac{\partial^2 C}{\partial R^2} + \frac{1}{R}\frac{\partial C}{\partial R} + \frac{1}{R^2}\frac{\partial^2 C}{\partial \theta^2}\right)$$

$$C(R_0\ ,\ \theta) = C_0$$

$$C(R,\ \pm\ \theta_0) = C_e$$

$$\frac{\partial C}{\partial R}(R,\ 0) = 0$$

where the radial velocity is related to the potential function by

$$U = \frac{\partial \Phi}{\partial R}$$

With the usual transformation for diffusion in potential flow, in which the potential and stream functions are taken as the independent variables, and with diffusion along the stream tubes neglected, there follows

$$\frac{\partial C}{\partial \Phi} = \mathfrak{D}\frac{\partial^2 C}{\partial \Psi^2}$$

$$C(\Phi_0\ ,\ \Psi) = C_0\ ,\qquad \Phi_0 = R_0 U_0 \ln R_0$$

$$C(\Phi,\ \pm\ \Psi_0) = C_e\ ,\qquad \Psi_0 = R_0 U_0 \theta_0$$

$$\frac{\partial C}{\partial \Psi}(\Phi,\ 0) = 0$$

which is virtually identical to the problem of diffusion into an infinite sheet, the solution of which is well known. For small values of $\Phi_0 - \Phi$ (short exposure times) the local rate of absorption is expressed conveniently as

$$N = (C_e - C_0)\cdot\sqrt{\frac{\mathfrak{D}U_0}{\pi R_0 (R/R_0)^2 \ln (R_0/R)}}\cdot\left\{1 + 2\sum_{n=1}^{\infty}(-1)^n \cdot \exp\left[\frac{n^2 R_0 U_0 \theta_0^{\,2}}{\mathfrak{D}\ln (R/R_0)}\right]\right\}$$

If the distance $R_0 - R$ is sufficiently short, the penetration depth of absorbed material is small compared with the width of the flow and only the first term within the braces need be retained. Then the local absorption rate is given by

$$N = (C_e - C_0)\cdot\sqrt{\frac{\mathfrak{D}U_0}{\pi R_0 (1-x)^2 \ln [1/(1-x)]}}$$

where now $x = (R_0 - R)/R_0$.

This problem can also be solved by the method presented herein. Instead of the polar coordinates just used, rectangular coordinates with the origin in the free streamline at R_0 are employed. With this transformation the surface velocity is

$$U_s = \frac{R_0 U_0}{R_0 - X}$$

and the velocity normal to the free streamline is

$$V = -\frac{R_0 U_0 Y}{(R_0 - X)^2 + Y^2}$$

For shallow penetration depths Y is small in the region of interest, and V is given to a good approximation by

$$V \cong -\frac{R_0 U_0 Y}{(R_0 - X)^2}$$

which can also be obtained with the use of Equation (14). From Equations (27) and (29) for local absorption rate, given the surface velocity, the result is again found to be

$$N = (C_e - C_0)\cdot\sqrt{\frac{\mathfrak{D}U_0}{\pi R_0 (1-x)^2 \ln [1/(1-x)]}}$$

There is of course no flow across the streamlines (lines of constant Ψ), but for $Y > 0$ there is a velocity component in the direction normal to the interface which must be accounted for when the diffusion equation is written in rectangular coordinates with the origin in the interface.

NOTATION

a = dimensionless constants, Equations (7) and (8)
b = δ/R_0, dimensionless boundary-layer thickness
B = constant in Equation (27), cm.^{4}/sec.^{2}
C = concentration, g.-moles/cc.
C_0 = initial concentration
D = jet diameter, cm.
$\mathfrak{D}$ = diffusion coefficient, sq. cm./sec.
f = function defined by Equation (27)
g_L = local acceleration of gravity, cm./sec.^{2}
h = jet length, cm.
l = equivalent length of flat plate, cm.
N = local absorption rate, g.-moles/(sq. cm.)(sec.)
$\mathfrak{N}_F$ = $g_L X/U_0^2$, Froude number
$\mathfrak{N}_P$ = $U_0 X/\mathfrak{D}$, Peclet number
$\mathfrak{N}_u$ = U_∞/U_0, velocity ratio
$\mathfrak{N}_l$ = $4l/X$, nozzle-drag number
q = volumetric flow rate, cc./sec.
R = jet radius, cm.
U = axial component of velocity, cm./sec.
V = radial component of velocity, cm./sec.
x = $(X/4l) + 0.13$, dimensionless variable, Equation (8)
X = axial coordinate, cm.
Y = radial coordinate, cm.

Greek Letters

δ = boundary-layer thickness, cm.
η = dimensionless variable, Equation (20)
ν = kinematic viscosity, sq. cm./sec.
ξ = $(X/4l)^{1/3}$, dimensionless variable, Equation (7)
ϕ = total absorption rate, g.-moles/sec.

Subscripts

e = equilibrium
0 = nozzle exit
s = surface
∞ = core
$*$ = ideal jet

LITERATURE CITED

1. Birkhoff, Garrett, "Hydrodynamics," Princeton Univ. Press, Princeton, N. J. (1950).
2. Cullen, E. J., and J. F. Davidson, *Trans. Faraday Soc.*, **53**, 113 (1957).
3. Danckwerts, P. V., and A. M. Kennedy, *Trans. Inst. Chem. Engrs. (London)*, **32**, S49 (1954).
4. Dirken, M. N. J., and H. W. Mook, *Biochem. Z.*, **219**, 452 (1930).
5. Edwards, G., R. Robertson, F. Rumford, and J. Thomson, *Trans. Inst. Chem. Engrs. (London)*, **32**, S6 (1954).
6. Eipper, J. E., thesis, Univ. Delaware, Newark (1955).
7. Goldstein, Sydney, *Proc. Cambridge Phil. Soc.*, **26**, 1 (1930).
8. ———, *Proc. Roy. Soc. (London)*, **A142**, 545 (1933).
9. Hammerton, D., and F. H. Garner, *Trans. Inst. Chem. Engrs. (London)*, **32**, S18 (1954).
10. Hughes, R. R., and E. R. Gilliland, *Chem. Eng. Progr. Symposium Ser.* No. 16, **51**, 101 (1955).
11. Lynn, Scott, J. R. Straatemeier, and H. Kramers, *Chem. Eng. Sci.*, **4**, 49, 58 (1955).
12. Manogue, W. H., Ph.D. dissertation, Univ. Delaware, Newark (1957).
13. Matsuyama, Takuzo, *Mem. Fac. Eng. Kyoto Univ.*, **15**, No. 11, 142 (1953) (in English).
14. Rideal, E. K., and K. L. Sutherland, *Trans. Faraday Soc.*, **48**, 1109 (1952).
15. Schlichting, Hermann, "Boundary Layer Theory," McGraw-Hill, New York (1955).
16. Scriven, L. E., Ph.D. dissertation, Univ. Delaware, Newark (1956).
17. ———, and R. L. Pigford, *A.I.Ch.E. Journal*, **4**, 439 (1958).
18. Vielstich, Wolf, *Chem.-Ing.-Tech.*, **28**, 543 (1956).
19. Vivian, J. E., and D. W. Peaceman, *A.I.Ch.E. Journal*, **2**, 437 (1956).

Manuscript received July 22, 1958; revision received January 20, 1959; paper accepted January 22, 1959.

Film Boiling of Helium I and Other Liquefied Gases on Single Wires

T. H. K. FREDERKING

Institut für Kalorische Apparate und Kältetechnik, Swiss Federal Institute of Technology, Zurich, Switzerland

Heat transfer coefficients have been obtained for natural-convection film boiling of helium I on single wires with a diameter ranging from 5 to 50 μ. The measurements covered temperature differences of 30° to 1,000 °K. between the heating surface and the saturated liquid under atmospheric pressure. The results are correlated in dimensionless form (Nusselt number vs. the product of the Grashof and Prandtl numbers) and compared with data for nitrogen and measurements of other investigators on film boiling of liquefied gases.

In recent years technical developments where large quantities of heat are transferred across comparatively small areas have increased the interest in all types of heat transfer at high flux densities and have focused attention on boiling.

In continuation of previous studies in the nucleate boiling region (*1*) measurements were made on stable film boiling of helium I under atmospheric pressure. There are some advantages in the use of helium I as a test liquid: its low boiling point permits a wide range of temperature differences without appreciable radiation influence and it has a well-known simple structure and does not attack the heating surface, although the low heat of vaporization necessitates a small heating device in order to keep the amount of vaporized gas within tolerable limits.

APPARATUS EMPLOYED

Electrically heated platinum wires were soft-soldered to copper current and potential leads. For the smaller units Wollaston wires were used. To reduce the chance of breakage the silver layer was etched off after soldering. The diameters were determined by microscope, measurements being made with both horizontally and vertically mounted wires. All experiments were carried out in a Dewar vessel of 6 cm. I. D. The tests were conducted by gradually increasing the current until stable film boiling was reached. By varying the power input and measuring the current and potential drop, one obtained the stable film-boiling curve. The average temperature of the test section was determined by resistance thermometry. The resistance-temperature characteristic was obtained from resistance measurements at the ice point and at liquid helium temperature, with the validity of Matthiessen's rule assumed and the data for pure platinum in the standard reference works (*2*) used. In most cases the power was increased until the wire burned out.

RESULTS OBTAINED

Table 1* gives a sample of the measured data for a single wire and the calculations made to obtain the heat transfer coefficient. In Figure 1 the experimental results for horizontal wires are presented as a plot of the average heat transfer coefficient, defined by the equation $q/A = h\,\Delta T$. (W = watt; 1 $W/(°K.)(sq.\ cm.) = 1{,}761$ B.t.u./(hr.)(sq. ft./°F.); 1 $W/(°K.)(sq.\ cm.) = 8{,}600$ kcal./(°K.)(sq. m./hr.).

At the highest temperature reached one obtains the order of magnitude of the film thickness by calculating $B = k/h$ (k at average film temperature), which yields B of about two times the wire diameter. The temperature gradients within the film reach values of the order of magnitude of 10^6 °K./cm. The mean free path of the gas molecules changes considerably across the film [from about (30 to 6,000) 10^{-8} cm.], causing changes in the transport properties for momentum and heat. At the burnout point current densities up to 5×10^5 A/sq. cm. were reached.

The heat transfer coefficients for some vertically mounted wires show no great differences compared with those for horizontal ones, the maximum observed difference being about 15% less for the vertical wires. (The lengths used were 3.60 cm. for 30-μ nominal diameter, 3.07 cm. for 10-μ wire, and 0.625 cm. for 5-μ wire.) The effect of wire length on h is very weak, as was observed in additional measurements with wires of 15-μ nominal diameter. Within the range of lengths from 3 to 10 cm. only a slight increase of h with increasing length was found; however it is difficult to give an exact quantitative relationship because scattering of data in these measurements is inevitable. A vertical cylinder is defined by two linear dimensions, the diameter and length. (Only for very short horizontal cylinders are end effects noticeable.) Generally it is to be expected that the influence of the ratio of length to diameter will not be the same at very small and very large diameters. A further complication comes from the existence of a laminar- and turbulent-flow region. (For long vertical cylinders the mean heat transfer coefficient is nearly unaffected by the mean h value of the relatively short viscous-flow path.) Thus for all diameters the h values on vertical cylinders will not be superior to those on horizontal ones, as was found by Hsu and Westwater (*8*) in film boiling on vertical tubes with $\frac{3}{8}$ to $\frac{3}{4}$ in. O.D. (9.5 to 19 mm.). A better knowledge of the critical Reynolds number of the film and the turbulent heat transfer would give a better explanation of the vertical film-boiling heat removal.

In addition to the helium measurements some experiments were conducted with nitrogen. In Figure 2 the heat transfer coefficients for thin horizontal wires measured by the author and by other authors (*3*, *4*) are presented. The shape of the nitrogen curve is similar to that obtained for oxygen (*5*). Beyond the heat-flux minimum (Leidenfrost point) h gradually decreases with increasing temperature difference toward a flat minimum. At higher temperatures of the heating surface the shape of the curve becomes steeper and steeper with increasing radiation. Compared with the helium data, the temperature range between the minimum of h and the beginning of radiation is considerably smaller.

THEORETICAL ANALYSIS

A theoretical solution of film-boiling heat transfer was given by Bromley (*3*), who treated the problem in analogy to the film-condensation theory of Nusselt. He has shown that the mean coefficient of heat transfer without radiation influence for the film boiling on horizontal cylinders is given by

$$h = 0.62 \cdot \left[\frac{k^3 \rho(\rho_L - \rho) g \lambda'}{D\mu\,\Delta T}\right]^{\frac{1}{4}} \qquad (1)$$

*Tabular material has been deposited as document No. 5972 with the American Documentation Institute, Photoduplication Service, Library of Congress, Washington 25, D. C., and may be obtained for $1.25 for photoprints or 35-mm. microfilm.

TABLE 1. SAMPLE OF MEASURED DATA AND CALCULATION OF THE HEAT TRANSFER COEFFICIENT

Wire, F 52
Diameter, D = 5.5 μ
Length, L = 0.537 cm.
Surface area, A = $9.28 \cdot 10^{-4}$ sq. cm.
Ice-point resistance, R_{273} 25.8 ohms
Resistance at liquid helium temperature, $R_{4.2}$ 0.61 ohm

Measured data power Amperes	Volts	Watts	Heat flux density watts/ sq. cm.	Wire resistance, ohms	Resistance function $\frac{R - R_{4.2}}{R_{273} - R_{4.2}}$	Wire temperature* (absolute), °K.	Temperature difference, °K.	Heat transfer coefficient h, watts/ (sq. cm.) (°K.)
0.0906	0.680	0.0616	66.4	7.50	0.274	97.4	93.2	0.711
0.0892	0.900	0.0803	86.4	10.1	0.376	121	117	0.739
0.0898	1.09	0.0979	105.5	12.1	0.456	140	136	0.776
0.0915	1.28	0.117	126	14.0	0.531	158	154	0.818
0.0911	1.46	0.133	143	16.0	0.611	176	172	0.831
0.0917	1.65	0.151	163	18.0	0.690	198	194	0.840
0.0923	1.95	0.181	194	21.1	0.815	227	223	0.869
0.0941	2.20	0.207	223	23.4	0.905	250	246	0.906
0.0965	2.67	0.258	278	27.6	1.07	291	287	0.969
0.0964	3.02	0.292	315	31.3	1.22	330	326	0.966
0.0972	3.54	0.344	371	36.4	1.42	380	376	0.986
0.0989	4.05	0.400	431	41.0	1.60	428	424	1.02

*Taken from standard tables (2).

The physical properties of the vapor are taken at the average temperature of the film. The effective latent heat of vaporization was taken in first approximation as $\lambda_1' = \lambda + 0.5\, c_p \cdot \Delta T$. A later (6) derived effective enthalpy difference $\lambda_2' = \lambda \cdot [1 + 0.4\, c_p\, \Delta T/\lambda]^2$ gives a better fit with observed data. Apart from the effect of diameter the boiling heat transfer can be described fairly well by Equation (1), which has been derived under the assumption of negligible film thickness in comparison with the diameter. Bromley's experimental results on cylinders 0.19 to 0.47 in. (4.8 to 12 mm.) O.D. are in good agreement with the theoretical prediction that h should be proportional to $D^{-1/4}$. For thin wires, however, the assumption of negligible film thickness is not valid. Measurements on boiling oxygen by Banchero, Barker, and Boll (5) gave heat transfer coefficients which were some 10% higher than those calculated by the Bromley equation for the smallest diameter used (0.025 in., or 0.0635 mm.). The data for the present tests on helium are up to 3.5 times larger for the thinnest wire than the theoretical values obtained by the insertion of λ_2' in Equation (1). In the diameter range used here [(5 to 50) $\times$ 10^{-3} mm.] h is proportional $D^{-0.7}$.

Vapor-layer Formation

In natural-convection film boiling at an inclined heating surface a continuous vapor film is flowing from the lower edge upward along the surface under the action of the gravity field, in contrast to the nucleate boiling mechanism. The driving temperature difference between the heating surface and the saturated liquid must exceed a certain value in order to establish a stable flow pattern. For the derivation of Equation (1) it is essential that the vapor film be sufficiently thin. Under this assumption the increase in thickness due to evaporation at the phase boundary corresponds immediately to the heat supply from the heating surface. In first approximation the temperature profile of the laminar flowing vapor is linear; the superheat and the heat capacity of the vapor are taken into account by the insertion of λ_2' instead of λ into Equation (1). In accordance with the equation the increase in film thickness for a given heat input, other variables being unchanged, is higher the lower the heat of vaporization. Other factors which are important for nucleation, such as surface roughness, do not enter the theory. Its important variables are the physical properties of the vapor within the film. Considering the good agreement with the experiments in the range of moderate diameters one may conclude that the rate-controlling mechanism must be the transfer of heat across the vapor film.

Natural-Convection Mechanism

Since the vapor resistance is controlling, there is some analogy to natural convection of a horizontal cylinder by a gas without boiling if other phenomena caused by the presence of the denser phase are neglected. This becomes evident for the limiting case of a liquid boiling under a pressure approaching the critical (vanishing latent heat of vaporization, vanishing phase boundary). Within the film the vapor is rising under the action of buoyant and viscous forces. The motion of the vapor is caused by gravitation in association with the density variations which occur as a result of the temperature difference produced by the heat-dissipating cylinder. Consequently the dimensionless groups $N_{Nu} = hD/k$ and the product of $N_{Gr} = D^3\rho^2\beta g\, \Delta T/\mu^2$ and $N_{Pr} = c_p\mu/k$, governing the natural-convection heat transfer without boiling, have been used to correlate the film-boiling data in dimensionless form. All physical properties are taken at the arithmetic mean temperature; in this sense $\beta = 1/T_m$.

The range of applicability of this correlation may be seen when one rewrites Equation (1) in dimensionless form for a liquid with negligibly low latent heat of vaporization ($\lambda \ll 0.5\, c_p\, \Delta T$) and

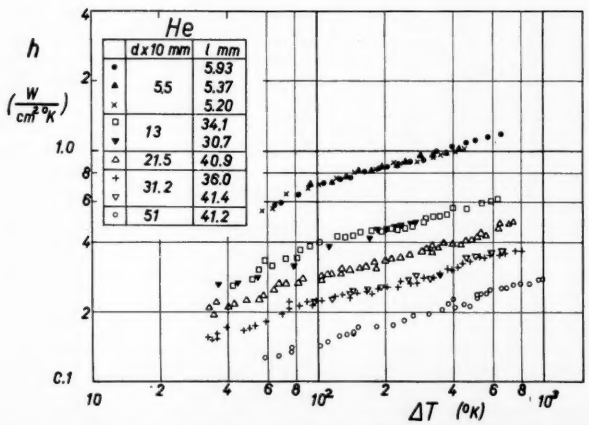

Fig. 1. Heat transfer coefficient for film boiling of helium on horizontal thin wires under atmospheric pressure.

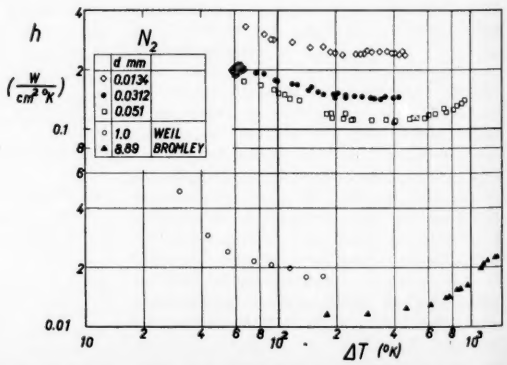

Fig. 2. Heat transfer coefficient for film boiling of nitrogen on horizontal wires and tubes under atmospheric pressure.

uses the approximate expression λ_1'. The Bromley equation can be written

$$N_{Nu} = 0.62\left[\frac{D^3\rho(\rho_L - \rho)g\lambda'}{k\mu\ \Delta T}\right]^{\frac{1}{4}} \quad (2)$$

and approximately with $\lambda' \approx 0.5\ c_p\ \Delta T$

$$N_{Nu} \approx C_1\left[\frac{D^3\rho(\rho_L - \rho)g}{\mu^2}\ \frac{\mu c_p}{k}\right]^{\frac{1}{4}} \quad (3)$$

By definition the coefficient of thermal expansion is $\beta = -(1/\rho)(\partial\rho/\partial T)$. For purposes of comparison one takes a modified coefficient $\beta^* = (1/\rho)[(\rho_v - \rho)/\Delta T]$. Thus $N_{Gr}{}^* = D^3g\ \Delta T\rho^2\beta^*/\mu^2 = D^3\rho g(\rho_v - \rho)/\mu^2$, and the approximate form of the Bromley equation for negligibly low λ becomes

$$N_{Nu} \approx C_1(N_{Gr}{}^* N_{Pr})^{\frac{1}{4}} \cdot \left[\frac{\rho_L - \rho}{\rho_v - \rho}\right]^{\frac{1}{4}} \quad (3a)$$

The last factor on the right side approaches unity near the critical pressure, where $\rho_v = \rho_L$. Equation (3*a*) in terms of the argument $N_{Gr}N_{Pr}$ used in this correlation becomes

$$N_{Nu} \approx C_1(N_{Gr}N_{Pr})^{\frac{1}{4}} \cdot \left[\frac{\beta^*}{\beta}\ \frac{\rho_L - \rho}{\rho_v - \rho}\right]^{\frac{1}{4}} \quad (3b)$$

with

$$\frac{\beta^*}{\beta} \cdot \frac{\rho_L - \rho}{\rho_v - \rho} = \frac{\rho_L - \rho}{\rho} \cdot \frac{T_m}{\Delta T}$$

$\beta = 1/T_m$ being used. For helium with its low boiling point (4.2°K. under atmospheric pressure) at sufficiently high temperatures with $\Delta T/T_m \approx 2$ and $\rho \ll \rho_L$

$$N_{Nu} \approx C_1(N_{Gr}N_{Pr})^{\frac{1}{4}} \cdot \left(\frac{1}{2} \cdot \frac{\rho_L}{\rho}\right)^{\frac{1}{4}} \quad (3c)$$

In Figure 3 a plot of N_{Nu} vs. $N_{Gr}N_{Pr}$ is presented for helium and nitrogen data and for published data on other liquefied gases boiling under atmospheric pressure. The experimental results for stable film boiling of helium can be represented by

$$N_{Nu} = C_2(N_{Gr}N_{Pr})^m \quad (4)$$

with $C_2 = 2.5$ and $m = 0.11$ for the range of variables $10^{-7} < N_{Gr}N_{Pr} < 10^{-1}$. The thin-wire nitrogen data can be approximated by a similar relation with a somewhat greater constant. Known film-boiling results for oxygen (*5*), nitrogen (*3*, *4*), and hydrogen (*4*) with larger diameters are added covering $N_{Gr}N_{Pr}$ values larger than unity. (The plotted nitrogen data of Bromley are the corrected values excluding the influence of radiation.)

Effect of Diameter

A general trend of the data is observable similar to the well-known curve for natural-convection cooling on horizontal cylinders without boiling (*7*). At low valuse of $N_{Gr}N_{Pr}$ the Nu values increase with an increase of $N_{Gr}N_{Pr}$ at a very slow rate. For values of the argument greater than unity this rate increases until N_{Nu} becomes proportional to $(N_{Gr}N_{Pr})^{1/4}$. In this region h is proportional to $D^{-1/4}$, as predicted by Bromley's equation. If the heat transfer coefficient is proportional to D^{-n}, then from Equation (4) this exponent becomes $n = (1 - 3m.)$. In this way the dimensionless correlation permits an estimate of the influence of diameter on the heat transfer coefficient without radiation.

For the greatest diameter used by Banchero (0.750 in. or 19.05 mm.) deviations of the h values calculated by the Bromley equation were also observed. In the dimensionless correlation of these data m approaches $\frac{1}{3}$, and h is nearly independent of the diameter. In natural convection without boiling this means turbulent flow. As for this diameter, no detailed observations regarding turbulence were made, and the exact value of m cannot be taken from this single run; conclusions on the transition laminar-turbulent are not possible, and the data were omitted in Figure 3.

One may note that in general for any given diameter of the cylinder an extension of the boiling curve to either lower or higher ΔT, corresponding to higher or lower values of $N_{Gr}N_{Pr}$, would lead to values of N_{Nu} lying above the general curve shown. At the higher $N_{Gr}N_{Pr}$ this occurs because the curve is continued into the transition region; at the lower values of the same dimensionless number the N_{Nu} values, calculated with the total heat transfer coefficient including radiation, increase toward the burn-out point. The presented points in this way have the character of a lower limit for the heat transfer coefficient.

Effect of Fluid

For the case of heat transfer by convection without phase change the Nusselt numbers are known to be entirely independent of the nature of the gas. It is not surprising, however, that in the case presented here there should be differences in the N_{Nu} values for different gases because the heat transfer process in film boiling is much more complicated than that without phase change. Of all gases investigated helium shows the greatest similarity in Nusselt numbers for film boiling and natural-convection cooling. This becomes understandable from its very low heat of vaporization [under atmospheric pressure about 20 joules/g. and c_p about 5 joules/(g.)(°K.)] [1 joule/g. = 0.431 B.t.u./lb.] and a ratio of pressure to critical pressure of about 44% at 1 atm. For nitrogen and oxygen this ratio is considerably smaller (about 3 and 2% respectively), and the latent heat of vaporization is about ten times larger than for helium. The curves for oxygen and nitrogen in Figure 3 at low temperature differences already show small deviations due to the influence of the latent heat of vaporization. [For the range of higher $N_{Gr}N_{Pr}$ a smooth curve for oxygen is obtained when one multiplies N_{Nu} with the correcting factor $[\lambda/(c_p\ \Delta T) + 0.5]^{-1/4}$ or $[\lambda/(c_p\ \Delta T) \cdot (1 + 0.4\ c_p\ \Delta T/\lambda)^2]^{-1/4}$ according to Equation (1).] When one considers the complicated conditions caused by the presence of the denser liquid separated from the gas by a more or less irregularly shaped phase boundary, the variation of vapor flow due to vaporization along this boundary, and the bubble-discharge mechanism and notices the various pressure-ratio values, the differences in the N_{Nu} numbers for the various liquefied gases are remarkably small. In general, the author's results show that great similarity exists in the behavior of these gases at the same film Reynolds number.

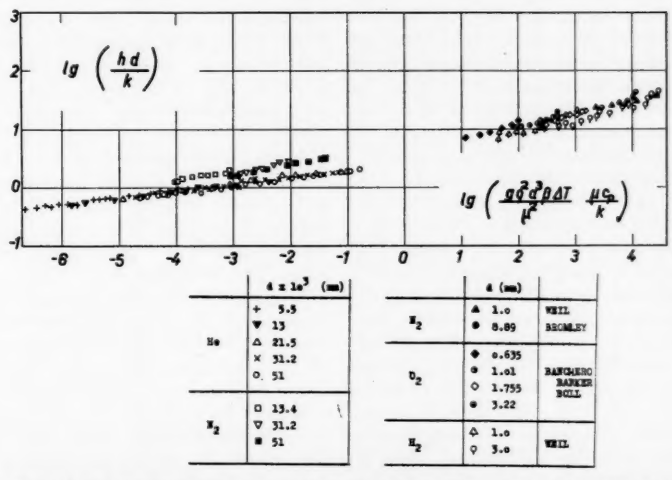

Fig. 3. The Nusselt number as a function of the product of the Grashof and Prandtl numbers for film boiling on horizontal cylinders under atmospheric pressure.

ACKNOWLEDGMENT

The work was supported by the schweizerischen Nationalfonds. Thanks are due to Professor P. P. Grassmann and Dr. J. L. Olsen for helpful discussions and support in the preparation of this paper.

NOTATION

A = area of heating surface
B = film thickness
C_1 = numerical constant
C_2 = numerical constant
c_p = specific heat at constant pressure
D = diameter ($d = D$ in figures)
g = acceleration due to gravity
h = mean heat transfer coefficient, 1 W./(°K.)(sq. cm.) = 1,761 B.t.u./(sq. ft.)(hr./°F.)
k = heat conductivity of vapor
L = length of test section ($l = L$ in figures)
m = exponent of empirical correlation
n = empirical exponent
$N_{Gr} = D^3 \cdot \rho^2 \beta g \, \Delta T / \mu^2$

$$N_{Gr}^* = \frac{D^3 g \rho (\rho_v - \rho)}{\mu^2}$$

modified Grashof number
$N_{Nu} = hD/k$
$N_{Pr} = c_p \mu / k$
q = rate of heat flow
R = electrical resistance
R_{273} = electrical resistance at ice point
$R_{4.2}$ = electrical resistance at liquid-helium temperature
T = absolute temperature
T_m = mean temperature of vapor
ΔT = temperature difference

Greek Letters

β = Coefficient of thermal expansion
β^* = Modified coefficient of thermal expansion
ρ = density of vapor
ρ_L = density of saturated liquid
ρ_v = density of saturated vapor
μ = viscosity of vapor
λ = latent heat of vaporization
λ' = effective heat of vaporization

LITERATURE CITED

1. Karagounis, Aristides, *Suppl. Bull. de l'Institut International du Froid*, Annex 2, 195 (1956).
2. "American Institute of Physics Handbook," pp. 4–13 (1957); "Handbook of Chemistry and Physics," 34 ed., p. 2190 (1952–1953); G. K. White, and S. B. Woods, *Rev. Sci. Instr.*, **28**, 640 (1957).
3. Bromley, L. A., *Chem. Eng. Progr.*, **46**, 211 (1950).
4. Weil, Louis, "IVe Congr. Intern. du Chauf. Industr. Paris," No. 210 (1952).
5. Banchero, J. T., G. E. Barker, and R. H. Boll, *Chem. Eng. Progr. Symposium Ser. No. 17*, **51**, p. 21 (1955).
6. Bromley, L. A., *Ind. Eng. Chem.*, **44**, 2966 (1952).
7. Jakob, Max, "Heat Transfer," vol. I, John Wiley, New York (1949); Hermann Senftleben, *Z. angew. Phys.*, **3**, 361 (1951).
8. Hsu, Y. Y., and J. M. Westwater, *A.I.Ch.E. Journal*, **4**, 58 (1958).

Manuscript received September 11, 1958; revision received December 8, 1958; paper accepted December 29, 1958.

COMMUNICATIONS TO THE EDITOR

The Uselessness of Raffinate Reflux

J. F. WEHNER

The Catholic University of America, Washington, D. C.

The theory behind the separation of liquid mixtures into their constituents by solvent extraction is based on the relatively simple, exact, material-balance calculation which may be done graphically for a two-component system. In this operation a feed stream is separated into two streams by contact with a partially miscible solvent in a countercurrent cascade (*1, 2*). Ideally one component is extracted into a solvent rich phase and the other is obtained in a solvent poor or raffinate phase. The separation is complete when the solvent is recovered from each stream. In a finite cascade each constituent is contaminated by a certain portion of the other constituent, which can be made as small as desired if the solvent is partially miscible with each component. Even so, to achieve this degree of separation the cascade must be modified by feeding into an intermediate stage and refluxing a portion of the product recovered from the extract.

A number of expositions of this theory show a countercurrent cascade which also includes reflux from the raffinate phase as a useful method of operation. This mode of operation is a needless generalization of the reflux concept, as it cannot achieve any degree of separation which cannot be obtained in its absence. The number of theoretical stages required for a desired separation is the same with or without raffinate reflux. In addition the use of raffinate reflux requires an extra solvent mixing stage. The saturation of the solvent that is achieved in this mixing stage can in no way aid the possible degree of separation. That the number of theoretical stages other than the mixing stage depends only on the degree of separation and an extract reflux ratio great enough to avoid a pinch point at any stage along the cascade is shown by locating the operating points and stepping off stages starting from the raffinate end. Alternately it can be seen that the number of stages is exactly the same when the material balances are started from the extract end and the reflux ratio is adjusted by trial and error until an integral number of stages is achieved. This latter condition is in reality the only situation in which the solution is exact mathematically. The nonintegral number of stages generally obtained for an arbitrary reflux ratio is only an approximation.

The lack of usefulness of raffinate reflux applies also in the case of extraction with a solvent that is immiscible with only one of the constituents of a binary system. In this case extract reflux may or may not be used. Without extract reflux, raffinate reflux achieves with an extra mixing stage only that separation which an adequate solvent-to-feed ratio already assures. Extract reflux can improve the degree of separation by a considerable amount if a solvent of low selectivity must be used but will not greatly aid the separation if a highly selective solvent is available.

ACKNOWLEDGMENT

The author is grateful to Professor M. R. Fenske for his constructive review.

LITERATURE CITED

1. Treybal, R. E., "Liquid Extraction," McGraw-Hill, New York (1951).
2. Perry, John H., ed., "Chemical Engineers' Handbook," 3 ed., p. 713 (1950).

The Uselessness of Total Reboiling

J. F. WEHNER

The Catholic University of America, Washington, D. C.

It has been shown (*1*, *2*) that solvent extraction and rectification are analogous operations. The operation analogous to raffinate reflux discussed in the previous note is total reboiling (*3*). In this operation a liquid stream from the bottom of a rectifying tower is split into two streams; one is vaporized and sent back to the tower, and the other is a bottoms product. Total reboiling also is subject to the same objections; it does not aid the degree of separation and requires one extra plate in a tower. It is not widely claimed as being useful and is not discussed in any authoritative works on distillation.

In constructing a McCabe-Thiele diagram for a desired separation it may be noted that the intersection of the lower operating line with the diagonal has physical significance only for the total reboiling operation. This significance has been obtained at the expense of an extra theoretical plate. The McCabe-Thiele diagram is identical for the case of partial reboiling, which is advantageous with regard to equipment. However in this case this same intersection of the operating line with the diagonal has no physical meaning. The use of total reboiling to give a meaning to this intersection should not lead one to believe that it has practical usefulness.

ACKNOWLEDGMENT

The author is grateful for the constructive review by Professor M. R. Fenske.

LITERATURE CITED

1. Varteressian, K. A., and M. R. Fenske, *Ind. Eng. Chem.* **29**, 270 (1937).
2. Maloney, J. O., and A. E. Schubert, *Trans. Am. Inst. Chem. Engrs.*, **36**, 741 (1940).
3. Randall, Merle, and Bruce Longtin, *Ind. Eng. Chem.*, **30**, 1188 (1938).

Semifluidization: Mass Transfer in Semifluidized Beds

LIANG-TSENG FAN, YUNG-CHIA YANG, and CHIN-YUNG WEN

Kansas State University, Manhattan, Kansas

It is the purpose of this communication to report the preliminary performance data of a new and unique type of fluid-solid contact operation which may be termed "semifluidization."

A state of fluidization results when the flow rate of fluid passing upward through a bed of solid particles becomes sufficiently high to buoy the solid particles, provided a sufficient space of free board is available for free expansion of the bed.

The characteristics of fluidization, especially its advantages over fixed-bed operation, are extensively discussed elsewhere. However the fluidization process is not immune from some serious defects of its own, such as loss of driving potential for the transport processes within the bed due to the back mixing of the solid particles, attrition and elutriation of the solid particles, necessity of considerable free board above the bed, and erosion of the containing vessel.

The present authors have speculated about the possibilities of eliminating those defects and attaining a type of solid-fluid contactor which compromises the features of both fixed and fluidized beds by partially restricting expansion of the fluidized bed.

Such possibilities are hinted from many of the correlations of transport processes (*1*, *4*) within the solid-particles-fluid contactors, which are claimed to be equally applicable both to the fixed bed and to the fluidized bed. For instance the mass transfer factor of J_d factor correlation of Chu and his co-workers (*1*) suggests that, irrespective of the type of operation (fixed bed or fluidization), the rate of mass transfer can be altered if the porosity of the bed can be changed.

However expansion of the bed, and consequently the porosity of the conventional fluidized bed, is a function of the geometrical characteristics of the solid particles, the physical properties of the solid particles and fluid, and the flow conditions of the fluid and is not subject to arbitrary control. In other words the porosity of the fluidized beds must be treated as a dependent variable rather than an independent variable.

A typical set of available data on bed expansion is plotted in Figure 1, in which the porosity of the beds is plotted against the rate of fluid flow (*2*).

While the expansion in a conventional fluidized bed is allowed freely, in a semifluidized bed the bed expansion is restricted by a porous or sieve plate introduced above the expanding bed, thus forcing formation of a fixed bed above the fluidized bed. By adjusting the position of the movable top sieve plate one can vary the over-all bed porosity. Therefore the desired heights of fixed and fluidized sections for optimum driving potential for mass, heat, and momentum transfer can be obtained.

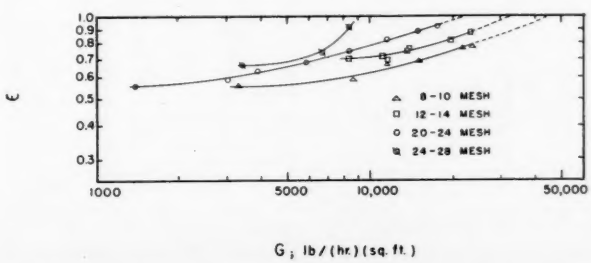

Fig. 1. Porosity of bed of benzoic-acid particle fluidized with water (*2*).

Chin-Yung Wen is at West Virginia University Morgantown, West Virginia.

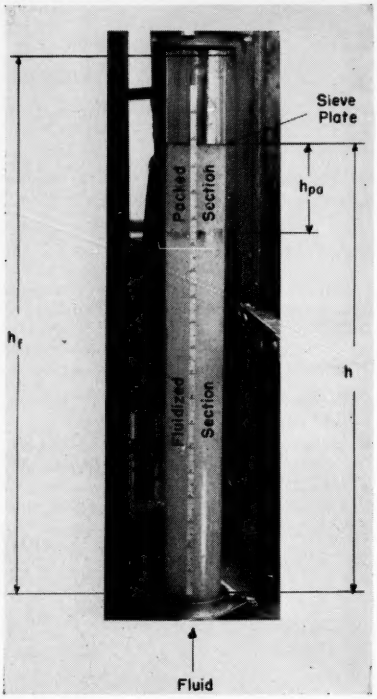

Fig. 2. Semifluidization of benzoic acid-water system.

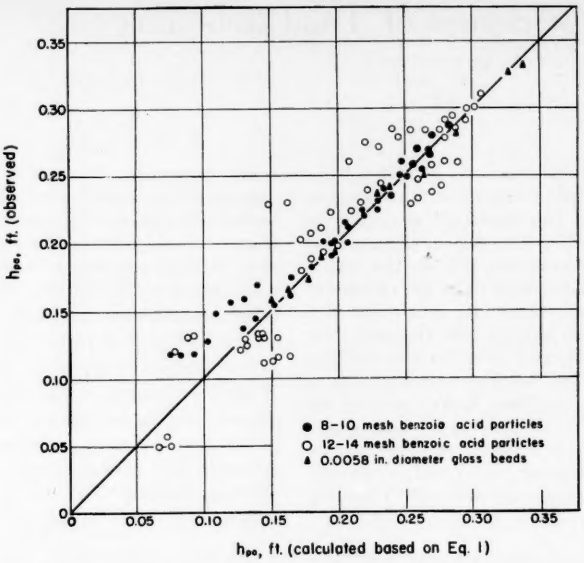

Fig. 4. Heights of packed-bed section whose calculation is based on Equation (1) and compared with that experimentally observed.

EXPERIMENTAL

The benzoic acid-water system was employed in the present investigation. The mass transfer in the fixed and fluidized beds of the system has been investigated by various researchers (*2, 3*).

The experimental apparatus, procedure for preparing solid particles, and the operating procedure employed by Evan and Gerald (*2*) were closely followed with the exception of the following modifications:

1. A movable top sieve plate was installed within the column containing the solid particles so that the expansion, and consequently the over-all porosity, of the bed could be controlled.

2. To minimize the change in geometry of the particles during the experimental runs none of the individual runs exceeded 80 sec. This resulted in a decrease of less than 3% of the initial weight of the solid particles for a single run.

A few preliminary test runs indicated that reproducibility of the Evan and Gerald data are excellent.

RESULTS OF EXPERIMENTS AND DISCUSSION OF RESULTS

As the picture in Figure 2 indicates it was found that a definite fraction of the solid particles formed a fixed bed immediately below the top sieve plate. The remainder of the particles remained in fluidized condition below the packed section. The name of "semifluidization" was taken from this phenomenon.

The segregation of the particles depended on factors such as the particle and fluid characteristics, flow conditions, and the expansion of the bed allowed. This is illustrated in Figure 3. The bed-expansion ratio is the height between the top sieve plate and the bottom of the expanded bed divided by the height of the bed before expansion.

Based on a simple material balance the height of the packed-bed section in the semifluidized bed can be derived. If the behavior of the particles in a column is assumed to be independent and uniform as is the case in a particulate type of fluidization, when one refers to Figure 2

$$h_{pa}\rho_s(1 - \epsilon_{pa}) = [h_{pa} + (h_f - h)]\rho_s(1 - \epsilon_f)$$

or

$$h_{pa} = (h_f - h)\frac{1 - \epsilon_f}{\epsilon_f - \epsilon_{pa}} \qquad (1)$$

The relationship concerning these quantities and operating conditions have been reported in literature (*5*). Figure 4 indicates the height of packed section calculated based on Equation (1) and that obtained from the experiments.

The weight fraction of solid in packed section can be calculated from

$$X = \frac{\rho_s A(1 - \epsilon_{pa})(h_f - h)}{W} \cdot \frac{1 - \epsilon_f}{\epsilon_f - \epsilon_{pa}} \qquad (2)$$

The agreement indicated in Figure 4 is good considering that the large-and irregular-size particles of benzoic acid were employed and that the data include $\epsilon_f > 0.8$ where the measurements of

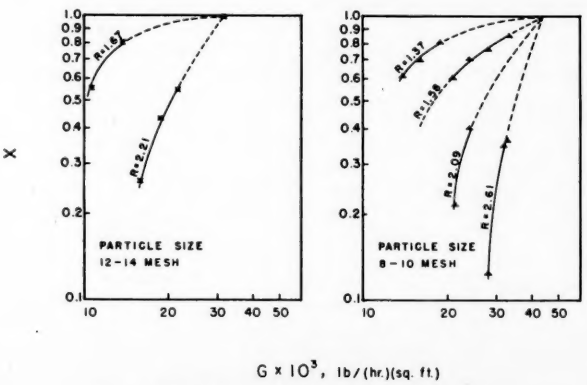

Fig. 3. Weight fraction of packed particles.

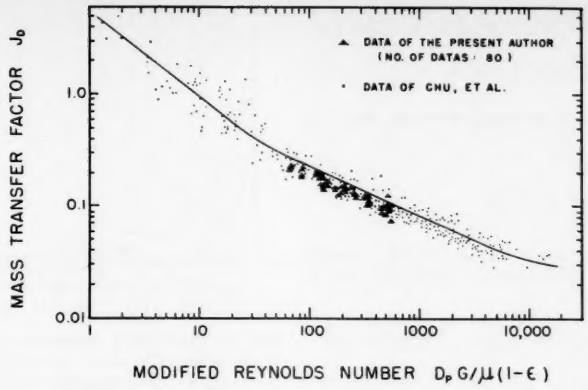

Fig. 5. Generalized correlation of mass transfer data (*1*).

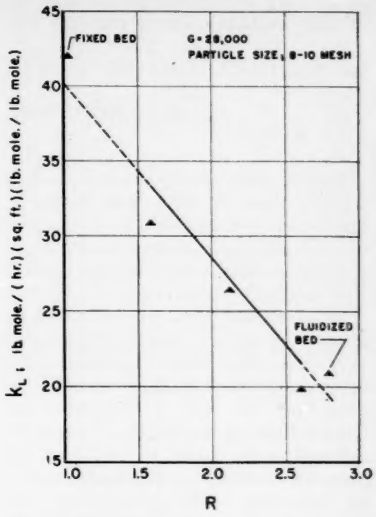

Fig. 6. Expansion ratio vs. mass transfer coefficient.

bed height could not be made accurately.

As indicated in the figure the deviation for the larger particles is greater than for the smaller ones.

The mass transfer data were correlated in terms of the J_d factor and the modified Reynolds number (*1*) (Figure 5). The mass transfer coefficients were calculated on the basis of the over-all logarithmic mean driving force, as was done by other investigators (*1, 2*) for both packed- and fluidized-bed mass transfer. The solid line in Figure 5 is a line of a generalized correlation used by Chu and his co-workers (*1*) to correlate the mass transfer data in both the fixed beds and the fluidized beds. The magnitude of the deviations from the line of the data by the present authors is of the same order as that of the data used by Chu, *et al.*

The axial concentration gradient within the semifluidized bed is being investigated.

To illustrate the effect of controlled expansion the mass transfer coefficients under approximately constant operating conditions are plotted against expansion ratios in Figure 6.

For a given fluid-flow rate a desired mass transfer coefficient can be selected by adjusting the position of the top sieve plate. The values of k_L for semifluidized bed lie between the limits corresponding to the fixed bed at one end and the fluidized bed (*2*) at the other. For a given expansion ratio the mass transfer coefficient was found to increase as the fluid flow rate is increased.

CONCLUSIONS

The following significant conclusions could be drawn from the results of the present investigation:

1. The segregation of the solid particles into two distinct sections, the fixed bed (upper section) and the fluidized bed (lower section), is caused within a fluidized bed by denying it full expansion. In other words it is possible to carry out the fixed bed and fluidization operations simultaneously within a single vessel.

2. The depth of the packed section, and consequently the fluidized section, are a function of the flow conditions, particle and fluid characteristics, and the expansion of the bed allowed.

The ratio of the depth of the fixed bed to the depth of the fluidized bed can be fixed arbitrarily for certain particles and fluids by controlling the expansion of the bed with the upper sieve plate.

3. The rate of mass transfer is also affected not only by the characteristics of the particles, fluids, and flow rate but also by the amount of expansion of the bed allowed. The magnitudes of mass transfer coefficients can be controlled approximately linearly and within the limits of a completely fixed bed and a fully fluidized bed by means of bed expansion alone.

The expansion of the bed can be introduced as an independent factor, in addition to such factors as temperature, pressure, and flow rate, in controlling the rate of mass transfer for any solid particles-fluid system.

The preliminary phase of the present investigation was concerned with the heights of fixed and fluidized sections and the aspect of mass transfer. However the result has very significant implications to the other aspects of this new operation, such as momentum transfer, heat transfer, and chemical reaction rate in the semifluidized beds. A comprehensive study of these phases of operation in semifluidized bed shall be reported in a paper to follow this communication.

The great possibility of the practical application of this new operation of semifluidization is beyond the need of much description since both fixed beds and fluidized beds are extensively employed in industry as catalytic reactors, ion exchange columns, heat exchangers, driers, solvent extractors, and other process equipments.

It is difficult to predict the occurrence of semifluidization for a large diameter column (of the order of 2 ~ 3 ft.) based on the evidence from the small laboratory-scale column. However it is believed that such phenomena are quite possible in a particulate fluidization but may not be possible in an aggregative fluidization.

NOTATION

D = diameter of particle, ft.
G = mass velocity of fluid, lb./(hr.)(sq. ft.)
J_d = mass transfer factor, dimensionless
h = depth or height of particle bed, ft.
k_L = mass transfer coefficient in liquid phase, lb. mole/(hr.)(sq. ft.)
R = bed expansion ratio, the height between the top sieve plate and the bottom of the expanded bed divided by the height of the bed before expansion, dimensionless.
X = weight fraction of particles in fixed bed, dimensionless
ϵ = void fraction or porosity in the bed of particles, dimensionless
μ = viscosity, lb./(hr.)(ft.)

Subscripts

f = fluidization
L = liquid
S = solid particle
pa = packed bed

LITERATURE CITED

1. Chu, J. C., *et al.*, *Chem. Eng. Progr.*, **49**, 141 (1953).
2. Evans, G. C., and C. F. Gerald, *ibid.*, 135 (1953).
3. Ishino, T., *et al.*, *Chem. Eng.* (*Japan*), **15**, 261 (1951).
4. Morse, R. D., *Ind. Eng. Chem.*, **41**, 1117 (1949).
5. Wen, C. Y., and Max Leva, *A.I.Ch.E. Journal*, **2**, 482, (1956).

The Ratio of Fluids to Solid Temperature and/or Concentration in Fixed-bed Processes

H. E. HOELSCHER, The Johns Hopkins University, Baltimore, Maryland

Design calculations related to heat transfer rates in fixed beds frequently involve the assumption that local values of solid and gas temperatures are equal. For the parallel mass transfer problem (for example, adsorption or ion exchange) gas and solid concentrations are often assumed to be directly proportional. It is obviously desirable to examine this assumption to determine under what conditions the ratio of fluid to solid temperature or concentration is negligibly different from unity. For at least one class of problems this question can easily be answered with information and techniques currently available in the technical literature.

Goldstein (*1, 2*) has developed the mathematics of wave-propagation rates through a fixed bed where there is no transfer across the containing wall, but a nonlinear surface rate equation is used; for example, in the case of adsorption, the latter corresponds to the use of a Langmuir type of isotherm. His results may be applied directly to determine the ratio of the solid to fluid concentration. The mathematical development presented by Goldstein is both lengthy and complex; however the useful results for the engineering student or for the research or design engineer are summarized below.

$$u = \frac{J(rx, y)}{e^{(1-r)(x-y)}\{1 - J(x, ry)\} + J(rx, y)} \quad (1)$$

$$v = \frac{1 - J(y, rx)}{e^{(1-r)(x-y)}\{1 - J(x, ry)\} + J(rx, y)} \quad (2)$$

where

$$J(x, y) \equiv 1 - e^{-y} \int_0^x e^{-s} I_0(2\sqrt{sy})\, ds \quad (3)$$

and

For adsorption	*For heat transfer*
$u = \dfrac{C_A - C_{A_0}^*}{C_{A_0} - C_{A_0}^*}$	$\dfrac{T_f - T_{s_0}}{T_{f_0} - T_{s_0}}$
$v = \dfrac{q_A - q_{A_0}}{q_{A_0}^* - q_{A_0}}$	$\dfrac{T_s - T_{s_0}}{T_{f_0} - T_{s_0}}$
$r = \dfrac{1}{1 + K_A C_{A_0}}$	1
$x = \dfrac{k\rho_B \rho_f q^* z}{G}$	$= \dfrac{h}{c_{p_f}} \dfrac{V}{GA}$
$y = \dfrac{k(1 + K_A C_{A_0})\alpha\rho_f}{KG}\left(\dfrac{G}{\alpha\rho_f} t - z\right)$	$= \dfrac{h}{C_{p_s}(1 - \alpha)}\left(t - \dfrac{\alpha\rho_f z}{G}\right)$

In this development the kinetic equation for the rate of adsorption by the solid is

$$\frac{\partial q}{\partial t} = k\left[C(q^* - q) - \frac{q}{K}\right]$$

This corresponds to the use of a Langmuir type of adsorption isotherm, that is

$$C^* = \frac{q/q^*}{K(1 - q/q^*)} = \frac{q}{K(q^* - q)}$$

with a rate equation for the surface adsorption expressed as

$$\frac{\partial q}{\partial t} = k(C - C^*)$$

Thus the ratio of fluid to solids temperature, for example, at any time and bed location may be calculated:

$$\frac{u}{v} \equiv \frac{T_f - T_{s_0}}{T_s - T_{s_0}} = \frac{J(x, y)}{1 - J(y, x)}$$

and, correspondingly, the ratio of fluid to solid concentration may be calculated:

$$\frac{u}{v} \equiv \frac{C_A - C_{A_0}^*}{q_A - q_{A_0}} = \frac{J(rx, y)}{1 - J(y, rx)}$$

To apply this method to the case of adsorption or ion exchange will require values of r and hence will require knowledge of the adsorption rate, data that are available in the literature. Thus the assumption regarding equality of fluid and solid concentrations can be checked.

Opler and Hiester (*3*) have prepared extensive tables of values for both u and v as a function of x and with parameters of v/x. From these tables values can be obtained for any specific problem of heating a fixed bed of solid particles with a hot gas from some initial temperature to an arbitrary final temperature. The ratio of u/v as a function of elapsed time for various values of bed length x is shown in Figure 1. This method may be applied to a specific problem as follows.

A bed is considered which is 4 in. in diameter, 2 ft. in length; a gas flow rate is 150 cu. ft./hr. at the inlet temperature, and particle size is approximately ⅛ in. A value of the convection heat-transfer coefficient of approximately (h =) 100 B.t.u./(hr.) (sq. ft./°F.) is calculated from standard equations in the chemical engineering literature. Values for solid- and gas-phase heat capacity and densities were taken from the handbook, and a fraction void of 0.4 was assumed. For an elapsed time of 1 hr. it was found that

$$\frac{u}{v} \simeq \frac{0.1}{0.07} \sim 1.44$$

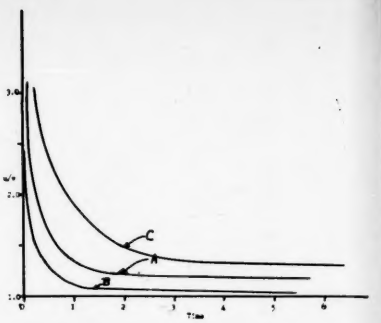

Fig. 1. Fluid/solid temperature ratio vs. elapsed time. Curve *A* : *X* = 18, *B* : *X* = 25, *C* : *X* = 10, time in hours.

NOTATION

A = cross-sectional area of bed = L^2
C = fluid phase concentration = M/L^3
c_p = heat capacity = heat units/M, °F.
G = mass rate of flow, $M/L^2\theta$
h = convection heat transfer coefficient (the analogue of k) = heat units/$L^3\theta$, °F.
k = adsorption rate constant = $L^3/\theta M$
K = adsorption equilibrium constant = L^3/M
q = solid phase concentration = M/g.
t = time
T = temperature
V = bed volume
z = bed length = L

Greek Letters

α = fraction void
ρ = density = M/L^3

Subscripts

0 = initial conditions
f = fluid
s = solid
B = bed

Superscript

* = equilibrium

LITERATURE CITED

1. Goldstein, S., *Proc. Roy. Soc.* (*London*), **A219**, 151 (1953).
2. *Ibid.*, 171.
3. Opler, Ascher, and N. K. Heister, "Tables for Predicting the Performance of Fixed Bed Ion Exchange and Similar Mass Transfer Processes," Stanford Research Institute, Stanford, Calif. (1954).

Thermodynamic Consistency Test for Multicomponent Solutions

J. M. PRAUSNITZ and G. D. SNIDER

University of California, Berkeley, California

In 1947 Herington (*1*) proposed a simple graphical method for testing the thermodynamic consistency of vapor-liquid equilibrium data for binary systems. Very shortly thereafter Redlich and Kister (*4*) independently proposed the same method. This convenient graphical test for thermodynamic consistency has won wide acceptance, and it is utilized with increasing frequency by workers in the field of phase equilibria.

Some years ago Herington showed how his consistency test might be applied to a ternary system (*2, 3*). The purpose of this work is to show how the Herington-Redlich-Kister method may be generalized for application to a system of any number of components.

For a given solution the general technique of the consistency test is to plot a particular function of the activity coefficients of all the components in that solution against the mole fraction of one of the components. If the thermodynamic data are consistent, then the area under the resulting curve is equal to the excess free energy of a solution containing one component less than the number of components in the solution being tested. In the case of a binary the data for the two-component solution are related to the excess free energy of a one-component solution which is zero. In the general case data for a solution of n components are related to the excess free energy of a solution of $n-1$ components.

A liquid-phase solution of n components is considered. The excess free energy for the solution is related to the activity coefficients by

$$\frac{\Delta G^E}{RT} = \sum_{i=1}^{n} x_i \ln \gamma_i \qquad (1)$$

M_i is defined by

$$M_i = \frac{x_i}{x_1} \qquad (2)$$

For a solution of n components $n-2$ such parameters are required for components $i = 2$ to $i = n-1$. In the discussion all M_i are constants, although not necessarily equal to one another.

Substituting (2) into (1) and noting that

$$x_n = 1 - x_1(1 + M_2 + M_3 + \cdots M_{n-1})$$

one obtains

$$\begin{aligned}\frac{\Delta G^E}{RT} &= x_1 \ln \gamma_1 + x_1 M_2 \ln \gamma_2 \\ &+ x_1 M_3 \ln \gamma_3 \\ &+ \cdots x_1 M_{n-1} \ln \gamma_{n-1} \\ &+ [1 - x_1(1 + M_2 \\ &+ M_3 + \cdots M_{n-1})] \ln \gamma_n\end{aligned} \qquad (3)$$

When Equation (3) is differentiated at constant temperature and pressure holding all M constant

$$\begin{aligned}\frac{1}{RT}\left(\frac{\partial \Delta G^E}{\partial x_1}\right)_{T,P,M_i} &= x_1 \frac{\partial \ln \gamma_1}{\partial x_1} + \ln \gamma_1 \\ &+ x_1 M_2 \frac{\partial \ln \gamma_2}{\partial x_1} \\ &+ M_2 \ln \gamma_2 + \cdots \\ &+ x_1 M_{n-1} \frac{\partial \ln \gamma_{n-1}}{\partial x_1} \\ &+ M_{n-1} \ln \gamma_{n-1} \\ &+ [1 - x_1(1 + M_2 + M_3 \\ &+ \cdots M_{n-1})] \frac{\partial \ln \gamma_n}{\partial x_1} \\ &- [1 + M_2 + M_3 \\ &+ \cdots M_{n-1}] \ln \gamma_n\end{aligned} \qquad (4)$$

At constant temperature and pressure the Gibbs-Duhem equation is

$$\sum_{i=1}^{n} x_i \frac{\partial \ln \gamma_i}{\partial x_1} = 0 \qquad (5)$$

When one substitutes (5) into (4)

$$\begin{aligned}\frac{1}{RT}\left(\frac{\partial \Delta G^E}{\partial x_1}\right)_{T,P,M_i} &= \ln \gamma_1 + M_2 \ln \gamma_2 \\ &+ M_3 \ln \gamma_3 \\ &+ \cdots M_{n-1} \ln \gamma_{n-1} \\ &- (1 + M_2 + M_3 \\ &+ \cdots M_{n-1}) \ln \gamma_n \\ &= \ln \gamma_1/\gamma_n \\ &+ M_2 \ln \gamma_2/\gamma_n \\ &+ M_3 \ln \gamma_3/\gamma_n \\ &+ \cdots M_{n-1} \ln \frac{\gamma_{n-1}}{\gamma_n}\end{aligned} \qquad (6)$$

Equation (6) is now integrated with respect to x_1 holding all M constant. The integration is performed from $x_1 = 0$ to

$$x_1 = \frac{1}{1 + \sum_{i=2}^{n-1} M_i}$$

At constant M, when $x_1 = 0$, $x_n = 1$ and the solution consists of pure component n. At $x_1 = 0$ therefore $\Delta G^E = 0$.

When

$$x_1 = \frac{1}{\left(1 + \sum_{i=2}^{n-1} M_i\right)}$$

$x_n = 0$ and the solution of n components is in the special state where it contains only $n-1$ components. When $x_n = 0$, ΔG^E is given by

$$\frac{\Delta G^E}{RT} = \sum_{i=1}^{n-1} x_i \ln \gamma_i$$

= function of a solution containing $n-1$ components (7)

WILEY BOOKS

1. PROCESS EQUIPMENT DESIGN: Vessel Design

By LLOYD E. BROWNELL and EDWIN H. YOUNG, both of Univ. of Michigan. Unifies basic concepts, industrial practice, and analytical aspects. Covers simple vessels for low-pressure and vacuum use, through thick-walled vessels for high-pressure application. Equations are completely derived and methods of analysis given. 1959. 408 pages. $19.50

2. HANDBOOK OF CHEMICAL MICROSCOPY

VOL. I. Third Edition

Principles and Use of Microscopes and Accessories; Physical Methods for the Study of Chemical Problems. By the late EMILE CHAMOT and CLYDE W. MASON, Cornell Univ. Completely revised to include material on electron microscopy, particle size, colloids, and aggregates—plus a new polarization color chart. 1958. 502 pages. $14.00

3. KINETICS OF HIGH-TEMPERATURE PROCESSES

Edited by W. D. KINGERY, M.I.T. Stresses high-temperature processes in general, nonmetal systems in particular, to form an integrated record of the field's status, and to help apply the data to often complex systems. A Technology Press Book, M.I.T. 1959. 326 pages. $13.50

4. THE PETROLEUM CHEMICALS INDUSTRY

SECOND EDITION

By RICHARD FRANK GOLDSTEIN. 1958. 458 pages. $16.50.

5. ANALYSIS OF PIPE STRUCTURES FOR FLEXIBILITY

By JOHN W. GASCOYNE. 1959. 181 pages. $7.50

6. SCIENTIFIC RUSSIAN

By GEORGE E. CONDOYANNIS. 1959. 228 pages. $3.50

JOHN WILEY & SONS, Inc.
440 Fourth Ave., New York 16, N. Y. AICE 99
1 2 3 4 5 6

Send on 10 day's approval the books circled. Within 10 days I'll remit full price plus postage or return books postpaid.

Name.....
Street.....
City.....Zone.....State.....

☐ Check here to save postage. Remit full price with order and we pay postage. Same return privilege.

Equation (6) therefore becomes

$$\sum_{i=1}^{n-1} x_i \ln \gamma_i = \int_0^{1/(1+\sum_{i=2}^{n-1} M_i)} \left[\ln \frac{\gamma_1}{\gamma_n} + M_2 \ln \frac{\gamma_2}{\gamma_n} + M_3 \ln \frac{\gamma_3}{\gamma_n} + \cdots M_{n-1} \ln \frac{\gamma_{n-1}}{\gamma_n} \right] dx_1 \quad (8)$$

The consistency test is carried out by the arbitrary selection of a set of parameters and the numerical (or graphical) evaluation of the integral in Equation (8) with activity-coefficient data for the solution of n components utilized. This integral must then be equal to the excess free energy of a solution of $n - 1$ components having the composition

$$x_1 = \frac{1}{1 + \sum_{i=2}^{n-1} M_i} \; ; \quad x_2 = M_2 x_1 \; ;$$

$$x_3 = M_3 x_1 \; ; \cdots x_{n-1} = M_{n-1} x_1$$

If this equality is met, the data tested are thermodynamically consistent. To cover a large section of the data it will of course be necessary to repeat the calculation several times with new sets of parameters each time. For a system of many components the calculations are necessarily quite tedious. However the form of this consistency test is very well suited for programming on an electronic computer.

NOTATION

ΔG^E = excess free energy
M = parameter defined by Equation (2)
n = number of components in solution
R = gas constant
T = absolute temperature
x = mole fraction in the liquid phase
γ = activity coefficient

Subscript

i = component i
$1,2 \cdots n$ = component $1,2 \cdots n$

LITERATURE CITED

1. Herington, E. F. G., *Nature*, **160**, 610 (1947).
2. ———, *Research*, **3**, 41 (1950).
3. ———, *J. Appl. Chem.*, **2**, 11 (1952).
4. Redlich, Otto, and A. T. Kister, *Ind. Eng. Chem.*, **40**, 345 (1948).

ERRATA

Vapor-Liquid Equilibria and Heat of Mixing: n-Octane-Ethylbenzene-Cellosolve System. P. S. Murti and Matthew Van Winkle.

Figure 4 of the above paper is in error. The corrected plot is presented below.
This article appeared on page 517 of the December, 1957, issue of the Journal.

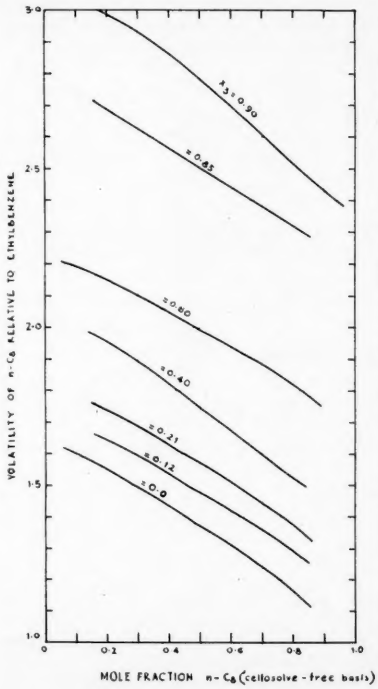

Fig. 4. Relative volatility parameter: mole fraction Cellosolve in ternary mixtures

Liquid-Side Mass Transfer Coefficients in Packed Towers. Kakusaburo Onda, Eizô Sada, and Yasuhiro Murase.

Equation (3) of the above paper is in error. It should read

$$a_w/a_t = 1 - 1.02e^{-0.278(L/a_t\mu)^{0.4}}$$

This article appeared on page 235 of the June, 1959, issue of the Journal.

(*Continued from page 276.*)

Fluid Dynamics and Heat Transfer, James G. Knudsen and Donald L. Katz, McGraw-Hill Book Company, Inc., New York (1958). 576 pages. $12.50.

The need for solving problems concerned with fluid heat transfer has always faced many engineers. In the past, because of the complex nature of fluids in motion, solutions to these problems have been found by an approach which was basically empirical. One illustration of this approach is an early edition of McAdams's comprehensive book "Heat Transmission." However there has been a growing awareness that fluid heat-transfer could best be understood by first understanding the

(*Continued on page 9S.*)

(*Continued from page 88.*)

nature of fluid flow in the turbulent and transiton regions. Although much of the treatment of turbulence has only progressed to the semitheoretical, substantial progress has been made in many areas of fluid dynamics—including transition and boundary layer flow. Nevertheless the record of accomplishments, which is spread through technical journals, has not been available in a textbook until recently.

Texts concerned with flow problems have appeared in the past five years, but most are too specialized for the purpose of introducing chemical engineers to those aspects of fluid flow which are useful for fluid heat transfer.

Recognizing this need for presenting the fundamentals of fluid dynamics basic to an understanding of convection heat transfer, Knudsen and Katz have prepared this text. In doing so the authors have codified and selected their choice of topics from the fluid dynamics literature. Since the material was organized and used in a specific graduate course in chemical engineering, the form has been arranged for class presentation. This form is also useful for the practicing engineer.

The title was probably intended to denote the relationship between heat transfer and fluid dynamics, for the authors make no attempt to be comprehensive in either field. Since the authors restrict themselves to certain fluids, many topics frequently included in a graduate course on fluid flow and heat transfer have been omitted; for example only incompressible liquids under forced convection are described. The authors clearly explain this narrowed scope as necessitated by the limitations of a one-semester course and also imply that this more integrated approach to heat transfer and fluid flow is a good basis for further, more comprehensive study of the applications of these two areas of study.

The greater part of the book is devoted to fluid dynamics, which is the subdivision of fluid mechanics concerned with the forces acting on the fluids. Starting with the partial differential equations of motion, using both the usual notation and the vector notation, the authors demonstrate some of the solutions to these equations, such as those for nonviscous flow and laminar pipe flow. The discussion of conduit turbulent flow is centered around the universal velocity profile obtained from Prandtl's mixing-length theory. From an introduction to boundary-layer theory immersed body flow is developed and is followed by an important chemical engineering application of immersed body flow, that is, flow on the shell side of heat exchangers.

The approach used throughout this section is one of presenting the theory briefly and then justifying or criticizing the theory with substantial experimental results. It is presumed that a reader interested in detailed, rigorous solutions of the applicable equations may refer to more theoretical references such as Schlichting's "Boundary Layer Theory."

Since the heat transfer section builds on the concepts and the developments described in fluid flow, and since only forced convection transfer is discussed, this section comprises only the last third of the text. General equations are developed and examples solved for the case of heat transfer through laminar films. Turbulent flow heat transfer is first discussed in terms of empirical correlations and then in terms of the analogy between momentum and heat transfer and for cases of immersed body heat transfer. Although the discussion of the empirical correlations does not require the previous fluid flow developments, discussions of the analogy and the immersed body heat flow rely heavily on the university velocity profile and Prandtl mixing length developed earlier in the text. A section on liquid metals is also included, ostensibly to illustrate low Prandtl Number heat transfer and because of current commercial interest, but also to fulfill a need for discussion of this new field in a textbook.

Perhaps the greatest limitations to this book, especially for teaching purposes, are the topics omitted, such as compressible fluids and radiation. Some of these other topics might feasibly be included if some of historical-developments discussions were condensed, especially in the area of turbulence where only an approximate solution to the theory is currently available. Another limitation is the treatment of the terms which contain the phrases "boundary layer." Since terms such as "laminar boundary layer," which is not a "boundary layer" at all but rather the "boundary to the laminar sublayer," are included, there is a need for either revised terminology or precise description of the interrelation of all the "boundary" terms used. Perhaps boundary-layer theory could have been presented before rather than after the discussion of conduit flow and laminar and buffer layers.

Nevertheless this book is an excellent basis for a course on fluid dynamics and heat transfer. It is clearly written; its continuity is strong, and its development proceeds smoothly. It is the first book on fluid flow suitable for chemical engineering needs. The authors are also to be commended for filling the gap between the rigorous detailed treatment of fluid flow and the empirical approach of forced convection heat transfer. As such this book is a welcome addition to the engineering literature.

JOHN A. TALLMADGE, JR.

(*Continued on page 108.*)

spinbars

magnetic stirring bars

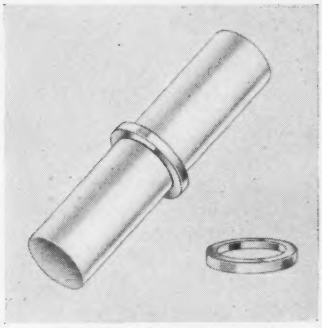

Pivot Ring at no extra cost.

teflon® kel-f® tygon® polyethylene high temp

The most widely accepted, lowest priced stirring bars on today's market.

Four years in research . . . research that has developed Spinbars with a powerful Alnico V Magnet encased in a solid one-piece capsule, each electrically and vacuum tested and absolutely leak proof. Available at any Laboratory Supply House.

SPINBARS, TEFLON	SPINBARS, KEL-F	SPINBARS, TYGON	SPINBARS, POLYETHYLENE
5/16" Dia. ½" Lg. to 2" Lg. ⅜" Dia. ⅜" Lg. to 2⅛" Lg. ½" Dia. 1⅝" Lg. to 3" Lg. ⅝" Dia. 1¾" Lg. to 1⅞" Lg.	¼" Dia. ½" Lg. to ⅞" Lg. 5/16" Dia. ½" Lg. to 2" Lg. ⅜" Dia. ⅜" Lg. to 2⅛" Lg. ½" Dia. 1⅝" Lg. to 3" Lg. ⅝" Dia. 1¾" Lg. to 1⅞" Lg.	⅜" Dia. ⅜" Lg. to 2⅛" Lg. ⅝" Dia 1¾" Lg.	5/16" Dia. ½" Lg. to 2" Lg. ⅜" Dia. ⅜" Lg. to 2⅛" Lg.

*Trademarks DuPont Kellog U. S. Stoneware

Stirring Bars for every requirement in Teflon, Kel-F, Tygon and Polyethylene—all leak proof, laboratory tested.

Spinbars are available, like all better products through Laboratory Supply Houses.

SPINBARS . . . designed for greater movement and agitation.

LPF LABORATORY PLASTICWARE FABRICATORS

714 BALTIMORE • P. O. BOX 213 • KANSAS CITY 5, MO.

(*Continued from page 9S.*)

Recent Advances in the Engineering Sciences, Proceedings of Conference on Science and Technology for Deans of Engineering, Purdue University, September, 1957, McGraw-Hill Book Company, Inc., New York 1958). 257 pages. $4.75.

With the rapidly developing science and technology of today there is an increasing demand for engineers having an educational background built on a more solid foundation of mathematics and science than is provided by the usual engineering curriculum. This demand is being met in part today by men whose first training is in mathematics and science and who later develop the required interest and background in engineering and in part by men who start their education in engineering school and later acquire interest and background in mathematics and science. It has been proposed that the education of these men might be better accomplished by a program which recognizes from the beginning the duality of interests. The concept of the engineering sciences arises naturally from the demand for such a program, and the general nature of the engineering sciences can be surmised from the requirements noted above. Because the concept, which has been adopted in several institutions, is of interest to many schools and because it is still in its formative stages the conference which is the subject of this book was held.

The basic plan of the conference involved first the selection of seven topics which might be regarded as engineering sciences. Two speakers were then selected for each topic, one to present a survey of the field and the other to discuss the impact of this field on engineering education. The selection of topics should not be taken as a definition of the fields of engineering science, either by inclusion or omission. It will be apparent that some of these topics might well be combined into more general headings and that some areas have not been included. The particular areas which were chosen for this conference are automation and automatic control; operations research and systems engineering; thermodynamics; mass, momentum, and heat transfer; nuclear engineering; solid state physics and engineering materials; and computer development and application.

The articles vary considerably in depth. In general however they are written for an engineering audience without specialized training in the various topics. Most engineers will find the surveys of the various fields to be of interest. Also of interest to engineers in practice and in education will be the authors' opinions as to trends in engineering education.

CHARLES A. WALKER

INDEX OF ADVERTISERS

Academic Press 6S
Eimco Corporation, The ..... Inside Back Cover
Electronic Associates, Inc. .... Inside Front Cover
Hevi Duty Electric Company 276
Industrial Research 4-5
Kellogg Co., M. W., The ... Outside Back Cover
Laboratory Plasticware Fabricators 9
Stearns-Rogers Mfg. Co., The 10
Wiley & Sons, Inc., John 8

Advertising Offices

New York 36—Paul A. Jolcuvar, Adv. Sales Mgr., Carl G. Lassen, Asst. Adv. Sales Mgr., Donald J. Stroop, Dist. Mgr., Robert S. Bugbee, Dist. Mgr.; 25 W. 45th St., COlumbus 5-7330.

Philadelphia—Lee W. Swift, Jr., Dist. Mgr.; 1207 Broad-Locust Bldg., PEnnypacker 5-5560.

Chicago 4—Martin J. Crowley, Jr., Dist. Mgr.; Robert Kliesch, Dist. Mgr.; 53 West Jackson Blv., Room 504, HArrison 7-3760.

Cleveland 15—Harry L. Gebauer, Dist. Mgr., 1501 Euclid Ave., SUperior 1-3315.

Pasadena 1, Calif.—Richard P. McKey, Dist. Mgr., 465 East Union St., MUrray 1-0685.

Dallas 18—Richard E. Hoierman, Dist. Mgr., 9006 Capri Drive, DIamond 8-1229.

Birmingham 9, Ala.—Fred W. Smith, Dist. Mgr., 1201 Forest View Lane, Vesthaven, TRemont 1-5762.

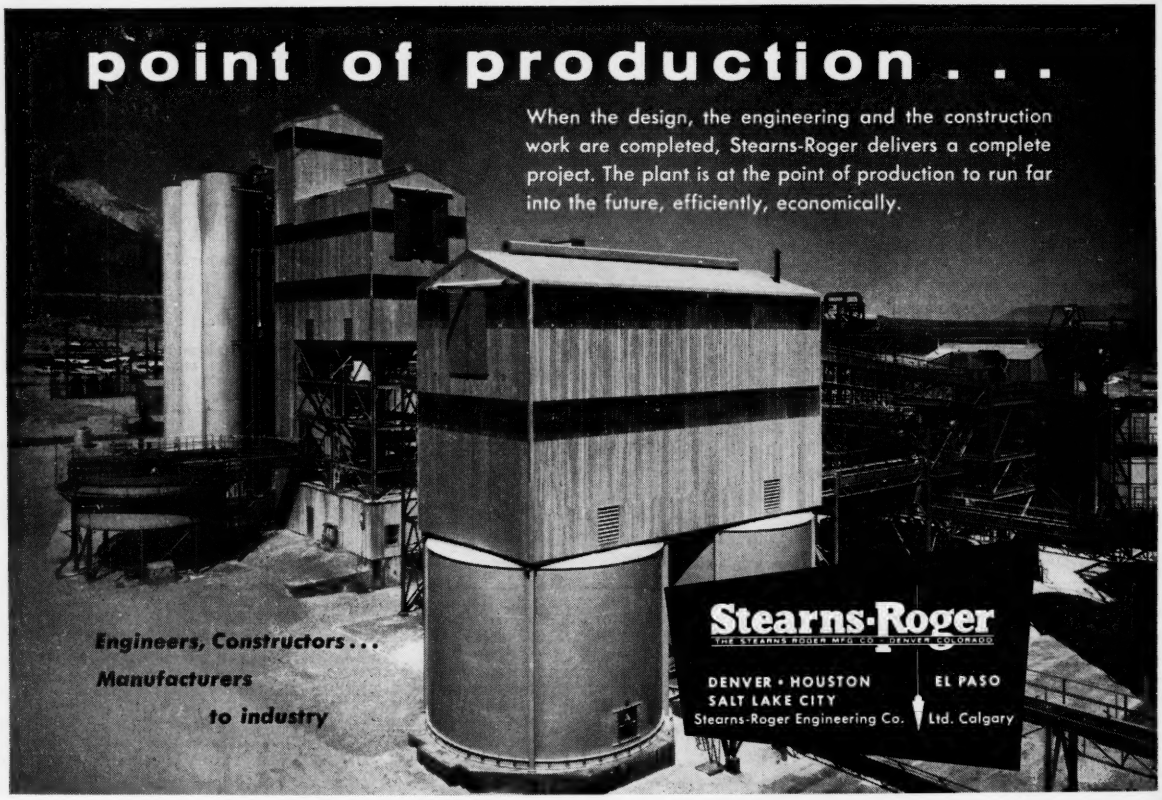
point of production . . .
When the design, the engineering and the construction work are completed, Stearns-Roger delivers a complete project. The plant is at the point of production to run far into the future, efficiently, economically.
Engineers, Constructors . . .
Manufacturers
to industry
Stearns-Roger
THE STEARNS-ROGER MFG. CO. DENVER, COLORADO
DENVER • HOUSTON
SALT LAKE CITY
EL PASO
Stearns-Roger Engineering Co. Ltd. Calgary

..6S
over
over
.276
.4-5
over
...9
..10
...8

Sales
Sales
obert
CO-

Mgr.;
5560.
Mgr.;
kson

Mgr.,

Dist.
5.
Mgr.,

Dist.
aven,